

UNIVERSITÀ DELLA CALABRIA



UNIVERSITA' DELLA CALABRIA

Dipartimento di Biologia, Ecologia e Scienze della Terra

Dottorato di Ricerca in
SCIENZE E INGEGNERIA DELL'AMBIENTE,
DELLE COSTRUZIONI E DELL'ENERGIA - SIACE

CICLO

XXIX

**SOME CALABRIAN STONES AS BUILDING MATERIALS:
CHARACTERIZATION, DURABILITY AND USE SUGGESTIONS**

Settore Scientifico Disciplinare GEO/09

(Georisorse Minerarie e Applicazioni Mineralogico- Petrografiche per l'Ambiente ed i Beni Culturali)

Coordinatore: Ch.mo Prof. PIETRO SALVATORE PANTANO



Tutor: Ch.mo Prof. MAURIZIO PONTE



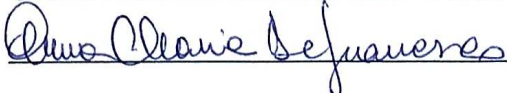
Co-Tutors: Ch.ma Prof.ssa MONICA ÁLVAREZ DE BUERGO BALLESTER



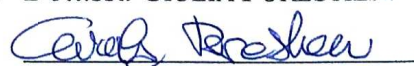
Ch.mo Prof. ALESSANDRO CAMPOLONGO



Ch.ma Prof.ssa ANNA MARIA DE FRANCESCO



Dottoranda: Dott.ssa GIULIA FORESTIERI



Index

Index	II
Acknowledgements	VII
Abstract	IX
Executive summary	XII
Sintesi	XVII
Articolazione e contenuti	XXI
Abbreviations	XXVI
1. Objectives	2
2. Introduction – Building stones in architecture	5
2.1 Natural stone uses in Architecture	7
2.2 Stone deterioration.....	13
3. Stones selection	18
3.1 Criteria for the selection	18
3.2 Historical background and architectural models	18
3.2.1 <i>The school of stonemasons of San Giovanni in Fiore</i>	19
3.2.2 <i>The school of stonemasons of Basilicata and the northern part of Calabria</i>	26
3.2.3 <i>The schools of stonemasons of Rogliano and Altilia</i>	29
3.2.4 <i>The school of stonemasons of Fuscaldo</i>	36
3.3 Quarries and materials – Calabria and Cosenza Province	44
3.3.1 <i>Natural stones</i>	44
3.3.2 <i>Italian and Calabrian stone market</i>	46
3.3.3 <i>Ancient quarries of Cosenza Province</i>	53
3.3.4 <i>Italian and Calabrian quarry standards</i>	58
3.3.5 <i>Types of quarries of Cosenza Province</i>	60
3.3.6 <i>Extraction methods of Cosenza Province</i>	63
3.3.7 <i>Traditional types of stone finishing of Cosenza Province</i>	68
<i>Rock faced</i>	69
<i>Rough pointed with/without chiseled margin</i>	69
<i>Furrowed surface</i>	69
<i>Bush-hammered</i>	69
3.4 Selected stones – Architectural and geological setting.....	70
3.4.1 <i>San Giovanni in Fiore granite</i>	70
<i>Geological setting and stone extraction</i>	72

3.4.2	<i>Grisolia stone</i>	77
	<i>Geological setting and stone extraction</i>	79
3.4.3	<i>San Lucido calcarenite</i>	81
	<i>Geological setting and stone extraction</i>	83
3.4.4	<i>Fuscaldo sandstone</i>	88
	<i>Geological setting and stone extraction</i>	89
4.	Cosenza Province masonries: construction techniques	92
4.1	Uncoursed random rubble masonry	93
4.2	Coursed random rubble	101
4.3	Ashlar masonry	103
5.	Methods and materials	106
5.1	Sampling and sample preparation	106
5.2	Techniques applied for the material characterization (NDT and laboratory tests) and rock fabrics (anisotropy)	109
5.3	Petrographic description	110
5.4	Chemical and mineralogical characterization	111
5.5	Surface properties	113
5.5.1	<i>Chromatic parameters</i>	114
5.6	Petrophysical properties	118
	<i>Porosity</i>	118
5.6.1	<i>Porosity accessible to water and real and bulk densities</i>	119
5.6.2	<i>Mercury intrusion porosimetry (MIP)</i>	121
5.6.3	<i>Air permeability</i>	123
5.7	Hydric properties	124
5.7.1	<i>Capillary water absorption – (Infrared Camera)</i>	125
5.7.2	<i>Water absorption/desorption at atmospheric pressure</i>	126
	<i>Water absorption</i>	126
	<i>Water desorption</i>	128
5.7.3	<i>Natural hydrophobicity by water static contact angle</i>	129
5.8	Mechanical properties	130
	<i>Anisotropy</i>	130
5.8.1	<i>Ultrasound propagation velocity (P waves)</i>	132
5.8.2	<i>Ultrasound propagation velocity (S waves)</i>	134
	<i>Hardness</i>	136
5.8.3	<i>Micro-hardness (Equotip), drilling resistance measuring system (DRMS) and Schmidt Hammer test</i>	137

<i>Micro-hardness</i>	137
<i>Drilling resistance</i>	138
<i>Schmidt hammer test</i>	140
<i>Strength properties</i>	142
5.8.4 <i>Uniaxial compressive strength</i>	142
5.8.5 <i>Flexural strength</i>	144
5.8.6 <i>Indirect Tensile strength test (Brazilian test)</i>	146
5.8.7 <i>Point Load test</i>	148
<i>Abrasion Resistance</i>	149
5.8.8 <i>Polished Stone Value</i>	150
<i>Los Angeles</i>	150
<i>Micro-Deval</i>	152
6. Characterization: results	156
6.1 Petrographic description.....	156
<i>San Giovanni in Fiore granite (GF)</i>	156
<i>Grisolia stone (DG)</i>	165
<i>San Lucido calcarenite (CS)</i>	168
<i>Fuscaldo sandstone (AF)</i>	171
6.2 Chemical and mineralogical characterization.....	174
6.3 Surface properties	175
6.3.1 <i>Chromatic parameters</i>	175
6.4 Petrophysical properties	179
6.4.1 <i>Porosity accessible to water and real and bulk densities</i>	180
6.4.2 <i>Mercury intrusion porosimetry (MIP)</i>	181
6.4.3 <i>Air permeability</i>	184
6.5 Hydric properties	186
6.5.1 <i>Capillary water absorption – (Infrared Camera)</i>	186
6.5.2 <i>Water absorption/desorption at atmospheric pressure</i>	196
<i>Water absorption</i>	196
<i>Water desorption</i>	202
6.5.3 <i>Natural hydrophobicity by water static contact angle</i>	206
6.6 Mechanical properties.....	207
6.6.1 <i>Ultrasound propagation velocity (P waves)</i>	207
6.6.2 <i>Ultrasound propagation velocity (S waves)</i>	209
6.6.3 <i>Leeb Micro-hardness (Equotip), Drilling resistance and Schmidt hammer test</i>	211
6.6.4 <i>Uniaxial compressive strength</i>	221

6.6.5	<i>Flexural strength</i>	230
6.6.6	<i>Indirect Tensile strength test (Brazilian test)</i>	235
6.6.7	<i>Point Load test</i>	239
6.6.8	<i>Polished Stone Value</i>	240
	<i>Los Angeles and Micro-Deval</i>	240
7.	Discussion and summary of stone properties	244
	<i>Mineralogical, chemical and petrographic correlation</i>	244
	<i>Pore system and correlation between porosity and mechanical properties</i>	247
	<i>Hydric behavior</i>	265
	<i>Correlation between ultrasonic velocities, petrographic properties and stiffness</i>	267
	<i>Correlation between Drilling resistance and mechanical properties</i>	272
	<i>Correlation between compressive, tensile and flexural strengths</i>	276
	<i>Correlation between Point Load and mechanical properties</i>	283
8.	Durability	288
8.1	Action of salts.....	288
8.2	Salt crystallization process	289
8.3	Salt crystallization test.....	290
8.3.1	<i>Procedure</i>	290
8.3.2	<i>Results of the salt crystallization test</i>	291
8.3.3	<i>Discussion of the salt crystallization test</i>	297
8.4	Ice crystallization process.....	304
8.5	Freeze-thaw test.....	306
8.5.1	<i>Procedure</i>	306
8.5.2	<i>Results of the freeze-thaw test</i>	307
	<i>Visual changes</i>	307
	<i>Weight loss</i>	308
	<i>Ultrasound velocity</i>	308
	<i>Mechanical properties</i>	310
8.5.3	<i>Discussion of results of freeze-thaw test</i>	312
9.	Limitations of the study and techniques used	316
	<i>Surface properties</i>	316
	<i>Hydric properties</i>	317
	<i>Hardness properties</i>	318
	<i>Ultrasound propagation velocity</i>	318
	<i>Mechanical properties</i>	319
10.	Use suggestions and conclusions	322

10.1	<i>Use suggestions</i>	324
10.1.1	<i>Water absorption and porosity</i>	325
10.1.2	<i>Uniaxial compressive strength</i>	325
A)	<i>Slabs</i>	325
B)	<i>Masonry</i>	327
10.1.3	<i>Flexural strength</i>	330
10.1.4	<i>Micro-hardness</i>	332
10.1.5	<i>Frosting</i>	333
10.2	<i>Conclusions</i>	335
	<i>San Giovanni in Fiore granite (GF)</i>	336
	<i>Grisolia stone (DG)</i>	339
	<i>San Lucido calcarenite (CS)</i>	342
	<i>Fuscaldò sandstone (AF)</i>	344
	<i>General conclusions</i>	347
	Symbols used	350
	Bibliography	352
	<i>Websites</i>	371

Acknowledgements

The research was carried out in Italy and Spain. In Italy: at the Department of Civil Engineering of the University of Calabria, where Peppino Sposato, Pasquale Pedace and Tonino Carrozzino helped me very much with the mechanical tests; at the Department of Territory and Environment of the University of Calabria, where Fortunato Crea and Ivan Iacobini were helpful with the portable mechanical tests; at the Department of Biology, Ecology and Earth Sciences of the University of Calabria, where Mauro and Silvio worked with me for the durability tests; at the IPG Laboratory “Istituto Prove Geotecniche” of Castrolibero with Sergio Soleri and his colleagues to perform mechanical tests on aggregates. In Spain, in Madrid, at the Petrophysics Laboratory IGEO (CSIC-UCM), “Centro Mixto del Consejo Superior de Investigaciones Científicas (CSIC) y de la Universidad Complutense de Madrid (UCM)”, where I performed the petrophysical, chemical and mineralogical characterization of the analyzed samples, thanks to the supports of “Programa de Geomateriales 2 (S2013/MIT-2914)” and to the Fellowship “Fondi 5 per mille D.P.C.M. 23/04/2010”. I received a lot of professional help from the researchers of the Applied Petrology for Heritage Conservation Research Group, especially from my tutor Mónica Alavarez de Buergo and from Rafael Fort that taught me professionally and humanly new scientific aspects. I am very grateful for it. David, Natalia, Du, Inma, Andrés, Elena, Mari Carmen, Arancha, Miguel, Luz, Maria José, Blanca, Patricia, all my fellow workers from the same group also deserve my gratitude. Without IGEO Group I would have never learnt and achieved the half of what I did. Thank you all. I am very grateful to them to welcome me so warmly and to be willing to co-operate any time. From the same department I have to express my thanks to the technical staff for the several thin sections and samples they prepared for me.

Quiero dar las gracias a todas las personas en Madrid que me ayudaron a adaptarme a esta cultura y sociedad científica tan maravillosa. Me han transmitido mucho, a nivel profesional y sobre

todo a nivel personal. La estancia en Madrid ha sido una de las etapas más importantes de este trabajo y que me ha cambiado la vida. A parte las personas que ya están mencionadas quiero dar mis gracias a Conchita por su cariño y a muchos más.

Vorrei inoltre ringraziare i miei tutor e co-tutors per avermi supportata ed aiutata durante questi tre anni. I professori Maurizio Ponte, Alessandro Campolongo, Anna Maria De Francesco dell'Università della Calabria e nuovamente Mónica Alvarez De Buergo dell'IGEO, per avermi trasmesso le basi scientifiche e l'appoggio morale per portare avanti questo progetto di dottorato.

Un ringraziamento speciale e di cuore va alle persone che ci sono sempre state al mio fianco: i miei genitori, che da sempre con il loro amore mi hanno supportata ed hanno creduto in me e nelle mie capacità sin dal principio, appoggiando le mie scelte standomi sempre vicina; la famiglia, i miei amici, Simona, per aver vissuto da lontano le esperienze di questi tre anni ma sempre con la vicinanza incredibile che contraddistingue la nostra amicizia, Veronica e Concetta per avermi ascoltata anche nei momenti più difficili e per aver condiviso e riso con me delle diverse avventure di questo periodo; a tutte quelle persone “nuove” che sono arrivate grazie a questa esperienza; Carlos (por supuesto) per l'amore immenso che mi ha regalato cambiando totalmente la mia vita con la sua energia, travolgendomi e facendomi innamorare di un nuovo mondo meraviglioso che ignoravo potesse esistere; la sua famiglia ed i suoi amici che sono entrati nella mia vita e che mi hanno accolta come “una di loro” sin dal primo istante; Nilla e Neil per l'aiuto ed i preziosi consigli che mi hanno regalato, come solo i veri amici sanno fare. Grazie davvero per tutto ciò che mi avete dato durante questi meravigliosi anni.

Thank you all!

¡Gracias a todos!

Grazie a tutti voi!

Abstract

The aim of this PhD thesis is to provide new scientific data regarding the use of certain Calabrian stones as building materials. This investigation included specific local stones used by the most important schools of Stonemasons of Calabria, in particular in the Cosenza Province; focusing on how properties of different building materials have influenced the figurative and architectural models.

In this study, stones commonly used as building materials are selected according to two important criteria:

1. The large employment of these materials in the past as building and decorative elements. Studying the use of selected stones in the centuries assists in identifying four lithotypes largely used by the most important Calabrian Schools of Stonemasons in the Cosenza Province:

- *San Giovanni in Fiore granite* - in the Sila area by the school of San Giovanni in Fiore and famous for its severe style due to “Joachim of Fiore” rules, and to material hardness.
- *Grisolia stone* – known as “gold stone” for its gold inclusions; limestone that represents the principal building material of the majority of the historical centers of the northern Tyrrhenian part of the Calabrian region and a small part of the Basilicata region.
- *San Lucido stone* - biocalcarene known in the past as “*biancolella*”; employed as a building material in the historical center of San Lucido and in the historical center of Cosenza, to build structural and decorative elements such as portals and arches.
- *Fuscaldo stone* - sandstone commercially known as “sweet stone” and utilized by artisans of the 14th century school of Fuscaldo; principally known for the construction of portals of noble palaces, built in the Spanish “plateresco” (plateresque) style for ornamental elements.

2. Lithotypes belonging to the different active and non-active important quarry areas of the Cosenza Province. Also taken into account is the possibility that these quarries may still be exploited for a local limited use, or a possible diffusion on a large scale out of the Region.

Special attention is dedicated to the characterization, durability, and to the building techniques employed in the past of the selected stones.

The petrophysical and mechanical characterization of these stones are performed by means of studying the petrographic characteristics, chemical and mineralogical composition, hydric properties; and the physical and mechanical behavior, with special attention to possible anisotropies. For this purpose, laboratory and non-destructive tests on quarry samples complying the current standards for “natural stones” and for the “conservation of cultural property” are performed.

Salt crystallization and freeze-thaw tests are performed to assess the durability of the stones and to relate the investigated stone properties with their behavior towards decay agents.

Among all the investigated lithotypes, San Giovanni in Fiore granite and Grisolia stone result the stones with a better mechanical and resistance behavior than the other lithotypes. In terms of durability, they are the most durable stones, and in terms of mechanical strength resistance, the strongest stones, both suitable for indoor and outdoor uses. But, petrographically, in the case of San Giovanni in Fiore granite, the oriented sets of microcracks demonstrate that microcracks influence the physical and mechanical behavior of this lithotype. In fact, comparing San Giovanni in Fiore granite with other similar granites, this stone presents worse properties and an anisotropic strength behavior, connected to the different orientation of its intracrystalline and intercrystalline microcracks. San Lucido calcarenite is classified as a stone with better mechanical features than petrophysical and hydric properties, so, the recommended use is for structural purposes, especially inside rather than for ornamental and external uses, in general where salts are not present. Concerning both petrophysical-mechanical properties and

durability, Fuscaldo sandstone is the stone with the worst behavior, if compared with the other investigated lithotypes. Its mineralogical composition connected to the susceptibility of some minerals, its high open porosity, the presence of a lot of micropores, its anisotropic hydric behavior, the high degree of ultrasonic anisotropy and its low mechanical strengths, makes this stone sensitive to decay processes and the recommendation is to use this stone for inside purposes and where no salts are present.

Results demonstrate that anisotropy and porosity are the main influencing factor in the stone behavior and durability. The way in which stones are positioned can avoid decay processes and improve their petrophysical-mechanical properties. In particular, it is suggested positioning the most anisotropic lithotypes (*e.g.* Fuscaldo sandstone) with the Z-direction parallel to the loading direction to obtain higher strengths and, simultaneously, to minimize water absorption. Moreover the pore structure, the pore-size distribution, the open porosity and the hydric behavior influence directly the stone resistance in front of decay agents. Microporous stones (*e.g.* Fuscaldo sandstone) or stones with high capillary coefficients (*e.g.* San Lucido calcarenite) have been classified as more susceptible to decay agents.

Furthermore, an attempt is made to consider possible modifications of current standards and performed non-destructive techniques, strictly focusing on the applied methods and the tested material of this research. In conclusion, all obtained results indicate the optimum use and the best methodology to perform, for the four investigated stones as building materials with regards to the stones' properties and with particular attention to different behaviors towards the anisotropy.

Keywords: characterization; destructive and non-destructive tests; durability; cultural heritage; new constructions; engineering geology; use suggestions.

Executive summary

The thesis “Some Calabrian stones as building materials: characterization, durability and use suggestions”, is divided into 10 chapters.

(1) Chapter 1 – presents the main objectives of this thesis:

- I. Objective 1 - establishes the history of use, quality, and quarriability of four building stones from the Cosenza Province, which are widely used in the vernacular architecture and monumental buildings.
- II. Objective 2 - characterizes the four selected stones by means of laboratory and non-destructive tests to obtain a complete petrophysical, chemical, mineralogical, and mechanical characterization; highlighting the most influential factors on the resistance for each lithotype, with a special attention to the anisotropy.
- III. Objective 3 - defines the durability of the four lithotypes.
- IV. Objective 4 - obtains the most adequate methodology for the characterization.
- V. Objective 5 - defines recommendations and suggests uses for the studied stones as building materials according to the properties obtained through characterization and durability tests.

(2) Chapter 2 – Presents an overview of the building stones’ usage throughout the centuries.

Since the prehistoric age, stones have been used for their unique durability to erect monuments of extraordinary and mostly religious importance. Until the 19th century, principally local stones were used from nearby sources, due to the lack of transportation facilities. Only rare and ornamental stones, such as marble, were transported from long distances and employed in exceptional cases. In all building types, the common factor was the adaptability of the building structure to the mineralogical, physical, and mechanical properties of stone. Medieval builders that succeeded in the erection of high and light structures such as Gothic church choirs or spires, could only stabilized the

construction with the help of hidden steel anchors. In fact, the high compressive strength and the low tensile strength of stone required special techniques to overarch gateways and to erect vaults. Only with the use of steel and reinforced concrete, the limits that stone properties posed to building structures had been overcome, and a new era of architectural building design began.

A precise description of all alteration types is presented; a definition of the distinction among the terms of “decay”, “deterioration”, “degradation”, “alteration”, “weathering”, and “damage”; and the most influencing ageing factors affecting stone durability.

- (3) Chapter 3 – Considers and illustrates the principal criteria in selecting the four lithotypes: Historical importance and the role of building stones in the Cosenza Province; most important Schools of Stonemasons working in the study area and their architectural models; role of the quarry activity in the past and the actual number of active quarries; and the stones’ quarriability for a possible diffusion out of the Province, both for architectural and engineering purposes.

The selected stones are: San Giovanni in Fiore granite (GF); Grisolia stone (DG); Fuscaldo sandstone (AF); and San Lucido calcarenite (CS).

A thorough literature review is conducted on the exploitation and use of these stones, which form part of many monuments, buildings, engineering elements, streets, and almost all vernacular architectures of the Cosenza Province. These include ancient building and modern engineering or civil structures (streets, milestones, portals, vaults, bridges).

- I. GF – grey granite named “Sila granite” belonging to the Sila Batholith, was principally employed by the School of Stonemasons of San Giovanni in Fiore, for ordinary masonries and engineering purposes.
- II. DG – “gold stone”, named for its yellow veins; a grey crystalline carbonate, geologically belonging to the Verbicaro Unit was exploited by the tradition of the School of Stonemasons of

Basilicata and the northern part of Calabria, to realize common buildings and noble portals of the Pollino Area, Tyrrhenian coast, and of old towns out of Region.

III. AF – reddish sandstone known as “sweet stone” due to its easy workability; belonging to the Miocenic Succession of the Tyrrhenian Coast, was principally employed by the School of Stonemasons of Fuscaldo.

IV. CS – whitish biocalcarene commercially known as “Mendicino tuff”; used by the School of Stonemasons of Rogliano and Altilia, belonging to the Miocenic Successions of the Tyrrhenian Coast, was principally employed for vernacular and monumental architectures of Cosenza Province.

- (4) Chapter 4 – Illustrates the usage of the selected four stones in the past, the principal constructive techniques adopted by Stonemasons, and considers important realized examples, such as the masonries of four old towns (San Giovanni in Fiore, Scalea, Fuscaldo, San Lucido).
- (5) Chapter 5 – Describes methods, methodologies, and followed adopted standards to perform the characterization of the four lithotypes. Non-destructive (NDT), micro-destructive (MDT), and destructive techniques (DT) are performed according to the following Standards: CEN/TC 246 “Natural stones” and CEN/TC 346 “Conservation of cultural heritage”.
- (6) Chapters 6 and 7 – Illustrate the principal properties obtained from the performed tests and the most significant results. In particular, details of each lithotype petrographic characteristics highlight fabric elements and discontinuities (microcracks for GF) with the following estimated properties: surface (hardness); petrophysical (chromatic parameters, open porosity, real and bulk density, air permeability); hydric (capillary and total water absorption, water desorption, natural hydrophobicity); and mechanical with a special attention to the anisotropy behavior (ultrasound P- and S-waves velocities; hardness characteristics like micro-hardness, drilling resistance and Schmidt

hammer rebound; strength properties such as uniaxial compressive, flexural, tensile strength, Point Load strength; abrasion resistance). Properties are individually analyzed and correlated to define the relationship between the considered properties.

- (7) Chapter 8 – Commences with a bibliographical study of salt crystallization and frost damage. Freeze–thaw and salt crystallization tests are performed to evaluate the decay suffered by stones. The salt crystallization test is performed on each lithotype, while the freeze-thaw test is only performed for GF and DG, employed in the colder parts of the Region. The general theories for salts and ice-crystallization are briefly exposed and the topics of interest are raised. The durability of the four lithotypes are evaluated through the salt crystallization test as it is identified that crystallization of salt solutions and ice are the most important decay mechanism that affect many buildings (Winkler & Singer, 1972; Rodriguez Navarro & Doehne, 1999). The performed tests defined the most resistant materials against the salt crystallization and freezing process.
- (8) Chapter 9 – Deals with consideration about possible modifications of current standards and non-destructive techniques performed, strictly focusing on the applied methods and the tested material types of this research. Additionally, the limitations of certain non-destructive performed techniques are described.
- (9) Chapter 10 – Represents the concluding summary of this thesis. All the obtained parameters are illustrated in a final table and distinguished for each lithotype (Table 10.1). The most important characteristics and the weakest properties are summarized for each lithotype. The properties that fundamentally control the decay processes, and thus the durability of stones are identified: the mineralogical and chemical composition, the hydric properties (especially the water uptake and drying; void space structure, especially the void size and aperture size distribution, and the connectivity of the porous space); and the mechanical properties, the anisotropy, and the presence of

microcracks. In accordance with all analyzed factors, recommendations and suggested usage of the four stones are reported.

Sintesi

L'obiettivo della presente Tesi di Dottorato è quello di apportare nuovi dati scientifici riguardanti l'utilizzo di alcuni materiali lapidei Calabresi come materiali da costruzione. La ricerca si focalizza su alcuni materiali lapidei locali impiegati dalle principali scuole di Scalpellini in Calabria, in particolare nella Provincia di Cosenza e su come le proprietà dei diversi materiali da costruzione abbiano influenzato i modelli figurativi ed architettonici.

Nel presente studio i materiali lapidei comunemente impiegati come materiali da costruzione sono stati scelti secondo due importanti criteri:

1. Il loro largo impiego in passato come materiali da costruzione e materiali ornamentali. Attraverso lo studio dell'utilizzo nei secoli dei materiali lapidei, nel territorio preso come caso di studio, sono stati individuati i quattro litotipi maggiormente impiegati dalle più importanti scuole di Scalpellini della Provincia di Cosenza:

- *granito di San Giovanni in Fiore* – utilizzato nell'area della Sila dalla scuola di San Giovanni in Fiore e famosa per il suo stile austero, in parte legato alle regole di Gioacchino da Fiore ed alla durezza del materiale lavorato.

- *pietra di Grisolia* – nota commercialmente come “pietra d'oro” per le vene di colore giallastro al suo interno; pietra calcarea che rappresenta il materiale lapideo principale della maggior parte dei centri storici calabresi dell'Alto Tirreno cosentino e di alcuni centri storici della confinante Regione Basilicata.

- *pietra di San Lucido* - biocalcareneite, nota commercialmente in passato tra gli scalpellini come “biancolella”; impiegata come materiale da costruzione predominante nel centro storico di San Lucido ed in quello di Cosenza per la realizzazione di elementi strutturali e decorativi quali portal e archi.

- *pietra di Fuscaldo* – arenaria conosciuta commercialmente come “pietra dolce” e utilizzata dagli Scalpellini della scuola di Fuscaldo del XXIV secolo; principalmente impiegata per la costruzioni di portali e palazzi nobiliari, realizzati con elementi decorativi assimilabili allo stile “plateresco” spagnolo.

2. I litotipi appartenenti alle principali cave attive e dismesse della Provincia di Cosenza. Tenendo in conto, anche, la possibilità di poter continuare ad estrarre materiali lapidei per un uso limitato oppure per una diffusione su larga scala al di fuori dei confini della Regione.

Particolare attenzione è dedicata alla caratterizzazione, alla durabilità dei materiali analizzati ed alle tecniche costruttive impiegate in passato.

La caratterizzazione petrofisica e meccanica dei litotipi prescelti ha riguardato lo studio delle caratteristiche petrografiche, chimiche, composizione mineralogica, proprietà idriche e comportamento fisico e meccanico, con particolare attenzione a possibili anisotropie. A questo scopo, su campioni di cava sono stati eseguiti numerosi test di laboratorio e test non-distruttivi, in conformità con le normative vigenti nell’ambito dei “materiali lapidei naturali” e della “conservazione dei beni culturali”.

Test d’invecchiamento accelerato (quali test di cristallizzazione dei sali e di gelo-disgelo) sono stati eseguiti allo scopo di definire la durabilità dei materiali lapidei e di correlare le principali proprietà dei litotipi analizzati con il loro comportamento, nei confronti degli agenti di degrado.

Tra i vari litotipi analizzati, il granito di San Giovanni in Fiore e la pietra di Grisolia sono risultati i materiali che hanno dimostrato il miglior comportamento fisico – meccanico e proprietà di resistenza migliori rispetto agli altri materiali studiati. In termini di durabilità, sono risultati essere i materiali più durevoli e, in termini meccanici, i materiali più “resistenti”, adatti per essere impiegati nell’ambito delle costruzioni, sia per usi interni che esterni. Dal punto di vista petrografico, però, nel caso del granito di San Giovanni in Fiore, è emerso che la presenza di microfratture ne influenza il

comportamento fisico e meccanico. Infatti, confrontando il granito di San Giovanni in Fiore con altri graniti simili, esso presenta proprietà meccaniche inferiori e comportamenti talora marcatamente anisotropi, proprio a causa del diverso orientamento delle microfratture intercristalline ed intracristalline individuate attraverso l'analisi petrografica.

La calcarenite di San Lucido è classificata come un materiale con proprietà meccaniche migliori rispetto a quelle petrofisiche ed idriche, per cui ne viene raccomandato l'uso per elementi strutturali, per usi interni piuttosto che esterni, ornamentali e solo laddove non siano presenti sali. Riguardo le proprietà petrofisico-meccaniche e la durabilità, l'arenaria di Fuscaldo è risultato essere il materiale lapideo che ha mostrato il comportamento peggiore rispetto agli altri litotipi studiati. La facile alterabilità di alcuni dei suoi componenti minerali, la sua elevata porosità aperta, la presenza di numerosi micropori, il suo comportamento idrico anisotropo, l'elevato grado di anisotropia ultrasonica e le sue basse prestazioni meccaniche rendono questo litotipo sensibile ai processi di degrado, per cui se ne raccomanda un uso prettamente interno e non in presenza di sali.

I risultati ottenuti dimostrano che l'anisotropia e la porosità sono i fattori che maggiormente influenzano il comportamento dei materiali lapidei e la loro durabilità. La corretta orientazione dei materiali può evitare processi di degrado e migliorarne le prestazioni petrofisiche-meccaniche. In particolare, viene raccomandato di posizionare i litotipi anisotropi (come la pietra di Fuscaldo) con l'asse Z parallelo alla direzione di carico, in modo da ottenere le maggiori resistenze meccaniche e, contemporaneamente, minimizzare l'assorbimento d'acqua. Inoltre, la struttura porosa, la distribuzione dei pori, la porosità aperta ed il comportamento idrico influenzano direttamente la resistenza dei materiali lapidei nei confronti degli agenti di degrado. I materiali lapidei microporosi (per esempio la Pietra di Fuscaldo) o quelli con i maggiori coefficienti di assorbimento capillare (la Pietra di San Lucido) vengono, quindi, classificati come più suscettibili agli agenti di degrado.

Inoltre, vengono suggerite possibili modifiche alle normative vigenti ed alle tecniche non-distruttive adoperate, focalizzando l'attenzione sui metodi applicati e sui materiali testati all'interno della presente ricerca.

In conclusione, i risultati ottenuti permettono, per i quattro litotipi investigati, di fornire raccomandazioni metodologiche e d'uso da adottare, rispetto alle proprietà fisico-meccaniche con particolare attenzione all'anisotropia.

Parole chiave: caratterizzazione; test distruttivi e non-distruttivi; durabilità; beni culturali; nuove costruzioni; ingegneria geologica; raccomandazioni d'uso.

Articolazione e contenuti

La tesi dal titolo “Some Calabrian stones as building materials: characterization, durability and use suggestions”, ovvero “Alcuni materiali lapidei Calabresi: caratterizzazione, durabilità e consigli d’uso”, si compone di 10 capitoli.

(1) Capitolo 1 - presentare i principali obiettivi della presente tesi:

- Obiettivo 1 – stabilire la storia dell’utilizzo, della qualità e dell’estrazione dei quattro materiali lapidei nella Provincia di Cosenza, che sono stati ampiamente utilizzati sia nell’ambito dell’architettura vernacolare che per l’edilizia monumentale e specialistica.
- Obiettivo 2 – caratterizzare i quattro litotipi, attraverso test di laboratorio e test non-distruttivi, al fine di ottenerne una completa caratterizzazione petrofisica, chimica, mineralogica e meccanica; evidenziando i fattori più influenti sulla resistenza di ciascun litotipo, il tutto con una speciale attenzione nei confronti dell’anisotropia.
- Obiettivo 3 – definire la durabilità dei quattro litotipi.
- Obiettivo 4 – identificare le più adeguate metodologie diagnostiche per la caratterizzazione dei campioni.
- Obiettivo 5 – definire raccomandazioni e consigli d’uso dei materiali lapidei studiati come materiali da costruzione in relazione alle proprietà ottenute attraverso i test di caratterizzazione e di durabilità.

(2) Capitolo 2 – illustrare una panoramica degli usi storici dei materiali lapidei studiati attraverso i secoli. Sin dalla Preistoria, i materiali lapidei sono stati impiegati come principali materiali da costruzione per la loro durabilità per erigere monumenti dalla straordinaria importanza architettonica e religiosa. Fino al XXIX secolo, venivano impiegati principalmente materiali locali provenienti da località estrattive vicine al sito di costruzione, a causa soprattutto della mancanza di idonei mezzi di

trasporto. Solo alcune varietà litologiche rare ed ornamentali, quali ad esempio il marmo, venivano trasportate da località lontane ed impiegate per costruzioni di una certa importanza economica, monumentale e/o religiosa. In tutti gli edifici il fattore comune era l'adattabilità della struttura della costruzione alle proprietà mineralogiche, fisiche e meccaniche del materiale lapideo impiegato. I costruttori medievali sono riusciti ad erigere strutture snelle ed elevate, quali le chiese Gotiche e le loro guglie, abbinando al materiale lapideo sistemi di ancoraggio metallici nascosti all'interno della muratura. Infatti, l'elevata resistenza a compressione e la scarsa resistenza a trazione del materiale lapideo richiedeva l'impiego di speciali tecniche per erigere archi e volte. Solo con la comparsa dell'acciaio e del calcestruzzo armato, vengono superati i limiti costruttivi legati alle proprietà dei materiali lapidei, per la realizzazione delle strutture e comincia una nuova era architettonica nell'ambito delle tecniche costruttive e dei materiali impiegati.

All'interno del presente capitolo viene fornita una descrizione delle principali forme di alterazione, nonché una distinzione tra i vari termini impiegati quali "degrado", "deterioramento", "degradazione", "alterazione", "degrado meteorico", "danno" e, inoltre, i fattori di degrado più ricorrenti ed influenti sulla durabilità dei materiali lapidei.

- (3) Capitolo 3 – considerare e illustrare i principali criteri adottati ai fini della scelta dei quattro litotipi da analizzare: l'importanza storica ed il ruolo dei materiali lapidei nella Provincia di Cosenza; le più importanti Scuole di Scalpellini che lavoravano nell'area scelta come caso di studio ed i principali modelli architettonici elaborati; il ruolo dell'attività estrattiva in passato e l'attuale numero di cave attive; la possibilità di continuare ad estrarre i materiali cavati in passato per una possibile commercializzazione al di fuori della Provincia, sia per scopi architettonici che ingegneristici.

I materiali lapidei selezionati sono: granito di San Giovanni in Fiore (GF); pietra di Grisolia (DG); arenaria di Fuscaldo (AF); e calcarenite di San Lucido (CS).

Un accurato esame bibliografico è condotto sullo sfruttamento ed utilizzo di questi materiali, che formano parte della maggior parte di monumenti, edifici, elementi impiegati nell'ambito dell'ingegneria, strade ed architetture vernacolari della Provincia di Cosenza. Queste architetture comprendono sia edifici antichi che opere moderne dell'ingegneria civile (strade, pietre miliari, portali, volte, ponti).

- GF – granito dal colore grigiastro noto genericamente come “granito della Sila” appartenente all'Unità geologica del Batolite della Sila, è stato principalmente impiegato dalla scuola degli Scalpellini di San Giovanni in Fiore, per la realizzazione di murature ordinarie e per opere ingegneristiche.
- DG – nota come “pietra d'oro” per le venature giallastre al suo interno; carbonato cristallino dal colore grigio scuro, geologicamente facente parte dell'Unità di Verbicaro, veniva lavorato dalla Scuola degli Scalpellini della Basilicata e dell'Alto Tittreno Cosentino, per realizzare edifici comuni e portali di palazzi nobiliari nell'area del Pollino, della Costa Tirrenica e dei centri storici calabresi e lucani.
- AF – arenaria dal colore rossastro, nota come “pietra dolce” grazie alla sua facile lavorabilità; appartenente alla Successione sedimentaria Miocenica della Costa Tirrenica, principalmente impiegata dalla Scuola degli Scalpellini di Fuscaldo.
- CS – biocalcarenite dal colore biancastro nota anche come “tufo di Mendicino”; lavorata dalle Scuole di Scalpellini di Rogliano ed Altilia, facente parte della Successione sedimentaria Miocenica della Costa Tirrenica, principalmente impiegata per la realizzazione delle architetture vernacolari e monumentali della Provincia di Cosenza.

(4) Capitolo 4 – illustrare l'impiego dei quattro litotipi prescelti, le principali tecniche costruttive adoperate dagli Scalpellini ed analizzare gli esempi più significativi dei principali elementi tecnici

quali portali e murature, raccolti all'interno di schede di catalogazione per il restauro di quattro centri storici (San Giovanni in Fiore, Scalea, Fuscaldo, San Lucido).

- (5) Capitolo 5 – descrivere metodi, metodologie e normative adottate per la caratterizzazione dei quattro litotipi. Tecniche non-distruttive (TND), micro-distruttive (TMD) e distruttive (TD) vengono applicate in osservanza dei seguenti standard: CEN/TC 246 “Materiali lapidei naturali” e CEN/TC 346 “Conservazione dei Beni Culturali”.
- (6) Capitoli 6 e 7 – illustrare le principali proprietà ottenute mediante i test eseguiti ed i principali risultati ottenuti. In particolare, dettagliare per ciascun litotipo le caratteristiche petrografiche, mettendo in evidenza elementi di fabbrica e discontinuità (microfratture nel caso di GF) e le seguenti proprietà: di superficie (durezza); petrofisiche (parametri cromatici, porosità aperta, densità apparente e reale, permeabilità all'aria); idriche (assorbimento d'acqua per capillarità, assorbimento d'acqua a pressione atmosferica, essiccamento, idrofobicità naturale); e meccaniche con uno speciale riguardo per l'anisotropia (velocità di propagazione di onde ultrasoniche longitudinali e di taglio, P ed S; caratteristiche di durezza quali micro-durezza, resistenza alla perforazione e rimbalzo di Schmidt; proprietà di resistenza quali resistenza a compressione, flessione, trazione, Point Load ed abrasione). Le diverse proprietà vengono analizzate e correlate tra loro al fine di definire corrispondenze e legami tra le varie proprietà considerate.
- (7) Capitolo 8 – definire con uno studio bibliografico il degrado dovuto a cristallizzazione dei sali e gelo-disgelo. Test di invecchiamento accelerato di cristallizzazione dei sali e di gelo-disgelo vengono eseguiti per valutare il degrado dei materiali lapidei. Il test di cristallizzazione dei sali viene eseguito su ciascun litotipo, mentre quello di gelo-disgelo solo per GF e DG che rappresentano i litotipi impiegati nelle aree più fredde della Regione. Vengono espone le teorie alla base dei fenomeni di cristallizzazione dei sali e di gelo-disgelo. La durabilità dei quattro litotipi viene

valutata attraverso questi test di invecchiamento accelerato perchè ritenuti ricorrenti e pericolosi per il degrado degli edifici (Winkler & Singer, 1972; Rodriguez Navarro & Doehne, 1999). I test eseguiti permettono di definire i materiali più resistenti nei confronti dei processi di degrado considerati.

- (8) Capitolo 9 – prendere in considerazione, attraverso un’analisi critica, possibili modifiche da apportare agli standard vigenti ed alle tecniche non-distruttive eseguite, focalizzando l’attenzione sui metodi applicati e sui materiali testati all’interno della presente tesi. Inoltre, vengono illustrati i limiti di alcune tecniche non-distruttive adoperate.
- (9) Capitolo 10 – descrivere le conclusioni della presente tesi. Tutti i parametri ottenuti vengono raccolti all’interno di una tabella riassuntiva finale e distinti per ciascun litotipo (Tab 10.1). Le caratteristiche più importanti e le proprietà analizzate vengono riassunte per ciascun litotipo. Vengono identificate le proprietà alla base dei processi di degrado e di conseguenza alla base della durabilità dei materiali lapidei: composizione chimica e mineralogica, proprietà idriche (soprattutto assorbimento ed essiccamento d’acqua; porosità, in particolare dimensione e distribuzione dei pori e caratteristiche dello spazio poroso); proprietà meccaniche, anisotropia e presenza di microfratture. In funzione dei fattori analizzati, vengono riportate raccomandazioni e consigli d’uso dei quattro materiali lapidei studiati come materiali da costruzione.

Abbreviations

Stones

GF = San Giovanni in Fiore granite

DG = Grisolia stone (limestone)

CS = San Lucido calcarenite

AF = Fuscaldo sandstone

Characterization tests

NDT = non-destructive test

MDT = micro destructive test

DT = destructive test

Stone properties/tests

Chemical and mineralogical properties

XRD = X-ray diffraction

XRF = X-ray fluorescence

Surface properties

L^* = lightness

a^* = red-green coordinate

b^* = yellow-blue coordinate

C^* = chroma

h^* = hue angle

B^* = brightness

ΔE^* or ΔE^*_{94} = global/total colour variation

Petrophysical properties

ρ_{sk} = real or skeletal density

ρ_b = apparent or bulk density

ρ_{water} = density of water

p_o = open porosity or porosity accessible to water

I_c = compactness index (real density/ bulk density)

W_{vac} = water absorption under vacuum conditions

MIP = mercury intrusion porosimetry

AirP = air permeability

C_C or C_1 or C_2 = capillary water absorption coefficients

W_{Ab} = water content absorbed or imbibition coefficient (at atmospheric pressure)

S_i = saturation coefficient

W_{Ds} = water content evaporated

S = saturation degree

Mechanical properties

V_{Px}, V_{Py}, V_{Pz} = ultrasonic P-waves velocity

V_{Sx}, V_{Sy}, V_{Sz} = ultrasonic S-waves velocity

$dM_{Vp\%}$ = total anisotropy index (P-waves velocity)

$dM_{Vs\%}$ = total anisotropy index (S-waves velocity)

$dm_{Vp\%}$ = relative anisotropy index (P-waves velocity)

$dm_{Vs\%}$ = relative anisotropy index (S-waves velocity)

L_s = Leeb micro-hardness

HV = Vickers hardness

DR_i = Drilling Resistance

H_s = Schmidt hammer rebound values

σ_c or UCS = uniaxial compressive strength

R_{tf} = flexural strength

σ_t = indirect tensile strength

$Is_{(50)}$ = point load strength

PSV = polished stone value

LA = Los Angeles coefficient

M_{DE} = Micro-Deval coefficient

1. Objectives

Following are the listed objectives of the thesis.

(1) To establish the historical use of the most important building stones of Cosenza Province.

To achieve this objective, the following issues will be developed:

- historical role of the most important schools of stonemasons and the correlated architectural models
- historical quarries exploited in the past and the actual situation of the Calabrian quarry market, individuating the number of active/inactive quarries and their location
- traditional extraction methods and types of finishing of the selected stones
- geological and quarry setting of each lithotype
- constructive techniques and different types of masonries.

(2) To characterize the four selected lithotypes.

This objective consists of defining the quality and the petrophysical, chemical, mineralogical and mechanical properties of the investigated lithotypes, by performing characterization tests. To achieve this objective, the following issues will be developed:

- influence of stone fabrics and voids space highlighting the most influential factors on the stone resistance and on its physical and mechanical properties
- presence of oriented microcracks and internal discontinuities
- role of anisotropy and spatial variability of each investigated property along the three spatial axes.

(3) To define the durability of the four lithotypes.

Evaluate the effects of decay due to salt and ice crystallization processes and relate results to further physical properties (*e.g.* pore system).

(4) To find the most adequate methodology for the stones characterization.

The purpose of this objective is to highlight limitations of certain performed tests and related standards; and to improve methods and methodologies in the field of stone characterization.

(5) To provide use suggestions

The outcome of test results makes possible to detail recommendations regarding the best use of the investigated stones, for architectural and engineering purposes. This is particularly useful for the conservation of cultural heritage and for new constructions.

2. Introduction – Building stones in architecture

Most historical and many contemporary buildings have been constructed by using natural stone. Natural stone has an important role, not only for the economical and industrial importance, but also for its historical value when employed in the cultural heritage. In fact, this material has been used as the major part of the built cultural heritage in the world.

Cultural heritage plays an important and integral role in our lives. The optimal way to preserve cultural heritage whilst retaining world history intact for future generations, is to share diagnostic techniques, methodologies and results with colleagues and wider communities.

The conservation of our cultural heritage is a concept that has acquired importance throughout centuries. During centuries the first organizations for the protection of heritage were set up (Poblador, 2001). In the United Kingdom, the “Society for the protection of Ancient Buildings” known as “SPAB”, was set up in 1877 and the “National Trust” in 1896. The “SPAB Manifesto”, establishing the “general principles and doctrines relating to the protection of monuments”, was issued in 1877. RILEM standards (“Reunión Internacional de Laboratorios para Ensayo de Materiales”), employed for the stone characterization through laboratory tests, were born in the 1970s. The Italian Charter for the Restoration of Historic Monuments or “Carta del Restauro”, one of the first documents for the protection of heritage like the “SPAB Manifesto”, dates back to 1972 (Brandi, 1977). Most of Brandi’s scientific works have been published as Conference Proceedings for the famous “International Congress on the Deterioration and Conservation of Stone”. Nowadays there are numerous organizations around the world involved in the elaboration of standards, like ASTM International (American Society for Testing and Materials), CEN (European Committee for Standardization or Comité Européen de Normalisation), NIST (The National Institute for Standards and Technology), BS (British Standards), ISO (International Organization for Standardization), DIN (German Institute for Standardization), AFNOR (“Association

Francaise de Normalisation”), AENOR (“Asociación Española de Normalización y Certificación”), etc. The two most recognized ones are ASTM International and CEN. Within North America, the ASTM standards govern, and within Europe, the CEN standards, known as “EN”s, govern. Elsewhere in the world, many countries have adopted one or the other systems, or have their own testing and specification standards authored by a local organization. The CEN standards are then subdivided in two sections, one for “natural stones” and another for “the preservation of cultural heritage” even though the CES goes way beyond dealing with building materials and in fact has 443 Technical Committees.

Standards must be taken into account whenever a consolidating treatment is applied, a new material is assessed for replacement or the decay rate and causes of the elements of a monument are established. They are followed for the characterization of natural stones both in the field of cultural heritage and for contemporary architectures.

Most of the techniques for characterization are well established (Doehne & Price, 2010). Many are summarized by Robertson (1982) as well as Borelli & Umland (1999) and Svahn (2006). Adams & MacKenzie (1998) provide a useful atlas of petrographic sections, while petrographic atlas and applications of polarized light microscopy to building materials conservation are presented by Bläuer & Kueng (2007) and Reedy (2008). In the process of characterizing stone, it is important to recognize that while some stones have a similar composition, their behaviors may have few things in common. The contrasting modes of deterioration of similar stones depend on different factors like porosity, pore shapes, pore size distribution, and grain size or chemical composition. One division of stone types is based on the percentage and relative ratio of pore-shaped and fissure-shaped voids (Crocì & Delgado Rodrigues, 2002). A second division can be made on the basis of the degree of hygric swelling of the stone (Delgado Rodrigues, 2001; Duffus *et al.*, 2008), and a third division on the strength (Winkler, 1985; Bourgès, 2006). Subsequent divisions based on composition, texture, and homogeneity enable

further distinctions to be made, but they may be less important in rating overall performance than the first three. Those stones with high porosity, high rates of swelling, and low strength tend to be relatively poor building materials (*e.g.* Jackson *et al.*, 2005). A review of the relationship between pore structure and other stone characteristics is given by Bourgès *et al.* (2008). Gauri & Bandyopadhyay (1999) review the interpretation of mercury porosimetry data and cite a number of the seminal papers on pore structure determination. Analysis of the positive correlation between the fractal dimension, stone pore surface, and the degree of natural weathering has shown that increases in the surface fractal dimension are a more accurate descriptor of the degree of weathering than pore size distribution (Yerrapragada *et al.*, 1993; Pérez Bernal & Bello López, 2000).

2.1 Natural stone uses in Architecture

Since the prehistoric age, mankind has used stone for its unique durability to erect monuments of extraordinary, mostly religious, importance. Due to lacking transportation facilities until the 19th century, stones from nearby sources had to be chosen to build churches, castles and towns. So, the use of local stones was prevalent. Only for exceptional cases rare and decorative stones, like marble, were transported over long distances when stone of the same colour and beauty was not available in the near vicinity.

Many important architectures were made of stones. Stonehenge (United Kingdom) is one of the first examples of the expertise of Stone Age men. It was built with huge stone blocks even though the transportation method is now still under debate. Thick crossbeams were used to prevent crack formation as shown in Fig. 2.1. The Stonehenge part of the World Heritage Site covers 2600 hectares (6500 acres)

of chalk downland and arable fields in Wiltshire. It includes parts of Amesbury and Larkhill, and the villages of West Amesbury, Normanton, Wilsford and Lake in the Woodford Valley¹.



Fig. 2.1. View of Stonehenge in Wiltshire (United Kingdom), UNESCO listed (ca 2500 BC), (picture from <https://en.wikipedia.org/wiki/Stonehenge>).

Egyptians realized the largest stone building: the Cheops Pyramid. It consists of about 2300000 stone blocks, each of them weighing about 2.5 tons. The pyramid has a height of 146 m. In spite of the enormous height of the Cheops Pyramid, there is no risk that the stone in the undermost layer could break for the uniaxial compressive strength of the entirety of the blocks. The pressure at the base of the Pyramid is much lower than the compressive strength of the building limestone (Fig. 2.2).



Fig. 2.2. View of Cheops Pyramid in Egypt, UNESCO listed in 1979 (ca 2580-2560 BC), (picture from https://en.wikipedia.org/wiki/Great_Pyramid_of_Giza).

¹ <http://www.stonehengeandaveburywhs.org/about-us/stonehenge-avebury/>

Thanks to the Greek and Roman culture, two building solutions were introduced: the “false vault” and the “arch”. In the first case, in contrast to a real vault, stone blocks were put upon each other, the upper one always protruding a little over the lower one. In order to avoid the toppling of the layers, heavy stone blocks or earth filling had to be placed on the opposite side as counter weight. Examples of false vault constructions are the “Trulli” in Apulia in Italy (Fig. 2.3) or the Tomb of Atreus in Mykene in Greece. The Roman culture began to employ stone to build arches like long aqueducts as the Pont du Gard in France or Via Appia in Rome (Fig. 2.4), and bridges all around Europe. The stones of the arch are laid out upon the scaffolding, and only when the arch is closed the scaffolding can be demounted.



Fig. 2.3. View of “false vault” in a “Trullo” in Alberobello (Apulia, Italy), UNESCO listed in 1996, (picture from <https://en.wikipedia.org/wiki/Trullo>).



Fig. 2.4. View of the Roman arch system in the Via Appia aqueduct in Rome (Italy), (ca 350 BC), (picture from https://en.wikipedia.org/wiki/Roman_aqueduct).

Romanesque and Gothic styles employed stones in two different ways. In the first case stones have been used to realize thick walls and narrow window openings. Portals and window frames are terminated with round arches. The stone is not loaded up to its strength limits. Romanesque buildings provide an impression of solidity and compactness (Fig. 2.5). On the other hand, Gothic structures are slim and light, thanks to the use of the pointed arch and iron ring anchors. The elongated structures of Gothic cathedrals go to the limits of the mechanical properties of stone (Fig. 2.6).



Fig. 2.5. View of the Romanesque Cathedral in Modena (Italy), UNESCO listed in 1997, (ca 1184), (picture from https://en.wikipedia.org/wiki/Modena_Cathedral).



Fig. 2.6. View of the Gothic Cathedral in Tournai (Belgium), UNESCO listed in 2000, (ca 12th century), (picture from [https://it.wikipedia.org/wiki/Cattedrale_di_Notre-Dame_\(Tournai\)](https://it.wikipedia.org/wiki/Cattedrale_di_Notre-Dame_(Tournai))).

The final point of building with natural stone was reached with Gothic architecture. In fact, the low bending strength of stone did not allow extreme building constructions. Therefore, during the Industrial Revolution, stone was replaced by new building materials such as steel and concrete. Stones maintained a modest role in the field of civil engineering, especially for the construction of arched bridges.

In the contemporary architecture natural stone recovered a new role especially as ornamental or covering material. The structural use of stones is limited due the industrialization process that realized thin and light covering elements.

During the 60s, the new system of the “ventilated façade” was introduced. It consists of a sandwich system composed by: external thin industrially processed slabs, detached from the bearing structure by means of metal supports; empty space for the air flow; structural elements of the internal façade. The most employed stone material was marble, especially Carrara marble. One of the most important architects was Alvar Aalto, who used this material as covering clads for his designs (Fig. 2.7).



Fig. 2.7. View of Stephanuskirche in Wolfsburg (Germany), completed in 1968 and designed by Alvar Aalto. This modern religious building has a façade clad in Carrara marble, (picture from <http://www.archdaily.com/372492/ad-classics-stephanuskirche-alvar-aalto>).

During the 80s, especially in Germany, many architects like Arata Isozaki, Aldo Rossi, James Stirling and others, started to employ lithotypes different than the white marble, with a variety of textures (Fig. 2.8).



Fig. 2.8. Views of Neue Staatsgalerie in Stuttgart (Germany), completed in 1984 and designed by James Stirling. This modern cultural center has a façade in designed travertine elements, (pictures from <http://www.archdaily.com/124725/classics-neue-staatsgalerie-james-stirling>).

During the 90s and the 21st century, a new trend to discover natural characteristics of stone, without superficial treatments or traditional types of finishing, experimented new technologies. Stones were principally employed with three different uses: semi-opaque and thin covering slabs (Fig. 2.9 a); local stones combined with structural metallic systems (Fig. 2.9 b); structural stone ashlar (Fig. 2.9 c).

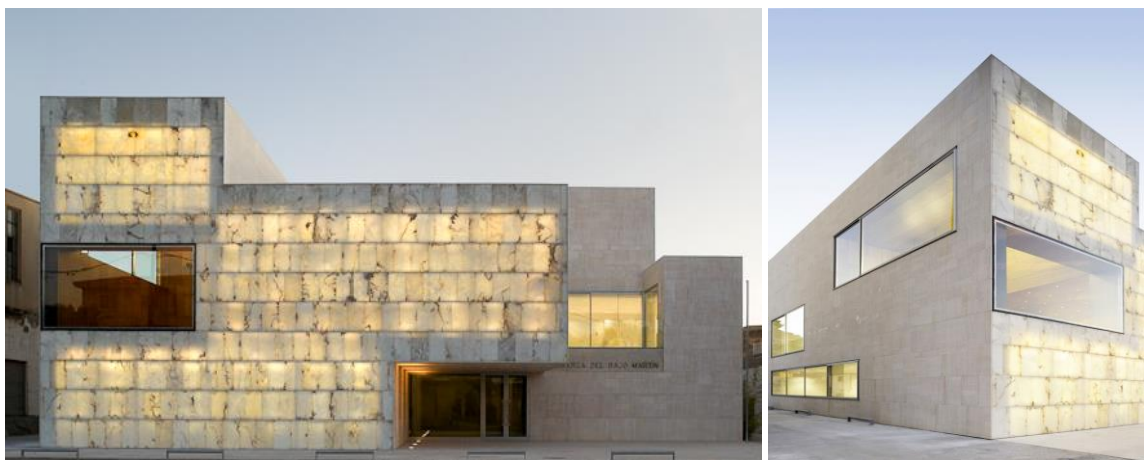


Fig. 2.9 a. Views of the Bajo Martin region Headquarters in Hjar (Teruel, Spain), completed in 2006 and designed by Magén Arquitectos. This administrative center has a façade in semi-opaque alabaster elements (pictures from <http://www.archdaily.com/206751/bajo-martin-county-magen-arquitectos>).



Fig. 2.9 b. Views of Dominus Winery in Yountville (California, USA), completed in 1998 and designed by Herzog & de Meron. It is characterized by gabion baskets filled with local field stone, hand stacked- to form the skin of the building which allows natural light to filter into the interior spaces, (pictures from <https://www.dezeen.com/2007/09/09/dominus-winery-by-herzog-de-meuron/>).



Fig. 2.9 c. Views of “Padre Pio Sanctuary” in San Giovanni Rotondo (Italy), completed in 2004 and designed by Renzo Piano. The supporting structure consists of two intermeshing rows of Apricena stone arches arranged in a circle, a total of 21, that form an inner and an outer ring with the arches of the outer ring representing scaled-down copies of the inner ones (pictures from <http://www.arcspace.com/features/renzo-piano-/padre-pio-pilgrimage-church/>).

2.2 Stone deterioration

Ancient and contemporary constructions, built with natural stones, can suffer decay processes. In order to choose the best intervention methods, to reply original materials or to employ new building

stones it is important to understand stone behaviour through a complete characterization. This process helps not only to define petrophysical and mechanical properties of stones but also to individuate possible factors influencing stone decay in order to apply suitable conservation treatments.

Stone deterioration is a function of the stone properties and the aggressiveness of the external conditions (Kühnel, 2002). Weathering is a natural and continuous process due to differences between the conditions of rock formation and the conditions to which they are exposed on the surface of the Earth (outcrops). It is a result of physical, chemical and biological mechanisms conditioned by the interaction between the rock and the atmospheric agents (Kühnel, 2004). Another deterioration form that influences stone deterioration refers to all the human activities, starting from the quarrying of the stone to the effects of vandalism or warfare on built constructions (Siegesmund *et al.*, 2002), including the indirect consequences of air pollution, etc.

One of the problems inherent in discussing stone decay is finding a common language above the terms mentioned above. Even in English, there are a bewildering number of terms that may mean different things to different people. A significant advance in this area is the publication of a stone decay glossary by the ICOMOS Stone Committee under the editorship of Véronique Vergès-Belmin (2008). Another effort to produce a glossary of decay terms is that of the Italian Commission NORMAL (UNI 11182:2006). Earlier work in this area came from the building stone industry in an effort to standardize terminology (Stone Federation of Great Britain, 1991), governmental organizations (Grimmer, 1984), and research groups (Fitzner *et al.*, 1997).

The ICOMOS-ISCS Illustrated Glossary on Stone Deterioration Patterns (Vergès-Belmin, 2008) helps define and clarify usage across languages and within the stone community, providing useful definitions of terms such as “scaling”, “spalling” and “flaking”. “Weathering” is used for the natural process of rock disintegration by external factors, usually in natural environments, while “deterioration”

implies the impairment of value and use and is “process of making or becoming worse or lower in quality, value, character, etc.”. Thus, rocks weather while stones deteriorate because the difference is that man has intervened in producing and using the stones. “Alteration” is used to indicate a modification of the material. “Degradation” and “decay” imply a change for the worse. The first one implies disintegration, has specific meanings for chemists, physicists, and geologists and is “decline in condition, quality, or functional capacity”. The second one, decay, has the connotation of decomposition, as reflected in tooth decay and is “any chemical or physical modification of the intrinsic stone properties leading to a loss of value or to the impairment of use”. The last word that needs to be mentioned is “damage”. This is the most general term that in general refers to structural or mechanical damages (Steiger *et al.*, 2014).

A more guided approach than a glossary can be found in work on expert systems from the late 1990s, with Van Balen (1996; 1999) producing an atlas of damage to historic brick structures as part of an expert system for elucidating environmental effects on brick. The atlas evolved into a broader program known as the MDDS (Masonry Damage Diagnostic System) (Van Hees *et al.*, 2006; Van Hees *et al.*, 2009).

Fitzner has produced an important classification of weathering forms as a basis for mapping the deterioration across a building façade (Fitzner *et al.*, 1997). This system has also been presented in case studies (Fitzner *et al.*, 2004). Such complex systems have been criticized because of the number of parameters to be measured (Moraes Rodrigues & Emery, 2008) as well as “cost concerns and the extensive training they require” (Dorn *et al.*, 2008). Fitzner’s classification recognizes nineteen different weathering forms and goes some way toward recording the severity of each, based on visual inspection (Fitzner, 2004). Similar, but simpler systems have been described by Massa *et al.*, (1991) and by Vergès-Belmin (1992). Zezza (1990 a; 1994; 2002) has used digital image processing to map different forms of

surface decay. Starting with photographs and other nondestructive information, such as ultrasonic measurements, false color images are produced that identify particular forms of decay (Doehne & Price, 2010).

Laboratory investigations about stone weathering have proved that among the numerous properties that characterize a stone material, there is a few that especially plays an important role in its degradation (Esbert & Ordaz, 1985).

As a great part of the deteriorating agents are connected to water (such as salts crystallization, the effects of freezing or the wet deposition of atmospheric pollutants) void spaces and hydraulic properties play a crucial part in the weathering processes, but they are not the only ones to control the durability of a stone material. Microstructural characteristics such as the grain interlocking, grain size and shape, the presence of large fossils, changes in the texture (Dürrast & Siegesmund, 1999), the presence of clay minerals (Esbert & Valdeón, 1985), internal sets of microcracks (Freire & Fort, 2015), anisotropy (Fort *et al.*, 2011), represent another group of properties influencing the rate and degree of weathering.

Regarding mechanical characteristics, uniaxial compressive strength, tensile strength, flexural strength, ultrasonic pulse velocity, Young's modulus, Bulk and Shear modulus, are important parameters to assess the durability or the weathering stone degree (Goudie, 1999). Among mechanical properties, tensile strength is the weakest, because being much lower than the uniaxial compressive strength, will be more affected by weathering (Arikan *et al.*, 2007).

In this research four types of stones and their petrophysical and mechanical properties will be investigated, by means of laboratory, non-destructive and ageing tests, according to CEN/TC 246 and CEN/TC 346 standards. The resulting data are beneficial for the preservation of cultural heritage and also for engineering purposes in new constructions.

3. Stones selection

3.1 Criteria for the selection

For the selection of the stone types to investigate in this thesis different criteria have been considered. First of all, the historical importance and the role of building stone materials in the Calabrian context, in particular in the territory of Cosenza Province. The most important Calabrian schools of stonemasons and the main related architectural models have been considered. Another criterion has been the analysis of the role of the quarry activity in the past and how it still influences the Calabrian quarry market. The number and the types of quarries presently active and non-active in the area of Calabria and in the territory of Cosenza have been analyzed. Concerning the selection of the lithotypes the possibility that quarries may still be exploited for a local limited use or a possible diffusion on a large scale out of the Region has been also taken into account.

3.2 Historical background and architectural models

The purpose of historical and architectural analysis is to investigate some of the most influential Calabrian schools of stonemasons in order to choose local stones to be investigated.

Since the 19th century until nowadays, the lithological variety, the ability of the stone cutters of Calabria and the presence of a lot of quarries have influenced the history of the local economy, as testified in literature. The area of Cosenza Province is very rich in quarry areas and some of them are still used. They played a very important role in the past for the realization of the architectural heritage of the old towns and for their decorative elements.

Analyzing masonries in some old towns of the Province of Cosenza, taken as the case study, the presence of recurrent stone materials can be noticed: pebbles of the Crati River, belonging to granite or gneiss stones of the “Sila Batholith” formation, mainly used for ordinary masonries (Bruno, 1993) and engineering purposes; white and compact limestones, indicated as “biancolella” by stonemasons and

commercially known as “ Mendicino tuff”, mainly used for structural elements and its components (Rodolico, 1953); calcarenitic Miocenic limestones and sandstones, softer, whitish or yellowish or sharply reddish, which outcrop in the southern Tyrrhenian Coastal Range, mainly used for floors, doors and for all the elements exposed to weathering (Bruno, 1995; Anastasio, 1996); crystalline carbonates, dolomitic limestones, limestones and dolostones, which characterize the masonries of the historical centers of the Pollino Area, the Tyrrhenian coast and part of the old towns of the neighbouring Region of Basilicata (AA.VV., 2015; Forestieri *et al.*, 2016a).

During the past, in the Cosenza Province (Calabria) four quarry schools were recognized, which worked both for patrimonial architecture and vernacular architecture. Some of them reached a good level and became famous out of the Region (Bruno, 1995).

3.2.1 *The school of stonemasons of San Giovanni in Fiore*

One of the most important school of Calabrian stonemasons was the so called “San Giovanni in Fiore² school”. In the Sila area, the central part of the Cosenza Province, a lot of little outcrops of granite, granitoid and tonalite, were exploited in the past for the construction of the architectures. So, granite, the main building material of this part of the Province, was used for the construction of buildings and for its principal decorative elements such as portals and cornices. But it was also employed as an important material in the field of the civil engineering, to build fountains, structural walls, weirs and milestones (Di Benedetto & Greco, 1990).

In particular, the area of San Giovanni in Fiore was very famous in the past for its stonemasons, very able to work this material and for the relevant quarry extraction of granite, principally employed for the construction of milestones (Di Benedetto & Greco, 1990) and for portals and Baroque and

² San Giovanni in is a town in the Province of Cosenza in the Calabria Region of southern Italy, in the Sila mountain range. The town originates from the Florense Abbey, built here by the Calabrian monk Joachim of Fiore in 1188. (http://www.florense.it/Inglese/San_Giovanni_in_Fiore-Italy.asp)

Neoclassical altars (Frangipane, 1950). The school of San Giovanni in Fiore influenced the “Florense architecture” (Bruno, 1995), famous for its severe style, based on the Joachim of Fiore³ (“Gioacchino da Fiore”, in Italian) rule and on the module of the “pointed arch”. Stonemasons operated for a long time, principally in four periods, from the 12th century until the 20th centuries. The school of San Giovanni in Fiore is the only Calabrian school that survived during the ‘800s and the ‘900s thanks to the industrial use of granite, its primary building material (Bruno, 1995).

In the first period, from the 12th to the 16th century, known as the “Età gioachimita” (“Joachim’s Era”), the main important religious buildings of the monastic order of Gioacchino da Fiore were built. The most important building is the “Florense Abbey”, whose model of Gothic portal was employed in the others construction sites belonging to the same religious order.

During the second period, from the 16th to the 18th century, the “Età Rotariana” (“Rotary Era”), the principal centre of this school, the historical centre of San Giovanni in Fiore was built. The architectural solutions were characterized by the traditional models and severe rules of Salvatore Rota, the commendatory abbot of the town and by the introduction of building materials softer than granite.

In the third period, named “Età degli scalpellini immigrati” (“Immigrants stone cutters’ Era”), from the 18th to the 19th century, San Giovanni in Fiore experienced the immigration of stonemasons from different parts of Calabria, who introduced new architectural models belonging to the Schools of Rogliano, Serra San Bruno and Palmi.

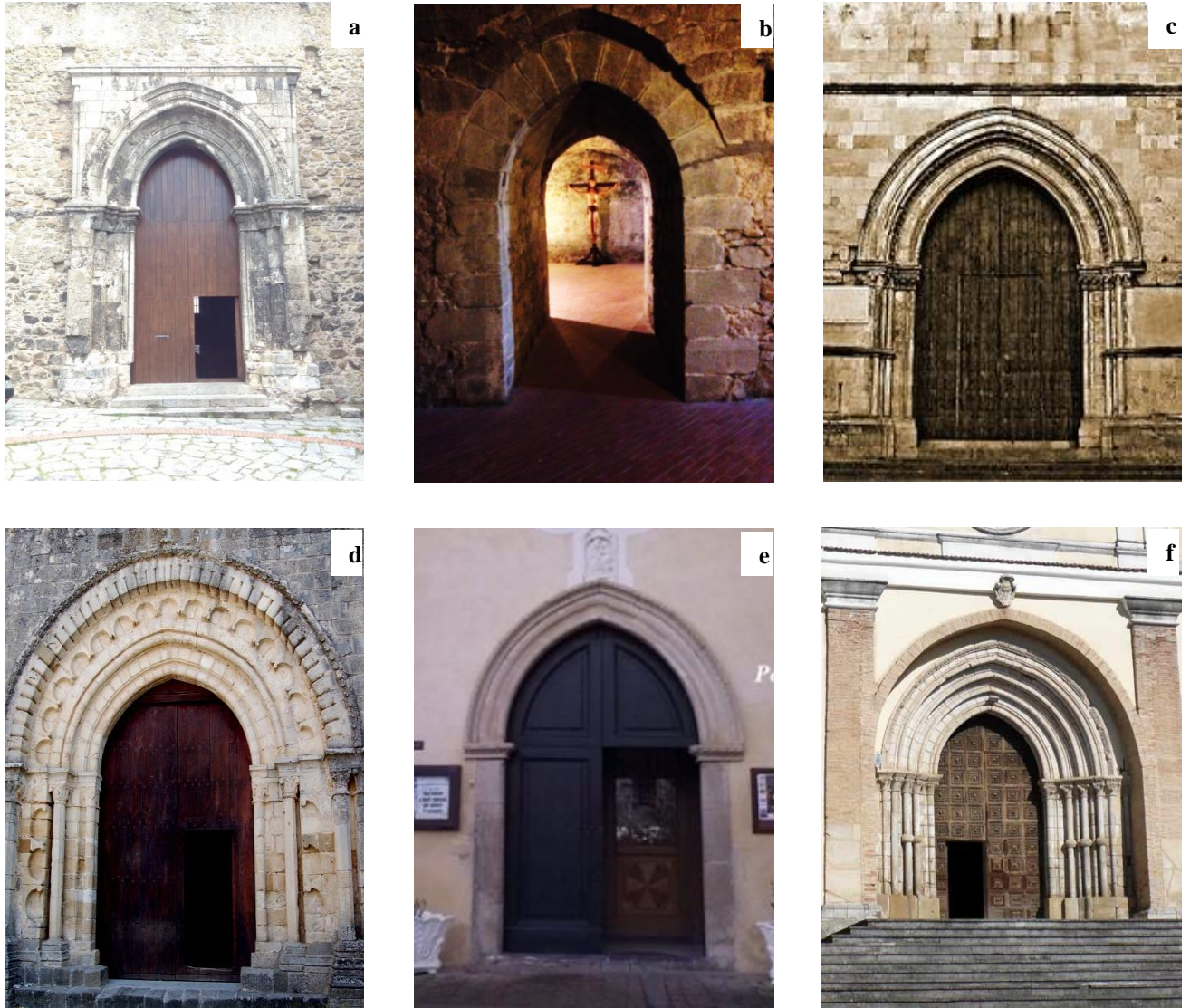
³ Joachim of Fiore, also known as Joachim of Flora and in Italian “Gioacchino da Fiore” (c. 1135 – 30 March 1202), was an Italian theologian and the founder of the monastic order of San Giovanni in Fiore. Born in the small village of Celico near Cosenza, in Calabria (at the time part of the Kingdom of Sicily), Joachim was the son of Mauro, a well-placed notary, and of Gemma, his wife. He was educated at Cosenza, where he became first a clerk in the courts, and then a notary himself. Later followers, inspired by his works in eschatology and historicist theories, are called Joachimites. He theorized the dawn of a new age, based on his interpretation of verses in the Book of Revelation, in which the Church would be unnecessary and in which infidels would unite with Christians. Members of the spiritual wing of the Franciscan order acclaimed him as a prophet. His popularity was enormous in the period, and some sources hold that Richard the Lionheart wished to meet him to discuss the Book of Revelation before leaving for the Third Crusade of 1189-1192. His famous Trinitarian “IEUE” interlaced-circles diagram was influenced by the different 3-circles Tetragrammaton-Trinity diagram of Petrus Alphonsi, and in turn led to the use of the Borromean rings as a symbol of the Christian Trinity (and possibly also influenced the development of the Shield of the Trinity diagram). (https://en.wikipedia.org/wiki/Joachim_of_Fiore)

In the last period, from the 19th to the 20th century, known as “Età dei Restauratori” (“Restorers’ Era”), due to the general crisis of the stone market, the stonemasons of the school of San Giovanni in Fiore were the only ones able to renew themselves and to work in restoration sites and to produce everyday granite objects.

But in the Sila Area, granite was also employed by another important school of the 16th and 18th century, the school of Rogliano, famous for the large use of granite, from decorative elements such as portals of churches and palaces, to elements able to resist weathering and wear and tear, like paving stones, stairs, balconies (Ceraudo, 1996). However, it can not be said that a real quarry activity existed, due to the less quantity of fresh rock that could be quarried, for physical, chemical processes cryoclastism and thermoclastism and hydrolysis and oxidation processes of weathering (Scarciglia *et al.*, 2008), onion-peel type exfoliation but, on the other hand, the granitoid boulders were widespread along the entire Sila Area, *boulders field* (Le Pera & Sorriso-Valvo, 2000). Nowadays, the extraction of this material is principally local and it is occasionally employed for local use (Di Benedetto, 1982).

The most famous architectural model of this school, that was handed down through the centuries was the model of the Portal with the “pointed arch” or “ogival arch”. This model is composed by a pointed arch with the presence or not of decorative elements. The most important architectural example with decorative elements is the Portal of the “Florense Abbey” in San Giovanni in Fiore (Fig. 3.1 a). This model, without ornamental elements (Fig. 3.2), is also present in the Crypt of the same building (Fig. 3.1 b) and in the Norman arch of the 1200 year that is the symbol of the town, whose arch structures were realized with San Giovanni in Fiore granite, squared ashlar with a smooth finishing surface, placed and arranged according to the construction technique of the “dry-stone wall” (without mortared courses). The Florense model of portal, with the pointed arch, has been proposed again in others buildings, like the “Cosenza Cathedral” in Cosenza (Fig. 3.1 c), the “Sambucina Abbey” in Luzzi

(Fig. 3.1 d), the “Sanctuary of the Madonna of the Castle” in Castrovillari (Fig. 3.1 e), and the “Bisignano Cathedral” in Bisignano (Fig. 3.1 f).



Figs. 3.1 (a, b, c, d, e, f). Models of portal with “ogival arch” belonging to the school of stonemasons of San Giovanni in Fiore: “Florense Abbey”, San Giovanni in Fiore (a); Crypt of the “Florense Abbey”, San Giovanni in Fiore (b); “Cosenza Cathedral”, Cosenza (c); “Sambucina Abbey”, Luzzi (d); “Sanctuary of the Madonna of the Castle”, Castrovillari (e); “Bisignano Cathedral”, Bisignano (f).

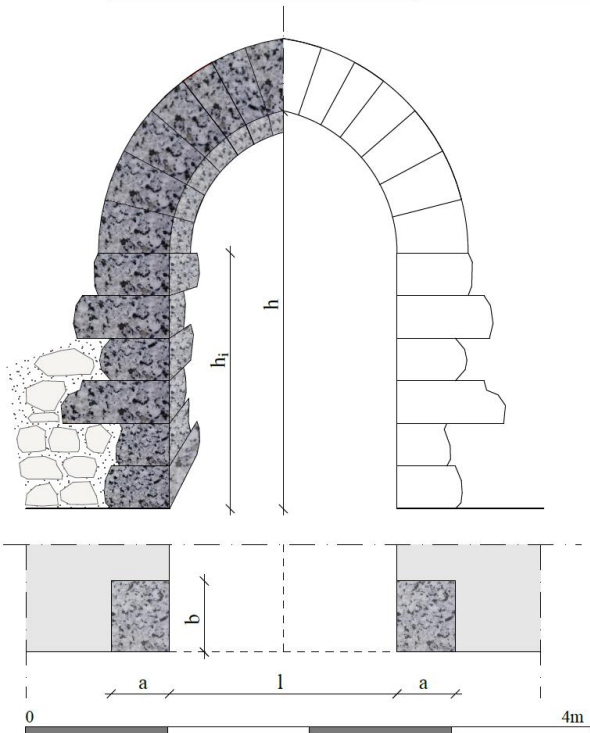


Fig.1. Front of portal with pointed arch



Fig. 2. Map of the town of San Giovanni in Fiore with the location of the portals of the same typology



Fig.3. Norman Arch, San Giovanni in Fiore (CS), XIII century

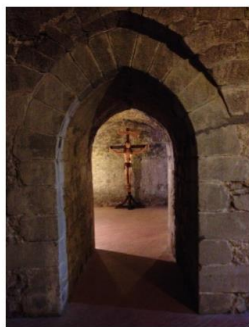


Fig.4. Building 1: "Crypt of Abbey Florense", San Giovanni in Fiore (CS)

Location:	"Crypt of Florense Abbey", San Giovanni in Fiore
Date:	XIII century
Typology:	pointed arch
N° portals reported in the map above:	2
Town:	San Giovanni in Fiore.
Dimensions:	l= 1.60m; h _i = 1.80m; h=2.80m; a= 0.40m; b=0.50m
Description:	Pointed arch composed by ashlar with a structural function and the keystone for the arch.
Materials and building techniques:	Local building stone. Dry-stone technique without mortared courses.
Finishing:	Smooth surface.
Decorative elements:	/
Description of decay:	Very slight decay. Patinas.
Building material:	"Granite of San Giovanni in Fiore" (GF): granite

Fig. 3.2. Model of portal with "pointed arch" belonging to the school of stonemasons of San Giovanni in Fiore, present in the Crypt of the "Florense Abbey" and in the Norman Arch, as reported in Fig.3 and Fig.4.

Another architectural model of this school is the Portal with the “semicircular arch” (Fig. 3.3). This model has been introduced during the period of “Età Rotariana” and the most important example is the main door of the “Chiesa Matrice” (“Matrix Church”) of the 18th century. The portal of “Chiesa della Cona” (Cona Church), of the 18th century too, was realized according to the same style. Thanks to the introduction in San Giovanni in Fiore of new building materials like the tuff of Acquafredda, from a little town in Sila, near San Giovanni in Fiore, stonemasons were able to chisel and carve the stone with more decorative detail. Comparing the two models of portals, the pointed and the semicircular one, the difference in ornamental elements is evident, due to the different level of hardness of the sculpted building material.

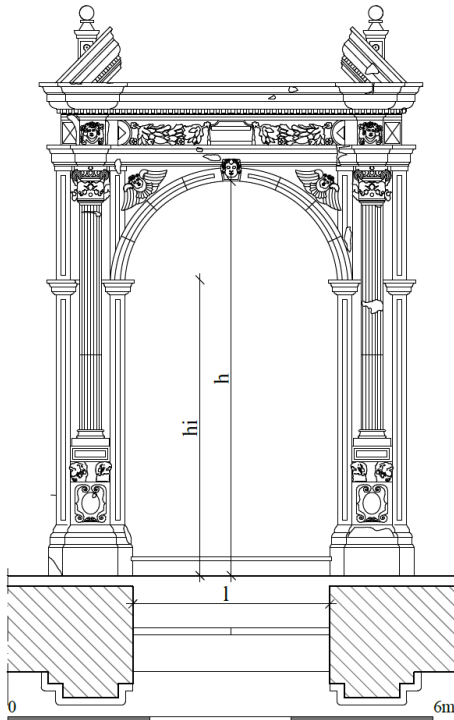


Fig.1. Front of portal with semicircular arch



Fig. 2. Map of the town of San Giovanni in Fiore with the location of the portals of the same typology



Fig.3. "Cona Church", San Giovanni in Fiore (CS), XVIII century



Fig.4. Building 1: "Matrix Church", San Giovanni in Fiore (CS)

Location:	"Matrix Church", San Giovanni in Fiore
Date:	XVIII century
Typology:	semicircular arch
N° portals reported in the map above:	2
Town:	San Giovanni in Fiore.
Dimensions:	l= 2.80m; hi= 4.20m; h=5.60m
Description:	Semicircular arch composed by ashlars with a structural function. The portal is framed by lateral columns and trabeation.
Materials and building techniques:	Sila building stone. Dry-stone technique without mortared courses.
Finishing:	Rock-faced surface with chiselled margin; furrowed surface; smooth surface.
Decorative elements:	Capitals, flowers, angels, lions, frames
Description of decay:	Medium decay. Erosion, efflorescences, missing parts, biological colonization, crusts.
Building material:	"Acquafredda sandstone" (AS): sandstone

Fig. 3.3. Model of portal with "semicircular arch" belonging to the school of stonemasons of San Giovanni in Fiore, present in the "Matrix Church" and in "Cona Church" of the 18th century, as reported in Fig.3 and Fig.4.

3.2.2 *The school of stonemasons of Basilicata and the northern part of Calabria*

In the towns of the northern part of Calabria and in some towns of Basilicata, there was a local school of stonemasons that worked in the period between the '700s and the '800 century. This school, was especially famous for the realization of portals of noble palaces and houses, in a local version of the style of the school of stonemasons of Naples. The main building materials employed were the local stones and in particular the “Grisolia⁴ stone”. The most important stonecutter lived in Aieta and one of them was Gerardo Rea, who in 1756 realized the portal of the Church of “S. Maria della Visitazione” in Aieta.

The model of portal developed by this school may be found in many portals of the old towns of the part of the Calabrian territory from Aieta to Scalea, to the towns of Latronico, Senise, Corleto Perticara, San Severino Lucano in the Basilicata region. In particular, this model is present in the following portals: in Aieta in Via Cantogrande n.41 (Fig. 3.4 a) and n.6 (Fig. 3.4 b), being built in 1860; in Scalea in the “Cupido Palace” (Fig. 3.4 c) and in other four portals of the same style concentrated in the higher part of the old town, near the Norman castle (Figs. 3.4 d, e, g, h); in Senise in “Barletta Palace” of the '700s (Fig. 3.4 f); in Tortora in the “Lomonaco Palace” of the '700s (Fig. 3.4 i); in Corleto Perticara in the palace of “Carminio and Tommaso Senise”, of 1880 (Fig. 3.4 l); in San Severino Lucano (Fig. 3.4 m); in Latronico in “Arcieri Palace” of the 19th century (Fig. 3.4 n). This model of portal is characterized by a “semicircular arch” (Fig. 3.5) composed by three ashlar with a structural function of piers, one ribbed vouissor for the impost, two lateral vouissors with spirals and the engraved keystone in the top of the arch with the family emblem or the engraving date. Due to the hardness of the building material employed, the ornamental elements are very few and concentrated in some details like the lateral volutes or the stoke emblem. The other structural elements are marked by linear grooves.

⁴ Grisolia is a town in the Province of Cosenza in the Calabria Region of southern Italy at an elevation of 480 a.s.l. (<http://www.visitsitaly.com/calabria/grisolia/>)



Figs. 3.4 (a, b, c, d, e, f, g, h, i, l, m, n). Models of portal with “semicircular” arch belonging to the school of stonemasons of Basilicata and the northern part of Calabria: Via Cantogrande n.21, Aieta (a); Via Cantogrande n.6, Aieta (b); “Cupido Palace”, Scalea (c); “Casa Famiglia Cupido”, Scalea (d); “Palazzo della Diocesi”, Scalea (e); “Barletta Palace”, Senise (f); Via del Castello n.24, Scalea (g); “Armentano Palace”, Scalea (h); “Lomonaco Palace”, Tortora (i); “Carmine e Tommaso Senise Palace”, Corleto Perticara (l); San Severino Lucano (m); “Arcieri Palace”, Latronico (n).

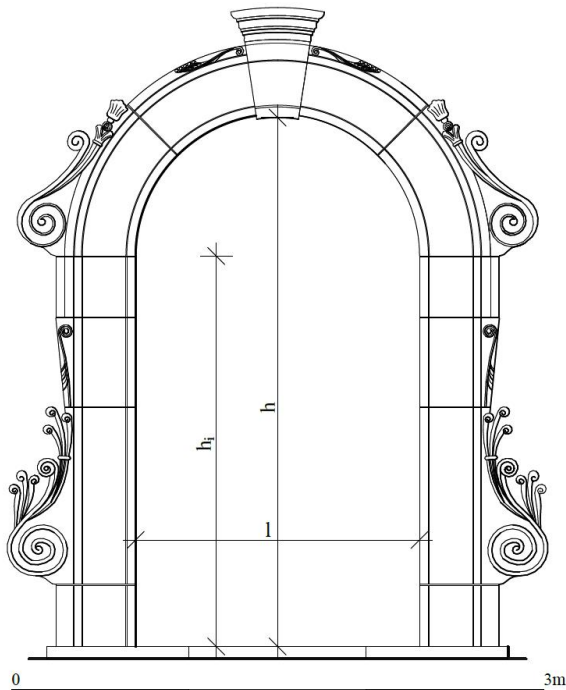


Fig.1. Front of portal with semicircular arch



Fig. 2. Map of the old town of Scalea with the location of the portals of the same typology



Fig.3. Building 1: "Cupido Palace", Scalea (CS)

Location:	"Cupido Palace", Via Castello, Scalea
Date:	XIV century
Typology:	semicircular arch
N° portals reported in the map above:	5
Towns:	Scalea, Aieta, Tortora (Calabria); Latronico, Senise, Corleto Perticara, San Severino Lucano (Basilicata).
Dimensions:	l= 1.60m; h ₁ = 2.20 m; h=3.00m
Description:	Semicircular arch composed by three ashlar for each side with a structural function of piers, one ribbed voussoir for the impost, two voussoirs with spirals and the keystone for the arch.
Materials and building techniques:	Local building stone. Dry-stone technique without mortared courses.
Finishing:	Rough-pointed surface without chiselled margin.
Decorative elements:	Emblem of the noble family on the top of the keystone.
Description of decay:	Very slight decay. Patinas and biological colonization by plants.
Building material:	"Grisolia stone" (DG): crystalline carbonate

Fig. 3.5. Model of portal with "semicircular arch" belonging to the school of stonemasons of Basilicata and the northern part of Calabria, present in many buildings, as reported in Fig.3.4.

3.2.3 *The schools of stonemasons of Rogliano and Altilia*

The “Mendicino calcarenite”, usually known as “tuff”, was employed by the important schools of stonemasons of Rogliano and Altilia. The school of Rogliano, influenced by the models of both Tuscan and Neapolitan schools, introduced three types of portals: the “framed portal”; with “advanced pilasters”; with “triumph arch and triple order”. The first one is characterized by a semicircular arch with lateral frames and a superior trabeation (Fig. 3.7). It can be found in many important buildings, such as the “S.Giorgio Church in Rogliano” (Fig. 3.6 a) of the 16th century “Cappuccinelle Convent” in Cosenza of 16th century (Fig. 3.6 b), “Annunziata Church” in Cosenza, 15th century (Fig. 3.6 c).

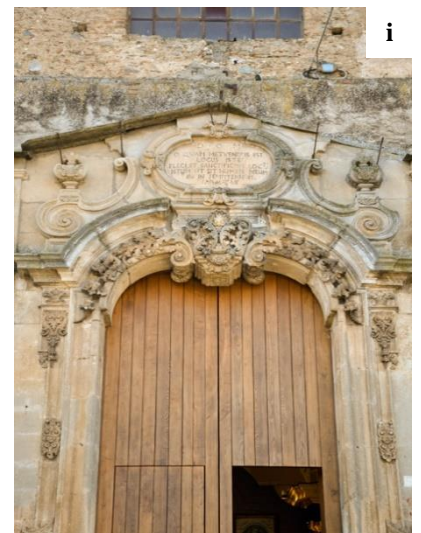
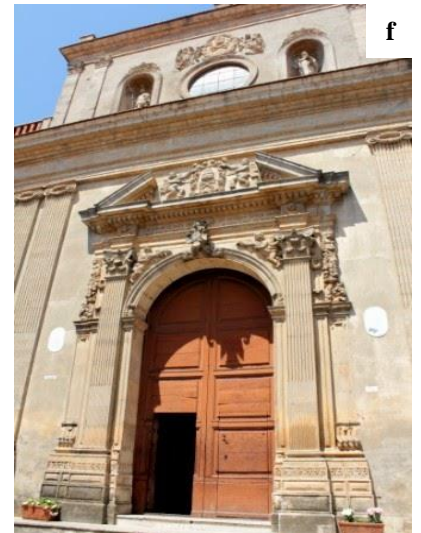
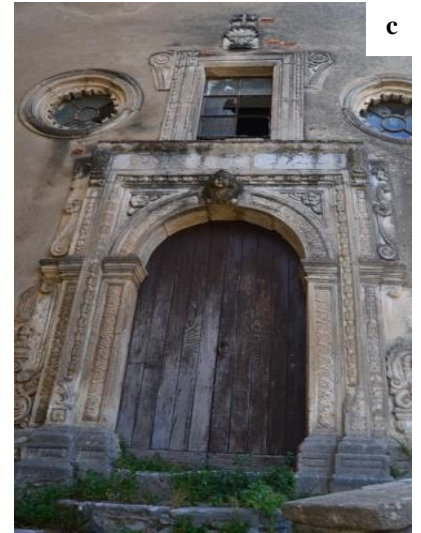
The second portal model is characterized by a flat ogee arch or semicircular arch with lateral advanced pilasters laying on jambs (Fig. 3.8). During the ‘700s this portal increased its ornamental elements like flowers and vegetal motifs, similar to the decorative elements of the carving art of wood (Leone, 2015). This kind of portal is visible in: “Santa Maria delle Grazie Church” in Cosenza of the 17th century; “Vergini Convent” in Cosenza (Fig. 3.6 d) of the 16th century realized by the stonemasons of Pietro Celeste and Domenico La Cava (Bruno, 1995) and reformed by Sansonetto Belsito (Altomare, 2015); “Santo Spirito Church” in Cosenza of the 16th century; “Quintieri Church” in Carolei of the 16th century (Fig. 3.6 e); “SS. Pietro and Paolo Church” in Rogliano of the 17th century (Fig. 3.6 f).

The third model of portal is composed by a “triumph arch and triple order” (Fig. 3.9). This portal is rich of decorative elements like capitals, spirals, frames, flowers and vegetal elements. It can be observed in many towns: Montalto Uffugo (“Santa Maria della Serra Church”, Fig. 3.6 g); Rogliano (“S. Ippolito Church”, Fig. 3.6 h); Cosenza (“Santissimo Salvatore Church”); San Fili (“Santissima Annunziata Church”, Fig. 3.6 i). In particular, “Santa Maria della Serra Church” in Montalto Uffugo was realized by the Niccolò Ricciuli in 1722, who was the most famous stonemason of the Rogliano School. The same author realized, in the same style: the portal of “Santissima Annunziata Church” in

San Fili of the 18th century; the portal of the “Montevergine Church in Paola” in 1704; “San Domenico Church” in Montalto Uffugo of 1717; “Immaculate Church” in Fuscaldo of the 17th century; the lateral and central portal of the “San Francesco di Paola Sanctuary” in Paola (Ameduri, 2015).

Probably, it is possible to identify a fourth model of “Roglianese portal”: the “diamond-shaped bosses” (Fig. 3.10). This portal is the main entrance of the “Vergini Convent” in Cosenza and was realized during the 16th century. Probably it was realized by the school of stonemasons of Rogliano for its rich decorative elements, such as the bosses and the lateral frames, and as the building material is the calcarenite, the same employed for the realization of the monastic building.

The school of stonemasons of Altilia was another important Calabrian school that built several portals in the same style of the Rogliano school. It was less famous than the first school but employed the same techniques and the same building materials (“Mendicino tuff”). The “Altiliese” portal was characterized by a semicircular arch in its different varieties: “cistercense frames”; “simple or double order”; “arch with the emblem” (Ameduri, 2015). These portals are concentrated in the towns of Altilia and Grimaldi.



Figs. 3.6 (a, b, c, d, e, f, g, h, i). Models of portal belonging to the school of stonemasons of Rogliano, with: “framed portal”, “S.Giorgio Church in Rogliano” (a), “Cappuccinelle Convent” in Cosenza (b), “Annunziata Church” in Cosenza (c); “advanced pilasters”, “Vergini Convent” in Cosenza (d), “Quintieri Church” in Carolei (e), “SS. Pietro and Paolo Church” in Rogliano (f); “triumph arch and triple order”, “Santa Maria della Serra Church” in Montalto Uffugo (g), “S. Ippolito Church” in Rogliano (h), “Santissima Annunziata Church” in San Fili (i).

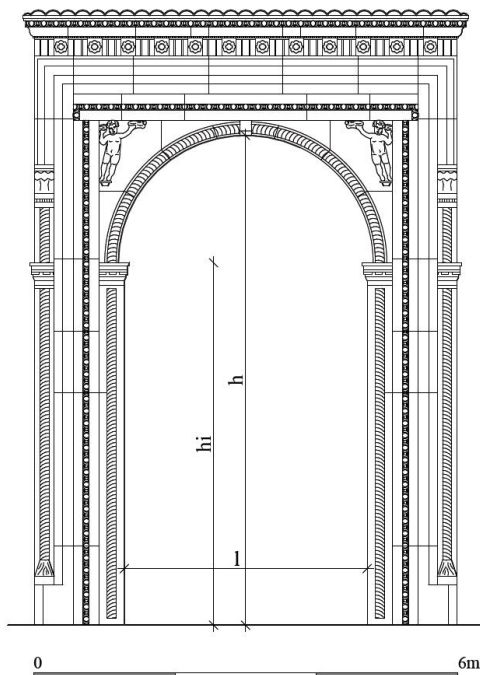


Fig.1. Front of framed portal



Fig. 2. Map of the town of Cosenza with the location of the portal



Fig.3. "S.Giorgio Church", Rogliano (CS), 1544



Fig.4. Building 1: "Cappuccinelle Convent", Cosenza

Location:	"Cappuccinelle Convent", Cosenza
Date:	1582
Typology:	semicircular framed arch
N° portals reported in the map above:	1
Towns:	Cosenza; Rogliano.
Dimensions:	$l= 3,00m$; $h_i= 4.70m$; $h=6,20m$
Description:	Semicircular arch composed by ashlar with a structural function. The portal is framed by lateral columns, frames and trabeation.
Materials and building techniques:	Calcarenite. Dry-stone technique without mortared courses.
Finishing:	Chiselled margin; furrowed and smooth surface.
Decorative elements:	Capitals, flowers, angels, lions, frames
Description of decay:	Medium decay. Missing parts, biological colonization, crusts.
Building material:	"Mendicino tuff" (CS): calcarenite

Fig. 3.7. Model of "framed portal" belonging to the school of stonemasons of Rogliano, present in many buildings, as reported in Figs.3.6 (a, b, c).

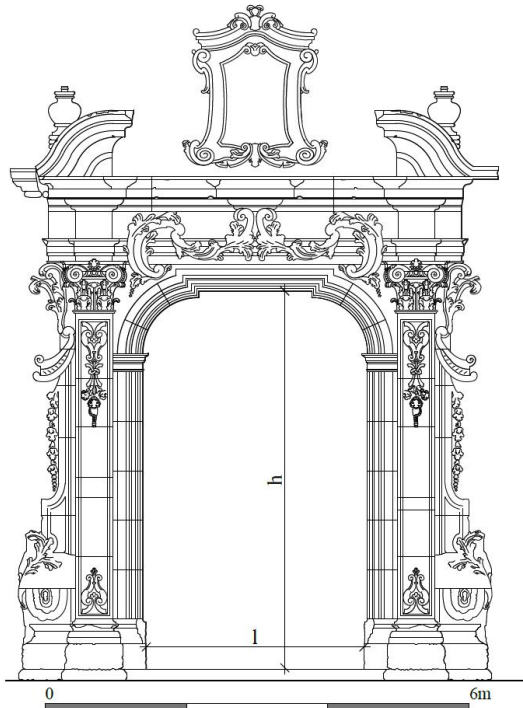


Fig.1. Front of portal with advanced pilasters



Fig. 2. Map of the town of Cosenza with the location of the portal



Fig.3. "SS. Pietro and Paolo Church", Rogliano (CS), XVII century



Fig.4. Building 1: "Vergini Convent", Cosenza

Location:	"Vergini Convent", Cosenza
Date:	1515 - 1517
Tipology:	advanced pilaster
N° portals reported in the map above:	1
Towns:	Cosenza; Rogliano.
Dimensions:	l= 2.80m; h= 4.20m.
Description:	Reverse ogee flat arch with advanced pilaster laying on jambs. The portal is framed by lateral columns with a structural function. Superior trabeation. Calcarenite. Dry-stone technique without mortared courses.
Materials and building techniques:	Calcarenite. Dry-stone technique without mortared courses.
Finishing:	Chiselled margin; furrowed and smooth surface.
Decorative elements:	Capitals, flowers, spirals, frames.
Description of decay:	Medium decay. Missing parts, biological colonization, crusts.
Building material:	"Mendicino tuff" (CS): calcarenite

Fig. 3.8. Model of portal with "advanced pilasters" belonging to the school of stonemasons of Rogliano, utilized for the realization of portals of many religious buildings, as reported in Figs.3.6 (d, e, f).

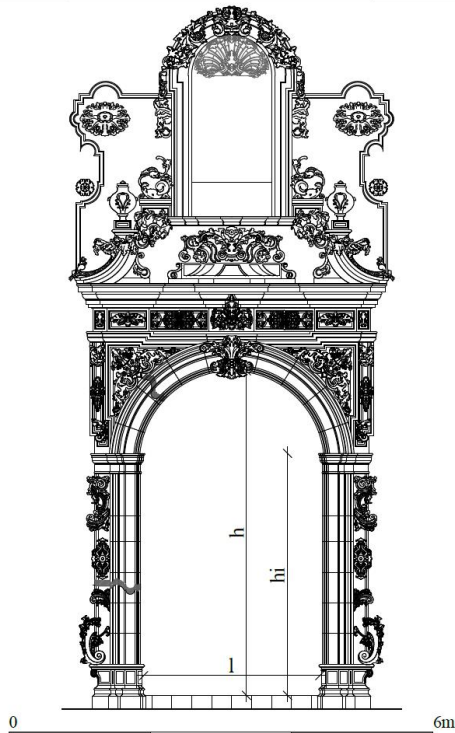


Fig.1. Front of portal with triumph arch and triple order



Fig. 2. Map of the town of Montalto with the location of the portal



Fig.3. "S. Ippolito Church", Rogliano (CS), 1709



Fig.4. Building 1: "Santa Maria della Serra", Montalto Uffugo (CS)

Location:	"Santa Maria della Serra Church", Montalto Uffugo (CS)
Date:	1722
Tipology:	triumph arch and triple order
N° portals reported in the map above:	1
Towns:	Montalto Uffugo, Cosenza; Rogliano; San Fili
Dimensions:	l= 2.50m; hi= 3,40; h= 4.60m.
Description:	Semicircular arch with lateral and superior frames. Trabeation and triple order.
Materials and building techniques:	Calcarenite. Dry-stone technique without mortared courses.
Finishing:	Chiselled margin; furrowed and smooth surface.
Decorative elements:	Capitals, flowers, spirals, frames.
Description of decay:	Medium decay. Missing parts, biological colonization, crusts.
Building material:	"Mendicino tuff" (CS): calcarenite

Fig. 3.9. Model of portal with “triumph arch and triple order” belonging to the school of stonemasons of Rogliano, utilized for the realization of portals of many buildings, as reported in Figs.3.6 (g, h, i).

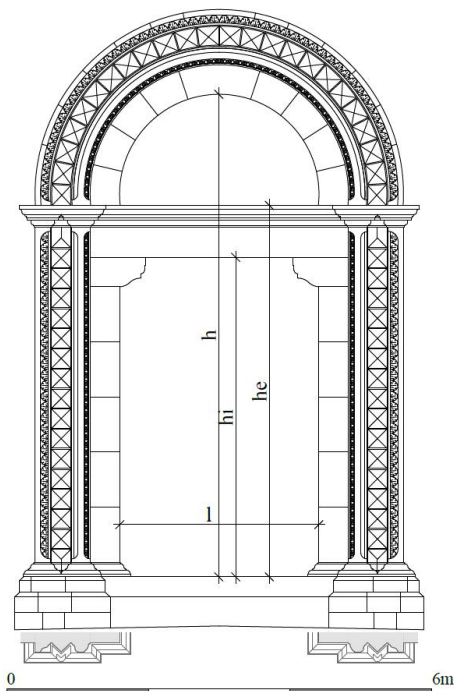


Fig.1. Front of portal with "diamond-shaped bosses"



Fig. 2. Map of the town of Cosenza with the location of the portal



Fig.3. "Vergini Convent" (external portal), Cosenza

Location:	"Vergini Convent" (external portal), Cosenza
Date:	XVI century
Typology:	diamond-shaped bosses
N° portals reported in the map above:	1
Town:	Cosenza.
Dimensions:	l=2.80m;hi=4.50m;he=5.20m;h=6.80m.
Description:	Semicircular arch with architrave and shelf elements. The portal is framed by lateral columns and inferior jambs.
Materials and building techniques:	Calcarenite. Dry-stone technique without mortared courses.
Finishing:	Chiselled margin; smooth surface.
Decorative elements:	Capitals, diamond-shaped bosses, ornamental vegetal elements.
Description of decay:	Medium decay. Disaggregation, missing parts, biological colonization, crusts, mass loss.
Building material:	"Mendicino tuff" (CS): calcarenite

Fig. 3.10. Model of portal with "diamond-shaped bosses" belonging to the school of stonemasons of Rogliano.

3.2.4 The school of stonemasons of Fuscaldo

Since the 12th until the 18th century, in Fuscaldo there was an important school of stonemasons that realized many artifacts with the local stone (sandstone) of “Pietra di Fuscaldo” (Fuscaldo stone) or “Pietra dolce”. The activity of this school, important for the realization of several portals⁵, can be resumed in three periods (Bruno, 1995). During the first period, from the 12th until the 15th century, called as “Età dei Cavatori” (“Quarry men Age”), many quarry sites situated in Fuscaldo were exploited to extract cut stones for military and religious buildings. There were only two figures of stonemasons: quarry men and rough-cutters. During the second period, from the 15th to the 16th century, known as the “Età dei modellatori” (“Stonemasons Age”), stonemasons introduced the first model of portal with a “simple order”. But the third period, from the 16th until the 18th century called as “Età dei capomastri” (“Master builders Age”), was the most important and the richest for the types of introduced portals. The proof of the influence of this school for the Calabrian architecture is the variety of models of portal, belonging to five categories: “simple order”; “cassettoni”; “diamond-shaped bosses”; “hanging flowers”; “with architrave”. The most important portals in Fuscaldo, for each category, are:

- “simple order” with two versions (Fig. 3.12): with *semicircular arch* (a) in “Marzano Palace” (Fig. 3.11 a) (15th century); “Porta del Sangue” in Guardia Piemontese (16th century); “Vaccari Palace”; “Mazzei Palace” (18th century); “Baldino Palace” (16th century); “Raimundo Palace” (16th century); “D’Andrea Palace” (16th century); “Santoro Palace” (15th century); “Apicella Palace” (18th century); “Raimundo G. Palace” (14th century); “Coscarelli Palace” (14th century); “Carnevale Palace” (Fig. 3.11 b) (14th century); with *flat arch* (b) in “Cariolo Palace” (18th century); “Vilardo Palace” (15th century); “D’Aqui Palace” (18th century).

⁵ Due to the several realization of portals in Fuscaldo by the school of stonemasons of Fuscaldo, the town has been called as the town of “Cento Portali” (“Hundreds of Portals”).

- “cassettoni” (Fig. 3.13): “Calabria Palace” (16th century); “Valenza Palace” (1585); “Ariani Palace” (17th century); “Vilardo Palace”; “Martini Palace”; “Mazzei (Don Ferdinando) Palace”; “Mazzei (Don Domenico) Palace”; “Lanzillotta F. Palace” (18th century); “Cariolo G. Palace” (18th century); “Lanza Palace” (19th century); “Iannuzzi R. Palace” (18th century); “Gentile Palace” in Acquappesa (18th century); “De Bernardis-Frassetto Palace” in Fuscaldo Marina (19th century); “De Caro Palace” in Itavolata; “Panza House” in Fiumefreddo Bruzio; “Perrone Palace” in Aieta; “Montesani Palace” (Fig. 3.11 c) in Fuscaldo Marina (18th century); “Sarpi Palace” in S. Marco Argentano;
- “diamond-shaped bosses” (Fig. 3.14): “Porta S. Francesco” (Fig. 3.11 d) (17th century); “Martini G. Palace” (17th century); “Lanzillotta F. Palace” (18th century); “Cariolo (ex carcere)” (18th century); “Trifilio F. Palace” (17th century);
- “hanging flowers” (Fig. 3.15): “Vairo Palace” (18th century); “De Simoni Palace” (18th century); “Ariani Palace” (17th century); “Valenza Palace”, (16th century); “Vilardo Palace”, (16th century); “De Seta House” (Fig. 3.11 e) in Itavolata (‘700s); “Lippo House” in Malvito (‘700s);
- “with architrave” (Fig. 3.16): “Immacolata Concezione Church”⁶ (Fig.3.11 f) by Niccolò Ricciulli⁷ (18th century); “Santa Maria Maggiore Church”⁸ in Paola; “Palace in via Vaccari” (15th century) in Fuscaldo; “Vilardo Palace” (15th century); “D’Aqui Palace” (18th century).

⁶ The same design of the “Immacolata Concezione Church” in Fuscaldo has been reproduced, by the school of stonemasons of Rogliano, in the churches of “Madonna della Serra” in Montalto Uffugo and “Montevergine” in Paola.

⁷ Niccolò Ricciulli is one of the most important stonemasons of the school of Rogliano. He worked for the realization of the “Royal Palace” in Naples during the kingdom of Carlo III Borbone.

⁸ Realized by the school of stonemasons of Fuscaldo.



Figs. 3.11 (a, b, c, d, e, f). Models of portal belonging to the school of stonemasons of Fuscaldo, with: “simple order - semicircular arch” in “Marzano Palace” (a) and “Carnevale Palace” (b) in Fuscaldo; “cassettoni” in “Montesani Palace” (c) in Fuscaldo Marina; “diamond-shaped bosses” in “Porta S. Francesco” (d) in Fuscaldo; “hanging flowers” in “De Seta House” (e) in Intavolata; “architrave” in “Immaculate Church” (f) in Fuscaldo.

P1_AF Class: *Portal*

Subclass: *Portal "simple order"*

P1_AF(a): *semicircular arch*

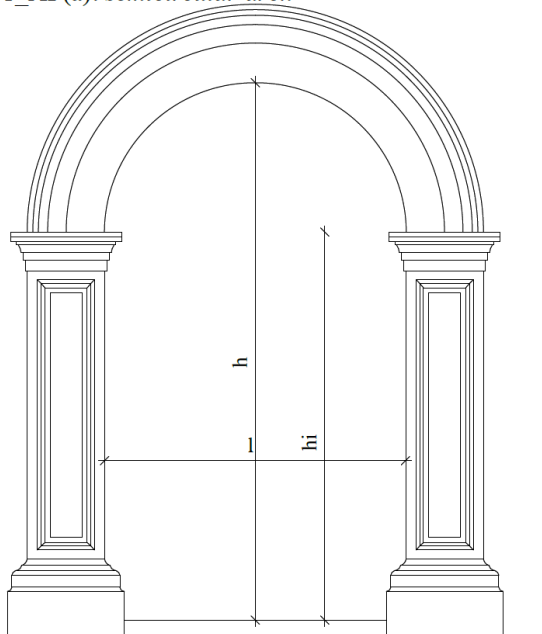


Fig.1. Front of portal with semicircular arch

P1_AF(b): *flat arch*

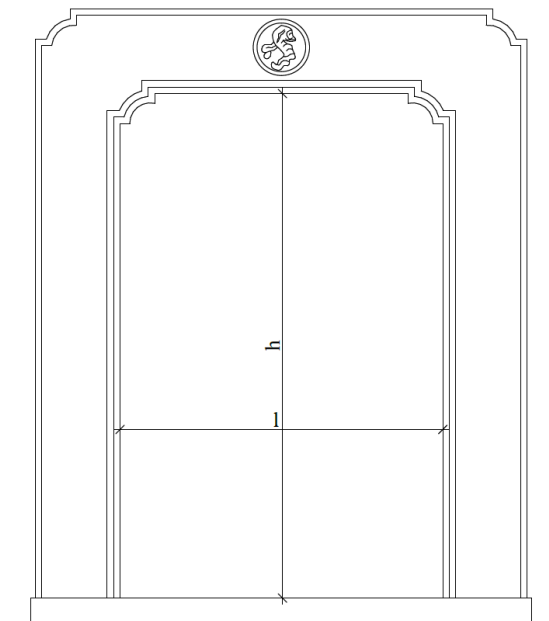


Fig.2. Front of portal with flat arch



Fig. 2. Map of the town of Fuscaldo with the location of the portals of the same typology (a, b)

Location:	P1_AF(a) "Baldino Palace", Spirito Santo area, Fuscaldo P1_AF(b) "D'Aqui Palace", C.Garibaldi, Fuscaldo
Date:	XVI century; XVII century
Typology:	semicircular arch (a); flat arch (b)
N° portals reported in the map above:	>10 (a); 3 (b)
Towns:	Fuscaldo; Guardia Piemontese
Dimensions:	$l=1.40m; h_i=2.00m; h=2.70m$ (a); $h=2.50; l=1.70m$ (b).
Description:	(a): piers laying on plinthes, capitals and semicircular arch; (b) linear piers and flat arch.
Materials and building techniques:	Fuscaldo sandstone. Dry-stone technique without mortared courses.
Finishing:	Furrowed (a) and smooth surface (a,b).
Decorative elements:	Capitals and linear slight grooves (a); linear grooves (b)
Description of decay:	Medium/high decay. Erosion, efflorescences, missing parts, biological colonization, crusts (a, b).
Building material:	"Fuscaldo sandstone" (AF): sandstone

Fig. 3.12. Model of "simple order" with semicircular and flat arch, belonging to the school of stonemasons of Fuscaldo, present in many buildings, as reported in Figs.3.11 (a, b).

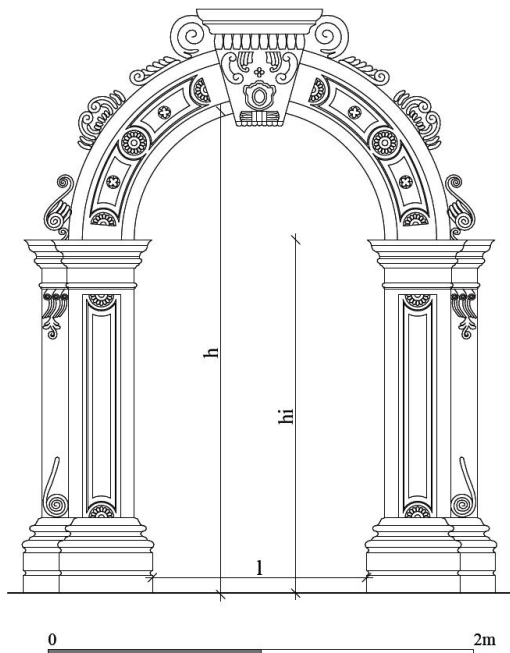


Fig.1. Front of portal with "cassettoni"

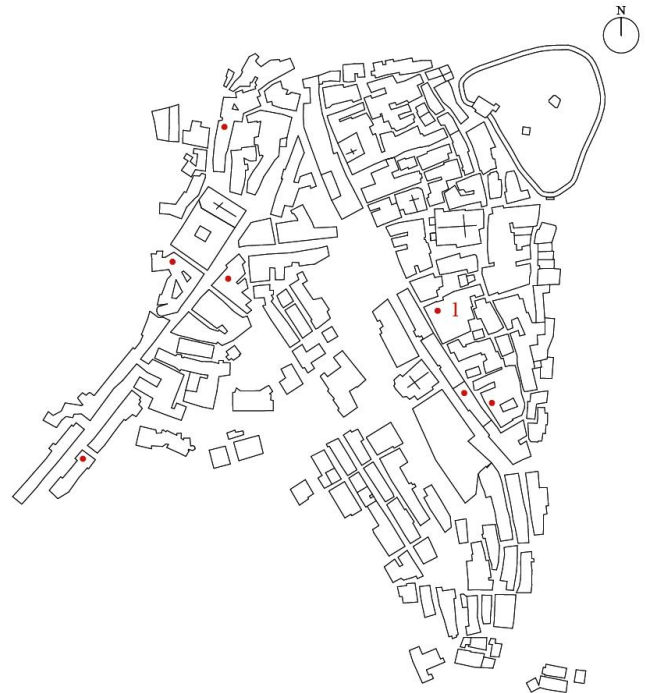


Fig. 2. Map of the town of Fuscaldo with the location of the portals of the same typology



Fig.4. "Valenza Palace", Fuscaldo (CS), 1585



Fig.3. Building 1: "Calabria Palace", Fuscaldo (CS), XVI century

Location:	"Calabria Palace", via Fanuele, Fuscaldo
Date:	XVI century
Typology:	semicircular arch with "cassettoni"
N° portals reported in the map above:	7
Towns:	Fuscaldo; Acquappesa; Intavolata; Fiumefreddo; S.Marco Argentano; Aieta
Dimensions:	l=1.40m; h _i =2.00m; h=2.70m.
Description:	semicircular arch with "cassettoni"; keystone with the emblem; structural piers; capitals and spirals.
Materials and building techniques:	Fuscaldo sandstone. Dry-stone technique without mortared courses.
Finishing:	Smooth surface with grooves and chiselled margins.
Decorative elements:	Capitals, grooves, spirals, family emblem.
Description of decay:	Medium/high decay. Erosion, efflorescences, missing parts, biological colonization, crusts.
Building material:	"Fuscaldo sandstone" (AF): sandstone

Fig. 3.13. Model of portal with "cassettoni", belonging to the school of stonemasons of Fuscaldo, present in many buildings, as reported in Fig.3.11 (c).

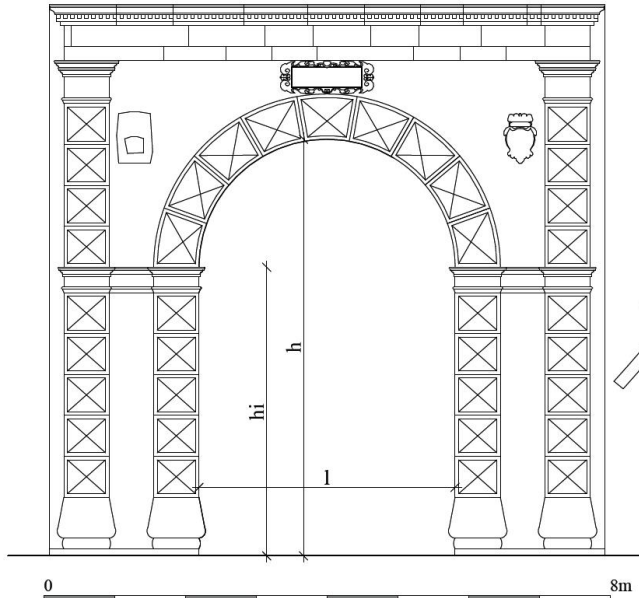


Fig.1. Front of portal with "diamond-shaped bosses"



Fig. 2. Map of the town of Fuscaldo with the location of the portals of the same typology



Fig.4. "Martini G. Palace", Fuscaldo (CS), XVII century



Fig.3. Building 1: "Porta S. Francesco", Fuscaldo (CS), XVII century

Location:	"Porta S. Francesco", quartiere Croce, Fuscaldo
Date:	XVII century
Tipology:	semicircular arch with "diamond-shaped bosses"
N° portals reported in the map above:	5
Town:	Fuscaldo.
Dimensions:	$l=3.60m$; $h_i=4.10m$; $h=5.90m$.
Description:	semicircular arch and pilasters with "diamond-shaped bosses"; capitals; architrave; structural pilasters; trabeation.
Materials and building techniques:	Fuscaldo sandstone. Dry-stone technique without mortared courses.
Finishing:	Smooth surface and bosses
Decorative elements:	Capitals, bosses, cornices, emblem.
Description of decay:	Medium/high decay. Differential erosion, delamination and granular disaggregation, exfoliation, efflorescences, micro-cracks and missing parts, crusts.
Building material:	"Fuscaldo sandstone" (AF): sandstone

Fig. 3.14. Model of "diamond-shaped bosses" portal, belonging to the school of stonemasons of Fuscaldo, utilized for the realization of many portals, as reported in Fig.3.11 (d).

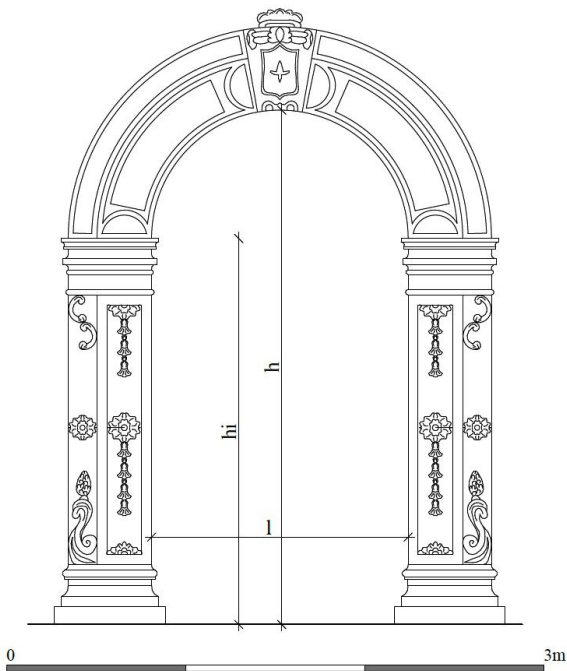


Fig.1. Front of portal with "hanging flowers"



Fig. 2. Map of the town of Fuscaldo with the location of the portals of the same typology



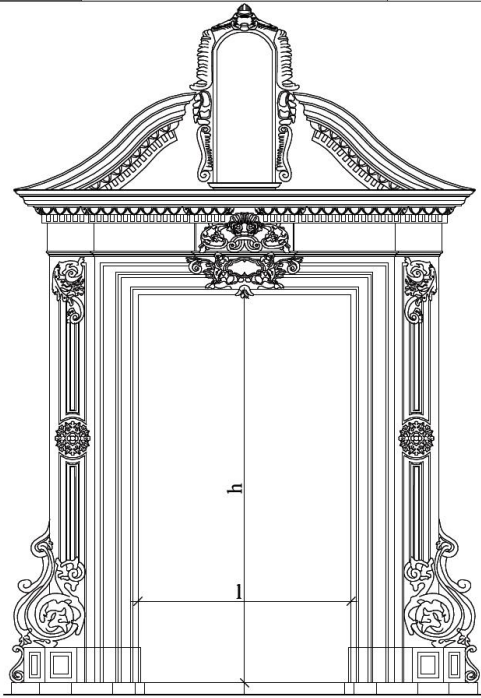
Fig.4. "Ariani Palace", Fuscaldo (CS), XVII century



Fig.3. Building 1: "De Seta House", Intavolata (CS), XVIII century

Location:	"De Seta House", Intavolata
Date:	XVIII century
Typology:	semicircular arch with "hanging flowers"
N° portals reported in the map above:	4
Towns:	Fuscaldo, Intavolata, Malvito.
Dimensions:	l=1.80m; h _i =2,70m; h=3.60m.
Description:	semicircular arch and "hanging flowers"; capitals; structural pilasters and plinths.
Materials and building techniques:	Fuscaldo sandstone. Dry-stone technique without mortared courses.
Finishing:	Smooth surface with grooves and chiselled margins.
Decorative elements:	Capitals, flowers, cornices, emblem.
Description of decay:	Medium/high decay. Differential erosion, delamination and granular disaggregation, exfoliation, efflorescences, micro-cracks and missing parts, crusts.
Building material:	"Fuscaldo sandstone" (AF): sandstone

Fig. 3.15. Model of portal with "hanging flowers", belonging to the school of stonemasons of Fuscaldo, utilized for the realization of many portals, as reported in Fig.3.11 (e).



0 6m

Fig.1. Front of portal with "architrave"



Fig. 2. Map of the town of Fuscaldo with the location of the portals of the same typology



Fig.4. "Palace in via Vaccari", Fuscaldo (CS), XV century



Fig.3. Building 1: "Immaculate Church", Fuscaldo (CS), XVIII century

Location:	"Immaculate Church", Fuscaldo
Date:	XVIII century
Typology:	portal with "architrave"
N° portals reported in the map above:	4
Town:	Fuscaldo.
Dimensions:	l=2,40 m; h=5.10m.
Description:	Tympanum with an aedicule in the centre. Architrave and structural pilasters.
Materials and building techniques:	Fuscaldo sandstone. Dry-stone technique without mortared courses.
Finishing:	Smooth surface
Decorative elements:	Inscription, spirals, rosettes.
Description of decay:	Medium/high decay. Differential erosion, delamination and granular disaggregation, exfoliation, efflorescences, micro-cracks and missing parts.
Building material:	"Fuscaldo sandstone" (AF): sandstone

Fig. 3.16. Model of portal with "architrave", belonging to the school of stonemasons of Fuscaldo, utilized for the realization of many important portals, as reported in Fig.3.11 (f).

3.3 Quarries and materials – Calabria and Cosenza Province

In this chapter, attention will be focused on the natural stone market and the quarry activity in Italy. Moreover, the active quarries in Cosenza Province will be reported and the traditional stone extraction and types of stone finishing will be mentioned.

3.3.1 *Natural stones*

Natural stone is a term employed for various stones used for structural or decorative purposes in construction and monumental applications (Merke, 2000). According to the Technical Committee for Natural Stones of the European Committee of Standardization (CEN/TC 246) and to the Decision 2002/272/EC definitions, a natural stone is a piece of naturally occurring rock. According to UNI-EN 12670 (2003), it is defined as *a natural resource rock with use in construction and for the restoration and reconstruction of monuments*.

The physical and mechanical properties of natural stone refer to its use as building material. Stone should mainly be loaded with compressive forces, for its high compressive strength. On the contrary stones can't be loaded with bending forces because the tensile strength is about 10 – 30 times lower than the compressive strength, so structures could easily crack causing failures. Therefore the products of the stone market analysis consider slabs, blocks, cladding panels and elements used for ornamental and decorative purposes. In particular, it is possible to identify three ranges based on quality grades of stones (Sousa, 2010): individual blocks; gravestones; building industry. For the first category aesthetic and surface properties are considered as important for the selection of the stone type; for the second, petrography has a principal role; for the last, physical and mechanical properties are considered as predominant.

A common commercial classification separates stone into: calcareous materials, including travertines, limestones and metamorphic stones as marbles; siliceous materials (granites, sandstones and quartzites); and slates. The commercial term “granite” includes not only granites but also igneous stones with distinguishable grains to the naked eye and some metamorphic stones such as gneiss (Hora, 2007), while the term “marble” is commercially defined as any crystalline stone composed predominantly of calcite, dolomite, or serpentinita that is capable of being polished (Sutphin & Orris, 2007).

The major producers of natural stones (Fig. 3.17) in the world are: Asia (China), followed by Europe; non EU countries like India, Iran, Turkey; South America; USA and South Africa. The major consumers of finished products are China, USA, India, Italy, Spain, South Korea, Germany, France, Japan, Taiwan, Brazil and UK (Montani, 2007). The stone production, as can be observed in Fig. 3.17, is mainly concentrated in areas where there is an historical use of these building materials through centuries like the Mediterranean and Eastern countries. The market of natural stones in Europe has shown an increase in production and regarding to the main European producers, Italy is one of the most important one followed by Spain. Similar to the European trend, Italian stone market is growing too and marble and granite are the most exported natural stones (Evangelista et al., 2007).

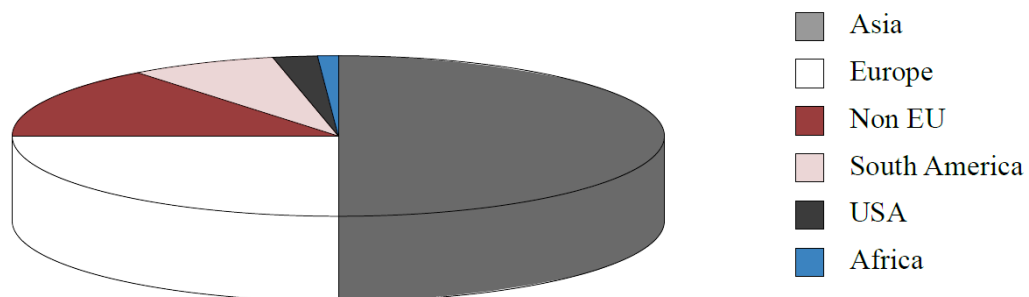


Fig. 3.17 Stone world production with respect to countries (Montani, 2007, modified): Asia (50-51%); Europe (27-28%); Non-European countries (10-11%); South America (8-9%); USA (2-3%); Africa (1-2%).

Natural building stone products range from unfinished raw to semi-finished blocks up to polished and refined dimensional stone that can be used for various applications (Siegesmund & Török,

2014). As it is shown in Fig. 3.18 main products are flooring tiles, cladding panels for internal and external façades, stairs, or other architectural elements. Other important sectors are: the production of gravestones that mainly uses semi-finished small blocks; the urban design with different stone types and craftworks for ornamental purposes.

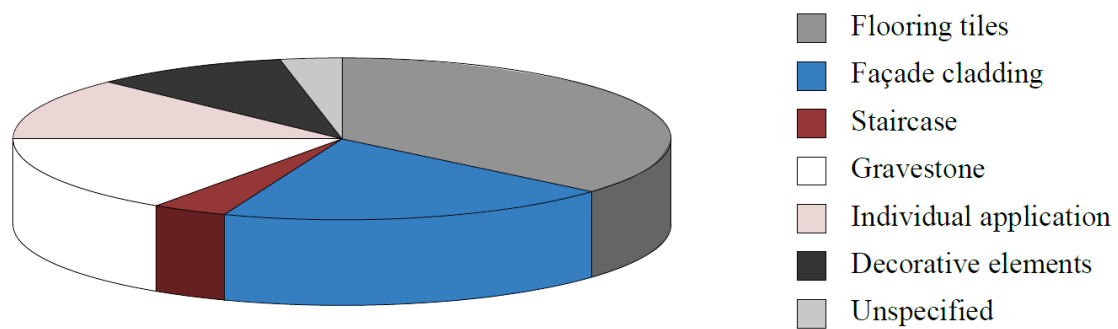


Fig. 3.18 Natural world stone uses (Siegesmund & Török, 2014, modified).

3.3.2 Italian and Calabrian stone market

Italy has been the dominating producer in the natural stone industry for a long time. It is one of the most important European exporter of stone materials, building and ornamental stones (especially the Carrara District), and at the same time it is a great consumer of finished products and importer of raw materials (Ashmole & Motloun, 2008). However, its dominance has been overcome by the Chinese and the Indian market, whose production is rapidly increasing.

According to the Italian extracted materials “Rapporto Cave” – Quarry Report (Legambiente, 2014), the number of Italian active quarries was 5592, while 16.045 was the number of the inactive ones. Data of inactive quarries referred only to those available in the regions where there was a monitoring activity (Calabria and Friuli Venezia Giulia did not have any monitoring activity⁹). Among stone materials, 80 million cubic meters were extracted in 2012 only for sand and gravel, followed by high quantities of limestone (31.6 million cubic meters) and ornamental stones (over 8.6 million cubic

⁹ LEGAMBIENTE. *Rapporto Cave 2014: I numeri, il quadro normativo, il punto sull'impatto economico e ambientale dell'attività estrattiva nel territorio italiano*, Roma, 2014, p.5

meters). The extraction of sand and gravel represents the 62.5% of the Italian stone extraction, mainly concentrated in the regions of Lazio, Lombardia, Piemonte and Puglia. 50% of the extractive industries are located in northern Italy; the remaining 50% belongs to the Centre and the South, with 24.8% and 28.4% respectively (Ceruti & Di Gregorio, 2014).

The number of active and inactive quarries in Calabria has been determined from a statistical analysis carried out by “Laboritt” research group (2014) on 633 extraction Calabrian sites. The number of active quarries ranges between 237 (Legambiente, 2014) to 273 (Laboritt, 2014). From the graphic reported in the Fig. 3.19, it can be observed that Calabria has not a developed quarry activity because the number of inactive quarries is higher than the active ones.

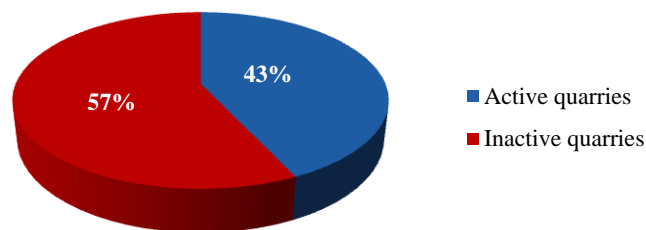


Fig. 3.19 Number of active and inactive quarries from a total of 633 Calabrian extraction sites (Laboritt, 2014, modified).

The highest number of active quarries is concentrated in the Cosenza Province (43%), followed by the Provinces of Catanzaro (23%), Reggio Calabria (19%), Vibo Valentia (10%). Crotona Province has the lowest number of quarries, with only the 5% (Fig. 3.20). On the other hand, analyzing the number of inactive extraction sites, Cosenza Province has the lowest number with only the 1% while Reggio Calabria the highest with the 36%. Vibo Valentia and Catanzaro show similar percentages, 28% and 24%, respectively. For Crotona has been registered the 11% of inactive quarries (Fig. 3.21).

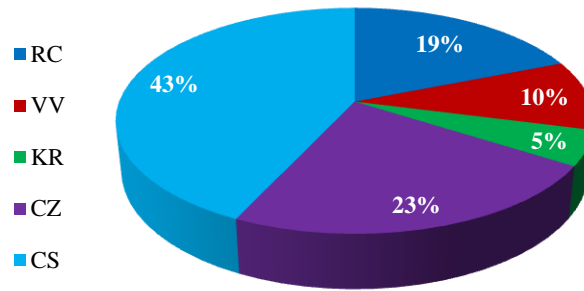


Fig. 3.20 Number of active quarries in the five Provinces of Calabria: RC (Reggio Calabria); VV (Vibo Valentia); KR (Crotona); CZ (Catanzaro) and CS (Cosenza). (Laboritt, 2014, modified).

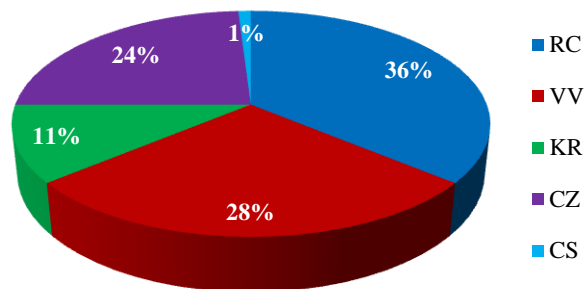


Fig. 3.21 Number of inactive quarries in the five Provinces of Calabria: RC (Reggio Calabria); VV (Vibo Valentia); KR (Crotona); CZ (Catanzaro) and CS (Cosenza). (Laboritt, 2014, modified).

Among quarried stone materials (Fig. 3.22), sand accounts for approximately the 60% of the Cosenza Province stone extraction, with quarries distributed over the entire territory (Figs. 3.23 a, b). It is followed by limestone (approximately 20%), arenaceous limestone (6%) and clay (4%). Clayey limestone, crystalline carbonate, dolomitic and reddish limestone and gypsum account for 1-2% of the stone extraction (Table 3.1).

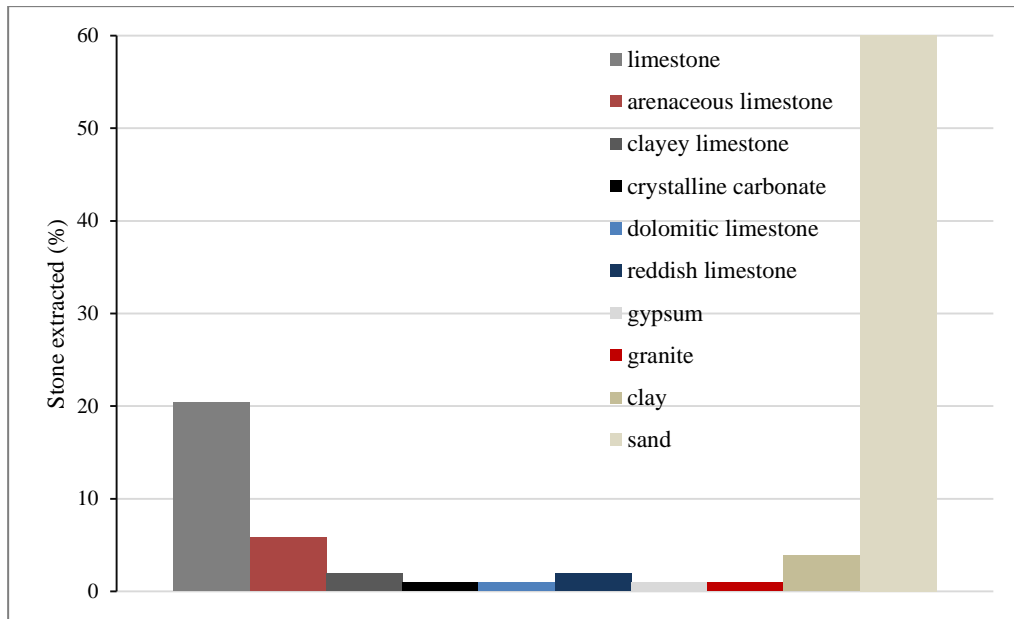


Fig. 3.22 Stone materials extracted (%) in Cosenza Province. (Laboritt, 2014, modified).

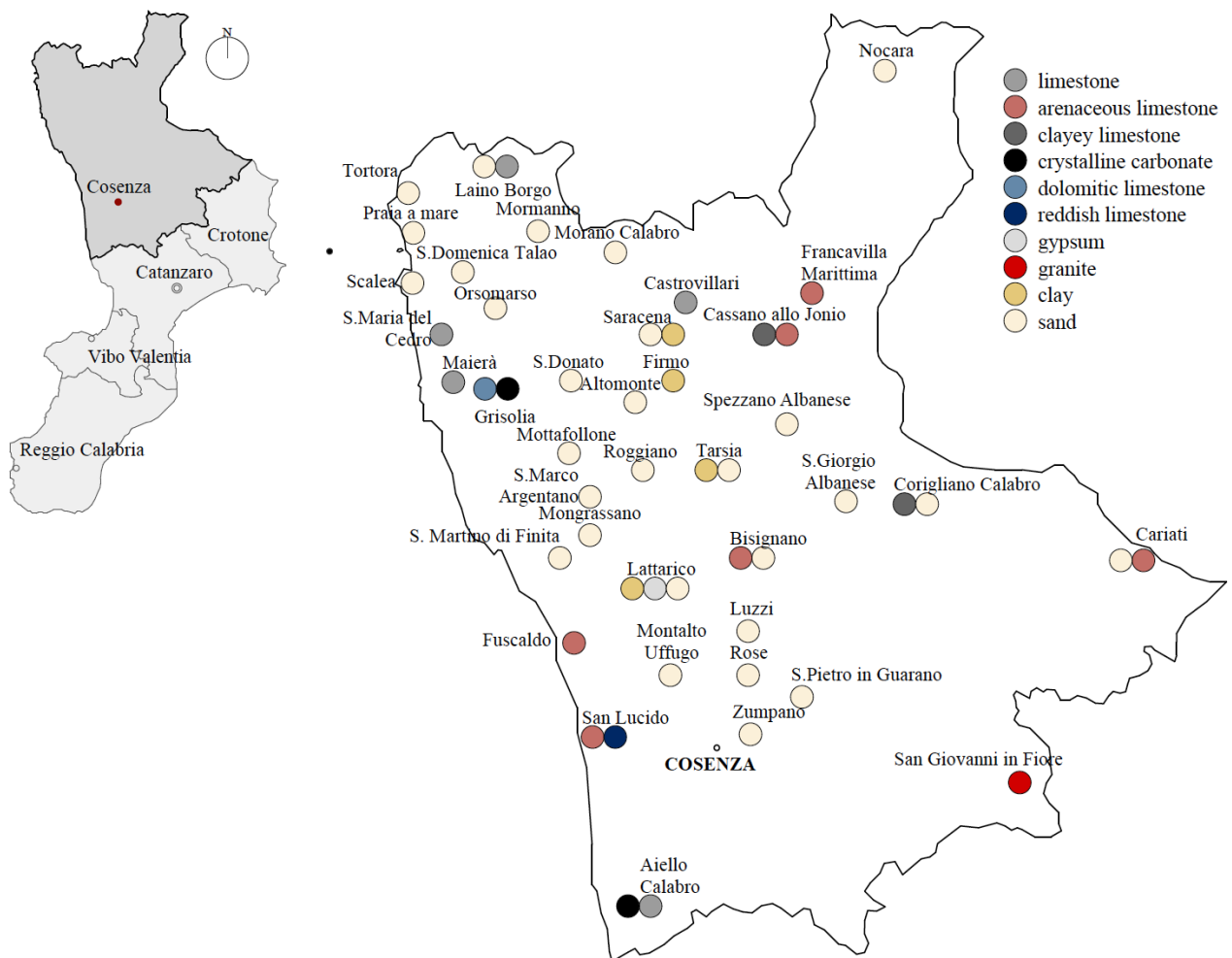


Fig. 3.23 a. Map of the active extraction sites of Cosenza Province, subdivided for lithology. (Laboritt, 2014, modified).

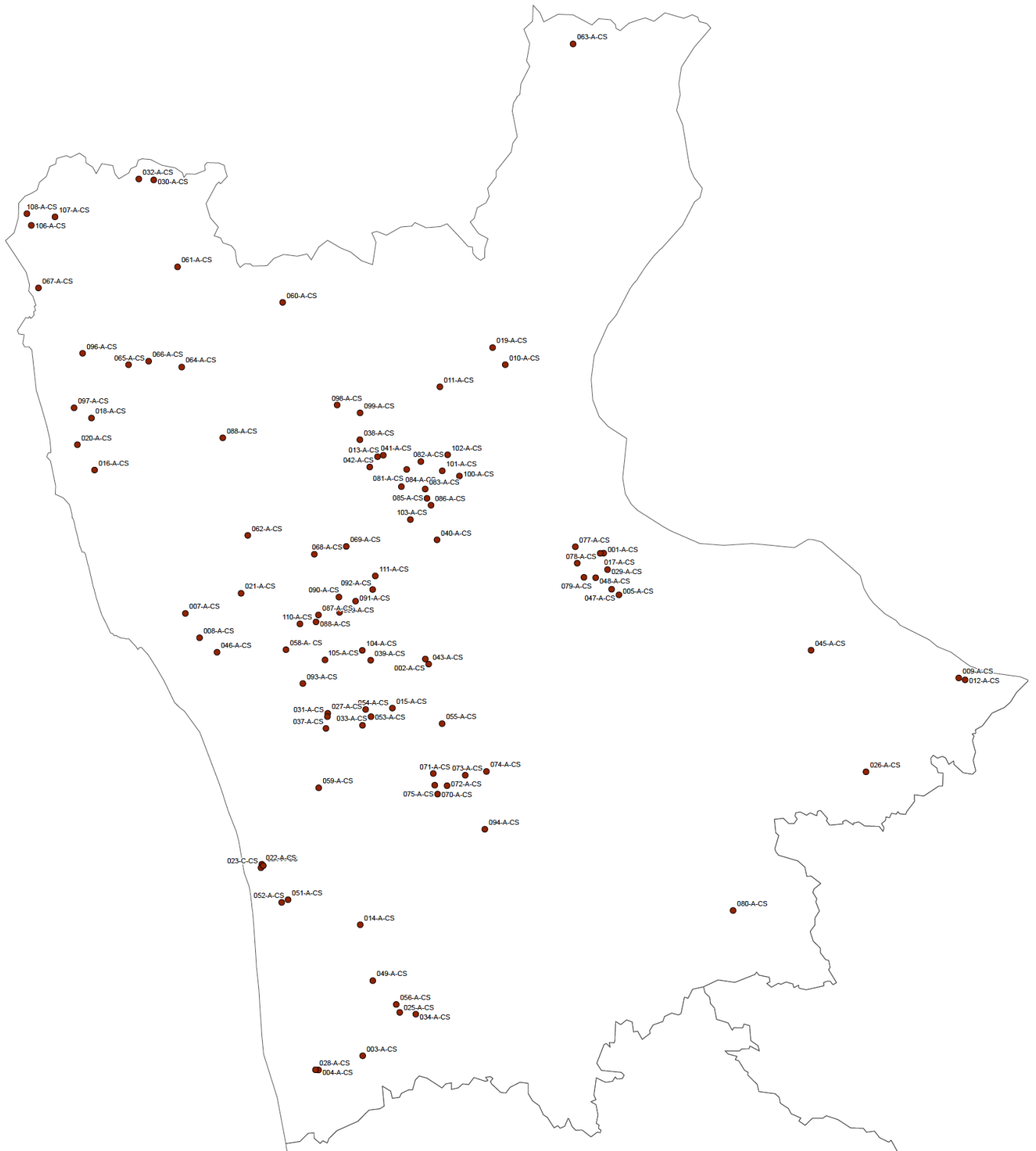


Fig. 3.23 b. Map of the active extraction sites of Cosenza Province, subdivided for the code. (Laboritt, 2014, modified).

Table 3.1. Active quarries of Cosenza Province, typology of stones and quarries (Laboritt, 2014, modified).

n. Code	Name	Town	Address	Stone	Typology	Position
1 028-A-CS	Osso Estrattive Srl	Aiello Calabro	Torrente Spinoso-Cozzo Opera	crystalline carbonate	escarpment	low hill
2 004-A-CS	O.S.F.E. snc	Aiello Calabro	Petrone	limestone	escarpment	low hill
3 003-A-CS	Cava di calcare in località Giani di Coccimiglio C	Aiello Calabro	C/da "Giani"	limestone	trench	coastal quarry
4 042-A-CS	ditta Fiore Antonio	Altomonte	Cacciatelle	sand		
5 041-A-CS	ditta Bilotti Leonardo	Altomonte	Serragiumenta	sand		
6 044-A-CS	ditta Spina Antonio	Bisignano	Campanaro	sand	escarpment	
7 002-A-CS	Boscarelli Michele	Bisignano	Chio	arenaceous limestone	escarpment	low hill
8 006-A-CS	Loise Ermanno	Bisignano	Curno	sand	escarpment	coastal quarry
9 043-A-CS	ditta Loise Ermanno	Bisignano	Curno		trench	
10 009-A-CS	Calcestruzzi Cariatese Snc	Cariati	Martello- Serre Boscose	arenaceous limestone	trench	coastal quarry
11 012-A-CS	Beton Nicà	Cariati	Montagnola Prato	alluvial sand	trench	coastal quarry
12 011-A-CS	Straface S.r.l.	Cassano allo Ionio	C/da Caccianova località Sacramento	arenaceous limestone	trench	coastal quarry
13 010-A-CS	Società Sposato P&P S.r.l.	Cassano allo Ionio	Le Venicelle	clayey limestone	escarpment	coastal quarry
14 045-A-CS	Italcementi Spa	Castrovillari	Le Serre	limestone		
15 007-A-CS	Bianco Serafina- Ruggiero Simone	Cetraro	Bosco- Difesa	limestone	terrace	hill
16 008-A-CS	Rossi Antonio Mariano	Cetraro	Marino	limestone	escarpment	low hill
17 046-A-CS	ditta Foresta Mario	Cetraro	Bosco	limestone		
18 005-A-CS	Jonica Lavori s.n.c.- Cofone Giovanni	Corigliano Calabro	C/da Marcoliva	clayey limestone	escarpment	coastal quarry
19 029-A-CS	Citrea Srl	Corigliano Calabro	Costa Mangini	alluvial sand	escarpment	coastal quarry
20 048-A-CS	Tecno Scavo	Corigliano Calabro	Gabelluccia-Serra Cardillo	sand		
21 017-A-CS	Società F.M.F. di Fortunato Francesco & C.	Corigliano Calabro	C/da Malupienzo-Muzzolito	arenaceous limestone	escarpment	coastal quarry
22 001-A-CS	Perri Santo	Corigliano Calabro	Castello	limestone	escarpment	coastal quarry
23 047-A-CS	ditta Esposito Michelangelo	Corigliano Calabro	Serra Cardillo	sand		
24 049-A-CS	Società Inerti Potame	Domanico	Magari	limestone		
25 021-A-CS	Rossi Tulio	Fagnano Castello	Lamberto-Mulino	limestone	escarpment	low hill
26 051-A-CS	ditta Ventura Francesco	Falconara Albanese	Manche-Covoni	limestone		
27 050-A-CS	CEIAM Costruzioni Srl	Falconara Albanese	Diamante-Mortella	limestone		
28 052-A-CS	ditta Sotero Rosario	Falconara Albanese	Malpertuso	limestone		
29 013-A-CS	Società Laterizi Meridionali	Firmo	Cerzitello	clay	escarpment	coastal quarry
30 019-A-CS	ionica Inerti S.r.l.	Francavilla Marittima	Timpone della Motta	arenaceous limestone	escarpment	low hill
31 113-A-CS	LG stone di Lucio Ghio	Fuscaldo	Scarcelli	sandstone	outcrops	
32 020-A-CS	La Pietra S.r.l.	Grisolia	Anania	limestone	escarpment	middle hill
33 030-A-CS	Forte Domenico Antonio	Laino Borgo	San Filpo	sand	escarpment	low hill
34 032-A-CS	Impresa Costruzioni geom. Vincenzo Papaleo	Laino Borgo	Arena Bianca	limestone	escarpment	hill
35 054-A-CS	ditta Nuove Pavimentazioni Srl	Lattarico	Ministalla-Zagarellaro	sand		
36 031-A-CS	Società Eurobitumi Srl	Lattarico	Cozzo del Carbonaro	sand	escarpment	coastal quarry
37 037-A-CS	Italcementi Spa di Bergamo	Lattarico	Striscioli-Vullo Bivio Regina	gypsum	escarpment	low hill
38 033-C-CS	RDB Fantini Srl	Lattarico	Scavello		escarpment	coastal quarry
39 027-A-CS	ALA Fantini Srl	Lattarico	Loreto	clay	escarpment	coastal quarry

n. Code	Name	Town	Address	Stone	Typology	Position
40	053-A-CS ditta Nuove Pavimentazioni Srl	Lattarico	Ischitella	sand		
41	015-A-CS Calabria Calcestruzzi Srl	Luzzi	Ischia Del Principe	alluvial sand	escarpment	coastal quarry
42	055-A-CS ditta Ferrise Annalisa	Luzzi	Petrini	sand		
43	016-A-CS Camp-Tor sas di Campagna Fedele & C	Maiera'	Scavo Romano	limestone	escarpment	low hill
44	056-A-CS Cave Petrusella	Malito	Petrusella	limestone		
45	034-A-CS Spina Franco	Malito	Scannelle	limestone	escarpment	hill
46	025-A-CS Malito Frantumati Srl	Malito	Petrone	dolomitic limestone	trench	hill
47	014-A-CS Mendicino Cave srl	Mendicino	Petrone	arenaceous limestone	escarpment	hill
48	058-A-CS Edil Scavi	Mongrassano	Cocchiato	sand		
49	035-A-CS Armado Sposato & C. sas	Mongrassano	Colombra	sand	trench	middle hill
50	057-A-CS ditta Eredi di Senna Eugenio	Mongrassano	Colombra	sand		
51	059-A-CS ditta Massimo Aceto	Montalto Uffugo	Santa Maria di Settimo	sand		
52	060-A-CS ditta F.Ili Verbicaro	Morano Calabro	Vidente	sand		
53	061-A-CS ditta Sola Carmine	Mormanno	Cagliostroza	sand		
54	062-A-CS ditta Contarino Orazio Carmelo	Mottafollone	Caccia	sand		
55	063-A-CS Mineraria Cave Sud	Nocara	Flaga	sand		
56	066-A-CS ditta Settecerze Vincenzo	Orsomarso	Grottone	sand		
57	064-A-CS ditta Magurno Saturnino	Orsomarso	Serra Bonangelo	sand		
58	065-A-CS Si.GE.CO.	Orsomarso	Vallementa	sand		
59	067-A-CS M.A.L.V.I.R.	Praia a Mare	Campo delle Rose	sand		
60	068-A-CS ditta Ambrosio Silvio	Roggiano Gravina	Setto Avena	sand		
61	069-A-CS ditta Ruffo Angiolino	Roggiano Gravina	Prunito	sand		
62	071-A-CS ditta Vitaro Natale	Rose	Arente	sand		
63	074-A-CS ditta Salerno Salvatore	Rose	Pizzilara	sand		
64	070-A-CS Calabria Calcestruzzi Srl	Rose	Cuculo-Pizzilara	sand		
65	072-A-CS ditta Vitaro Salvatore	Rose	Arente	sand		
66	073-A-CS DEMAR	Rose	Pizzilara	sand		
67	075-A-CS EUROCEM	Rose	Cuculo	sand		
68	076-A-CS ditta Viggiani Innocenzo	San Donato di Ninea	Crocciaro	sand		
69	035-A-CZ Sanseverino Carlo	San Floro	Ficaria	sand	escarpment	middle hill
70	077-A-CS ditta Murano Natale	San Giorgio Albanese	Malfrancato	sand		
71	079-A-CS ditta Terranova Francesco	San Giorgio Albanese	Podere	sand		
72	078-A-CS ditta Godino Giorgio	San Giorgio Albanese	Podere	limestone		
73	080-A-CS ditta Rao Francesco	San Giovanni in Fiore	Patia	granite	boulders	
74	112-A-CS LG stone di Lucio Ghio	San Giovanni in Fiore	Colle dei Fiori	granite	boulders	
75	085-A-CS ditta Pellicori Francesco	San Lorenzo del Vallo	Terzo di Firmo	sand		
76	084-A-CS ditta Santoro Mario	San Lorenzo del Vallo	Laccata	sand		
77	083-A-CS BI.CA.MIS.	San Lorenzo del Vallo	Valle Cupa	sand		
78	082-A-CS BI.CA.MIS.	San Lorenzo del Vallo	Cozzo Tornata	limestone		
79	081-A-CS BI.CA.MIS.	San Lorenzo del Vallo	Peschiera	sand		
80	086-A-CS Piano Lago Calcestruzzi	San Lorenzo del Vallo	Laccata	sand		
81	022-A-CS Albanese Massimo	San Lucido	Mottalupo	reddish limestone	escarpment	middle hill
82	023-C-CS Metallo Ottavio	San Lucido	Mottalupo-Cinnirello-Deuda	reddish limestone	escarpment	middle hill

n.	Code	Name	Town	Address	Stone	Typology	Position
83	024-A-CS	Metallo Ottavio	San Lucido	San Nicola	limestone	escarpment	low hill
84	088-A-CS	ditta Vuono Giuseppe	San Marco Argentano	Scarniglia	sand		
85	111-A-CS	Ditta Amodio Franco	San Marco Argentano	Maiolungo			
86	110-C-CS	Ditta Vuono Giuseppe	San Marco Argentano	Cimino	sand	escarpment	coastal quarry
87	092-A-CS	COEM	San Marco Argentano	Prato	sand		
88	091-A-CS	ditta Vuono Giuseppe	San Marco Argentano	Serra D'Asino	sand		
89	089-A-CS	ditta Fiore Antonio	San Marco Argentano	Molocco	sand		
90	087-A-CS	ditta Vuono Giuseppe	San Marco Argentano	Colabello	sand		
91	090-A-CS	ditta Fiore Antonio e Fiore Italo	San Marco Argentano	Piparo	sand		
92	093-A-CS	Costruzioni Idrauliche	San Martino di Finita	Timpe	sand		
93	094-A-CS	Nuova Pavimentazioni Srl	San Pietro in Guarano	Ventracqua	sand		
94	095-A-CS	CIMA Costruzioni Srl	San Sosti	Cavarina	sand		
95	096-A-CS	EDILSET	Santa Domenica Talao	Sovareta	sand		
96	097-A-CS	La Pagaria	Santa Maria del Cedro	Destri	limestone		
97	018-A-CS	Russo Salvatore	Santa Maria del Cedro	Destri		escarpment	coastal quarry
98	038-A-CS	Italcementi Spa di Bergamo (Cemensud Spa)	Saracena	Stamiota	clay	escarpment	hill
99	098-A-CS	Beton Calabria	Saracena	Porcile	sand		
100	099-A-CS	ditta Costabile Franco Orlando	Saracena	Salso	sand		
101	101-A-CS	ditta Sposato Armando	Spezzano Albanese	Stragolia Piccola	sand		
102	100-A-CS	C.I.D.E.	Spezzano Albanese	Valle dei Bufali- Stragolia Piccola	sand		
103	102-A-CS	Sud Strade	Spezzano Albanese	Stragolia Mordillo	sand		
104	103-A-CS	Abbruzzese Elio-Mauro Salvatore	Tarsia	Canicella	sand		
105	040-A-CS	ditta Fratelli Scaglione Domenico Francesco & Carlo	Tarsia	Serra della Guardia	clay	escarpment	low hill
106	107-A-CS	Inerti Costruzioni	Tortora	Acqualisparti	sand		
107	106-A-CS	ditta Olivieri Mario	Tortora	Capo D'Acqua	sand		
108	108-A-CS	ditta Iaselli Michele	Tortora	Orchidella	sand		
109	036-A-CS	Fratelli Dodaro snc	Zumpano	Pietra Giulia	sand	escarpment	

3.3.3 Ancient quarries of Cosenza Province

Since the pre-Hellenic Age, the territory of Cosenza Province was full of many quarries that have conditioned the architecture of Calabria. In fact, it was rich in quarries of limestones, sandstones and other building stones. These materials were employed by local artisans and by many schools of stonemasons. During the '500 century (Table 3.2) there were 40 quarries of marble, alabaster and gypsum principally utilized to build military, religious monuments and noble buildings¹⁰. During the

¹⁰ http://web.provincia.cs.it/ptcp/struttura_ambiente/sist_ris_stor_cult/ralazione1.pdf

Modern age, until the 19th century, there were 21 quarries¹¹, extracting the following materials: travertine, sand, sandstone, millstones (Altomare, 2015).

Table 3.2. Active quarries of Cosenza Province during the 16th century

(http://web.provincia.cs.it/ptcp/struttura_ambiente/sist_ris_stor_cult/ralazione1.pdf).

Town	stone
Aiello	marble, gypsym
Aieta	flint stone, millstone, marble
Altilia	marble, gypsum, tuff
Altomonte	gypsum, gold, silver, salt, crystal, turquoise
Belmonte	marble
Belsito	lapis specularis
Bocchigliero	flint, millstone, lapis phrigius
Caloveto	gypsum
Campana	flint, millstone
Carolei	flint, tuff
Cariati	millstone
Castrolibero	gypsum, flint
Castrovillari	gypsum
Cassano	millstone
Celico	gold
Cerchiara	salt
Cetraro	gypsum
Cirella	lapis phrigius
Cleto	salt
Cropalati	millstone, gypsum
Fuscaldo	lapis phrigius, sandstone
Grisolia	marble, limestone
Guardia Piemontese	gypsum
Lattarico	millstone, gypsum, flint
Longobucco	silver
Malvito	lapis phrigius, gypsum
Mendicino	flint, tuff
Montalto	alabaster, millstone
Morano	lapis phrigius, gypsum, talc
Orsomarso	millstone
Paludi	alabaster, salt
Paola	millstone
Pedace	gold
Pietrafitta	salt
Rende	salt
Rossano	gypsum
S.Donato Ninea	lapis phrigius, salt, flint

¹¹ G. BARRIO, *Antichità e luoghi della Calabria*, Cosenza, Brenner, 1979, p.160

Town	stone
S.Lucido	tuff, flint
S.Giovanni in Fiore	granite
S.Marco Argentano	millstone, flint
S.Vincenzo la Costa	salt
S.Agata d'Esaro	lapis phrigius
S.Maria del Cedro	millstone
Scalea	lapis phrigius
Spezzano grande	marble
Verbicaro	lapis phrigius, sand

The most important Calabrian quarries were situated in Mendicino, Altilia and San Lucido¹² (Lico, 2015). Mendicino quarries, actually not active, belonged to the Middle Age and were exploited until 1950. Also Altilia and Carolei quarries were utilized until the last century. From these quarries two lithological varieties of the calcarenitic stone known as “Mendicino tuff” were extracted: the more compact *whitish*, and the softer *reddish*, principally cut for thin slabs principally employed for floors, doors and other elements not exposed to weathering¹³. San Lucido quarries were situated in the area between Deuda and Torbido streams, where the ancient quarry was located. From the 1950s the quarry

¹² «...tuttavia la roccia tipica della città bisogna cercarla nel miocene che ampiamente affiora nel versante tirrenico della Calabria, da Amantea a Grimaldi, da San Lucido a Dipignano. Appartiene ai sedimenti di questa età un calcare arenaceo, od arenaria che dir si voglia, di colore biancastro o giallastro o nettamente rossastro, a grana minuta, riccamente fossilifero (aculei d’achini, denti di squalo, ecc), tenero, appena cavato, tanto che lo si può persino piallare, e che poi si indurisce. Forma una serie di sottili strati della potenza complessiva d’alcuni metri, dove le varietà più compatte si trovano generalmente in basso. Risalgono al Medioevo le cave più note, quelle di Mendicino nella vallata del Caronte (a otto chilometri della città di Cosenza), onde il nome di *tufo di Mendicino*, che tuttavia comprende anche la roccia d’altri luoghi (Domanico, Carolei, Vada, ecc.)» F. RODOLICO, *Le pietre delle città d’Italia*, Second Edition, Firenze, Ed. Le Monnier, 1995, p.427.

¹³ «L’ora molto avanzata non ci ha permesso di estenderci al prossimo villaggio di Carolei, per osservare le cave di una pietra calcare porosa rossiccia di natura tufacea, che impiegasi a Cosenza ed in gran parte di quella provincia nella fabbrica degli edifizii. Anche presso Mendicino ci si è detto trovarsi altre cave di quell’istessa pietra, ma di tessitura alquanto più compatta. In effetti, a Cosenza ne abbiamo riconosciute due varietà: una più compatta di color bianco, che gli scalpellini distinguono col nome di *biancolella*, e l’altra di grana più grossolana e di color rossiccio, che disegnano semplicemente col nome di tufo. Questo secondo, per esser più tenero, può segarsi in lastre della spessezza! di un pollice e mezzo, e somministra così ottimi quadroni per i pavimenti delle abitazioni; della stessa pietra si tagliano anche le imposte delle porte, e tutto il resto delle analoghe costruzioni che possono restare al coperto delle intemperie; mentre per le ginelle, per gli archi, per le mostre, e tutto altro, che deve rima nere all’aria aperta si preferisce la pietra bianca, perchè meno della prima soggetta ad essere attaccata dalle meteore». L. PETAGNA, G. TERRONE, M. TENORE, *Viaggio in alcuni luoghi della Basilicata e della Calabria Citeriore effettuato nel 1826*, Tip. Francese, Napoli, 1827, pp. 84-85

activity started, in the upstream area with three quarries, belonging to the category of “open cut mining” quarries. Nowadays the quarry activity in San Lucido is intense.

In the territories of “Pollino” mountain and the Coastal Tyrrhenian Range, limestones, dolomitic limestones, dolostones and others lithologies used for obtaining artificial stones were exploited. Along the Tyrrhenian area there was the “pietra di paragone o indice”, a stone employed for comparing the goodness of silver or gold¹⁴. This stone was extracted in many towns such as S. Maria del Cedro, Grisolia, Cetraro, Guardia Piemontese, Fuscaldo, Paola, San Lucido and Belmonte Calabro. In Belmonte Calabro and in Aiello marble was also present. In Verbicaro, another Tyrrhenian town, there was one of the most important quarries of sand employed until the 20th century, for the realization of mortars, named “arena” (sand) quarry. Others Calabrian towns such as Grisolia, Belmonte Calabro and Aieta were full of stones for the realization of millstones. In Castrovillari and Morano, in the “Pollino” area, also gypsum was extracted¹⁵.

Sandstone quarries were mainly concentrated in Fuscaldo and surroundings. According to Bruno (1995) and Anastasio (1996) there were a lot of ancient quarries: “Cava Scarcelli”, utilized until the 1937 approx.; “Cava Castello”, exploited until the 1945; “Cava Cuozzu Russu”, situated near the graveyard and in use until the 1995; “Cava del Pesco”, active until the 1940; “Cava Codemma”, situated in “Fuscaldo Marina”; “Cava piccolo” in “Via Roma”, utilized until the 1937 (Bruno, 1995). Other quarries were located in the area of “zona Castello”, “via Piana degli artisti”, “via Croce”, “via Sotto il Convento”, from which it was transported to the construction site (Anastasio, 1996).

In the Sila area, precisely in San Giovanni in Fiore, there were important quarries of granitic and granitoid rocks. In the past there were many “Boulders fields” of granite concentrated in San Giovanni in Fiore (Bruno E., 1993), especially exploited for the extraction of granitic material for millstones, for

¹⁴ «...col suo attrito si indica la bontà dell'oro e dell'argento». (cit.) G. BARRIO, *Op. cit.*, p.160

¹⁵ *Ibidem*

oil industries and for watermills (Di Benedetto & Greco, 1990). According to the same authors (Di Benedetto & Greco, 1990), there were “good granites” in the southern area of San Giovanni in Fiore, in the area “Gigante” in Cotronei (CS). Other ancient quarries were situated in “località Palla Palla” (Fig. 3.24 a), in “località Guglielmo” (Fig. 3.24 b), where weathering planes are visible, from the most weathered up to the less ones in the lower part, in località “Colle dei Fiori” (Figs. 3.24 c, d), in “località Macchia di Lupo”. The last one was active during the 20th century and has been closed for the lack of additional quarry material. Other ancient quarries were “Abetina Scura”, “Ferulia”, “Colle di Jure”, “Olivaro”, “Garga”, “Serrisi”, “Campanelli”, where there was a legendary big boulder called “Pietra Pizzi” where stonemasons were used to engrave on its surface (Bruno E., 1993). In the “Colle dei Fiori” ancient quarry (Figs. 3.24 c, d), in particular, boulders fields can be seen, with quarrying prints grooves in where wedges and quarry bars acting as levers were inserted to favour the stone breaking, as well as holes where steel strand cables were put for transporting the broken blocks. Nowadays there are active quarries in San Giovanni in Fiore in “Cagno” (Fig. 3.24 e), and in “Colle dei Fiori” (Fig. 3.24 f), the last one near the ancient quarry for the extraction of granite blocks for building and ornamental uses; in “Macchia di Lupo”, near to the ancient quarry, for aggregates; in Palla Palla” for the extraction of granite blocks for decorative uses.

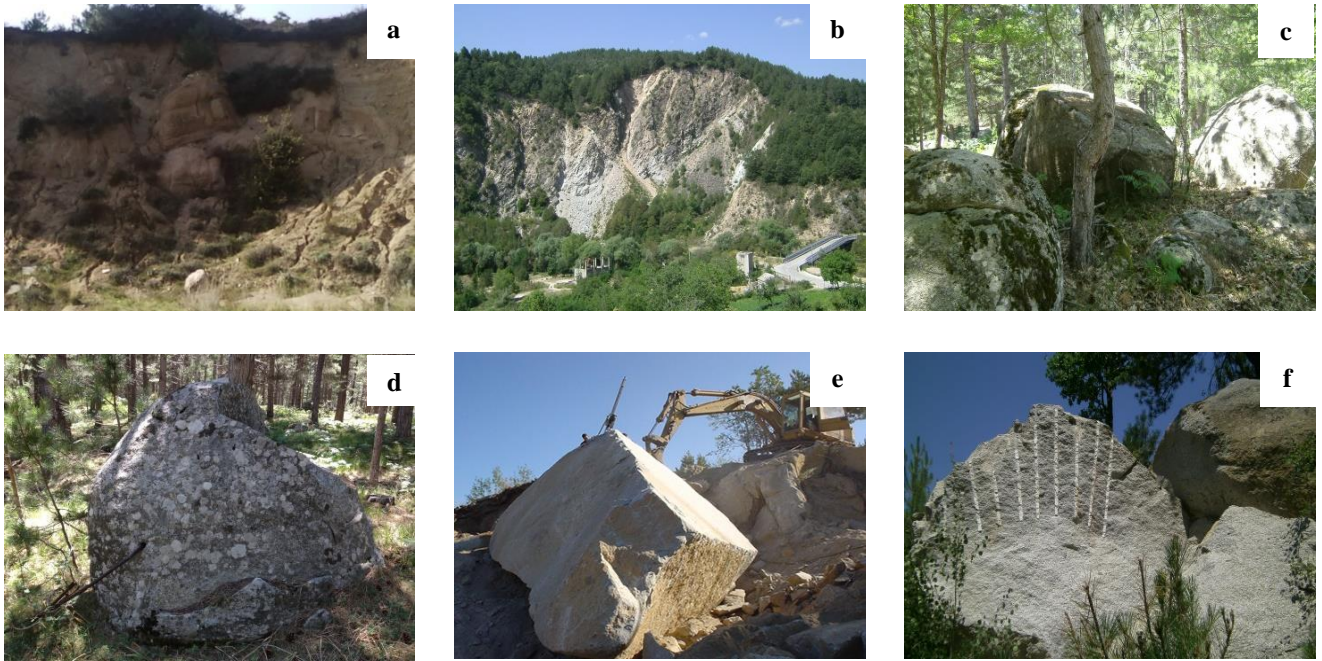


Fig. 3.24. Palla Palla (a), Guglielmo (b), Colle dei Fiori (c, d), Cagno (e), new Colle dei Fiori (f) quarries in San Giovanni in Fiore.

In the territory of Cosenza Province, stones were also employed not only as building materials. For example, quarries of Cassano allo Jonio, in the area of Jonic Sea, or Cropalati and Lattanico were exploited for the extraction of millstones (Sole, 1985). In the central-northern area of the Province, in the localities of Cirella, San Donato di Ninea, Bocchigliero, Martirano, Fuscaldo, Malvito, Sant’Agata d’Esaro, Morano, Verbicaro and Scalea there was an important stone commercially used by dyers and named *lapis phrygius* (Salerno, 2015).

3.3.4 Italian and Calabrian quarry standards

In Italy, quarry standards regarding mining activities are regulated by the Royal Decree “R.D. of the 29th July of 1927, n. 1443”. Since that decree there wasn’t a national legislation in order to establish uniform criteria for the whole country. In the ‘70s regional regulations were approved, which transferred the power of this field from the central government to the Regions. The opening of new quarries is

actually regulated according to the European Directives that introduced the “Valutazione d’Impatto Ambientale” that refers to an Environmental Impact Assessment (Dir . 85/337/EEC).

Through the Presidential Decree of the 24th July of 1977 n.616, the mining activity is governed by Regions that have to create a Regional Plan of Mining Activities (“Piano Regionale Attività Estrattive – P.R.A.E.”).

These plans for mining activities (PRAE) must be subjected to the advance of the “Strategic Environmental Assessment” (“Valutazione Ambientale Strategica – VAS”). Many Regions have introduced the “Environmental Impact Assessment” (Valutazione d’Impatto Ambientale - VIA) in the case of large quarry sites and the “Incidence Assessment” (Valutazione di Incidenza – VIC) in the case of areas with an environmental European relevance.

Mining activity in Calabria is normed by the Regional Law n.40 of the 5th November of 2009 concerning “Attività estrattiva nel territorio della Regione Calabria” and by “Regolamento di attuazione Legge Regionale 5 novembre 2009, n. 40 – Attività estrattiva nel territorio della regione Calabria”.

These laws preserve the environment, safety of workers and in general the health in the extraction areas. The art. 5 of this law instituted the “Regional Observatory of Mining Activities” (Osservatorio Regionale Attività Estrattive – ORAE), able to manage an Information System for Mining Activities (Sistema Informativo delle Attività Estrattive – SITRAE) that collects information and data about quarry sites present in Calabrian territory. With the art. 6 is identified the content of the basic regional programming instrument (PRAE) that indicates: dimension of quarry areas and volume of extracted material; the final destination of the areas subject to mining activities; the methods of cultivation; strategies for the restoration of abandoned quarry sites; the rent related to the quantity and quality of the extracted materials .

3.3.5 *Types of quarries of Cosenza Province*

Depending on the quarry site, it is possible to differentiate in Cosenza Province among trench, escarpment quarries and boulder field.

Trench quarries are typical extraction sites of sand, gravels and aggregates. They are quite shallow with faces up to 5-10m high. They are valley bottom quarries and are visible from the nearby valley sides and hill tops depending on the local relief. Generally, they have been individuated nearby the rivers (Fig. 3.25).



Fig. 3.25. Trench quarry of sand in Scalea, near the Lao River.

Depending on the position of the quarry site related to the topography, individuated escarpment quarries belong to one category, the hillside quarries. They consist of two typologies. The first one can be associated to a basic form of a three sided notch into a hillside (Fig. 3.26 a). One of these faces is the highest and the other two are endwalls. The structural relief of the outcrop corresponds to the steepest slope. They develop laterally, following the uppermost layer closest to the edge. They have been

individuated as very common for geological deposits of limestones, crystalline carbonates and sandstones.



Fig. 3.26 a. Hilltop quarry of limestones in San Lucido: typology of defined shape. It is an active quarry, commercially known as “Albanese quarry”.

The second typology of hilltop quarry has not a defined shape (Fig. 3.26 b). It is similar to the result of a landslide. It is typical of weathered soil and the extracted material is generally utilized for aggregates.



Fig. 3.26 b. Hilltop quarry of granitic aggregates in San Giovanni in Fiore: typology of undefined shape. It is an inactive quarry, commercially known as “Guglielmo quarry”.

Regarding igneous rock, the typology of individuated quarry has been “boulderfields”. They consist of spread granite blocks. They are very common in the hilltops of the Sila area and include suites of forms, widespread and isolated, scattered over flat-topped hills, or more commonly, grouped on the crests of hills. Boulder shape is spheroidal or almost cubic with a medium diameter ranging from 0.5 to more than 3 m, consisting of a corestone surrounded by concentric rough exfoliation sheets (Le Pera & Sorriso Valvo, 2000). It is possible to find isolated boulders or forming regular ridges.



Fig. 3.27. Boulderfield of “Colle dei Fiori” in San Giovanni in Fiore (Sila area).

3.3.6 Extraction methods of Cosenza Province

Regardless of the digging method, each type of quarry involves its own working system or method of advancing.

The extraction method of trench quarries involves a single workface on a single surface layer (Fig. 3.28), with the side slopes being abandoned as the workface progressed. The dip plane has a variable shape, normally linked to a linear trench of up 100-300 m in length, depending on the dimensions of the extraction site, with a workface of 50-100 m and sidewalls up to 2-3 m high.

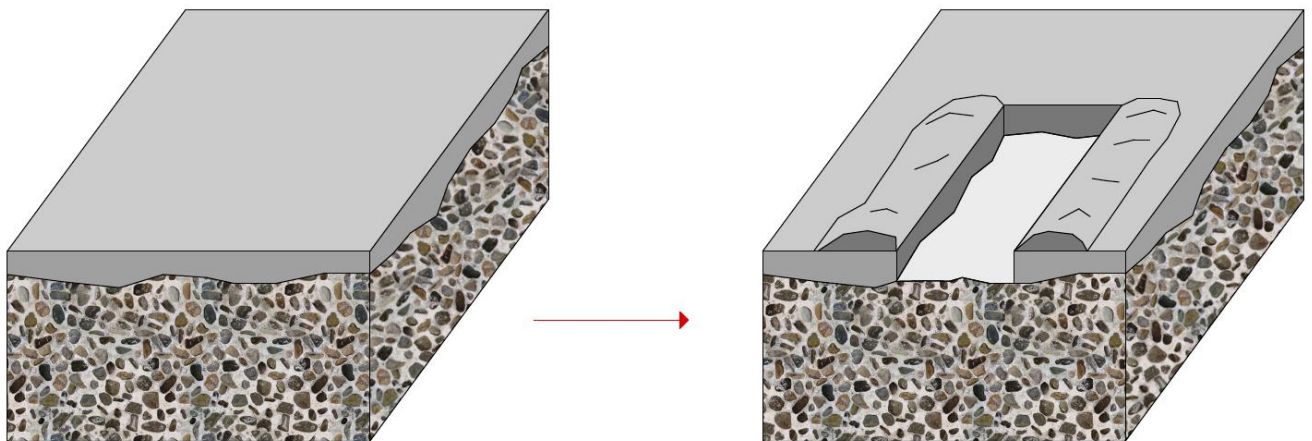


Fig. 3.28. Block schematic diagram representing extraction method of sand/aggregates for a trench quarry.

Advancement of the workface in the hillside quarries is limited by the extent of the top layer. Depending on it or on the presence of topsoil, the workface is abandoned and continues laterally. When the top layer has been extracted, the resulting surface is used to start extraction work on the level below (Fig.3.29). The employed digging method is a descending technique. The excavation starts with the topmost layer descending progressively to lower layers. Along lateral sides, the maximum length of the quarry depends on the dimensions of the escarpment terminating at a point where the layer has been

eroded or the relief is so steep that it prevents access. At the end of the escarpment generally there is the work plane with the presence of quarry vehicles.

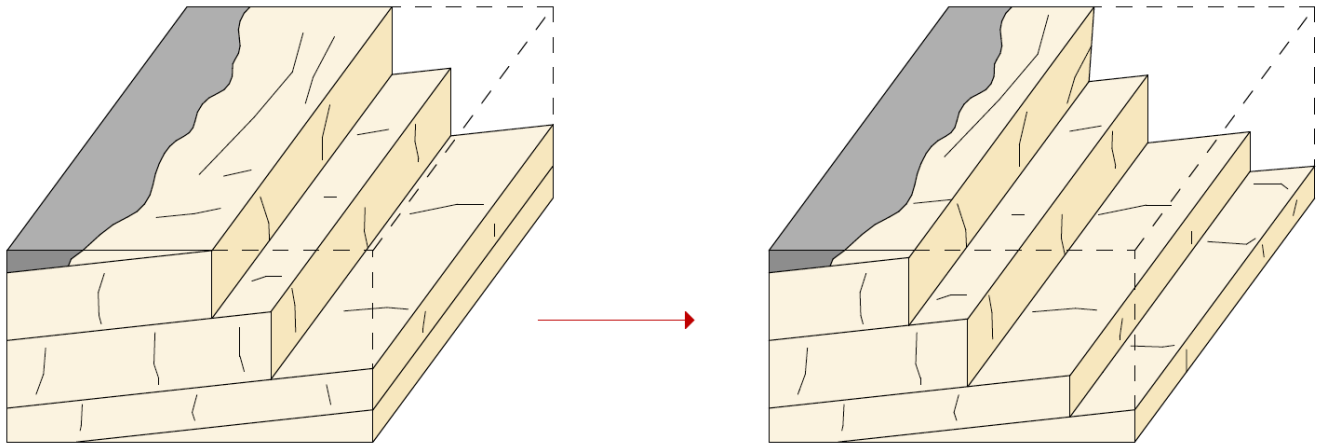


Fig. 3.29. Block schematic diagram representing extraction method of an escarpment quarry.

The result of an escarpment quarry is a notched profile, composed by alternating horizontal and sloping planes (Fig. 3.30).

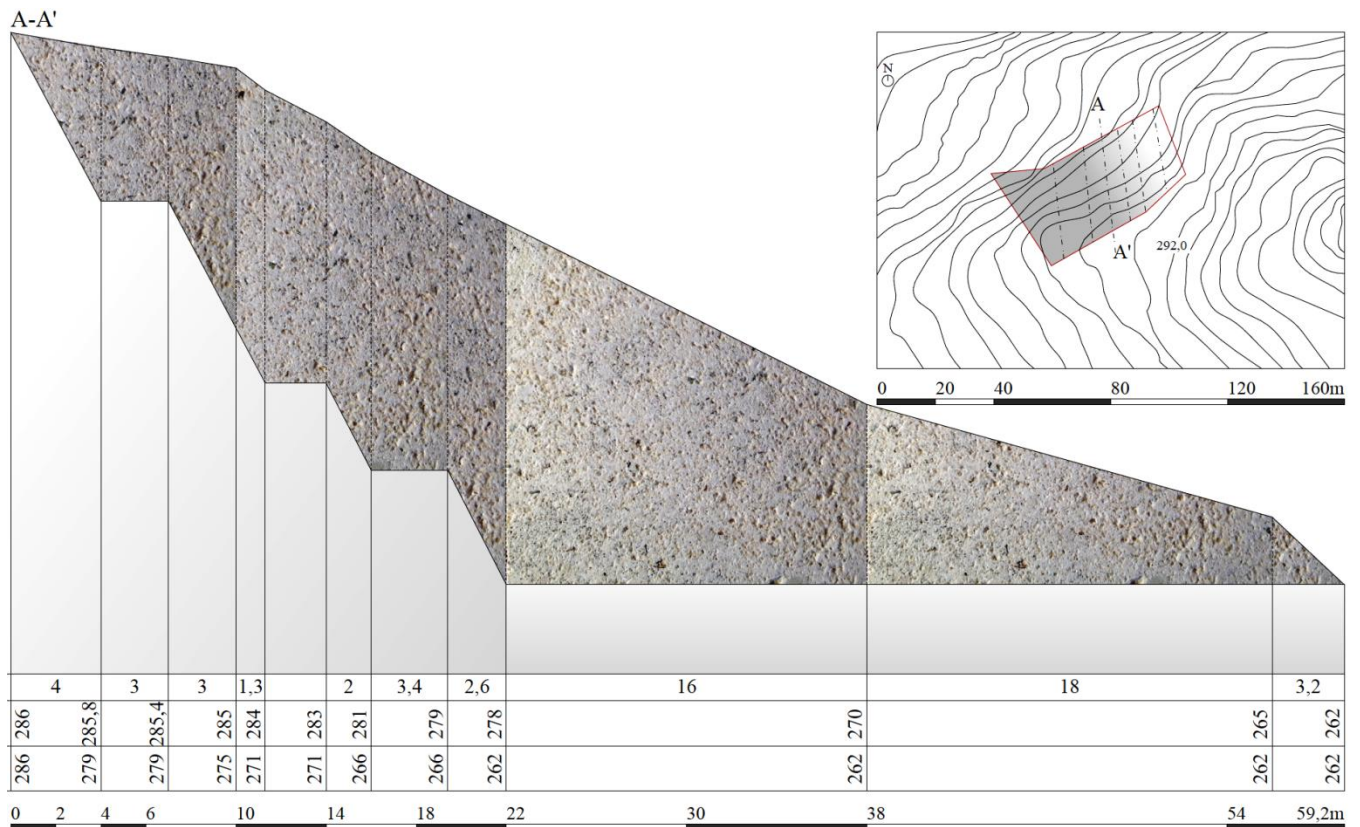


Fig. 3.30. Schematic section representing the active calcarenitic quarry of “Motta Lupo” in San Lucido.

Marks on some of the abandoned quarry boulders provide insight into the employed digging methods. Digging methods were simple and sophisticated such as explosives or wire saws. Usually, joints on boulders surfaces were not continuous. So metal or wooden wedges soaked with water would have been used, following lines of potential fracture (Fig. 3.31). Wedges or chisels were inserted into the building material and then split with striking-hammers (Fig. 3.32).



Fig. 3.31. Granite boulder of the ancient boulderfield of “Colle dei Fiori” in San Giovanni in Fiore with the marks of the wedges soaked along joints.



Fig. 3.32. Splitting devices: point chisel (a); standard chisel called “pungiotto” (b); wedge (c); toothed chisel (d); striking-hammer (e). Hammers and chisels employed by the stonemason Silvio Ferrari, belonging to the school of stonemasons of Altilia.

The fracture lines were established according to the anisotropy planes. Masons have traditionally used granite anisotropy to identify the cut planes (Freire-Lista & Fort, 2015). As reported in Fig. 3.33, in a granite block cut from a boulder, it is possible to distinguish three surfaces: the hardway plane (the most resistant), the grain plane and the rift plane (the softest). Usually, the ashlar were extracted along the easiest splitting plane, corresponding to the rift direction. The order of splittability (decreasing) was: rift, grain and hard-way.

The hard-way plane is the YZ plane along the X-axis; the grain plane is the XZ along the Y-axis and the rift plane is the XY plane along the Z-axis. The “rift plane”, “grain plane” and “hard-way plane” follow the quarrymen convention for granites. With the identification of the natural anisotropy degrees, the quarrymen, without knowing it, have used since past times this natural anisotropy, which has favor granite extraction, carving and placing the stone blocks in a building, decreasing efforts and improving the stone resistance against decay (Freire-Lista & Fort, 2015, 2016).

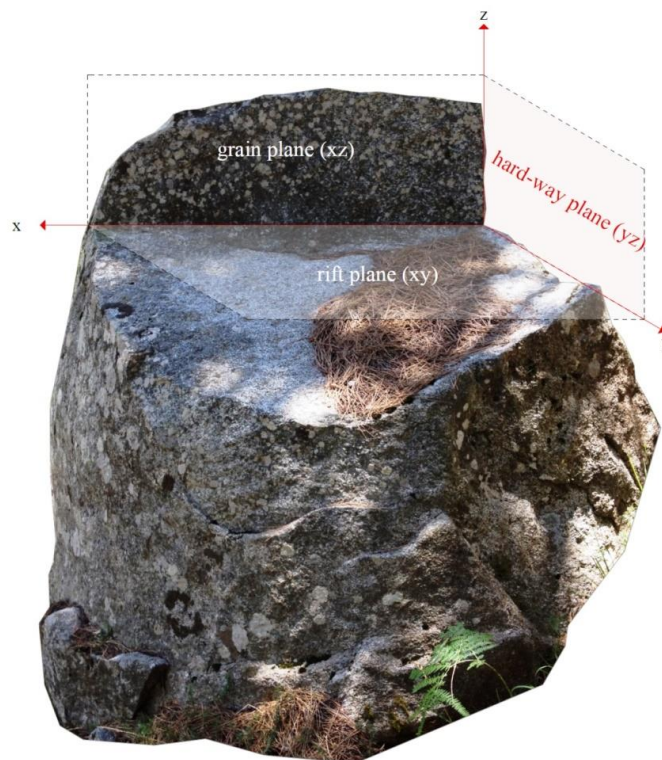


Fig. 3.33. Distribution of cutting planes of the historic boulderfield of “Colle dei Fiori” in San Giovanni in Fiore, where the granite boulders were mined.

3.3.7 Traditional types of stone finishing of Cosenza Province

To be used in construction, quarried stone blocks must be readily split, pitched and hewn (Shadmon, 1989).

Types of stone finishing employed by Calabrian stonemasons can be resumed in: “rock faced”; “rough-pointed”; “rough-pointed with chiseled margin”; “furrowed surface”; “bush hammered”.

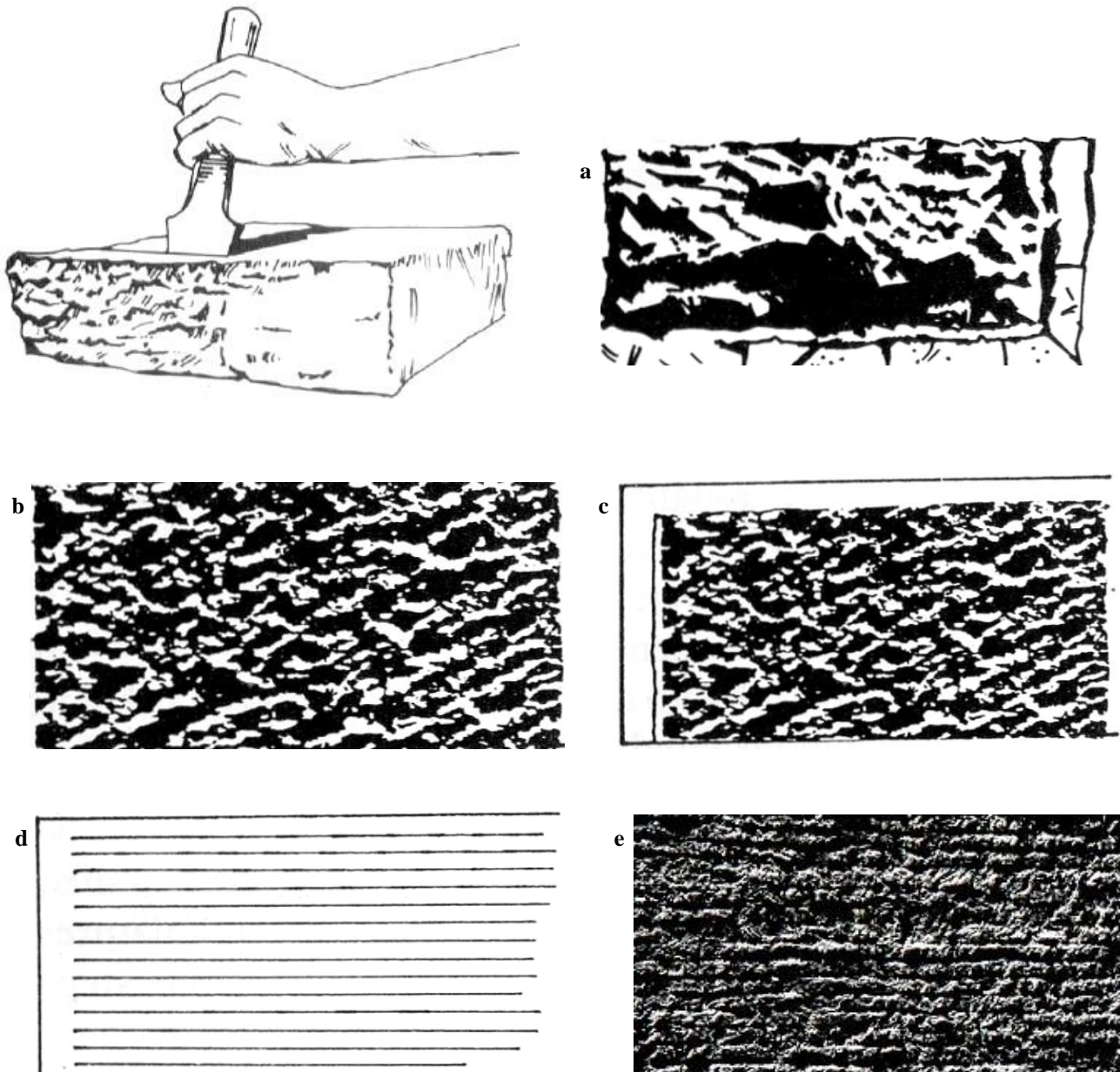


Fig. 3.34. Types of stone finishing employed by stonemasons of Cosenza Province: “rock faced” (a); “rough pointed” (b); “rough pointed with chiseled margin” (c); “furrowed surface” (d); “bush-hammered” (e).

Rock faced

The surface of the rock was made to resemble the natural break as it comes from the quarry (Fig. 3.34 a). This type of finishing was obtained by hand through hammer striking a chisel along the outer surface. The joint edges were straightened and no tool marks were left on the stone.

Rough pointed with/without chiseled margin

The result of this type of dressing was of a fine-pointed surface (Fig. 3.34 b). In order to obtain this effect a chisel point or pick was employed, leaving a pock-marked dressing. The pick was used for finer work than the chisel, through direct and short strokes. In the type of dressing “rough pointed and chiseled margin” (Fig. 3.34 c) there were drafted margins, cut a few centimeters from the edge, with a chisel. This kind of finishing was typical of large ashlar, employed for masonry of important buildings for the typical dynamism of this type of stone finishing.

Furrowed surface

The furrowed finishing (Fig. 3.34 d) was obtained through horizontal or vertical lines, cut at a constant distance. Grooves were done through a chisel with short strokes. Generally, grooves were oriented parallel to the building height and were usually made on portal pilasters, in order to emphasize the height of the portal.

Bush-hammered

For granite and hard materials, as mentioned before, quarrymen split planes to improve the workability of building materials. The anisotropy was used to identify the outdoor surface of granite ashlar. Usually the hardway and the grain planes were positioned parallel to the inner wall surface or to

the horizontal axis. Consequently, the rift plane was the preferred as outer surface on ashlar and for hewing. The traditional Calabrian quarrying practice consisted of polishing granite surfaces as bush-hammered (Fig. 3.34 e). This technique, similar to the traditional Madrilanian quarrying practice, which consisted of different stages process of bush-hammering using hammers with a tooth of increasing size (Freire-Lista & Fort, 2016).

3.4 Selected stones – Architectural and geological setting

Taking into account the historical importance of building stones in Cosenza Province, four lithotypes have been selected to be studied by means of the characterization techniques described in Chapter 5.

3.4.1 *San Giovanni in Fiore granite*

The first selected stone is the San Giovanni in Fiore granite (GF) from the Sila Area. Granite has been one of the most used building material of European historical buildings and monuments because of its abundance and great variety of colour and textures (Vicente *et al.*, 1996), and, in some countries, because of quarry proximity to cities, and in many others as a high quality imported building material (Fort *et al.*, 2013; Freire-Lista *et al.*, 2015b).

Macroscopically, San Giovanni in Fiore granite is grey, with slight variations in tone. It is commercialized under the same name or generically as “Sila Granite”.

This granite was employed in the past in the Cosenza Province for different uses, as a building and decorative material, not only in the Sila area. The most famous and relevant building, built mainly with granite and that is an example of the architectural heritage “silana”, is the Abbey of San Giovanni in Fiore (Fig. 3.35 a). One of its most decorative and original elements is the main portal, built around 1220 (Bitonti, 1994) and the crypt, accessibly from the right side chapel on the first level, divided into

two chambers (Crisci *et al.*, 2002), connected by a vaulted elements gallery, whose pointed arch portals are entirely made of blocks of granite. Furthermore, the entire old town of San Giovanni in Fiore was built with this granite, from masonries of building and portals to urban design elements, like fountains, balconies and streets. Granite was also employed as an important building material in civil engineering in different sites, such as bridges and railway bridges in San Giovanni in Fiore like “Ponte della Cona” (Fig. 3.35 b), over the Neto River, 18th century, and “Ponte ferroviario dei Ceretti”, in 1956, entirely built with granite blocks (Argentieri, 2013). Other important railway bridges were built with this granite, not only in San Giovanni in Fiore but also in San Pietro in Guarano (CS), for the structural elements of the bridges in “località Pozzillo” and in “località Fiumara”, and in Cosenza for “Ponte Alarico” (Fig. 3.35 c), reformed in 1947 by Santelli industry, with concrete and local materials like bricks, Mendicino stone and this granite. Granite of S. Giovanni was also employed for the milestones in the street from “Cuturelle and Pettinascura” in San Giovanni in Fiore in the 1953-1954; for squared blocks for the realization of the dams of Sila lakes and for the realization of the river banks of Saraceno and Raganello rivers in Trebisacce; for the realization of the Tarsia dam in the 1954 through 6000 square meters of squared blocks called “bolognini”; for the construction of ports like the one in Crotona in the 1968 (granite blocks coming from the “Campanelli” quarry) and the port of Reggio Calabria in the 1970 using ashlar called “bagnasciuga”; for trapezoidal ashlar to build bridges and tunnels of the railway lines between San Giovanni in Fiore and Cosenza (Bruno, 1993). Since 1958 and 1970 granite was exported out of Calabria as millstones and olive-presses to Bari, in Italy, and to Greece and Albania, too (Bruno, 1993). Granite of San Giovanni in Fiore was also employed, in the past, as a decorative and ornamental material to build monuments in Cosenza like the monument to “Bernardino Telesio” of the 1914 by Achille D’Orsi (AA.VV., 1980), whose lower parts are made of blocks of granite; “Il monumento ai caduti” (Fig. 3.35 d) of the 1936 dressed by marble and granite elements and actually for statues like

“Ferro rosso” by Pietro Consagra in 2010 in the Outdoor museum “Museo all’aperto Bilotti (MAB)” in Cosenza. Moreover, local stonemasons, nowadays, continue the ancient local stone tradition realizing architectural and urban elements, like stone sills and listels.



Figs. 3.35 (a, b, c, d). Architectural and engineering buildings built with San Giovanni in Fiore granite: Abbey of San Giovanni in Fiore (a), “Ponte della Cona” (Cona bridge), San Giovanni in Fiore (b), “Ponte di Alarico” (Alarico bridge), Cosenza (c), “Monumento ai caduti” (war Memorial), Cosenza (d).

Geological setting and stone extraction

The investigated granite is located in the area of San Giovanni in Fiore, at an altitude of about 1.100 m a.s.l., in Sila Massif uplands. Sila Massif is a section of the Hercynian orogenic belt of Western Europe (Amodio-Morelli *et al.*, 1976) and is part of the Calabrian terraces (Messina *et al.*, 1994; Van Dijk *et al.*, 2000; Tansi, Muto, Critelli, & Iovine, 2007; Critelli, Muto, Tripodi, & Perri, 2013). This territory is constituted by plutonic rocks of Sila Batholith (Fig. 3.36), belonging to the Northern Sector of “Arco Calabro-Peloritano” (Messina *et al.*, 1991 a, b).

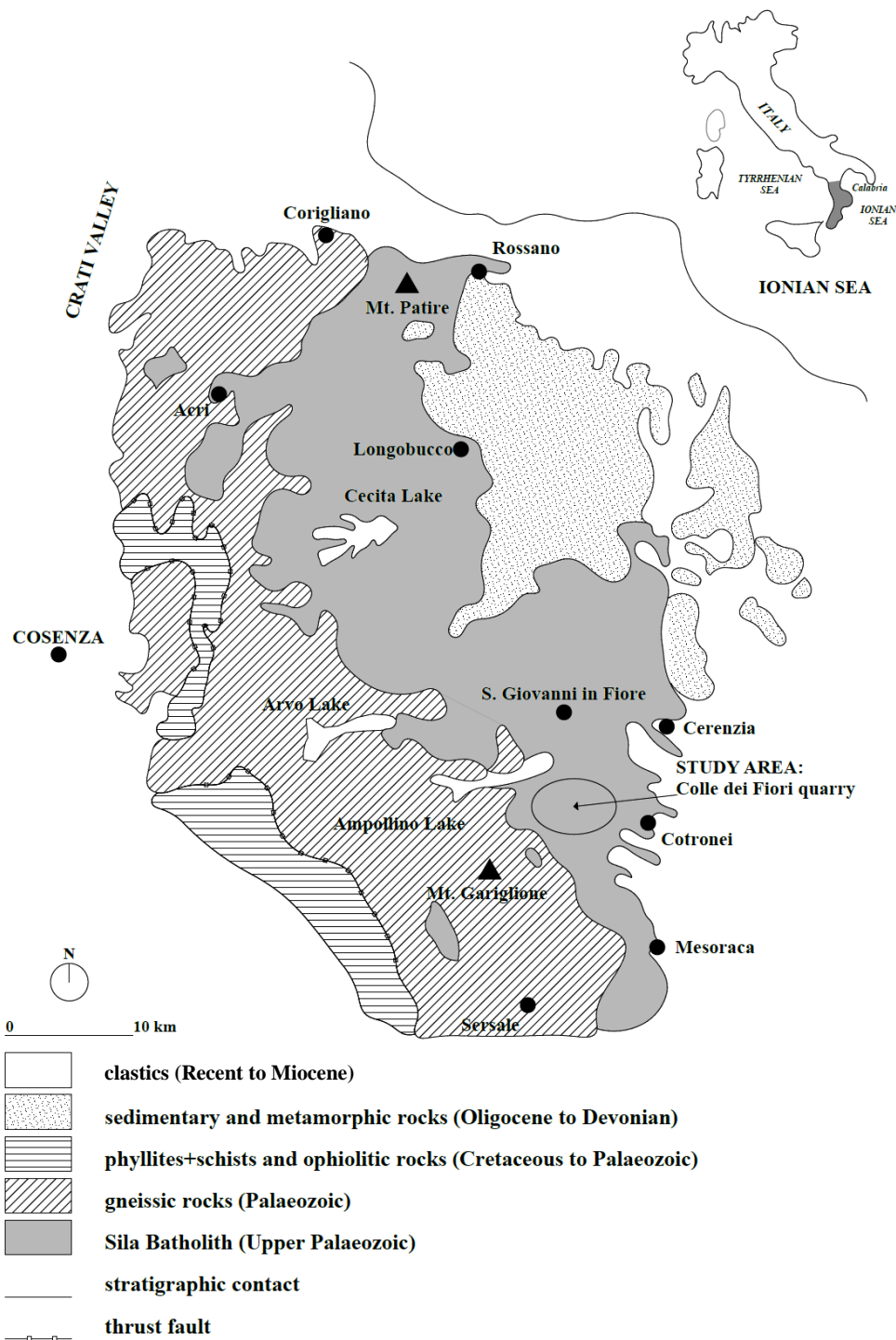


Fig. 3.36. Geological sketch map of Sila Massif (Apollaro *et al.*, 2009, modified) and location of the active quarry “Colle dei Fiori”.

Sila batholith, belonging to the Upper Paleozoic, consists of nested and cross-cutting intrusive bodies. The batholith has a regional NE-SW elongation and an area of about 600 km² (Messina *et al.*, 1991 a, b). The batholith intruded low grade Cambrian to Ordovician country rocks (eastern side) and medium-to high-grade metamorphic rocks (western side). Country rocks contain a wide contact-

metamorphic thermal aureole up to amphibolite-hornfels, consistent with emplacement of the batholith at relatively shallow depths (Ayuso, 1994).

The previously well-characterized petrology and geochemistry of unweathered granodiorite of Sila Massif was carried out by Messina *et al.* (1991 a). It consists of a biotite granodiorite with a medium-grain sized, unevenly grained fabric, composed of coarse K-feldspar phenocrystals (up to 2 cm long) plus smaller zoned plagioclase, subhedral and greenish-brown biotite, large interstitial to poikilitic crystals of quartz; accessory minerals are allanite, apatite, zircon and magnetite. Alkali feldspar phenocrystals are large Carlsbad-twinned and poikilitic with well-developed myrmekite (vermicular quartz intergrowths) at the plagioclase contact or micropertthitic poikilitic crystals. Plagioclase feldspars are zoned and partially sericitized; biotite is chloritized probably as a result of deuteritic alteration during igneous cooling of Sila plutonites (Messina *et al.*, 1991 a). The granodiorite boulders frequently exhibit a typical onionlike structure: it consists of an unweathered inner core, usually surrounded by a moderately-weathered outer shell, with millimeter-to centimeter-thick exfoliation sheets or flakes (Scarciglia *et al.*, 2012). According to Borrelli *et al.* (2015), some weathering studies were performed on granitoid stones samples of San Giovanni in Fiore and of Sila Massif (Apollaro *et al.*, 2009). Resultant maps of the weathering grade of the granitoid and studied profiles showed that they are formed by rocky masses varying from moderately weathered rocks (along the cut slopes of the stream incisions 783–930 m a.s.l.) to completely weathered rocks (along the cut slopes of the highest reliefs, above 1000 m a.s.l.) (Borrelli *et al.*, 2015). This weathering has been explicated, by different authors, like the combination of tectonic and climate variation (between the Late Miocene and Pleistocene) that played an important role in the development of granitoid weathering profiles of the area (Critelli *et al.*, 1991; Ietto & Ietto, 2004; Matano *et al.*, 1999). Petrographic analysis of weathered samples of granitoid rocks showed a subhedral

granular texture, composed by K-feldspar, plagioclase, quartz, biotite, and minor constituents of chlorite, muscovite with accessory epidote, apatite, and titanite (Borrelli *et al.*, 2015).

Analyzed samples belong to spheroidal granitoid blocks, named as “sferoidi granitici della Sila” (Di Benedetto, 1982), characterized by a mainly rounded shape. The smallest have a spheroidal shape, with a diameter from 0.80 m to 1.50m. The biggest have an ellipsoidal shape, with a diameter from 1.50-2.00 m to 2-3m. Exfoliated boulders are widespread and by thousands. They are more frequent on the hill tops, most probably due to concentration by selective erosion and probably because the lowest parts were quarried first. The studied samples were provided from the extraction site (Upper Paleozoic) as indicated in the geological sketch-map (Fig. 3.37): unweathered boulders of granite, located in San Giovanni in Fiore, in “Colle dei Fiori” belonging to Sila Unit (Fig. 3.38), that extends from about 1275 to 1400 m above the sea level. From the granite boulders in “Colle dei Fiori”, 10 blocks were extracted and then cut in the laboratory to obtain regular specimens. According to the geological map reported in the Fig. 3.37, in the quarry area of “Colle dei Fiori”, fine to medium-grained granites and acid porphyritic rocks, with a variable composition between quartz diorite and granite, can be found. In this geological map and in the others that follow, just the legend related to the interested lithotypes is shown. The geological Unit is also composed by pink metagranodiorites, with K-feldspar crystals, by granodiorites and gabbros.

Most of the granitic historic quarries in Sila area are boulder fields, not very big, where the stone was traditionally removed manually from the inner core of the boulders through the splitting devices reported in Fig. 3.32. Metal wedges or wooden wedges soaked with water would have been used, following lines of potential fracture; then wedges or chisels were inserted into the building material and successively split with striking-hammers. Traditional types of dressing employed by Calabrian stonemasons for granitic blocks were “furrowed surface” and “bush hammered”. Whereas in the past,

quarrying consisted of removing only whale-back formations (granite boulders) (Fig. 3.31), more recently, with their gradual depletion, extraction has involved quarrying at greater depths or from outcrops. Today very few traditional family-run quarries co-exist with the mechanized variety.

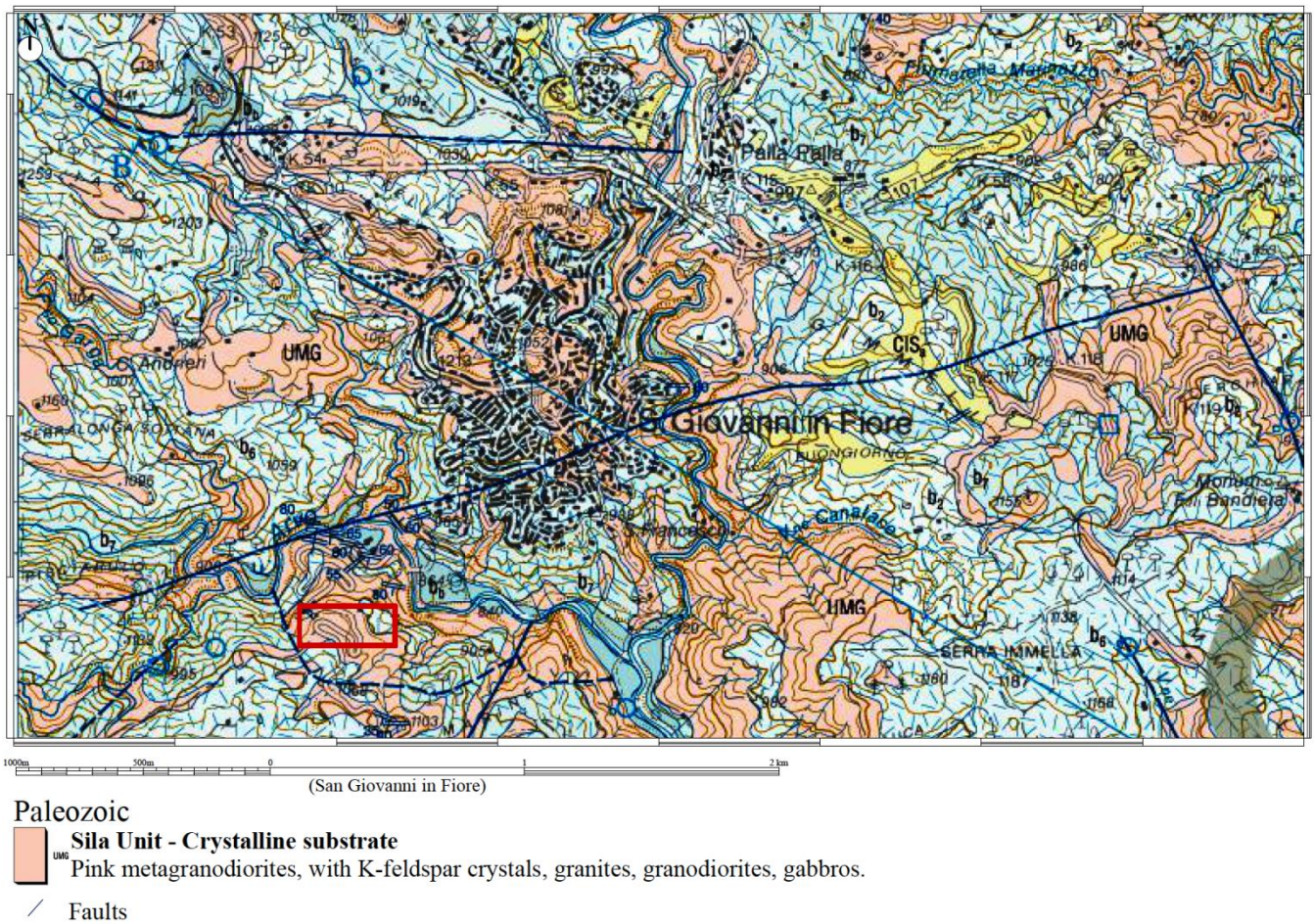


Fig. 3.37. Geological sketch map of the studied area of San Giovanni in Fiore (red rectangle shows the studied area and the quarry of “Colle dei Fiori”). Sheet 561 “San Giovanni in Fiore”, Scale 1:50000 [ISPRA, 2010 (a)].



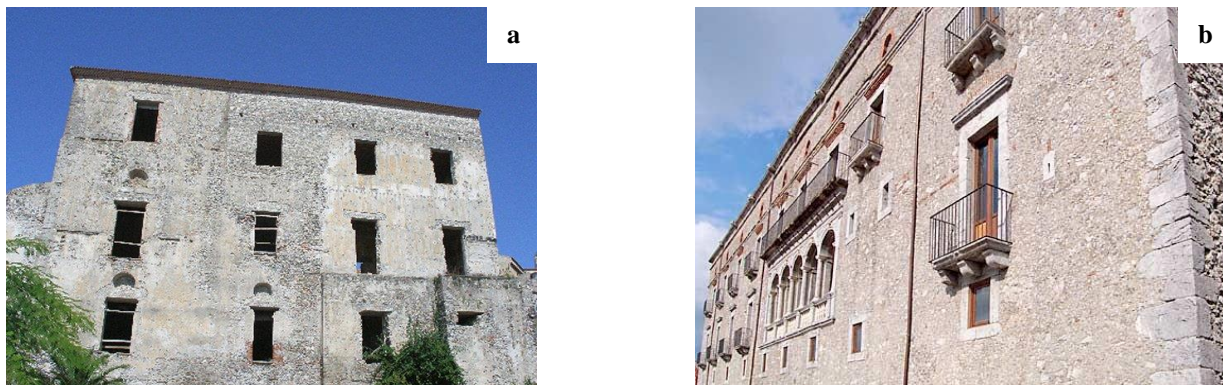
Fig. 3.38. Granite unweathered boulders extracted from the active quarry of “Località Colle dei Fiori” in San Giovanni in Fiore.

3.4.2 *Grisolia stone*

Macroscopically, Grisolia stone, commercialized under that same name or as “Pietra d’oro” (Gold stone) for its yellow intrusions (AA.VV., 2015), is a grey limestone, with slight variations in tone.

This stone has been used in the past to build the old towns of the Upper Tyrrhenian part of Cosenza Province and old towns spread in towns of Basilicata that are situated near the Grisolia formation (Forestieri *et al.*, 2016 a).

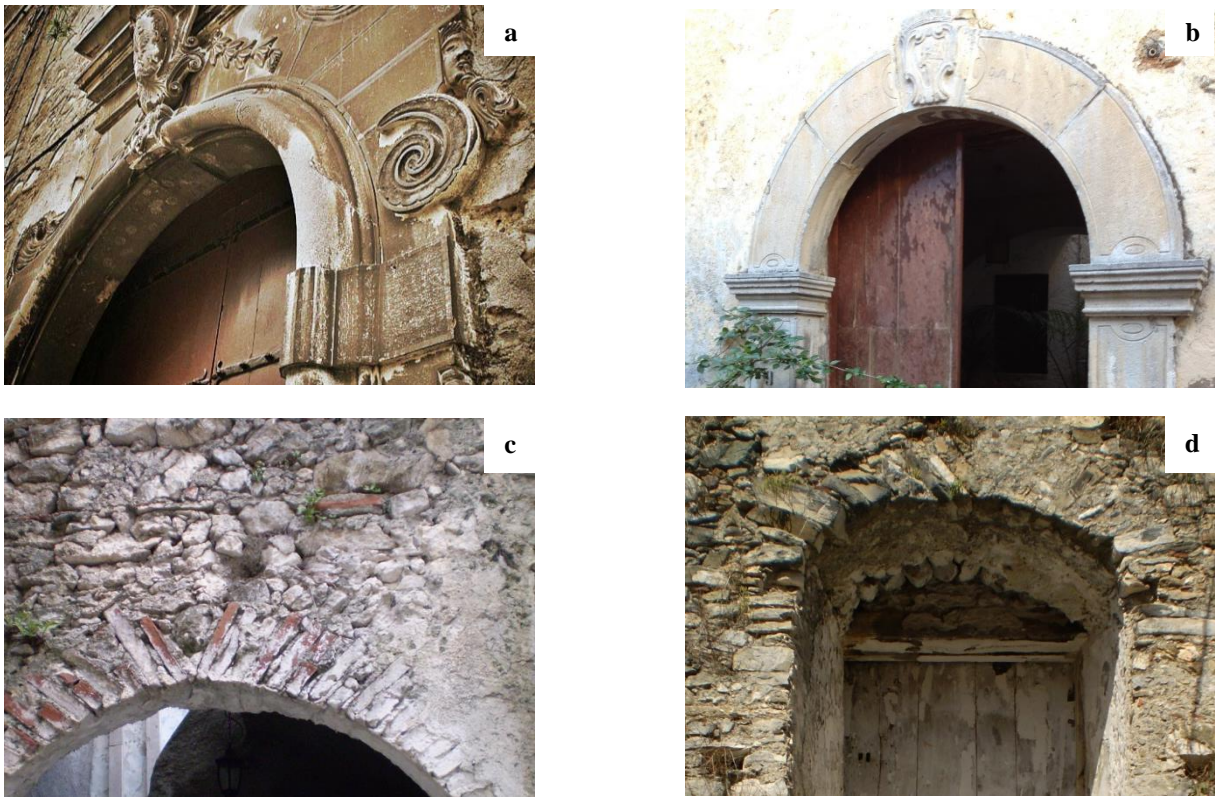
It has been employed not only for the construction of the majority of the masonries of the old above mentioned towns, but also for the realization of important religious and noble buildings of the Calabrian architecture. One of them is the church of “San Francesco”, of the 14th century, in Aieta, where the main building material is the Grisolia stone¹⁶. Others examples of the noble architecture are the famous “Palazzo dei Principi Spinelli” of the 13th century, in Scalea (Fig. 3.39 a) and “Palazzo Martirano-Spinelli” of the 14th century, in Aieta (Fig. 3.39 b).



Figs. 3.39 (a, b). Examples of Calabrian noble buildings built with Grisolia stone: “Palazzo dei Principi Spinelli”, Scalea (a); “Palazzo Martirano-Spinelli”, Aieta (b).

Grisolia stone has been used for both decorative, such as covering elements of façade and portals of noble palaces (Figs. 3.40 a, b), and structural uses for the construction of masonries, arches and retaining walls (Figs. 3.40 c, d).

¹⁶ Cit. <http://www.mpsrl.net/publicazioni/comunita-montana-alto-tirreno-appennino-paolano/grisolia/80-itinerario-turistico.html>



Figs. 3.40 (a, b, c, d). Decorative and structural uses of Grisolia stone: Portal of “Palazzo Barletta”, Senise – decorative use (a); Portal of 18th century (1780) with a rough-pointed surface, Scalea - decorative use (b); example of a random rubble uncoursed masonry, Scalea – structural use (c); example of stone arch and vertical elements built with trimmings stones (war Memorial), Cosenza (d).

Geological setting and stone extraction

Geologically, Grisolia stone is to be referred to the carbonatic deposits of the Upper Triassic, belonging to the “Verbicaro Unit” (Amodio Morelli *et al.*, 1976). These deposits have been also named “Trias Dolomitique” by Grandjacquet & Grandjacquet (1962) and successively as “Dolomie scure” (dark dolostones) by Damiani (1970). According to Damiani (1970) the upper part of the Verbicaro Unit, corresponding to the Grisolia Formation, is characterized by a succession of grey limestones alternating with marls and argillites with a yellowish/reddish colour (Mastandrea *et al.*, 2003). Grisolia Formation extends from the “Lao” River to Papisidero; outcrops can be found in locality called “Serra la Limpida” and between the Lao River and the road that connects San Domenica Talao to Papisidero.

It is considered as a transition from the dark dolostones Unit to grey limestones, with an average thickness of 50-60m (Damiani, 1970). According to Mastandrea *et al.* (2003), Grisolia Formation is characterized by fine grained, usually thin bedded limestones alternating with yellow-red marls and shales and the upper part is characterized by a reduction in pelite layers and contemporaneous increase in fine grained limestones, locally strongly recrystallized. From a detailed point of view, according to the geological map reported in the Fig. 3.41, samples collected from the active quarry of “Via Anania” in Grisolia (Fig. 3.42), belong to the “Frido Formation” characterized by clayschists, quartzarenites and a few presence of crystalline carbonates with a grey-dark colour and containing microfossils.

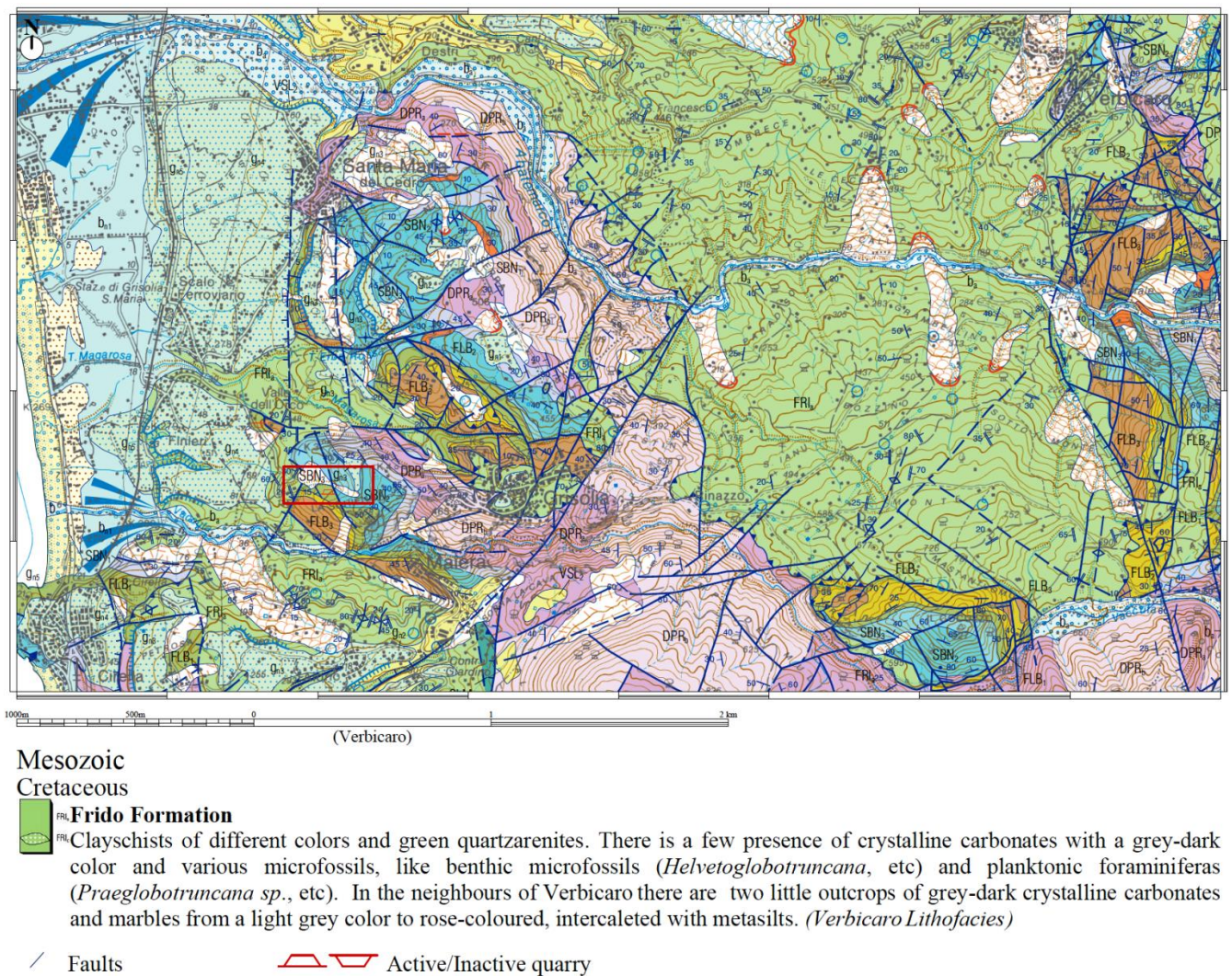


Fig. 3.41. Geological sketch map of the studied area of Grisolia (red rectangle shows the studied area and the quarry of Via Anania). Sheet 542 “Verbicaro”, Scale 1:50000 [ISPRA, 2010 (b)].



Fig. 3.42. Active quarry of Grisolia stone, of “Via Anania” in Grisolia.

The extracted samples come from to the active quarry reported in [Fig. 3.42](#) belonging to the category of the hillside quarries. 10 blocks were extracted and then cut in the laboratory. The quarry is characterized by Grisolia stone blocks quarried mechanically. The extraction method is the digging method with the descending technique.

3.4.3 *San Lucido calcarenite*

The third selected stone is the San Lucido calcarenite (CS) from the Coastal Tyrrhenian Range, the coastal part of Cosenza Province. This stone has been one of the most used building materials of the Calabrian architecture.

Macroscopically, San Lucido calcarenite appears to be compact and shows a white/reddish-cream colour, with visible fossils at naked eye. It is commercialized under the name of “Pietra di San Lucido” (San Lucido stone) or generically as “Pietra o tufo di Mendicino” (Mendicino stone or tuff).

“Mendicino calcarenite”, commonly named as “tuff” (Rodolico, 1995) due to its easy workability, was widely employed as building material by the most important Calabrian schools of stonemasons to realize structural and ornamental elements, such as masonries, arches and portals of many Calabrian historical centres of the Coastal Tyrrhenian area and the central area of the Crati River (Italy). The outcrops of this building material, quarried in the past, are situated near the town of Cosenza, in an area including the southern part of the Coastal Tyrrhenian Range, from San Lucido to Domanico, and the right side of the Crati River, from Laurignano to Altilia (Crisci *et al.*, 2003). The ancient quarries were situated in Mendicino, Altilia and San Lucido (Lico, 2015). Mendicino and Altilia quarries were exploited until the last century, but nowadays are not active anymore. San Lucido quarries were situated in the area of the “Deuda stream” and the “Torbido stream”, where there was one of the ancient quarries. Since the 50s of the last century has started the quarry activity in the northern area of San Lucido with three new quarries that are still in use (Forestieri *et al.*, 2016 a).

San Lucido calcarenite has been employed by the schools of stonemasons for the realization of the vernacular architecture of many historical centres of Cosenza and to build important noble palaces, religious buildings and in the field of the civil architecture. Some of the examples of palaces realized with this stone can be found in San Lucido and are reported in the Figs. 3.43 a, b, c, d with: Palazzo Zagarese”, of the 19th century (Figs. 3.43 a, b); “Palazzo Manes”, built in the 18th century that is one of the most important Palace (Forestieri *et al.*, 2016 b) in the town of San Lucido (Fig. 3.43 c); the most important example of the civil architecture, the castle of San Lucido, that actually, the only visible part, is the west tower because many parts collapsed for the earthquake of the 1905 (Fig. 3.43 d).



a



b



c



d

Figs. 3.43 (a, b, c, d). Examples of buildings built with “San Lucido Calcarenite” in San Lucido: “Palazzo Zagarese” (a, b); “Palazzo Manes” (c); the ruins of the castle “Castello di San Lucido”(d).

Geological setting and stone extraction

San Lucido calcarenite belongs to the Sedimentary Successions of the Upper Oligocene-Middle Pliocene of the Coastal Tyrrhenian Range that includes not only calcarenites but also sandstones (arkose), conglomerates, clays, marls, gypsums and evaporitic limestones, from 200 m to over 1.500 m in thickness (Critelli & Le Pera, 2000). This Tortonian-Messinian sedimentary succession represents the

infilling of the basins opened during the Lower Tortonian in the western area of the Calabrian Arc. The area belongs to the high Crati Valley, between the Coastal Range in the West and Sila Massif in the East (Mastandrea *et al.*, 2002). According to many authors, the succession can be divided into four lithostratigraphic units: the first unit consists of coarse siliciclastic deposits; the second unit is made up of mixed carbonate/terrigenous sediments; the third unit consists mainly of marlyclayey deep-water sediments, rich in planktonic foraminifera alternated with some turbiditic levels; the fourth unit, of Messinian age, is characterized by evaporitic sediments interlayered with pelite beds (Mastandrea *et al.*, 2002). The generic “Calcare di Mendicino” belongs to the second one, made up of mixed carbonate and terrigenous sediments (Colella, 1995).

Regarding petrographic characteristics of calcarenite, showing a carbonate matrix, it can be defined as *biocalcarenite/calcirudite* (Mastandrea *et al.*, 2002) or *biolitite/boundstone* (Crisci *et al.*, 2003), with a presence of microfossils (*e.g.* shells fragments). It's a porous material, almost resistant, with a colour ranging from whitish to reddish, variable for the presence or not of iron minerals. The Altilia calcarenite, belonging to the same “Calcare di Mendicino”, can be defined as a calcarenite with a high content of calcium carbonate and it is partially dolomitized (Lico, 2015). The San Lucido calcarenite can be classified as biocalcarenite.

According to the geological map of the Fig. 3.44, the Miocenic succession is composed by whitish and dark-reddish limestones, mainly calcarenites; sandstones and sands, well stratified; conglomerates, made of rounded to sub-angular pebbles of igneous and metamorphic rocks. Quarry samples analyzed in this study belong to 10 blocks extracted from the active quarry of “Motta Lupo” in San Lucido (Fig. 3.45).

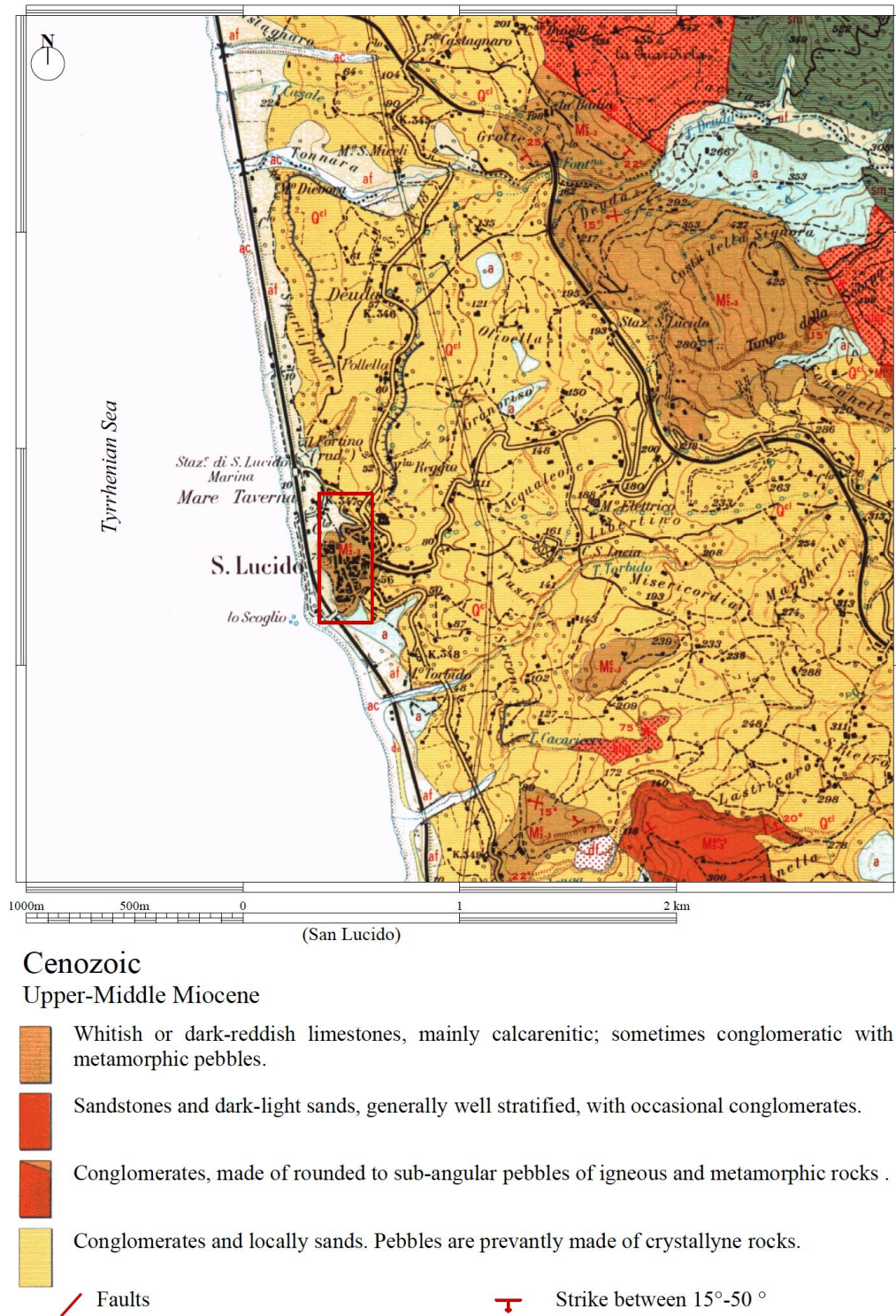


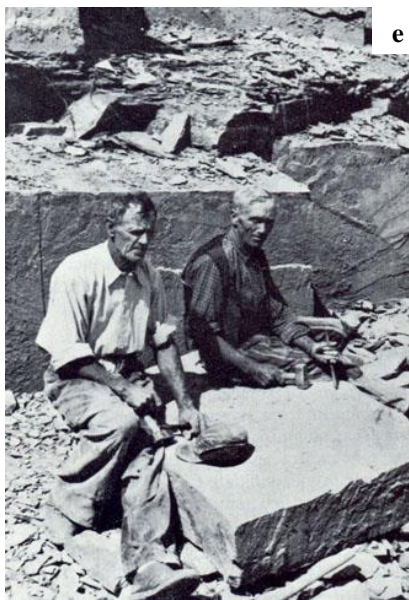
Fig. 3.44. Geological sketch map of the studied area of San Lucido (red rectangle shows the studied area and the quarry of “Motta Lupo”). Sheet 236, IV N.W. “San Lucido”, Scale 1:25000 [Casmèz, 1967 (a)].



Fig. 3.45. Active quarry of San Lucido stone, “Motta Lupo” in San Lucido.

The examined active quarry of “Motta Lupo” belongs to the category of three sided notch into a hillside. The relief of the quarry corresponds to the steepest slope. It develops laterally and the advancement of the workface is digged laterally through a descending technique. At the end of the escarpment, as can be seen in [Fig. 3.45](#), there is the work plane with the presence of vehicles.

As well as the active quarry, ancient quarries reported in [Figs. 3.45 a, b](#), situated in Mendicino and Altilia, respectively, belong to the category of hillside quarries. The traditional extraction method, reported in [Figs. 3.45 c, d, e, f](#), consisted in the using of metal wedges soaked with water, following stratification lines of potential fracture; then wedges or chisels were inserted into the building material and successively split with striking-hammers.



Figs. 3.45 a, b, c, d, e, f. Ancient quarries of San Lucido stone in Mendicino (a) and Altilia (b) [Lico, 2015]. Traditional extraction methods of San Lucido stone (c, d, e, f) [AA.VV., 2015].

3.4.4 Fuscaldo sandstone

Macroscopically Fuscaldo sandstone is compact, has a yellow/brownish-colour. It is commercialized under the name of “Pietra di Fuscaldo” (Fuscaldo stone) or as “Pietra dolce” (Sweet stone) due to its easy workability.

Fuscaldo sandstone, commonly named as “tuff”, was utilized in the past by the most important Calabrian schools of stonemasons to realize structural and ornamental elements, such as buildings, arches and portals of many Calabrian historical centers (Forestieri *et al.*, 2015). The most important architectural elements that were built with this material are the portals. The main portals are situated in the old town of Fuscaldo and for this reason the city is also called “La città dei cento portali” that means the “town of hundreds portals”. The most famous realizations are the portals of: Carnevale Palace of the 14th century (Fig. 3.46 a); Valenza Palace of the 17th century (Fig. 3.46 b); Vaccari Palace of the 17th century (Fig. 3.46 c).



Figs. 3.46 (a, b, c). Examples of portals built with “Fuscaldo sandstone” in Fuscaldo: Carnevale Palace (a); Valenza Palace (b); Vaccari Palace (c).

Geological setting and stone extraction

Fuscaldo sandstone belongs to the same Sedimentary Successions of the Upper Oligocene-Middle Pliocene of the Coastal Tyrrhenian Range of San Lucido calcarenite.

According to the geological map of the Fig. 3.47, the Upper Miocenic sedimentary succession in this area is composed by dark and light sandstones with a calcareous cement, locally conglomeratic (Critelli & Le Pera, 2000); dark and light sandstones with a calcareous cement, with sandy horizons; dark-light to dark-reddish conglomerates, composed by rounded pebbles and fragments of granite, gneiss into an arkosic matrix. Quarry samples belong to 10 irregular blocks extracted from the outcrops situated in “Località Scarcelli” in Fuscaldo (Fig. 3.48).

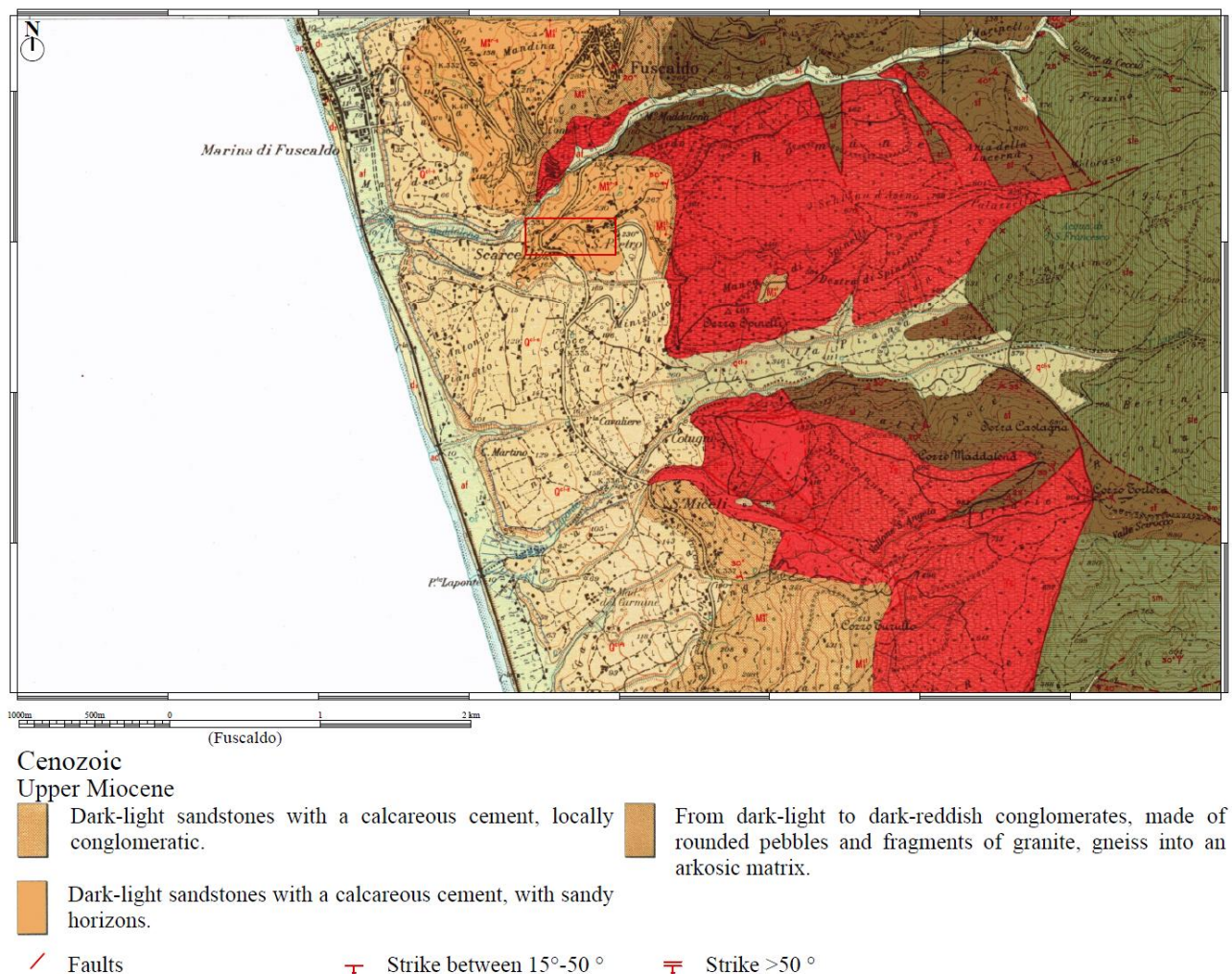


Fig. 3.47. Geological sketch map of the studied area of Fuscaldo (red rectangle shows the studied area and the outcrop of “Scarcelli”). Sheet 228, III S.W. “Paola”, Scale 1:25000 [Casméz, 1967 (b)].

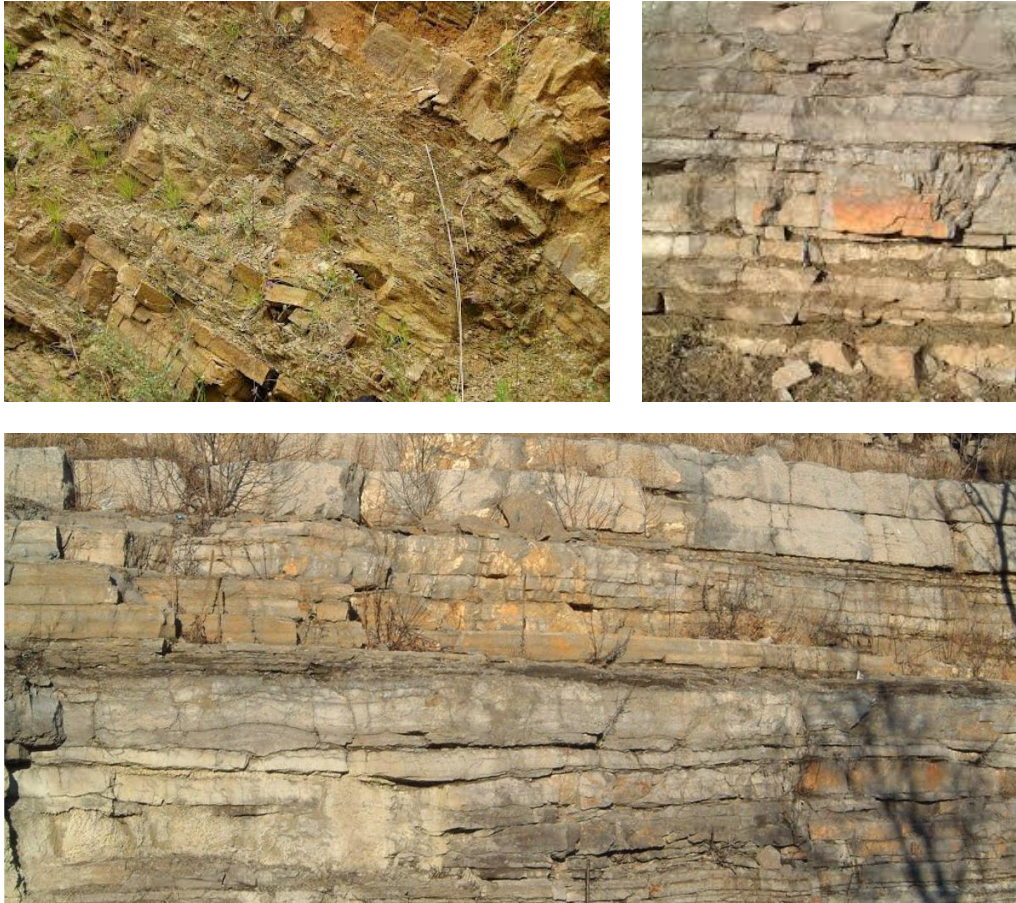


Fig. 3.48. Sandstone outcrops of Fuscaldo sandstone, “Località Scarcelli” in Fuscaldo.

The outcrops situated in Località Scarcelli in Fuscaldo are characterized by stratified sandstones. They are spread in different points of the area and they are few in numbers due to the intense urbanizations. In the past, in the same area, there were a lot of ancient quarries, exploited by the school of stonemasons of Fuscaldo (Bruno, 1995). Due to the low hardness of the Fuscaldo stone, blocks are extracted through simple mechanical tools.

4. Cosenza Province masonries: construction techniques

This chapter analyzes masonries built with the selected lithotypes. Masonries have been classified according to the thickness of joints, continuity of courses and finish of face. Analyzed masonries belong to four historical centres where the four studied stones have been employed. In particular, two categories, in common for the four lithotypes, have been individuated:

1. Rubble or irregular masonry;
2. Ashlar masonry or regular texture.

The first category corresponds to masonry consisting of stones either undressed or roughly dressed and having wider joints. The most common employed stones are pebbles, cobbles and rubbles and rarely blocks and ashlar (Fig. 4.0). Masonry is in general composed by a single leaf. Further random rubble masonry is also divided into the following types:

- 1.1 Uncoursed random rubble masonry;
- 1.2 Coursed random rubble masonry.

Reported masonries of the four investigated old towns will be shown for each category with the following abbreviations: GF. San Giovanni in Fiore (San Giovanni in Fiore granite); DG. Scalea (Grisolia stone); AF. Fuscaldo (Fuscaldo sandstone); CS. San Lucido (San Lucido calcarenite). Pictures are also marked with progressive small letters to differentiate every masonry category (e.g. a, b, etc.).

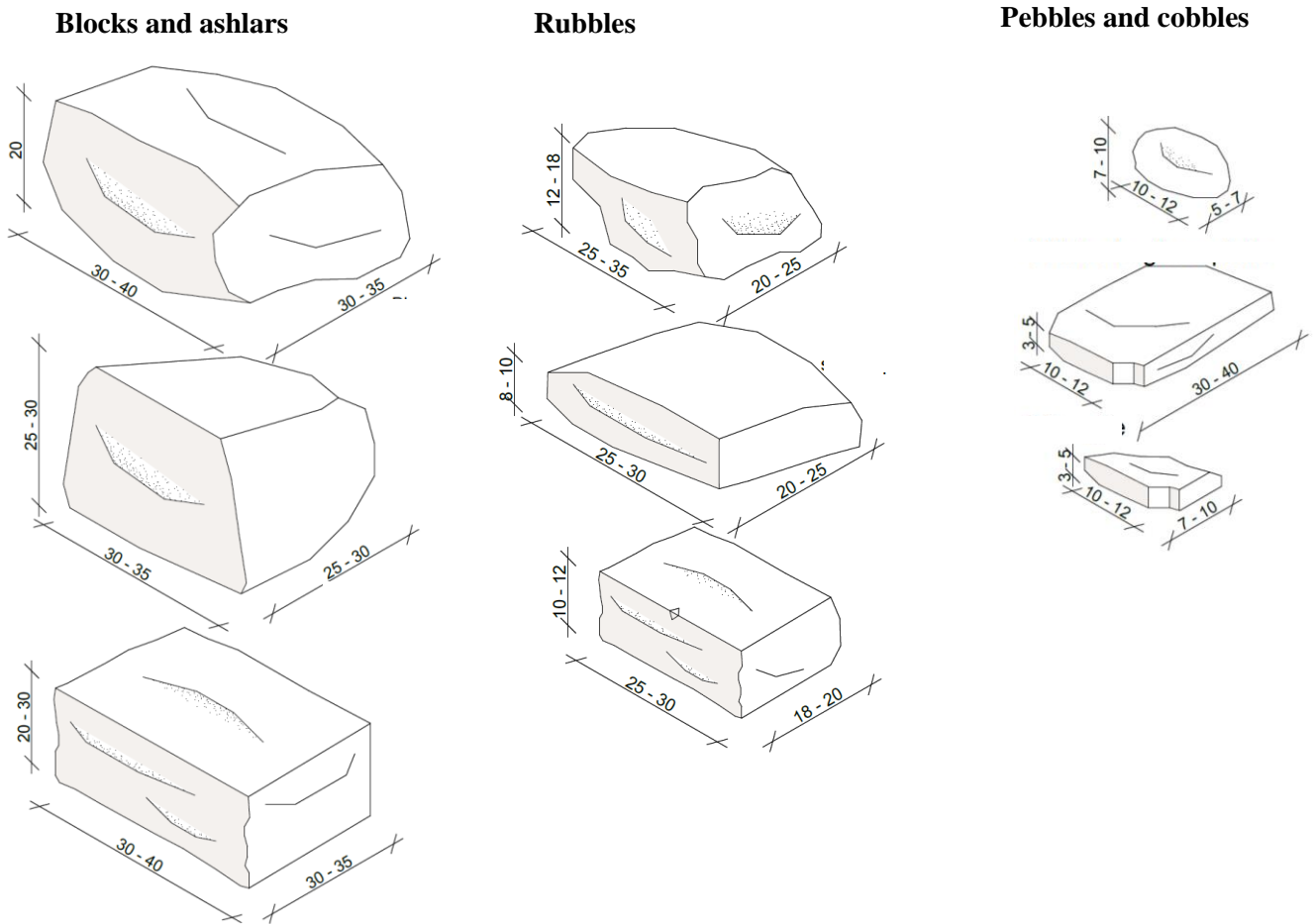


Fig. 4.0. Different types and sizes of stones employed as building materials in the investigated old towns.

4.1 Uncoursed random rubble masonry

The random rubble masonry in which stones are laid without forming courses is known as uncoursed random rubble masonry. This is the roughest and cheapest type of masonry and is of varying appearance. The stones used in this masonry are of different sizes and shapes. Before lying, all projecting corners of stones are slightly knocked off.

Below are shown some masonry examples belonging to this category realized with San Giovanni in Fiore granite and represented with technical details.

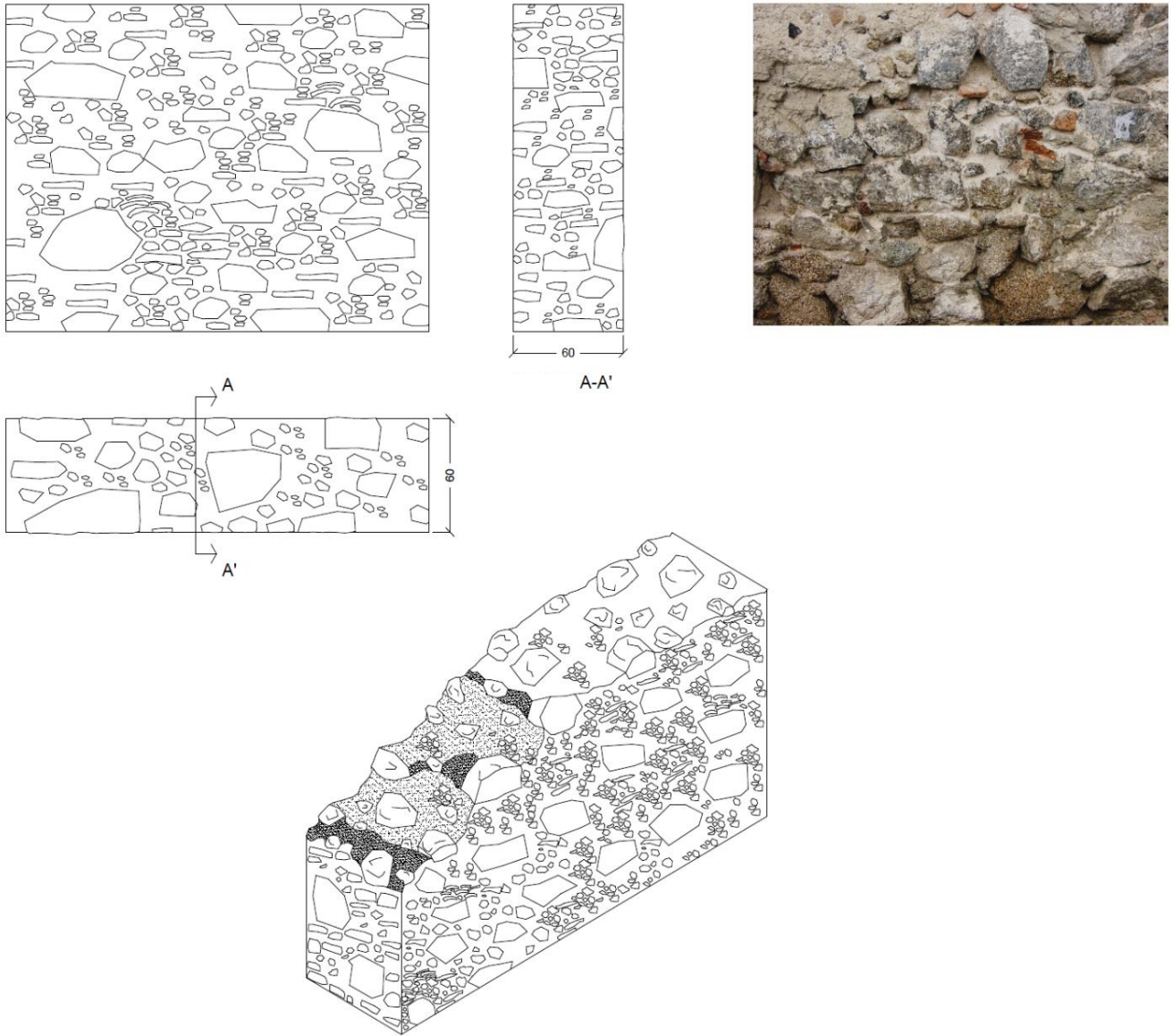


Fig. 4.1 a – GF. Uncoursed random masonry realized with San Giovanni in Fiore granite, San Giovanni in Fiore (CS). Masonry is composed by pebbles and rubbles of different sizes. High amount of mortar. Bricks fragments to fill empty spaces.

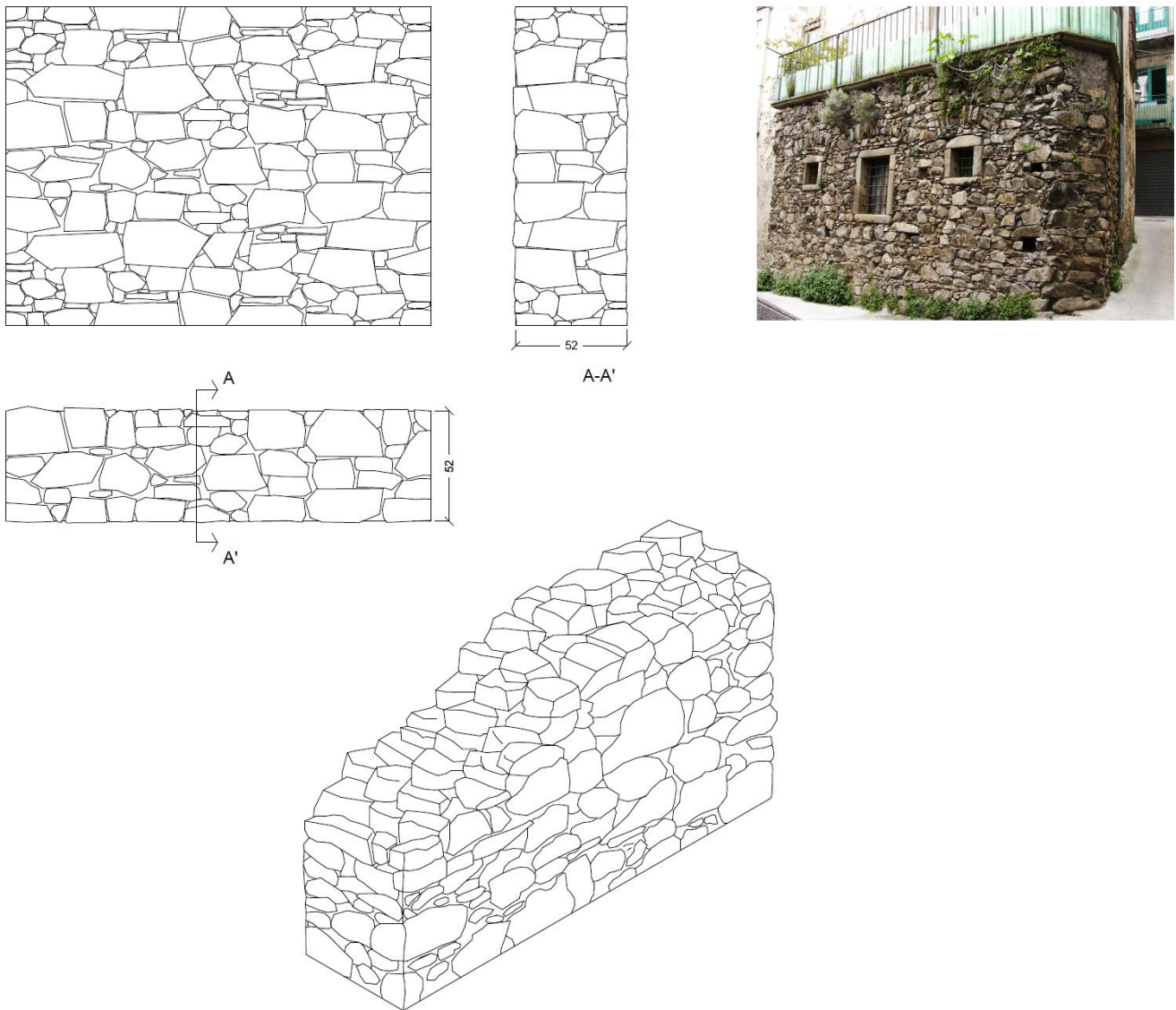


Fig. 4.1 b – GF. Uncoursed random masonry realized with San Giovanni in Fiore granite, San Giovanni in Fiore (CS). Masonry is composed by rubbles of medium and big dimensions, with sharp edges. Medium amount of mortar. Absence of bricks fragments to fill empty spaces.

The difference between masonry of [Fig. 4.1 a – GF](#) and [Fig. 4.1 b – GF](#) is the amount of mortar employed to fill empty spaces and the dimensions of rubbles. Regarding masonry resistance, the second one has a higher resistance due to the less presence of mortar than the first one. In this category of masonry, in San Giovanni in Fiore, have been found rare examples of employment of large stones used at corners and at jambs to increase their strength ([Fig. 4.1 c – GF](#)).

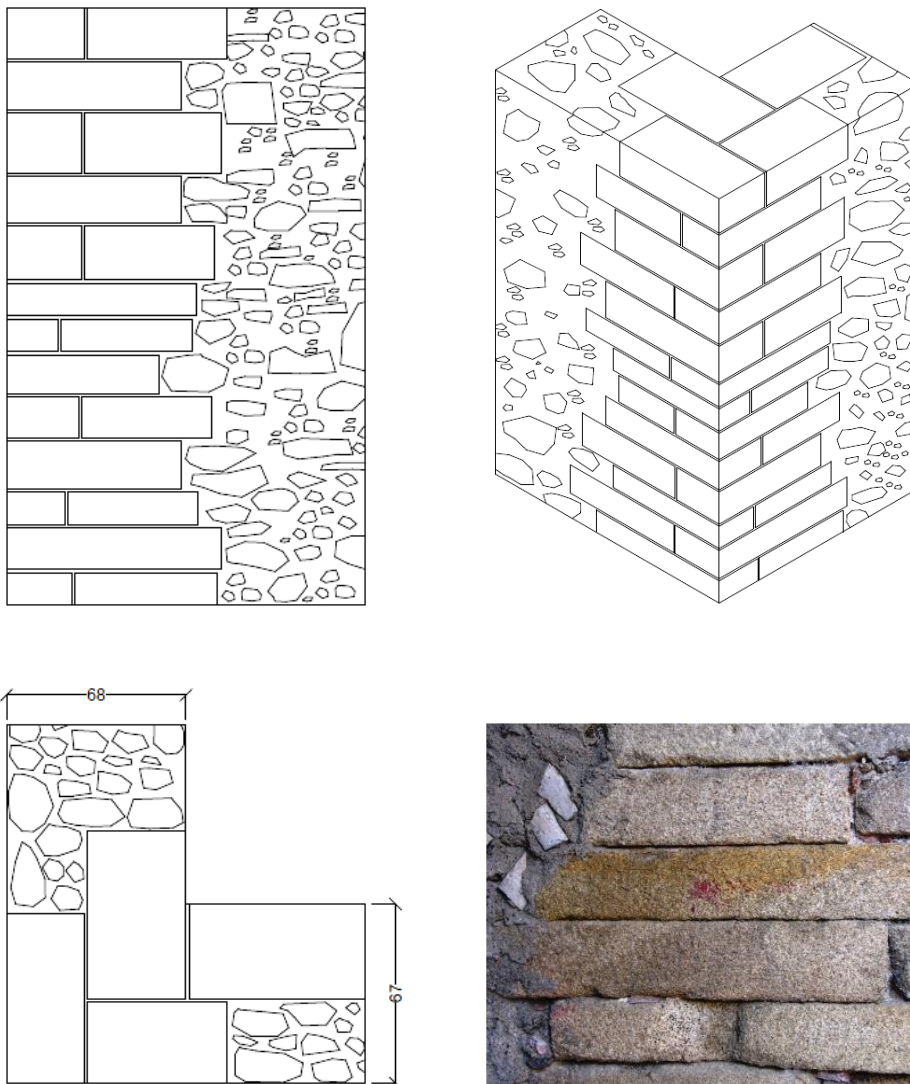
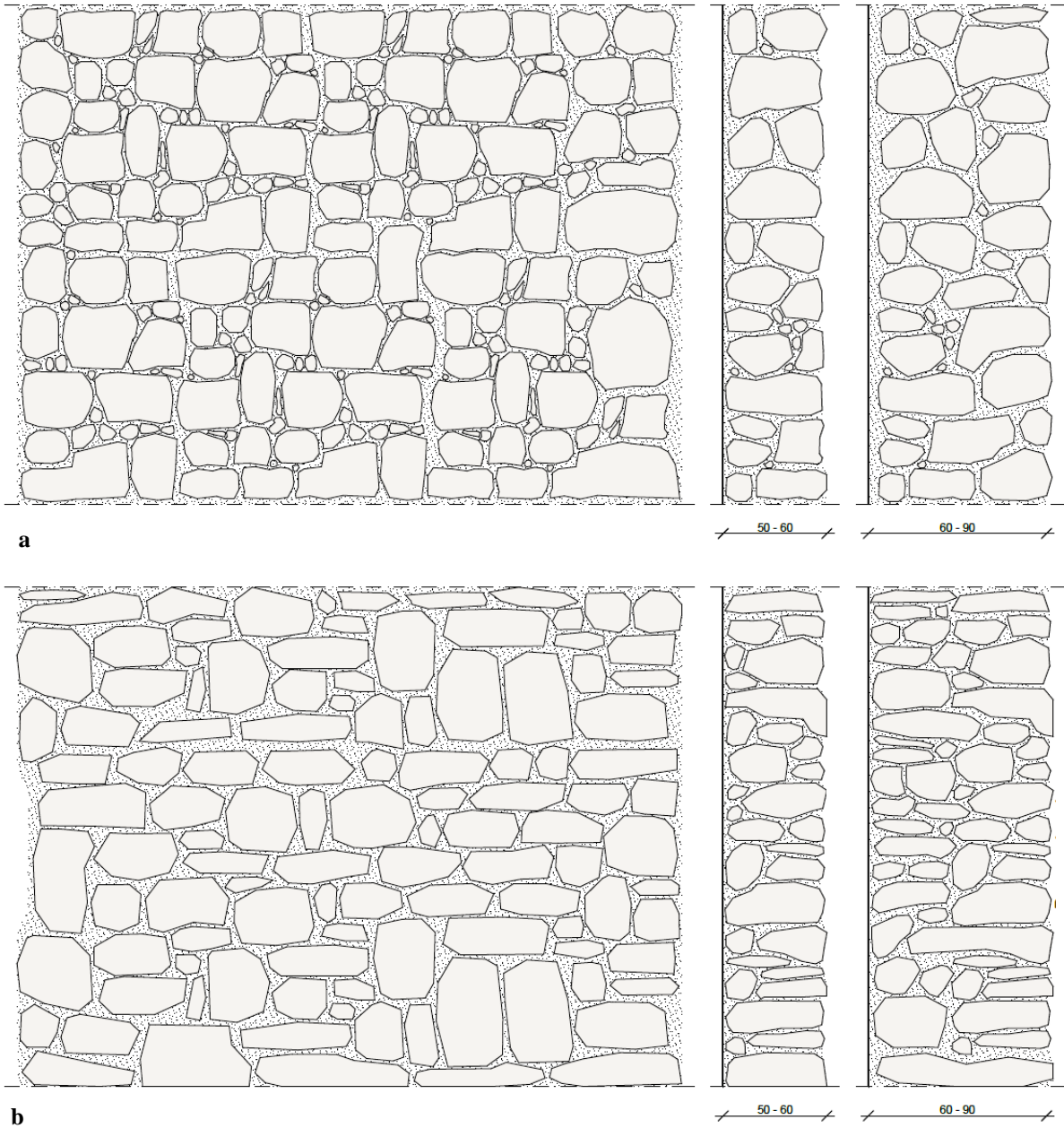
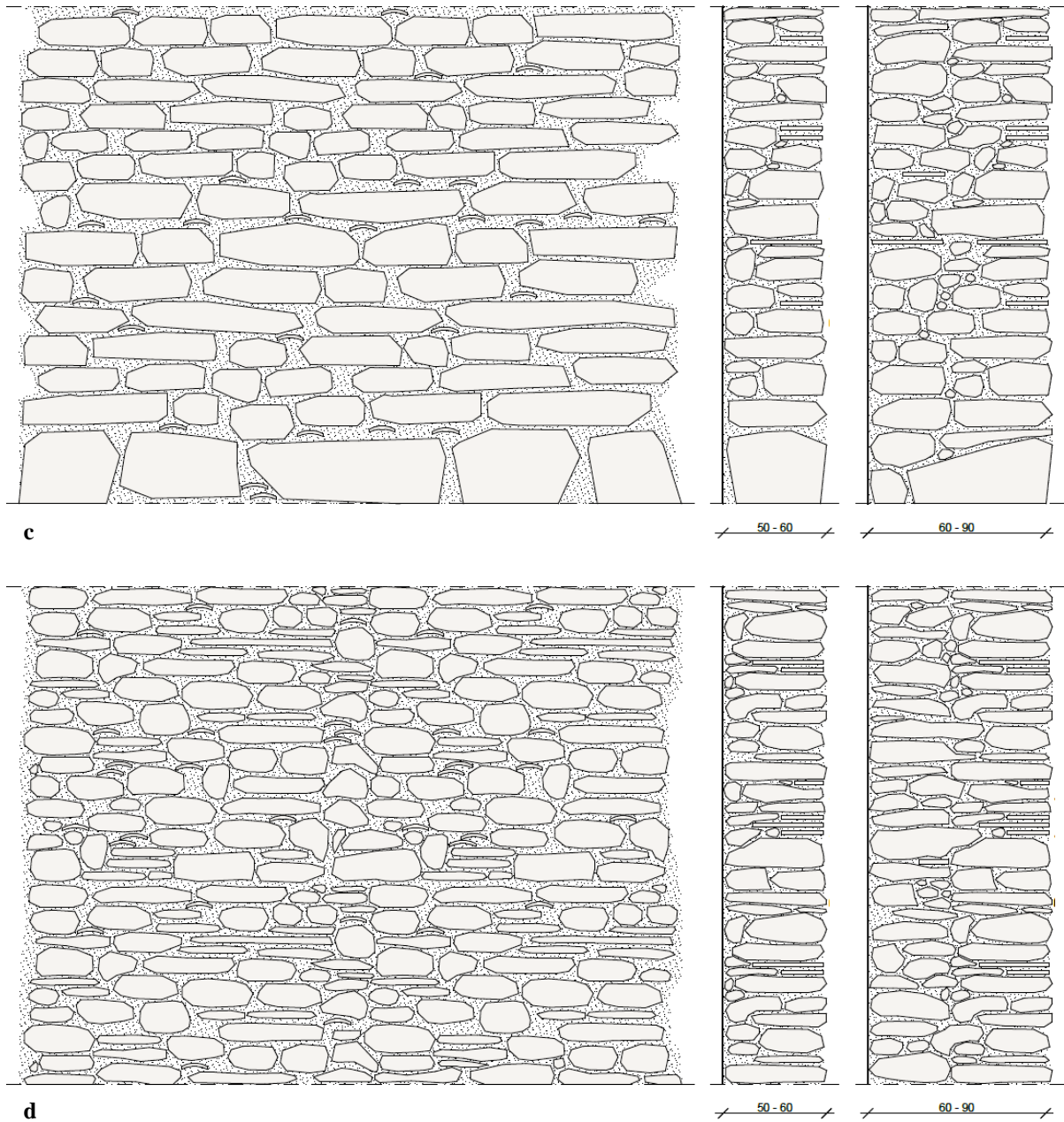


Fig. 4.1 c – GF. Example of an uncoursed random masonry realized with San Giovanni in Fiore granite, San Giovanni in Fiore (CS), with the rare presence of ashlars elements in the corner.

Irregular masonries of the historical centres of Scalea built with Grisolia stone are characterized by rubbles and cobbles of different sizes (Figs. 4.2 a, b - DG) or by extended large blocks and rubbles, with the interposition of small bricks elements to fill empty spaces (Figs. 4.2 c, d - DG).



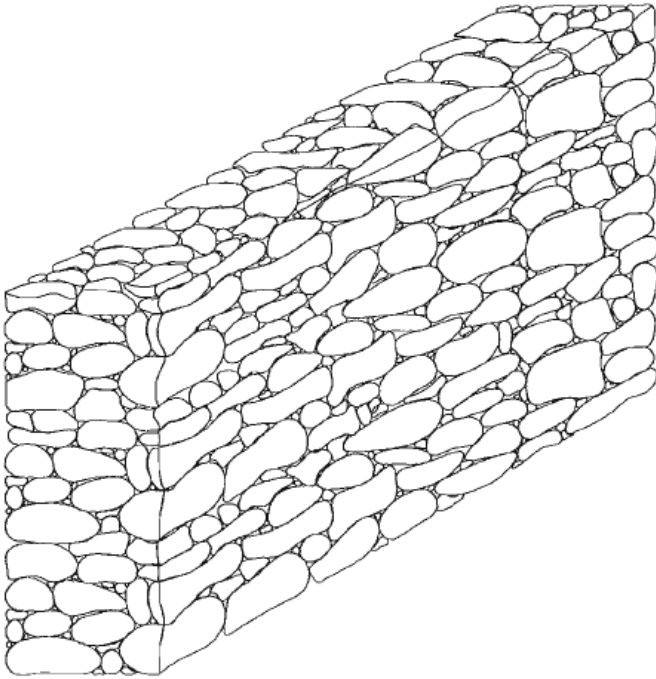
Figs. 4.2 a, b – DG. Examples of uncoursed random masonry realized with Grisolia stone, Scalea (CS), with rubbles and cobbles of different sizes.



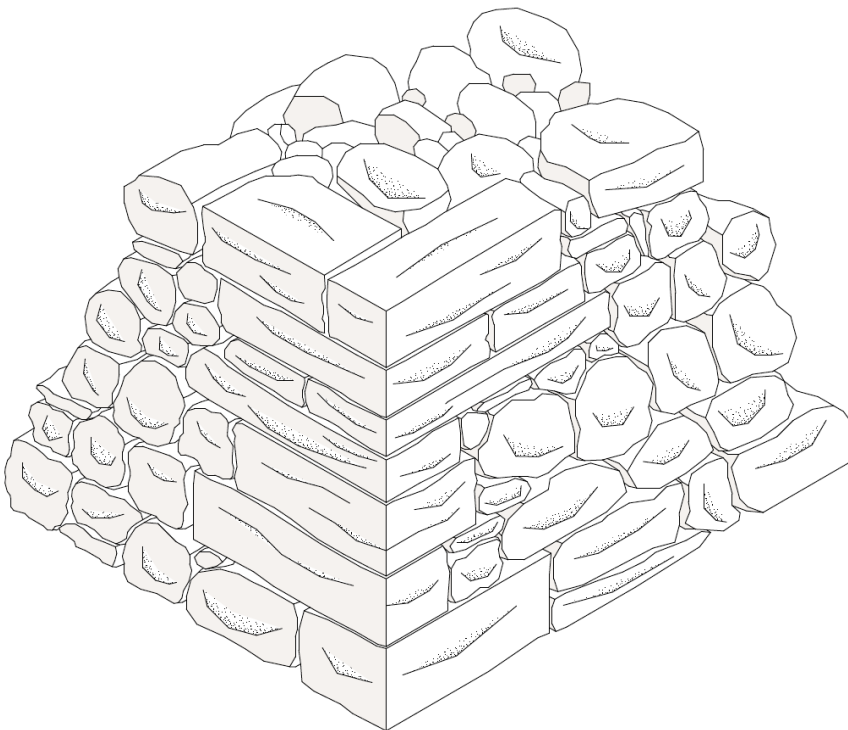
Figs. 4.2 c, d – DG. Examples of uncoursed random masonry realized with Grisolia stone, Scalea (CS), with extended blocks and rubbles, with the interposition of small bricks elements to fill empty spaces.

In the old town of San Lucido only one type of irregular masonry has been individuated (Figs. 4.3 a - CS) realized with blocks, rubbles and pebbles of different sizes. In rare cases the corner is strengthened by squared blocks (Fig. 4.3 b - CS).

a

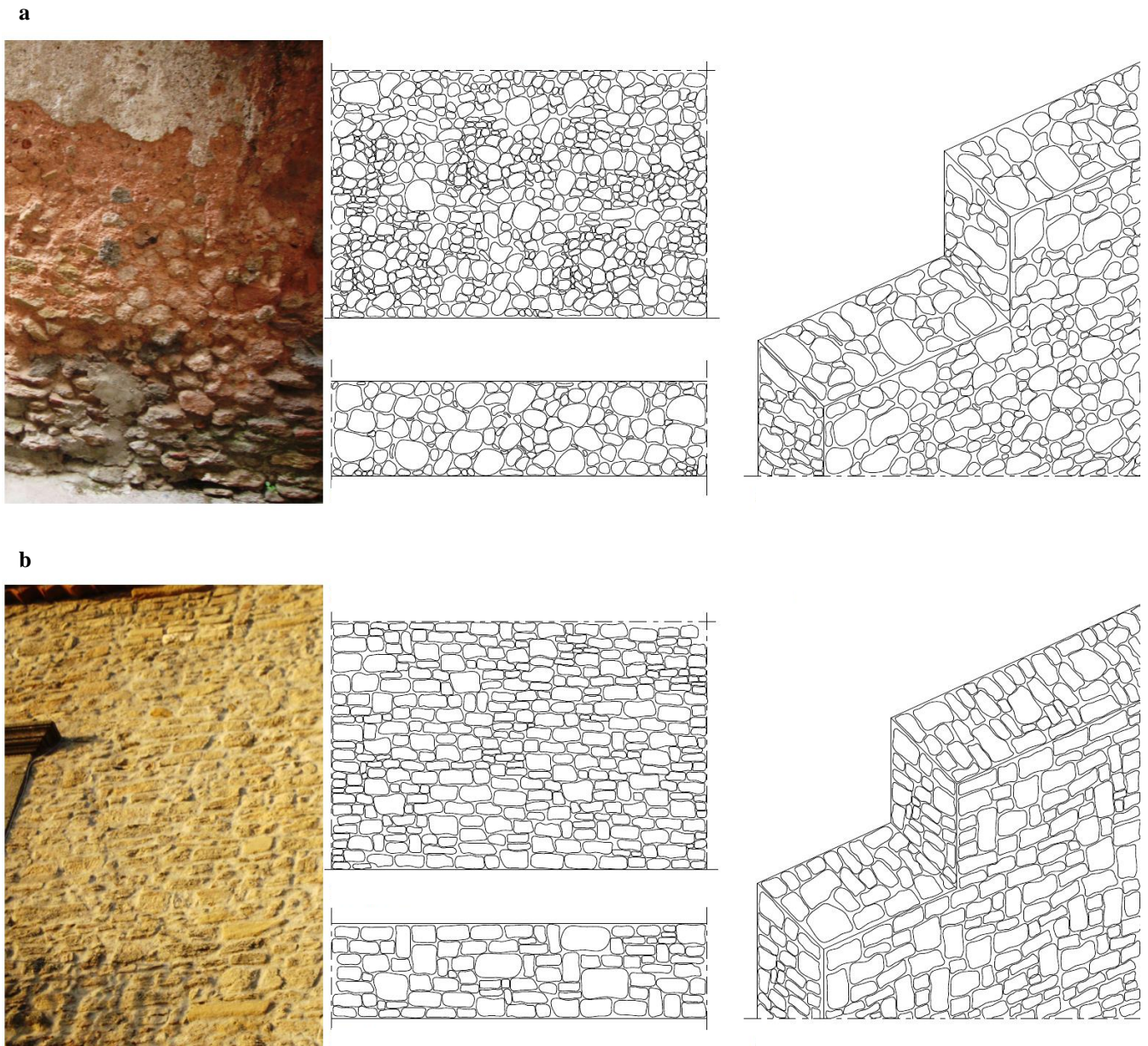


b



Figs. 4.3 a, b – CS. Example of uncoursed random masonry realized with San Lucido calcarenite, San Lucido (CS), with blocks, rubbles and pebbles (a). Detail of the corner realized with squared (b).

In Fuscaldo two different types of irregular masonries have been selected. The first typology is composed entirely by rounded pebbles (Fig. 4.4 a - AF); the second one with semi-squared extended blocks (Fig. 4.4 b - AF).



Figs. 4.4 a, b – AF. Example of uncoursed random masonry realized with Fuscaldo sandstone, Fuscaldo (CS), rounded pebbles (a) or with semi-squared extended blocks (b).

4.2 Coursed random rubble

The random rubble masonry in which stones are laid in layers of equal height is called *random rubble masonry*. In this type of masonry, the stones are laid in somewhat level courses. Headers of one coursed height are placed at certain intervals.

Regular courses, in all investigated old towns, were realized according to two different patterns. In the first one, the entire masonry is composed by semi-squared blocks laid in regular courses (Figs. 4.6a - DG; 4.7 a - CS).

The second typology is constituted by a mixed masonry with semi-squared blocks and brick coursing to realize single or double regular courses (Figs. 4.5 - GF; 4.6 b, c - DG; 4.7 b - CS; 4.8 - AF).

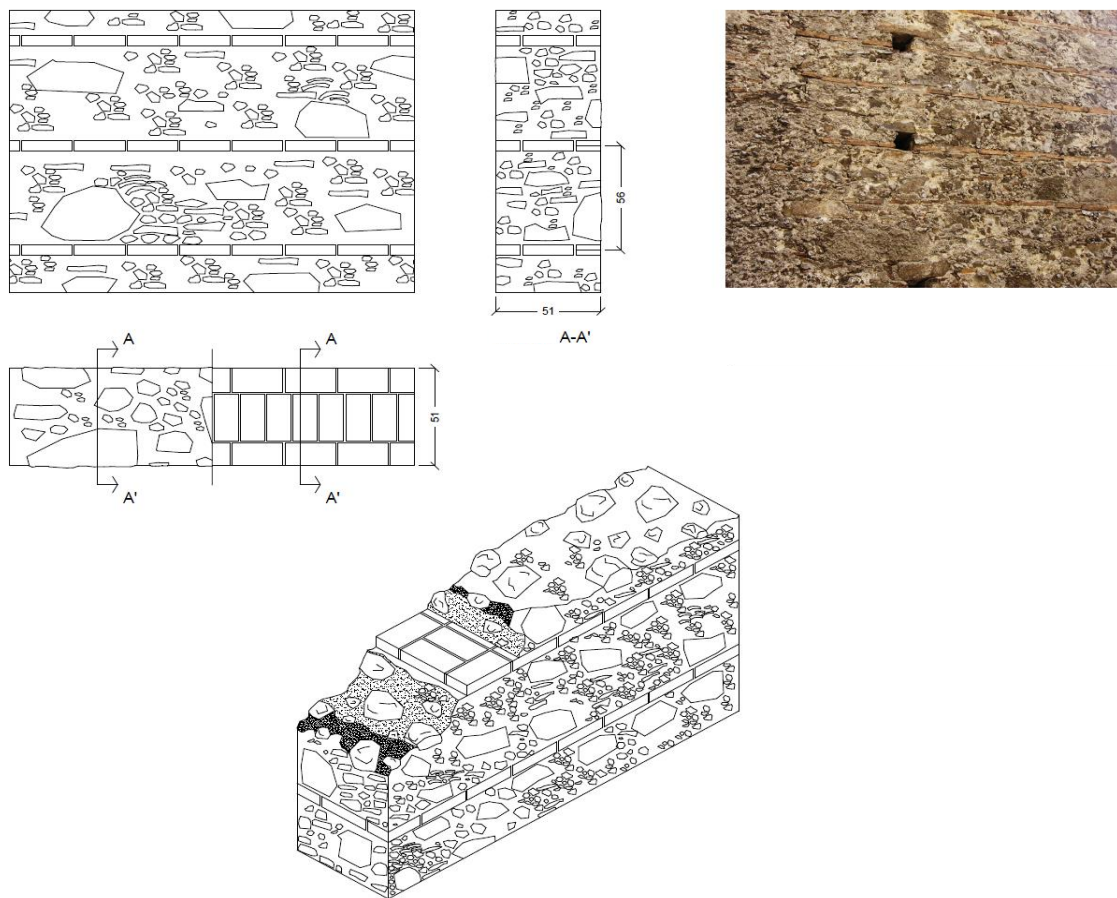
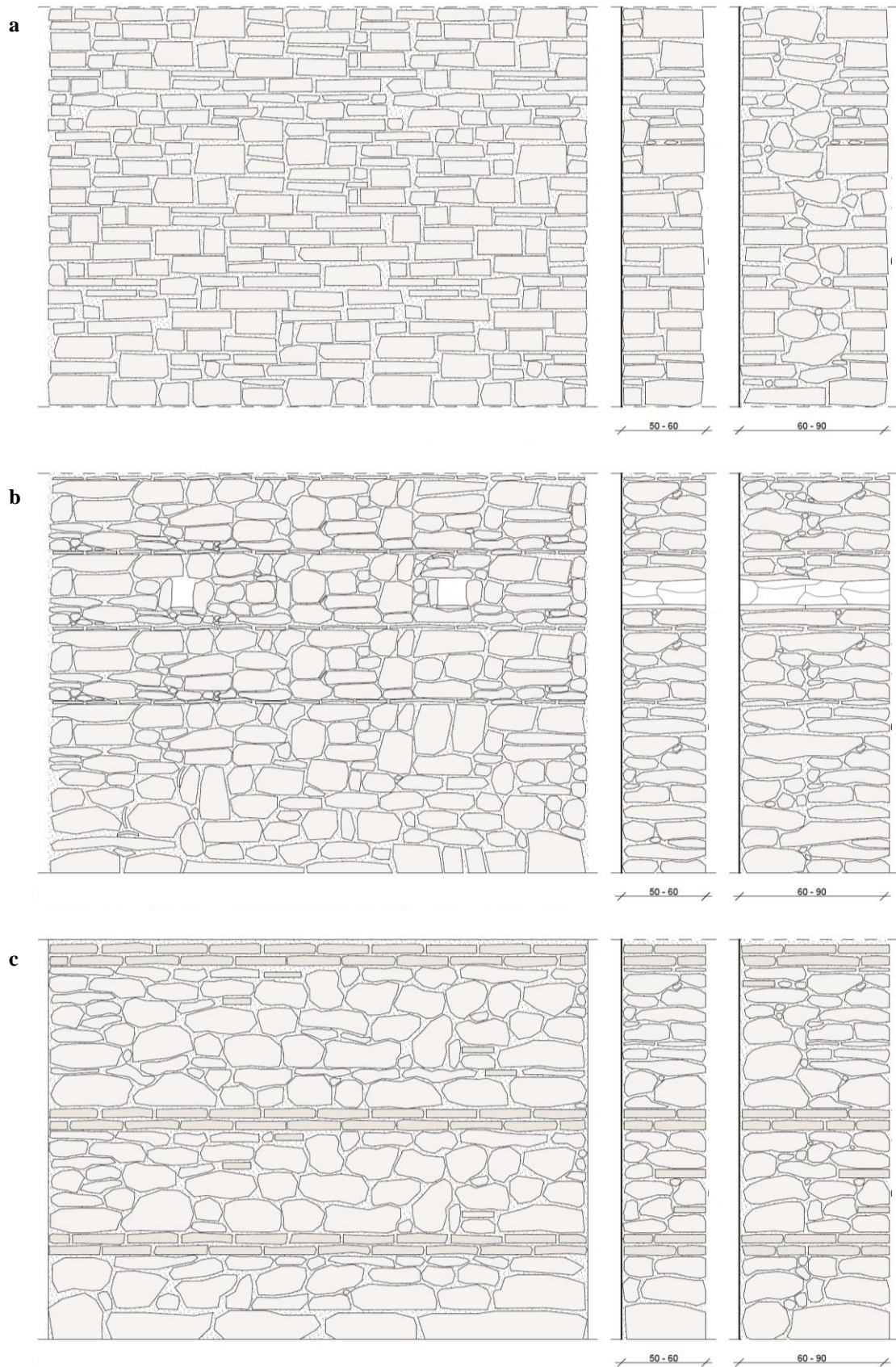
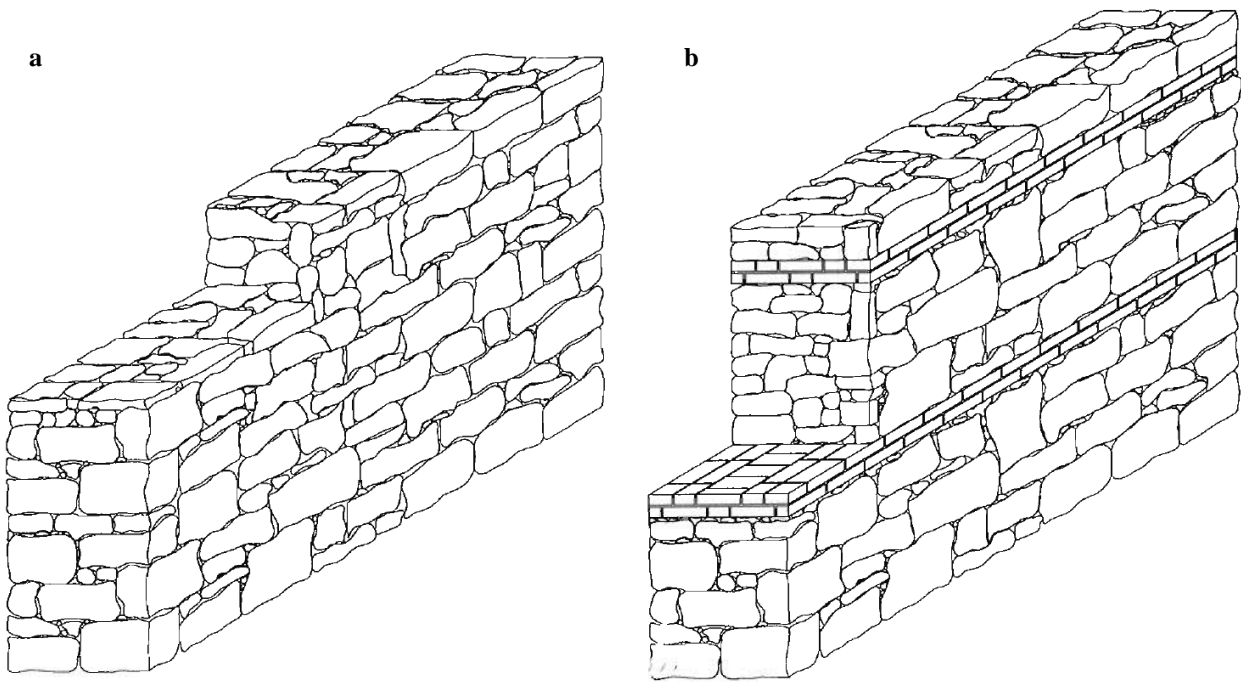


Fig. 4.5 – GF. Coursed random masonry realized with San Giovanni in Fiore granite, San Giovanni in Fiore (CS). Mixed masonry is composed by pebbles and rubbles of different sizes with single brick courses.



Figs. 4.6 a, b, c – DG. Coursed random masonry realized with Grisolia stone, Scalea (CS). Stone masonry with semi-squared blocks (a), mixed masonry composed by single brick courses (b) and double courses (c).



Figs. 4.7 a, b – CS. Coursed random masonry realized with San Lucido calcarenite, San Lucido (CS). Stone masonry with semi-squared blocks (a), mixed masonry composed by double brick courses (b).

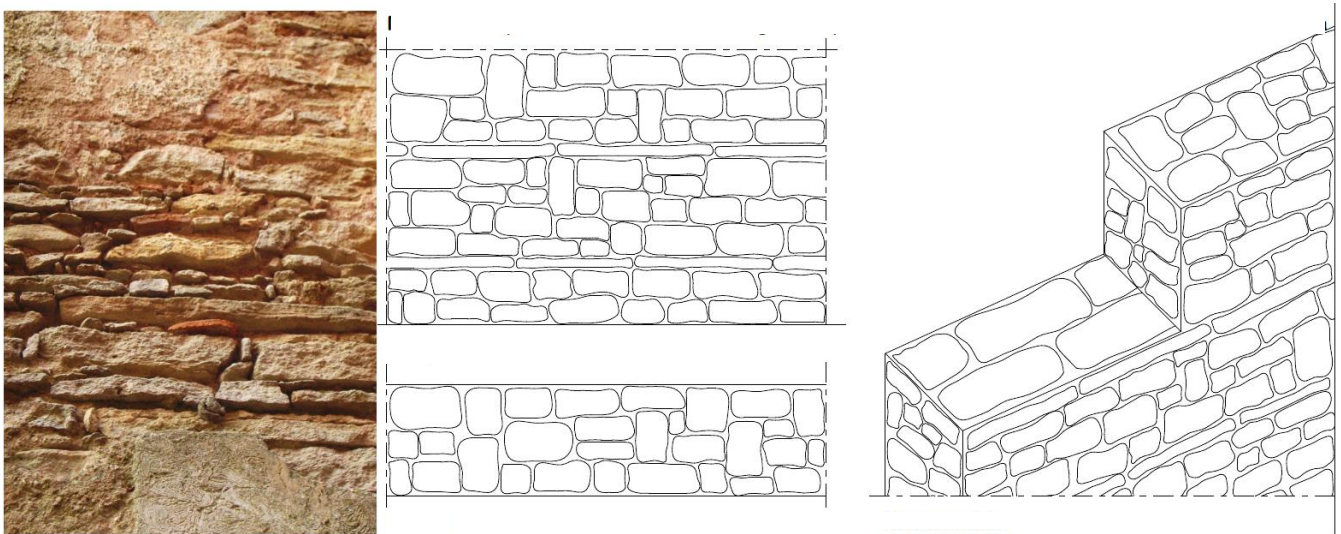


Fig. 4.8 – AF. Coursed random masonry realized with Fuscaldo sandstone, Fuscaldo (CS). Stone masonry with semi-squared blocks and single stone courses realized by extended and thin stone elements.

4.3 Ashlar masonry

The stone masonry in which finely stones are dressed and squared is known as *ashlars masonry*.

In this masonry the courses are of uniform height, all the joints are regular, thin and have uniform

thickness. As this type of masonry is much costly as it requires dressing of stones, it has been found only in the old towns of Fuscaldo and is the typical masonry of only religious or architectural buildings (Fig.4.9 - AF). In fact, this kind of masonry is totally absent for the vernacular architecture.

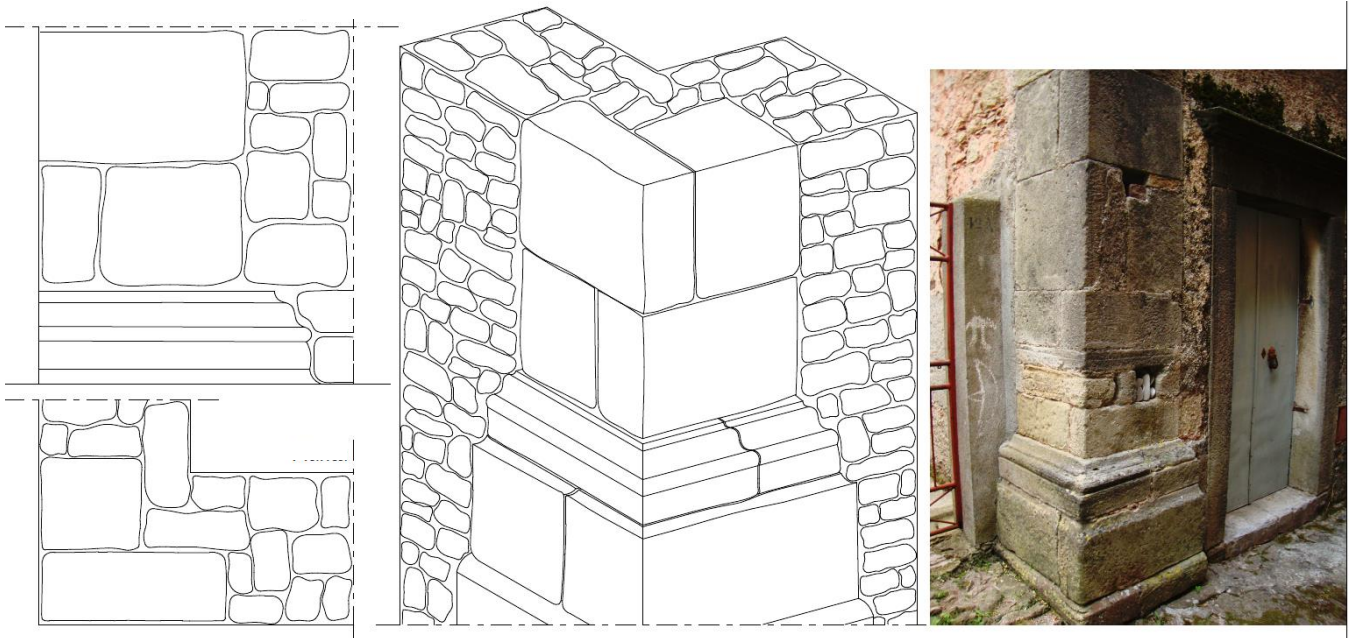


Fig. 4.9 – AF. Ashlar masonry realized with Fuscaldo sandstone, Fuscaldo (CS). Stone masonry with ashlar and ornamental stone elements to strengthen building corners.

5. Methods and materials

To understand stone behavior, it is important to have a thorough knowledge of its properties. For this purpose, many tests on “fresh” stone materials, belonging to active quarries, have been performed. Sample collection and preparation is explained in the following paragraph (5.1).

The most important characteristics of the stones which have been investigated are: petrographic, mineralogical and chemical composition, texture, anisotropy, homogeneity, physical properties, features of its void space, strongly connected to hydric properties, surface and mechanical properties. All these properties have been related to the anisotropy planes in order to obtain the variability of stone properties along the three spatial axes. Applied methodologies for the determination of these properties are described in the second part of this chapter (5.2).

5.1 Sampling and sample preparation

Specimens come from active quarries and outcrops of Cosenza Province, as described in the Paragraph 3.4. For each quarry or outcrop, 10 blocks for each lithotype have been extracted. For the “San Giovanni in Fiore granite” blocks belong to the unweathered boulders of the active quarry of “Colle dei Fiori” in San Giovanni in Fiore (Upper Paleozoic); for the “Pietra di Grisolia” to the active quarry in Grisolia in “Località Anania” (Mesozoic); for the “San Lucido calcarenite” to the active quarry of “Motta Lupo” in San Lucido (Upper-middle Miocene); for the “Fuscaldo sandstone” to the outcrops in Fuscaldo in “Località Scarcelli” (Upper Miocene). The sampling has been carried out, for each quarry, on the same unweathered stratigraphic horizon or on similar unweathered boulders (only in the case of San Giovanni in Fiore granite), in order to preserve a compositional homogeneity of the samples.

Stones were cut in the laboratory with a diamond cutting wheel to separate from blocks:

- fragments for the preparation of thin sections of 30 μm thick;
- cubic specimens of 5 cm and 10 cm sides;
- disks specimens/cylinders of 5x1cm and 6x3 cm;
- prismatic specimens of 5x5x30 cm;
- aggregates of 11.2-8 mm, 8-4 mm, 6.3-10 mm and 4-6.3 mm.

Thin sections were utilized for the petrographic description; cubic and prismatic specimens were employed for physical and mechanical tests; disks for the tensile tests and the hydric properties (natural hydrophobicity); aggregates for mechanical tests such as Los Angeles and Micro-Deval tests, performed only on San Giovanni in Fiore granite specimens.

Lengths of the specimens were measured in the three orthogonal directions with a Mitutoyo digital caliper with a precision of ± 0.01 mm (Fig. 5.1).



Fig.5.1 Mitutoyo digital caliper

Specimens were named with a letter and a progressive number. For the “San Giovanni in Fiore granite” the letters GF were used, for the “Pietra di Grisolia” the letters DG, for the “San Lucido calcarenite” the letters CS and for the “Fuscaldo sandstone” the letters AF. Abbreviations employed for the mean values for each lithotype are:

- GF for the San Giovanni in Fiore granite;
- DG for the Grisolia stone (limestone);

- CS for the San Lucido calcarenite;
- AF for the Fuscaldo sandstone.

Specimens were also marked with orthogonal axes of the co-ordinate system (X, Y, and Z axes) referring to the internal fabric of the stone (if visible) and to the internal orientation of the foliation, obtained by the ultrasonic test (Fig. 5.2).

Fabric co-ordinates of granite were related to the dominant sets of joints expressed here in the terms used by quarrymen (Hills, 1972; Prikryl, 2001). The X-direction is perpendicular to the direction of hardway plane which is the most resistant plane in plutonic stones. The Y-direction is oriented perpendicular to the grain plane, and the Z-direction is normal to the plane of the easiest splitting (rift plane). In the past, the oldest ashlar, were extracted from the subaerial granite boulders along the rift plane.

For the other specimens, the sedimentary stones (limestone, calcarenite and sandstone), fabric co-ordinates X, Y, Z were marked as: the X-direction is parallel to the lineation, the Y-direction is normal to the lineation in the plane of foliation and the Z-direction is perpendicular to the foliation and lineation.

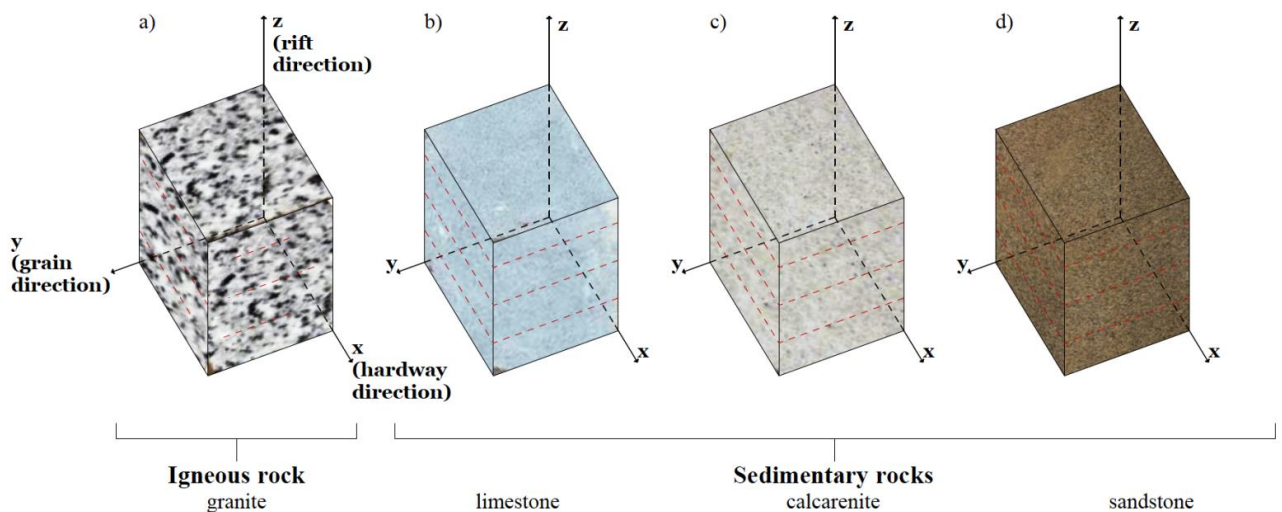


Fig. 5.2 Orientation of the specimens of (a) San Giovanni in Fiore granite, (b) Grisolia stone (c) San Lucido calcarenite, (d) Fuscaldo sandstone. For the granite: X = hardway direction; Y = grain direction; Z = rift direction.

5.2 Techniques applied for the material characterization (NDT and laboratory tests) and rock fabrics (anisotropy)

Performed tests belong to the NDT (non-destructive), MDT (micro-destructive) and laboratory tests.

The use of NDT and MDT tests has many advantages. In the cases of in-situ analysis, tests are performed without sampling and without alteration (or less alteration in the case of MDT) of the analyzed material surfaces. Another advantage consists in the portability of instruments, which can be used almost. Moreover, in the last years, various non-destructive investigation methods have been successfully tested for the maintenance and preservation of buildings and historical monuments (Binda *et al.*, 2007). Tests on stone samples also provide direct, more reliable information about material properties and their changes due to weathering. In the case of laboratory tests, using NDT or MDT tests, it is possible to reanalyze the same samples for different techniques comparing results.

Laboratory tests have been also carried out for the petrographic, chemical and mineralogical characterization. Tests were performed in the following laboratories: Petrophysics Laboratory IGEO (CSIC-UCM), “Centro Mixto del Consejo Superior de Investigaciones Científicas (CSIC) y de la Universidad Complutense de Madrid (UCM)” of Madrid (Spain) for the petrophysical stone characterization; Department of Biology, Ecology and Earth Sciences of the University of Calabria (Italy) for the chemical-mineralogical characterization and for durability tests; Department of Civil Engineering and Department of Territory and Environment of the University of Calabria (Italy) for the mechanical characterization; IPG Laboratory “Istituto Prove Geotecniche” (Geotechnical test Institute) of Castrolibero (Italy) for the mechanical characterization on San Giovanni in Fiore aggregates.

5.3 Petrographic description

The petrographic analyses were performed by means of a Olympus BX 51 polarized light microscope (PM), fitted with a DP 12-coupled camera, on 12 uncovered and polished thin sections (3 thin sections for each lithotype). These analyses aimed to identify primary minerals and to petrographically describe stone samples (UNI EN 12407, 2007).

Thin sections, with a thickness of 30 μm , were cut parallel to the three spatial directions in order to investigate the grain shape and crystals orientation.

GF thin sections were also analyzed in order to highlight intracrystalline and intercrystalline microcracks along the three spatial directions, counting the total number of microcracks and their prevalent orientation. The presence of voids in the stone, especially microcracks, affects physical and mechanical properties and may be responsible for the anisotropy detected in many granites (McWilliams, 1966; Engelder & Plumb, 1984; Almeida *et al.*, 1998).

All GF thin sections were characterized by means of an Zeiss Axiolab 40 polarized light microscope (PM), fitted with a DP 12-coupled camera (6 V/2.5 \AA) and an Olympus DP-Soft software (version 3.2) (Fig. 5.3); to obtain the mosaics of micrographs the Image Software Processor “Photoshop” has been used. The mosaic comprised approximately 50 micrographs measuring 2 cm^2 . Then, a colour inversion has been produced, followed by the image transformation to high dynamic range (HDR) to highlight more clearly the luminance variations between the lightest and the darkest areas and to individuate the microcracks. In the HDR converted image, the inter- and the intracrystalline microcracks have been marked with the yellow and the red colour, respectively. Five equidistant vertical scale lines were drawn for the micromosaic of the XZ and YZ planes. For the XY planes these lines, of a length of approximately 1 cm, were horizontal lines. The total number of microcracks intersected with these lines has been calculated, distinguishing between inter- and intracrystalline microcracks. The

linear microcrack density (LMD) was found by dividing the total number of microcracks with the lines lengths (Sousa *et al.*, 2005; Freire-Lista and Fort, 2016). According to the obtained LMD value has been classified the weathering class of GF, taking into consideration the classification based on the LMD, proposed by Sousa *et al.* (2005).

Table 5.1. Classes of weathering based on linear crack density (Sousa *et al.*, 2005).

Linear microcrack density (LMD)	Degree	Rock weathering class
<1.5	I	Sound
1.5-3.0	II	Slightly weathered
3.0-4.5	III	Moderately weathered
4.5-6.0	IV	Weathered
>6.0	V	Highly weathered



Fig. 5.3. Petrographic analysis: Zeiss Axiolab 40 polarized light microscope in transmitted polarized light – Department of Petrology of the Complutense University of Madrid (Spain).

5.4 Chemical and mineralogical characterization

The most important internal factors that determine the deterioration of a material are its mineralogical and chemical composition.

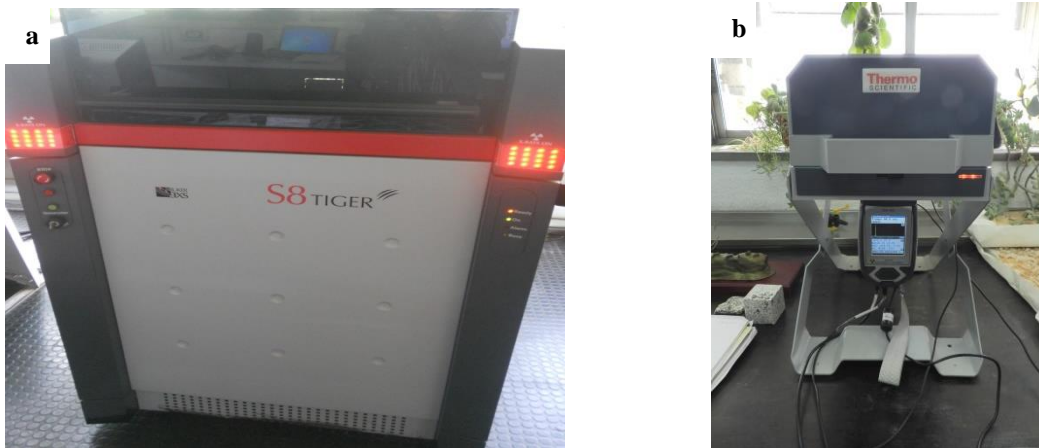
The qualitative mineralogical composition of samples was determined through X-ray diffraction (XRD). The XRD analysis was carried out using a Bruker diffractometer D8 Advance (Fig. 5.4) with a

tube of copper. The obtained diffractograms were studied through a software for the qualitative and quantitative analysis (PC-ADP DIFFRACTION).

The chemical composition was obtained by means of X-ray fluorescence (XRF) analysis using a Bruker S8 Tiger XRF spectrometer (Fig. 5.5 a) and a portable XRF instrument – Niton XL3 - ThermoScientific (Fig. 5.5 b). Anions and cations were detected by means of ion chromatography analysis using the tester Metrohm 761 Compact IC (Fig. 5.6). 16 powdered samples (4 for each lithotype from disks of 5x1cm) were accurately weighed, leached, added with 10 ml aliquot of de-ionized water and subjected to test anions (fluoride, nitrite, chloride, nitrate, sulphate) and cations (sodium, potassium, calcium). Two/three milliliters sample were injected into the chromatography machine, through a 0.45 μm filter and analyzed. Measurements for both anions and cations were standardized and expressed in ppm.



Fig. 5.4. X-ray diffraction analysis: Bruker diffractometer D8 Advance.



Figs. 5.5 a, b. X-ray fluorescence analysis: Bruker S8 Tiger XRF spectrometer (a); portable XRF instrument – Niton XL3 - ThermoScientific (b).

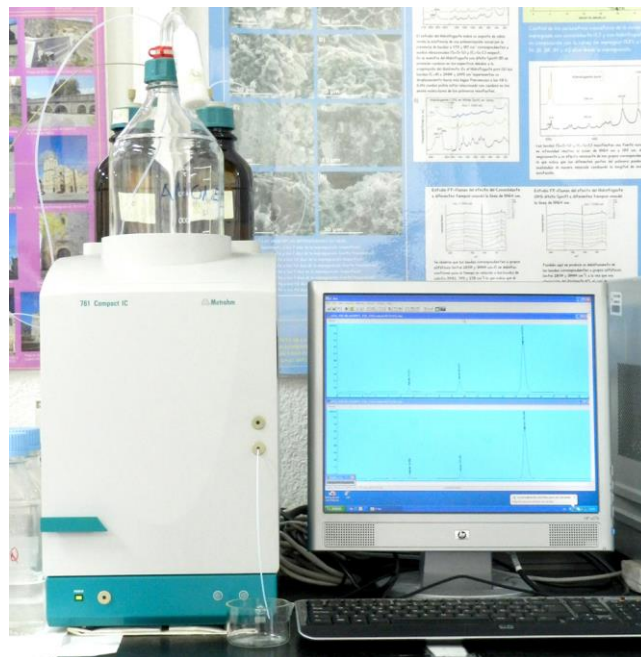


Fig. 5.6. Ion Chromatography analysis: Metrohm 761 Compact IC tester.

5.5 Surface properties

Surface properties such as colour, texture, brightness and roughness are very important for the building stones behavior and durability. These properties also influence the aesthetical and the economic value of the stones themselves. In this chapter the chromatic parameters of the four types of lithotypes

have been investigated in order to describe colour properties through mathematic parameters. Colour is a very important characteristic, especially for decorative stones, conditioning their economic value.

5.5.1 Chromatic parameters

Colour constitutes a fundamental petrophysical characteristic of the four different types of investigated stones (Fort, 1996). Colour is, also, one of the most important properties of the ornamental or monumental stones. Its change, during the degradation, seriously influences the aesthetical value of the stone. As colour can be a very subjective characteristic, it is necessary to quantify it in order to avoid the mistakes of the human eye (MacAdam, 1985). There are many colour charts like that of Munsell, which permit a semi-quantitative colour analysis, or instrumental techniques (colourimeters or spectrophotometers) for quantitative analysis (Grossi *et al.*, 2007).

In this study the chromatic analysis was carried out with the aid of a spectrophotometer (Minolta CM-700d) (Fig. 5.7) with a Colour Data Spectramagic™ NX CM-S100W Software, on the surface specimens.



Fig. 5.7. Spectrophotometer Minolta CM-700d

Thirty readings were taken from each cubic specimen (32 samples, 8 specimens for each lithotype), in particular five readings for each face of the cube (Fig. 5.8) to provide an average result that could be representative of each series of tested samples (UNI-EN 15886, 2010).

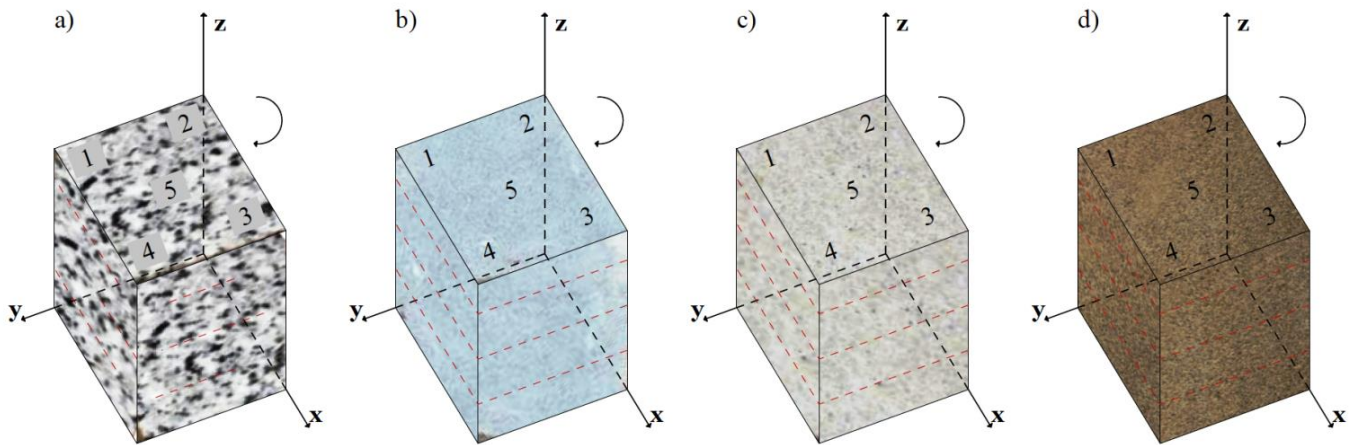


Fig. 5.8. Readings orientation of colour measurements. (a) San Giovanni in Fiore granite, (b) Grisolia stone (c) San Lucido calcarenite, (d) Fuscaldo sandstone.

The method which has been utilized for the colour test was the CIE 1976 $L^*a^*b^*$ and the CIELCH systems (CIE= Commission Internationale de l'Eclairage = International Commission on Illumination), that better represent human sensibility to colour than other colour encoding systems (Grossi *et al.*, 2007). The CIE 1976 $L^*a^*b^*$ chromatic scale was used to measure parameters L^* , a^* , and b^* . Through this method, colour space can be visualized as a three dimensional space, where every colour can be uniquely located. The location of any colour in the space is determined by its colour coordinates; L^* , a^* , and b^* , the variable L^* represents the lightness within a range of values between 0 (black) and 100 (white), the a^* parameter corresponds to a green/red axis (with a range between -60: green and +60: red) and b^* to a blue/yellow axis (with a range between -60 and +60). The CIELCH system is an alternate method, based on L^* , C^* (chroma), and h^* (hue) coordinates. In this method, the L^* coordinate is the same as in $L^*a^*b^*$, while the C^* and h^* coordinates are computed from the a^* and b^* coordinates. The same colour is still in the same location in the colour space, but there are two

different ways to describe its position ($L^*a^*b^*$ or $L^*C^*h^*$). The $L^*C^*h^*$ colour space is also three dimensional, but the colour is located using cylindrical coordinates, as follows:

L^* - the lightness coordinate, same as in $L^*a^*b^*$.

C^* - the chroma coordinate, the distance from the lightness axis, calculated by the equation:

$$C^* = \sqrt{(a^{*2} + b^{*2})}$$

h^* - the hue angle, expressed in degrees, with 0° being a location on the $+a^*$ axis, then continuing to 90° for the $+b^*$ axis, 180° for $-a^*$, 270° for $-b^*$, and back to $360^\circ = 0^\circ$.

For testing specimens the attributes of chroma (C^* : saturation or colour purity) from the polar system CIELCH have been utilized.

Moreover, WI and YI, the whiteness and yellow indices, respectively (ASTM, [E313-1998](#)), have been measured. According to ASTM Standards the whiteness index indicates the degree of departure of an object colour from that of a preferred white while the yellowness index indicates the degree of departure of an object colour from colourless or from a preferred white, toward yellow.

Furthermore, for each sample the parameter B^* (the brightness) has been evaluated.

The standard test conditions were: medium diameter of 1 cm according to the paragraph 8.2 of UNI-EN 15886:2010 for heterogeneous materials (such as granite), 10° observer (CIE 1964) and standard illuminant D65, equivalent to daylight with ultraviolet radiation. The environmental conditions for the readings were: dry test specimens, dried at a temperature of 70°C for 24 hours and after 1 hour in the desiccator, tested at an environmental temperature of $T=24 \pm 1^\circ\text{C}$ and a relative humidity of $\text{RH}= 53 \pm 5\%$.

For the granite samples, the colour of some specimen surfaces tends to yellow shades (increase b^*) due to the presence of natural alteration of granite in nature for biotite oxidation. So, there were separated measurements of the two kind of surfaces, in natural and altered, in order to calculate ΔE

(total/global colour variation), the chromatic variations between two measurements ($L_1^*a_1^*b_1^*$ and $L_2^*a_2^*b_2^*$) (Fig. 5.9) which allows to set a numerical comparative value between these different surfaces.

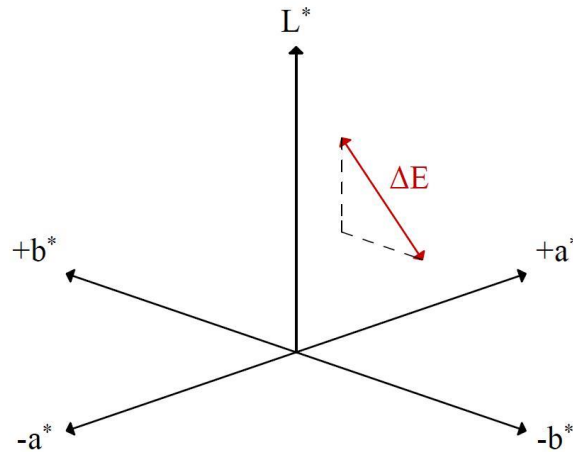


Fig. 5.9. ΔE value representation as the distance between two points in a three-dimensional colour space.

The determined value is based on the following mathematical formula:

$$\Delta E_{2,1}^* = \sqrt{(\Delta L^{*2} + \Delta a^{*2} + \Delta b^{*2})}$$

where:

- $\Delta L^* = L_2^* - L_1^*$
- $\Delta a^* = a_2^* - a_1^*$
- $\Delta b^* = b_2^* - b_1^*$

The final value (ΔE^*) is obtained by calculating the average of all measured points. It is understood that the change is visible to the human eye when it exceeds the value 5, although it may vary according to different authors (Perez Ema *et al.*, 2013).

According to UNI-EN 15886:2010 it was calculated the chromatic variation not only with ΔE^* but also with ΔE_{94}^* , introduced by the CIE in 1994. This formula uses the L*C*h*-notation for calculating colour differences and introduces k-coefficients as parametric factors and S-coefficients to

improve chromatic variations (Habekost M., 2013). Changes in chroma can also be expressed in ΔC^* and in lightness as ΔL^* (Schilling M.R., 1993) and the colour difference in ΔE^*_{94}

$$\Delta E^*_{94} = \sqrt{\left(\frac{\Delta L^*}{k_L S_L}\right)^2 + \left(\frac{\Delta C^*_{2,1}}{k_C S_S}\right)^2 + \left(\frac{\Delta H^*_{2,1}}{k_H S_H}\right)^2}$$

The final value (ΔE^*_{94}) is obtained by calculating the average of all measured points.

5.6 Petrophysical properties

Porosity

The porosity of a stone is defined by the ratio of the pore volume (pores and open cracks) to the volume of the whole stone. Porosity has a direct and indirect effect on most of the physical properties of stones and is considered one of the most important stone parameter (Siegesmund & Dürrast, 2014).

Porosity can be determined through different methods that allow to measure different pore diameter distributions in different ranges of pores.

Porosity can be related to two different types: the porosity accessible to water and the open porosity. The porosity accessible to water, of primary interest for weathering processes (Weiss, 1992) has been determined by the non-destructive test of the water absorption by total immersion under vacuum conditions, based on the Archimedes principle which considers all pore spaces accessible to fluids and gases. The open porosity has been calculated by the destructive test of the mercury intrusion porosimetry. This test also allows determining the size of pores and the pore radius distribution in a range of 0.001 to 400 micrometers approximately.

Obtained porosity values have been compared to classification in the literature. Concerning the effective porosity value, it has been taken into account the classification of von Moos and De Quervain (1948) that classifies stones in: compact ($p_o < 1\%$); few pores ($1 < p_o < 2.5\%$); slightly porous ($2.5 < p_o < 5$

); significantly porous ($5 < p_o < 10$ %); many pores ($10 < p_o < 20$ %); high amount of pore space ($p_o > 20$ %).

According to several previous studies, typical porosity values are the following (Mosch & Siegesmund, 2007): porosity from 0.1% to 29% for sedimentary stones (sandstones); from 1% to 20% for carbonate stones (limestones, ooliths, dolomites, breccias); from 1% to 50% for volcanic stones (andesites, basalts, rhyolites, dacites, trachytes and tuffs with the highest values); from 0.05% to 1.65% for plutonic stones; $\leq 1\%$ for some metamorphic stones. The majority of the pore spaces in plutonic and metamorphic stones can be defined as crack porosity (Siegesmund & Dürrast, 2014).

Regarding the pore size, the classification of De Quervain (1967) has been used, that distinguishes pores into: micropores ($< 5\mu\text{m}$); mesopores ($5-200\mu\text{m}$); macropores ($200-2000\mu\text{m}$); large pores ($> 2000\mu\text{m}$). The pore-size distributions of stones can be classified, according to Ruedrich & Siegesmund (2006), into three types: unimodal; uneven; bimodal. For the capillarity and fluid transport in the pore space, the pores with a radius in the range of 1 mm to ca. $0.1\ \mu\text{m}$ are of great significance. Micropores are important for questions related to the drying of stones and for the penetration of substances with a defined molecule size for conservation and impregnation. Stones with a smaller percentage of micropores can be more resistant to ageing tests as the salt crystallization test than those with a larger percentage. In the macropores, however, water loses its interconnectivity and, thus, can no longer move freely (Siegesmund & Dürrast, 2014).

5.6.1 Porosity accessible to water and real and bulk densities

The density and the porosity are strongly connected parameters. By using the classical water imbibition under vacuum method (water saturation method), the apparent density and the open porosity can be measured (Fig. 5.10).

As known the density of a material is the ratio of the mass to the volume. Real or skeletal density refers to the density of the solid fraction excluding the voids while for the apparent or bulk density pores are included. The difference between the real and the apparent density is strictly related to the porosity of the material and its ratio provides the compactness index.

Real and bulk density and open porosity, have been determined through the water absorption test by total immersion under vacuum conditions. 32 cubic-shaped specimens (8 samples for each lithotype) were dried at a temperature of (70 ± 5) °C until reached constant mass (UNI EN 1936, 2001). After drying, samples were saturated by imbibition in an evacuation vessel during 24 h, by complete immersion during a day in outgassed water, at a constant pressure of 2.7 kPa (RILEM, 1980). Real and bulk density, porosity, saturation and compactness values were obtained calculating three mass-values of samples: dried (m_d), saturated under vacuum (m_s) and saturated and weighted in water (m_h) with the following equations:

$$\rho_{sk} = \frac{m_d}{m_s - m_h} \times \rho_{water}$$

$$\rho_b = \frac{m_d}{m_d - m_h}$$

$$p_o = \frac{m_s - m_d}{m_s - m_h} \times 100$$

$$I_c = \frac{\rho_{sk}}{\rho_b}$$

$$W_{vac} = \frac{m_s - m_d}{m_d} \times 100$$

where:

- ρ_{sk} is the real or skeletal density (g/cm^3);
- ρ_b is the apparent or bulk density (g/cm^3);
- ρ_{water} is the density of water = 0.998 g/cm^3 ;

- p_o is the open porosity (%);
- I_c is the compactness index as the ratio of the two densities;
- W_{vac} is the water absorption under vacuum (%).



Fig. 5.10. Evacuation vessel employed for the water absorption by total immersion test under vacuum.

5.6.2 Mercury intrusion porosimetry (MIP)

The pore diameter distribution, the total cumulative mercury volume, the average pore diameter, the open porosity have been determined by using mercury injection porosimetry to find out the pore size and the pore diameter distribution of 12 samples (3 specimens for each lithotype). This test, moreover, furnishes information about specific surface of pores and apparent and skeletal density. The last ones have been compared to those determined by performing the first test (water absorption under vacuum). Conversely than the first method performed, this test is defined as destructive, because requires a small amount of sample which then can not be further used as it is impregnated with mercury.

This method is based on the principle of measuring the volume of mercury penetrating a dehydrated and degassed sample under increasing pressure. This technique is based on the use of a non-wetting fluid that can be pressurized in order to penetrate into the void space and on the fact that the geometry of the pores can be assimilated to cylinders. The equation for the determination of the pore diameter distribution is the equation of Washburn (Washburn, 1921):

$$D = \frac{-4\gamma\cos\theta}{P}$$

where: D is the pore diameter; γ the surface tension at the liquid interface; θ the liquid–solid contact angle; P the applied pressure (Dubois et al., 1998). Test was performed with an Autopore IV Micromeritics mercury porosimeter (Fig. 5.11).



Fig. 5.11 Autopore IV Micromeritics mercury porosimeter.

5.6.3 Air permeability

Air permeability describes how a fluid (air) flows through a specific section of porous media. The air permeability test has been performed by the handheld air permeameter “TinyPerm II” (Fig. 5.12). It consists of a rubber nozzle, that was pressed against the specimen and withdrew a specific volume of air from it with a single stroke of a syringe. As air is pulled from the sample, a microcontroller unit simultaneously monitored the syringe volume and the transient vacuum pulse created at the sample surface. To optimize measurements, it was put a seal between probe tip and sample surface, to prevent leakage and the device was mounted in an upright static position to provide reproducible testing conditions and a uniform contact pressure during laboratory test. According to the TinyPerm II operational manual, TinyPerm values (T) registered by the microcontroller, were linked to air permeability through this equation:

$$T = -0.8206\log_{10}(K)+12.8737$$

where K is the permeability in millidarcys (mD). The permeability measurement range is from approximately 10 millidarcys to 10 darcys, with recommended measuring period from 1 minute to 4 hours (Filomena C.M., 2014). Test was carried out on dried cubic specimens, according to standards recommendations (RILEM, 1980), along two principal anisotropic directions X and Z. The test was performed on 32 cubic specimens (8 for each stone type).



Fig. 5.12. Air permeameter TinyPerm II.

5.7 Hydric properties

Hydric properties represent the main factors involved in the majority of the weathering processes (Snethlage, 1984; Weiss, 1992; Siegesmund & Dürrast, 2014). The presence of water is responsible of many decay processes such as salt crystallization, frost, hygric expansion, dry-wet cycles and has an important role related to the durability of building stones. The effect of water on materials is strictly connected to the pore space and pore system (Siegesmund & Dürrast, 2014) and to the anisotropy behavior of building stones (Poschold, 1990; Ruedrich *et al.*, 2010).

Four elemental properties related to water transport within the stone have been determined according to the following standards: capillarity water absorption (UNI-EN 1925: 2000); water absorption (UNI-EN 13755:2002; RILEM, 1980; ICR CNR NORMAL 7/81) and desorption at atmospheric pressure (ICR CNR NORMAL 29/88); and natural hydrophobicity determined by water static contact angle (UNE-EN 15802:2010). The water adsorption at atmospheric pressure is determined by the interconnected pores (Bell & Dearman, 1988; Tuğrul, 2004). The water desorption process has an important role for dry cycles, especially for the salt crystallization (Ruedrich and Siegesmund, 2006). The desorption is influenced by the evaporation rate from the surface and by the water transport in the material (Pender, 2004). The hydrophobicity is influenced by the water transport on the material surface and on its roughness. It is very important to evaluate the effect of hydrophobic stone treatments (Snethlage & Wendler, 1996).

In the two first tests, cubic specimens were tested (5 cm side). In the other two tests disks of 5x1 cm were used. In the capillarity test, the coefficients were obtained in the two principal directions (X and Z), and the final values were considered as the average of the measurements in all the samples and directions investigated.

5.7.1 Capillary water absorption – (Infrared Camera)

The procedure of the test has been carried out according to the UNI-EN 1925: 2000 on 32 cubic specimens (8 samples for each stone type), orientated along the two anisotropic directions (X and Z). Specimens have been placed in water of 3 (± 1) mm height and the weight increase has been measured continuously at the following time intervals: 1, 3, 5, 10, 15, 30, 60, 180, 480, 1.440, 2.880 minutes until reach constant mass (Fig. 5.13).

The weight increases have been plotted in graphs in order to obtain the capillary water absorption curve for each material. Then, starting with the real curves, the curves with linear sections have been calculated and plotted. The capillary coefficients correspond to the slope of the initial part of the curve. Capillary coefficients, parallel and perpendicular to the anisotropy planes (X and Z, respectively, obtaining C_2 and C_1 , respectively too) and the average coefficient C , have been compared to the classification of Snethlage (Siegesmund & Dürrast, 2014), in order to describe the capillary water absorption behavior of the materials tested. Concerning to the coefficient C , it can be defined the stone with a: slightly absorbing ($C < 0.5 \text{ kg/m}^2\text{h}^{0.5}$); medium absorbing ($0.5 < C < 3.0 \text{ kg/m}^2\text{h}^{0.5}$); highly absorbing ($C > 3.0 \text{ kg/m}^2\text{h}^{0.5}$).

The capillary coefficients C_1 , C_2 and C have been calculated with the equation:

$$C_1, C_2 \text{ or } C = \frac{m_i - m_d}{A * \sqrt{t_i}}$$

where:

- m_i is the weight at the i moment (g);
- m_d is the dry weight at the time 0 (g);
- A the surface of the sample in contact with water (m^2);
- t_i is the time at the i moment (s).

Moreover test has been registered by an infrared camera Thermacam B4 - Flir Systems in order to visualize how water it is absorbed in relation to the anisotropy.

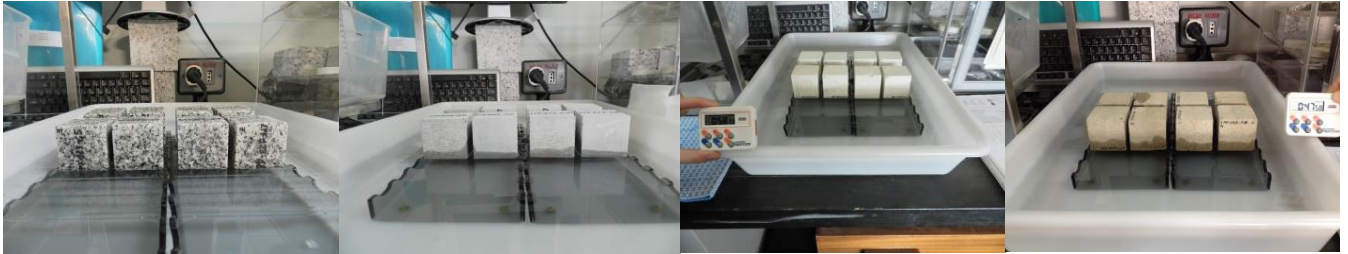


Fig. 5.13. Capillary water absorption test. From left to right: granite of San Giovanni in Fiore; Grisolia stone; San Lucido calcarenite; Fuscaldo sandstone.

5.7.2 Water absorption/desorption at atmospheric pressure

Water absorption

The aim of this test is to evaluate the quantity of water that the stone is able to absorb by complete immersion under atmospheric pressure. The test has been carried out according to the UNI-EN 13755:2002 European standard and to the RILEM 1980 and ICR CNR NORMAL 7/81. 32 cubic specimens (8 samples for each stone type), after dried, have been gradually covered by distilled water: at the time t_0 until the half of their height; at $t_0 + 60$ minutes till the $2/3$ of their height; at $t_0 + 120$ minutes have been completely covered. For each time interval the increase of weight has been registered until reach the constant mass at the complete saturation. The weights have been plotted through curves as a function of time in order to describe the water absorption behavior and the kinetics of the process.

The water content absorbed ($W_{i(Ab)}$) has been calculated with the following equation:

$$W_{i(Ab)} = \frac{(m_i - m_d)}{m_d} \times 100$$

where:

- m_d : weight of the dried sample;

- m_i : weight of the sample at the time i .

The water absorption coefficient (W_{Ab}) or imbibition coefficient has been calculated with the following equation (ICR CNR NORMAL 7/81): :

$$W_{Ab} = \frac{(m_s - m_d)}{m_d} \times 100$$

where:

- m_d : weight of the dried sample at the time t_{final} ;
- m_s : weight of the saturated sample at the time t_0 .

The saturation of the samples, at the time intervals i , has been evaluated as:

$$S_{i(t)} = \frac{(m_i - m_d)}{(m_s - m_d)} \times 100$$

while the saturation coefficient (S) or saturation degree (Hirschwald, 1912) has been calculated as the ratio of the water absorption at atmospheric pressure (W_{Ab}) and the water absorption under vacuum (W_{vac}), using the following equation:

$$S = \frac{W_{Ab}}{W_{vac}}$$

The saturation coefficient is important for the evaluation of the stone resistance to weathering. It describes how much of the total pore space is accessible to water absorption, thus providing a value for the frost resistance evaluation. For frost resistance, Hirschwald (1912) proposed the following guideline values using the saturation coefficient: when $S < 0.75$, the stone is not weathered and is frost resistant; for values ranging between 0.75 and 0.90, it is uncertain, and further investigations are necessary; when $S > 0.90$, the stone is weathered and is not frost resistant (Siegesmund & Dürrast, 2014).

Water desorption

The drying characteristic of a building stone is a very important factor related to the weathering resistance. Drying of wet building stone is a multistage process that is mainly governed by air humidity and movement. The faster and the more thoroughly a stone is dried, the lower the probability that the stone will experience frost or salt damage (Siegesmund & Dürrast, 2014). The theory of the drying of building materials has been studied by many authors (Vos, 1978; Snethlage, 1984; Buj *et al.*, 2007; Siegesmund & Dürrast, 2014) that describe the desorption behavior as a curve composed by two parts: the first part is characterized by a rapid decrease in moisture content with a linear trend; the second one is characterized by a less slope. This first linear trend represents the period when sufficient moisture is transported to the surface by capillarity to keep up a continuous evaporation. During the second phase of the drying process, the capillary moisture transport is completely replaced and determined by water vapour transport within the stone (Ruedrich & Siegesmund, 2006), related to the evaporation of inner surfaces of the pores. The critical moisture content can be defined graphically and is given by the changing point of the curve and the velocity of the drying process is given by the ratio between the critical moisture content and the moisture content in total saturation conditions.

The water desorption was determined following the Italian standard ICR-CNR NORMAL 29/88. After reaching the saturated conditions through the water absorption test, the same 32 cubic samples (Fig. 5.14) have been dried under constant laboratory conditions (temperature and relative humidity).

Their weight loss has been registered in the same given time intervals of the absorption test performed and plotted as a function of time.

The evaporated water content ($W_{i(Ds)}$) has been calculated using the following equation:

$$W_{i(Ds)} = \frac{(m_i - m_s)}{m_s} \times 100$$

where:

- m_i : weight the sample at the time i ;
- m_s : weight of the saturated sample at the time t_0 (at the starting time of the test).

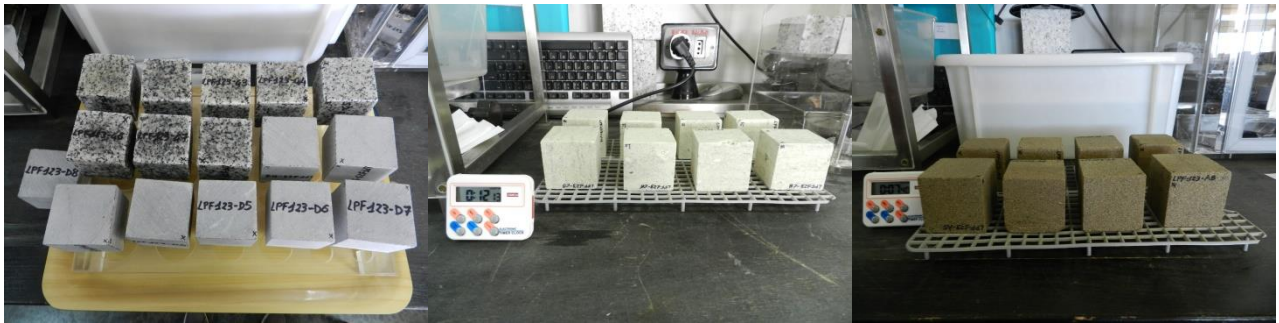
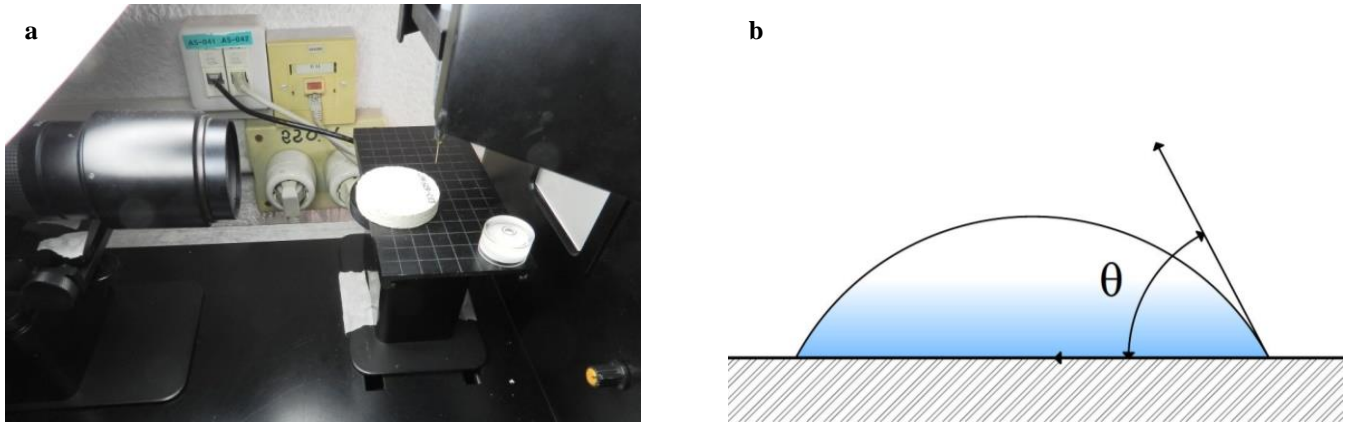


Fig. 5.14. Water desorption test. From the left to right: granite of San Giovanni in Fiore and Grisolia stone; San Lucido calcarenite; Fuscaldo sandstone.

5.7.3 *Natural hydrophobicity by water static contact angle*

This test measures the degree of the hydrophobicity of materials and is especially performed in the field of the cultural heritage for evaluating the durability or the effectiveness of water repellent products (Ferreira Pinto & Delgado Rodrigues, 2000).

For this study, the test of the water static contact angle has been performed in order to evaluate the degree of natural hydrophobicity of the samples, according to UNE-EN 15802:2010 standards. The test has been carried out on 24 disks specimens, 6 disks for each stone type (5x1cm), with a water contact angle analyzer Phoenix 300 Seo - Surface Electro Optics (Fig. 5.15 a) that measures the angle between the specimen surface and the tangent to the water drop, in the contact point (Fig. 5.15 b). If the contact angle between water droplet and stone surface is zero, it means that the water droplet has been completely spread out and the material has a hydrophilic surface. On the contrary, if the contact angle between the droplet and the surface is above 90° or 180° (ideal case), the material does not absorb water on the surface for short times and the water droplet cannot spread out because the attractive forces acting between the water molecules and the stone surface are blocked by the hydrophobic surface.



Figs. 5.15. Static contact angle test: disk of San Lucido calcarenite sample (a); schematic graph representing the angle (θ) between the specimen surface and the tangent to the water drop, in the contact point (b).

5.8 Mechanical properties

Anisotropy

All tests have been carried out with a special attention to the anisotropy. Anisotropy has an important role in the stone characterization, behavior and durability, because material properties may exhibit a distinct directional dependence and variability along the anisotropic directions (Benavente *et al.*, 2009). This is very important for the practical application of natural building stones. These include the tensile, compressive, and flexural strength, the abrasion strength, thermal properties, susceptibility to weathering, and many more. Ascertaining anisotropy in natural stone and how it develops is of utmost importance, since this information is essential to determine the following issues (Fort *et al.*, 2011):

- a) how the stone should be quarried and most efficiently processed;
- b) the quality of the stone products and their suitability for use as ashlar or ornamental elements;
- c) its placement/arrangement on buildings.

This is the reason why the use of natural stone in construction is influenced by its anisotropy index. Likewise, the directions of anisotropy have a bearing on stone material decay and consequently on its quality and durability (Sheremeti-Kabashi & Sneathlaga, 2000; Fernandez-Revuelta *et al.*, 2008; Fort *et al.*, 2008, 2011). These issues must be considered when planning restoration works on the

architectural heritage, or when a certain type of natural stone is to be used for structural, aesthetic or insulation purposes in new construction, whether of buildings or civil works (Fort *et al.*, 2011).

The anisotropy of stones is related to structural factors as well as compositional differences (Siegesmund & Török, 2014). Anisotropy of physical properties of stones may originate from other possible factors such as: the aligned grain fabric, crystallographically preferred orientation within the grains or the geometry of the void space (Tourenq *et al.*, 1971; Sousa *et al.*, 2002; Benson *et al.*, 2005). Macroscopic fabric elements, that can be macroscopically recognizable, are typical of sedimentary and metamorphic stones (especially gneiss) and are called as bedding, schistosity, foliation, and lineation, depending on the type of rock and its genesis. They are related to the orientation of planes parallel to the external stresses occurring in the formation of the stone. Moreover, in sedimentary rocks, the anisotropy is not mainly due to tectonic efforts but is also due to the stratification planes. Microfabric elements related to anisotropy can be resumed as: the preferred orientation of mineral grains or their grain boundaries, the grain shape orientations, the arrangement of microcracks or the crystallographic preferred orientation of mineral grains. These anisotropic elements related to microfabric can be detected through microscopic or physical analyses. Shape-preferred orientations describe the anisotropic spatial distribution of the axes of shape-anisotropic crystals. Especially for gneissic stones crystals are stretched and oriented parallel to the foliation determining a planar fabric. Microcracks, generally present a preferred orientation and occur either along the grain boundaries (intergranular) or within the mineral grains (intragranular). They can be due to external factors like the continuous growth of macrocracks that can provoke internal microcracks. Furthermore they can be related to the geological process or the evolution of the stone when occur later mineralization. Mineralized cracks can be differentiated into “healed” microcracks (filled with the same material as the host grain) or “sealed” microcracks (filled with a foreign material). Microcracks are a major contributor to the anisotropy in a

stone. In fact they can be related to the porosity and permeability, especially in very dense crystalline stones (plutonic and metamorphic stones) and, because of their parallel orientation, often cause anisotropic fracture behavior (Vollbrecht *et al.*, 1993). Moreover sedimentary stones like slats and schists show anisotropic behavior due to their foliation planes.

The anisotropy of the material determines some deterioration processes as it strongly influences some kind of behavior, such as the capillary absorption one. Thus, it should be considered when placing and orienting new stone material on ancient structures as a preventive conservation method (Fort *et al.*, 2008).

5.8.1 *Ultrasound propagation velocity (P waves)*

The ultrasound propagation velocity determination is a non-destructive test and it can be considered one of the most important tool to investigate physical properties of building materials (Benavente *et al.*, 2006; Vasconcelos *et al.*, 2008). It is useful, in situ and in laboratory, to identify many properties of materials such as the directions of anisotropy (Fort *et al.*, 2011), the compactness, the alteration degree if comparing fresh and deteriorated parts, the homogeneity, the presence of discontinuities (cracks, fractures, presence of different materials, joints) (Saka & Uchikawa, 1995), and the effectiveness of treatment products (Esbert *et al.*, 1997; Valdeón *et al.*, 1997; Sousa *et al.*, 2005).

P-wave velocity measurements (UPV) were obtained by the ultrasonic test portable equipment Pundit CNS Electronics (Fig. 5.16), with an accuracy of 0.1 microseconds and equipped with two transducers (1.5 cm of diameter) having 1 MHz frequency (UNI EN 14579, 2005).



Fig. 5.16. Pundit CNS Electronics portable equipment.

During measurements, in order to improve coupling of the transducers-transmitter and receiver, it was applied an ultrasound couplant Farnell Gel on the opposite faces of the cubic samples (direct mode). Five measurements were taken in each of three orthogonal directions (Fig. 5.17) and averaged, in order to obtain the spatial variability of P-wave velocity values and to identify anisotropies on the set of three axis (coded by X, Y and Z). Measurements were taken after the specimens were dried in an oven at 70 °C to a constant weight (when the difference between two consecutive measurements, taken 24 h apart, was <1%). The total number of examined samples was 56:

- 32 cubic specimens (5 cm sides), 8 for each lithotype;
- 24 cubic specimens (10 cm sides), 6 for each lithotype.

Material anisotropy has been determined by the anisotropy indices proposed by Guldader and Denis (1986) (Guldader & Denis, 1986) and utilized by Zezza for the first time in 1990 (Zezza, 1990 b), as shown below:

$$dM\% = [1 - (2V_{Pmin}/(V_{Pmean} + V_{Pmax}))] * 100$$

$$dm\% = [(2 * (V_{Pmax} - V_{Pmean}))/ (V_{Pmean} + V_{Pmax})] * 100$$

where V_{pmax} is the mean maximum velocity, V_{pmin} is the mean minimum velocity and V_{pmean} is the intermediate value; $dM\%$ is the total anisotropy that takes the three spatial axes into consideration while

dm% is the relative anisotropy considering only two axes, excluding the axis for which the smallest V_p value was found.

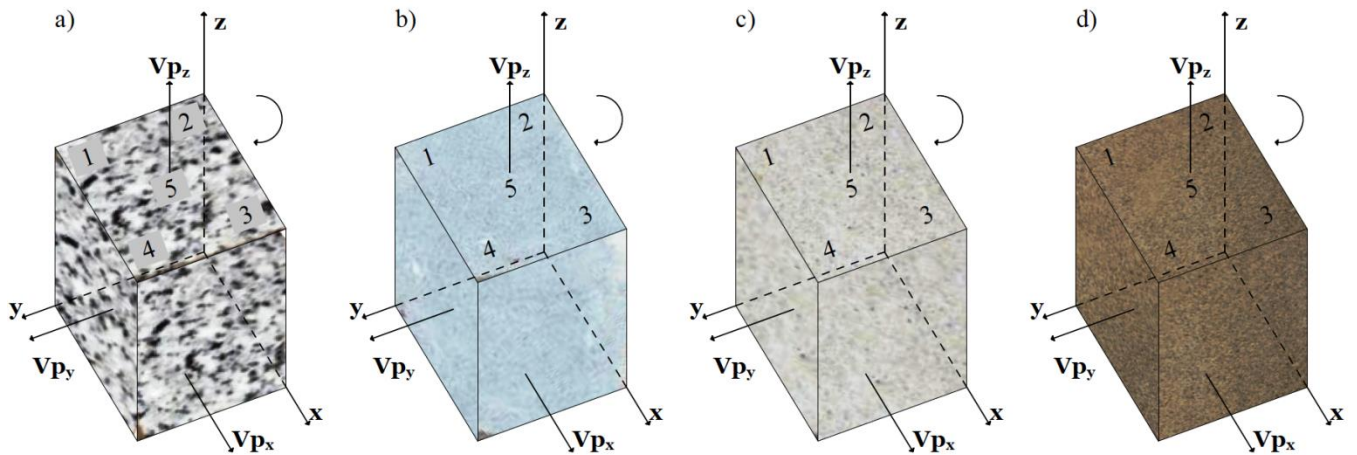


Fig. 5.17. Readings ultrasonic measurements. (a) San Giovanni in Fiore granite, (b) Grisolia stone (c) San Lucido calcarenite, (d) Fuscaldo sandstone.

Obtained ultrasonic velocity mean values have been compared to the classification of Anon (Anon, 1979; Vasanelli *et al.*, 2015) that distinguishes five different classes of stone velocities: class 1 of “Very low velocity” with ultrasonic velocity values <2500 m/s; class 2 of “Low velocity” with values of 2500-3500 m/s; class 3 of “Middle velocity” with values of 3500-4000 m/s; class 4 of “High velocity” with values of 4000-5000 m/s; class 5 of “Very high velocity” with values >5000 m/s.

5.8.2 Ultrasound propagation velocity (S waves)

Ultrasonic pulse velocity (UPV) testing of S-waves has been reported by several authors (Hassan *et al.*, 1995; Sack *et al.*, 1995) as an useful and reliable non-destructive tool for assessing indirectly the mechanical characteristics of materials, such as the modulus of elasticity and the compressive strength. This aim has been accomplished by means of empirical correlations between the ultrasonic pulse velocity and the compressive strength and modulus of elasticity (Uchida *et al.*, 1999; Yasar & Erdogan, 2004).

Elastic properties have been determined using ultrasonic pulse Test (velocity of S-waves). It was applied a Tektronix TDS 3012B Oscilloscope (Fig. 5.18) with transmitters/receivers (frequency 1 MHz) for S-waves, respectively. Velocity of P-and S-waves was measured on 32 cubic samples (8 specimens for each stone type), dried at 70°C for 24 hours. Five measurements were made in each of three orthogonal directions of each sample. In order to improve coupling of the transducers-transmitter and receiver, it was applied an ultrasound couplant Farnell Gel on the opposite faces of the cubic samples (direct mode).

Elastic properties are usually necessary in the evaluation of the performance of built structures and V_p and V_s are commonly used in the estimation of the strength of concrete (Komloš *et al.*, 1996). Concerning the assessment of the stone properties by means of non-destructive techniques, some results revealed the dependence of the mechanical properties, namely the modulus of elasticity and compressive strength, on ultrasonic pulse velocities (Tuğrul & Zarif, 1999; Kahraman S., 2001).

Therefore, statistical correlations between ultrasonic pulse velocity and mechanical parameters measured in each specimen were employed.

To compute Young's modulus (E_{dyn}) has been utilized the equation of the Darracott and Orr (1976), employed by many authors (Hammam & Eliwa, 2013; Barton N., 2007).

$$E_{dyn} = \rho_b V_s^2 \frac{3(V_p/V_s)^2 - 4}{(V_p/V_s)^2 - 1}$$

where V_p is the longitudinal wave value (m/s); V_s is the transverse wave value (m/s); E_{dyn} is the Young's modulus (MPa); and ρ_b , is the bulk density (kg/m^3).

To compute Shear modulus (G_{max}) has been utilized the equation (Chuanchenga Y., 2012; Hammam & Eliwa, 2013).

$$G_{max} = \rho_b * V_s^2$$

where V_s , is the transverse wave value (m/s); G_{\max} , is the Shear modulus (MPa); and ρ_b , is the bulk density (kg/m^3).

To calculate Poisson's ratio (ν) (Hammam & Eliwa, 2013) and Bulk modulus (K) (Alvarez Manilla Aceves *et al.*, 2003; Barton N., 2007; Molina *et al.*, 2013), have been employed the following equations:

$$\nu = \frac{0.5(V_p/V_s)^2 - 1}{(V_p/V_s)^2 - 1}$$

$$K = \rho_b(V_p^2 - 4/3V_s^2)$$

where V_p , is the wave longitudinal velocity (m/s); V_s , is the transverse wave (S) velocity (m/s); ν , is the Poisson's ratio; ρ_b , is the bulk density (kg/m^3); and K is the Bulk modulus (MPa).



Fig. 5.18. Oscilloscope Tektronix TDS 3012B.

Hardness

Because the surface hardness measured by this means is the result of the hardness of the stone constituents and its internal cohesion, this parameter can be considered to be an indicator of the stone's mechanical properties, for fresh stones (Aoki & Matsukura, 2007).

Stone hardness is a material property that can be defined as a measurement of the ease with which a smooth surface of a mineral can be scratched, or of its resistance to abrasion. It can be described

by different hardness scales (Mohs, Vickers, Knoop), which accounts for different techniques that can be related into each other through empirical relationships. Depending on the different use of materials, hardness scales varies (Siegesmund & Dürrast, 2014). The hardest stones are - in theory - igneous, as granite, due to the hardness of its minerals with a Mohs hardness of 7 (quartz), 6 (feldspar), and 2–3 (mica). Conversely, sedimentary stones, as sandstones or limestones, consist of minerals with a Mohs hardness of 2–3 for the presence of calcareous or siliceous cement/matrix or grains/crystals/skeleton.

In addition to the average hardness it can be determined the micro-hardness, that is a highly variable property due to the heterogeneity of natural stones and the diversity of minerals. It could be a useful tool for the characterization of stones with respect to the wear strength and processing performance, which is finally determined by the hardness of the individual stone-forming minerals in contrast to the average hardness (Primavori, 1999).

5.8.3 Micro-hardness (Equotip), drilling resistance measuring system (DRMS) and Schmidt Hammer test

Micro-hardness

The micro-hardness of samples has been measured using the micro-hardness tester Equotip 3 (Fig. 5.19). Equotip measurements were conducted on five of the surfaces of cubic specimens, with 5 consecutive impacts in each face. 32 cubic samples (8 specimens for each stone type) have been examined. Material hardness was obtained using Leeb hardness scale, as the value of rebound energy derived from the impact of the plunger device striking against tested material surfaces. Leeb hardness values were converted to the Vickers scale dividing the obtained values by the conversion factor of 3.5875. The test was carried out according to the “Single impact method” (Hisashi & Yukinori, 2007). Twenty five rebound values were obtained from different points for each sample by a single impact (the

microtester device placed perpendicularly to the stone surface) and the mean value of rebound hardness for each type of stone was obtained by 200 rebound points and denoted as Ls. Micro-hardness, even though is considered as a non-destructive method, it can be classified as micro-destructive because it could leave marks and little dots on the analyzed surfaces. Moreover, due to the little surface of the tester (only 2 mm²), for each sample a lot of measurements, 25 measurements exactly, have been taken.



Fig. 5.19. Micro-hardness tester Equotip 3 - Proceq.

Drilling resistance

Drilling test (Drilling resistance measurement system, DRMS) performed on quarry samples is a micro-destructive no-standardized test, useful to obtain the drilling material resistance that could be correlated to the physical-mechanical properties of stones (Theodoridou *et al.*, 2012). This test, in many countries, is performed to obtain the stone quality in situ or in laboratory (Exadaktylos *et al.*, 2000) or to determinate weathering depth on building materials (in Italy is not allowed to drill on building surfaces).

Many authors indicated that drilling resistance of natural building stones, measured by DRMS test, can be correlated with: porosity (Fratini *et al.*, 2006) and compressive strength (Fratini *et al.*, 2006; Exadaktylos *et al.*, 2000); Mohs hardness (Pamplona *et al.*, 2007); flexural strength (Wendler & Sattler,

1996); salt crystallization map on deteriorated surfaces (Modestou *et al.*, 2012); evaluation of consolidating treatments in monuments (Tiano *et al.*, 2000).

Drilling resistance was obtained through Drilling Resistance Measuring System (DRMS). A small diameter diamond (5 mm) twist drill type BOSCH CYL-9 (Fig. 5.20) was used to drill 5 mm deep holes in 32 cubic-shaped samples (8 specimens for each stone type). Operating test conditions were: drilling speed 1000 rpm; penetration rate 1 mm/min; number of 5 holes/face. Thrust and drift force, as well as the main and feed drive current sensors signals were synchronously recorded during each drilling cycle on external measuring system. As well as the micro-hardness test, drilling test followed the “Single impact method”. Five drilling values were made from different points for each sample by a single impact and the mean value of drilling resistance related to depth, denoted as DR_i, was obtained as the average of 40 drilling points for each series of stones. The drilling length was fixed to 5 mm in all specimens, even though the maximum length reached varied considerably for the hardest (granite of San Giovanni in Fiore) and the softest stone (Fuscaldo sandstone), from the value of 1.50 mm to 5 mm, respectively.



Fig. 5.20. Drilling Resistance Measurement System device: Drill Bosch Cyl-9. Sint Technology

Schmidt hammer test

The Schmidt hammer is a tool for micro-destructive testing that can be easily applied in situ for estimating rock strength. As well as micro-hardness, even though this test is considered as a non-destructive method, it can be classified as micro-destructive because it could provoke microcracks and fractures on the analyzed surfaces, especially for soft stones. Originally, it was developed for measuring the strength of hardened concrete (Schmidt, 1951) but, recently, it has been also applied to building stone surfaces (Queisser, 1986; Schneider *et al.*, 2008) and to determine weathering degree of rock outcrops (Borrelli *et al.*, 2015). The rebound hardness method provides a means for rapid classification of the hardness of rock during site characterization for engineering, design, and construction purposes, geotechnical mapping of large underground openings in rock. This test method is of limited use on very soft or very hard rocks, which is defined as having uniaxial compressive strengths lower than approximately 1 MPa or greater than 100 MPa (ASTM D5873-14).

Schmidt hammer test was used for in “situ” test on outcrops and quarries and on the specimens surfaces in the laboratory. The “in situ” mechanical tests included strength measurement of granite boulders and quarry surfaces of the other three types of rocks, by the Schmidt hammer Geohammer L-type (Fig. 5.21), according to ASTM D5873 standards (2014), to assess hardness characteristics of quarry boulders and to classify weathering state of granite boulders (from Grades I to V), according to weathering classes modified by Borrelli *et al.* (2015).

When the Schmidt hammer (consisting of a springloaded piston) is pressed orthogonally against a surface, the piston is automatically released onto the plunger. Part of the impact energy of the piston is consumed largely by absorption (work done in plastic deformation of rock material under the plunger tip) and transformation (into heat and sound). The remaining energy represents the impact penetration resistance (or hardness) of the surface and enables the piston rebound. The harder the surface, the

shorter the penetration time (*i.e.* smaller impulse) or depth (*i.e.* lesser work or energy loss), and hence the greater the rebound (*i.e.* smaller momentum change). The distance traveled by the piston after rebound (expressed as a percentage of the initial extension of the key-spring) is called the rebound value (R), which is considered to be an index of surface hardness (Aydin & Basu, 2005; Viles *et al.*, 2011).

Schmidt test was performed on four granite boulders of the active quarry and on four of the ancient, too, in order to compare rebound values. Moreover, it was carried out on the quarries of the other three types. The rebound test hammer housing was held firmly by hand in a position aligned horizontally downward (~0 degrees) so that the impact plunger struck at an angle perpendicular to the test surface of the portals. Eight points were examined, four for each quarry and twelve impact readings were recorded. After the plunger impact for each reading, the surface of the rock was examined. Readings were rejected if any individual impact test resulted in cracking or any other visible damage. The correlation between the uniaxial compressive strength and Schmidt hammer rebound values was determined by the relationship of Bieniawski (Bieniawski, 1984), that according to literature and empirical studies it is suggested to estimate the uniaxial compressive strength of rock on the basis of Schmidt hammer rebound, known the unit weight and the porosity of stone (Moomivand, 2011):

$$\sigma_c = 21.479 \cdot e^{0.0148 \cdot (H_s - P) \cdot \gamma}$$

where σ_c is the uniaxial compressive strength in MPa, H_s the Schmidt hammer rebound, P the porosity in %, γ the unit weight in g/cm^3 .



Fig. 5.21. Schmidt hammer: Geohammer L-Type.

Strength properties

Strength properties are the most important parameters for engineering purposes, used to classify the quality of natural stones. The results of the strength tests can be used directly to evaluate the suitability of the stones for construction purposes.

Tests carried out in this study have allowed estimating the uniaxial compressive strength, the flexural and the tensile strength. The flexural strength values are usually lower than the tensile strength values for a stone (Siegesmund & Dürrast, 2014), while the compressive are the highest. A material strength depends on the heterogeneity of the stone and its fabrics and is influenced by its composition, the shape and size of the material sample, the aging of the material, its storage conditions (Siegesmund & Dürrast, 2014) and to the anisotropy planes. The mechanical strength of a stone is considerably influenced by the angle of possible planes of anisotropy in relation to the loading axis (Broch, 1983; Saroglou *et al.*, 2004; Rigopoulos *et al.*, 2013). So, in order to consider the potential different effects of the anisotropy on mechanical tests strength, the tested specimens were prepared in such a way that the loading axis was both parallel and perpendicular to any plane of anisotropy.

5.8.4 Uniaxial compressive strength

The uniaxial compressive strength is the most common performance measure used by engineers for the quality assessment of stones. The uniaxial compressive strength (UCS) was determined on 96 cubic specimens (24 for each stone type), of 5 cm sides (UNI-EN 1926, 2000) along the three directions of anisotropy, X, Y and Z. The sample preparation and the sample dimension have been accurate according to the current standards, and the end-face was co-planar with an accuracy of 0.1 %. The maximum load applied is defined as the uniaxial compressive strength.

Prior to testing, specimens were oven-dried at 70°C to a constant weight for 24h. After reaching constant mass, the specimens were loaded to failure according to the three spatial directions obtained through the UPV test. Test was carried out on the machine at a constant speed rate of 1mm/min MFL SYSTEM (Fig. 5.22) with a maximum load capacity of 3000 kg. The uniaxial compressive strength values, $UCS_{max,x}$, $UCS_{max,y}$ and $UCS_{max,z}$, along X, Y and along Z respectively, of the tested stones were calculated by

$$UCS_{max,x,y \text{ or } z} = \frac{F_{max}}{A}$$

where F_{max} is the applied compressive load at failure and A is the cross-sectional area of the test specimen.

The mean uniaxial compressive strength UCS_{mean} was calculated from the values determined in the three principal orientations of samples as:

$$UCS_{mean} = \sqrt[3]{UCS_{min} \times UCS_{max} \times UCS_{inter}}$$

This mean value is reported as the characteristic compressive strength of each stone type (Prikryl, 2001).

Mean values have been compared to the classification of Anon (1977) that distinguishes stones as: very weak (VW) with compressive strength values from 0.60 to 1.25 MPa; weak (W) from 1.25 to 5.0 MPa; moderately weak (MW) from 5.0 to 12.5 MPa; moderately strong (MS) from 12.5 to 50 MPa; strong (S) from 50 to 100 MPa; very strong (VS) from 100 to 200 MPa; extremely strong (ES) higher than 200 MPa.

It was also calculated the anisotropy of stone strength expressed as a ratio of UCS_{max}/UCS_{min} and as the anisotropy ratio R_a (Douglass & Voight, 1969) that is

$$R_a = \frac{UCS_{max} - UCS_{min}}{UCS_{mean}}$$

Moreover, the stress–strain curves in unconfined state have been analyzed in order to describe stone behavior until failure. According to theory of stone failure (Bieniawski, 1967), regarding fracture initiation under compression, the fracture propagation during the test has been analyzed. The fracture patterns have been reported manually and shown schematically for all specimens investigated, using the photos of broken samples and indicating the fractures.



Fig. 5.22. Uniaxial compressive press machine MFL System.

5.8.5 *Flexural strength*

The flexural strength or bend strength is an important mechanical property of structural and decorative stones. Failures due to bending stress are more common than those caused by compressive or shear stresses and generate tensile stresses. These failures can be related to the action of the wind pressure, or strain forces operating for example for horizontal elements as architraves or vertical ones as covering stones for facades, load stones built in stairways.

Common flexural strength values range from 5 to 30 MPa (Mosch & Siegesmund, 2007), up to 40 MPa (Peschel, 1983) for plutonic and volcanic stones; from 13 to 28 MPa for granites, granodiorites,

monzo-granites and monzonites (Günes Yılmaz *et al.*, 2011); from 1 to 34 MPa for carbonate stones and sandstones (Siegesmund & Dürrast, 2014); lower values for crystalline marbles (Brosch *et al.*, 2000); from 6 to 82 MPa, a wide range, for metamorphic stones due to directional dependency of the flexural strength (Mosch & Siegesmund, 2007).

For the execution of flexural strength the three-point load bending strength test has been chosen, as described in the UNI-EN 12372:2001 European standard. The samples used in this mechanical strength test fully meet the dimensional requirement suggested in the above mentioned stone testing standard. The standards suggest that: the thickness (h) should be included between 25 and 100 mm and at least two times the maximum grain size; the total length (L) as six times the thickness; the span length (l) as five times the thickness; the width (b) between 50 mm and three times h. Thus, 54 prismatic test specimens of 50x50x300 mm in dimension were prepared (6 specimens for GF, 10 for DG, 12 for CS and 6 for AF) and oven-dried at 70 ± 5 °C until reach constant weight for 24 h.

The specimens were loaded to failure, with a INSTRON 1195 testing machine (Fig. 5.23), with a maximum load capacity of 5000 kg, at a constant speed rate of 1mm/min. The test has been performed along the three spatial directions, for each specimens and the flexural strength (R_{tf}) of each sample was calculated by the following equation:

$$R_{tf} = \frac{3Fl}{2bh^2}$$

where:

- R_{tf} is the flexural strength resistance (MPa);
- F is the load failure (N);
- l is the span length (mm) that is a constant value of the test performed (250 mm);
- b is the specimen width (mm);
- h is the thickness of the specimen (mm).

The average value of the test results of the mean values along the three directions investigated, was accepted as the flexural strength of stone.



Fig. 5.23. Three-point bending flexural strength testing machine, INSTRON 1195.

An anisotropic index of flexural strength is defined as the ratio of the maximum flexural strength to the minimum flexural strength within the three spatial directions.

$$Ra_{tf} = \frac{R_{tfmax}}{R_{tfmin}}$$

5.8.6 Indirect Tensile strength test (Brazilian test)

Tensile strength is not a common property used for engineering purposes but is essential for a complete characterization of the mechanical behavior of building stones and is strongly recommended to evaluate for determining strength parameters of anisotropic stones (Khanlari *et al.*, 2014).

The most common testing procedure for the determination of tensile failure strength (σ_t) is the Brazilian test or indirect tensile strength test (Ugur *et al.*, 2010), because easy to perform (Li & Wong, 2013), cheap, and take short testing time (Shalabi *et al.*, 2007). 30 disks specimens of 6x3 cm were used for this test (6 specimens for GF, 10 for DG, 8 for CS and 6 for AF), in accordance with the ISRM

(1997). The specimens were loaded to failure, with a MATEST C070 testing machine (Fig. 5.24), with a maximum load capacity of 30000 kN at a constant speed rate of 0.1 MPa/s. The Brazilian tensile strength (σ_t) was determined by the following equation:

$$\sigma_t = \frac{2P}{\pi Dt}$$

where:

- σ_t is the tensile strength (MPa);
- P is the maximum load recorded during the test (kN);
- D is the diameter and t is the thickness of specimen.

Specimens were placed in the Brazilian test machine with different anisotropy angles of loading directions ($\beta = 0^\circ, 45^\circ$ and 90°). The Brazilian anisotropy index (BAI) for indirect tensile strength was obtained from the ratio of tensile strength at strongest and weakest directions (Khanlari *et al.*, 2014).



Fig. 5.24. Tensile strength machine MATEST C070.

5.8.7 Point Load test

For the strength determination and classification of intact stone materials, according to Franklin & Broch (1972), it was performed the point load test (PLT), that is widely used in geotechnical practice (Günes Yılmaz *et al.*, 2009). A portable point load test machine (Fig. 5.25) connected to a barometer in order to register the maximum pressure, was used to test 24 cubic specimens of 10 cm sides (6 samples for each lithotype), along the three principal directions X, Y and Z. It was measured the Point Load Strength Index ($I_{s(50)x,y,z}$) along the three spatial directions (N/mm²), in the form of cut blocks (the block test) in accordance with the ISRM (1981) and according to ASTM D5731-08 (2008) as

$$I_{s(50)} = F * I_s$$

where F = size correction factor

$$F = \left(\frac{D_e}{50}\right)^{0,45}$$

And I_s is the uncorrected point load strength index (N/mm²)

$$I_s = \frac{P}{D_e^2}$$

where:

- P = failure load (N);
- D_e = equivalent core diameter (mm) and is given by:

$$D_e^2 = 4A/\pi$$

where: A = WD = minimum cross-sectional area of a plane through the platen contact points (mm²).

Furthermore it was determined the point load strength index anisotropy value ($I_{a(50)}$) as $I_{s(50)\max}/I_{s(50)\min}$ that is =1 for isotropic stones (ISRM, 1981).



Fig. 5.25. Point Load portable testing machine.

Abrasion Resistance

Another measure of stone hardness is the abrasion resistance. It is defined as the resistance of a stone against a grinding force. The abrasion resistance of a stone depends mainly on the mineralogical composition and the stone fabric (Siegesmund & Dürrast, 2014). The determination of the abrasion resistance it is important when the stone must resist to forces related to footsteps and walking. Abrasion tests are performed to determine quality of aggregate used as building materials, defined by European Standard test methods. The Los Angeles and the micro-Deval tests are the common methods used to define the mechanical properties of the aggregate (Erichsen *et al.*, 2011). The two methods are defined as drum test express, through thee degradation of the material occurring by rotation, the material resistance to fragmentation or wearing. The rotation happens between the test material (aggregates) and steel balls that rotating provoke the breakdown of the aggregate. Los Angeles and Micro-Deval tests have been performed only on the granite of San Giovanni in Fiore in order to evaluate its possible use as aggregate.

5.8.8 Polished Stone Value

Polished Stone Value (PSV) is one of the main factors in estimating the quality of aggregates used for wearing courses. It reflects the aggregate micro roughness, which is important for skid resistance and safe driving (Dokic *et al.*, 2015). In this study the PSV value has been obtained indirectly using models for predictions of PSV.

The PSV values has been determined only for GF samples because they represent one of the major geological formations of Calabria and they are close to the main roads that makes their exploitation and transport economically sustainable. So, they could be a significant source of aggregate material for wearing course construction in Calabria.

The PSV value has been obtained from the evaluated engineering mechanical properties: Los Angeles and Micro-Deval, according to the following equations (Dokic *et al.*, 2015):

$$PSV = 49.371 + 0.393 LA$$

$$PSV = 49.544 + 0.435 M_{DE}$$

where:

- LA = Los Angeles (%);
- M_{DE} = Micro-Deval (%).

Los Angeles

The Los Angeles test is a measure of degradation of mineral aggregates of standard gradings resulting from a combination of actions including abrasion or attrition, impact, and grinding in a rotating steel drum containing a specified number of steel spheres (Ugur *et al.*, 2010).

The test has been carried out according to the UNI-EN 1097-2:1999 European standard. The Los Angeles testing machine consists of a hollow steel cylinder, closed at both ends, having an inside length

of 508±5 mm and an inside diameter of 711±5 mm (Fig. 5.26). The interior of the cylinder has a shelf that picks up the sample and charge during each rotation and drops them on the opposite side of the cylinder, subjecting the sample to abrasion. The cylinder rotates for 500 revolutions at a constant velocity, from 31 to 33 rpm and after the prescribed number of revolutions, the machine will automatically be stopped by a counter switch. A graded aggregate sample is placed into this cylinder with 8–12 steel spheres weighing approximately 420 g each and having a diameter between 45 and 47 mm. The test has been performed on two graded size classes: the class between 8 and 11.2 mm and the fraction between 4 and 8 mm, for a total weight of 5000±5 g (Fig. 5.27). Charge requirements employed, for each sample size of grading, are given in Table 5.2.

Table.5.2 Los Angeles test conditions – granite of San Giovanni in Fiore

Grain size Φ (mm)	Steel sphere number	Steel sphere mass (g)	Revolution number	m ₀ (g)
8 - 11.2	10	4.260 - 4.420	500	5.000±5
4 - 8	8	3.410 - 3.540	500	5.000±5

Following the completion of the 500 revolutions, the material coarser than 1.6mm sieve was separated and weighed (m₅₀₀), to determine the amount of degradation that occurred during the test. The abrasion loss or Los Angeles coefficient (LA), expressed as a percentage of the original mass of the test sample after 500 revolutions, is calculated according to the following equation:

$$LA = \frac{m_0 - m_{500}}{m_0} \times 100$$

where:

- LA is the abrasion loss or the Los Angeles coefficient (%);
- m₀ is the original sample mass (g);
- m₅₀₀ is the sample mass at the end of 500 revolutions (g).



Fig. 5.26. Los Angeles testing machine.



Fig. 5.27. Graded sample of San Giovanni in Fiore granite.

Micro-Deval

The micro-Deval (M_{DE}) test (UNI EN 1097-1, 2004) is widely used to determine the resistance of an aggregate to abrasion. The resistance to wear, the micro-Deval test, measures the ability of an aggregate to tolerate abrasive wear, and is developed to test aggregate products to establish the quality classification for resistance to wear. It determines the abrasion loss in the presence of water and an abrasive charge. The Micro Deval test incorporates the use of water in contrast to some other tests, which are conducted on dry aggregate, because many aggregates are more susceptible to abrasion when wet than dry.

The test machine used consists of a steel frame with four cylinders (Fig. 5.28), with an internal diameter of 200 ± 1 mm and a length of 154 ± 1 mm. During Micro-Deval testing, aggregates degrade when tumbled in a rotating steel drum with water and steel balls. During testing, the quantity of fines produced is measured.

Granite samples belong to two grain sizes: two samples between 8 and 11.2 mm; one with a grain size between 6.3 and 10 mm; one between 4 and 6.3 mm (Fig. 5.29). The weight of each sample is of 500 ± 2 g, according to the standard recommendation. In each cylinder has been put a sample in a container, with a sufficient number of steel spheres. Then has been put water and the test has been performed at a constant velocity for 12000 ± 10 revolutions. At the end of the test, samples have been separated to the abrasive charges and washed. The retained weight at 1.6 mm has been dried at a temperature of 110 ± 5 °C.

The wear coefficient or micro-Deval coefficient (MDE) has been calculated, for the three fractions investigated, through the following equation (UNI EN 1097-1, 2004):

$$MDE = \frac{500 - m}{5}$$

where:

- MDE is the micro-Deval coefficient (%);
- m is the mass retaining at 1.6 mm.



Fig. 5.28. Micro-Deval testing machine.

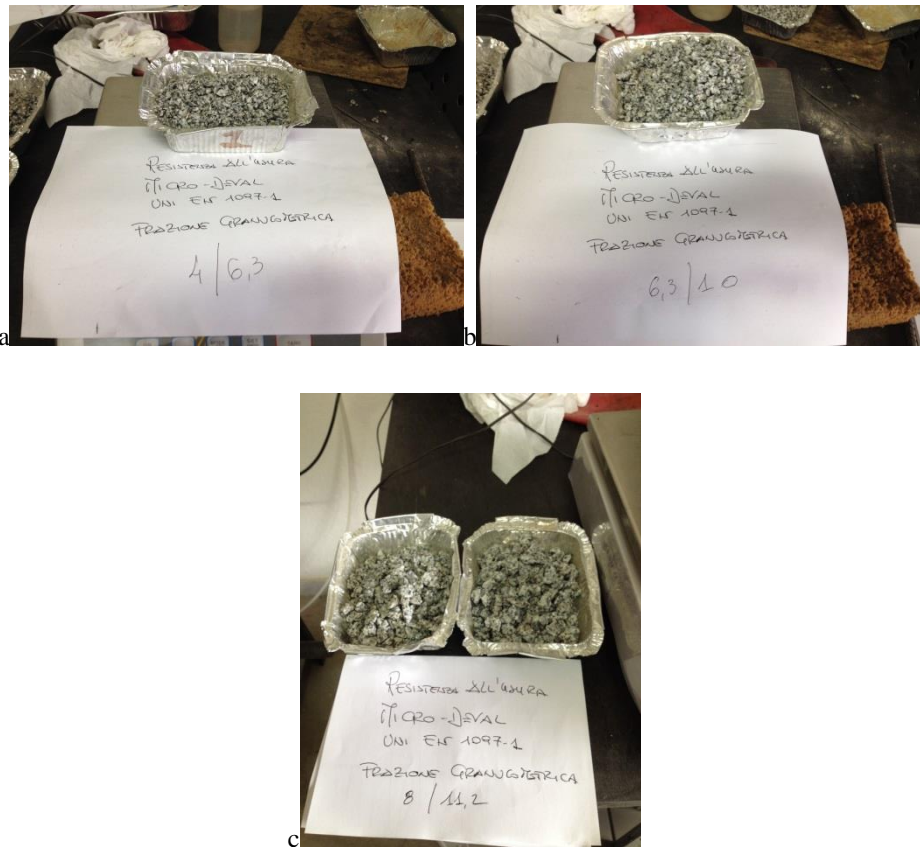


Fig. 5.29. Grain size classes investigated of San Giovanni in Fiore granite: (a) from 4 to 6.3 mm; (b) from 6.3 to 10 mm; (c) from 8 to 11.2 mm.

6. Characterization: results

6.1 Petrographic description

The petrographic description includes the textural and mineralogical characteristics of the materials, which play an important role in the determination of their susceptibility to degradation processes. Thin sections were oriented with respect to the macroscopic fabric elements (foliation and lineation) and according to the coordinate reference system established for the three orthogonal directions (X, Y and Z-axes), as described in [Par. 5.1](#) and as shown in [Fig. 5.2](#).

San Giovanni in Fiore granite (GF)

Macroscopically ([Fig. 6.0](#)), San Giovanni in Fiore granite (GF) is grey in colour and contains mafic enclaves, ellipsoidal, probably due to mingling of mafic and felsic magmas (Messina *et al.*, [1991\(a\)](#)). The boulders frequently exhibit a typical onion structure. They present an unweathered innercore, usually surrounded by a moderately-weathered outer shell, with millimeter to centimeter thick exfoliation sheets, often widely encrusted by lichens.

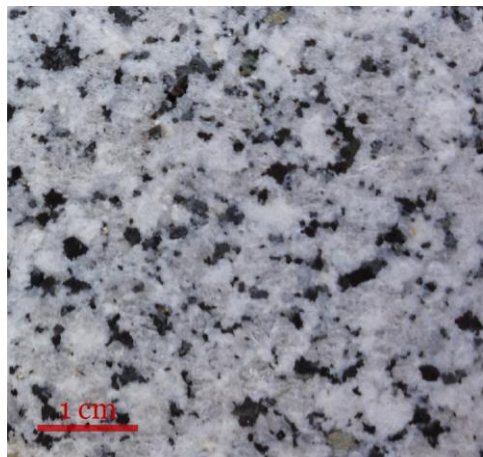


Fig. 6.0. San Giovanni in Fiore granite (GF) macroscopic appearance.

Texture

Petrographically (Fig. 6.0 a), the examined material shows a holocrystalline texture, is inequigranular, coarse-grained and micro-fractured.

Mineralogical composition

It contains quartz (30% vol.), plagioclase (30% vol.), potassium feldspar (30% vol.) and biotite (10% vol.). It can be classified as *granite* (Streckeisen, 1973).

Most significant accessory minerals are apatite and zircon.

Quartz exhibits allotriomorphic crystals, clear, without inclusions and with an undulating extinction.

The potassium feldspar (orthoclase and microcline) exhibits a poikilotopic texture, is large in size, subidiomorphic, with perthitic exsolutions and often shows albite-pericline twinnings.

The plagioclase has heterometric crystals, often zoned, a low level of sericitization and exhibits albite twinning. Myrmekitic exsolutions can be noticed.

The biotite is abundant and appears often chloritized. It exhibits pleochroism from yellow to brown. The petrographic analysis of GF is in agreement with previous studies on the same lithology (Scarciglia *et al.*, 2012).

Plane polarized light

Crossed Polarized light

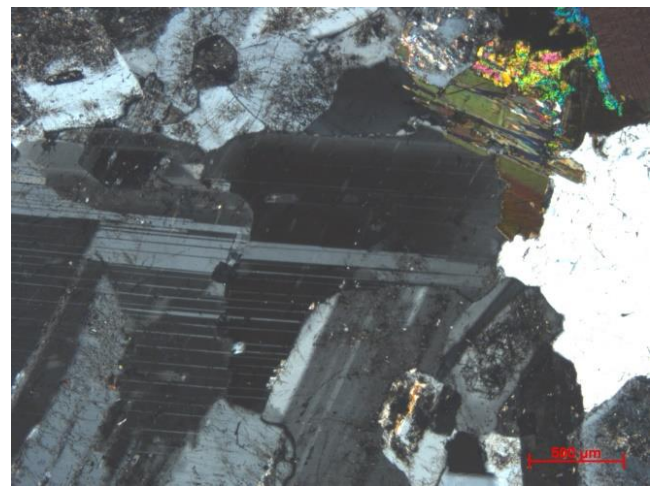
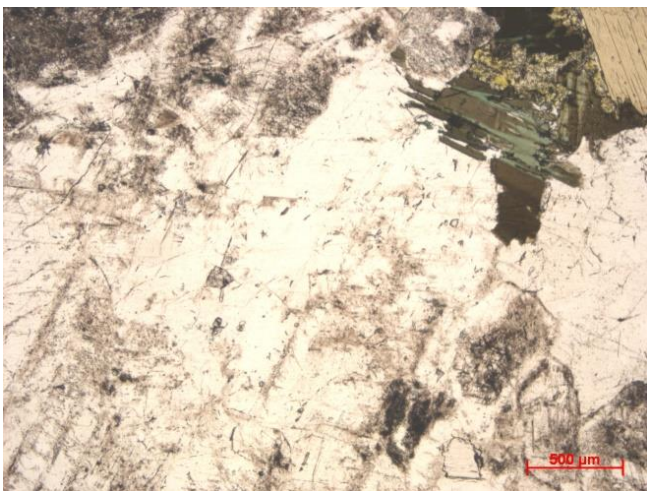
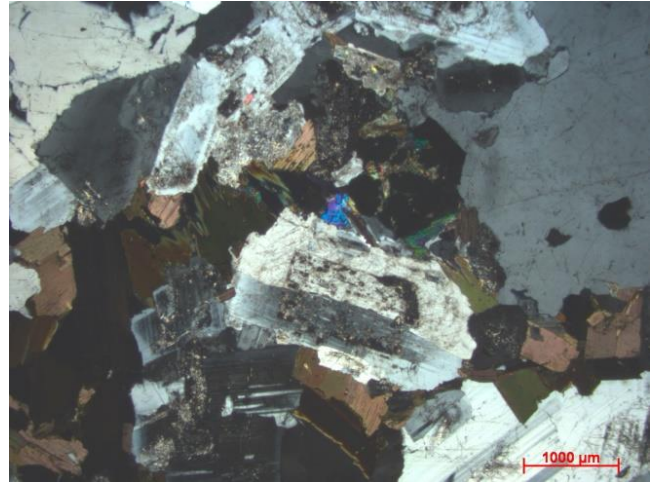
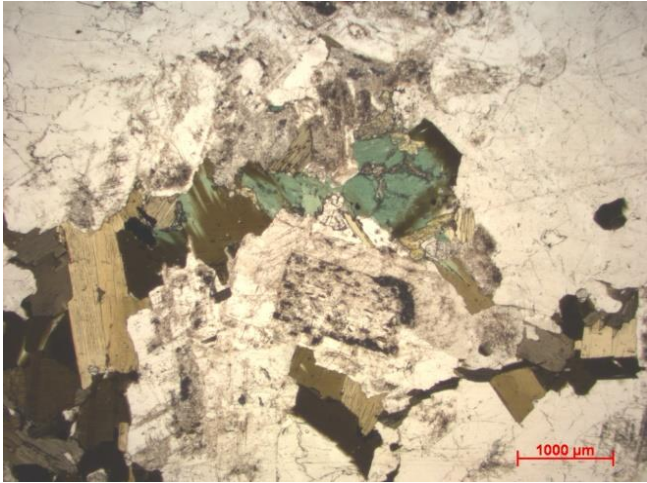


Fig. 6.0 a. Micrographs at the polarized optical microscope of thin sections from San Giovanni in Fiore granite.

X-direction

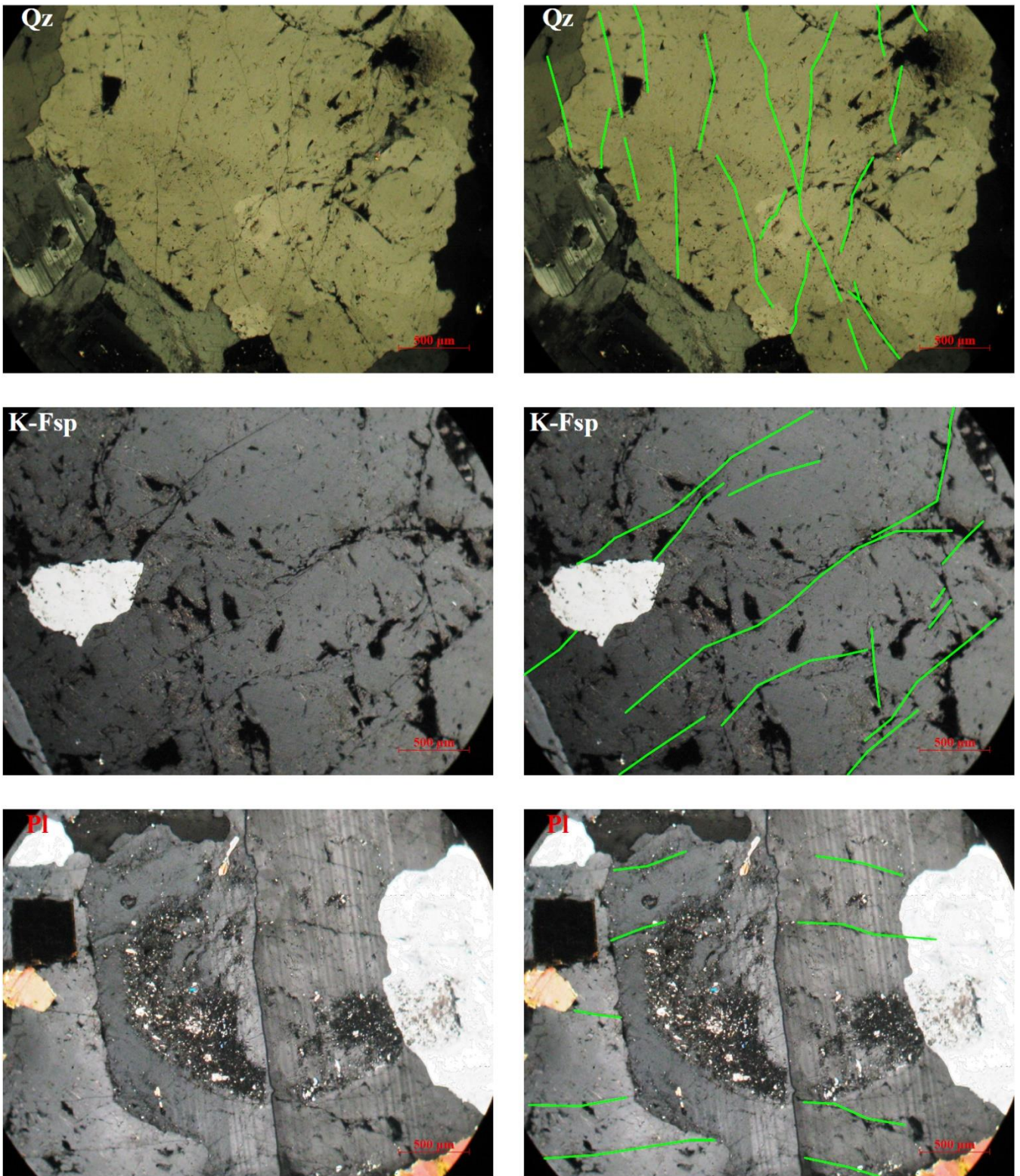


Fig. 6.0 b. Micrographs at the polarized optical microscope (crossed polarized light) of thin sections from San Giovanni in Fiore granite, along the X-direction, highlighting the intracrystalline microcracks for the following crystals of (from the top to the bottom): quartz (Qz); K-feldspar (K-Fsp); plagioclase (Pl).

Y-direction

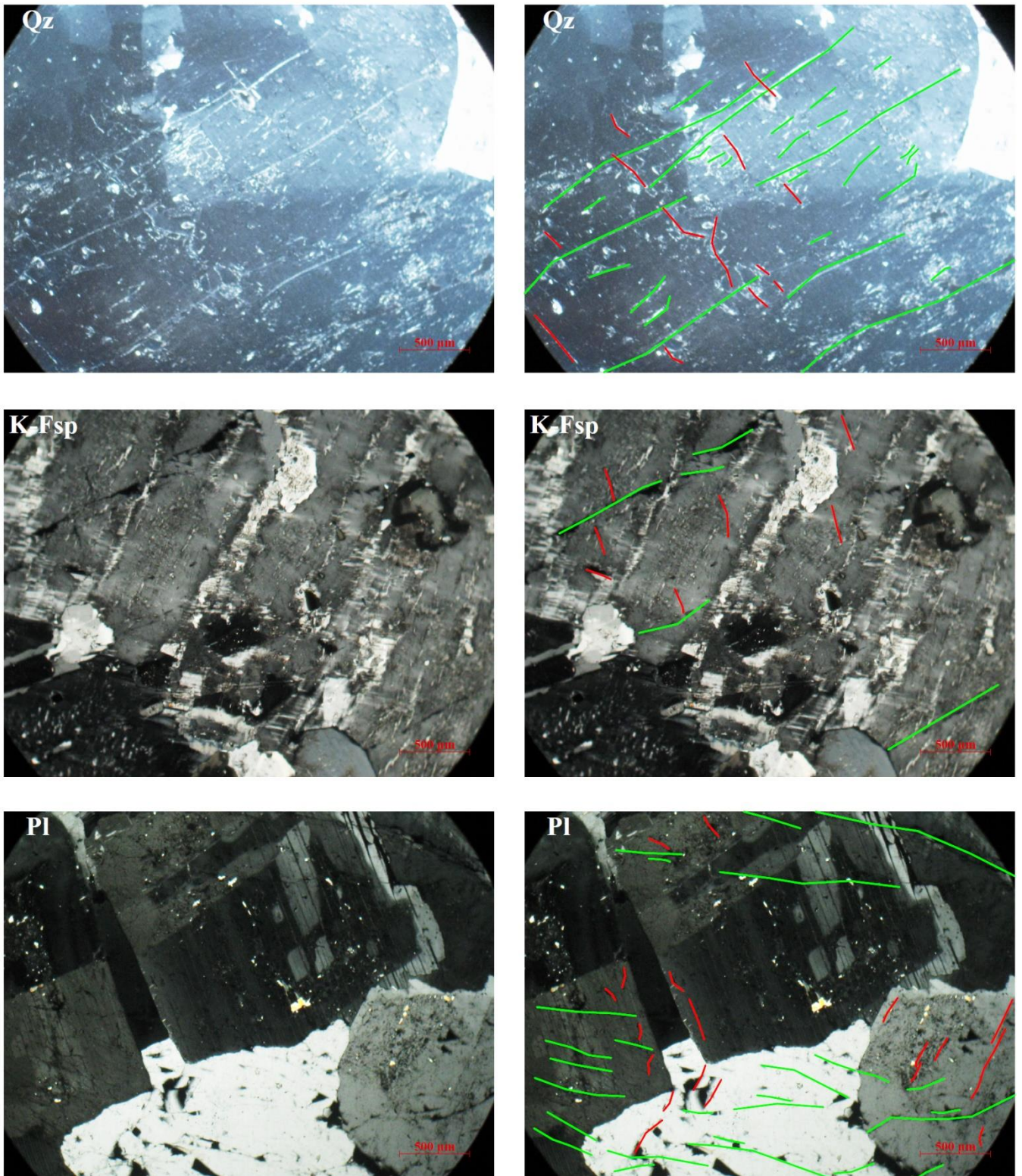


Fig. 6.0 c. Micrographs at the polarized optical microscope (crossed polarized light) of thin sections from San Giovanni in Fiore granite, along the Y-direction, highlighting the intracrystalline microcracks for the following crystals of (from the top to the bottom): quartz (Qz); K-feldspar (K-Fsp); plagioclase (Pl).

Z-direction

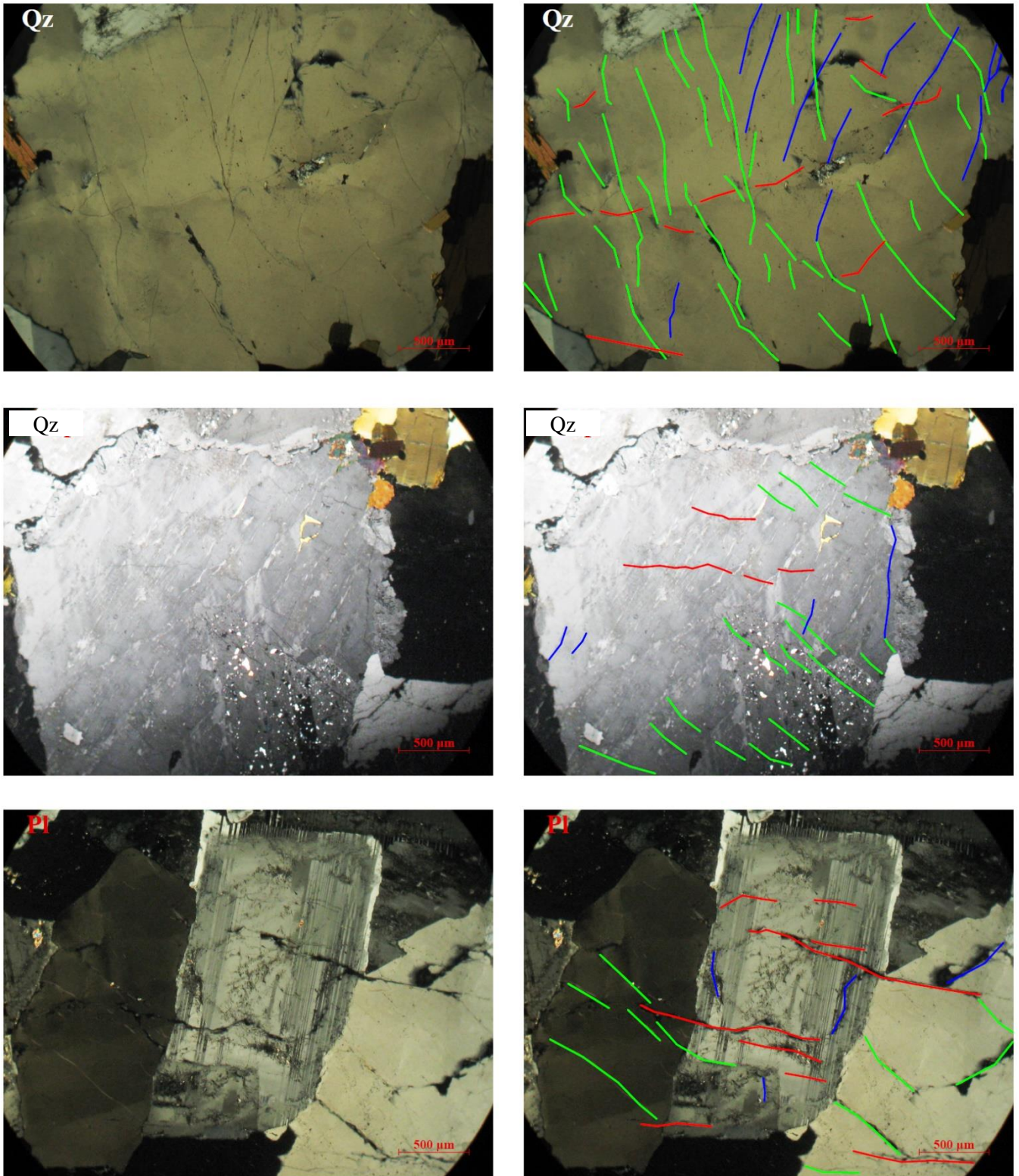


Fig. 6.0 d. Micrographs at the polarized optical microscope (crossed polarized light) of thin sections from San Giovanni in Fiore granite, along the Z-direction, highlighting the intracrystalline and intercrystalline microcracks for the following crystals of (from the top to the bottom): quartz (Qz); plagioclase (Pl) – intercrystalline microcracks.

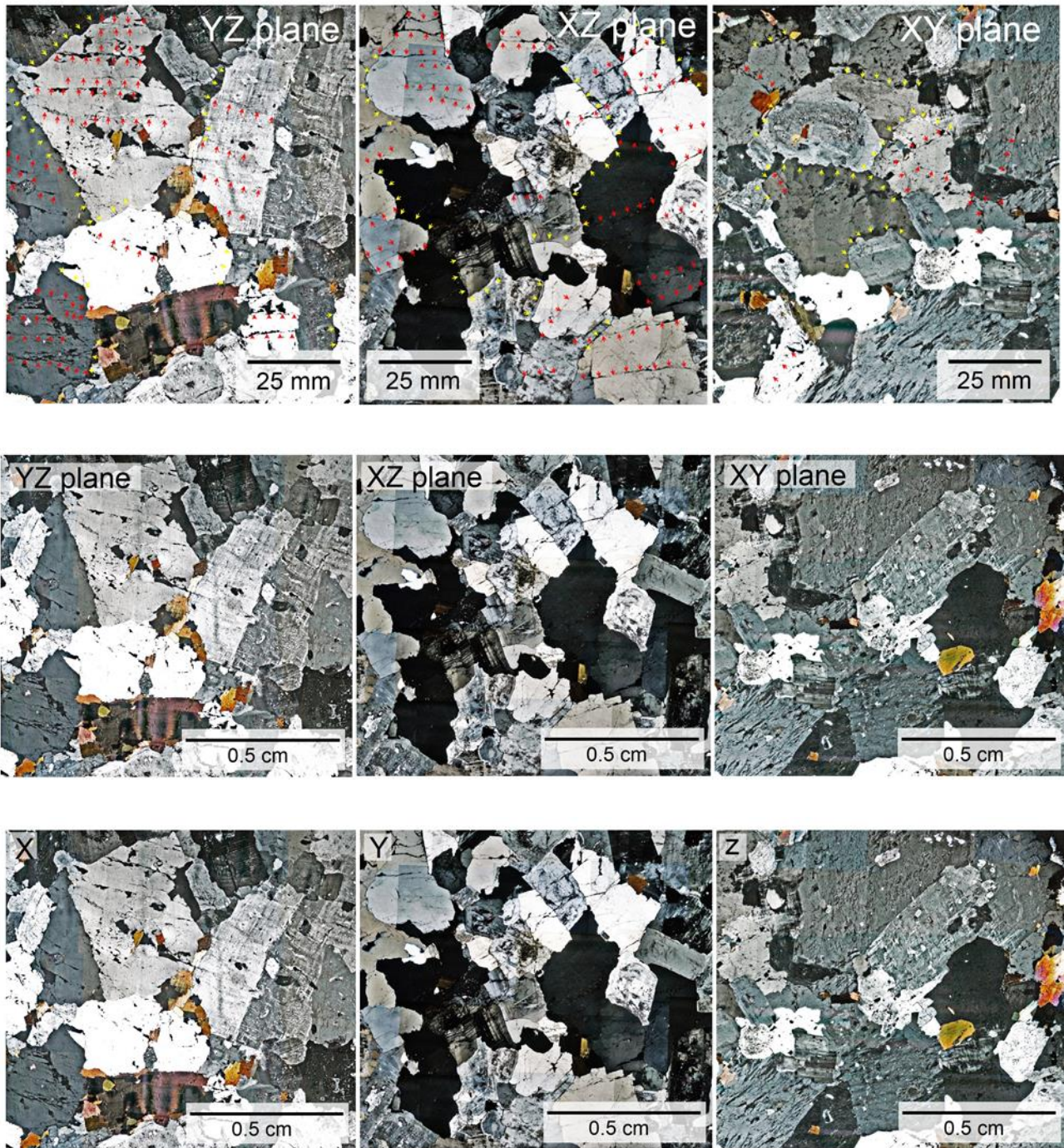


Fig. 6.0 e. Part of the micromosaic, analyzed at the polarized optical microscope (crossed polarized light) of thin sections from GF, along the YZ, XZ, XY planes, highlighting the inter- and intracrystalline microcracks. The red colour refers to the oldest microcracks while the yellow one to the most recent.

The exfoliation microcracks represent anisotropy planes in heritage granite ashlars. Along these weak lines the granite ashlar decay could develop. *Scaling*, as defined by ICOMOS (Vergès-Belmin, 2008) is the most common decay form of granite consisting in the detachment of stone as a scale or a

stack of scales, not following any stone structure and detaching like fish scales parallel or sub-parallel to the stone surface (Freire-Lista & Fort, 2015). For this reason, microcracks in San Giovanni in Fiore granite thin sections, their orientation and related weathering class have been individuated.

The thin section observations (Figs. 6.0 b, c, d) and the micromosaic (Fig. 6.0 e) have allowed gaining important information concerning GF characterization.

Along the X-direction a system of oriented microcracks in a prevalent direction may be detected, parallel to each other (Fig. 6.0 b). Along these intracrystalline microcracks, a secondary porous system and alteration forms can be detected. Above analyzed minerals, K-feldspar presents the highest number of fractures.

Along the Y-direction, two systems of intracrystalline microcracks have been observed (Fig. 6.0 c): one, more extensive, similar to that recognized along the X-directions; the other, smaller, perpendicular to the first one.

While along the X and Y-directions it is possible to individuate oriented systems of microcracks, along Z-direction (Fig. 6.0 d) is difficult to recognize a principal direction because of the presence of three prevalent directions. Moreover, many intracrystalline microcracks, concentrated in K-feldspar crystals, more than those along X and Y are also present. It has been also observed a system of intercrystalline microcracks, especially for quartz-feldspar crystals. Fractures generate the starting of alteration forms and the statement of voids.

The difference along the three spatial directions is that the intracrystalline microcracks in Fig. 6.0 b are straight and parallel, in Fig. 6.0 c are perpendicular, whereas the intracrystalline cracks in Fig. 6.0 d, are branched and run in no prevalent direction.

In other words, the rift plane (XY plane), the plane traditionally preferred for hewing and subsequent used as the outer surface on ashlar in heritage buildings (Freire-Lista & Fort, 2016), is the plane where there is a high number of intercrystalline microcracks running along the Z-direction.

Along the XZ and the YZ planes a system of oriented intracrystalline microcracks in a prevalent horizontal direction has been detected, parallel to each other (Fig. 6.0 e). Along the XY plane it is difficult to recognize a principal direction of the intracrystalline microcracks. Most of them are intercrystalline microcracks.

The difference along the three planes is that the intracrystalline microcracks of YZ and XZ planes are straight and pseudo-parallel, whereas the intracrystalline microcracks run in no prevalent direction.

Above analyzed minerals, quartz presents the highest number of horizontal microcracks according to the LMD value (Table 6.0).

Intracrystalline microcracks represent the majority of all cracks observed. Obtained microcracks data (Table 6.0) reveal that the studied granite has a mean value of linear microcrack density close to 1.0 corresponding to the class of “fresh or sound stone” (Sousa *et al.*, 2005).

Summarizing, the *rift plane* (XY along the Z-axis) is the plane with the dominant microcracks set (intracrystalline microcracks < intercrystalline); the *grain plane* (XZ along the Y-axis) is the plane with the secondary concentration of microcracks (intracrystalline microcracks > intercrystalline), while the *hard-way plane* (YZ along the X-axis) shows the lowest concentration of microcrack set (intracrystalline microcracks > intercrystalline).

Table 6.0. Number of intracrystalline and intercrystalline microcracks and linear crack density (LMD) along the three orthogonal directions.

Plane	Intracrystalline microcracks (%)				Intercrystalline microcracks (%)	LMD (microcracks/mm)
	K-feldspar	Plagioclase	Quartz	All	All	
XZ	9	6	22	37	11	1
YZ	10	5	23	38	10	1
XY	12	5	8	25	16	0.8
mean value	10	5	18	33	12	1

Grisolia stone (DG)

Grisolia stone, macroscopically, is a carbonate stone grey in colour with white and yellow inclusions. The commercial name of this stone is “pietra d’oro” (gold stone). It shows a compact structure with no visible pores (Fig. 6.1).

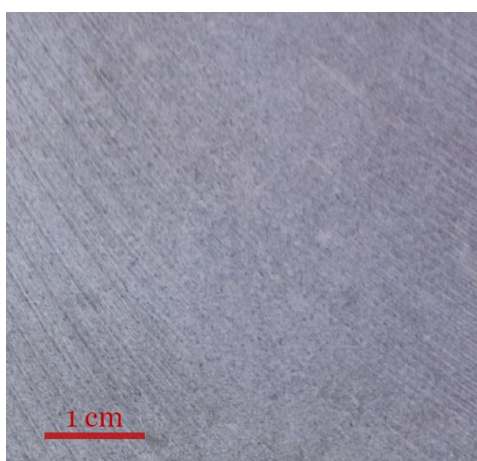


Fig. 6.1. Grisolia stone (DG)

Petrographically, DG (Fig. 6.1 a) is a compact limestone, with a very low porosity. It shows a non-recognizable depositional texture and a strong level of diagenesis. It can be classified as a *crystalline carbonate* (Dunham, 1962). Although it is fine grained, it shows coarser grained calcite crystals near the veins (Fig. 6.1 b).

Probably the diagenetic process - due to the recrystallization - can be related to “neomorphism”, in particular to an “aggrading neomorphism” that provoked the formation of coarser crystalline mosaics

(Tucker, 2010). The micritic matrix has been substituted by a neomorphic psuedosparite (between 10 and 50 μm crystal size), distinguishable for the irregular distribution of the granulometry composed by coarse mosaics and fine grained areas.

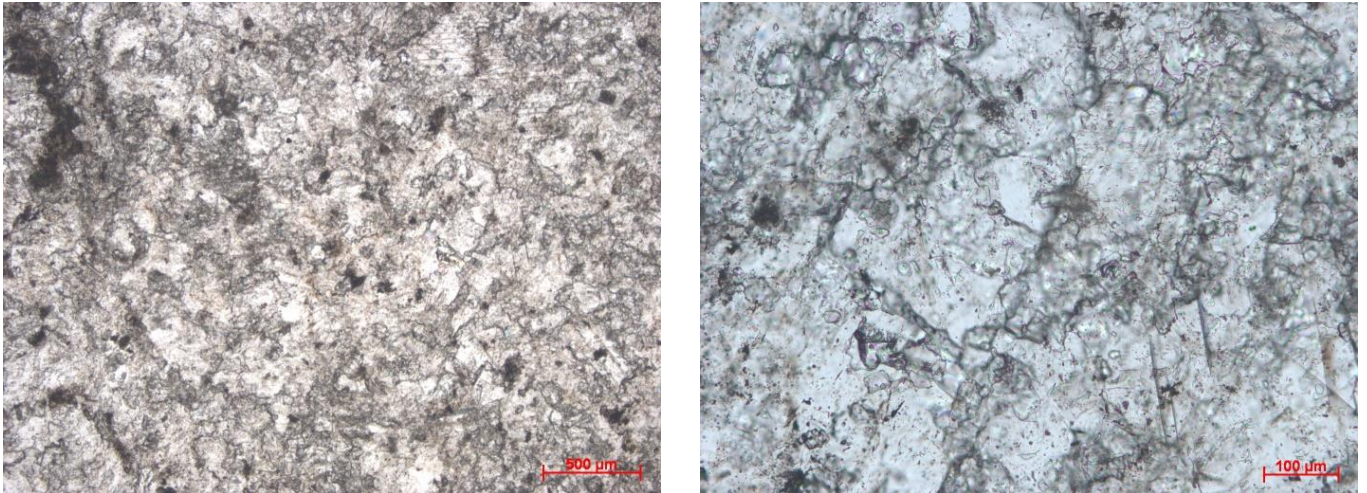


Fig. 6.1 a. Micrographs at the polarized optical microscope of thin sections of Grisolia stone. On the left plane polarized light and on the right crossed polarized light.

Analyzing the thin sections along the three directions (X, Y and Z), significant differences may not be observed (Fig. 6.1 b). Therefore, Grisolia stone can be considered as a homogeneous and isotropic material under a textural and mineralogical point of view at this microscopical level.

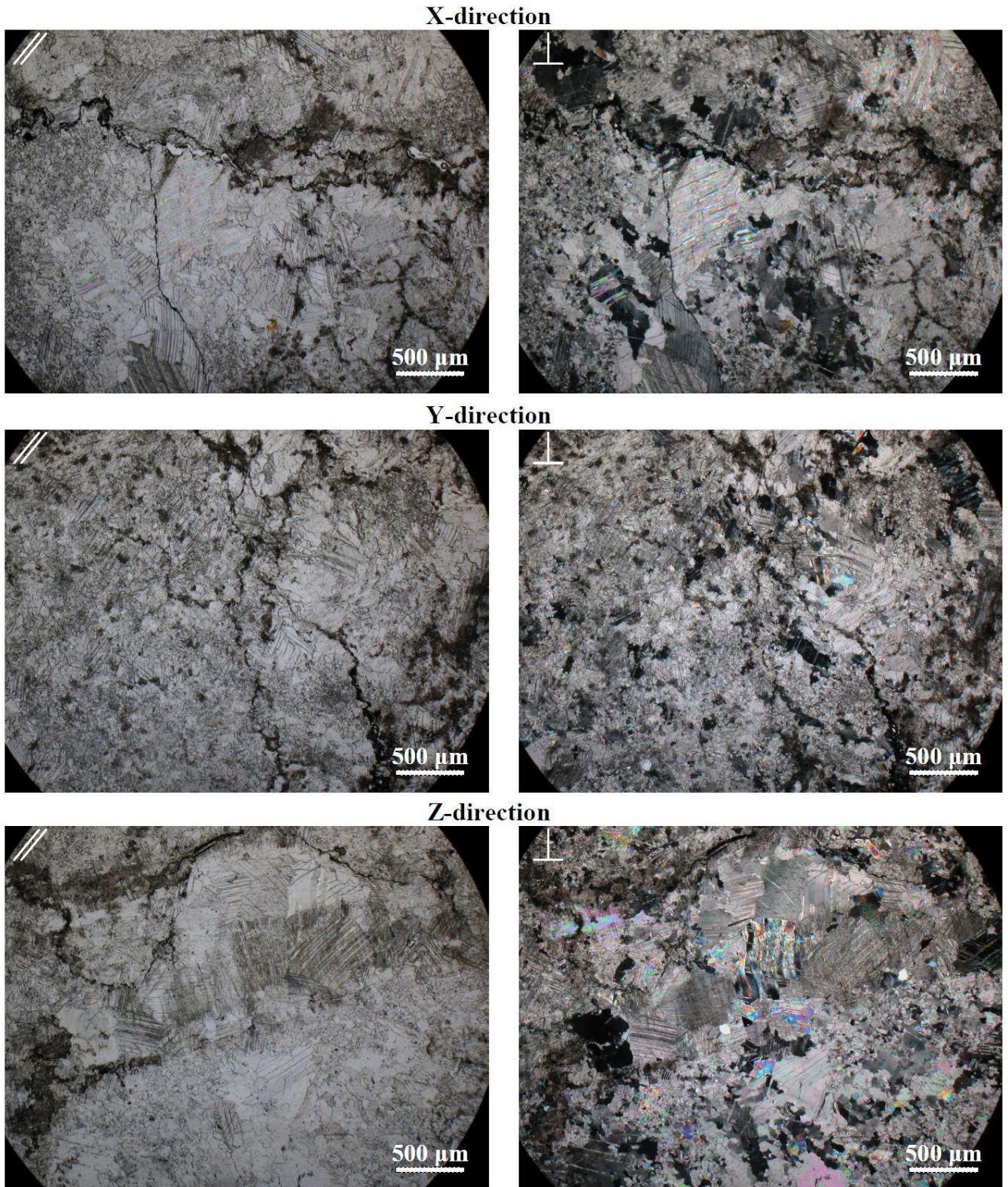


Fig. 6.1 b. Micrographs at the polarized optical microscope (on the left plane polarized light and on the right crossed polarized light) of thin sections from Grisolia stone, along the X, Y and Z-direction (from the top to the bottom).

San Lucido calcarenite (CS)

Macroscopically, San Lucido calcarenite exhibits a whitish colour, with a porous structure and visible fossils from 1 mm to 6.50 mm (Fig. 6.2).

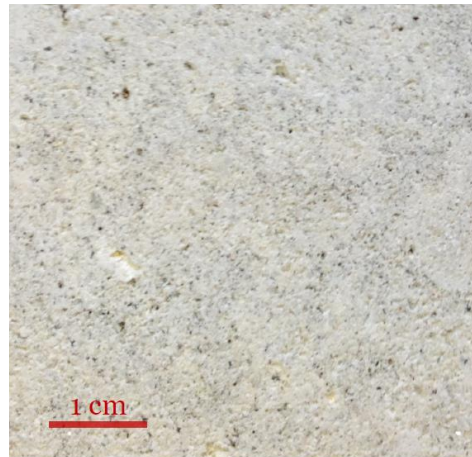


Fig. 6.2. San Lucido calcarenite (SC)

Petrographically, CS (Fig. 6.2 a) is a carbonate stone with bioclasts and peloids. The bioclastic component is more prevalent than the peloid one. The matrix is mainly composed of micrite, clayey to silty siliciclastic components that represent minor impurities. Fossils, like corals, echinoids, planktonic and benthic microforaminiferas, algae, bivalves and gastropods are also present. The pore system is distinguishable and associated with formation processes. The pores are irregular in shape. There are few interclastic pores and some are mold-like. In some cases, the porosity is associated with the internal structure of fossils. This stone varies between *biopelmicrite* and *biopelsparite*, according to Folk (1959), and can be classified as *packstone* according to Dunham (1962).

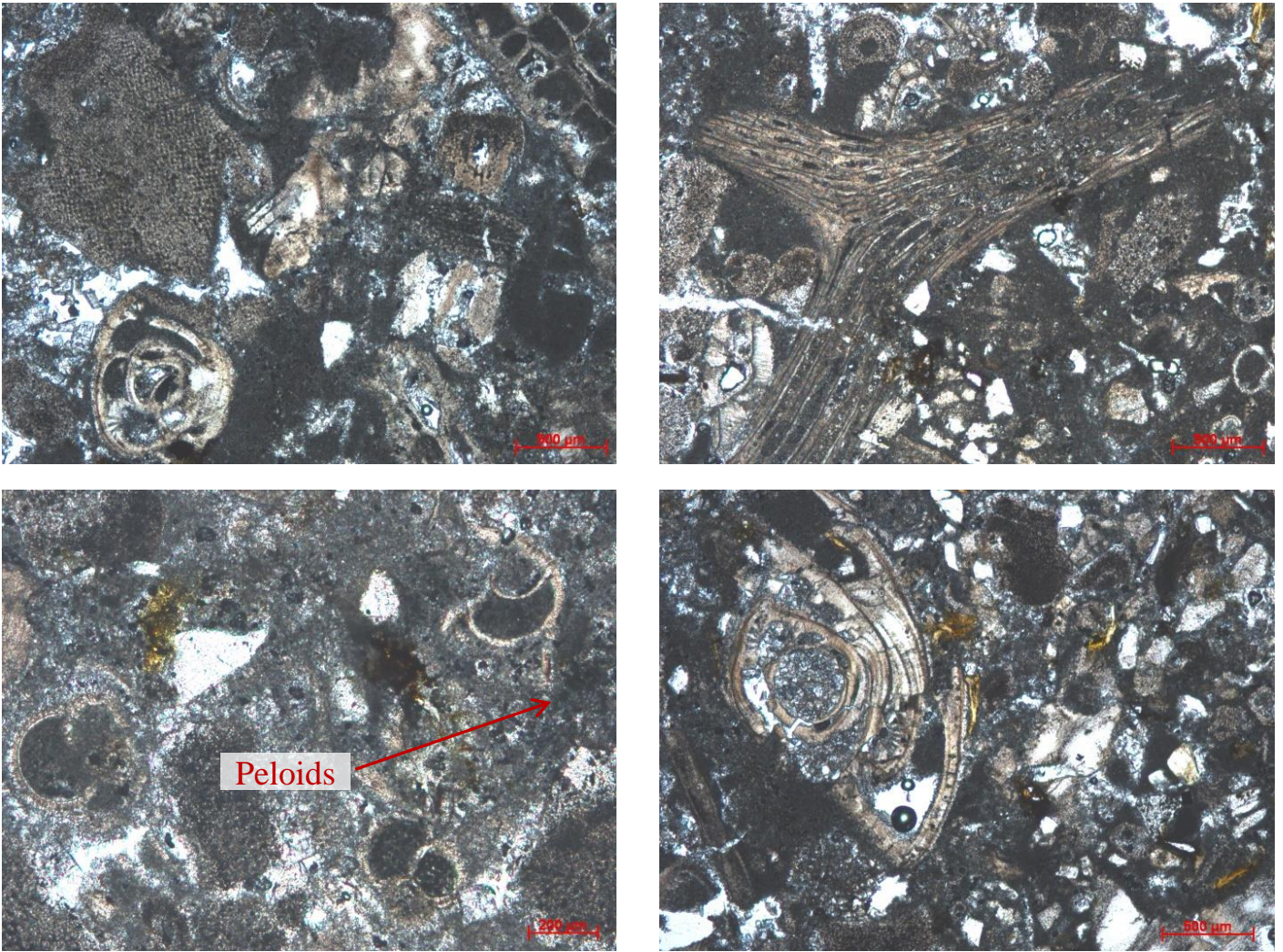


Fig. 6.2 a. Micrographs at the polarized optical microscope of thin sections from San Lucido calcarenite. Images at crossed polarized light.

Analyzing the thin sections along the three directions (X, Y and Z), no significant differences were detected (Fig. 6.2 b). So, San Lucido calcarenite is to be considered as a homogeneous and isotropic material.

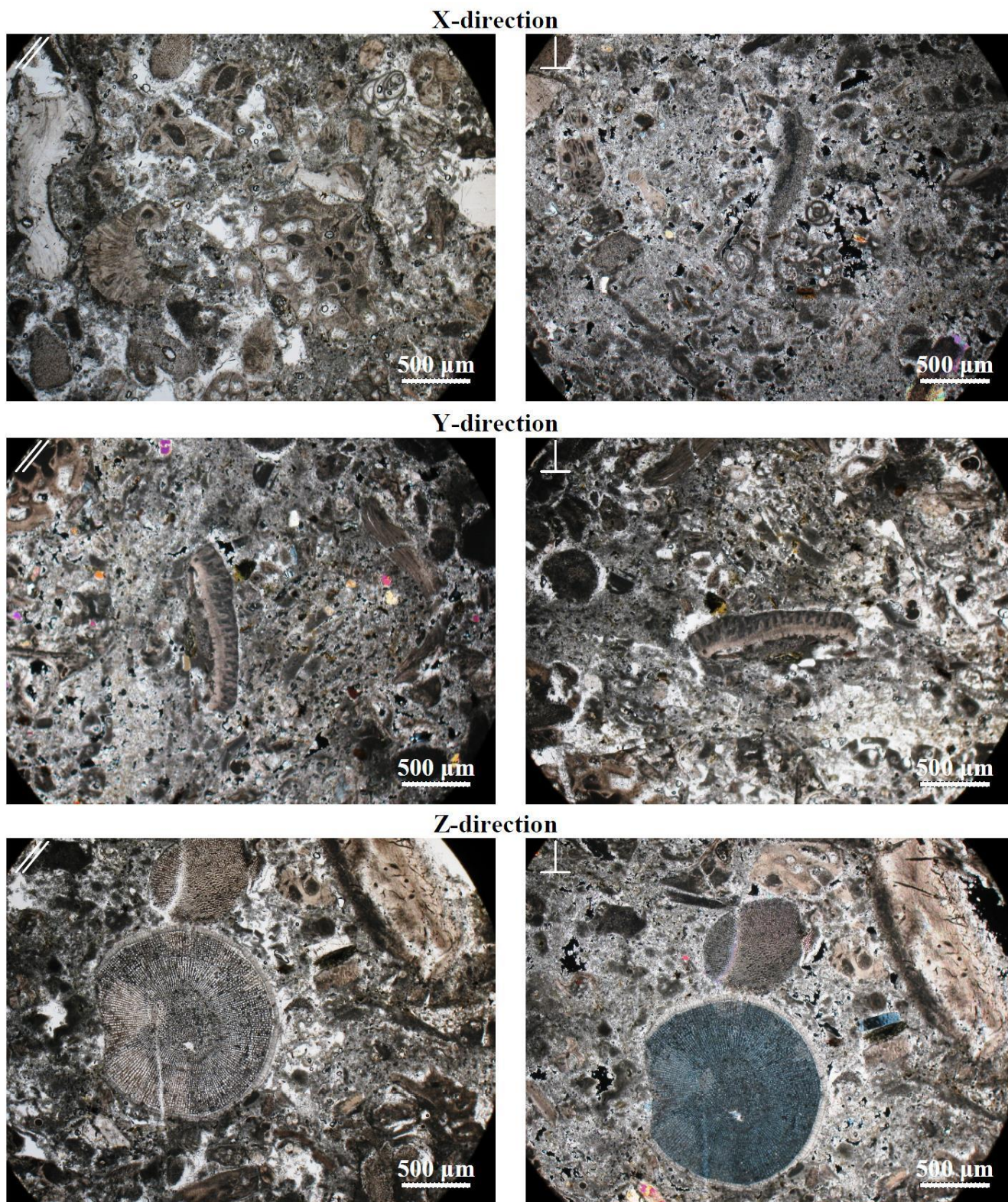


Fig. 6.2 b. Micrographs at the polarized optical microscope (parallel crossed polarized light) of thin sections from San Lucido calcarenite, along the X, Y and Z-direction (from the top to the bottom). On the left plane polarized light and on the right crossed polarized light.

Fuscaldo sandstone (AF)

Fuscaldo sandstone, macroscopically, shows a yellow-cream colour, with visible fossils and a porous structure (Fig. 6.3).

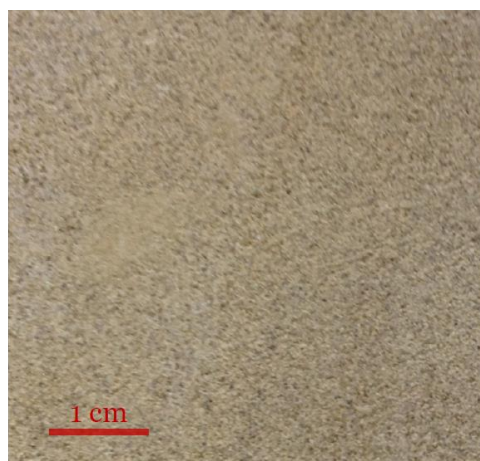


Fig. 6.3. Fuscaldo sandstone (AF)

Petrographically, AF contains a silico-clastic matrix (50%) and clasts (50%). It is characterized by a homogenous composition and texture (Fig. 6.3 a). Packing is moderate and quartz is the most abundant mineral phase. The quartz clasts are generally sub-angular to sub-rounded in shape. Some are irregular or oblong in size from 0.002 up to 1mm with a predominant value around 250 μm .

The quartz is mainly monocrystalline but also polycrystalline. Fragments of granitic stones, sub-rounded from 800 to 1000 μm , are also present. Feldspar crystals were observed in smaller concentrations, above all potassium feldspar with a large proportion of microcline and smaller amounts of orthoclase. Some of the feldspars crystals are altered. Plagioclase crystals with polysynthetic crystal twinning have been also identified. The micas are present, both biotite and muscovite in long laminar crystals around 250 μm , laid out in the same direction as the lamination of the stone. Some muscovite crystals are deformed or fractured. Biotite, which crystals are similar to muscovite ones in size and proportions has been also observed. In some cases, the biotite crystals are altered to iron oxyhydroxides and rarely to chlorite. Zircons have been detected as accessory phases.

A mainly micro-sparitic calcareous cement has been identified.

The pores are distinguishable with a mean value size of 25 μm ; dissolution areas parallel to the principal orientation of the stone are also present. Fossils attributable to microforaminiferas are also present. According to Pettijohn (1975), this stone can be classified as *greywacke*.

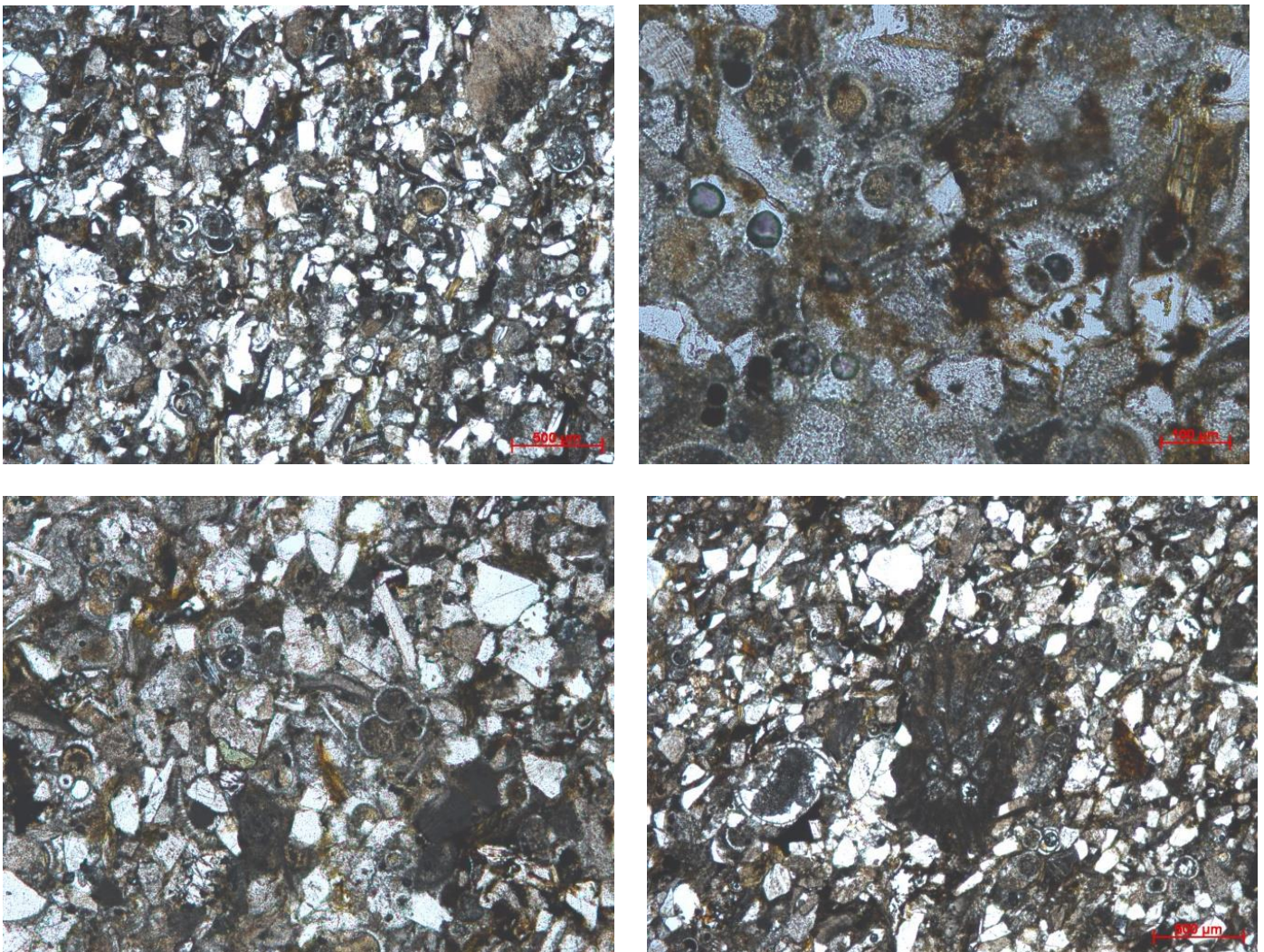


Fig. 6.3 a. Micrographs at the polarized optical microscope of thin sections from Fuscaldo sandstone. Images at crossed polarized light.

Analyzing the oriented thin sections (Fig. 6.3 b), along the X-direction a slight orientation of phyllosilicates along a prevalent direction can be observed, while for the other two directions (Y and Z) they are not well oriented.

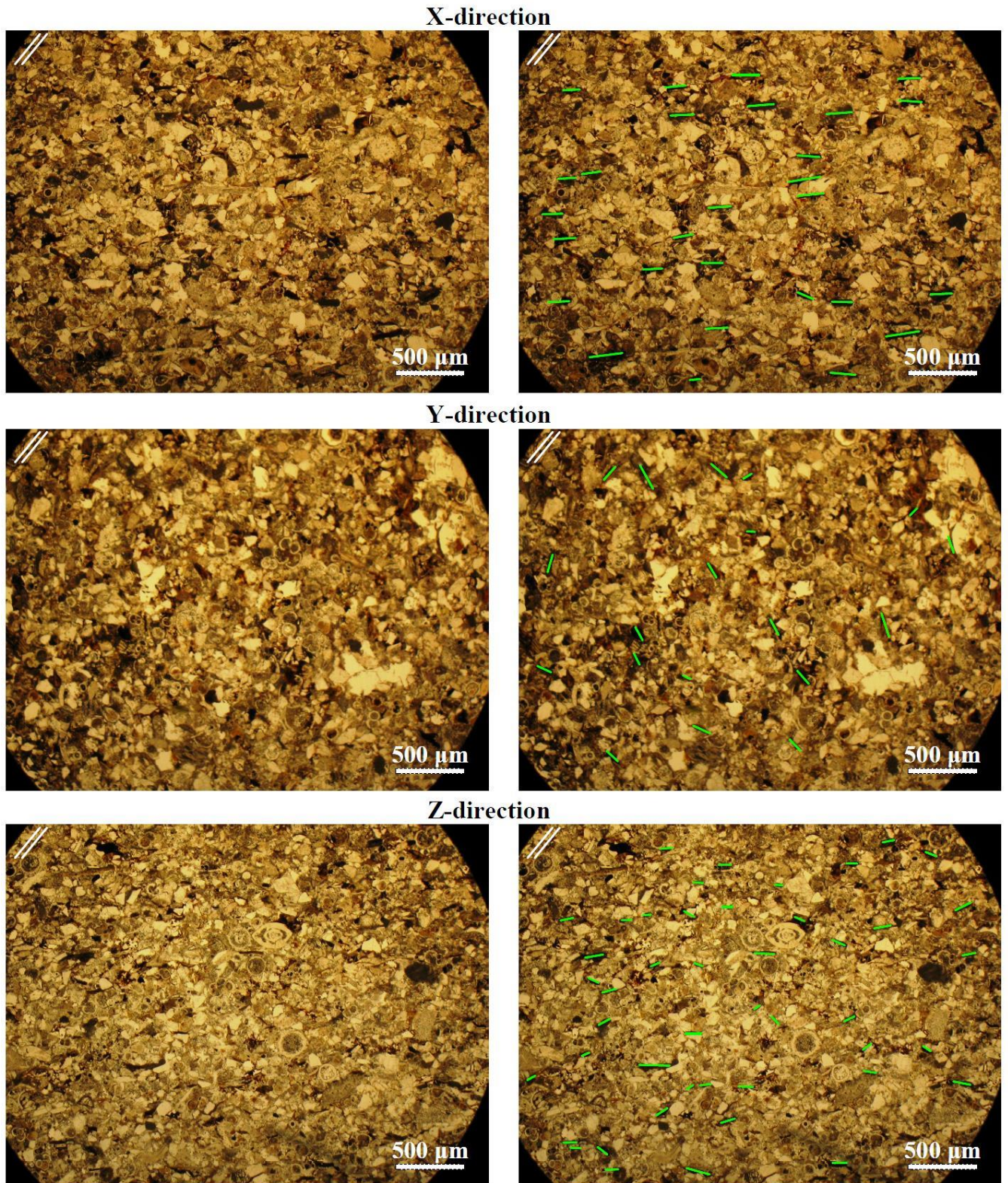


Fig. 6.3 b. Micrographs at the polarized optical microscope (parallel polarized light) of thin sections from Fuscald sandstone, along the X, Y and Z-direction (from the top to the bottom).

6.2 Chemical and mineralogical characterization

The mineralogical (XRD) composition of each stone and its chemical characterization (XRF), is shown in Table 6.1 and Table 6.2, respectively. Measurements are reported as weight percentages while trace elements are expressed in ppm (Table 6.2).

Table 6.1. The semi-quantitative mineralogical composition of the Granite of San Giovanni in Fiore (GF), Grisolia stone (DG), San Lucido calcarenite (CS) and Fuscaldo sandstone (AF), obtained by means of XRD analysis

Samples	Q	C	Chl	Bi	F	D
GF	xxxx	/	xx	xxx	xxx	/
DG	/	xxxx	/	/	/	tr
CS	x	xxxx	/	/	/	xx
AF	xxx	xxxx	x	x	xx	/

Q=quartz, C=calcite, Chl=chlorite, B=biotite, F=K-feldspar and plagioclase, D=dolomite; xxxx=very abundant, xxx=abundant, xx=present, x=scarce, tr=traces

Table 6.2. The chemical composition of San Giovanni in Fiore granite (GF), Grisolia stone (DG), San Lucido calcarenite (CS) and Fuscaldo sandstone (AF), obtained by means of XRF analysis. “n.d.” means “not detected”.

	GF	DG	CS	AF
SiO ₂	73.72	n.d.	n.d.	37.06
TiO ₂	0.25	n.d.	0.08	0.43
Al ₂ O ₃	12.51	0.07	1.18	7.57
Fe ₂ O ₃	3.15	0.06	0.79	3.73
MnO	0.11	0.01	0.07	0.51
MgO	0.61	0.77	3.68	2.07
CaO	1.62	98.95	93.71	45.43
K ₂ O	4.59	n.d.	0.46	2.06
P ₂ O ₅	0.06	0.15	0.03	0.14
Na ₂ O	3.39	n.d.	n.d.	0.99
TOT (%)	100.00	100.00	100.00	100.00
Rb (ppm)	195	5	11	63
Sr	83	395	740	662
Ba	467	n.d.	n.d.	304
Pb	26	2	7	12
Nb	17	3	3	6
Cu	9	9	9	12
Zr	125	7	14	103
Ni	12	3	11	25
Cr	239	n.d.	n.d.	120
V	23	7	12	43
Ce	48	25	20	42
Co	4	n.d.	n.d.	3
Y	46	5	5	19

XRD examinations indicate that: San Giovanni in Fiore granite (GF) is composed of quartz, K-feldspar and plagioclase, biotite and chlorite; Grisolia stone (DG) is composed of calcite and small amounts of dolomite, so it may be considered a *limestone*; San Lucido calcarenite (CS) is mainly composed of calcite, dolomite and quartz; Fuscaldo sandstone (AF) of calcite, quartz, K-feldspar and plagioclase and small amounts of biotite and chlorite (Table 6.1).

X-ray fluorescence has allowed the detection of (from the major to the minor): SiO₂ of 73.72% in GF, 37.06% in AF; CaO in DG with 98.95%, in CS with 93.71%, in AF with 45.43% and in GF with 1.62%; of Fe₂O₃ in AF with 3.73%, in GF with 3.15%, in CS with 0.79% and in DG with 0.06%; of Al₂O₃ in GF with 12.51%, in AF with 7.57%, in CS with 1.18% and in DG with 0.07%; of Na₂O in GF with 3.39% and in AF with 0.99%; of K₂O in GF with 4.59%, in AF with 2.06% and in CS with 0.46%; little amounts of MgO in CS with 3.68%, in AF with 2.07%, in DG with 0.77% and in GF with 0.61%; MnO in AF with 0.51%, GF 0.11%, CS 0.07% and DG 0.01%; very little amounts of P₂O₅ in DG with 0.15%, in AF with 0.14%, in GF with 0.06% and in CS with 0.03% (Table 6.2). In GF the presence of silica is prevalent while for DG, CS and AF calcite is prevalent than silica.

6.3 Surface properties

6.3.1 Chromatic parameters

The chromatic parameters were measured according to the CIE Lab system. The values are shown in Table 6.3. They are important to define the colour of each material as shown in Figs. 6.4 (a, b, c, d). Test results which have been obtained are plotted in Fig. 6.5.

For GF, the chromatic variations ($\Delta L^*_{2,1}$, $\Delta a^*_{2,1}$, $\Delta b^*_{2,1}$, $\Delta E^*_{2,1}$, $\Delta C^*_{2,1}$, $\Delta H^*_{2,1}$ and ΔE^*_{94}) between specimens not altered and those with yellow shades ($L_1^*a_1^*b_1^*$ and $L_2^*a_2^*b_2^*$), is reported in Table 6.4, in order to set a numerical comparative value between these different surfaces.

Table 6.3. Chromatic parameters of the granite of San Giovanni in Fiore (GF), Grisolia stone (DG), San Lucido calcarenite (CS) and Fuscaldo sandstone (AF), obtained by means of spectrophotometry analysis.

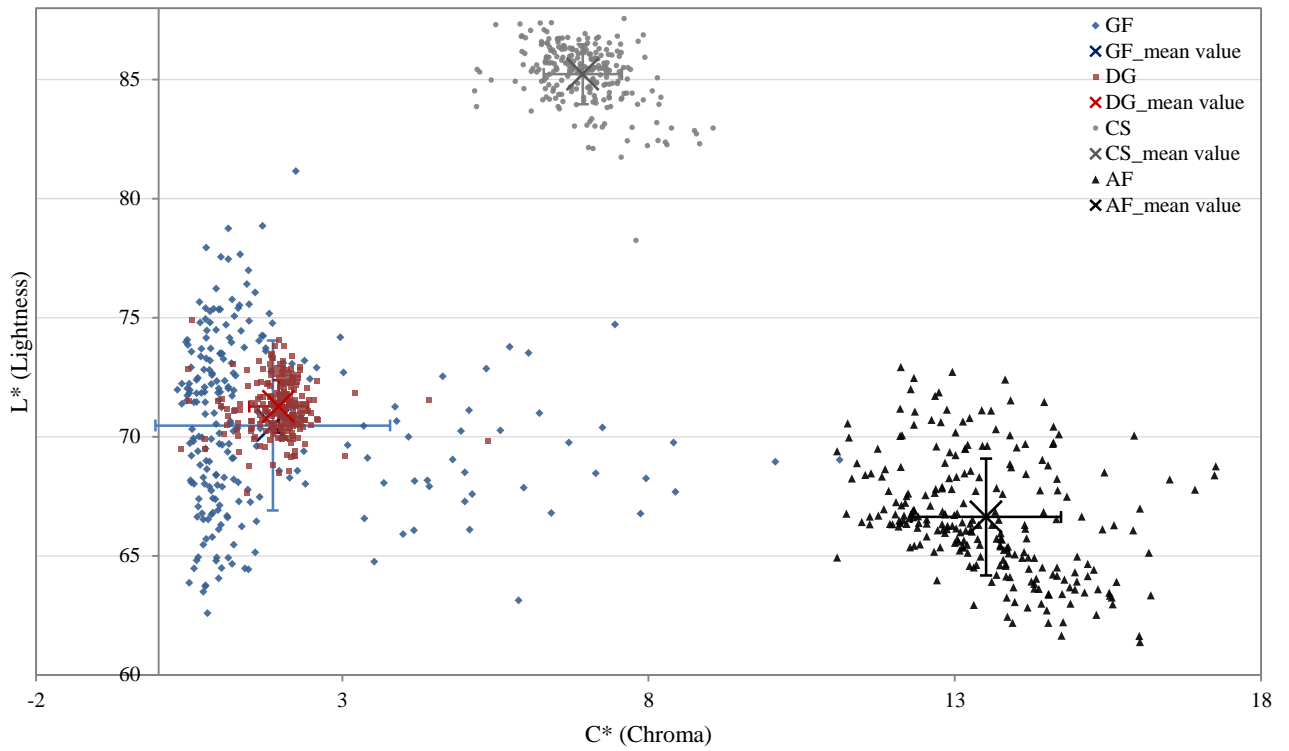
Samples		$L^*_{(D65)}$	$a^*_{(D65)}$	$b^*_{(D65)}$	$C^*_{(D65)}$	$WI_{(E313-73)}$	$YI_{(E313-73)}$	$B_{(ISO)}$
GF	mean value	70.48	-0.47	1.59	1.87	36.84	2.97	40.50
	st. dev.	3.57	0.38	2.07	1.92	8.47	4.15	5.42
DG	mean value	71.27	-0.24	-1.38	1.96	47.71	-3.03	43.74
	st. dev.	1.11	0.16	1.45	0.48	5.49	2.96	2.15
CS	mean value	85.23	0.14	6.92	6.93	36.15	11.51	59.40
	st. dev.	1.26	0.18	0.64	0.64	3.70	1.10	2.57
AF	mean value	66.63	2.45	13.28	13.51	-1.19	25.93	27.49
	st. dev.	2.46	0.38	1.19	1.22	3.47	2.41	3.03

L^* =the lightness coordinate; a^* = the red/green coordinate, with $+a^*$ indicating red, and $-a^*$ indicating green; b^* = the yellow/blue coordinate, with $+b^*$ indicating yellow, and $-b^*$ indicating blue; C^* =the chroma coordinate, the distance from the lightness axis; WI =the whiteness index; YI = the yellowness index; B =the brightness

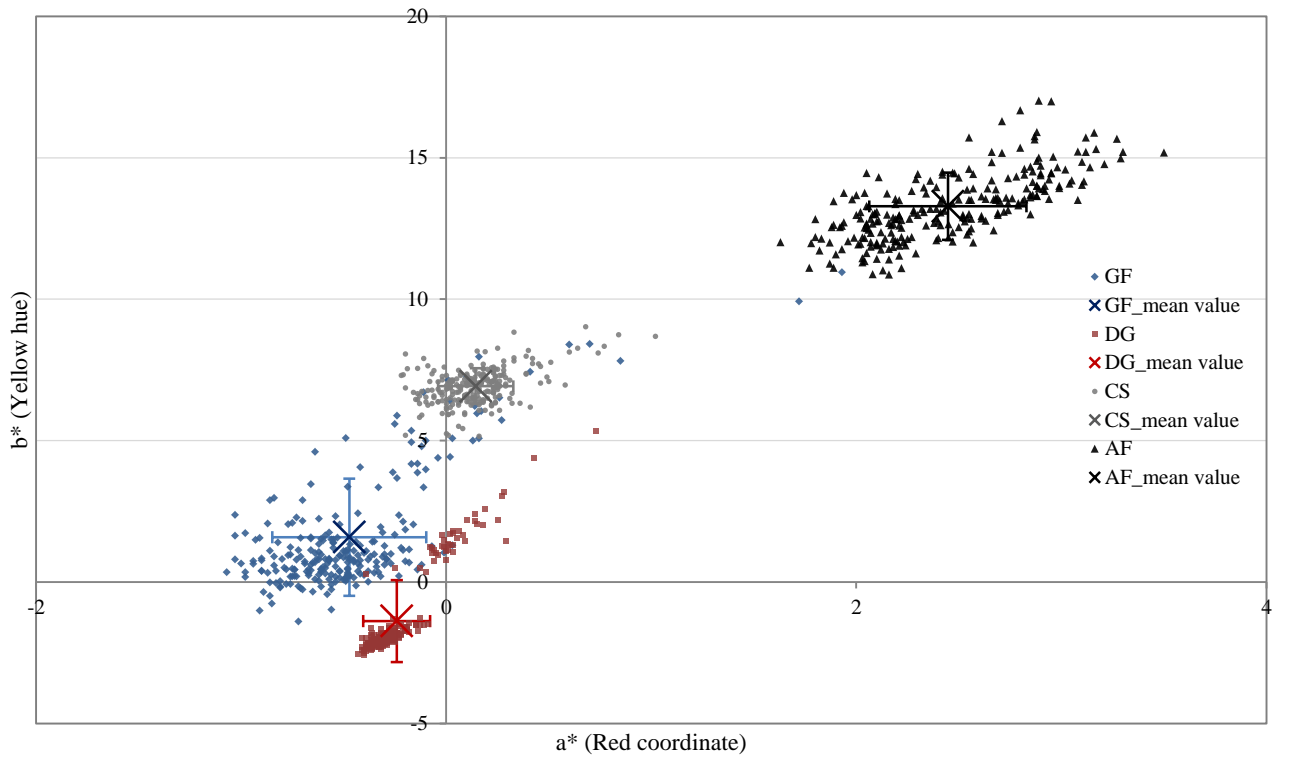
Table 6.4. Chromatic variations of the granite of San Giovanni in Fiore (GF): $\Delta L^*_{2,1}$; $\Delta a^*_{2,1}$; $\Delta b^*_{2,1}$; $\Delta E^*_{2,1}$; $\Delta C^*_{2,1}$; $\Delta H^*_{2,1}$ and ΔE^*_{94} .

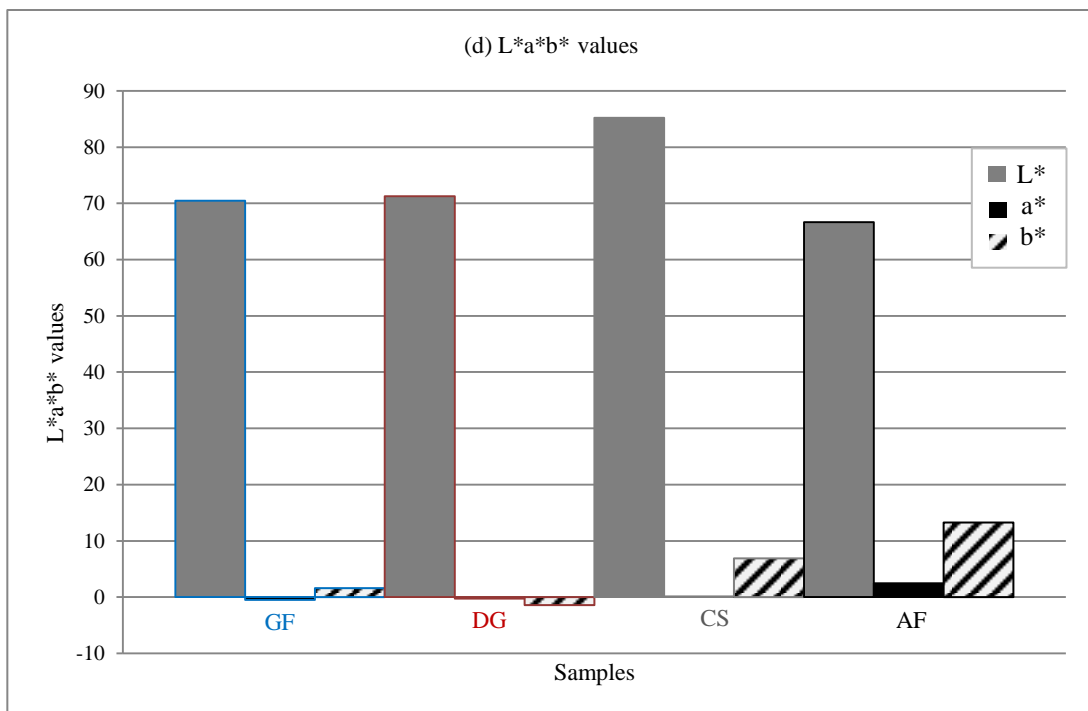
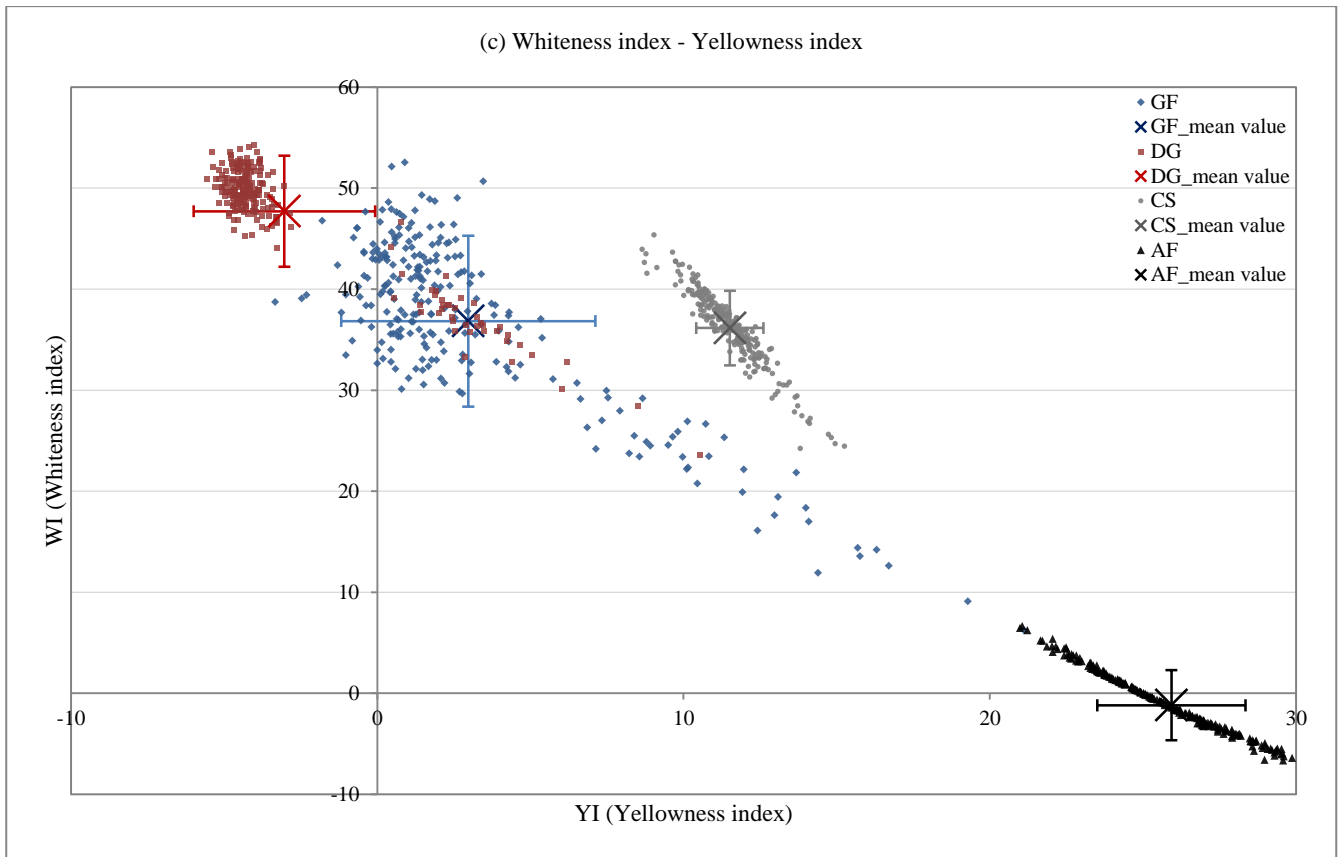
Samples	$\Delta L^*_{2,1}$	$\Delta a^*_{2,1}$	$\Delta b^*_{2,1}$	$\Delta E^*_{2,1}$	$\Delta C^*_{2,1}$	$\Delta H^*_{2,1}$	ΔE^*_{94}
GF	-1.95	0.62	4.76	5.18	4.44	1.83	4.79

(a) Lightness - Chroma



(b) Yellow hue - Red hue





Figs. 6.4 a, b, c, d. Chromatic parameters mean values of San Giovanni in Fiore granite (GF), Grisolia stone (DG), San Lucido calcarenite (CS) and Fuscaldo sandstone (AF): (a) C^* =Chroma and L^* =Lightness; (b) a^* =red hue and b^* =yellow hue; (c) YI =yellowness index and WI =whiteness index; (d) bar chart diagrams for L^* , a^* and b^* mean values.

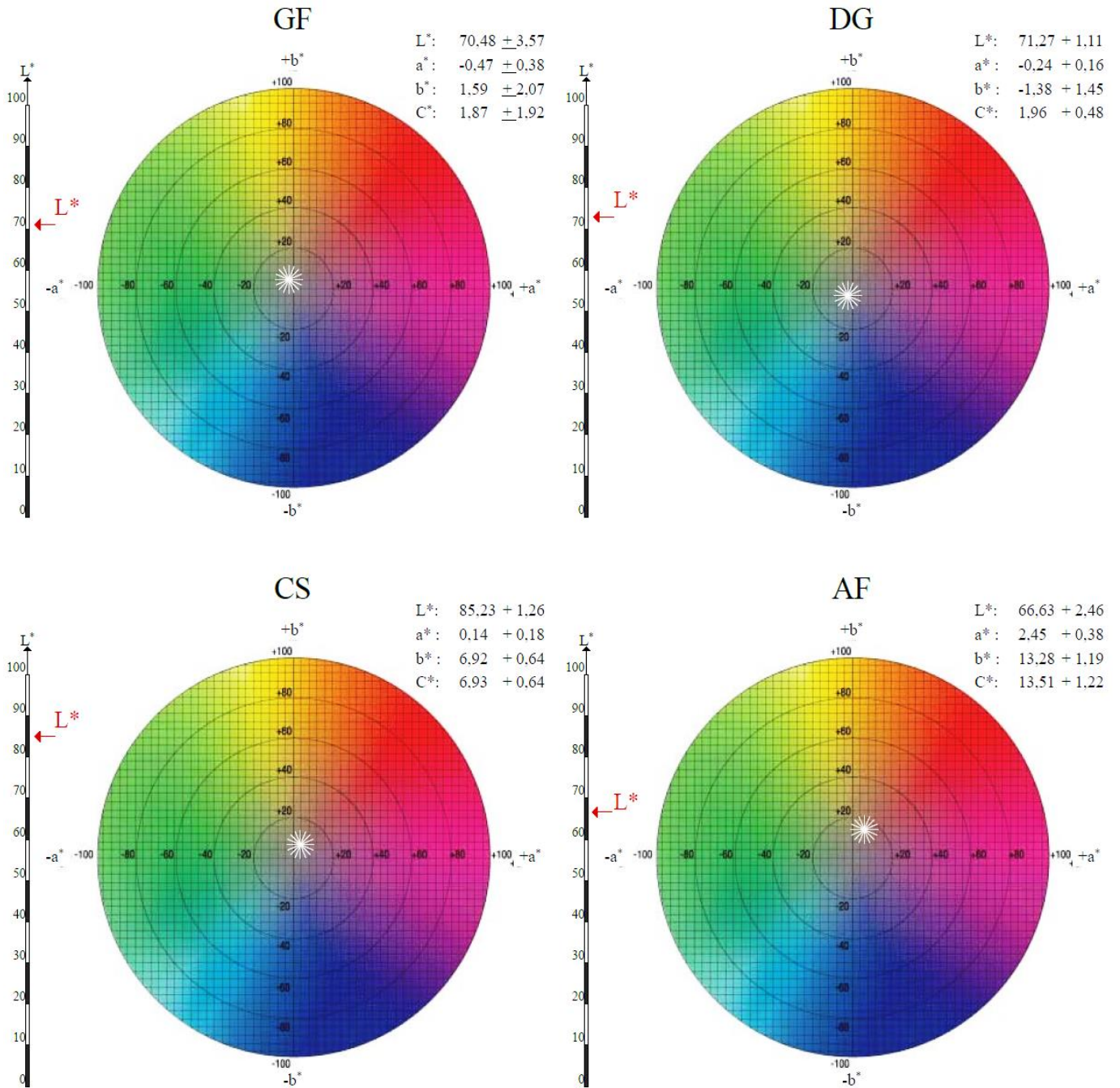


Fig. 6.5. Results of chromatic mean values of San Giovanni in Fiore granite (GF), Grisolia stone (DG), San Lucido calcarenite (CS) and Fuscaldo sandstone (AF).

6.4 Petrophysical properties

The typical features of the void space of the materials were observed and described by means of the porosity tests of real and bulk densities, mercury intrusion porosimetry and air permeability.

6.4.1 Porosity accessible to water and real and bulk densities

Mean values and standard deviations of open porosity, real and bulk density, water absorption under vacuum and compactness index are reported in Table 6.5, for the four materials.

Table 6.5. Results of the water absorption under vacuum test: ρ_{sk} = real or skeletal density (g/cm^3); ρ_b = apparent or bulk density (g/cm^3); p_o = open porosity (%); W_{vac} = water absorption under vacuum conditions (%); I_c = compactness index.

Samples	ρ_{sk} (g/cm^3)	ρ_b (g/cm^3)	p_o (%)	W_{vac} (%)	I_c
GF	2.72 \pm 0.01	2.68 \pm 0.01	1.35 \pm 0.06	0.50 \pm 0.02	0.98 \pm 0.00
DG	2.72 \pm 0.00	2.70 \pm 0.00	0.54 \pm 0.08	0.20 \pm 0.03	0.99 \pm 0.00
CS	2.74 \pm 0.01	2.29 \pm 0.02	16.18 \pm 0.81	7.05 \pm 0.41	0.84 \pm 0.01
AF	2.70 \pm 0.00	2.16 \pm 0.06	20.14 \pm 2.28	9.36 \pm 1.33	0.80 \pm 0.02

As can be seen, mean values of apparent and real density are similar for GF and for DG, due to their low open porosity, while there is a difference between the two average values for CS and AF, due to the higher porosity values. Also the content of water absorbed depends on the open porosity: the greater the porosity, the higher the amount of absorbed water. The highest porosity values have been registered for AF ($p_o=20.14\pm 2.28\%$), followed by CS ($p_o 16.18\pm 0.81\%$). Conversely, the lowest values belong to DG with a mean value of open porosity of $0.54\pm 0.08\%$ (p_o), that result on the most compact material ($I_c=0.99$), followed by GF with an open porosity of $1.35\pm 0.06\%$ (p_o) and a compactness index of 0.98 (I_c). Regarding the obtained mean values and according to the stone classification of von Moos & De Quervain (1948), it is possible to classify the four materials investigated as follows: DG as *compact* ($p_o < 1\%$); GF with *few pores* ($1 < p_o < 2.5\%$); CS with *many pores* ($16 < p_o < 20\%$); AF with *a lot of pores* ($p_o > 20\%$). Moreover, according to the classification of Anon (1979), it is possible to affirm that GF and DG exhibit *low porosity* ($1 < p_o < 5\%$), while CS and AF exhibit *high porosity* ($p_o > 15\%$) (Bell & Lindsay, 1999).

Concerning the standard deviation values, it is possible to define as “homogeneous” GF and DG for their low values and on the contrary as “heterogeneous” CS and AF for their higher values.

6.4.2 Mercury intrusion porosimetry (MIP)

Mercury intrusion porosimetry (MIP) was performed in order to characterize the porous media of the four stones.

The total cumulative volume, the average pore diameter, the open porosity, the apparent (ρ_{sk}) and the bulk density (ρ_b) of quarry samples, obtained by MIP analysis, are reported in Table 6.6 and in Fig.

6.6.

Table 6.6. Results of the mercury intrusion porosimetry test: Tot.intr.V. = total intrusion volume (mL/g); Av.pore diam. = average pore diameter (μm); p_o = open porosity (%); ρ_{sk} = real or skeletal density (g/cm^3); ρ_b = apparent or bulk density (g/cm^3).

	Samples	Tot. Intr. V. (mL/g)	Av. pore diam. (μm)	Po (%)	ρ_{sk} (g/cm^3)	ρ_b (g/cm^3)
GF	mean value	0.0036	0.29	0.94	2.66	2.66
	st. dev.	0.0003	0.10	0.08	0.05	0.02
DG	mean value	0.0010	0.70	0.21	2.38	2.38
	st. dev.	0.0011	0.03	0.24	0.37	0.38
CS	mean value	0.0583	0.49	12.93	2.22	2.55
	st. dev.	0.0116	0.08	2.53	0.01	0.07
AF	mean value	0.1030	0.15	20.94	2.04	2.57
	st. dev.	0.0063	0.00	0.71	0.06	0.05

Macro and micro porosity and the pore diameter distribution are shown in Table 6.7 and the pore size distribution in Figs. 6.7 (a, b, c, d), for each material. The obtained median pore diameters (Area) are: 0.1183 μm for GF; 0.0620 μm for DG; 0.2416 μm for CS; 0.0311 μm for AF.

Table 6.7. Macro and micro porosity and pore diameter distribution, by means of the mercury intrusion porosimetry test.

Samples	Macro >5 μm (%)	Micro <5 μm (%)	<0.1 μm	0.01-0.1 μm	0.1-1 μm	1-10 μm	10-100 μm	>100 μm
GF	28.10	71.90	/	7.45	41.44	29.11	14.19	7.82
DG	76.16	23.84	/	4.91	14.15	15.17	23.06	42.70
CS	31.41	68.59	/	2.68	43.46	43.40	8.77	1.69
AF	2.96	97.04	0.96	12.78	42.07	42.31	0.98	0.91

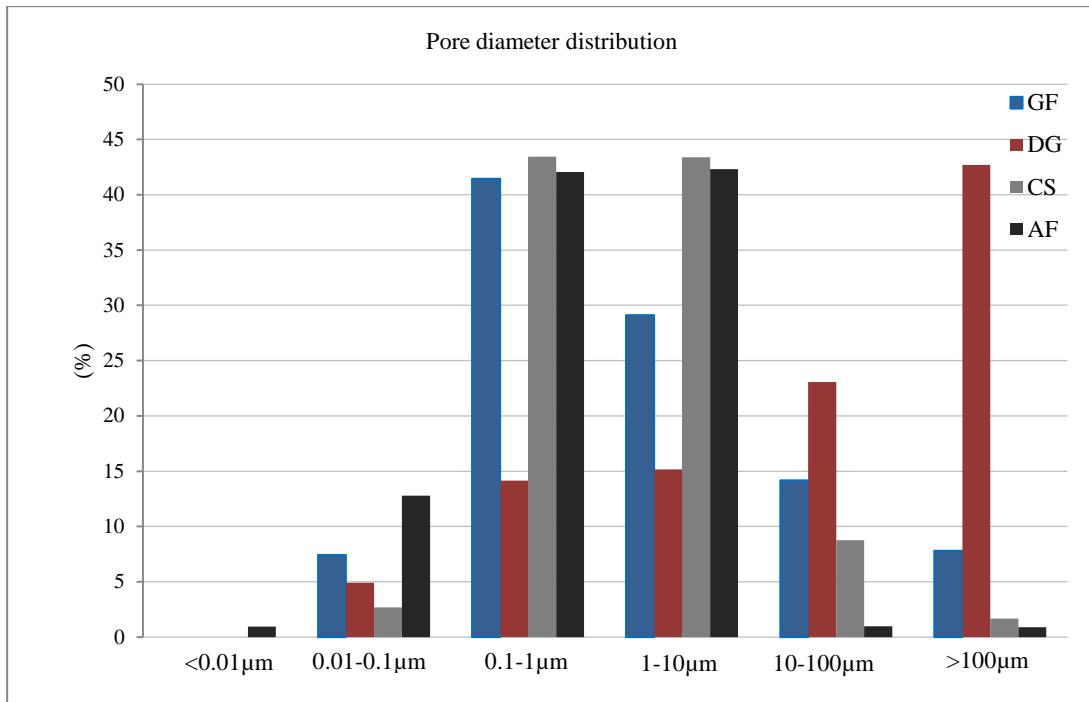
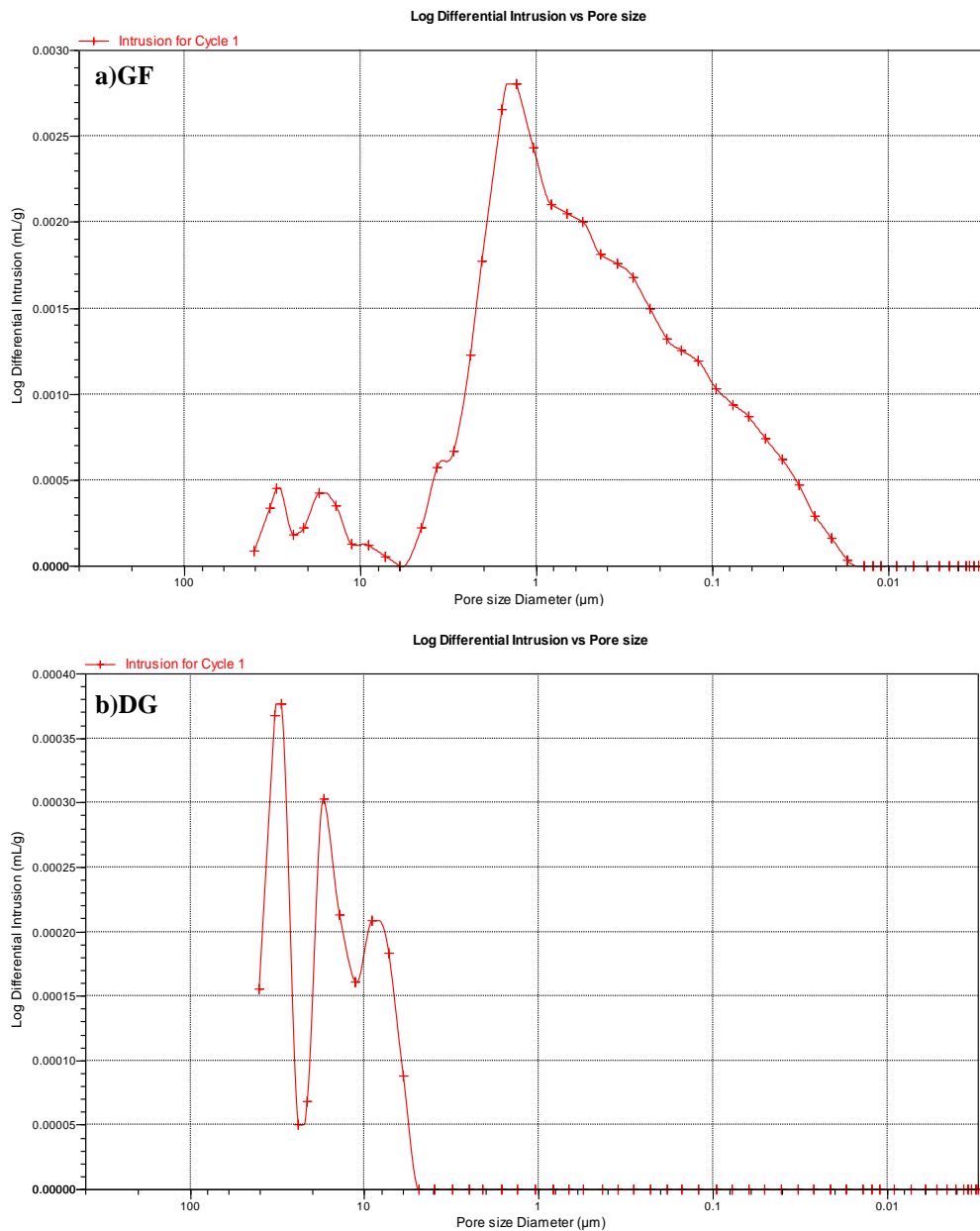


Fig. 6.6. The pore diameter distribution of the four stones based on mercury intrusion porosimetry.



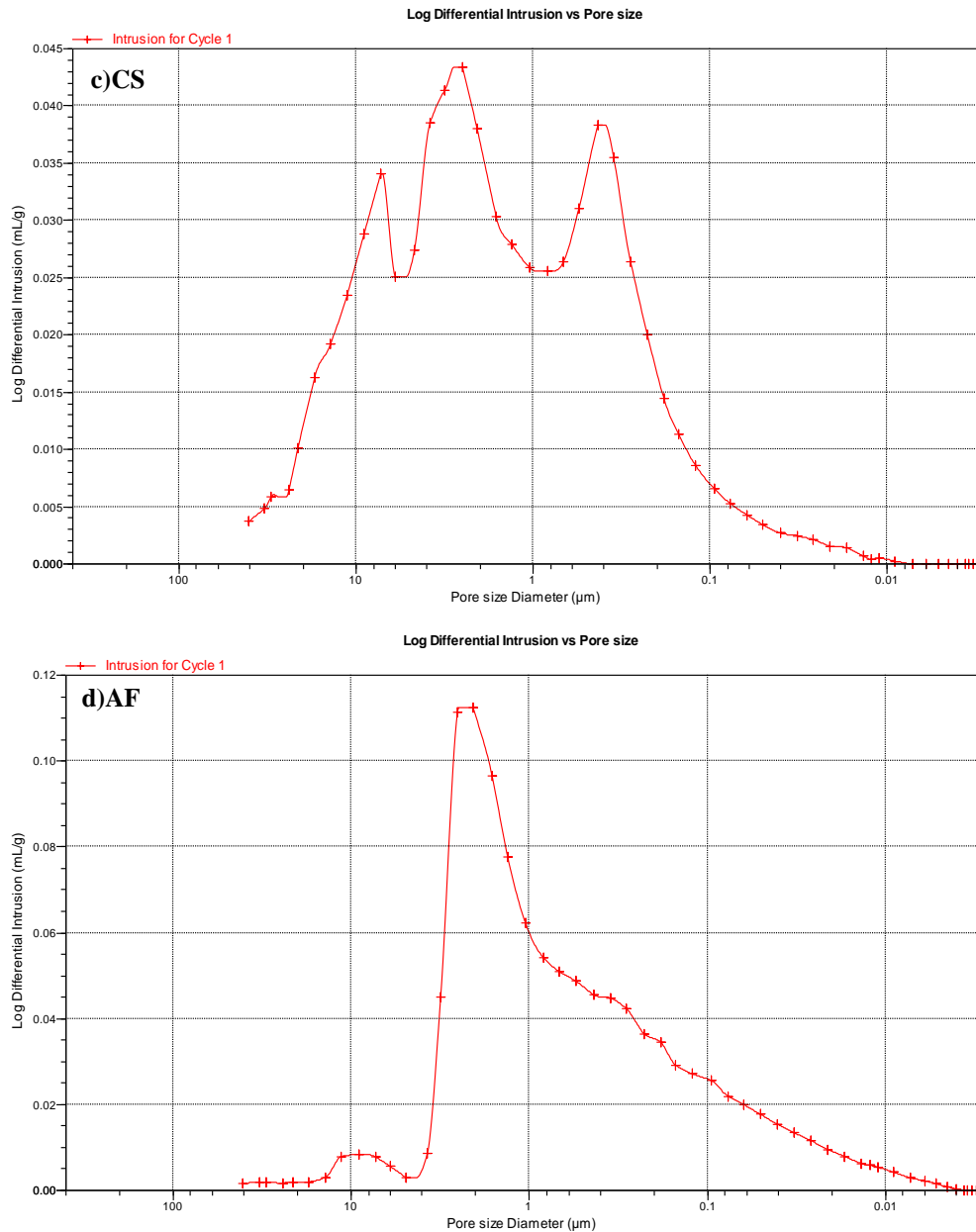


Fig. 6.7. Pore size distribution curves [Log differential intrusion (mL/g) vs. pore size diameter (μm)] obtained by MIP analysis of GF (San Giovanni in Fiore granite), DG (Grisolia stone), CS (San Lucido calcarenite) and AF (Fuscaldo sandstone).

As regards the pore size distribution, the results on the microporosity (<5μm; De Quervain, 1967) measured by MIP analysis, show: an unimodal distribution in the range 0.1–1μm for GF; a trimodal distribution for CS and AF in the ranges 0.1–1μm, 1–10μm and 10–100 μm for CS and in the ranges of 0.01–0.1μm, 0.1–1μm and 1–10μm for AF, respectively; an unimodal distribution for DG in the range of macroporosity, as reported in Table 6.7 and Fig. 6.6.

All analyzed samples present high values of microporosity, while only DG presents a lower percentage of microporosity as well as the highest value of macroporosity (76.16%). The highest value of microporosity has been reached by AF with 97.04%.

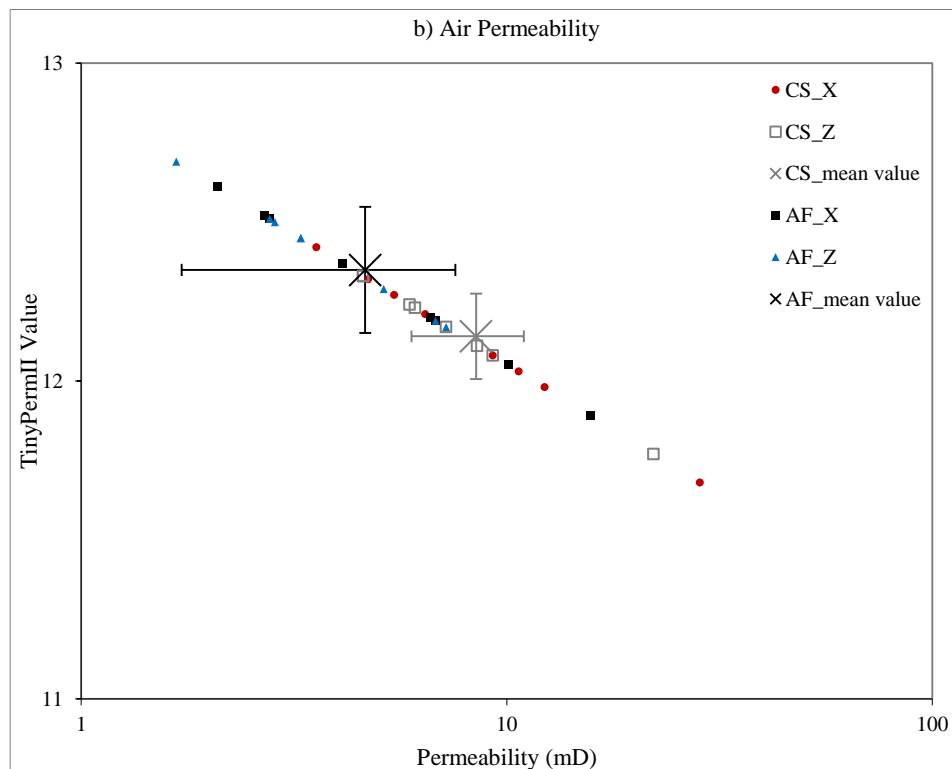
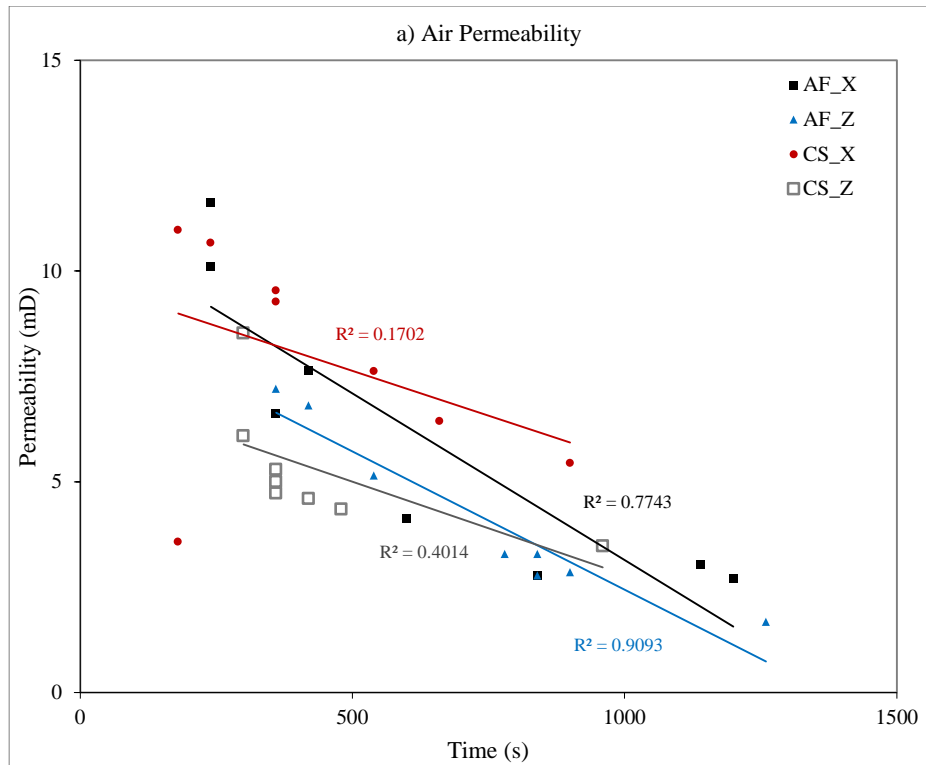
Regarding the obtained values of microporosity, it can be said that the stones that have a small percentage of micropores and a low porosity, like DG, could have a higher durability than those with a larger percentage of micropores and higher porosity like AF and CS. GF, even though it presents high values of microporosity, shows a very low porosity value (Ruedrich *et al.*, 2005).

6.4.3 Air permeability

Air permeability test was performed on eight cubic specimens, along two directions, X and Z, for each stone type. For GF and DG was reached a time longer than 4 hours without registering any values. So, it can be said that granite of San Giovanni in Fiore and Grisolia stone, show an impermeable behaviour (Filomena *et al.*, 2014). On the contrary, air permeability values and time, by means of air permeability test, are reported in Table 6.8. In Figs. 6.8 (a, b) the correlation between permeability and time and with Tiny Perm values, along the two directions and for AF and CS is shown.

Table 6.8. Air permeability values along the two directions X and Z: TP = Tiny Perm measurements; t = time registered (s); AirP = air permeability value (mD).

Samples	TP			t (s)			AirP (mD)			
	min	max	mean	min	max	mean	min	max	mean	
CS	mean value	12.02	12.43	12.23	180	960	435	3.47	10.97	6.60
	st. dev.	0.14 (X)	0.09 (Z)	0.13	255 (X)	217 (Z)	229	5.26 (Z)	7.94 (X)	2.50
AF	mean value	12.00	12.69	12.35	240	1260	686	1.67	11.61	5.10
	st. dev.	0.21 (X)	0.18 (Z)	0.20	388 (X)	294 (Z)	337	4.13 (Z)	6.07 (X)	2.50



Figs. 6.8 a, b. Binary diagrams showing the correlation between the mean values of air permeability (mD) and (a) the time (s), (b) Tiny PermII values, for San Lucido calcarenite (CS) and Fuscaldo sandstone (AF).

Regarding the correlation between air permeability and time for both materials (Fig. 6.8 a), it can be said that air permeability reach lower values for higher times. Fuscaldo sandstone (AF) reaches the

highest values of correlation of 0.77 (R^2) along the X-direction and 0,91 along Z-direction, as well as the highest values of air permeability along Z. Contrarily to the porosity values registered, CS showed higher values of air permeability than AF, mean values of $6.40 \pm 2.50 \text{mD}$ and $4.67 \pm 2.50 \text{mD}$, respectively. This fact could be explained with the average pore area measured by mercury intrusion porosimetry that is higher for CS ($0.2416 \mu\text{m}$) than AF ($0.0311 \mu\text{m}$). Therefore, as pore throat size increases, a subsequent increase in permeability occurs because the pore-throat distribution is closely related to the permeability of the samples (Allen, 1990; Giesche, 2006; Nooruddin *et al.*, 2014).

Coherently to the spatial directions, X-axis is the direction along which registered values of permeability are higher than those along the Z direction, where the air-flow trajectory is oriented orthogonal to the foliation planes.

6.5 Hydric properties

Hydric tests are widely used for the characterization of building materials as they provide information about pore structure, hydric behavior and hence degradability.

6.5.1 Capillary water absorption – (Infrared Camera)

Capillary water absorption test provides information about the velocity and the amount of the water uptake. The capillary coefficient is calculated from the slope of the first part of the capillarity uptake curve in a capillary water absorption vs. time plot.

According to the obtained porosity values obtained from the MIP test, water absorption by capillary test has shown some differences among the samples: Grisolia stone samples (DG) exhibit the lowest values of capillarity, with an average capillary absorption coefficient of $1.25 \pm 0.05 \text{ g/m}^2 \text{ s}^{0.5}$. Conversely, San Lucido calcarenite (CS) shows the highest values of capillarity, with a mean value of

48.86±0.82 g/m²s^{0.5}. San Giovanni in Fiore granite samples (GF) reach an average coefficient of 3.35±0.14 g/m²s^{0.5}, while Fuscaldo sandstone (AF) exhibits a mean value of 29.18±6.06 g/m²s^{0.5}. The capillary imbibition kinetics of the four stones is reported in Fig. 6.9. The slope of the initial stretch of the curve during capillary absorption is the capillary absorption coefficient (C_c). The first part of each curve defines the capillary water absorption, while the second part defines the saturation. The first part is linear for all samples while the second part is different for each material. Fig. 6.9 highlights that CS absorbs water more quickly than the other stone specimens (first part of the curve), while AF absorbs the major water quantity due to its higher open porosity (the second part). The difference of capillary suction rate depends on pore diameter (Siegesmund & Dürrast, 2014) and on porosity. Smaller pore diameters and smaller connected porosity values lead to lower coefficients (C_c) and slow water transport (López-Arce *et al.*, 2009, 2010). According to Winkler (1997), the pore involved in the capillary process ranges from 0.1 and 1000 μm. CS, due to the presence of larger pores (0.49μm), absorbs water faster than AF, characterized by smaller pores (0.15μm). The difference in the absorbed water quantity is to be related to the porosity: as AF that has higher open porosity than CS, absorbs more water. This difference explains the different velocity of AF and CS in the two parts of the curve (Fig. 6.9).

Data in Table 6.9 and the graph in Fig. 6.9 reveal that GF, DG and CS samples do not show any significant variations of the water absorption coefficient by capillarity along the two investigated directions (X and Z); hence it can be said that the stones do not exhibit a strong anisotropy related to the capillary absorption. On the contrary, AF, shows a different hydric behavior along the two directions, with an average coefficient along X (C₂) of 33.46±9.41 g/m²s^{0.5} higher than the coefficient value (C₁) of the Z direction with a mean value of 24.89±5.79 g/m²s^{0.5}, due to its hydric behavior anisotropy.

In relation to the obtained average values and according to the classification of Snethlage (Siegesmund & Dürrast, 2014), it is possible to identify two groups of stones: the “slightly absorbing” group, with GF and DG and the “medium absorbing” group, with CS and AF (Fig. 6.9).

Capillary absorption also exhibits a strong directional dependency which can be significant (Poschlod, 1990; Weiss, 1992; Ruedrich *et al.*, 2005, 2007, 2010). According to the results of the infrared thermography test performed during the capillary water absorption, it can be assumed that the lowest capillary water absorption values are measured perpendicularly to the textural and structural orientation. As it is shown in Figs. 6.11(a, b), capillary water absorption is faster along the X-direction than the Z-axis for the four materials. GF exhibits a little difference in the heights of water absorbed, higher along X direction than Z. Moreover along Z direction, GF does not reach the complete saturation after 72h, while along X direction it shows a capillary higher level of water at 24h. The same behavior is shown for short times while for long times the hydric behavior is different. Effectively, as shown in the Fig. 6.10 (a) and by infrared images, along Z direction the curve is composed by three parts that are the same of those along X, but along the X-direction the hydric curve presents a fourth part when the material reaches the full imbibition. DG does not absorb a significant quantity of water, coherently to the measured porosity values. It shows an isotropic hydric behavior (Fig. 6.10 b), so it does not exhibit any significant difference in the water heights reached along the two axes (Figs. 6.11 a, b). CS shows an isotropic hydric behavior, too. In fact, it saturates at 2h for both directions (Figs. 6.11 a, b). But for larger times, while along X direction the hydric behavior is characterized by only two parts, along Z direction there is a third part, probably due to the difficult water absorption in the direction oriented perpendicular to the foliation planes (Fig. 6.10 c). AF reaches a distinct saturation for the two anisotropic directions, at 8h along X direction while at 24h along Z direction. This fact is coherent with the anisotropic behavior shown in Fig. 6.10 (d), where it is possible to notice the different hydric

behavior along the two investigated directions. So, it is possible to say that Fuscaldo sandstone (AF) has an anisotropic hydric behavior.

Table 6.9. Hydric test. C_C = mean value of capillary water absorption coefficient ($\text{g/m}^2\text{s}^{0.5}$; $\text{kg/m}^2\text{h}^{0.5}$) of the two directions investigated (X and Z); C_2 and C_1 = capillary absorption coefficient along X and Z, respectively ($\text{g/m}^2\text{s}^{0.5}$; $\text{kg/m}^2\text{h}^{0.5}$). Capillary water absorption values are expressed in two units of measurement to be easily compared to the Snethlage classification (Siegesmund & Dürrast, 2014).

	Samples	C_2 ($\text{g/m}^2\text{s}^{0.5}$)	C_1 ($\text{g/m}^2\text{s}^{0.5}$)	C_C ($\text{g/m}^2\text{s}^{0.5}$)	C_2 ($\text{kg/m}^2\text{h}^{0.5}$)	C_1 ($\text{kg/m}^2\text{h}^{0.5}$)	C_C ($\text{kg/m}^2\text{h}^{0.5}$)	w-value - Snethlage
GF	mean value	3.45	3.25	3.35	0.21	0.20	0.20	slightly absorbing
	st. dev.	0.85	0.38	0.14	0.05	0.02	0.01	
DG	mean value	1.29	1.22	1.25	0.08	0.07	0.08	slightly absorbing
	st. dev.	0.22	0.12	0.05	0.01	0.01	0.00	
CS	mean value	49.44	48.27	48.86	2.97	2.90	2.93	medium absorbing
	st. dev.	10.11	3.38	0.82	0.61	0.20	0.05	
AF	mean value	33.46	24.89	29.18	2.01	1.49	1.75	medium absorbing
	st. dev.	9.41	5.79	6.06	0.56	0.35	0.36	

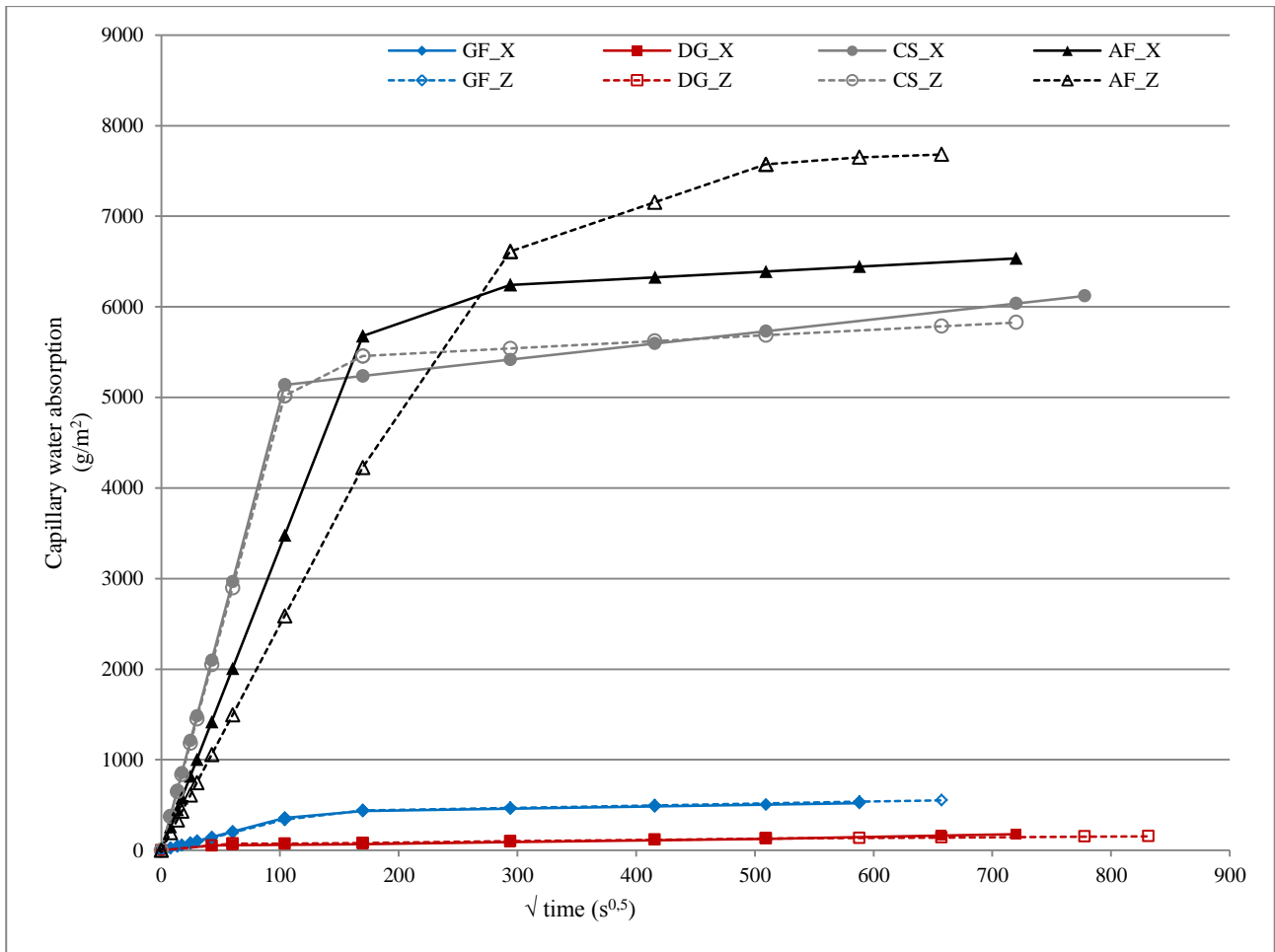
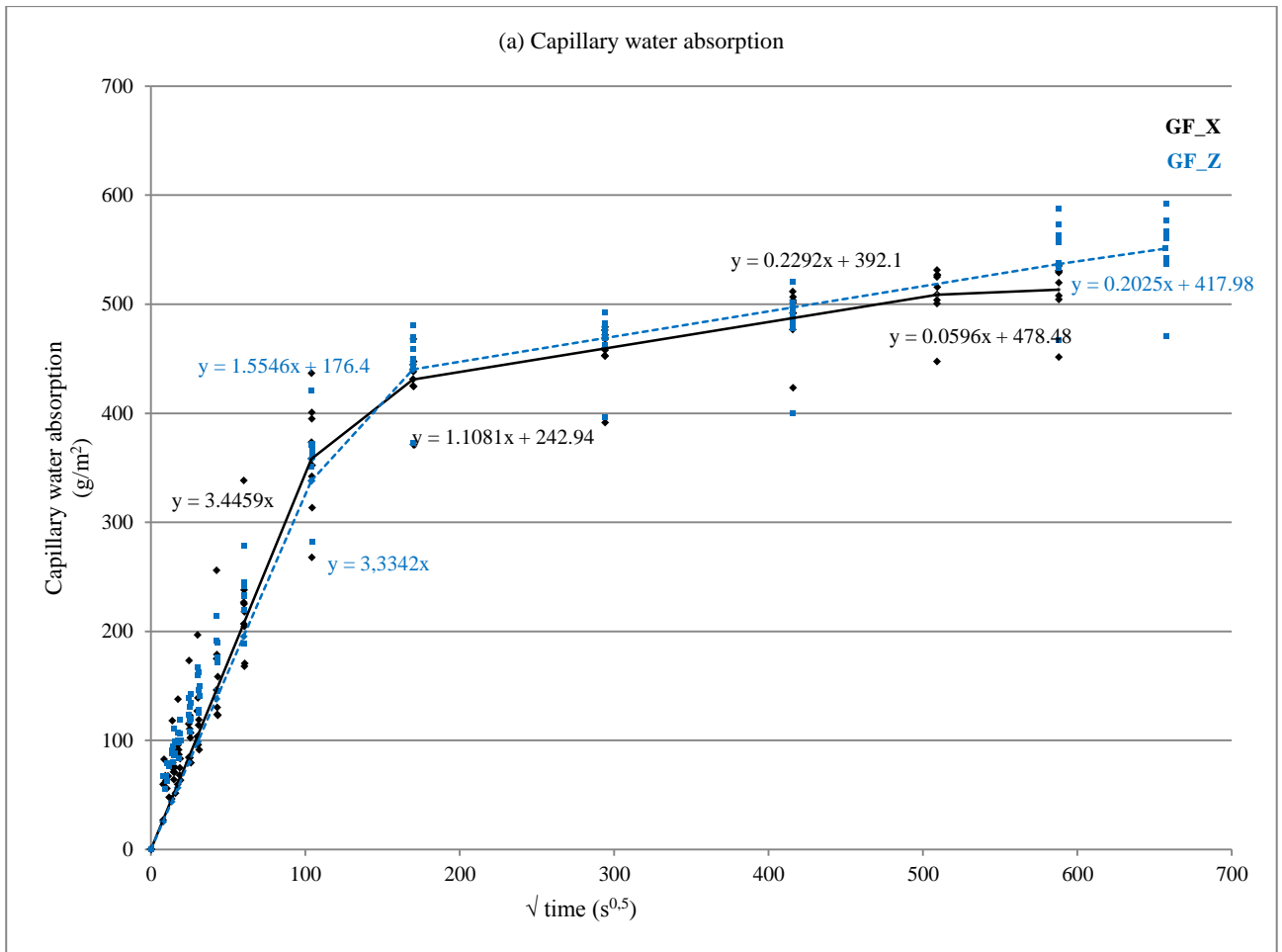
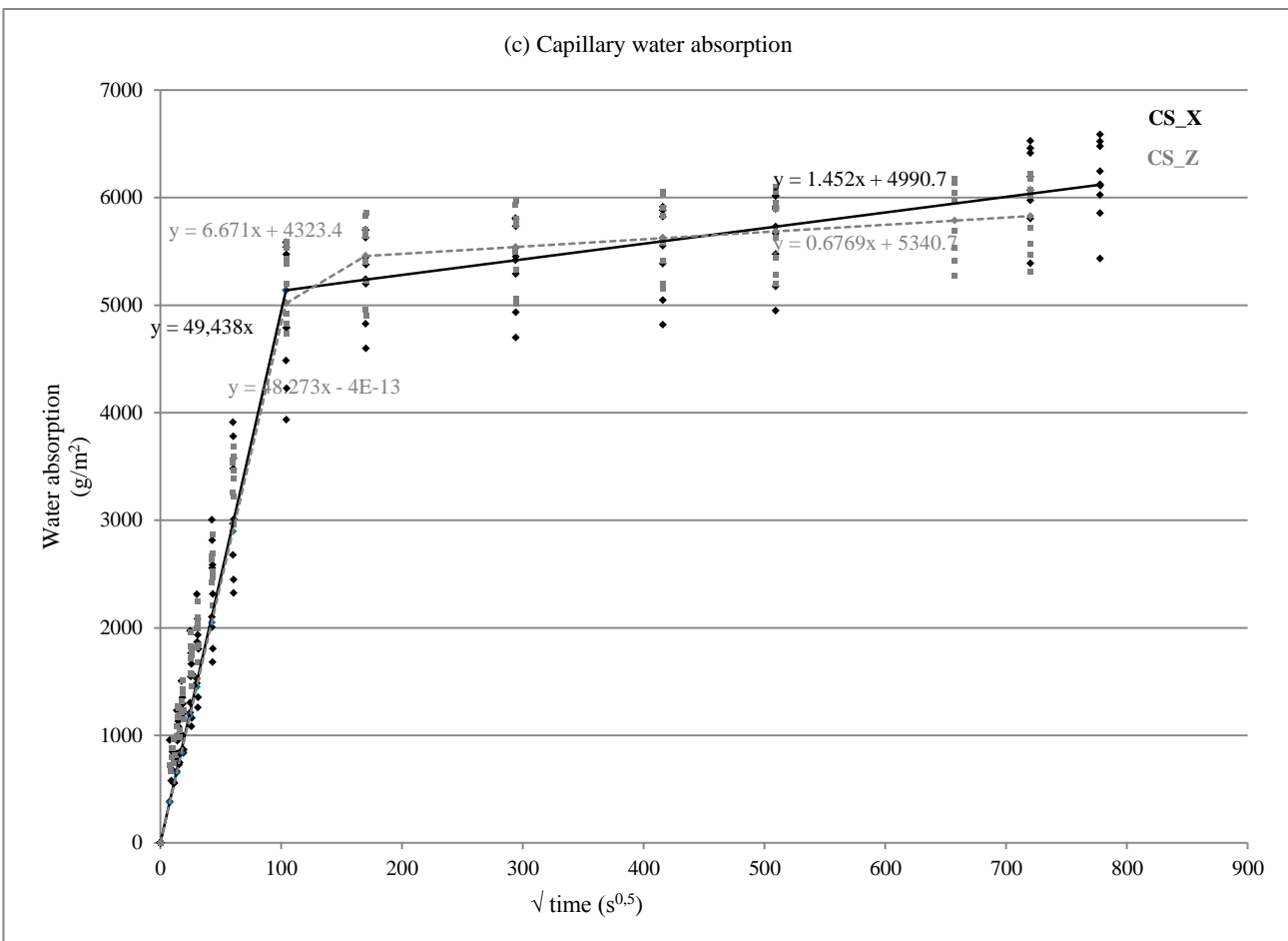
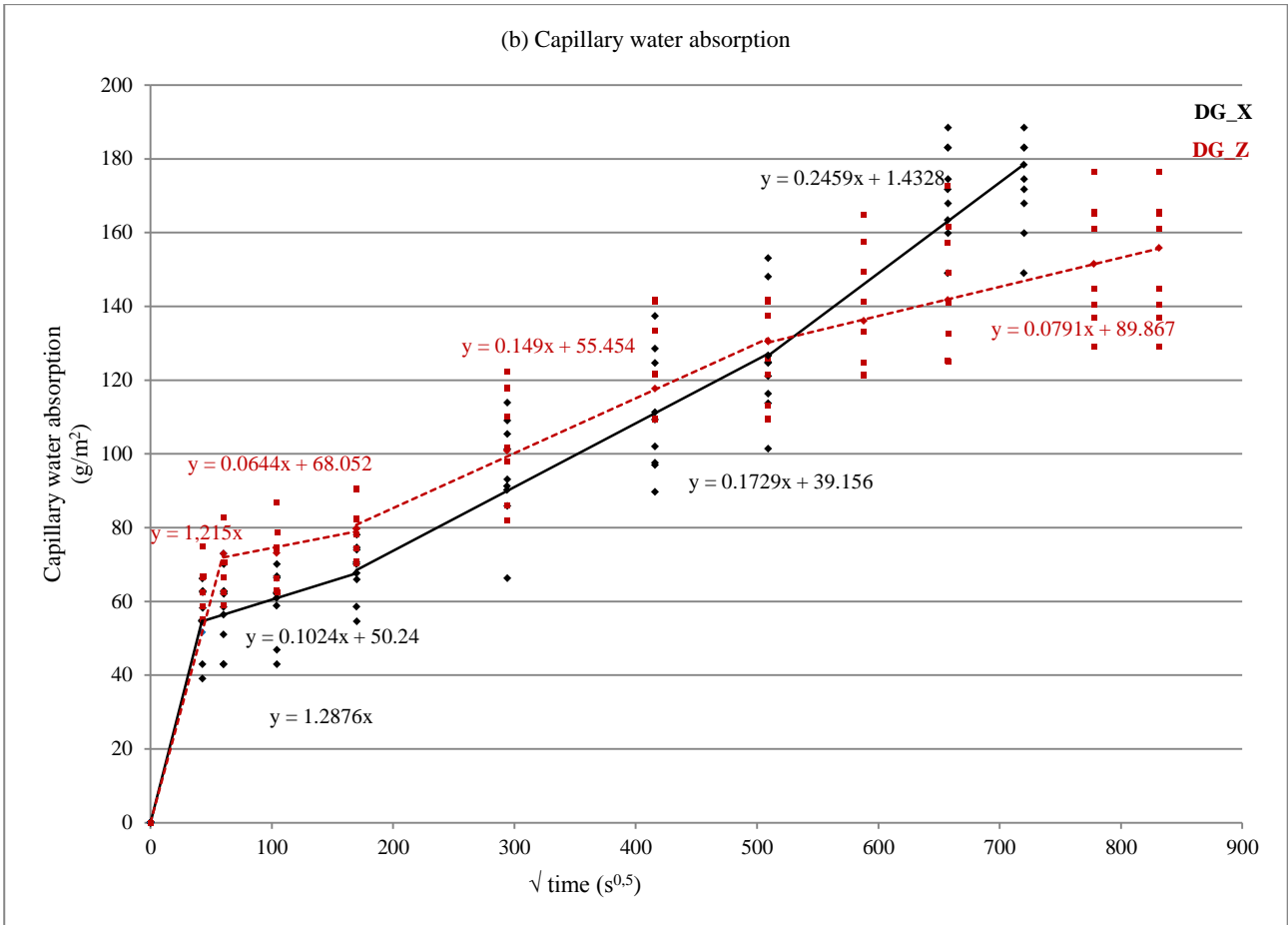
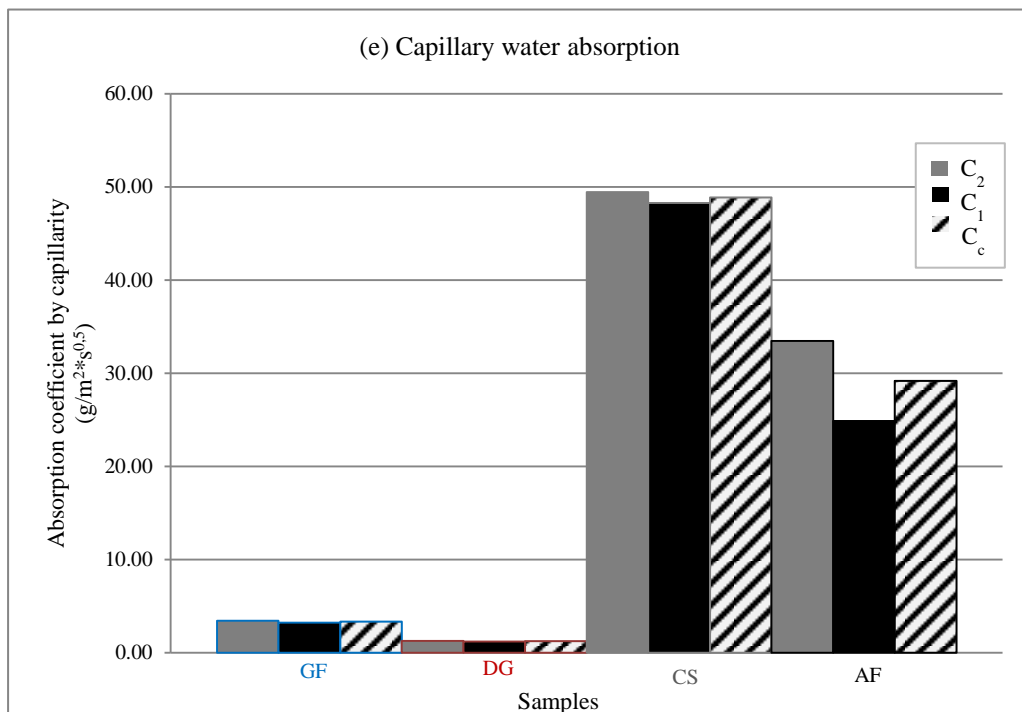
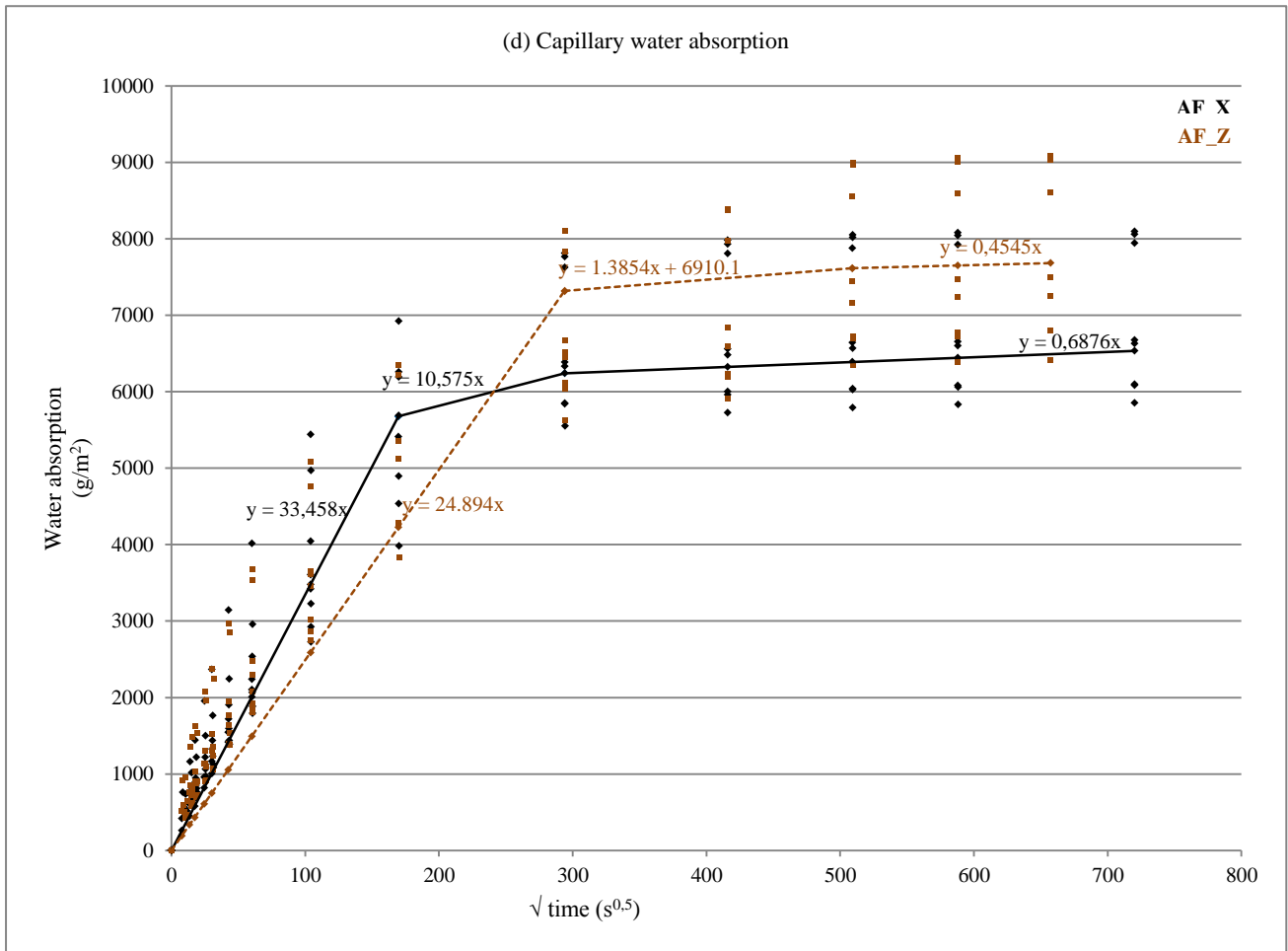


Fig. 6.9. Capillary water absorption average curves of the four selected stones, along the two spatial directions X and Z. The capillary water absorption is given in g/m^2 versus the square root of the time in seconds (after Franzen & Mirwald, 2004)

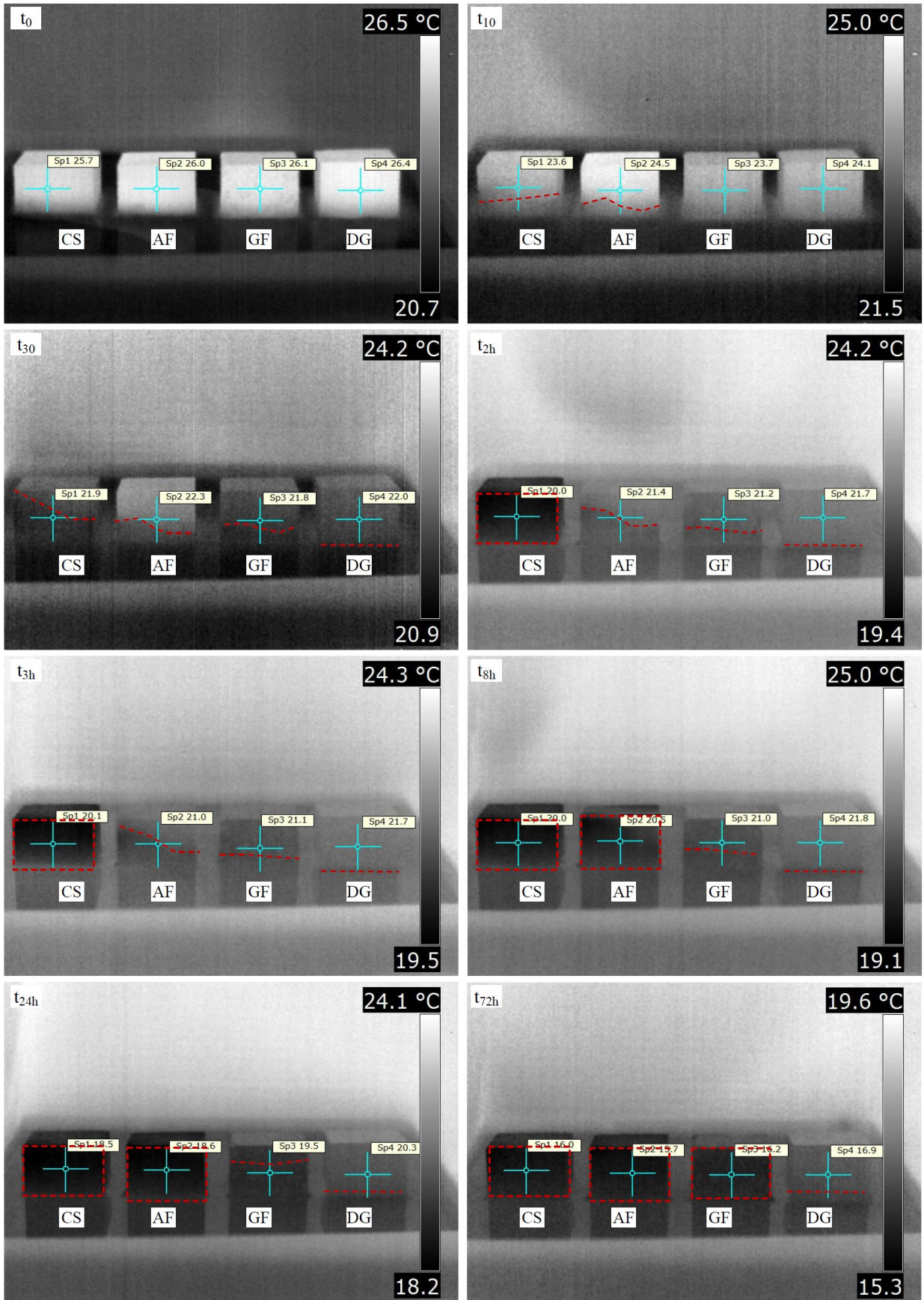




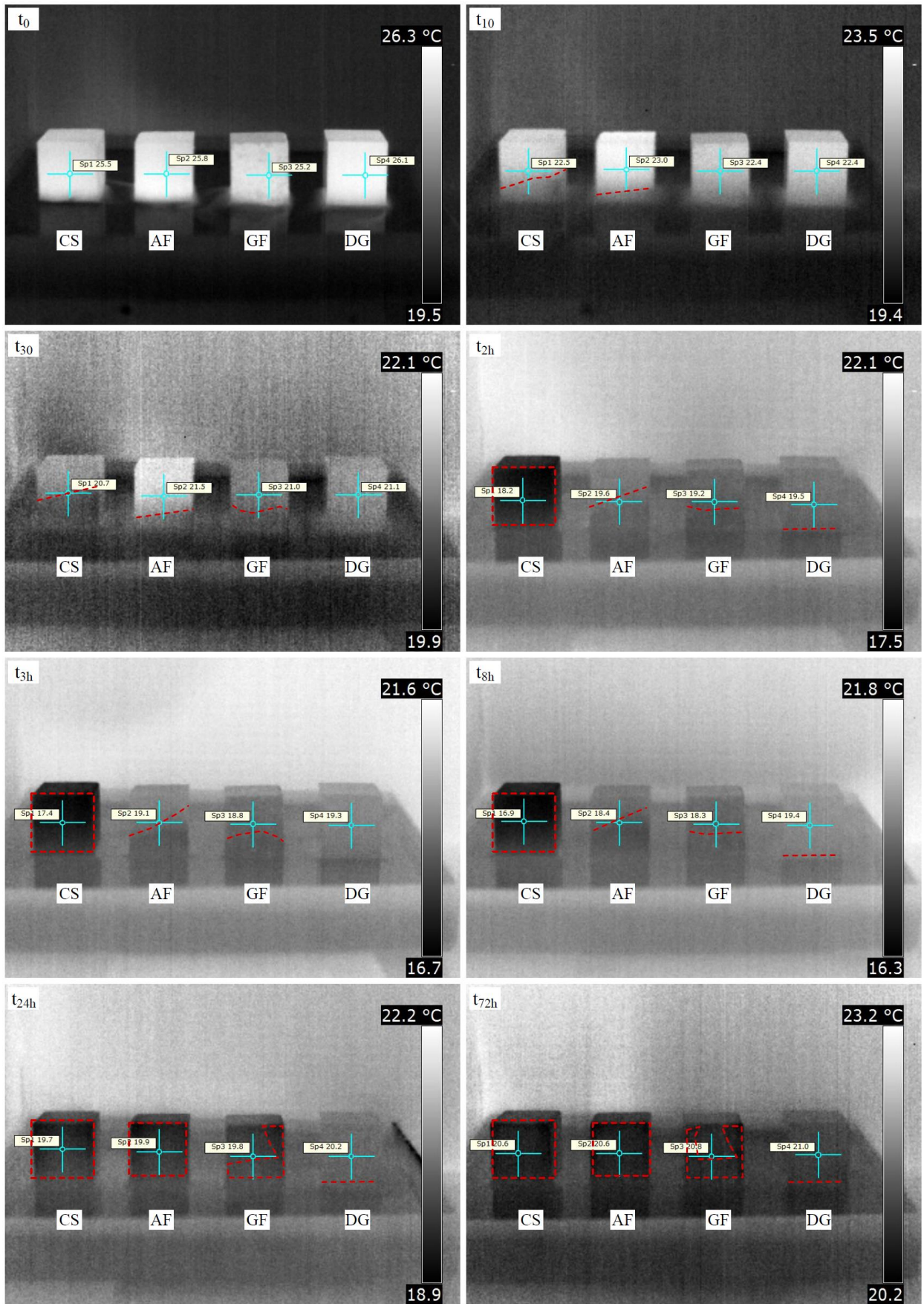


Figs. 6.10 a, b, c, d, e. Capillary water absorption average curves, along the two spatial directions X and Z, for each stone: (a) San Giovanni in Fiore granite (GF), (b) Grisolia stone (DG), (c) San Lucido calcarenite (CS), (d) Fuscaldò sandstone (AF). In the Fig. 6.10 (e) are reported the water capillary coefficients along X (C_2), along Z (C_1) and the average value (C_c).

(a) Capillary water absorption – X direction



(b) Capillary water absorption – Z direction



Figs. 6.11 a, b. Capillary water absorption for the four materials, along (a) X-direction and (b) Z-direction for the intervals of time: t_0 , t_{10} , t_{3h} , t_{8h} , t_{24h} , t_{72h} . The red line and the red rectangle are used to mark the height of the capillary rise with water.

6.5.2 Water absorption/desorption at atmospheric pressure

Water absorption and desorption by immersion tests are widely used for the characterization of building materials as they provide information mainly about the kinetics of the process and, indirectly about their pore structure and hence their durability resistance (Anania *et al.*, 2012). The water absorption, defined as the difference between the weight of a sample totally immersed in water and its dry weight, has been determined through the test of total immersion at atmospheric pressure conditions. The water absorption capacity of a stone is closely related to its open porosity that is the percentage of pores accessible to the water under normal conditions.

The drying characteristic of a stone (or evaporation kinetics) is a very important factor that clearly determines the weathering resistance (Siegesmund & Dürrast, 2014). Obtained values have been graphically shown into curves to highlight the different stages of the drying process.

Water absorption

Through absorption tests the following values of porosity and capillary absorption coefficients have been obtained (Table 6.10): Grisolia stone samples (DG) show the lowest values of water absorption, with an average imbibition coefficient (W_{Ab}) of $0.12 \pm 0.01\%$; conversely, Fuscaldo sandstone (AF) shows the highest values of water content absorbed, with a mean value of $5.35 \pm 0.92\%$; granite of San Giovanni in Fiore samples (GF) reach an average coefficient of $0.39 \pm 0.02\%$, while San Lucido calcarenite (CS) a mean value of $4.29 \pm 0.33\%$.

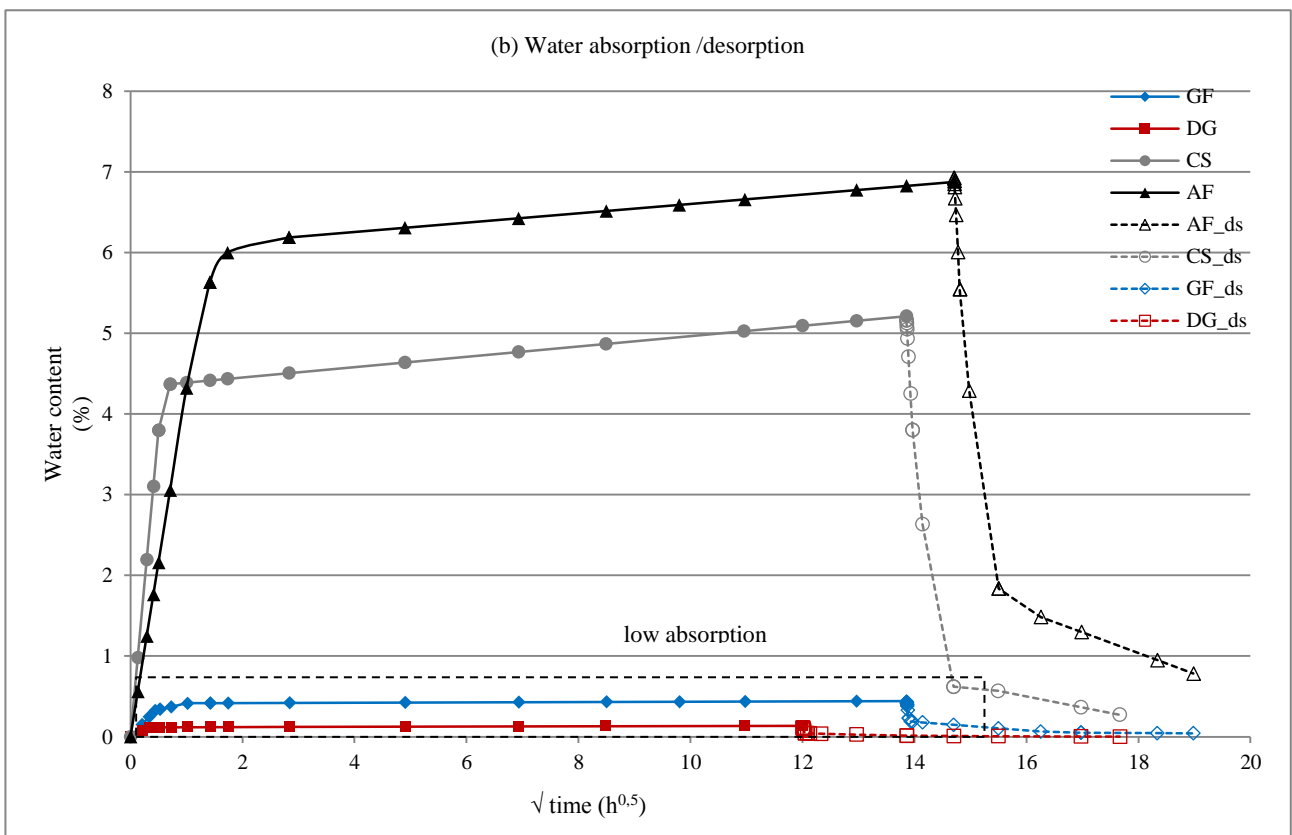
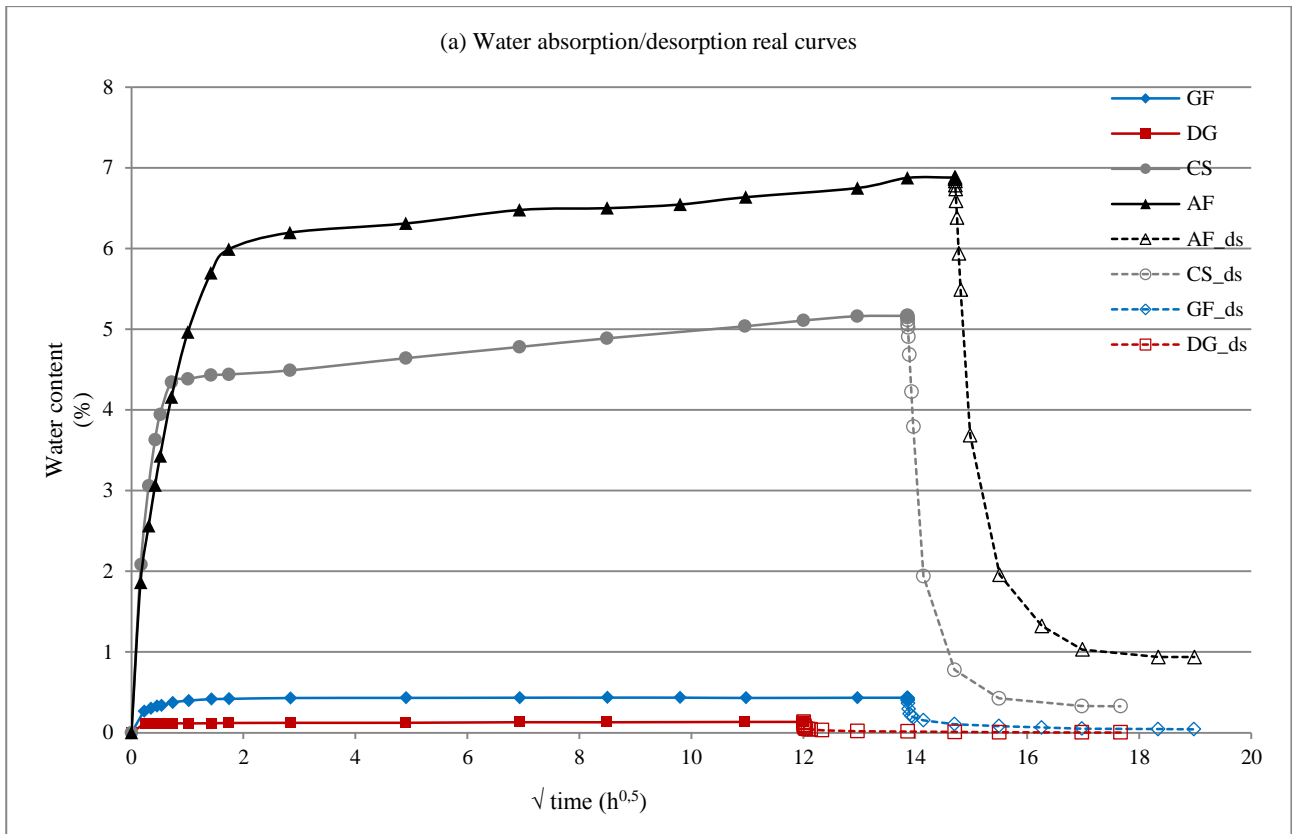
Table 6.10. Water absorption/desorption test. W_{Ab} = water content absorbed or imbibition coefficient (%); S_i = saturation coefficient; W_{vac} = water absorption under vacuum conditions (%) obtained through the test of the porosity accessible to water under vacuum conditions; W_{Ds} = water content evaporated (%); R_{mc} = moisture content ratio (%); S = saturation degree defined as the ratio of W_{Ab}/W_{vac} (Hirschwald, 1912).

Samples	W_{Ab} (%)		S_i (%)		W_{vac} (%)		W_{Ds} (%)		R_{mc} (%)		S
GF	0.39	± 0.02	90.92	± 1.62	0.50	± 0.02	-0.23	± 0.01	0.21	± 0.01	0.78
DG	0.12	± 0.01	91.08	± 4.06	0.20	± 0.03	-0.09	± 0.01	0.09	± 0.01	0.61
CS	4.29	± 0.33	83.11	± 0.39	7.05	± 0.41	-1.95	± 0.13	0.80	± 0.06	0.61
AF	5.35	± 0.92	77.74	± 1.75	9.36	± 1.33	-2.49	± 0.33	0.80	± 0.05	0.57

The saturation coefficient (S_i) follows the same order: the highest value has been $91.14 \pm 4.04\%$ for DG; the lowest for AF with a saturation of $77.74 \pm 1.75\%$; then $90.92 \pm 1.62\%$ for GF and $83.19 \pm 0.40\%$ for CS.

The calculated saturation degree (S), important for the evaluation of the frost resistance, is <0.75 for all samples, except for GF that is slightly higher than the other mean values ($S=0.78$). According to the frost resistance classification of Hirschwald (1912), it can be said that all the samples are “weathering and frost resistance”, while GF shows an uncertain frost behavior.

The sorption kinematic of the four stones is reported in Figs. 6.12 a, b, where the shape of the water adsorption curve furnishes information about the velocity and amount of the water absorption process. The major or the minor velocity depends on the connectivity of the porous network and on the pore size distribution. The major velocity has been registered for CS while the lowest for DG. Besides velocity of absorption, AF registered the maximum amount or absorbed water out of the 4 lithotypes, and DG, the lowest.



Figs. 6.12 a, b. Water absorption/desorption real curves (a) and schematic curves (b), obtained by mean values, for the four materials investigated.

Regarding the kinematic process it is possible to distinguish two groups of stones: the group of lower absorption (GF and DG) and the group with higher absorption (CS and AF).

As shown in Fig. 6.12 (b), for each group of stones, the velocity of water uptake process is similar. GF reaches the total saturation within 24 hours (Fig. 6.13), while DG reaches 90% at the same time and then the micropores continue to be slowly filled until the end of the test. On the other hand, the San Lucido calcarenite (CS) reaches approximately 85% saturation in 24 hours and needs approximately 7 days for the total saturation. But the highest values have been recorded by Fuscaldo sandstone (AF). In fact, it reaches only approximately 55% saturation in 24 hours and need approximately 9 days for the total saturation. This is due to the very small average void size of the sandstone and probably to the high tortuosity of its fissures and pores, which slow down the water movement in the material. The values of the saturation coefficient (S) presented in Table 6.10 express this velocity numerically.

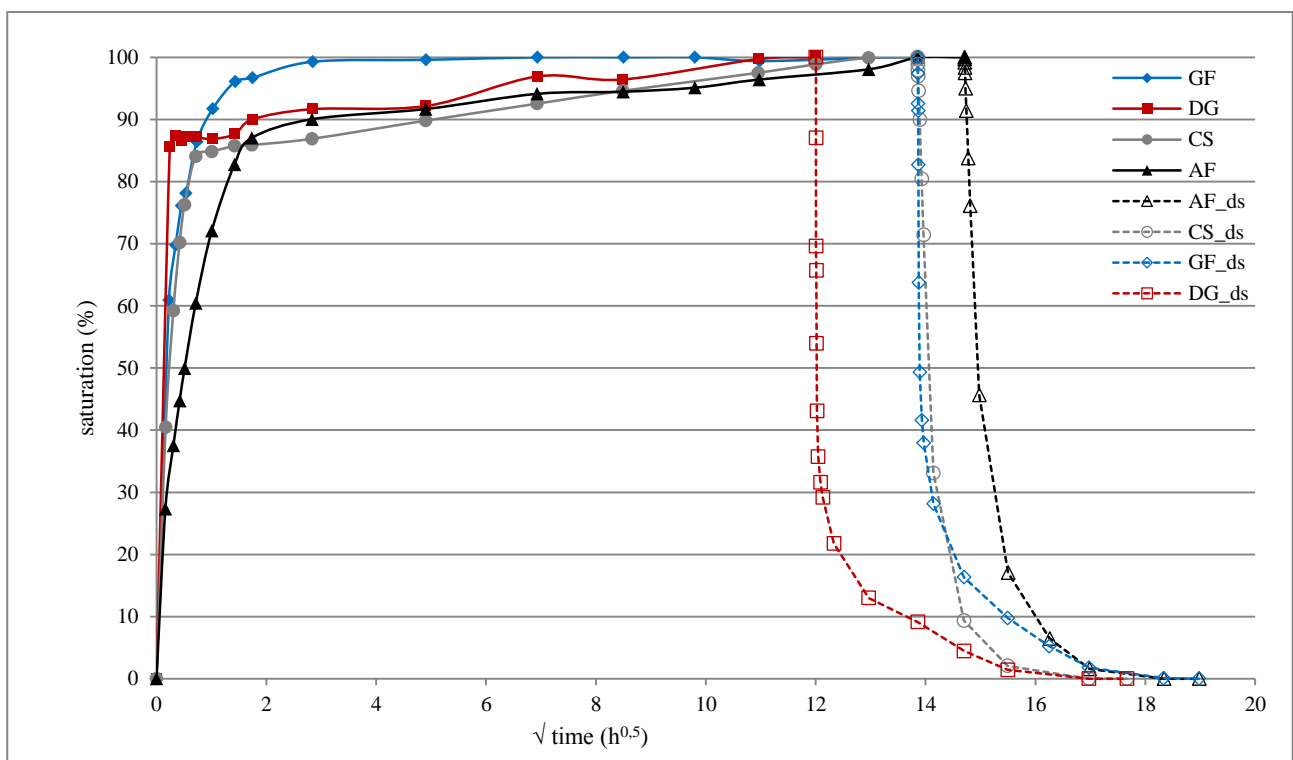
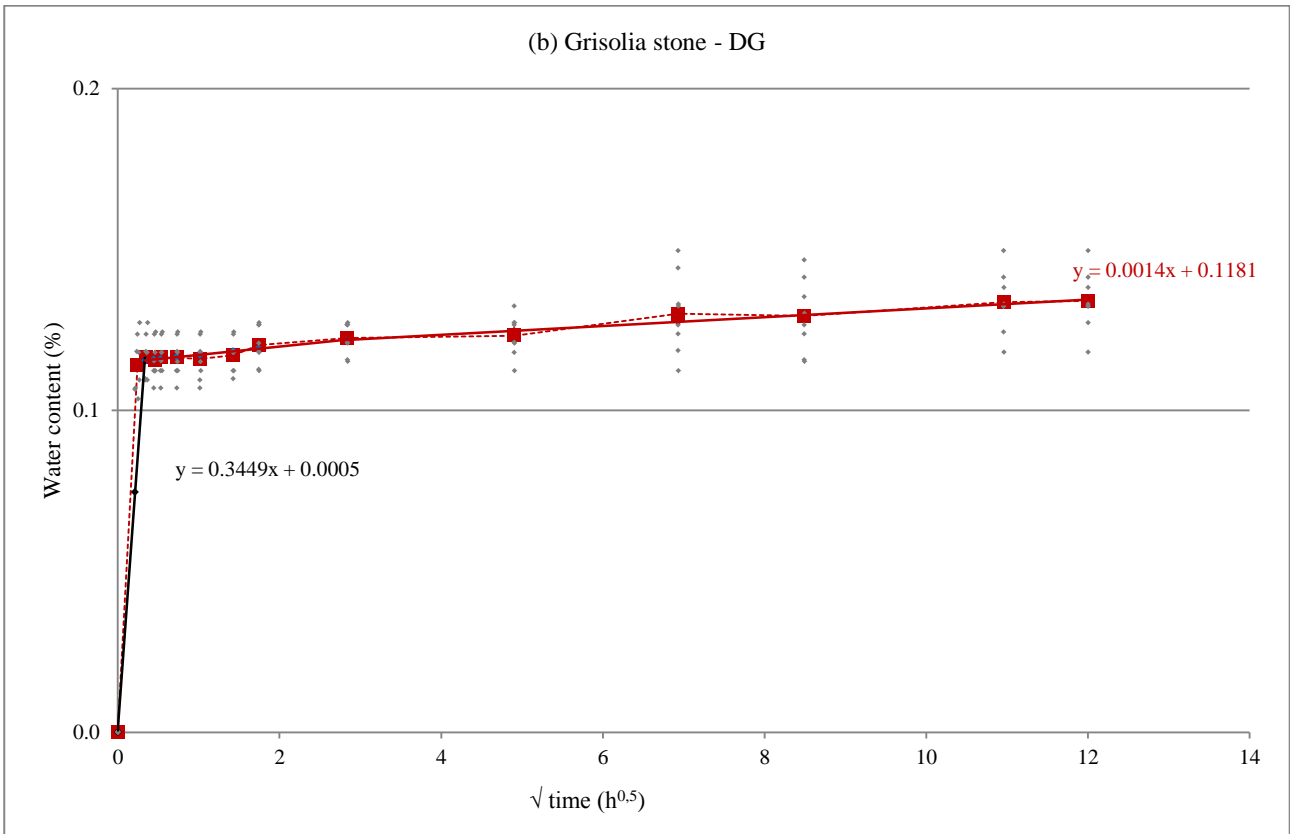
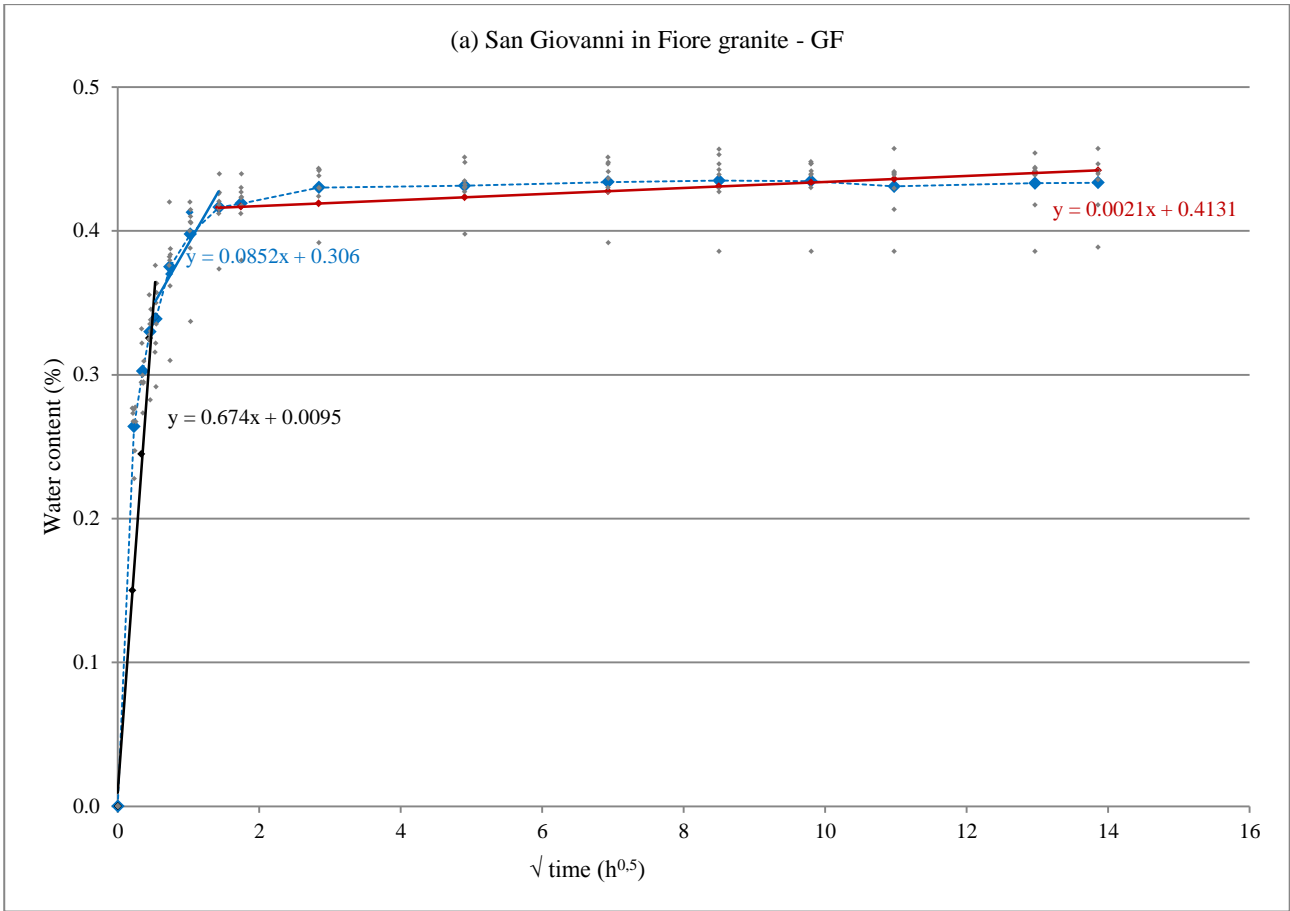
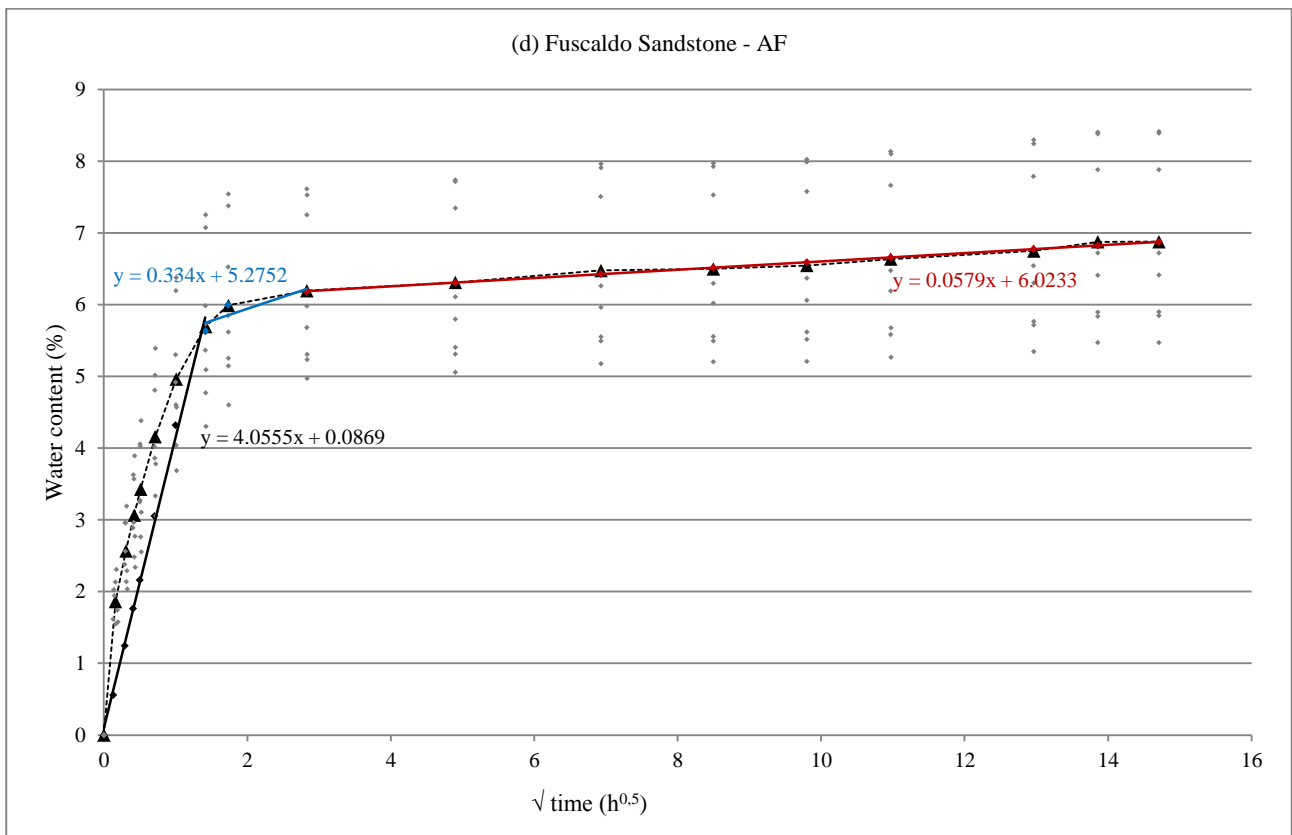
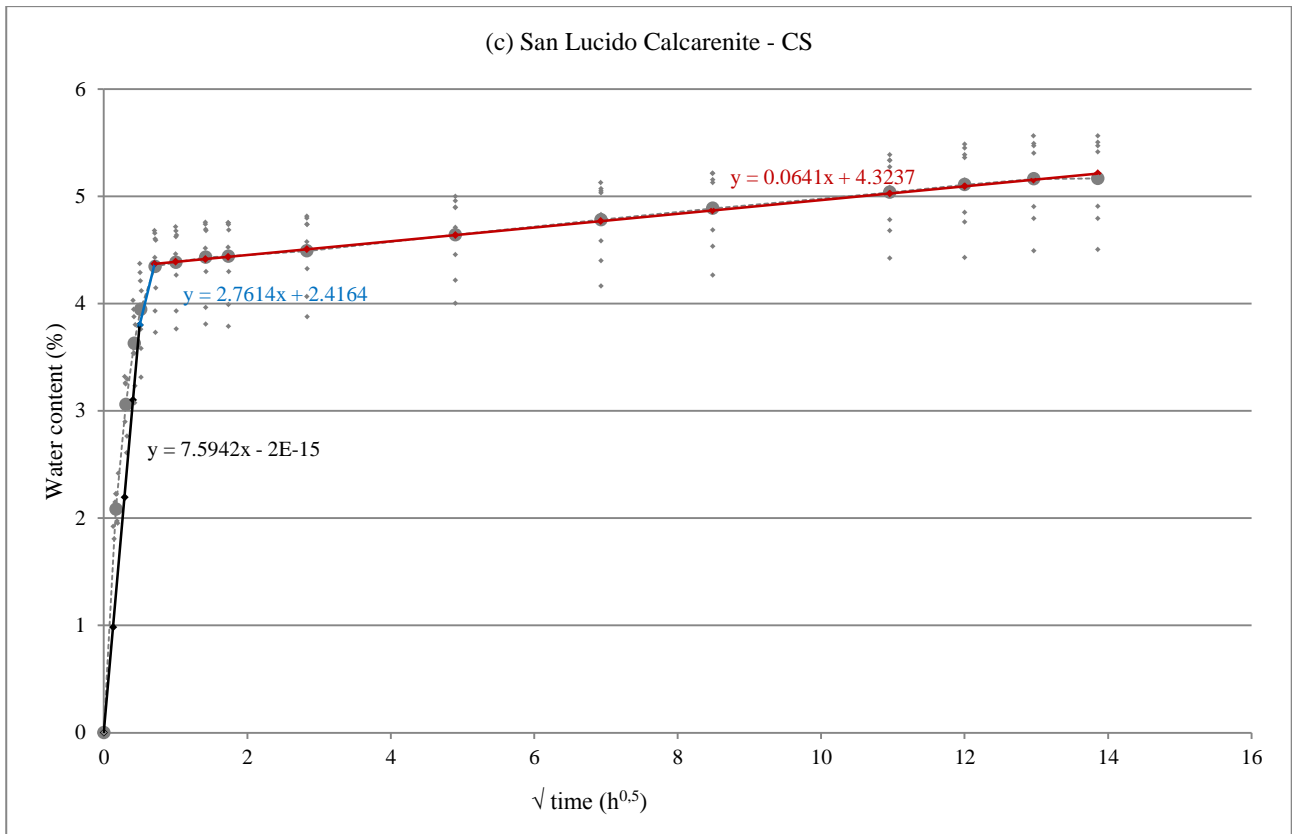


Fig. 6.13. Saturation of the water absorption/desorption process, for the four investigated materials.





Figs. 6.14 a, b, c, d. Kinematic of water absorption for each material with the different stages of absorbing: (a) San Giovanni in Fiore granite; (b) Grisolia stone; (c) San Lucido calcarenite; (d) Fuscaldo sandstone.

As reported in Figs. 6.14 (a, b, c, d), it is possible to analyze the different stages of water absorbing for each material. For all the samples may be recognizes three stages of absorbing, except for DG that presents only two stages. For all the samples, the first stage is characterized by higher velocity than the others and the highest values, as testified by the values contained in Table 6.10 too, has been reached for CS, while the lowest one for DG. Also the quickest velocity value of the second phase of absorbing belongs to CS, followed by AF, GF and DG. The velocity of the third phase is very similar for CS and AF. For GF, the velocity of this last phase is very low and comparable to the slope of the second phase of DG.

Water desorption

According to Snethlage (1984) and Tournier *et al.* (2000), it is possible to identify, for each material, three stages of drying (Fig. 6.15). As it can be seen, all the four curves (saturation versus time ratio) start with a steep phase, which corresponds to the evaporation of the water from the surface, but the length of these phases and the relative water amounts lost are very different for the different materials. In Figs. 6.16 (a, b, c, d) for each material the evaporated water content and the drying velocity rate are reported, numerically expressed by the moisture content ratio (R_{mc} %), shown in Table 6.10. The moisture content ratio (R_{mc} %) has been graphically determined for each lithotype and the correspondent number has been reported in Table 6.10. Graphically, the moisture content ratio (Ruedrich & Siegesmund, 2006) is given by the changing point of the curve between the first drying phase (evaporation due to capillarity) and the second one (evaporation due to water vapor transport).

Within the first 30 minutes Grisolia stone loses 60% of its water content by the evaporation process, followed by granite of San Giovanni in Fiore with a 40% of loss, while at the same time the saturation of the calcarenite of San Lucido and Fuscaldo sandstone is still about 90-95%. This first phase ends at about 2h for DG; at the same time its saturation is about 30%. The second drying phase of

the Grisolia stone is a lot slower: within approximately five days it reaches a constant value with a saturation of 10-20%. GF follows a similar trend to DG with a second drying phase slower and constant with a saturation of 10-15%. This is probably due to the pore size and morphology of DG and GF that causes obstructions that slow down water desorption. CS and AF show a first phase slower than the other two materials. After the evaporation of the water from their surfaces a pretty fast drying rate still keeps due to the internal absorbed water: within 21 hours (interval of time from 3h until 24h) they lose 60% of their water content. This can be due to a probable good connectivity of the porous system. After this point, there is an abrupt change in their drying rate with a constant saturation of 10-15%. Basically it could be summarized that higher the water absorption velocity the higher the water desorption velocity and *viceversa*.

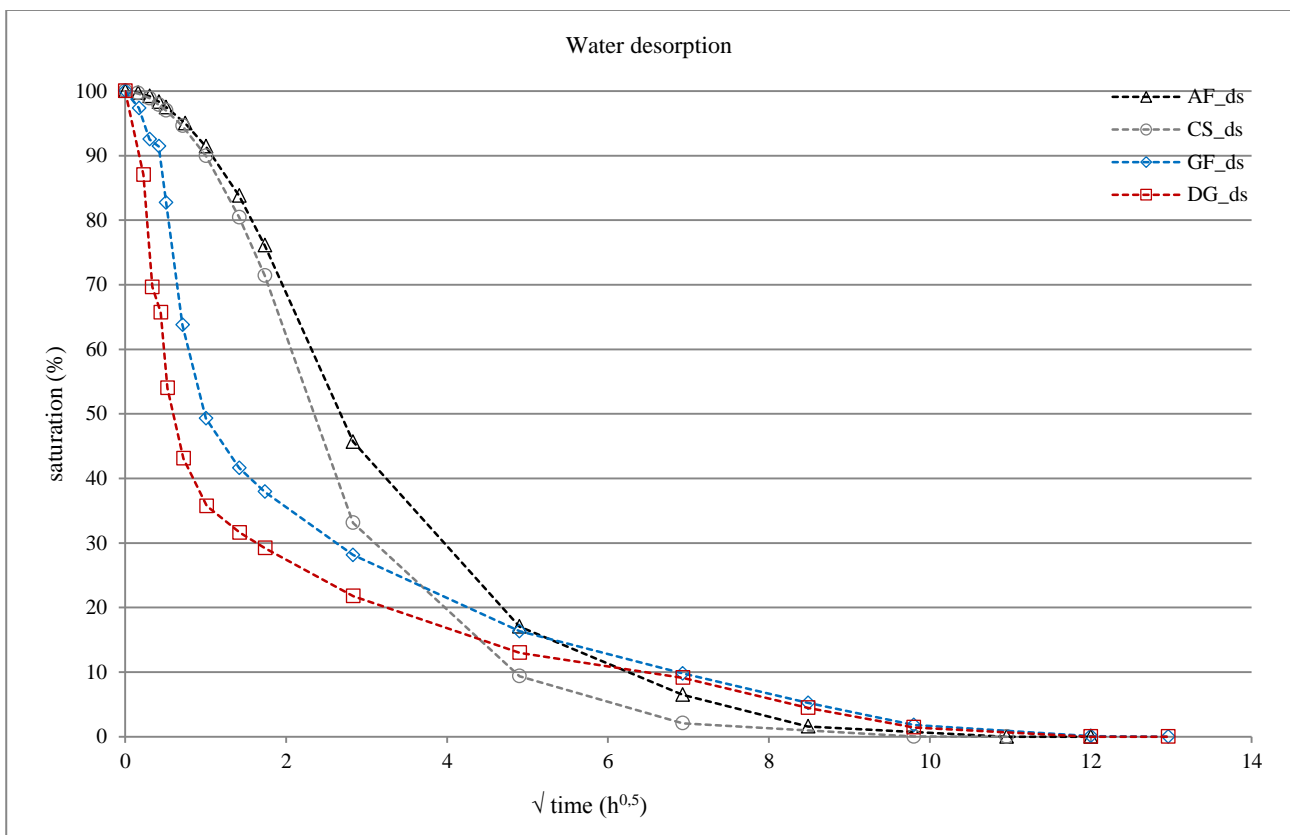
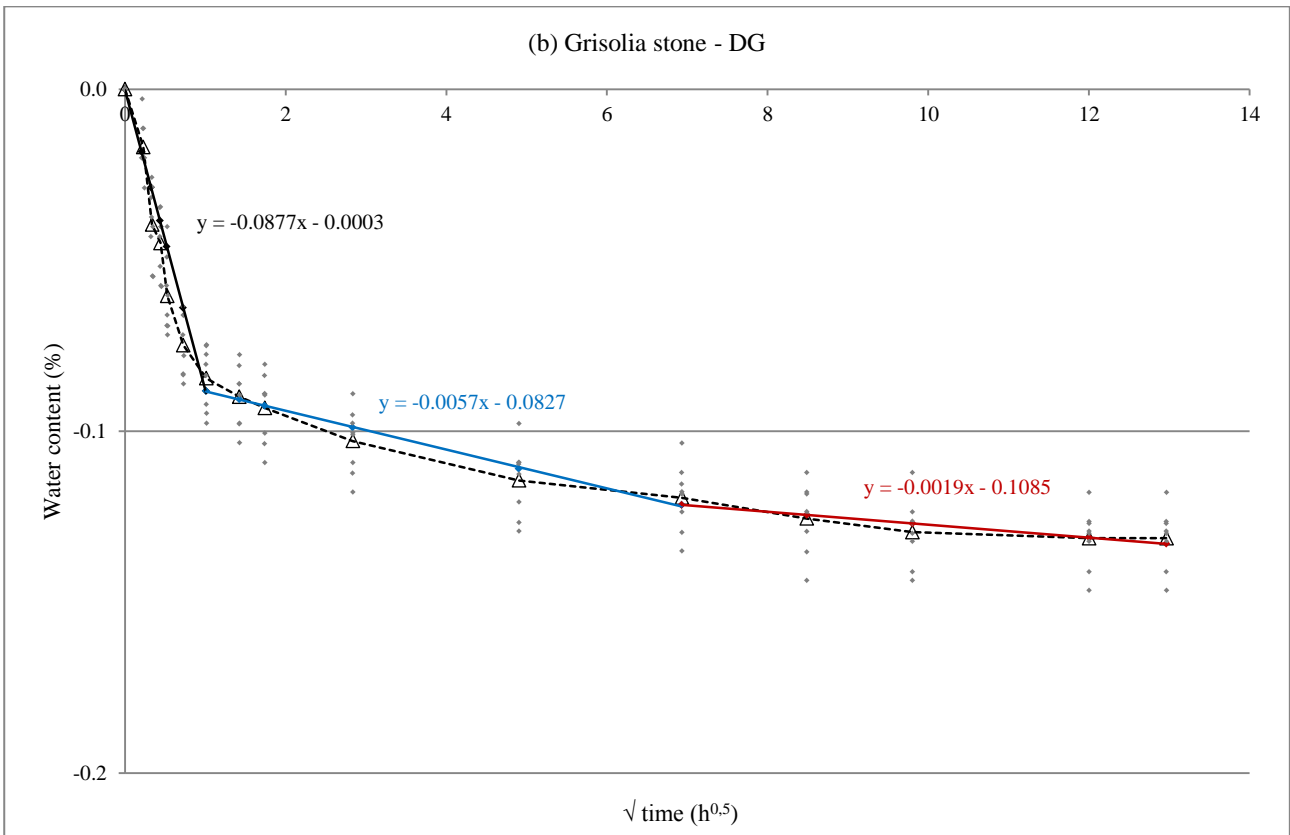
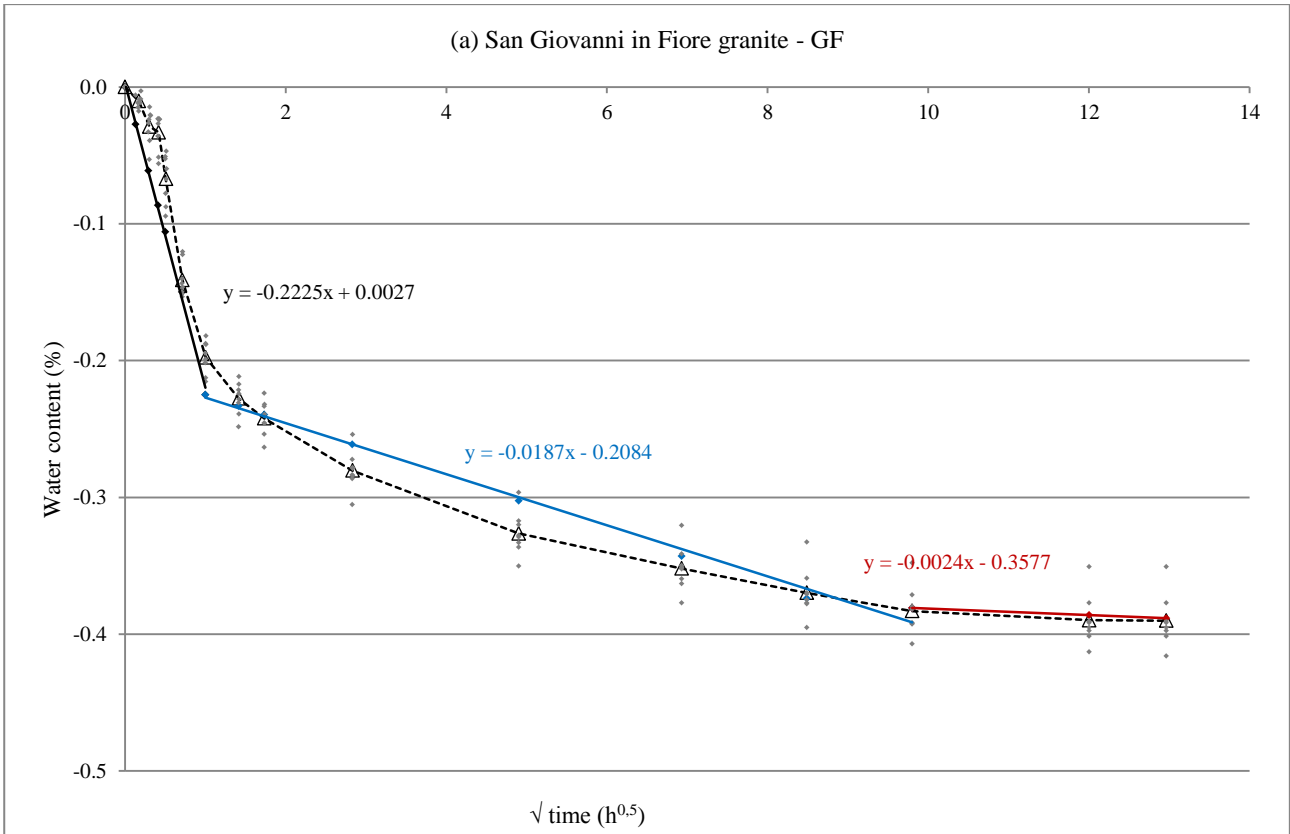
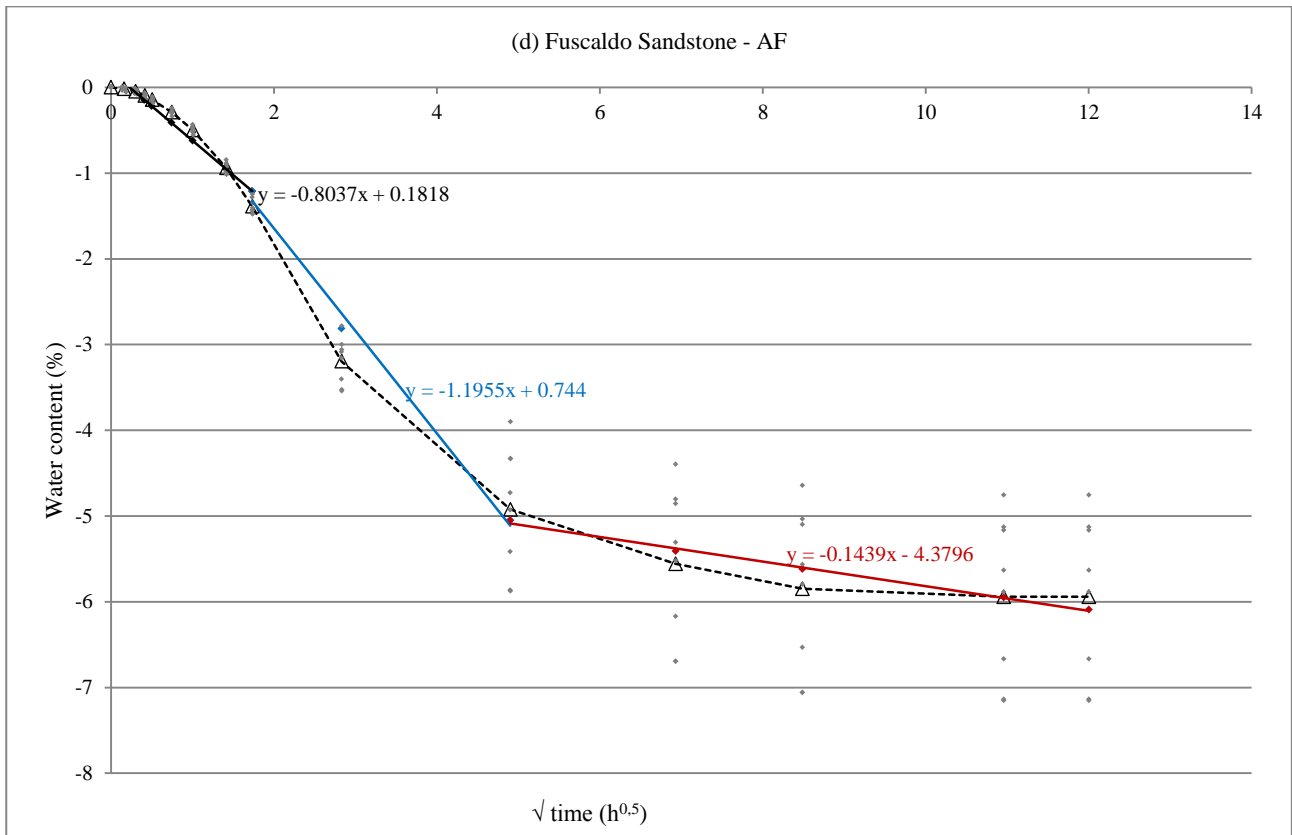
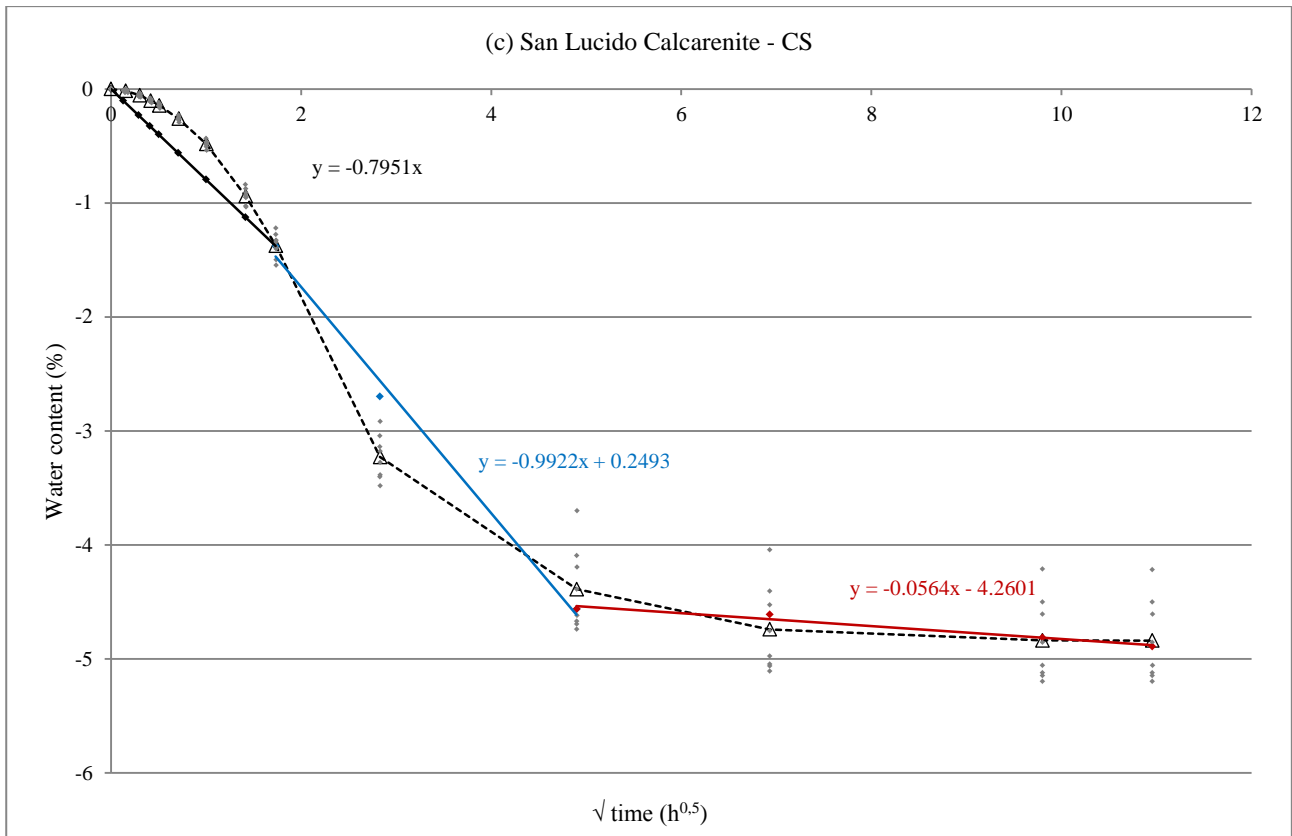


Fig. 6.15. Water desorption curves for: granite of San Giovanni in Fiore (GF_ds); Grisolia stone (DG_ds); San Lucido calcarenite (CS_ds); Fuscaldo sandstone (AF_ds).





Figs. 6.16 a, b, c, d. Kinematic of water desorption for each material with the different stages of drying: (a) San Giovanni in Fiore granite; (b) Grisolia stone; (c) San Lucido calcarenite; (d) Fuscaldo sandstone.

6.5.3 Natural hydrophobicity by water static contact angle

The water static contact angle is a test principally performed to evaluate the durability and the effectiveness of stone treatments. In this study this technique has been employed in order to estimate the natural hydrophobicity of the samples surfaces.

Contact angles mean, maximum and minimum values obtained, are reported in [Table 6.11](#), while in [Fig. 6.17](#) the relationship between the angle values ($^{\circ}$) and the drop volume (μl) is represented. Analyzing the values reported in [Table 6.11](#), it can be observed that it was impossible to perform the test on the surfaces of the samples of CS and AF because, according to UNE-EN 15802:2010 standards, the loss of drop water was $>50\%$ in the first 10s. So, it can be said that CS and AF do not present hydrophobic surfaces. Conversely, for the samples of GF and DG medium values of the static angle have been obtained, of 45.20° and 46.16° , respectively. In [Fig. 6.17](#) it can be noticed the major standard deviation of the angle values obtained for GF that indicate that this material has a more heterogeneous surface than DG. Anyway, these materials have not a natural hydrophobicity.

Table 6.11. Static contact angle values for: San Giovanni in Fiore granite (GF) and Grisolia stone (DG).

Sample	% loss drop water	Min	Max	St. dev.	Mean value
GF	-	29.92	63.55	7.16	45.20
DG	-	32.22	54.97	4.71	46.16
CS	51.67	/	/	/	/
AF	77.43	/	/	/	/

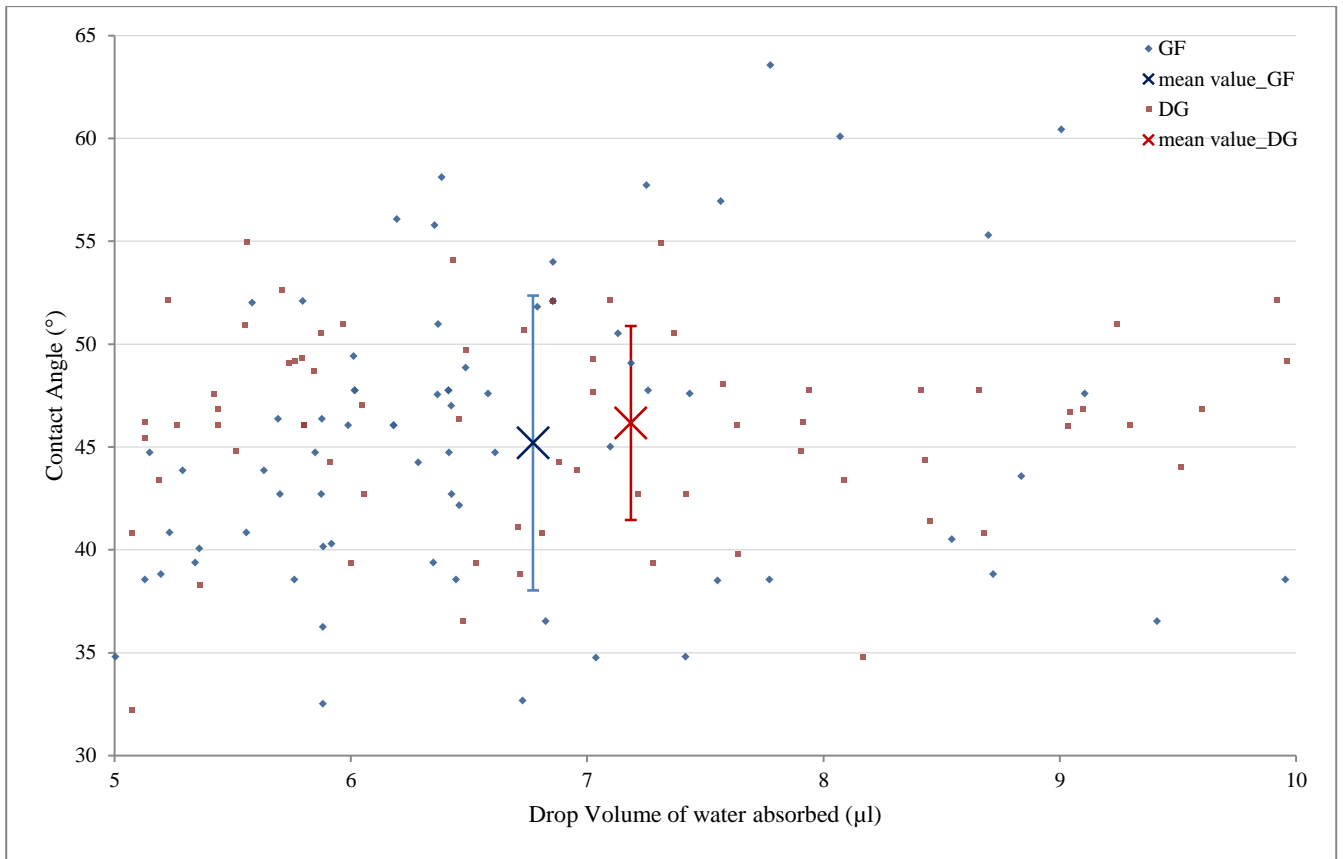


Fig. 6.17. Binary diagram showing the relationship between static contact angle values (°) and drop volume (μl), with the standard deviation, for San Giovanni in Fiore granite (GF) and Grisolia stone (DG).

6.6 Mechanical properties

The mechanical characterization of the four investigated materials has been performed through many non-destructive (NDT), micro-destructive (MDT) and destructive (DT), such as: ultrasonic pulse velocities, V_p and V_s waves (NDT), micro-hardness (NDT), drilling resistance (MDT), Schmidt Hammer hardness (MDT), uniaxial compressive strength (DT), flexural strength (DT), indirect tensile strength (DT), Point Load (DT), Los Angeles (DT), Micro-Deval (DT).

6.6.1 Ultrasound propagation velocity (P waves)

Mean values of ultrasonic pulse velocities, P and S-waves, and anisotropy indices, are shown in [Table 6.12](#). Relationship between V_s values and V_p values is reported in [Fig. 6.18](#).

Table 6.12. Ultrasonic velocities, P and S waves, measured in granite of San Giovanni in Fiore (GF), Grisolia stone (DG), San Lucido calcarenite (CS) and Fuscaldò sandstone (AF) specimens. P waves: V_{Px} , V_{Py} , V_{Pz} = ultrasonic velocity (m/s) registered in the directions X, Y and Z; V_p = average ultrasonic velocity (m/s); dM_{Vp} %: total anisotropy index and dm_{Vp} % relative anisotropy index. S waves: V_{Sx} , V_{Sy} , V_{Sz} = ultrasonic velocity (m/s) registered in the directions X, Y and Z; V_s = average ultrasonic velocity (m/s); dM_{Vs} %: total anisotropy index and dm_{Vs} % relative anisotropy index.

Samples	V_{Px}	V_{Py}	V_{Pz}	V_p	dM_{Vp}	dm_{Vp}	V_{Sx}	V_{Sy}	V_{Sz}	V_s	dM_{Vs}	dm_{Vs}	V_p/V_s
GF	4082	3744	3585	3804	8.4	8.7	2370	2185	2120	2225	6.9	8.1	1.7
<i>st. dev.</i>	124	191	160	258	1.2	2.4	279	83	49	199	4.1	14.3	
DG	6633	6600	6542	6592	1.1	0.5	3416	3406	3388	3404	0.7	0.3	1.9
<i>st. dev.</i>	56	76	73	76	0.5	0.5	26	24	15	24	0.4	0.6	
CS	4324	4282	4236	4281	1.6	1.0	2386	2376	2359	2374	0.9	0.4	1.8
<i>st. dev.</i>	235	229	240	234	0.9	0.6	91	88	73	84	0.7	0.6	
AF	3528	3463	2888	3293	17.4	1.9	2110	2096	1905	2037	9.4	0.7	1.6
<i>st. dev.</i>	350	331	611	517	10.8	1.3	168	161	244	214	6.4	2.6	

The highest mean values, for all the samples, were obtained along the X-axis, the medium along the Y-axis and the lowest along the Z-axis (Table 6.12).

Also the values of ultrasonic velocity of S-waves recorded the highest values along the X-axis and the lowest along the Z-axis. Average registered values were: 3404 ± 24 m/s for DG, the highest values; followed by 2374 ± 84 m/s for CS; 2225 ± 199 m/s for GF; 2037 ± 214 m/s for AF, the lowest mean values.

Concerning the anisotropy indices for P and S-waves, the obtained mean values indicate that DG and CS exhibit an isotropic ultrasonic behavior. The anisotropy values were low for both varieties of stone, as obtained by other authors for similar lithologies (Fort *et al.*, 2008). GF presents slightly higher values of anisotropy, for the total anisotropy and for the relative one, due to the microcracks. AF registered an anisotropic ultrasonic behavior (highest values of anisotropy indices). For AF the highest anisotropy values were obtained for total anisotropy, which means that anisotropy is more accentuated in one spatial direction due, perhaps, to a slight laminar orientation not perceptible to the naked eye and to the preferred phyllosilicates orientation detected by the petrographic analysis (Fort *et al.*, 2008).

Concerning the mean values of V_p , the samples of GF, DG, CS and AF belong to different stones category, respectively: “middle velocities” (class 3), “very high velocity” (class 5), “high velocity” (class 4) and “low velocity” (class 2) (Anon, 1979; Vasanelli *et al.*, 2015).

Regarding the ratio V_p vs. V_s , it can be observed that the lowest value was recorded for AF and the highest for DG. These values are coherent with the calculated anisotropy indices and confirm the different anisotropic behavior between AF and DG, as also shown in Fig. 6.18 a.

6.6.2 Ultrasound propagation velocity (S waves)

Determination of V_p and V_s values has allowed obtaining the elastic properties of the four materials. Young’s modulus (E), Poisson’s ratio (ν), Shear modulus (G) and Bulk modulus (K) are reported in Table 6.13, along the three directions (X, Y and Z) and their mean values. Relationship between V_s values, V_p values and Young’s modulus, are reported in Figs. 6.18 a, b, respectively.

Table 6.13. Young’s modulus (E), Poisson’s ratio (ν), Shear modulus (G) and Bulk modulus (K) measured along the three directions X, Y and Z, for the four materials: San Giovanni in Fiore granite (GF), Grisolia stone (DG), San Lucido calcarenite (CS) and Fuscaldo sandstone (AF). E, G and K modulus are expressed in GPa.

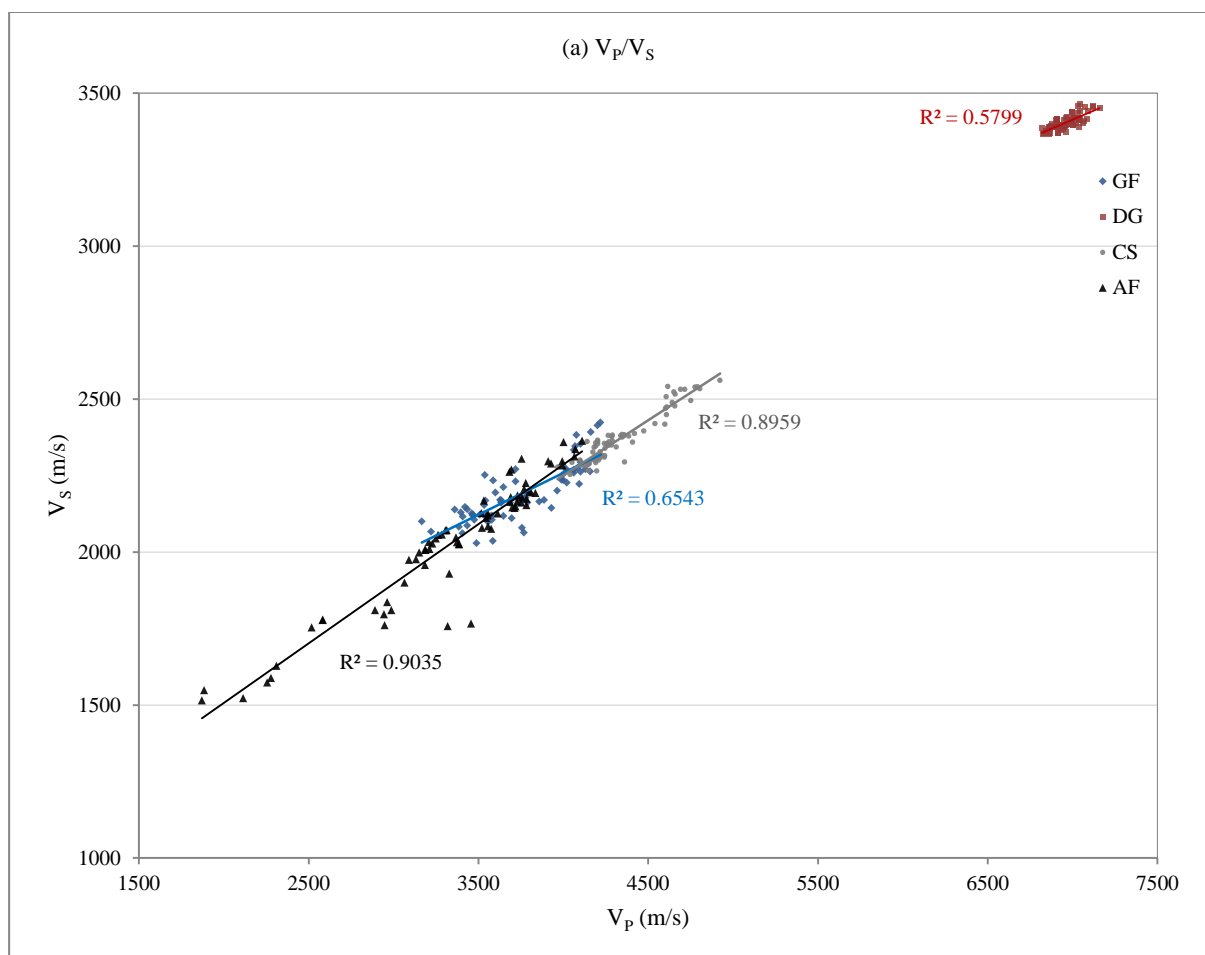
Samples	ν_x	ν_y	ν_z	ν	G_x	G_y	G_z	G	E_x	E_y	E_z	E	K_x	K_y	K_z	K
GF	0.27	0.24	0.20	0.24	15.27	12.83	12.06	13.39	36.61	31.69	29.01	32.44	24.24	20.19	16.54	20.32
<i>st. dev.</i>	<i>0.01</i>	<i>0.01</i>	<i>0.01</i>	<i>0.01</i>	<i>3.00</i>	<i>0.96</i>	<i>0.50</i>	<i>1.21</i>	<i>3.56</i>	<i>2.47</i>	<i>1.36</i>	<i>2.11</i>	<i>3.02</i>	<i>2.05</i>	<i>1.31</i>	<i>1.33</i>
DG	0.35	0.34	0.34	0.34	31.53	31.34	31.01	31.30	84.83	84.19	83.20	84.08	91.45	89.42	87.48	89.45
<i>st. dev.</i>	<i>0.00</i>	<i>0.00</i>	<i>0.00</i>	<i>0.00</i>	<i>0.47</i>	<i>0.43</i>	<i>0.26</i>	<i>0.45</i>	<i>1.13</i>	<i>1.21</i>	<i>0.76</i>	<i>1.24</i>	<i>1.54</i>	<i>2.32</i>	<i>2.12</i>	<i>2.58</i>
CS	0.29	0.29	0.28	0.29	13.10	12.99	12.80	12.96	33.84	33.41	32.79	33.35	27.15	26.13	25.13	26.14
<i>st. dev.</i>	<i>0.01</i>	<i>0.01</i>	<i>0.02</i>	<i>0.01</i>	<i>1.10</i>	<i>1.06</i>	<i>0.88</i>	<i>1.01</i>	<i>2.99</i>	<i>2.90</i>	<i>2.56</i>	<i>2.82</i>	<i>3.43</i>	<i>3.27</i>	<i>3.66</i>	<i>3.51</i>
AF	0.24	0.23	0.08	0.18	9.70	9.57	8.01	9.10	24.06	23.56	17.86	21.83	15.62	14.74	8.65	13.00
<i>st. dev.</i>	<i>0.03</i>	<i>0.03</i>	<i>0.19</i>	<i>0.13</i>	<i>1.70</i>	<i>1.64</i>	<i>2.18</i>	<i>1.99</i>	<i>4.43</i>	<i>4.21</i>	<i>6.73</i>	<i>5.90</i>	<i>3.72</i>	<i>3.26</i>	<i>4.53</i>	<i>4.93</i>

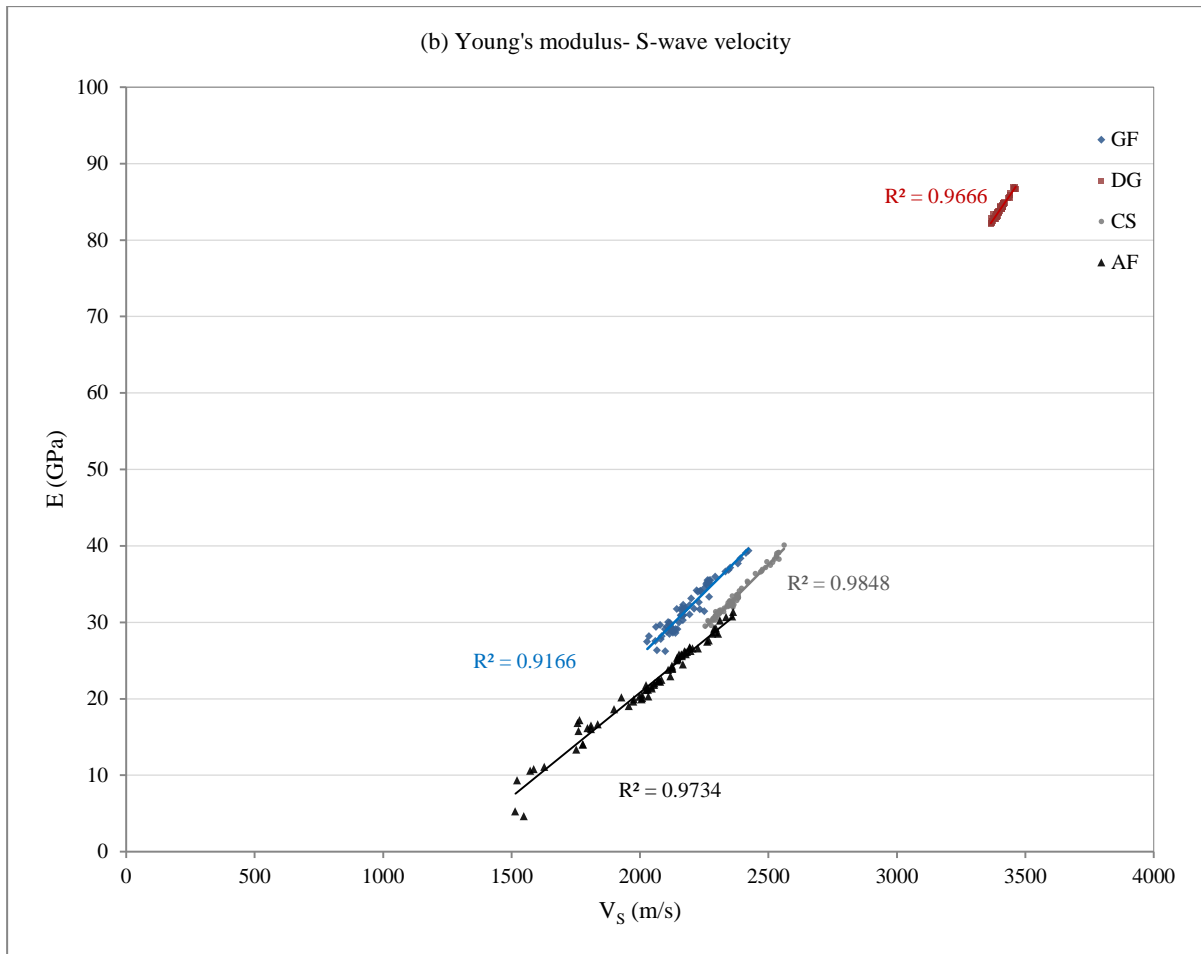
Regarding the elastic modulus obtained, mean values which have been recorded (Table 6.13) follow the same order of the ultrasonic velocities: the highest values for DG; intermediate values for CS followed by GF; the lowest values with the highest standard deviations for AF. The only values where

GF reaches a higher value than CS has been for the Shear modulus along the X-axis with 15.27 ± 3.00 GPa in contrast to 13.10 ± 1.10 GPa, respectively.

According to the classification of Anon (1979) based on the E values, the four lithotypes can be classified as: DG “very low deformable” ($E > 60$ GPa); GF and CS “low deformable” ($30 < E < 60$ GPa); AF “moderate deformable” ($15 < E < 30$ GPa), (Bell & Lindsay, 1999).

Regarding the relationship between ultrasonic velocities (S-waves) and Young’s modulus, it can be said that for the four materials a good correlation with high values of the correlation coefficient (R^2) has been recorded, as shown in Fig. 6.18 b.





Figs. 6.18 a, b. Binary diagrams showing the correlation between mean values of ultrasonic velocity V_s (m/s) and (a) mean values of V_p (m/s), (b) the Young's modulus (GPa)

6.6.3 Leeb Micro-hardness (Equotip), Drilling resistance and Schmidt hammer test

Mean values of micro-hardness and drilling resistance for the four investigated materials are reported in Table 6.14. Mean values of micro hardness are represented in Fig. 6.19. The relationships between drilling depth with force and drilling resistance are shown in Figs. 6.20 (a, b, c, d) and Figs. 6.21 (a, b, c, d), respectively, for each material. Mean values obtained have been reported in the binary diagrams of Figs.6.22 (a, b).

Table 6.14. Maximum and mean values of Micro-hardness (Ls), converted values in Vickers hardness (HV), Maximum Drilling Depth $Depth_{max}$ (mm), Drilling Force (N) and Drilling Resistance DR_i (N/mm) for the four materials: San Giovanni in Fiore granite (GF), Grisolia stone (DG), San Lucido calcarenite (CS) and Fuscaldo sandstone (AF).

Samples	L_s (HLD)	Vickers (HV)	$Depth_{max}$ (mm)	F (N)	DR_i (N/mm)
GF	761	212	0.5	53.9	116.1
<i>max</i>	783	218	1	65.9	133.6
<i>st. dev.</i>	13	4	0.2	8.3	18.7
DG	609	170	1.4	64.8	98.1
<i>max</i>	639	178	1.4	119.4	209.9
<i>st. dev.</i>	14	4	0.4	35.5	42.0
CS	438	122	2.5	42.2	33.9
<i>max</i>	505	141	5.0	45.8	271.4
<i>st. dev.</i>	32	9	1.5	6.7	47.3
AF	366	102	2.5	36.5	28.7
<i>max</i>	419	117	5.0	42.1	229.0
<i>st. dev.</i>	29	8	1.5	6.0	39.8

The harder the tested material, the higher the rebound value. So, GF resulted the hardest material, followed by DG, CS and AF (Table 6.19). The good characteristics of hardness of granite have been confirmed by the high mean values obtained by micro-hardness and drilling tests. In general, it can be said that granite is a hard stone, as granite consists of minerals with a Mohs hardness of 7 (quartz), 6 (feldspar), and 2–3 (mica). Micro-hardness, a highly variable property due to the heterogeneity of natural stones and the diversity of minerals, could be a useful tool for the characterization of stones with respect to the wear strength and processing performance, which is finally determined by the hardness of the individual stone-forming minerals in contrast to the average hardness (Primavori, 1999). Results of microdrilling and Equotip test highlight high values of hardness. Obtained mean values, 761+13 HLD and 116.13+18.71 N/mm, respectively, are related to minerals with Mohs hardness > 5, such as quartz. According to literature, for a 5 mm diameter drill bit the DRMS, until 100 N and drilling resistance until 20 N/mm, is restricted to minerals with a Mohs hardness ≤ 5 (Pamplona M., 2007). It can be also seen that there isn't a wide range of variation for the mechanical properties among the granite specimens, according to the low values of standard deviation. From the results of drilling force (Fig. 6.20 a) and

drilling resistance (Fig. 6.21 a), it can be observed a clear peak in all specimens due to the initial resistance of the material under drilling conditions. The DRMS curves indicate that this peak lies between approximately 0 and 0.1 mm below the surface of the material (Fig. 6.21 a). The high values of obtained drilling resistance and the low values of reached drilling depth are in agreement with the other hardness values which have been determined in this study.

Grisolia stone reached higher mean values of drilling force due to the different behaviour under drilling conditions. In fact, in spite of granite, Grisolia stone does not show a bilinear trend with the initial peak corresponding to the maximum force. The penetration force is lower in the initial part but increases during the steady state penetration and a significant random force oscillation (noise) has not been detected (Fig. 6.20 b). The maximum penetration depth is very low and similar to GF, so it can be said that Grisolia stone is a hard material, also according to the micro-hardness value (690 ± 14 HLD). Regarding the drilling resistance (Fig. 6.21 b), some samples reached very high values with a first phase characterized by an initial peak and a second phase with a horizontal trend composed by almost constant values.

Concerning the random force oscillation, it can be observed that San Lucido calcarenite and Fuscaldo sandstone behavior are characterized by an oscillation during the penetration. Once the peak has been reached, the penetration force decreased and the random force oscillation decreased too with depth (Figs. 6.20 c, d). Regarding drilling resistance, the two materials showed a similar behavior (Figs. 6.21 c, d) and comparable mean values. CS registered slight higher maximum and mean values than Fuscaldo sandstone. Micro-hardness mean values of 438 ± 32 HLD and 366 ± 29 HLD, respectively, indicate that they are material with a medium hardness and with minerals with Mohs hardness ≥ 5 , such as quartz and feldspar.

According to the hardness and drilling resistance mean values reported in Figs. 6.19 and 6.22, respectively, GF resulted the hardest material and with the highest drilling resistance, followed by DG and then by CS, while AF registered the lowest values.

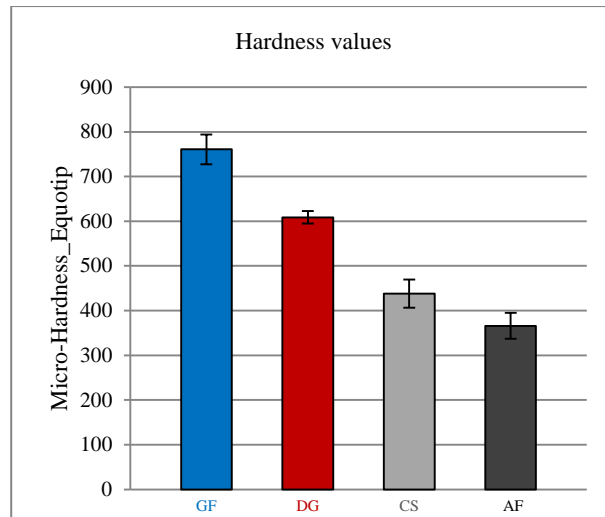
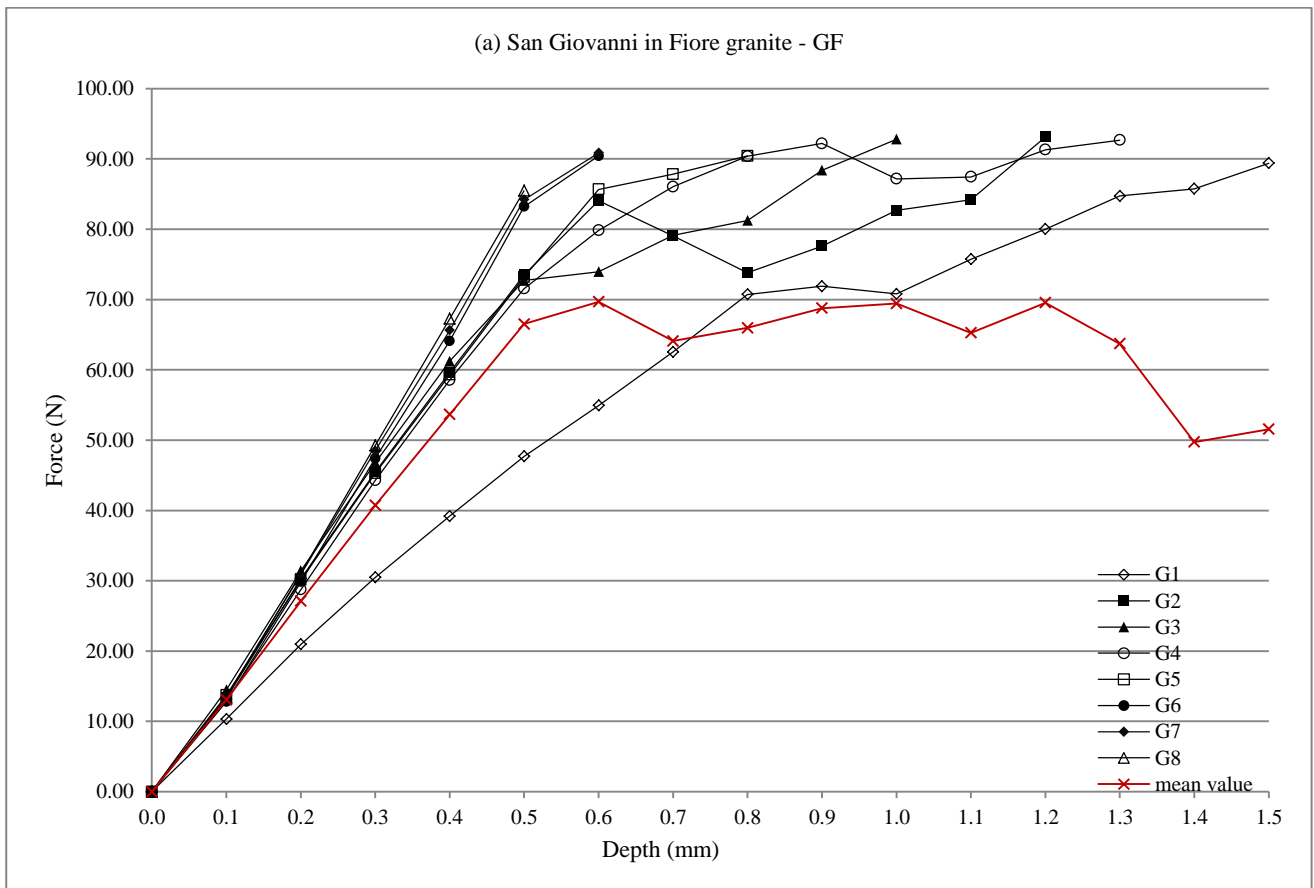
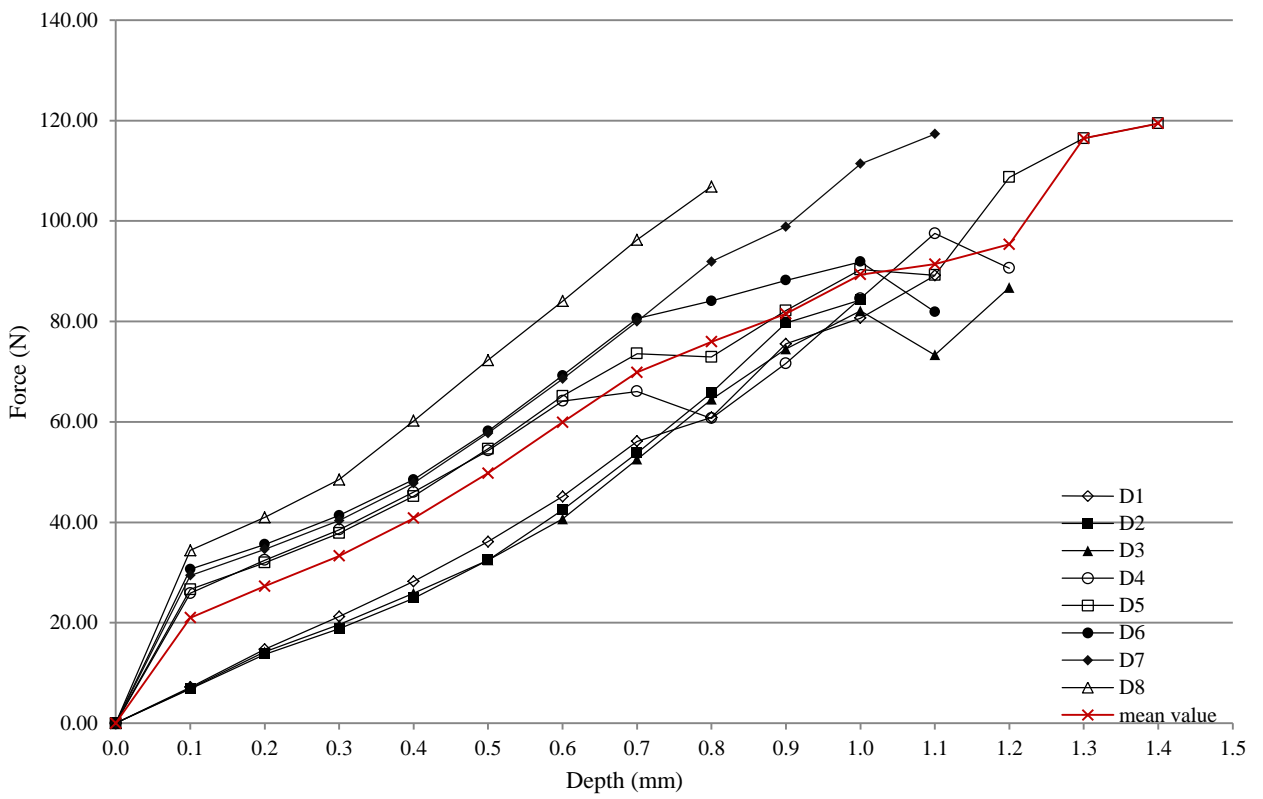


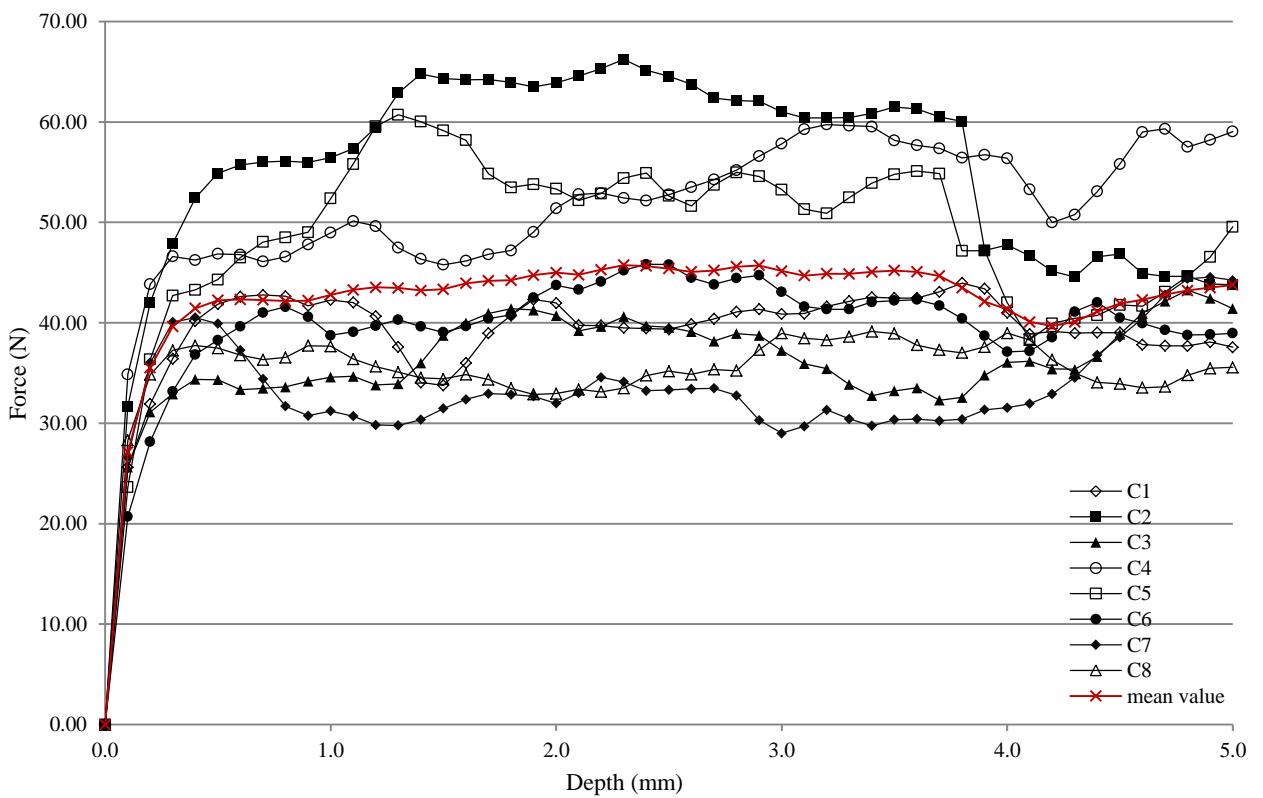
Fig. 6.19. Micro-hardness mean values of San Giovanni in Fiore granite (GF), Grisolia stone (DG), San Lucido calcarenite (CS) and Fuscaldo sandstone (AF).

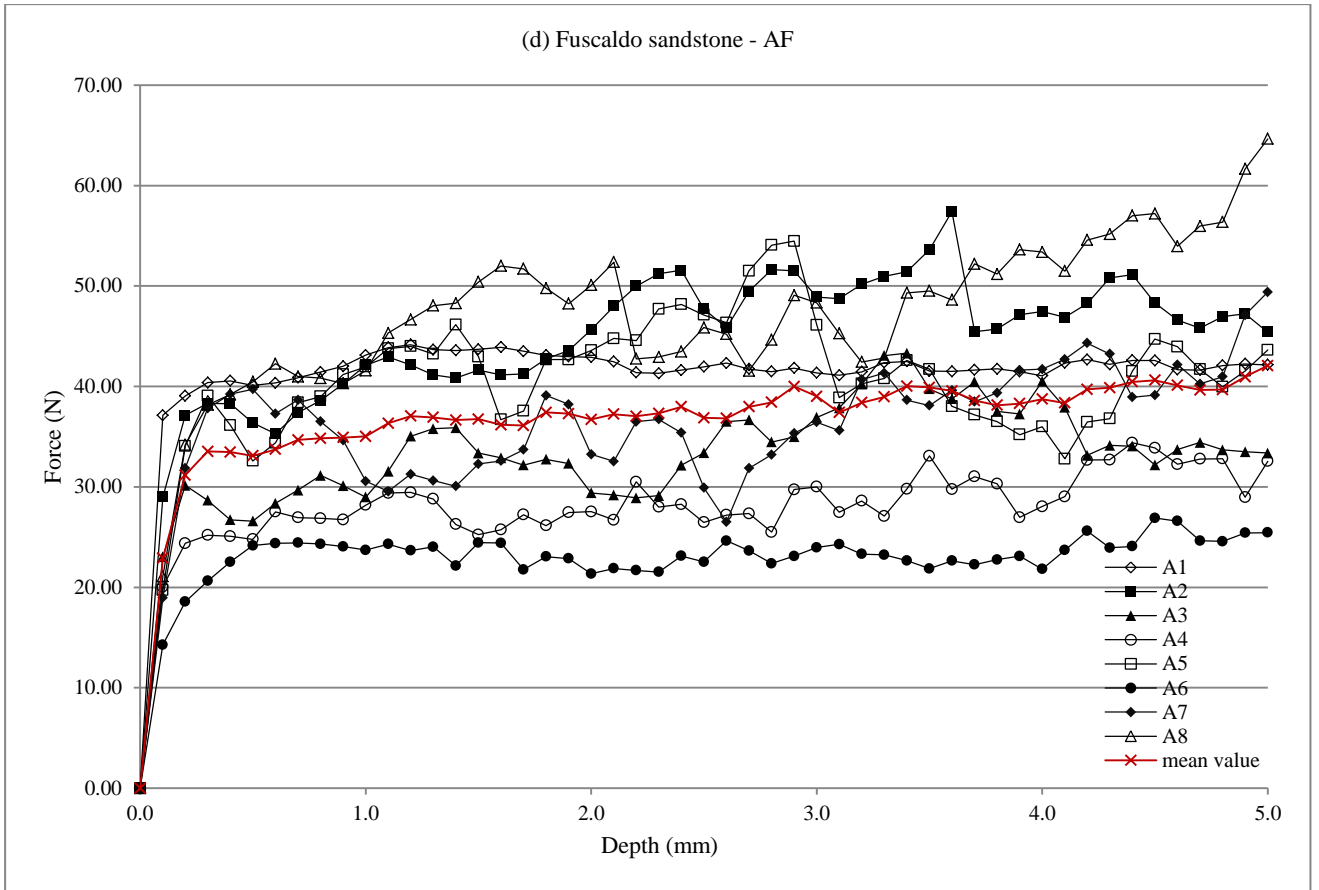


(b) Grisolia stone - DG

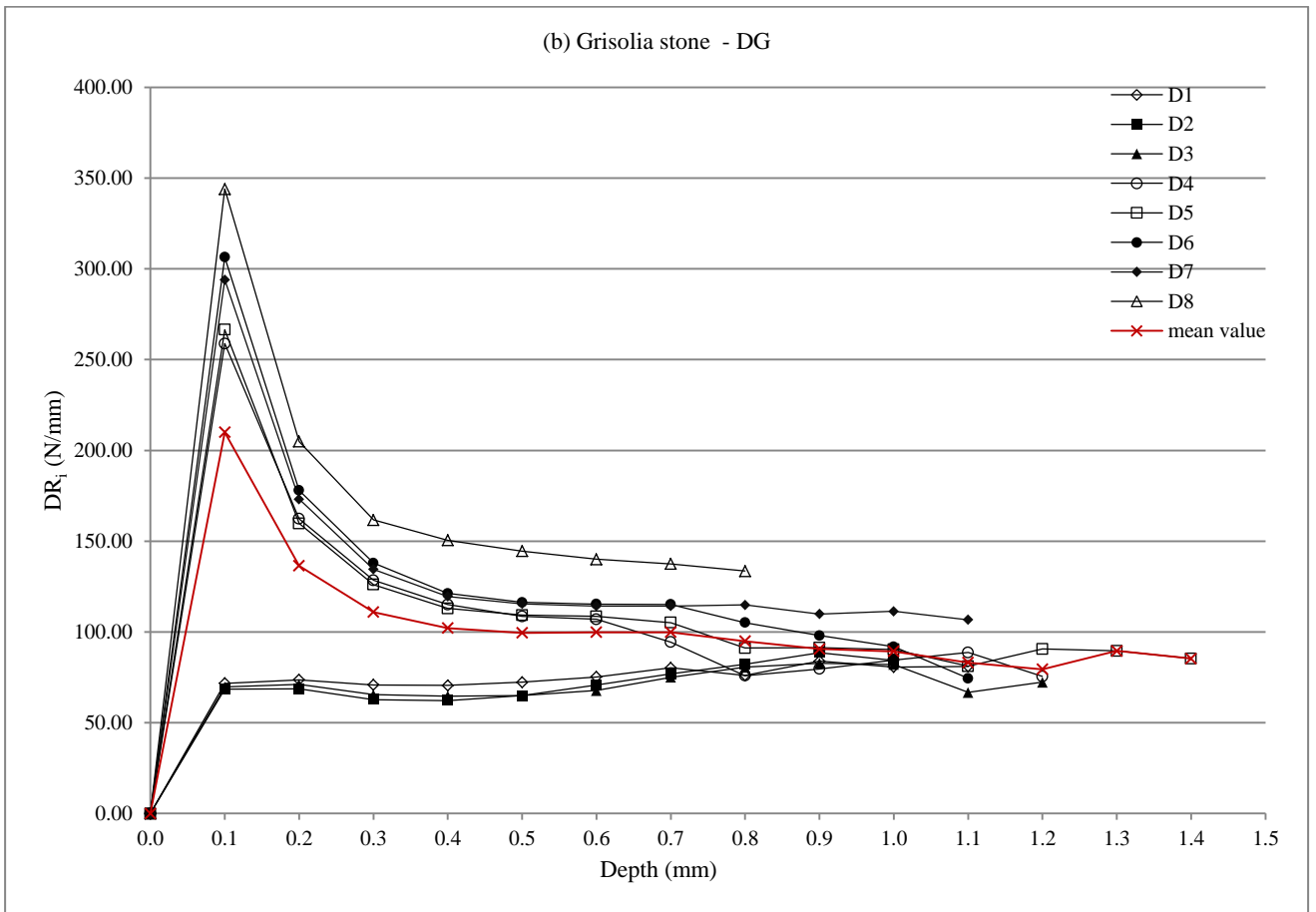
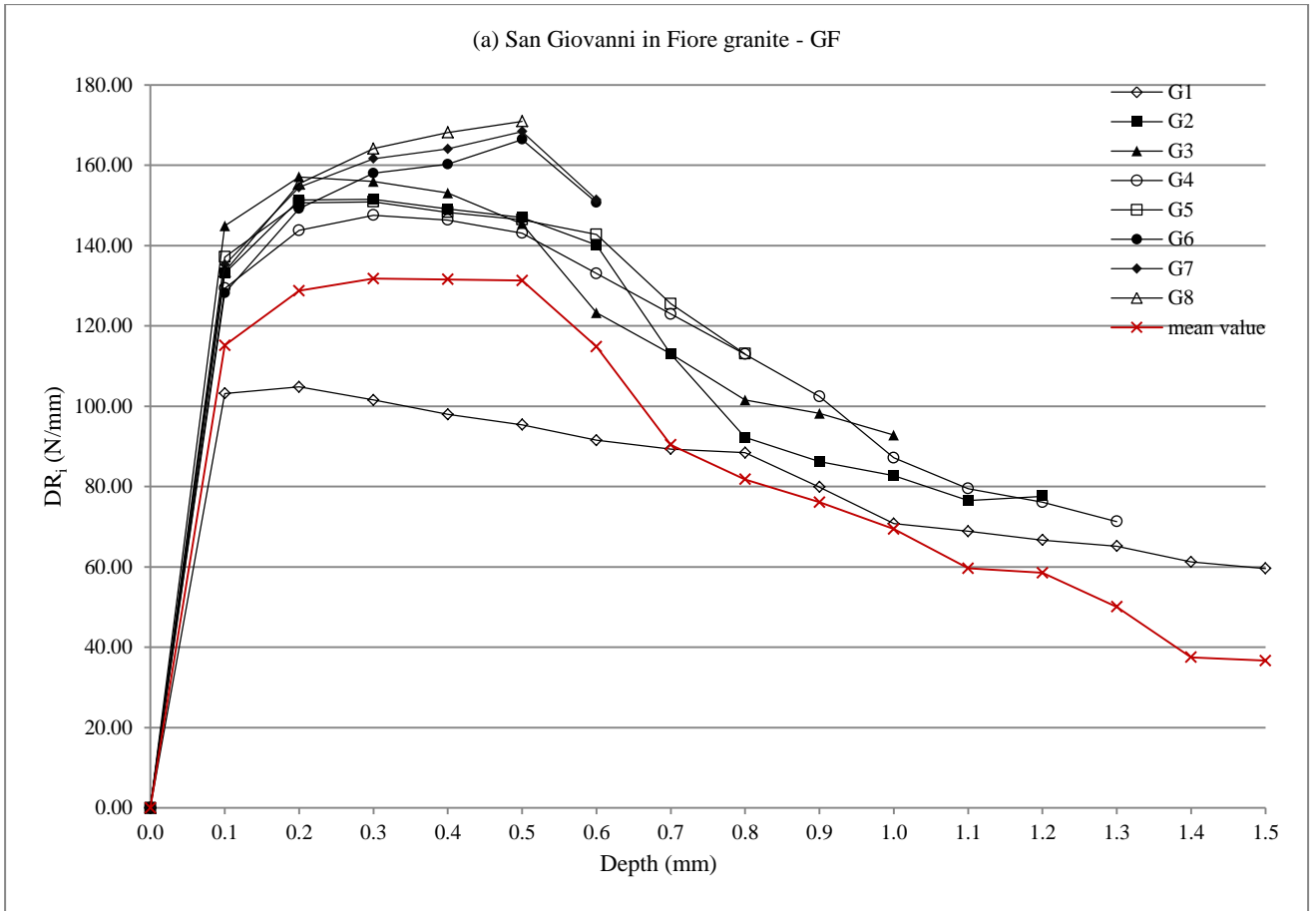


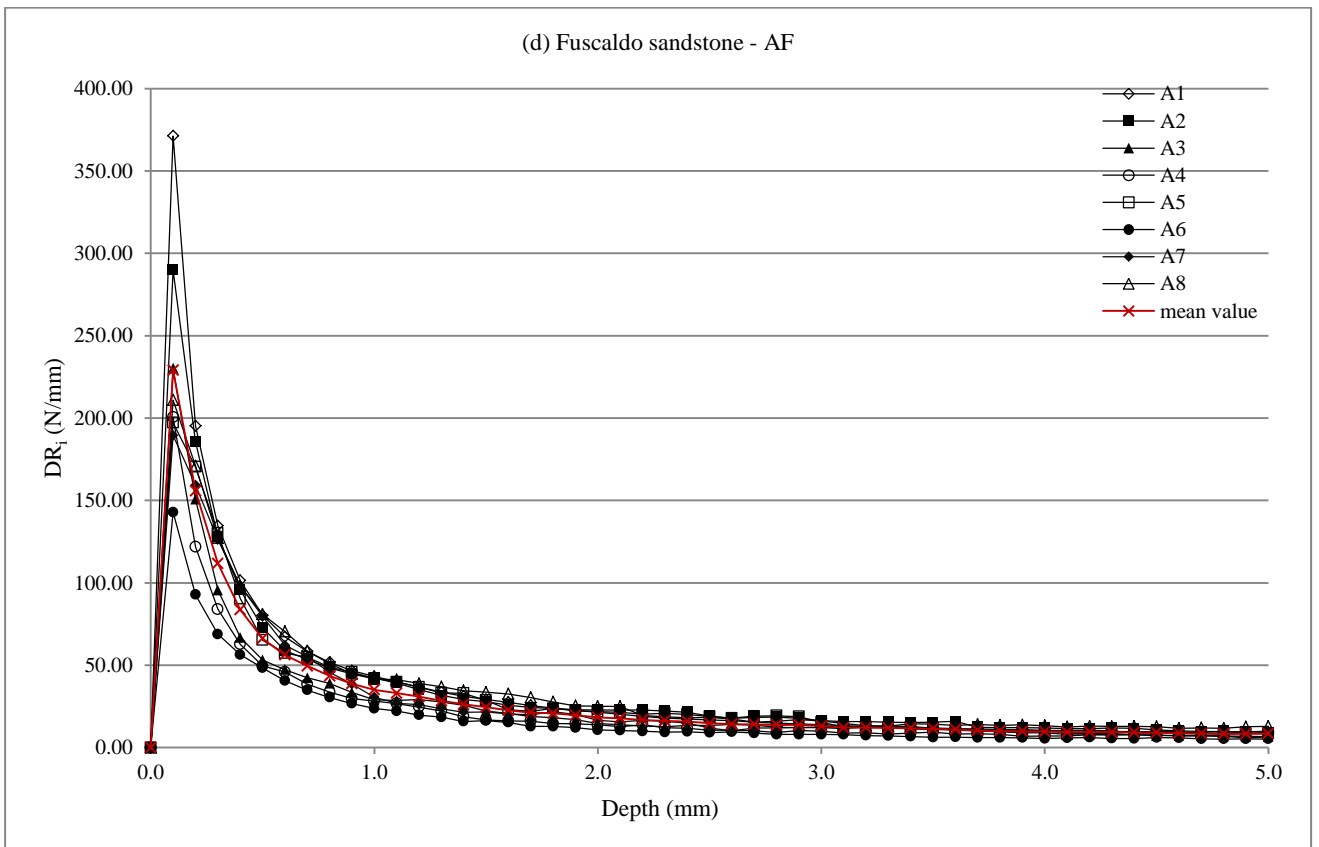
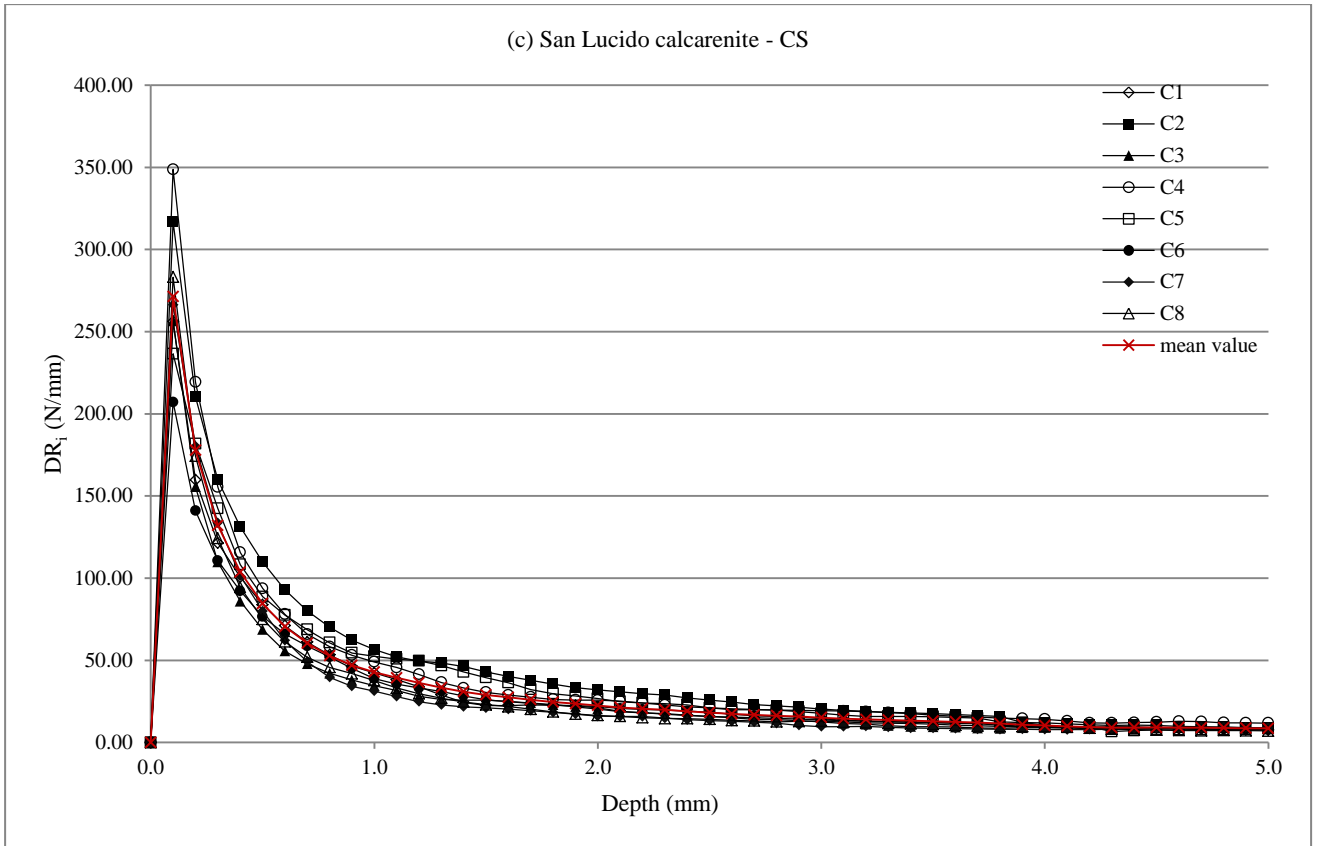
(c) San Lucido calcarenite - CS



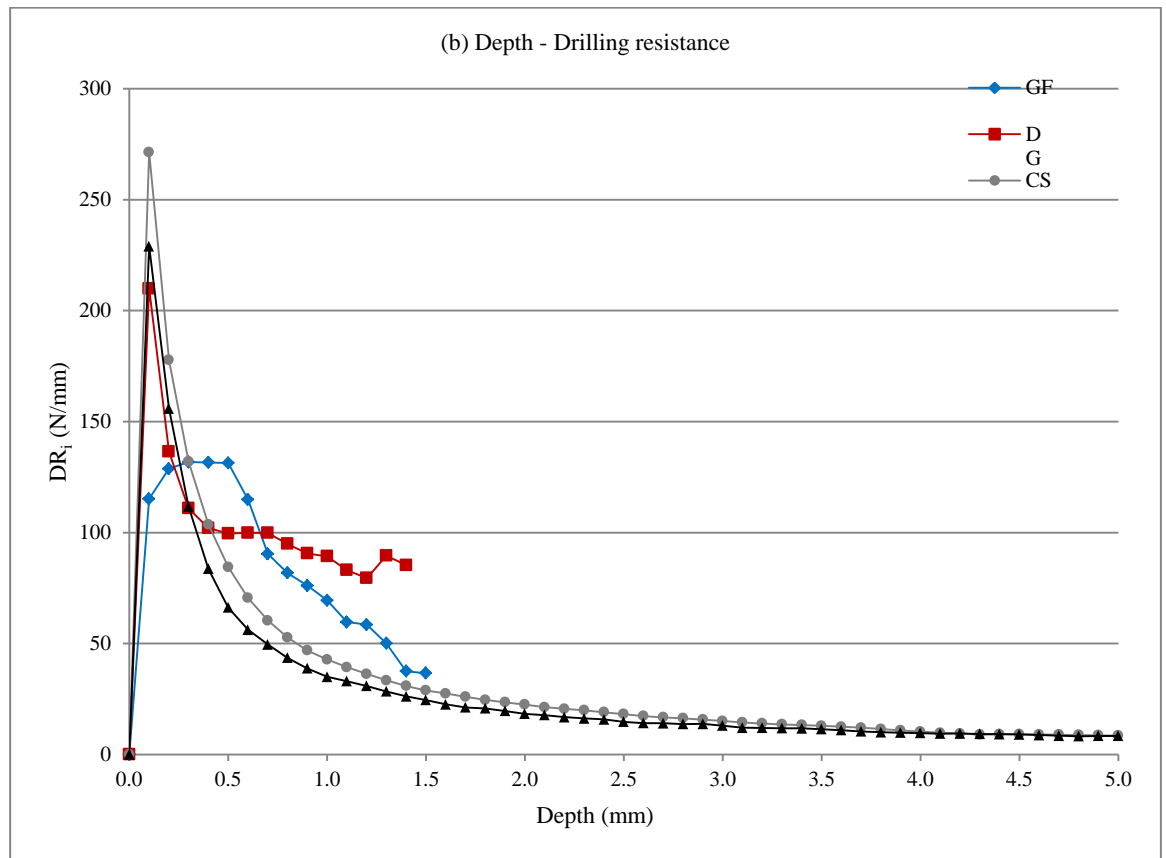
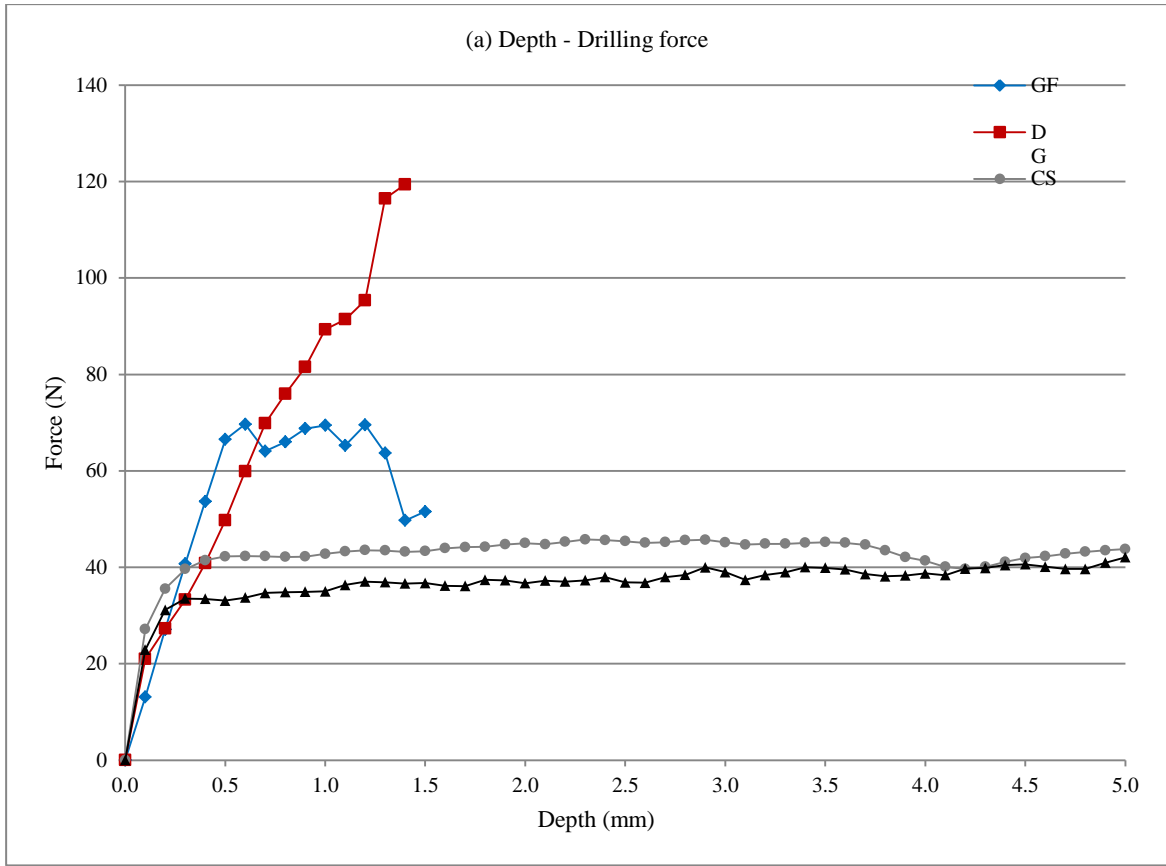


Figs. 6.20 a, b, c, d. Binary diagrams between Drilling Force (N) and Depth (mm) for each material: (a) San Giovanni in Fiore granite; (b) Grisolia stone; (c) San Lucido calcarenite; (d) Fuscaldo sandstone.





Figs. 6.21 a, b, c, d. Binary diagrams between Drilling Resistance DR_i (N/mm) and Depth (mm) for each material: (a) San Giovanni in Fiore granite; (b) Grisolia stone; (c) San Lucido calcarenite; (d) Fuscaldo sandstone.



Figs. 6.22 a, b. Binary diagrams of the four investigated materials representing the correlation between: (a) Depth (mm) and Drilling Force (N); (b) Depth (mm) and Drilling Resistance DR_i (N/mm).

The average values of Schmidt hardness test (H_s), carried out on granite boulders of the active and the ancient quarries are reported in [Table 6.15](#). For granite boulders, starting from rebound values, it was indirectly determined the uniaxial compressive strengths (σ_c) and the weathering class. The Schmidt hammer test, in fact, is a reliable indicator of the degree of decay in stone materials and Schmidt hammer rebounds are inversely proportional to the decay of stone materials and consequently to their porosity (Fort *et al.*, 2013). Measured Schmidt rebound hardness values range from 30 to 60 for granite boulders for the ancient quarry and from 30 to 54 for the active one. Uniaxial compressive strength, determined from rebound values, range from 68.1 to 227.6 MPa with a mean value of 126.3 ± 38.7 MPa for granite boulders of the ancient quarry and from 68.1 to 178.8 MPa with a mean value of 116.5 ± 30.4 for granite boulders of the active quarry. According to weathering classification, San Giovanni in Fiore granite of both quarries belongs to the “class II – Moderately weathered” (Schmidt Rebound mean values from 25 to 50) (Irfan & Dearman, 1978; Borrelli *et al.*, 2015). Moreover the mean value of Schmidt Rebound is in accordance with previous studies on the same granites that demonstrated that the mean value of H_s is related to the biotite content: as the biotite content increases, so does the weathering class (Le Pera & Sorriso-Valvo, 2000). H_s obtained demonstrates that the studied granite has a biotite content <15% vol. and as observed through the petrographic analyses too.

Table 6.15. Schmidt rebound values (H_s) and uniaxial compressive strength for the granite ancient quarry (H_{s1} and σ_{c1}) and for the active quarry (H_{s2} and σ_{c2})

	H_{s1}	σ_{c1} (MPa)	H_{s2}	σ_{c2} (MPa)
min	30	68.1	30	68.1
max	60	227.6	54	178.8
mean value	44	126.3	43	116.5
<i>st. dev.</i>	7	38.7	6	30.4

6.6.4 Uniaxial compressive strength

The uniaxial compressive strength of one stone can exhibit a strong directional dependence when determined in the different directions, due to the stone fabric elements (especially the lattice and shape preferred orientation of minerals), the degree of grain interlocking (*i.e.* grain boundary configuration) (Wenk, 1985; Siegesmund, 1996; Brosch *et al.*, 2000), the microcracks, the concentration of oriented minerals. For this reason the uniaxial compressive test, under unconfined condition, has been performed along the three spatial directions, X, Y and Z, parallel and perpendicular to anisotropy planes or microcracks. Stone strength values and anisotropy values (Ra), obtained for each direction, are shown in Table 6.16.

Most of the San Giovanni in Fiore granite samples (GF) under study exhibited maximum strength in the rift direction (Z-axis), *i.e.* in the direction that is reported as the strongest one for some Japanese granitic stones (Kudo *et al.*, 1987). Only few specimens reached maximum strength perpendicular to the hard-way (YZ section). The minimum values of uniaxial compressive strength probably do not represent the lowest possible strength. Stones exhibit the minimum strength when the plane of weakness (foliation, dominant set of microcracks) is oriented at a certain degree (30–45°) to the loading direction (Douglass & Voight, 1969; Singh, 1989; Kwasniewski, 1993; Rammamurthy, 1993; Prikryl, 2001). The range of unconfined compressive strength of samples varied between 76.4 and 143.3 MPa, with a mean value of 104.1 MPa, that is in the range of the average uniaxial compressive strength of plutonic stones found by other authors (Mosch & Siegesmund, 2007). Most of GF specimens can be classified as “strong” and others “very strong” along the X and Y-axes, according to the strength classification of Anon (1977) (Bell & Lindsay, 1999).

Regarding DG specimens UCS values obtained are very similar along the three spatial directions and with very slight differences. This fact is in agreement with the low anisotropy ratio (only 0.1), its

homogeneous features and its ultrasonic isotropic behavior. The maximum value of UCS of 64.7 MPa has been recorded along the Z-axis, the intermediate of 63.7 MPa along the Y-axis and the minimum 59.5 MPa along the X-axis, with an average value of 62.5 MPa. It can be classified as a “strong” stone.

San Lucido calcarenite (CS) and Fuscaldo sandstone (AF) registered similar mean values, 33.8 MPa and 31.0 MPa, respectively. But CS showed isotropic strength behaviour, with very slight difference of UCS along the three axes while AF an anisotropic behavior. Fuscaldo sandstone reached resistance to compression lower compared to the other variety of sandstones (Molina *et al.*, 2015).

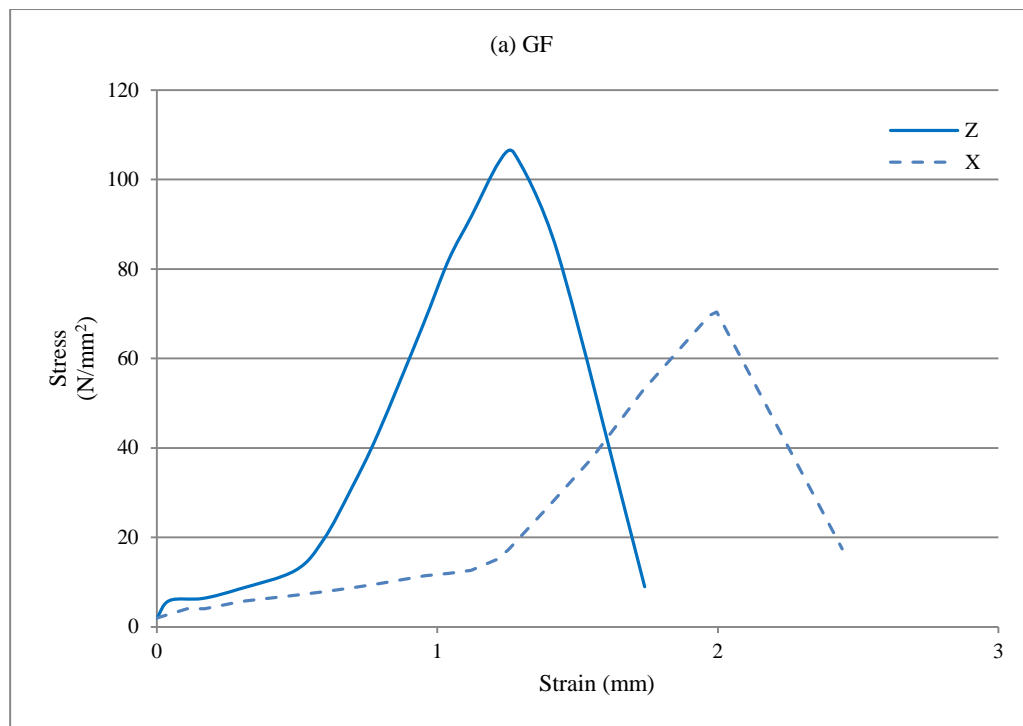
Table 6.16. Uniaxial compressive strength (UCS) and its anisotropy expressed as “Ra” and as the ratio “max/min” of the studied lithotypes. Letters in brackets (X), (Y) and (Z) indicate orientation of samples along axes X, Y and Z with respect to the fabric features. Letters in brackets (MS), (S) and (VS) mean: MS, “moderately strong” 12.5-50 MPa; S, “strong”, 50-100 MPa; VS, “very strong”, 100–200 MPa (Anon, 1977).

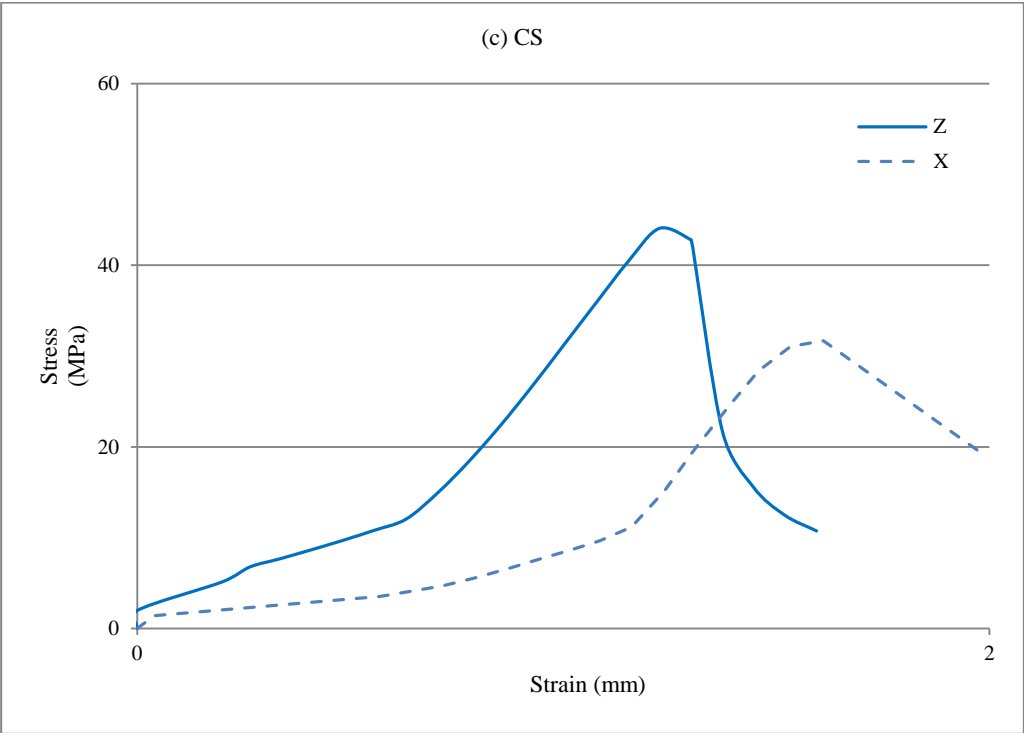
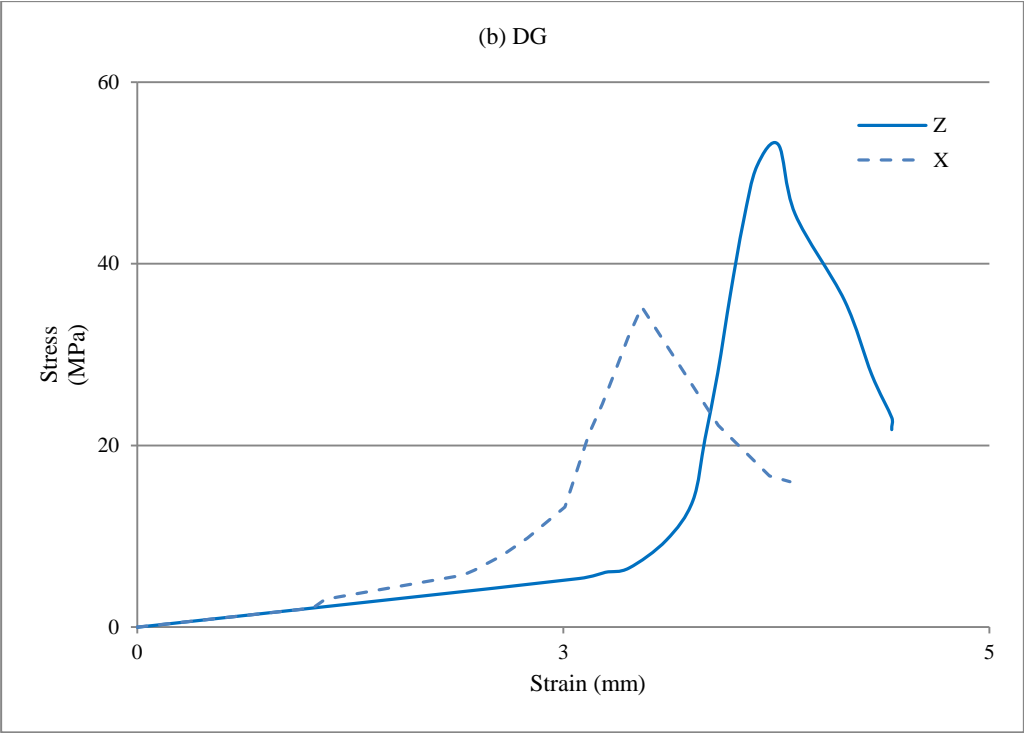
Samples	Uniaxial compressive strength (UCS) (MPa)										Anisotropy		
	min		inter				max		mean		Ra	max/min	
GF	69.0	(X)	(S)	109.4	(Y)	(VS)	161.5	(Z)	(VS)	104.1	(VS)	0.9	2.3
<i>st. dev.</i>	6.3			23.7			28.7			30.5			
DG	51.7	(X)	(S)	68.8	(Y)	(S)	99.1	(Z)	(S)	68.4	(S)	0.7	1.9
<i>st. dev.</i>	9.0			5.4			25.2			14.2			
CS	23.8	(X)	(MS)	33.1	(Y)	(MS)	48.3	(Z)	(MS)	33.8	(MS)	0.7	2.0
<i>st. dev.</i>	5.3			1.9			5.4			5.9			
AF	17.7	(X)	(MS)	44.1	(Y)	(MS)	50.6	(Z)	(MS)	31.0	(MS)	1.1	2.9
<i>st. dev.</i>	6.3			3.1			11.8			11.0			

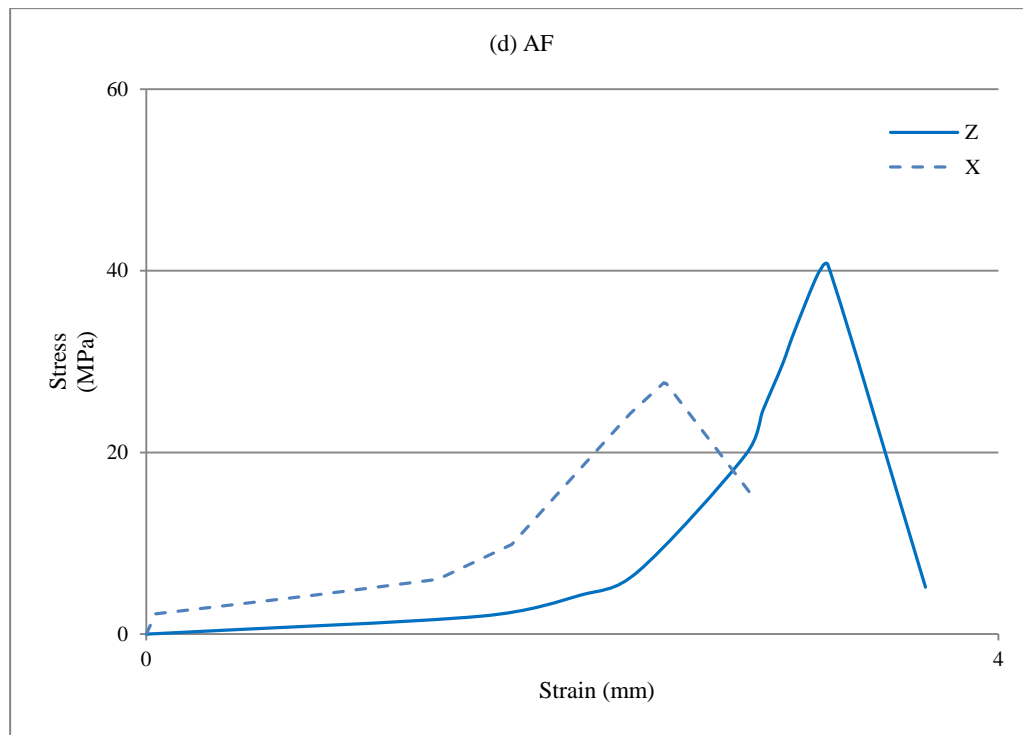
San Giovanni in Fiore granite (GF) and Fuscaldo sandstone (AF) exhibit a certain degree of strength anisotropy, as demonstrated analyzing UCS values along the three axes and by the anisotropy ratio. Comparing anisotropy values obtained for granite (about 19%) with the same lithology investigated by other authors, GF could be defined as a stone with “medium strength anisotropy” (Prikryl, 2001). This moderate strength anisotropy was observed for granites with the same fabric characteristic like GF: medium- to coarse-grained granites; well-pronounced sets of microcracks; no shape-preferred orientation of minerals. The presence of oriented sets of microcracks, individuated by the petrographic analysis, proved to have a moderate influence on the granite strength anisotropy.

As well as GF, Fuscald sandstone showed a medium anisotropy, probably due the preferred orientation of phyllosilicates, as demonstrated by the petrographic analysis.

The lowest anisotropy values (less than 10%) were observed for San Lucido calcarenite (CS) and Grisolia stone (DG). Both stones did not show a shape-preferred orientation of major stone-forming minerals, that is one of the most influential factors affecting strength anisotropy (Prikryl, 2001).







Figs. 6.23 a, b, c, d. Stress-strain curves for San Giovanni in Fiore granite (a), Grisolia stone (b), San Lucido calcarenite (c) and Fuscaldò sandstone (d), showing the correlation between the stress (MPa) and the strain (mm), for two directions (X-axis and Z-axis).

The stress-strain curves (Figs. 6.23 a, b, c, d) have been drawn for two spatial directions (Z and X), where the maximum and minimum values of UCS, respectively, have been recorded.

The anisotropic behaviour of GF is also confirmed by the analysis of the stress-strain curves (Fig. 6.23a) in the parallel and perpendicular direction to the rift plane. It is observed that a significant reduction of the UCS is found along the X-axis, whereas almost high values are found along the Z-axis. This fact is probably due to the presence of material discontinuities resulting from microcracking that develop, during tests, in planes oriented in the direction of axial loading, decreasing strength material in the planes perpendicular to the hardway direction. Moreover, the planar anisotropy and the presence of internal microcracks, influence considerably the strength material and its elastic properties (Vasconcelos *et al.*, 2007).

Also Fuscaldo sandstone exhibits an anisotropic behavior with a significant difference of maximum stress value along the two directions (Fig. 6.23 d), while Grisolia stone and San Lucido calcarenite confirm their isotropic behavior (Figs. 6.23 b, c).

The stress–strain curves in unconfined state (Figs. 6.23 a, b, c, d) for the two investigated directions show that the behavior of stone samples is almost quasi-linear-elastically until failure. It can be said, graphically, that initial tangent modulus, that is the slope of the initial part of the stress-strain curve, remains almost equal to the tangent modulus, at 50% of the failure strength. Furthermore, it can be noticed that samples showed the same quasi-elastically behaviour along the two axis. The only difference appears for the strain part, that is longer for the X-direction than the Z-direction one for GF and CS, while, contrarily, longer for Z-direction than the X-direction for DG and AF.

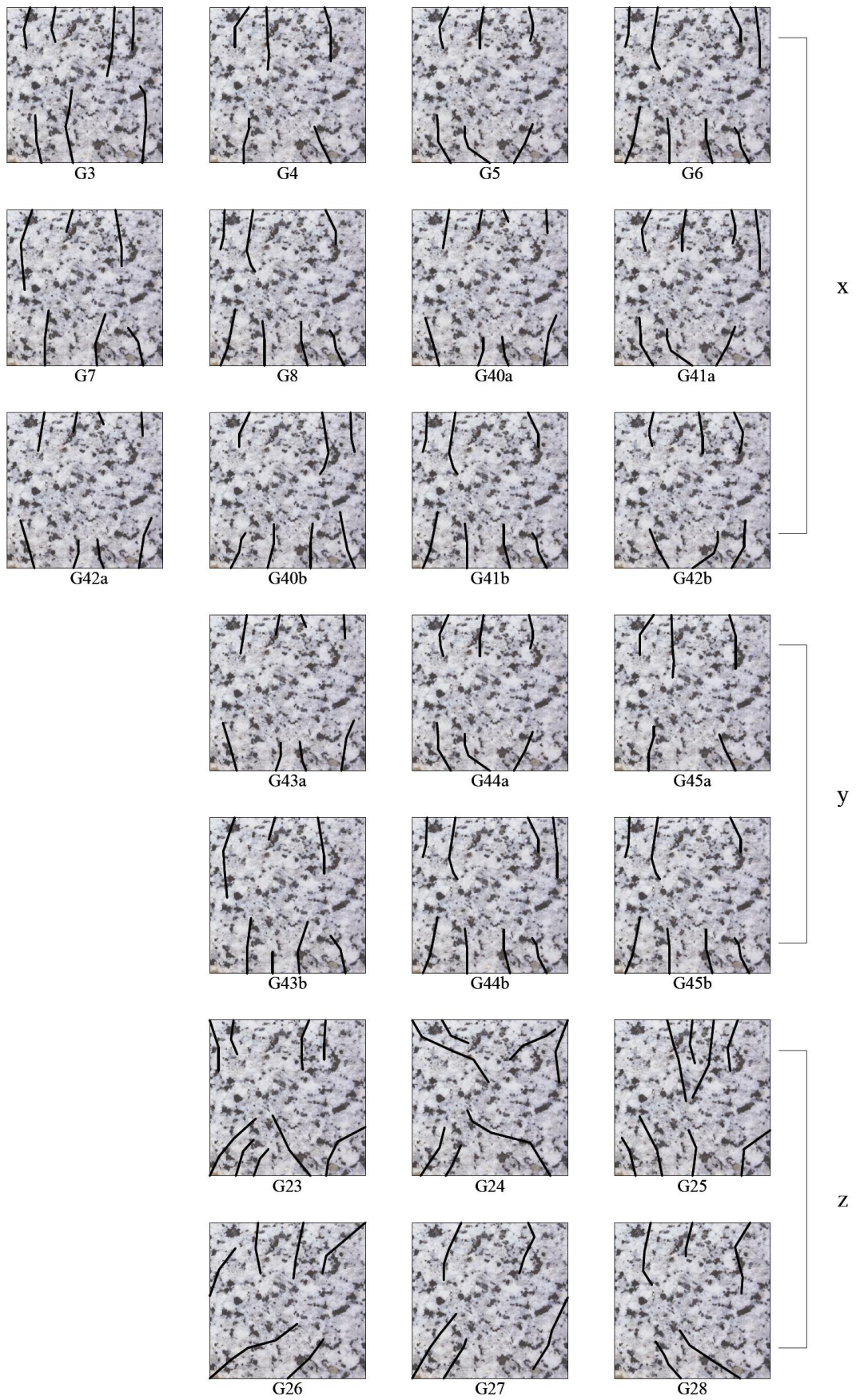


Fig. 6.24. Diagrammatic view of the fractures developed in granite specimens under uniaxial compressive conditions, along the three directions, X, Y and Z-direction.

The fracture propagation during test has been reported for San Giovanni in Fiore granite specimens along the three investigated directions (Fig. 6.24).

According to theory of stone failure (Bieniawski, 1967), regarding fracture initiation under compression, granite specimens showed an initial elastic deformation with a fracture initiation and at last a several propagation of fractures. Ultimately fail violently releasing the stresses instantaneously with axial tensile-fractures parallel to the direction of loading. The fracture patterns are shown schematically in Fig. 6.24 for the San Giovanni in Fiore granite specimens, where it can be noticed that fractures are little and mainly concentrated near top surface, generating an axial failure, as observed for other fresh Indian granites (Gupta & Seshagiri Rao, 2000). Moreover for the X-axis and Y-axis fractures are more parallel than for the Z-axis, probably due to the orientation of microcracks along the XY plane parallel to the direction of loading. According to the mode failure it can be determined the weathering grade of granite specimens (Gupta & Seshagiri Rao, 2000): fresh granite with a splitting and tensile failure.

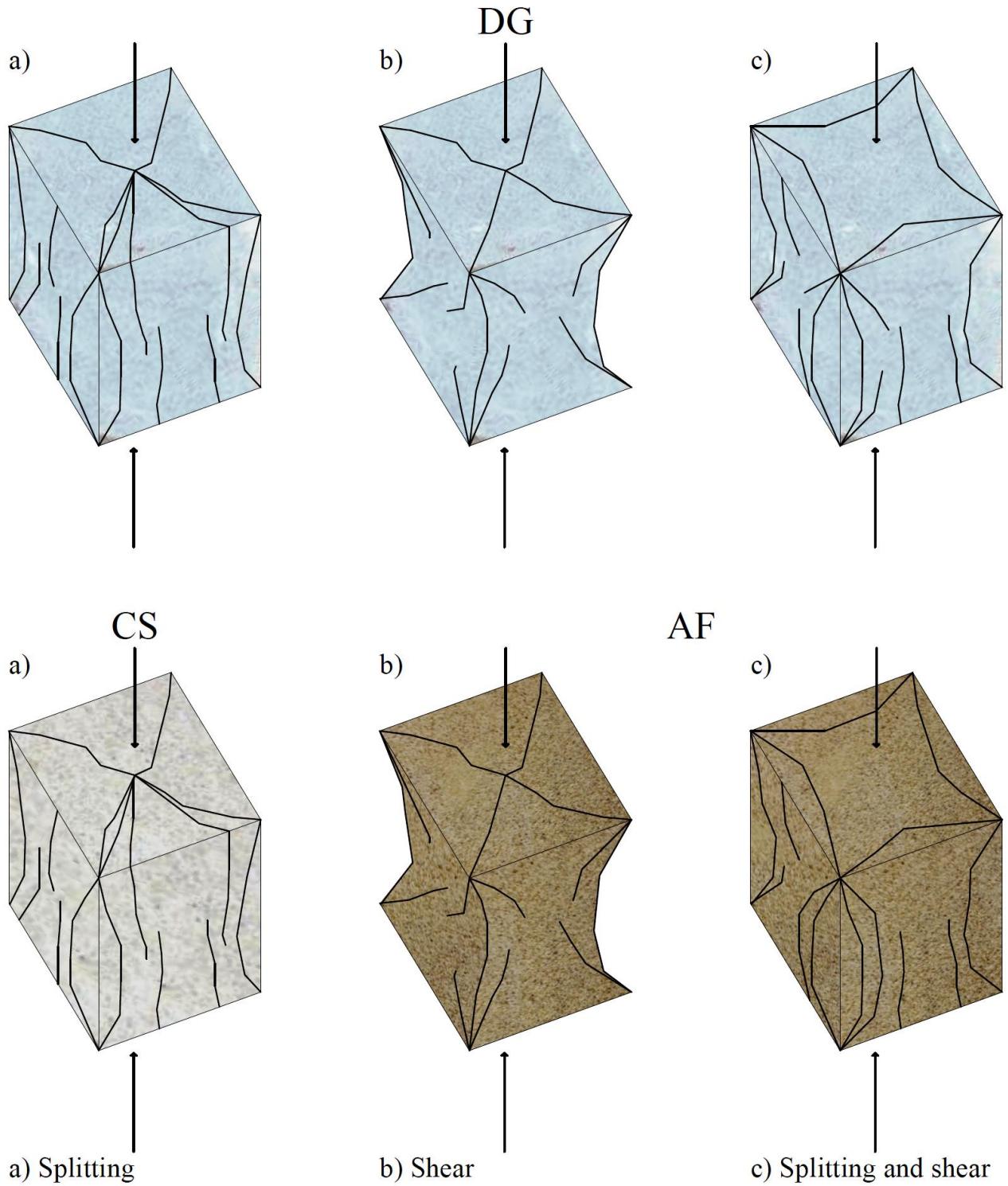


Fig. 6.25. Diagrammatic view of the fractures developed in Grisolia stone (DG), San Lucido calcarenite (CS) and Fuscaldo sandstone (AF) specimens under uniaxial compressive conditions.

For other specimens (DG, CS and AF) it has been observed a failure as a composite of shear and tensile, along the three directions (Fig. 6.25). For DG it has been observed that specimens broke in three

different ways (Fig. 6.25 a, b, c – DG): splitting; shear; splitting and shear. There is no difference along the three investigated directions and probably the difference in mode failure is due to the presence or not of internal weak planes. Fractures are long, extended for the height of the sample and mainly parallel to the direction of loading. In the case of shear failure fractures are oriented towards the inside of the sample and after the rupture the sample has hourglass shape. The shear failure, that is complex conjugate failures in terms of Gramberg (1989), took paths along planes of weakness.

San Lucido calcarenite specimens (CS) showed only a splitting mode failure (Fig. 6.25 a - CS). Specimens broke along planes that are characterized like thin layers parallel to the direction of loading. Some fractures are very short, mainly concentrated in the middle of specimens, near the surface in contact with the load plates and others long and spread along edges.

Fuscaldo sandstone (AF) exhibited two types of mode of failure (Fig. 6.25 b, c - AF): shear; splitting and shear. Fractures are long and oriented towards the inside of specimens. The final hourglass shape is typical of the shear failure. Probably the failure develops along weakness planes or following the internal distribution of phyllosilicates, oriented along a prevalent direction. The difference between the investigated spatial directions is only that along the Z-axis there is a no evident parallel distribution of fractures lines, more evident along the X and Y-axes.

6.6.5 Flexural strength

Stones are pretty weaker in tensile loads than in compressive loads. The mechanical properties resisting the tension type failure (*i.e.* tensile strength, flexural strength) bear much importance to stone engineering practice such as the stability of mining roofs, tunnel boring, crushing, drilling and blasting. It is thus important to characterize the tension-related properties of anisotropic stones and to find out the correlation between properties, the microcrack-induced anisotropy as well and the internal foliation planes (Dai *et al.*, 2013).

Flexural strength values along the three spatial directions and the anisotropy ratio are reported in

Table 6.17.

Table 6.17. Flexural strength (R_{tf}) values and its anisotropy expressed as “ $R_{a_{tf}}$ ” and as the ratio “max/min” of the studied lithotypes. Letters in brackets (X), (Y) and (Z) indicate orientation of samples along the axes X, Y and Z with respect to the fabric features.

Samples	Flexural strength (R_{tf}) (MPa)							Anisotropy	
	min		inter		max		mean	$R_{a_{tf}}$	max/min
GF	6.5	(X)	7.2	(Y)	9.0	(Z)	7.8	0.3	1.4
<i>st. dev.</i>	0.5		0.6		0.5		1.0		
DG	9.3	(X)	12.9	(Y)	15.1	(Z)	12.2	0.5	1.6
<i>st. dev.</i>	0.8		0.3		2.4		1.9		
CS	5.6	(X)	6.4	(Y)	7.0	(Z)	6.8	0.2	1.2
<i>st. dev.</i>	2.0		0.1		0.5		1.2		
AF	6.7	(X)	8.5	(Y)	11.0	(Z)	7.9	0.5	1.6
<i>st. dev.</i>	2.5		0.8		2.1		1.0		

For all investigated samples the maximum values were reached along the Z-axis, the intermediate along the Y-axis while the minimum along the X-direction, as expected because the loading directions parallel to the layering or foliation show the lowest flexural strength values (Siegesmund & Dürrast, 2014).

San Giovanni in Fiore granite reached lower values compared to other granites and higher values of anisotropy. The high values of the anisotropy ratio probably are due to the presence of the internal set of microcracks because, as known, the flexural tensile strength anisotropy of granite appears to be compromised by two factors competing either way: the loading rate effect; the anisotropic effects of the stone minerals and the microcracks (Dai *et al.*, 2013). Granites generally exhibit anisotropy due to anisotropic elasticity of stone forming minerals and the alignment of the pores and/or microcracks in preferred directions (Phillips & Phillips, 1980). The reason for the flexural strength anisotropy may be understood using the microcrack orientations reported by the petrographic analysis and the rate dependence of the anisotropy is explained with the microcrack interaction. The maximum measured flexural tensile strength was reached in the rift plane (Z-axis) with a mean value of 7.4 ± 0.5 MPa;

intermediate strengths are from the grain plane (Y-axis) with 7.1 ± 0.6 MPa; the minimum were from the hard-way plane (X plane) with an average value of 5.0 ± 0.7 MPa. The obtained strength distribution corresponds to previous studies on the anisotropy flexural strength by Goldsmith *et al.* (1976) and by Dai *et al.* (2013), although the nomenclature of principle directions in the more recent study is different (*e.g.* the Z-axis corresponds to the X-axis of this study).

Grisolia stone (DG) reached the highest mean value of flexural strength with 10.1 ± 3.9 MPa and a low value of anisotropy ($R_{af}=0.2$). The flexural average values recorded were: maximum value of 11.0 ± 3.9 MPa; intermediate of 10.0 ± 6.2 MPa; minimum of 8.9 ± 1.7 MPa.

San Lucido calcarenite (CS) recorded the minimum values of anisotropy with only 0.1 of R_{af} and the lowest value of flexural strength with 6.8 ± 1.2 MPa. Mean values along Z and Y are the same with 6.5 MPa while along X it was reached the maximum value with 7.1 ± 2.0 MPa.

Fuscaldo sandstone (AF), even though its resistance to compression was lower compared to the other variety of sandstones, exhibited a higher flexural resistance (Molina *et al.*, 2015). Its anisotropy ratio is high, probably for the internal foliation planes. The flexural average values recorded were: maximum value of 11.5 ± 1.0 MPa; intermediate of 8.7 ± 2.1 MPa; minimum of 8.2 ± 0.8 MPa.

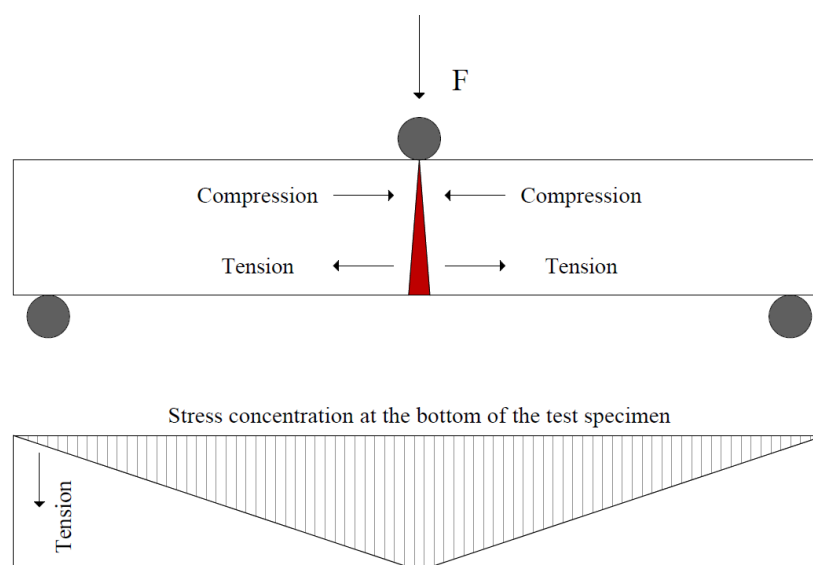
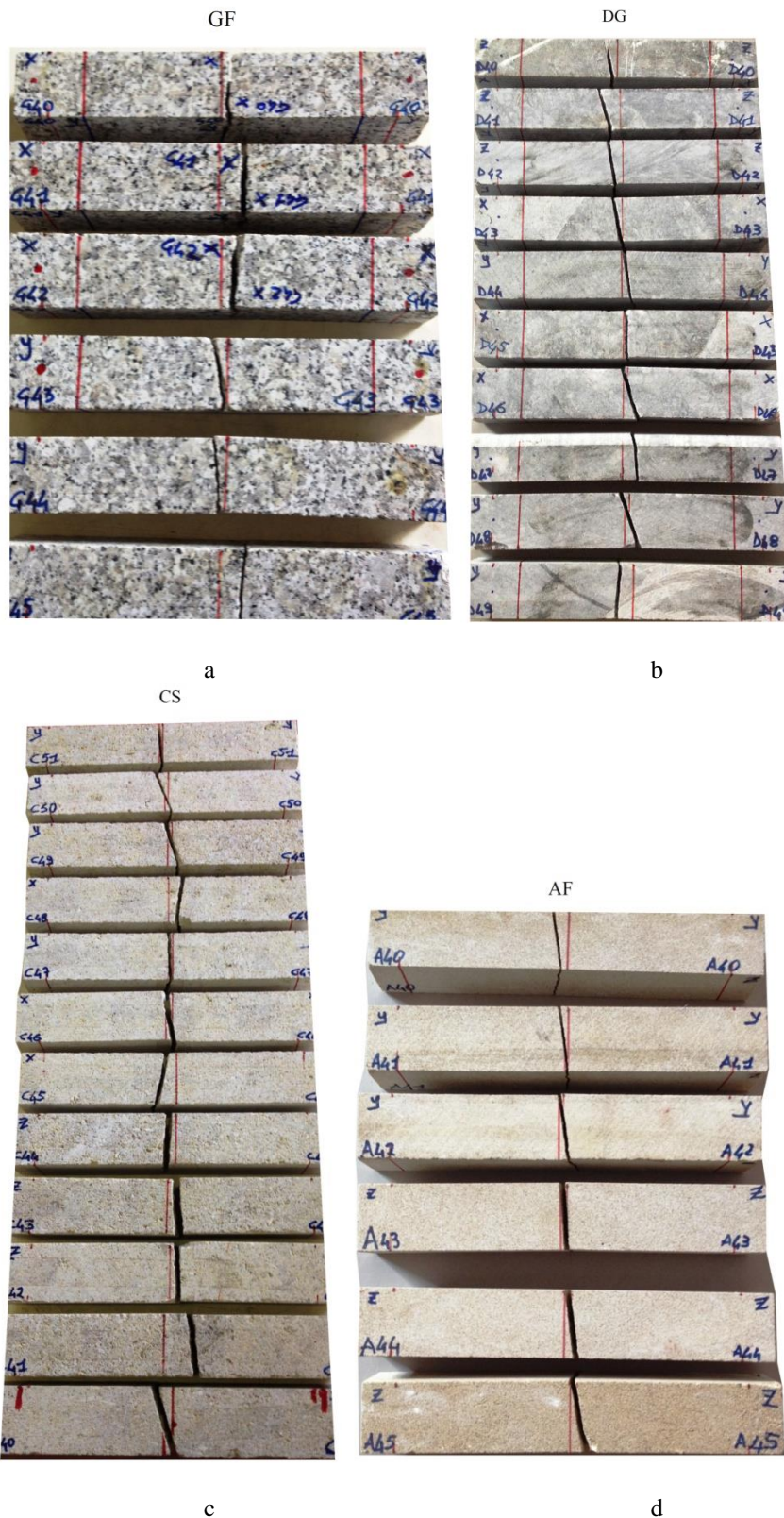


Fig. 6.26. Schematic picture of a sample under three-point load bending strength test, with regions of compression and tension indicated and where F is the loading force direction.

Regarding the mode of failure comparing uniaxial compressive strength test with the flexural one, crack interaction and coalesce mechanism are less complex compared to that of the compressive loading. In fact, only a limited number of critical cracks, mainly concentrated in the middle of specimen, are required to induce failure (Tsur-Lavie & Denekamp, 1982; Günes Yılmaz *et al.*, 2011). As shown in Fig. 6.26, the directions usually presented are the spatial orientation of the tensile vectors, which are perpendicular to the fracture surface. This macroscopic crack initiates from the centre of the sample, where the tensile stress is the maximum. After that, the macroscopic crack propagates along the loading axis, resulting in the final catastrophic failure of the sample. The fracture patterns of the analyzed samples for this test are shown in Figs. 6.27 a, b, c, d. Along the loading directions, the sample is split into two approximate half parallelepipeds. It should be pointed out that the position of the fracture in the specimen was very variable. This is probably related to different stress fields associated to the beam slenderness of each specimen geometry. For the calcarenite (CS) in few cases this was also influenced by the presence of inclusions, such as larger shells.

It should also be pointed out that the fracture never developed in the loaded section and that in that case Navier's equation should not be used for processing data. The tensile strength is then evaluated by means of applying the well-known Navier's equation to the furthestmost fiber from the neutral axis at rupture. It should be highlighted, however, that the validity of this equation has some limitations. In the de Saint-Venant solid the Navier's equation does not apply for sections which are closer than the cross section height to concentrated loads and, therefore, should not be used for interpreting flexural strength results. These theoretical considerations are also confirmed by experimental data; for example, Cardani & Meda (2004) have measured the profile of the axial normal strain along the specimen height under the concentrated load of a three pointed flexural strength test on Carrara Marble. Data clearly confirm the

theory and indicate that if the Navier's equation is used for this type of test, the maximum tensile stress is overestimated (Coviello *et al.*, 2005).



Figs. 6.27 a, b, c, d. Fracture patterns of the analyzed samples: San Giovanni in Fiore granite (a); Grisolia stone (b); San Lucido calcarenite (c); Fuscaldo sandstone (d).

6.6.6 Indirect Tensile strength test (Brazilian test)

The effect of anisotropy on indirect tensile strength determined by the Brazilian test has been investigated by many researchers such as Hobbs (1963), Barla & Innaurato (1973), Chaberlain *et al.* (1976), Behrestaghi *et al.* (1996), Khanlari *et al.* (2014).

In this research, the specimens were placed in a Brazilian test machine with different anisotropy angles of loading directions ($\beta = 0^\circ, 15^\circ, 30^\circ, 45^\circ, 60^\circ, 75^\circ$ and 90°). The loading direction was oriented: parallel to the foliation planes or microcracks (in the case of GF) for $\beta = 0^\circ$; perpendicular to those planes or microcracks for $\beta = 90^\circ$; with different orientations for $0^\circ < \beta < 90^\circ$. The resulting data of the Brazilian tensile strength (σ_t) at different angles, are summarized in Table 6.18, together with the Brazilian anisotropy index (BAI).

The correlation between Brazilian tensile strength (σ_t) and anisotropy angle (β) for all tested samples are shown in Fig. 6.28.

Table 6.18. Values of tensile strength σ_t (MPa) at different β ($^\circ$) for the tested samples and Brazilian anisotropy indices BAI.

Samples	Brazilian tensile strength (σ_t) (MPa)								Anisotropy BAI
	β (Deg.)							mean value	
GF	7.87	7.89	7.96	7.98	8.06	8.07	8.20	8.00	1.0
<i>st. dev.</i>	0.1	0.1	0.1	0.1	0.1	0.1	0.1	0.1	
DG	7.70	7.82	7.85	7.86	7.89	7.90	8.00	7.86	1.0
<i>st. dev.</i>	0.0	0.2	0.3	0.1	0.1	0.0	0.1	0.1	
CS	1.1	1.3	1.3	1.4	1.6	2.0	2.1	1.54	1.9
<i>st. dev.</i>	0.0	0.2	0.1	0.3	0.5	0.2	0.0	0.4	
AF	1.3	5.5	5.9	6.0	6.8	7.3	7.8	5.80	5.6
<i>st. dev.</i>	2.0	2.4	2.1	2.5	3.0	1.5	2.0	2.1	

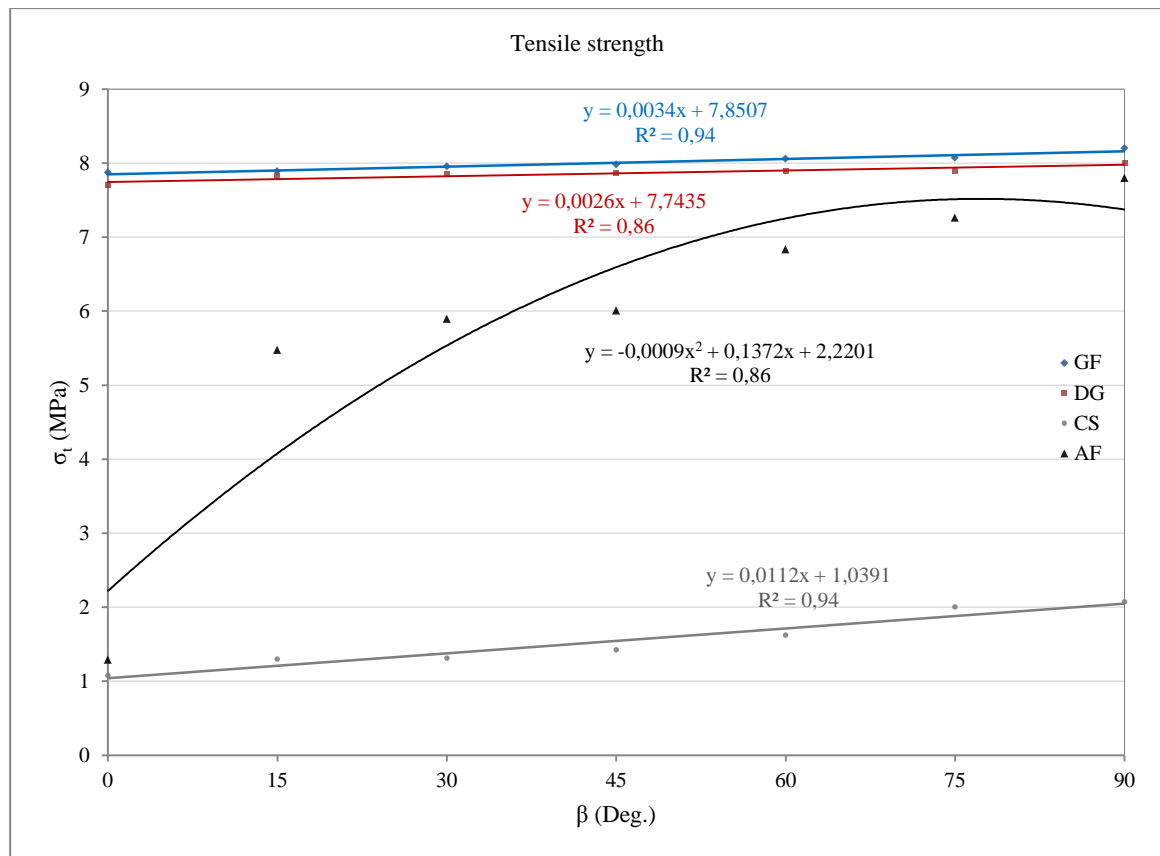


Fig. 6.28. Correlation between tensile strength (σ_t) and anisotropy angles (β) of the analyzed samples: San Giovanni in Fiore granite (GF); Grisolia stone (DG); San Lucido calcarenite (CS); Fuscaldo sandstone (AF).

Fig. 6.28 shows good linear correlations between the measured indirect tensile strength and angles of anisotropy (β). The maximum correlation coefficient has been reached by GF with 0,94 while the minimum by DG with 0,86, because for DG the obtained values for different angles are very similar, as demonstrated by the low standard deviation too. A linear relationship was obtained for GF, DG and CS while for AF a binomial-linear relationship.

Brazilian tensile strengths of anisotropic stones increase as β increases from 0° to 90° . The maximum values of σ_t was obtained for all the samples at $\beta = 90^\circ$. On the other hand, the minimum values of σ_t were obtained at $\beta = 0^\circ, 15^\circ, 30^\circ$ and 45° in different tested samples. These results match with those of Chen *et al.* (1998) and Khanlari *et al.* (2014). The BAI index values are very low and vary

between 1.0 and 5.6, for GF and AF, respectively. Low values of the BAI index indicate that the analyzed samples are isotropic except AF that shows tensile strength anisotropy.

According to the results of mechanical tests, the maximum strength values for all the samples were obtained perpendicular to the foliation planes and the internal set of microcracks and the minimum parallel to those planes, according to Khanlari *et al.* (2014).

After performing the Brazilian test, cracks in specimens tend to propagate parallel to anisotropy planes. These types of failures occurred at all anisotropy angles except specimens at $\beta = 90^\circ$. For example, Fig. 6.29, shows failure of some AF samples, where tensile anisotropy has been more evident than the other investigated lithologies (BAI = 5.6), at $\beta = 0^\circ$ (a) and at $\beta = 90^\circ$ (b).

Regarding the fracture propagation in GF, it has been observed that the initiation and the following propagation of the tensile failure happened in the weakest biotite zones. This observation is in agreement with the results of other authors studying cracks pattern in granites (Günes Yılmaz *et al.*, 2011) and with the results of numerical simulation about the influence of petrographic features on Brazilian tensile strength (Chen *et al.*, 2004).

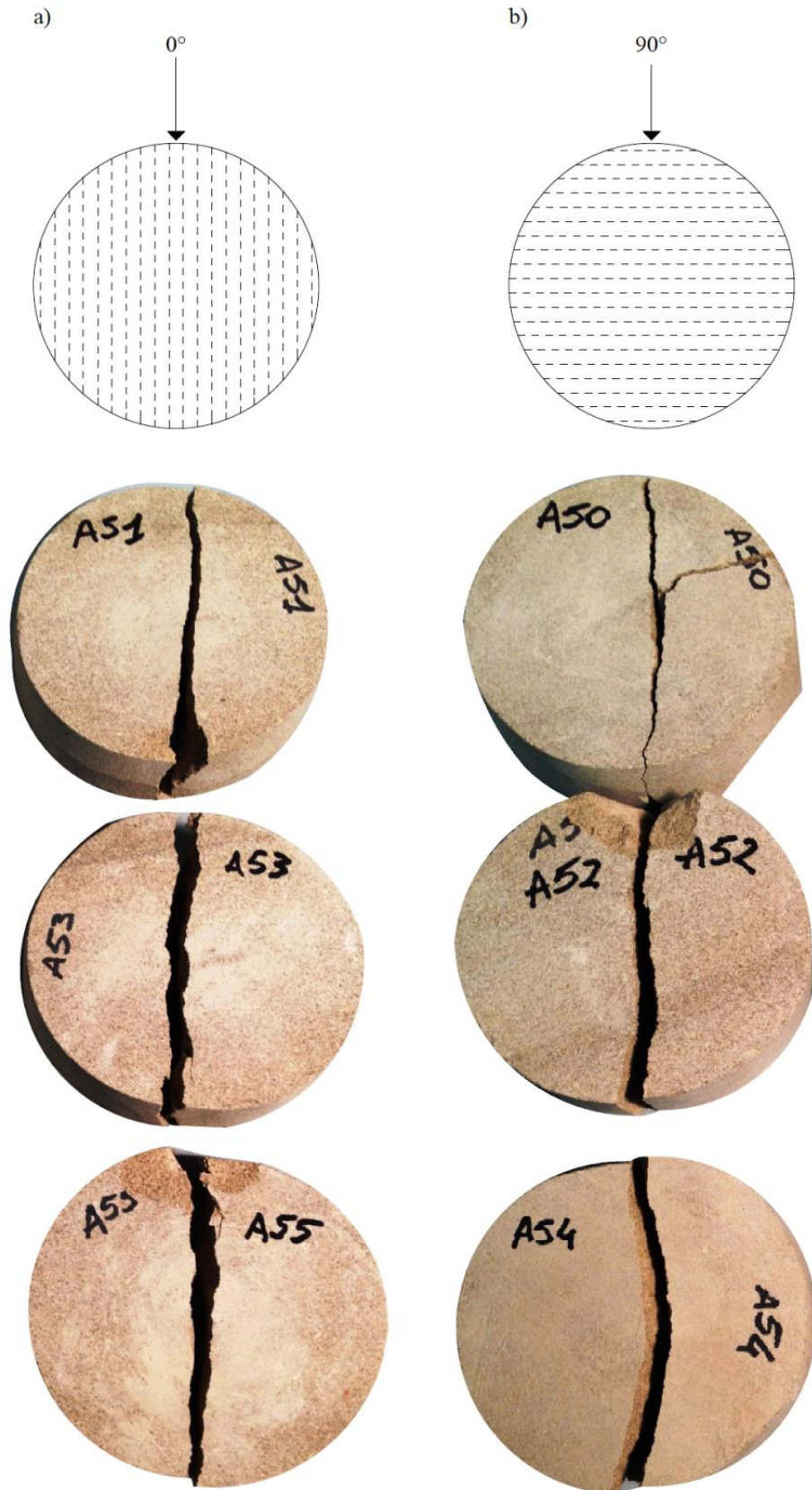


Fig. 6.29. Some AF samples' crack propagation, parallel to spatial directions at $\beta = 0^\circ$ (a) and perpendicular to the weakness planes at $\beta = 90^\circ$ (b).

6.6.7 Point Load test

The point load test is commonly used in practice because of the ease of testing, simplicity of specimen preparation and possible field application (Kahraman & Gunaydin, 2009; Khanlari *et al.*, 2014).

The obtained point load test index values ($I_{s(50)}$) are summarized in Table 6.19, together with the point load strength anisotropy index $I_{a(50)}$.

Table 6.19. Values of point load test index ($I_{s(50)}$) and the anisotropy indices ($I_{a(50)}$).

Samples	Point Load Test Index $I_{s(50)}$ (MPa)							Anisotropy
	min		inter		max		mean	$I_{a(50)}$
GF	1.55	(X)	2.05	(Y)	2.35	(Z)	2.1	1.5
<i>st. dev.</i>	0.3		0.2		0.2		0.1	
DG	0.87	(X)	1.16	(Y)	1.42	(Z)	1.2	1.6
<i>st. dev.</i>	0.2		0.2		0.2		0.2	
CS	0.56	(X)	0.76	(Y)	0.93	(Z)	0.8	1.7
<i>st. dev.</i>	0.2		0.2		0.1		0.2	
AF	0.37	(X)	0.47	(Y)	0.56	(Z)	0.5	1.5
<i>st. dev.</i>	0.1		0.1		0.1		0.1	

Foliation planes are characteristic of the stones, and it is expected that mechanical behaviors of these stones will be controlled by these planes under a certain state of stress (Khanlari *et al.*, 2014). Results show that, for all tested samples, maximum strength values have been reached along the Z direction (perpendicular to the foliation planes and the dominant set of microcracks) while, on the contrary, the minimum values have been recorded along the X-direction. As well as the UCS values, the most resistant stones under Point Load conditions, have been, in decreasing order: GF, DG, CS and AF (Table 6.19).

According to the point load strength anisotropy index, all the samples can be defined as isotropic due to the recorded values which are close to 1.0. In fact, as the strongest and weakest directions are perpendicular and parallel to planes of foliation, respectively, the point load strength anisotropy index

($I_{a(50)}$) is close to 1.0 for quasi-isotropic stones and achieve higher values for anisotropic stones (ISRM, 2007). DG and CS appeared to be the most anisotropic stones, with anisotropy index values of 1.6 and 1.7, respectively.

According to the classification of Franklin & Broch (1972), all samples belong to the category of “high strength” (Bell & Lindsay, 1999).

6.6.8 Polished Stone Value

Los Angeles and Micro-Deval

Among mechanical properties of aggregates, Los Angeles (LA) and Micro-Deval (M_{DE}) appear to play an important role in determining the aggregate Polished stone value (PSV).

Quality requirements for aggregate used for road pavements differ slightly from country to country and their values depend on the availability of raw material. For example, the concept of High Specification Aggregates in UK considers that natural or artificial coarse aggregates (P3 mm) suitable for road surfacing and surface dressing should have the following characteristics: frost resistance, polishing ($PSV \geq 58$) and resistance to fragmentation ($LA < 30$) (Thompson *et al.*, 2004; Thompson, 2008; Dokic *et al.*, 2015). According to their PSV, these stones are resistant to polishing, that makes them very usable in road pavement construction. Aggregates which exhibit a great resistance to abrasion and fragility tend to polishing.

LA coefficient is an important aggregate feature for hot asphalt mixes, because it indicates resistance to wear. The limiting value of LA abrasion coefficient is 20–25% for surface aggregates (heavy traffic roads). LA values of GF are reported in Table 6.20.

Table 6.20. Los Angeles coefficient values (LA) for the two grain size classes of San Giovanni in Fiore granite: from 8 to 11.2 mm; from 4 to 8 mm.

Grain size Φ (mm)	m_0 (g)	Passing weight at 1.6 mm (g)	Retained weight at 1.6 mm (m_{500}) (g)	LA (%)
8 - 11.2	5010	2336	2674	46.6
4 - 8	4983	2775	2208	55.7
<i>mean value</i>				51.2
<i>st. dev.</i>				6.4

M_{DE} provides better evaluation of PSV because it reflects more accurately changes of aggregates in the pavement during usage (Dokic *et al.*, 2015). M_{DE} values of GF are shown in Table 6.21 while in Table 6.22 are reported LA, M_{DE} and the correspondent PSV coefficient values (PSV values calculated from the equations reported in the Par. 5.8.8) for all the grain size classes of GF.

Table 6.21. Micro-Deval coefficient values (M_{DE}) for the three grain size classes of granite of San Giovanni in Fiore: from 8 to 11.2 mm; from 6.3 to 10mm; from 4 to 6.3 mm.

Grain size Φ (mm)	m_0 (g)	Passing weight at 1.6 mm (g)	Retained weight at 1.6 mm (m_{500}) (g)	M_{DE} (%)
8-11.2	500	84.7	415.3	16.9
6.3-10	500	111.3	388.7	22.3
4-6.3	500	150.3	349.7	30.1
<i>mean value</i>				23.1
<i>st. dev.</i>				6.6

Table 6.22. Los Angeles (LA), Micro-Deval coefficient (M_{DE}) and PSV values calculated from LA (PSV_{LA}) and from M_{DE} (PSV_{MDE}), for all the grain size classes of San Giovanni in Fiore granite.

Grain size Φ (mm)	LA (%)	PSV_{LA}	MDE (%)	PSV_{MDE}
8 – 11.2	46.6	67.7	16.9	56.9
4 - 8	55.7	71.3	/	/
6.3 - 10	/	/	22.3	59.2
4 – 6.3	/	/	30.1	62.6
<i>mean value</i>	51.2	69.5	23.1	59.6
<i>st. dev.</i>	6.4	2.5	6.6	2.9

PSV mean value for GF, obtained from the mean values of PSV_{LA} and PSV_{MDE} is 63.5.

To critically analyze the results of this study, the following limited values have been adopted: M_{DE} ranging 15–25% (Jacobs Engineering, 2009; Dokic *et al.*, 2015), LA ranging 20–25% and $PSV \geq 58$ (Thompson *et al.*, 2004).

According to the values reported in Table 6.22 and to the above considered limits, it can be said that GF has not good mechanical properties as aggregate. In fact, LA does not respect the engineering limit, even though the abrasion resistance of stone is not a decisive factor that controls the degree of resistance to polishing (Dokic *et al.*, 2015). M_{DE} and PSV values are slightly higher than the considered limits.

7. Discussion and summary of stone properties

The variation of physical and mechanical properties of a stone is very important to establish criteria for its use. Data analysis of the results obtained through the performed tests, give the possibility of: obtaining many correlations among petrophysical properties and stone fabrics or mechanical characteristics; evaluating stone behavior; estimating stone durability; defining use suggestions. The relationship between the analyzed properties can be established by the correlation coefficient (R). The best-fit curves is obtained by the least-squares method and the fitting quality is given by the determination coefficient (R^2). This value, ranging from 0 to 1, must be high if the curve is to be representative of the relationship between variables (Davis, 1986; Sousa *et al.*, 2005). For this study the correlation values have been defined as: statistically significant if $R^2 > 0.8$; approximately useful for the evaluation if $0.7 < R^2 < 0.8$; not considered if $R^2 < 0.7$.

Mineralogical, chemical and petrographic correlation

Table 6.1 shows the mineralogical composition as determined by XRD for each investigated stone. In San Giovanni in Fiore granite (GF) samples, quartz is the main mineral phase, while feldspar and biotite have been recognized in smaller quantities. Other identified phase was chlorite. In the case of Grisolia stone (DG) and San Lucido calcarenite (CS), calcite is the foremost mineral phase. Dolomite was identified in CS while was observed in very low quantities or in traces in DG. Moreover in CS has been detected the presence of a small amount of quartz. Regarding Fuscaldo sandstone (AF) calcite was the prevalent mineral phase followed by, in decreasing order, calcite, feldspar, biotite and chlorite.

As regards the clay fraction (Table 6.1), the most abundant mineral phase in GF and AF is chlorite. The possible presence of clay minerals could have important implications for the durability of stones (Molina *et al.*, 2015).

The analysis of the chemical composition via XRF ([Table 6.2](#)) corroborated the findings for mineralogical composition, such that for GF higher values in the elements related with silicates (above all quartz and feldspars) such as Si, Al and K have been obtained. Fe is also present and the low contents of Ca and Mg values are due to the presence of calcite and dolomite. In DG and CS, the most notable element is calcium from the calcite. In AF the most important elements are calcium followed by silicates (Si, Al and K). Mg has been detected in very low amounts; in CS has been registered the highest value while in DG the lowest value, even though DG is also commercially known as “dolostone”.

Petrographically, DG and CS are the materials with the most homogenous composition and texture. They are compact and petrographically isotropic. In fact, analyzing the oriented thin sections along the three directions, have detected no preferential orientation. This is in agreement with the other tests performed where the correspondent anisotropy indexes are very low (*e.g.* [Tables 6.8, 6.12, 6.13, 6.14, 6.15](#)).

The petrographic analysis of GF samples is in accordance with studied granites belonging to the same study area (Le Pera & Sorriso-Valvo, [2000](#); Scarciglia et al., [2012](#)). In fact, some granites from which the boulders are shaped are a massive, medium-grained equigranular-textured stone consisting mainly of quartz, K-feldspar, plagioclase, and, with a fairly constant 30% biotite content, as observed in the analyzed thin sections. Petrographically, GF has a variable composition between granites and granodiorites (Messina *et al.*, [1991a](#)). Even though GF samples look fresh with the naked eye, it presented alteration forms under the optical microscope. According to Le Pera & Sorriso-Valvo ([2000](#)) it was detected that quartz was unaffected by chemical alteration, although some intracrystalline microcracks appeared. It was found that the plagioclase has a low level of sericitization, the biotite is

slightly chloritized. This is one reason why the porosity is as quite high as 1.3%, if compared to other granites (Takemura *et al.*, 2003).

According to the micromosaic (Fig. 6.0 e), it is possible to individuate at least two sets of microcracks whose relative timing can be assessed by crosscutting relationships (Hooker *et al.*, 2014). The more recent microcracks cut the older ones. Summarizing, the intracrystalline microcracks detected in the XZ (grain direction) and YZ (hardway direction) planes correspond to the decompression microcracks, while the other microcracks, with a no prevalent direction and individuated in the XY plane (rift direction), are related to tectonic forces. The correspondence between microcracks and splitting planes results is in agreement with other authors that studied similar granites (*e.g.* “Barre granite”, Dai *et al.*, 2013). Since the Late Miocene, the basement stones of Sila Massif experienced intense weathering processes resulting in weathered landforms and deep weathering profiles, responsible for the intra- and intercrystalline microcracks detected through the petrographic analyses performed on San Giovanni in Fiore granite samples by Borrelli *et al.* (2015) and Perri *et al.* (2015).

CS and AF also showed big amounts of fossils and it is possible to distinguish pores. In the case of GF and DG the pores are difficult to distinguish since they are small (between 0,1 and 10 μm) and few in number. This is in agreement with the porosimetric analysis (Table 6.7).

Regarding the anisotropy, in contrast to DG and CS, GF and AF showed internal orientations. In the case of GF the anisotropy is related to the presence of internal sets of microcracks with prevalent directions along the X axis. The presence of microcracks is higher along the XY plane and without a prevalent direction. It is possible to individuate three sets of microcracks whose relative timing can be assessed by crosscutting relationships (Hooker *et al.*, 2014). The more recent microcracks cut the older ones. The oldest microcracks could be related to the intense mechanical and chemical weathering in Sila Massif, as investigated by many authors (Le Pera & Sorriso-Valvo, 2000; Borrelli *et al.*, 2015; Perri

et al., 2015). In fact, since the Late Miocene, the basement stones of Sila Massif experienced intense weathering processes resulting in weathered landforms and deep weathering profiles, responsible of the intra- and intercrystalline microcracks detected by the petrographic analysis performed on San Giovanni in Fiore granite samples by Borrelli *et al.* (2015). The oldest microcracks, individuated in this study, have been marked with green vertical lines and correspond to the rift plane. In other words, the rift plane (XY plane), is the plane where there is the highest number of intracrystalline microcracks representing the majority of all microcracks observed. The highest amount of microcracks has been registered for K-feldspar minerals. This is in agreement with the fact that feldspars are the minerals most vulnerable to decay processes (Freire-Lista *et al.*, 2015). The obtained mean value of LMD for GF, equal to 1.0, corresponds to the class of “sound granites” (Sousa *et al.*, 2005). Summarizing, the rift plane (XY, the plane normal to Z-direction) is the plane with the dominant microcracks set and with the more recent set of microcracks; the grain plane (XZ, the plane normal to Y-direction) is the plane with the secondary concentration of microcracks while the hard-way plane (YZ, the plane normal to X axis) has the least concentration of microcracks. This correspondence between microcracks and splitting planes result is in agreement with other authors that studied similar granites (*e.g.* “Barre granite”, Dai *et al.*, 2013). In the case of AF the anisotropy is due to the preferred orientation of phyllosilicates. Along the X-direction phyllosilicates are parallel while, on the contrary, along the Z-direction they have no preferred orientation.

Pore system and correlation between porosity and mechanical properties

Concerning the porosity distribution, in a combined view of Fig. 6.7 and the porosity values distributed in ranges in Table 6.7, GF and DG show a unimodal distribution while AF and CS a trimodal distribution with higher microporosity. AF and CS also show pores in the range 0.01 - 10 μm that may be a risk in terms of durability, due to the fact that salt crystallization or freeze-thaw processes cause

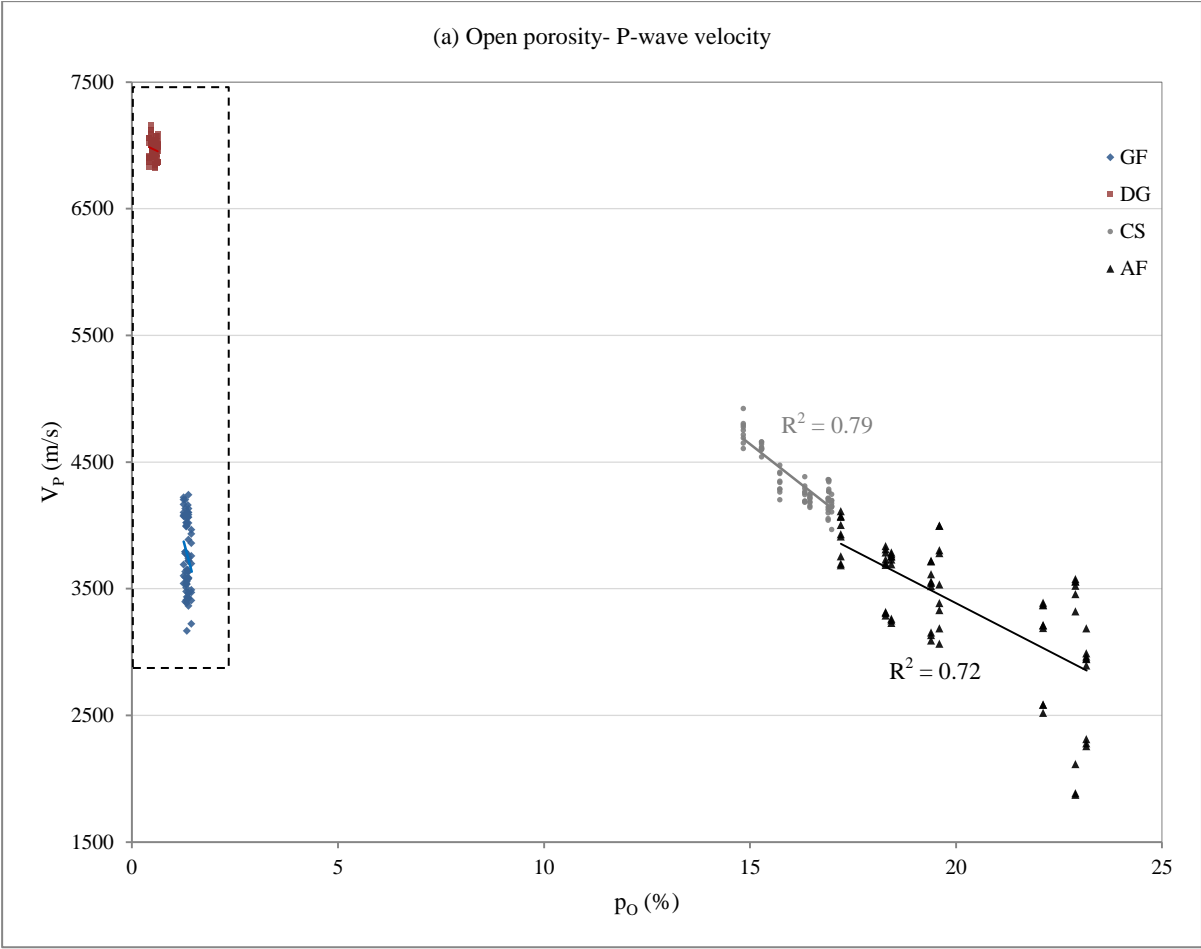
most damage in this pore range (Rodriguez-Navarro & Doehne, 1999). In the case of CS, the distribution is more heterogeneous, with 31% of macropores ($> 5\mu\text{m}$) and 69% of micropores, which means that the possible damage due to salt crystallization or freeze-thaw is undoubtedly much lower than in AF (Molina *et al.*, 2015). In addition, these values of microporosity are percentages of the porosity of the stone and the open porosity is lower in CS than in AF. These results have been confirmed by the salt crystallization test performed on 8 samples for each stone, as better described in Chapter 8. In the case of CS only 1 sample broke (Table 8.3) while, on the contrary, 6 specimens of AF broke (Table 8.4).

The highest apparent density values (ρ_b) were measured in GF and DG (Table 6.5). These values are in agreement with the fact that for the dominant phases in both stones, quartz in GF and calcite in DG, the apparent density value corresponds to the theoretical value ($2.65 \text{ g}\times\text{cm}^3$ for quartz and $2.71 \text{ g}\times\text{cm}^3$ for calcite). In the case of CS and AF, the measured apparent density values are a long way from the theoretical values of their dominant phases, as they are influenced by the other secondary phases. This difference is greater in AF as it is more porous than CS. In agreement with the porosity values there is also the compactness index that reached the highest values in GF and DG (approximately 0.99%), while the lowest in CS followed by AF. Air permeability values also confirms that AF and CS are the most porous lithotypes, even though this technique refers to other range of pores with respect to MIP or the other techniques related to porosity performed in this study.

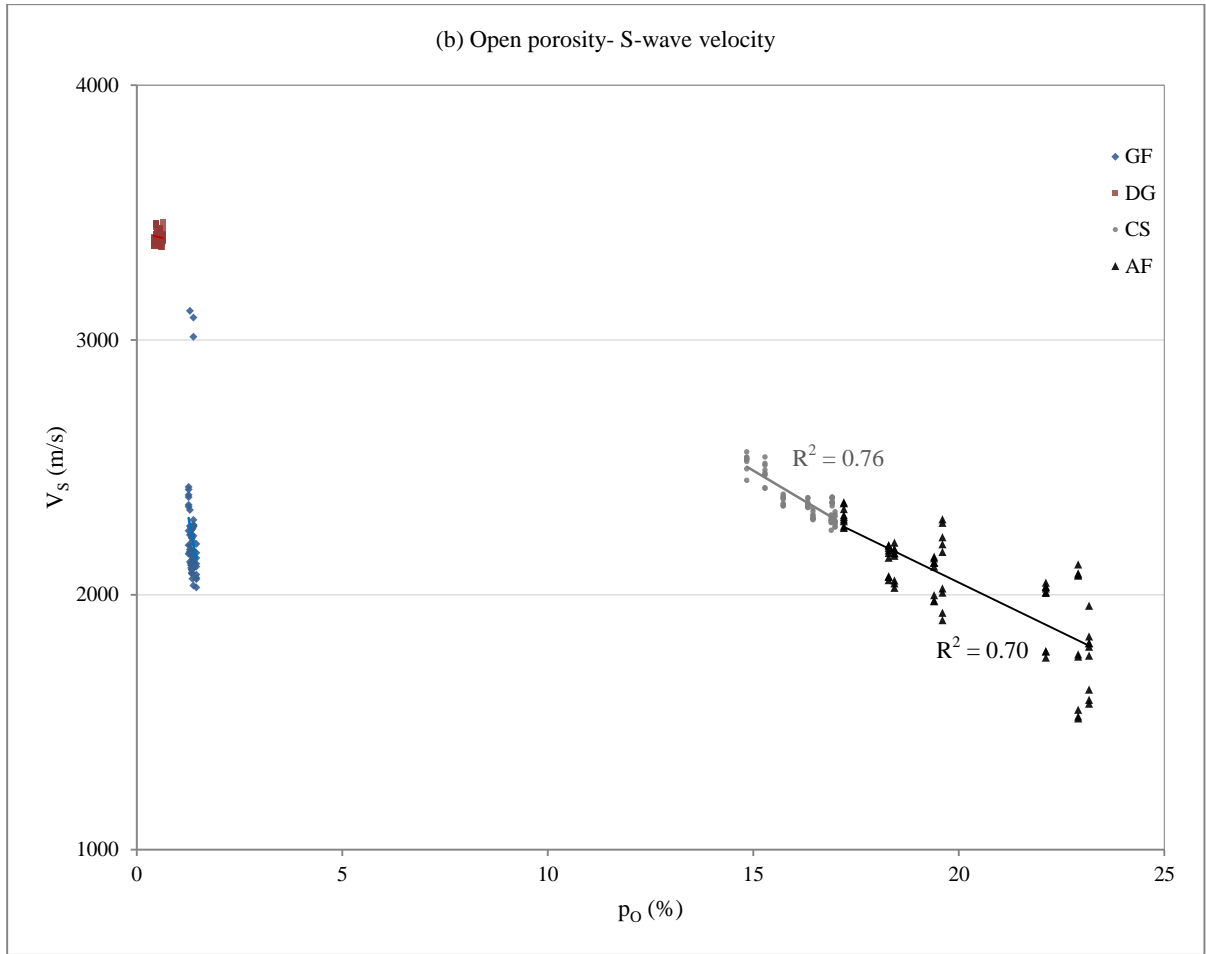
Regarding the correlation between porosity and ultrasound velocities (P and S waves), shown in Figs. 7.1 a, b, c, d, it can be said that there is a good correlation between the above mentioned properties for CS and AF, with correlation values for the P-waves of 0.79 and 0.72 and for the S-waves of 0.76 and 0.70, respectively for CS and AF. This means that there is an inverse relationship between porosity and ultrasound velocities for CS and AF. The lower porosity values, the higher the ultrasound propagation:

in the case of GF and DG, their low porosity values (instead of high porosity values like CS and AF) do not affect the ultrasound propagation velocity, as demonstrated by the very low values of correlation, considered as statistically insignificant. The non-linear relationship is in agreement with other authors, in particular for plutonic stones as GF and carbonate stones as DG, with low open porosity values (<2%) there is no significant correlation between porosity and ultrasound velocities (Siegesmund & Dürrast, 2014). Even though there isn't any linear correlation, it is possible to say that exists an inverse relationship between UPV and porosity, as has also been previously proved by several authors in different lithological types (Jermy & Bell, 1998; Sousa *et al.*, 2005). As porosity increases, ultrasonic velocity decreases; however, stones with the same porosity but with persistent network of microcracks like GF, present a lower propagation velocity. So, both pores and microcracks affect the ultrasound propagation velocity (Kelsall *et al.*, 1986; Sousa *et al.*, 2005).

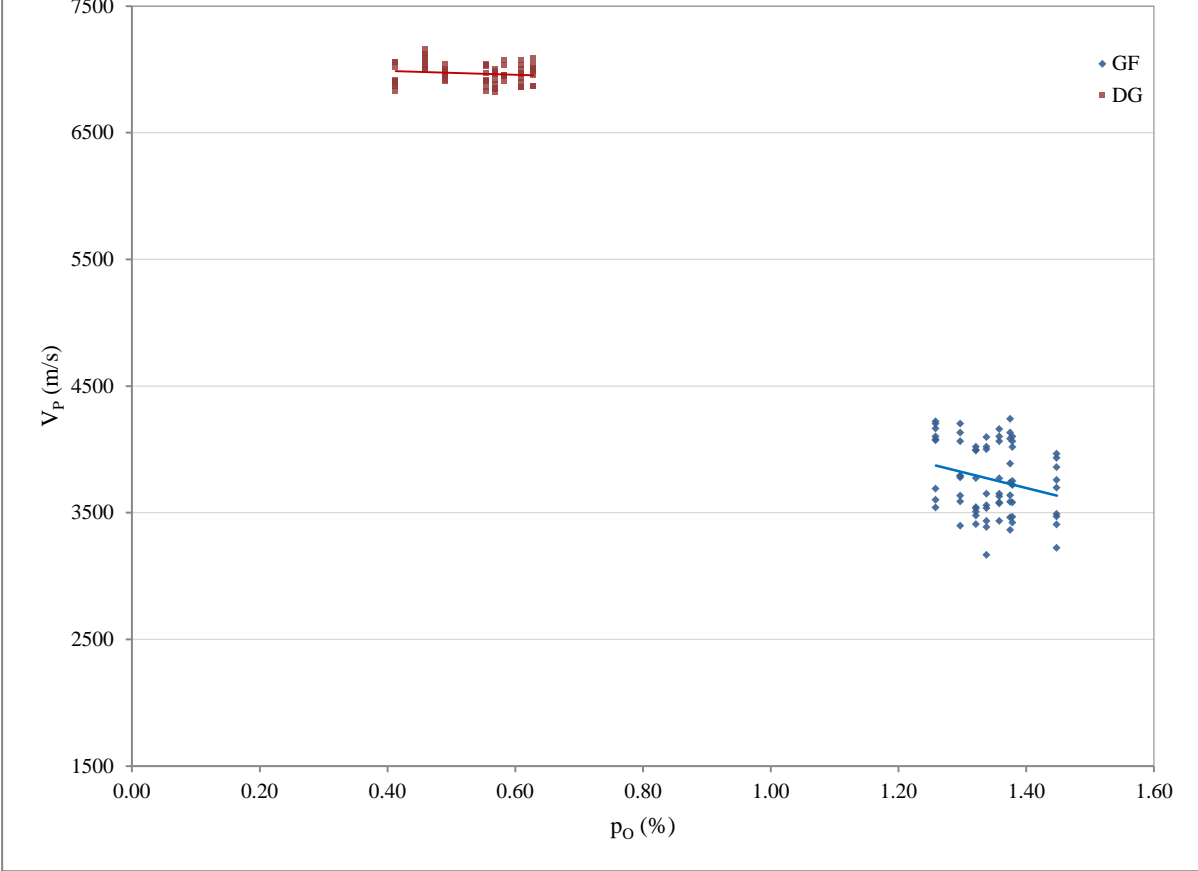
Furthermore, analyzing Figs. 7.1 a, b, c, d, it can be said that DG, in terms of V_p and open porosity, is the most homogeneous material while AF is the most heterogeneous.

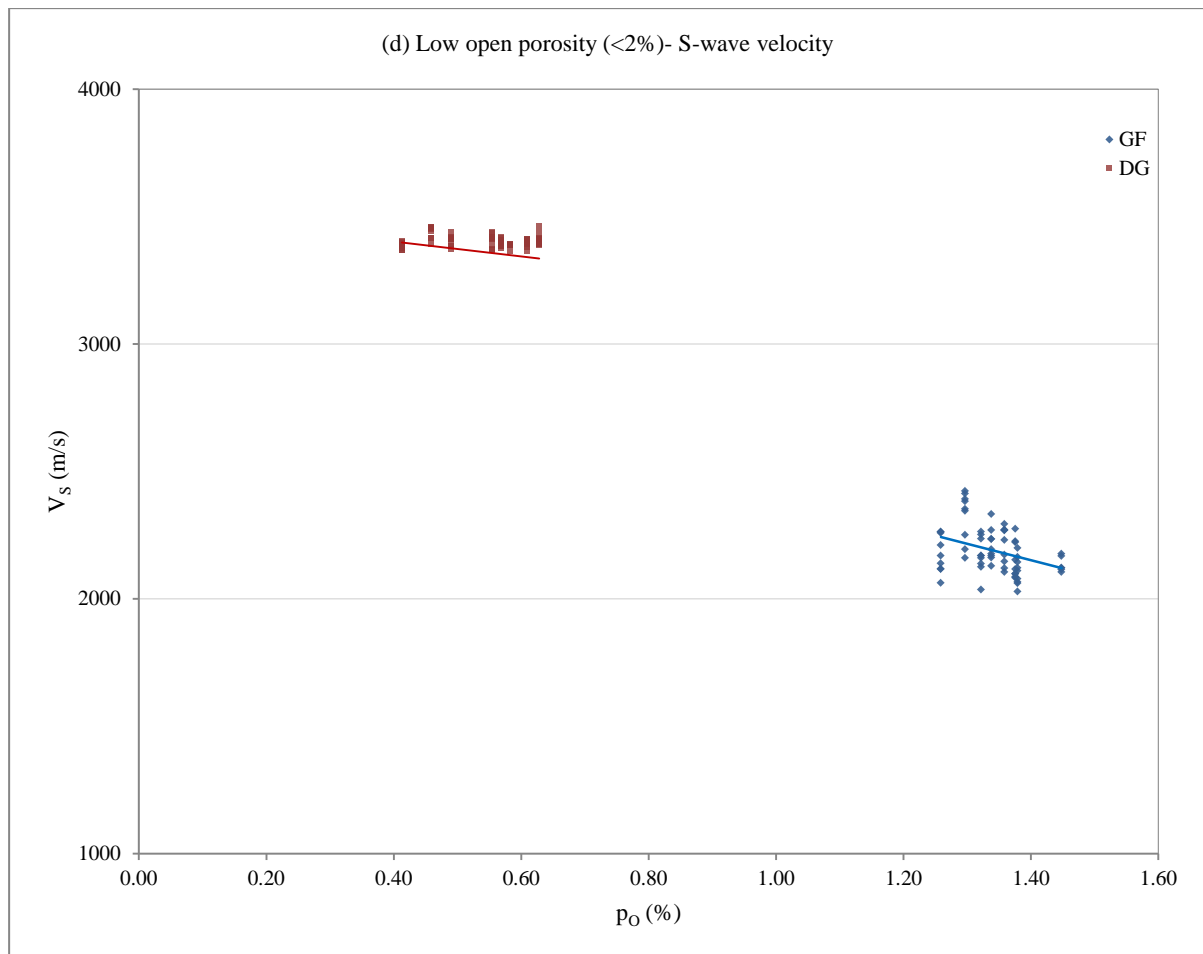


(b) Open porosity- S-wave velocity



(c) Low open porosity (<2%) - P-wave velocity



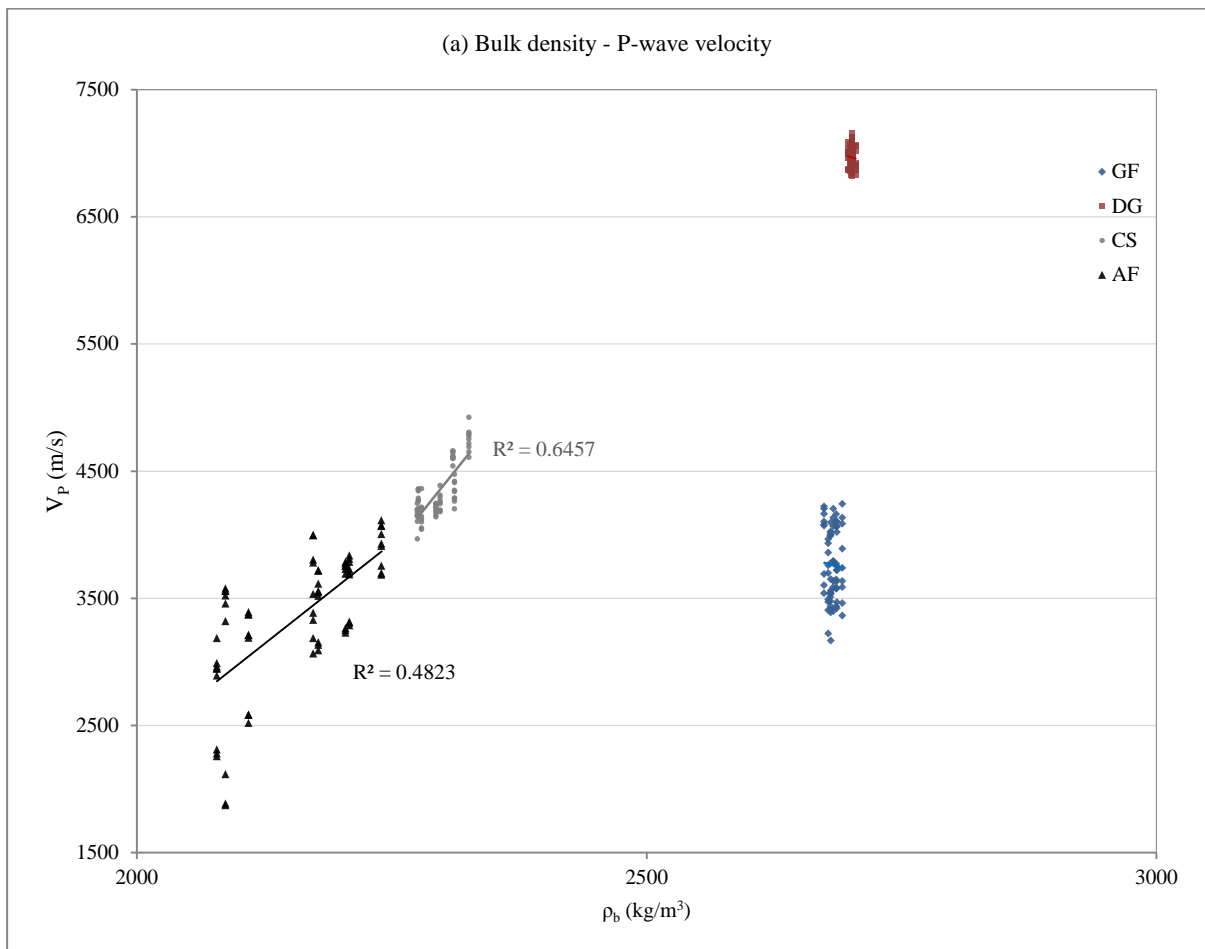


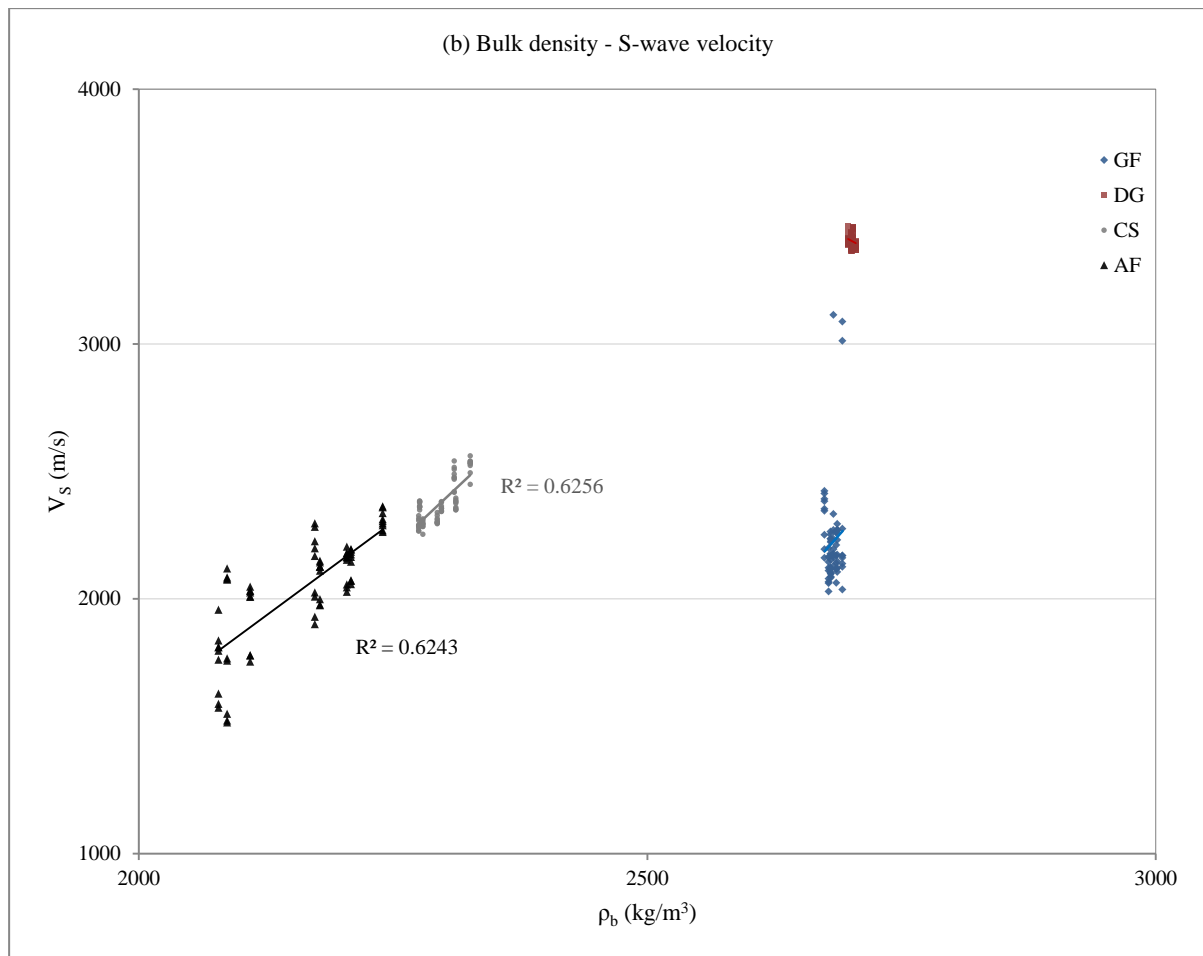
Figs. 7.1 a, b, c, d. Diagrams showing the relationship, for all investigated samples, between open porosity and: P-waves velocities (a, c); S-waves velocities (b, d).

Concerning the relationship between bulk density and ultrasonic velocities, correlation values lower than for the porosity have been obtained. As reported in Fig. 7.1, a linear relationship has been obtained only for CS and AF, while for GF and DG any significant relationship has been defined, as reported in Figs. 7.2 a, b. Velocity–density relations for plutonic, volcanic, and quasi-isotropic metamorphic stones were reported by Gebrande (1982), based on a quite larger data set, obtaining clear correlations for that lithotypes. The direct correlation between average V_p and average density is based on the assumption that, for most stones, a variation in the mineralogical composition has an effect on both parameters in the same way (Simmons, 1964). In this study the empirical equation obtained for plutonic stones by Gebrande (1982; Siegesmund & Dürrast, 2014) has been applied:

$$V_{P_{estim}} = (-6.73 + 4.36\rho_b \pm 0.03)km/s$$

Considering the mean value of the bulk density for GF ($\rho_b=2.68\pm 0.01 \text{ g/cm}^3$), the estimate ultrasonic P-wave velocity is $V_{P_{estim}}=5.33 \text{ km/s}$ that is considerably higher than the measured mean value of $V_p=3.80 \text{ km/s}$ ($3.804\pm 258 \text{ m/s}$). This remarkable difference between the two values could be due to the presence of microcracks. As mathematically demonstrated, the estimate value does not correspond to the measured value by means of the ultrasonic test. This also confirms the absence of a linear velocity-density relation for GF (Fig. 7.2 a).

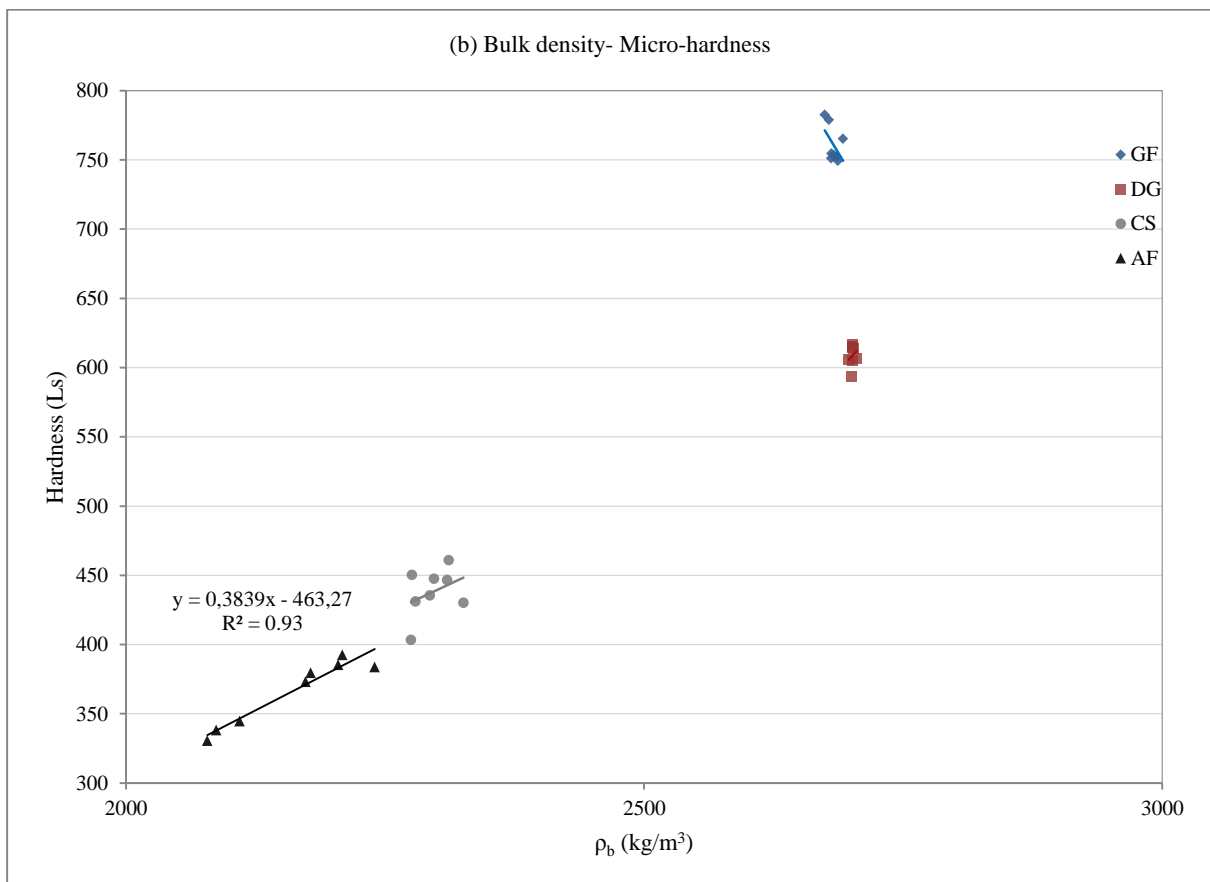
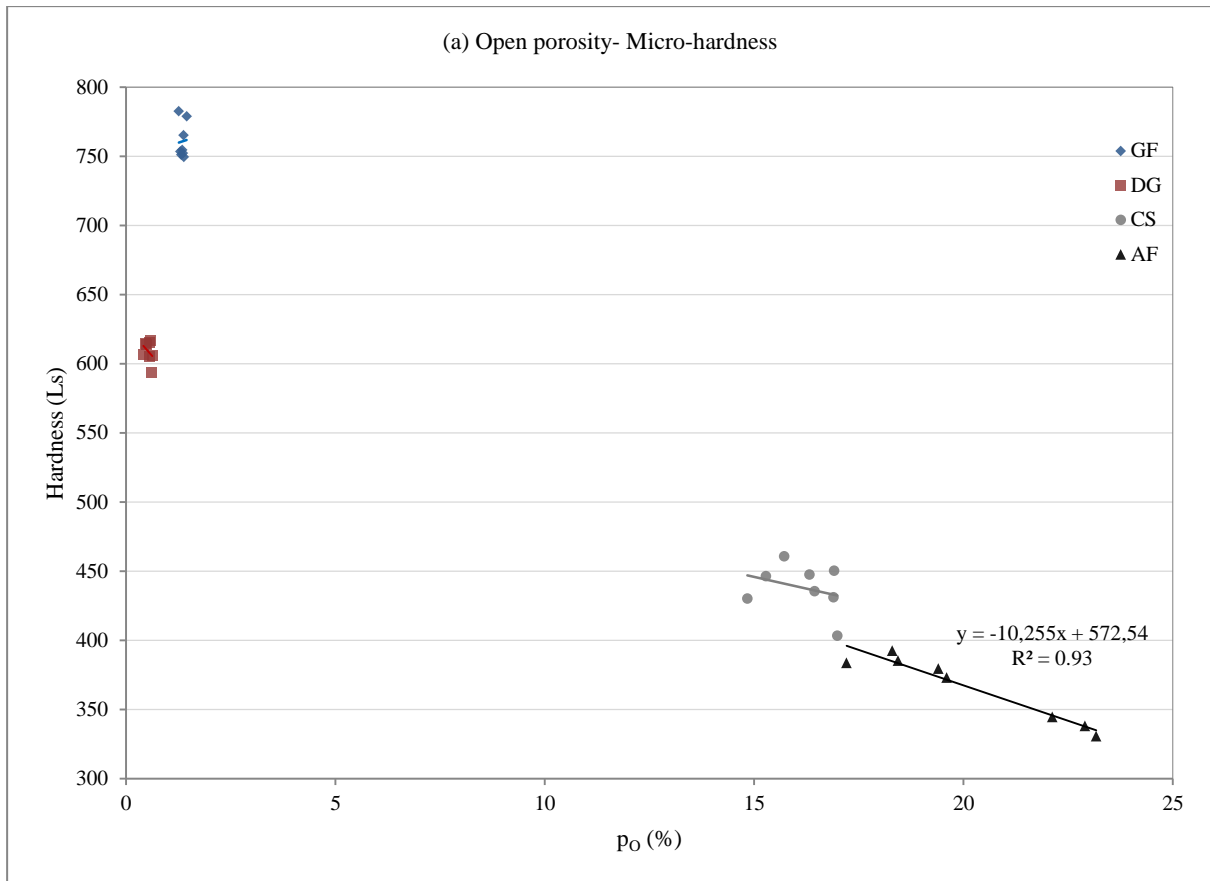




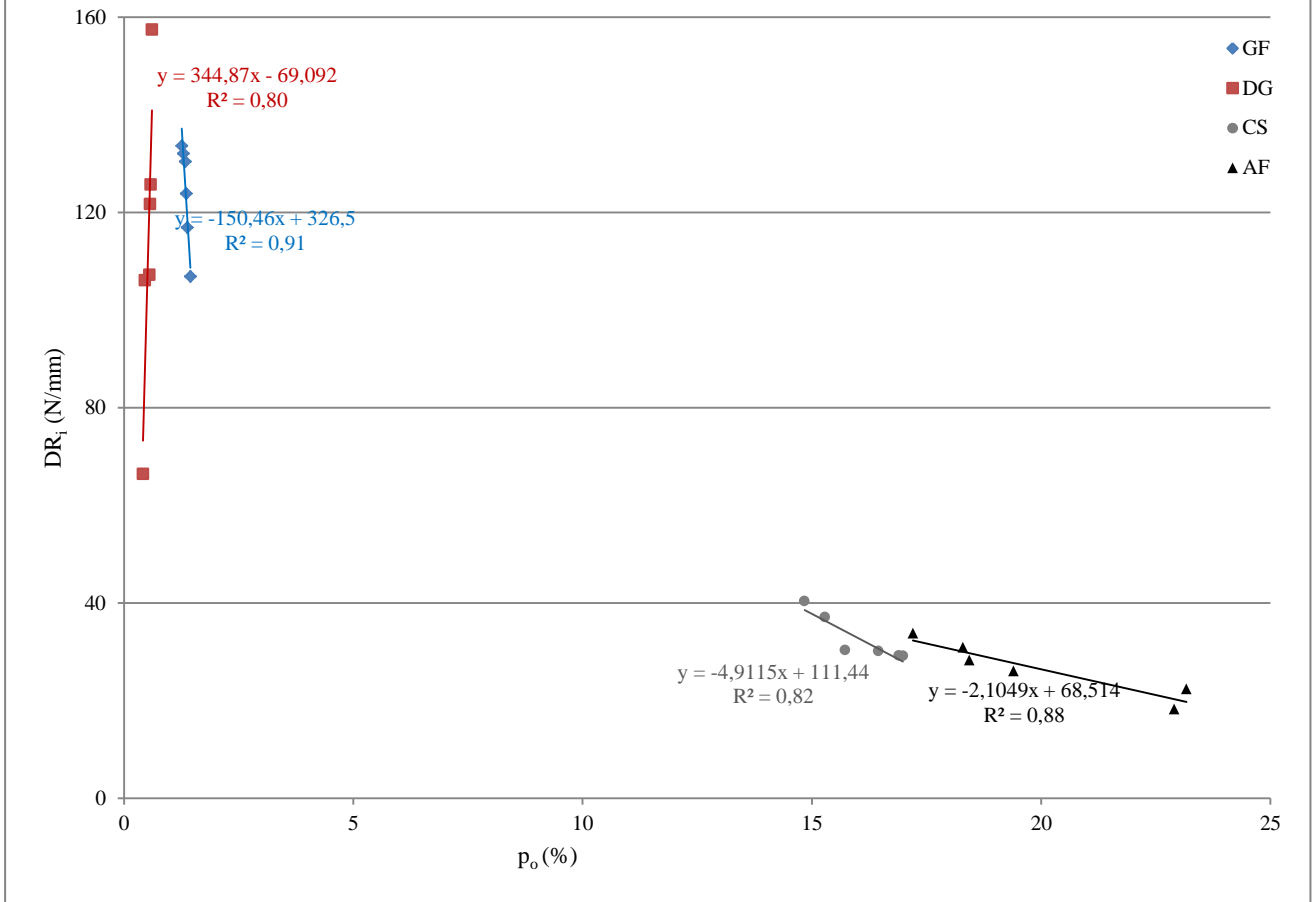
Figs. 7.2 a, b. Diagrams showing the relationship, for all investigated samples, between bulk density and: P-waves velocities (a); S-waves velocities (b).

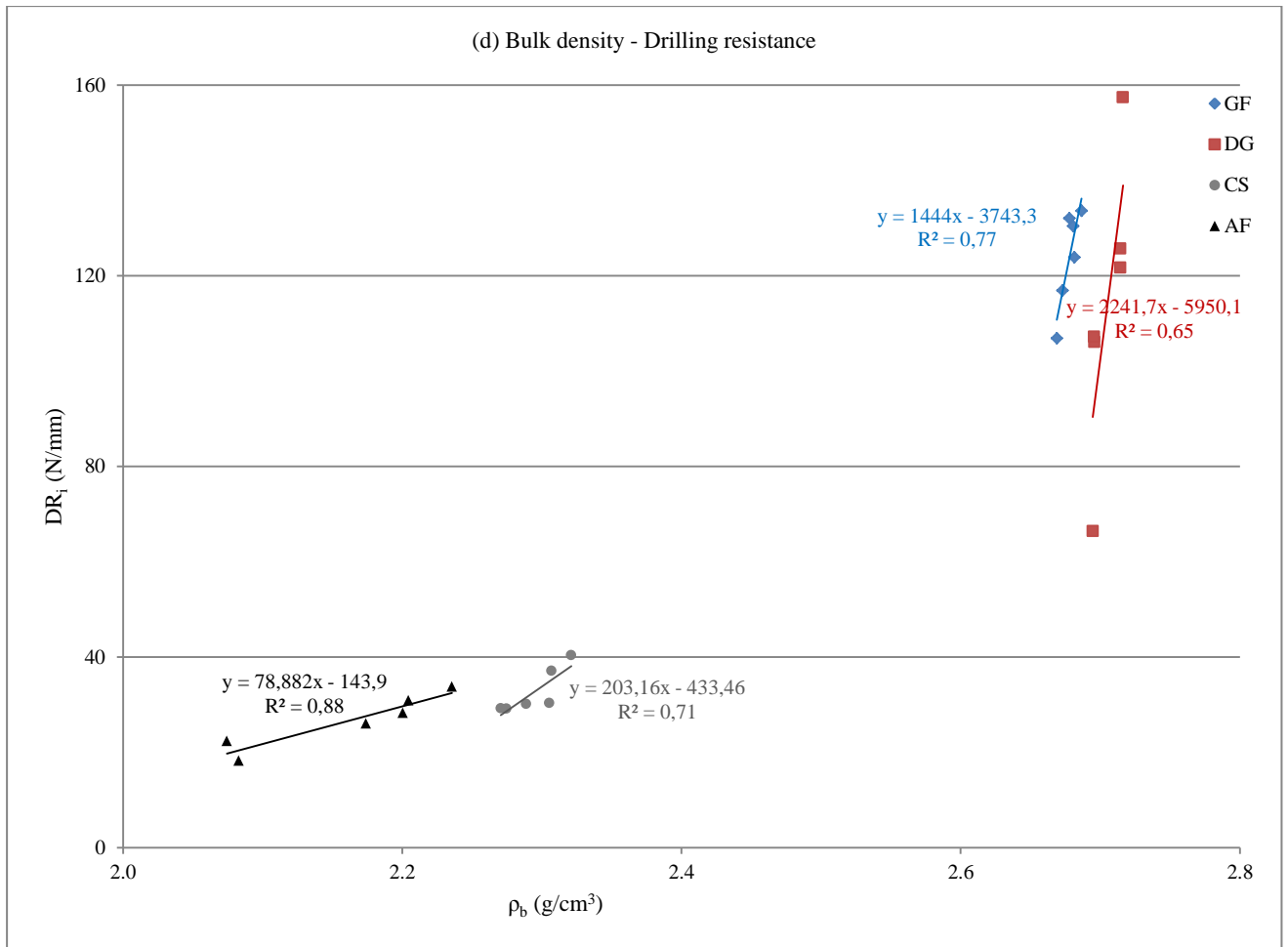
The relationships between porosity and bulk density with micro-hardness and drilling resistance, are reported in Figs.7.3 a, b, c, d. It is well established that two intrinsic stone properties, namely, *density*, representing the unit weight per unit volume of a stone including the inherent pores (voids) and *open porosity*, influence the strength and deformability of stone materials (Günes Yılmaz, 2013). The strength and deformability of stone materials generally increase with increasing density, whereas the reverse is observed with porosity. In rebound testing, the pores present in a stone material cause dissipation of energy during impact and affect the height of rebound (Aoki & Matsukura, 2008). From previous studies, it is also known that the hardness values obtained by using different rebound testing instruments (*i.e.* Schmidt hammer, Equotip) are sensitive to the variations in these two intrinsic stone

properties (Cargill & Shakoor, 1990; Aoki & Matsukura, 2008; Günes Yılmaz, 2013). Thus, in this section of the present study, it was attempted to include the possible effects of these intrinsic stone properties on the correlations established between each considered testing procedure and the properties of density and porosity. As seen in Fig. 7.3 b, combination of micro-hardness values with bulk density gives significant correlation only for AF while, as shown in Fig. 7.3 d, combination between bulk density and drilling resistance presents good correlations for all investigated materials, with the highest correlation value for AF. Similar considerations can be made about the relationship between open porosity and hardness (Figs. 7.3 a, c). This difference among correlation values for distinct materials, between the two testing procedures and the properties of bulk density and porosity, can be related to the different testing methods. In fact, in the case of micro-hardness, hardness values refer to the superficial layer of the tested material. On the other hand, for drilling test, the testing machine reaches higher depths. So, micro-hardness in the case of materials with very low porosity is not affected by porosity and apparent density due to the limited tested surface. On the contrary for materials with high porosity ($p_o > 20\%$) like AF, micro-hardness is influenced by the void space (and roughness) as well as is affected the drilling resistance.



(c) Open porosity - Drilling resistance

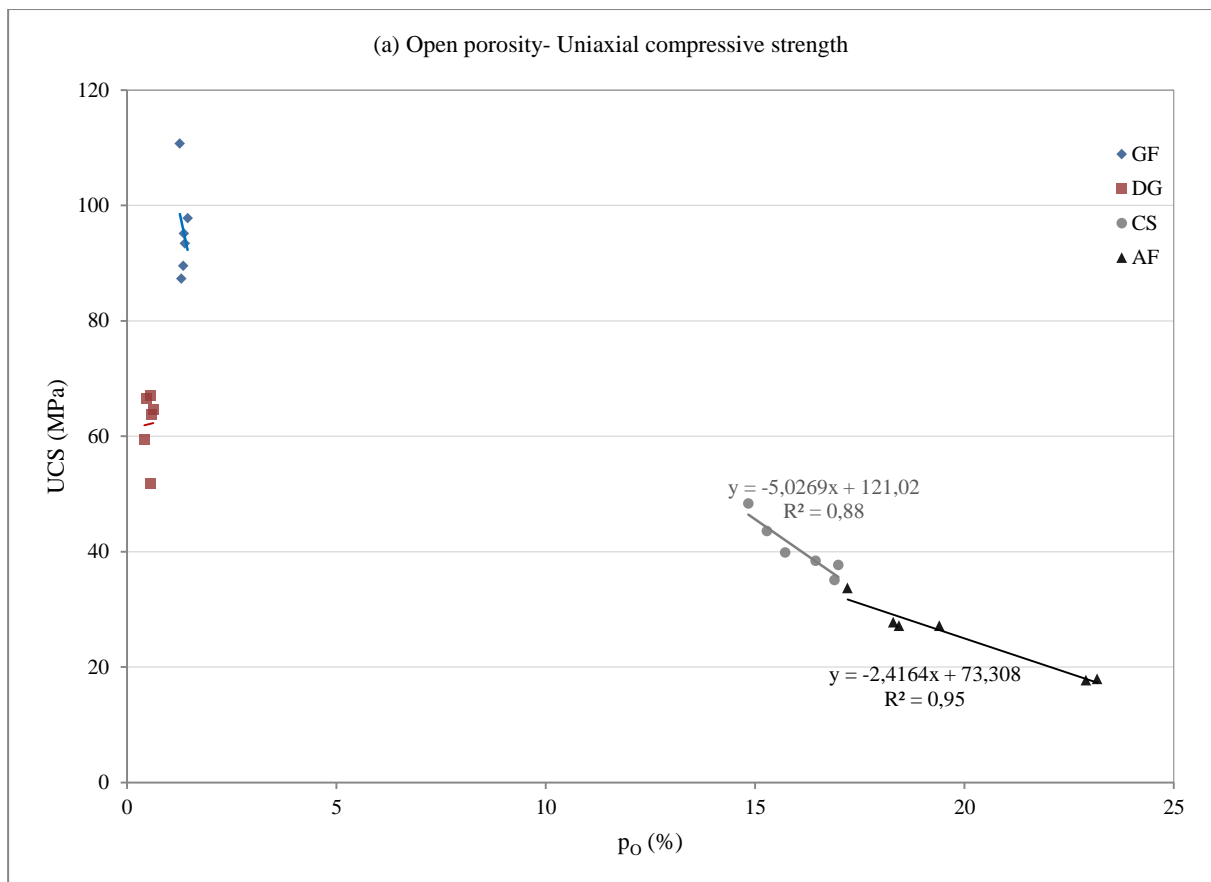


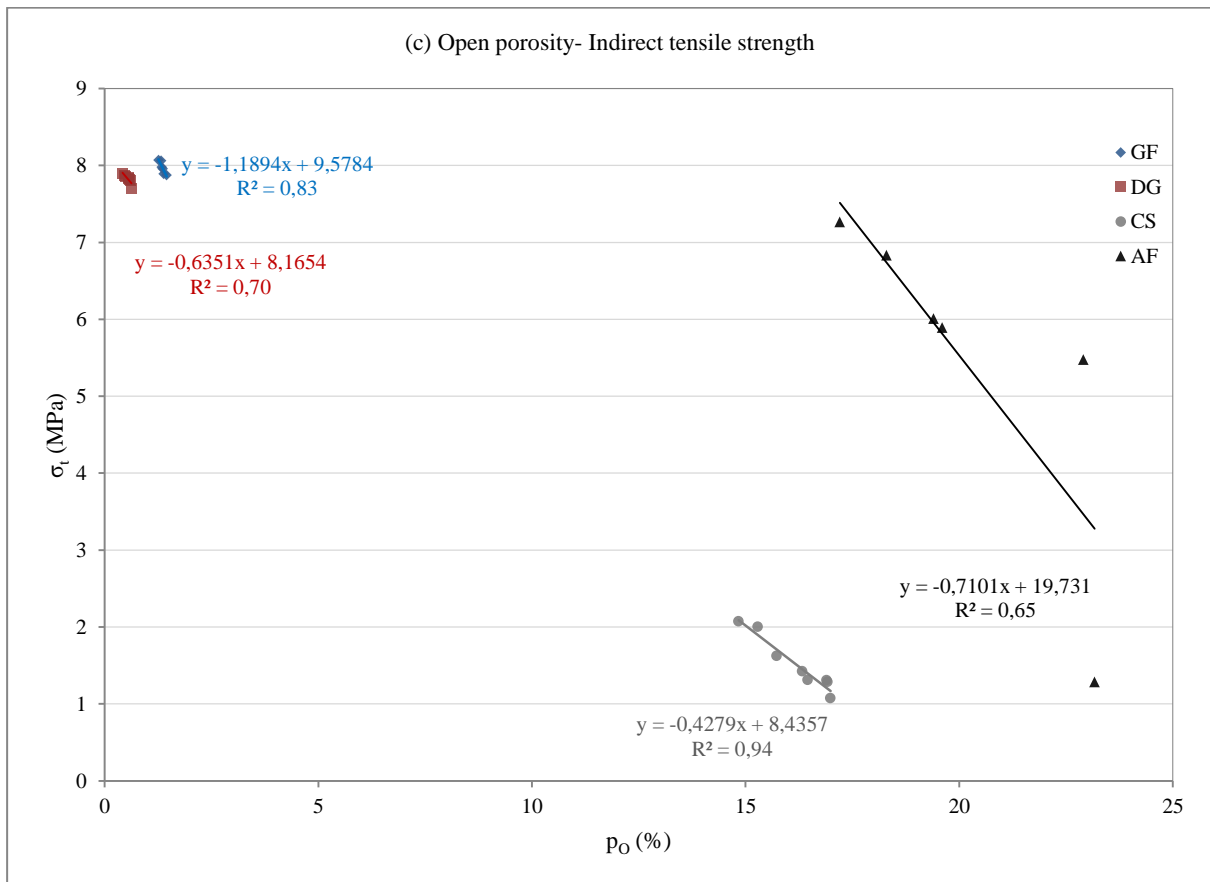
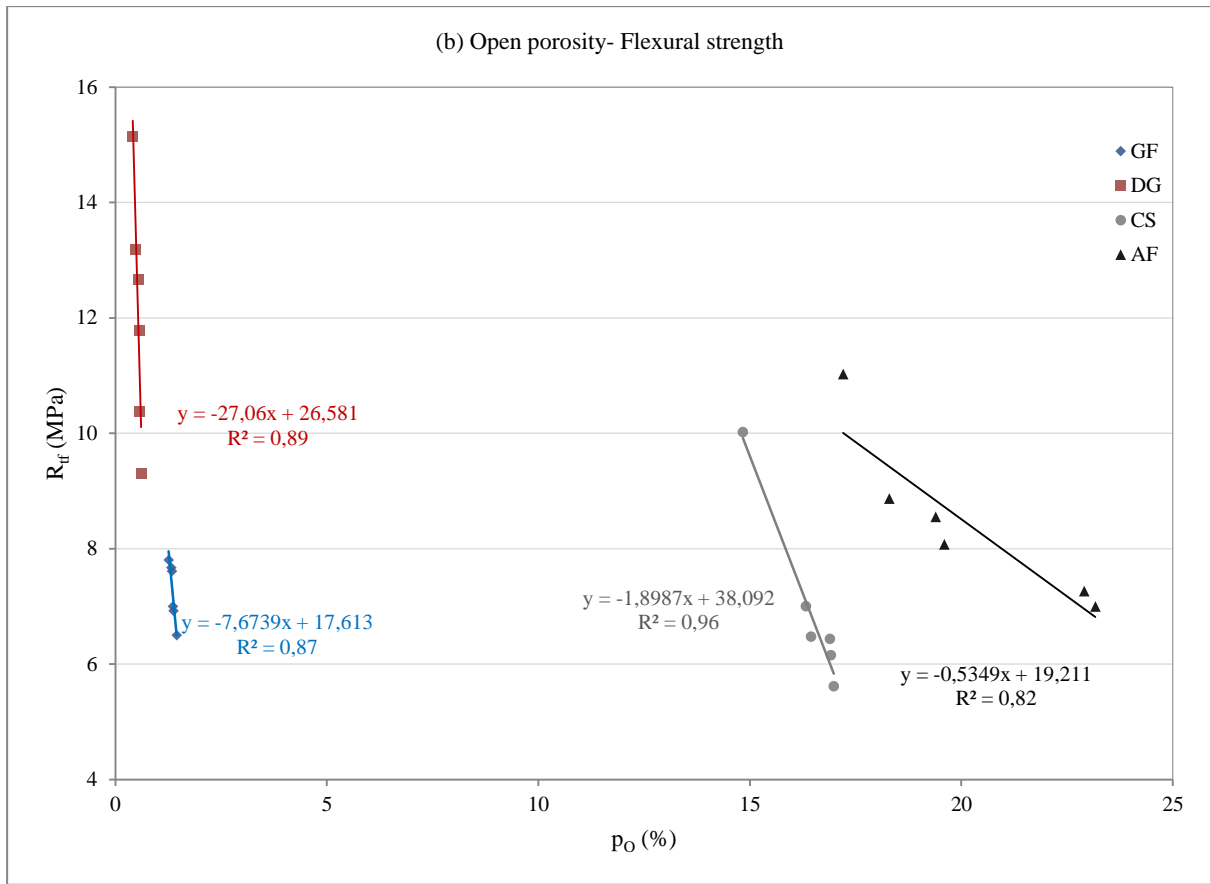


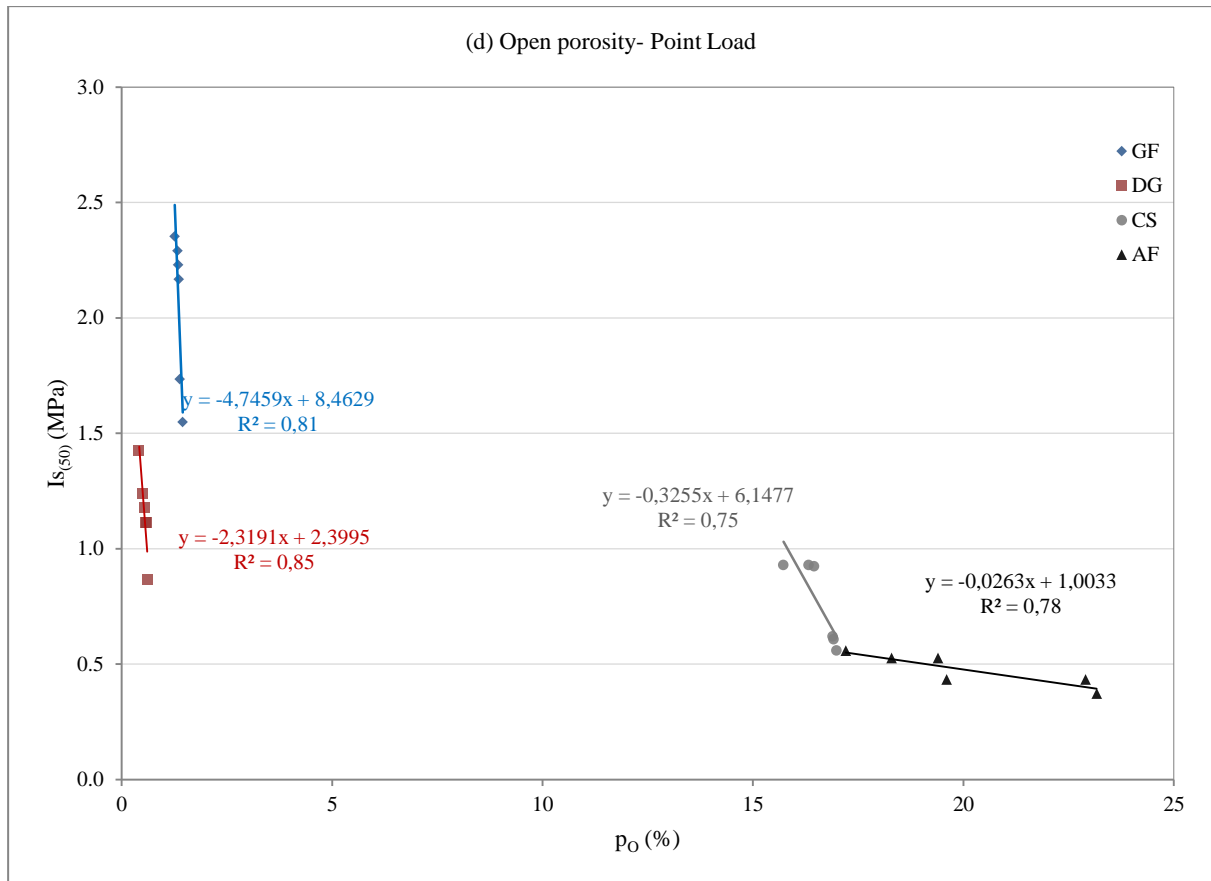
Figs. 7.3 a, b, c, d. Diagrams showing the relationship, for all investigated samples, between: open porosity and micro-hardness (a); bulk density and micro-hardness (b); open porosity and drilling resistance (c); bulk density and drilling resistance (d).

The relationships between porosity and mechanical properties (UCS , R_{tf} , σ_t , $Is_{(50)}$) are reported in [Figs. 7.4 a, b, c, d](#). Good correlations have been obtained for AF and for CS for all the investigated properties. This indicates that the lower the open porosity, the higher the strength values. So, when comparing some of the results of measured mechanical properties, it is possible first to conclude that uniaxial compressive and the other strength properties decrease as the porosity increases, as previously stated by several authors (Tuğrul & Zarif, 1999; Sousa *et al.*, 2005). In the case of materials with very low porosity as GF and DG, according to [Fig. 7.4 a](#), there isn't any linear relationship between porosity and UCS, even though as porosity increases the uniaxial strength decreases but without a linear

correlation. This result is in contrast with results of other researchers investigating similar lithotypes as granitic stones (*e.g.* Sousa *et al.*, 2005) or other lithotypes (Bell & Lindsay, 1999), but is in agreement with other researchers (*e.g.* Prikryl, 2001) who found that other factors like the variable grain size, and not the porosity, seem to be the main causes of the variability of uniaxial compressive strengths of low porosity stones.



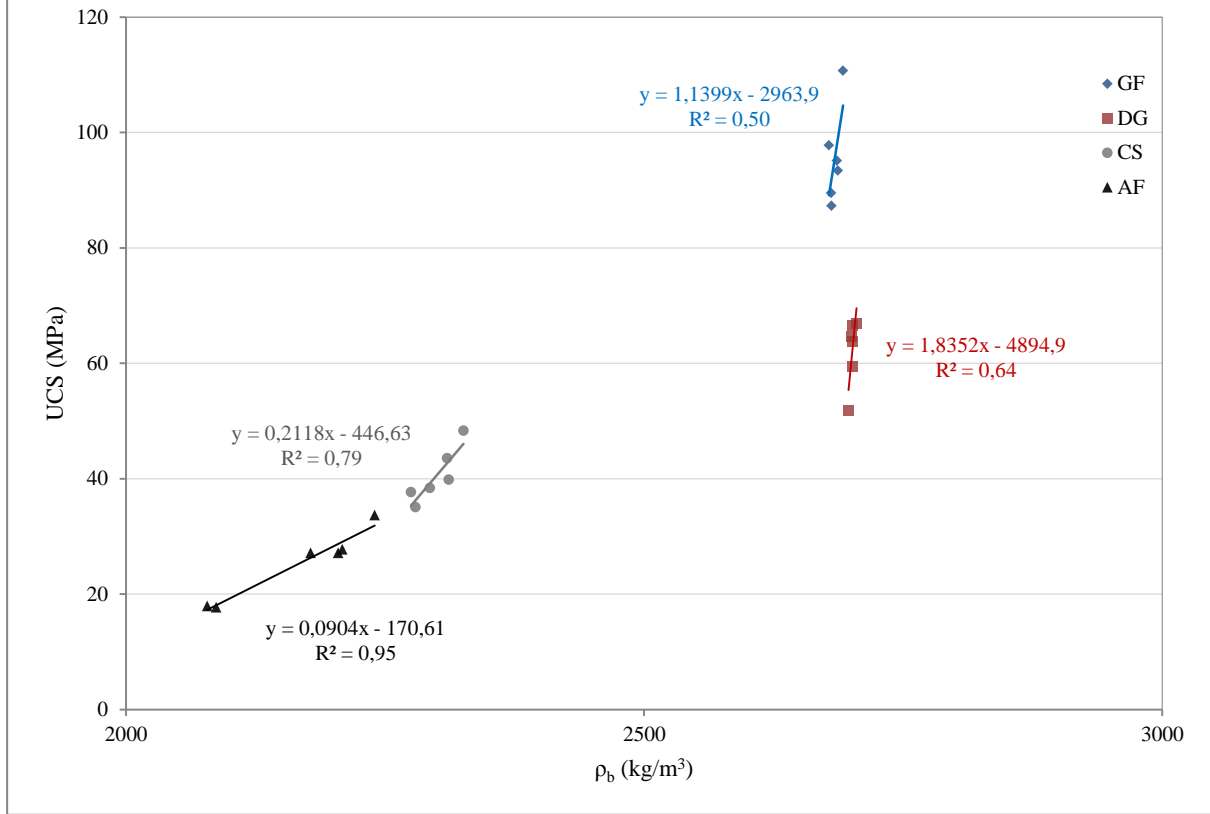


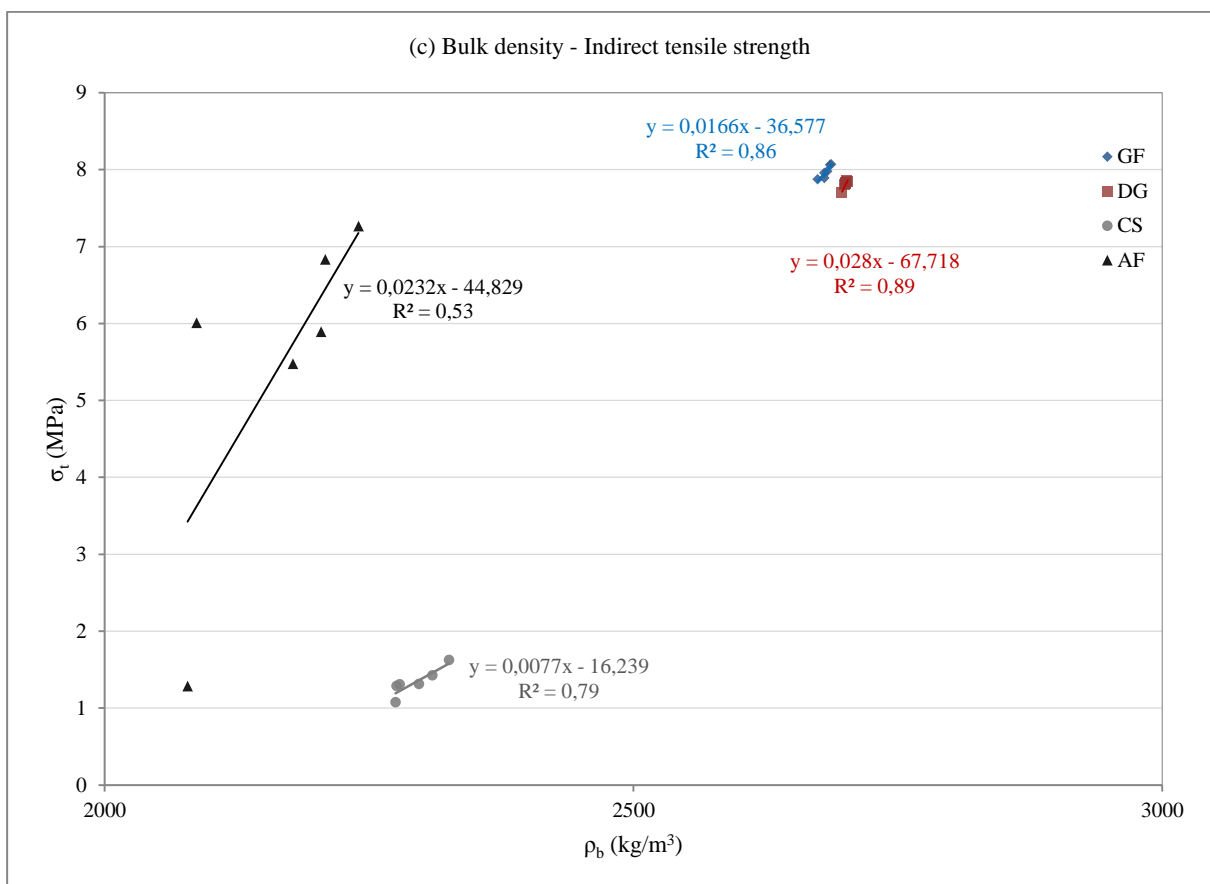
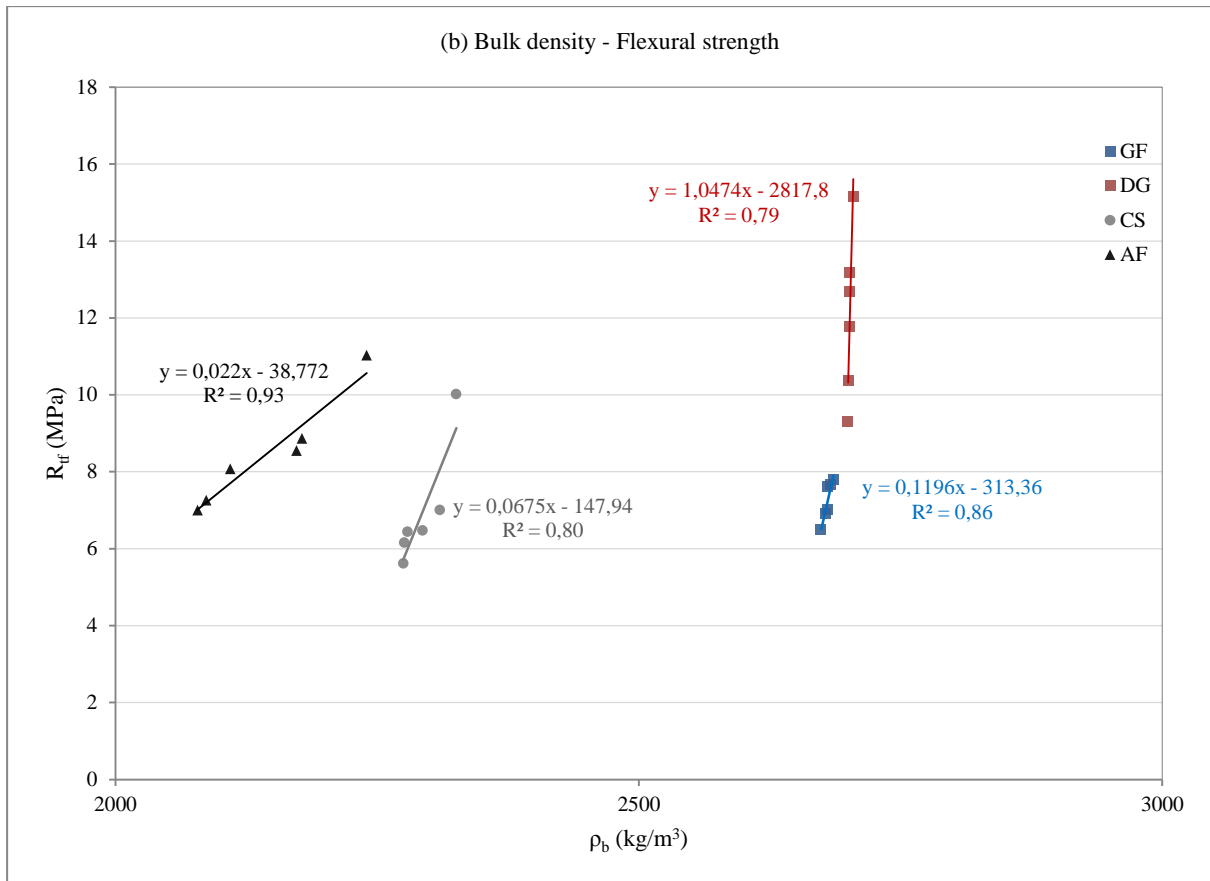


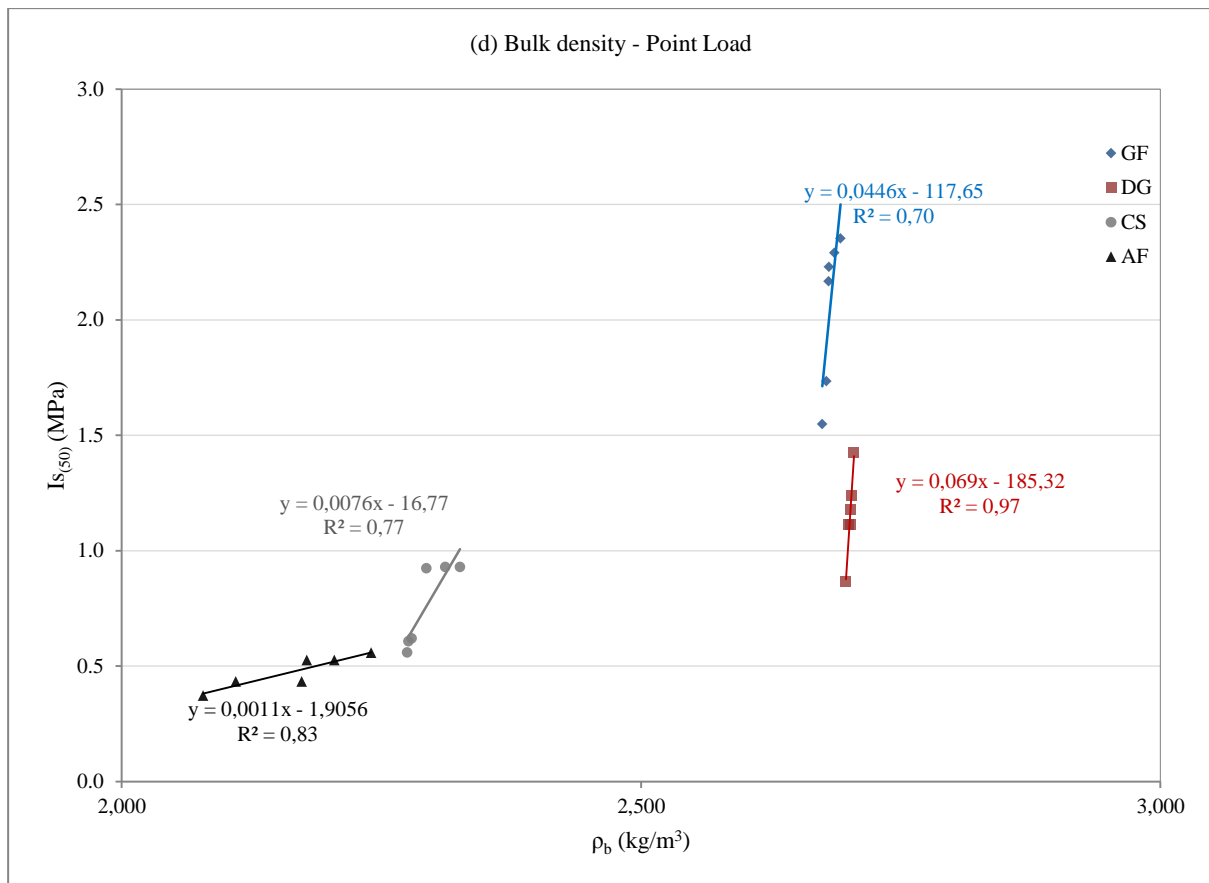
Figs. 7.4 a, b, c, d. Diagrams showing the relationship, for all investigated samples, between open porosity and: uniaxial compressive strength (a); flexural strength (b); indirect tensile strength (c); point load index (d).

The relationships between bulk density and mechanical properties (UCS , R_{tf} , σ_t , $IS_{(50)}$) are reported in Figs. 7.5 a, b, c, d. Bulk density plays a primary role in the mechanical behaviour of the investigated materials, as evidenced by the correlation factors between this parameter and the uniaxial compressive strength, flexural strength, tensile strength and point load (Figs. 7.5 a, b, c, d). The highest correlation values have been reached by AF both for UCS ($R^2=0.95$) and for R_{tf} ($R^2=0.93$) and by DG for σ_t ($R^2=0.89$) and for $IS_{(50)}$ ($R^2=0.97$). The higher the bulk density, the higher the strength values.

(a) Bulk density- Uniaxial compressive strength







Figs. 7.5 a, b, c, d. Diagrams showing the relationship, for all investigated samples, between bulk density and: uniaxial compressive strength (a); flexural strength (b); indirect tensile strength (c); point load index (d).

Hydric behavior

Coherently with porosity values obtained, the values of water absorbed by capillarity respect the same order: limestone DG shows the lowest values, followed by the granite GF and the calcarenite CS, while the sandstone AF exhibits the highest values. The lowest values reached by DG, suggest that the capillary pores are very few and not well connected. The values in the two investigated directions are very similar, meaning that the existing capillary pores do not have any special orientation. The second lowest value is that of GF (1.4 ± 0.2), which, similarly to the water absorption, may be due to the high tortuosity of the pores or their low connectivity. Finally, CS and AF show a fast and effective capillarity uptake, their coefficients being one order of magnitude larger than the other two. In this case, the difference between the coefficient in the two different directions (Table 6.9) shows the orientation of the

fractographic network of this stone; in the X direction the capillary pores probably are better connected. Furthermore, the pore size has an influence on the total water absorption. Relatively small pores, micropores detected by MIP, which are widely found in sandstones like AF and in granites like GF, are filled only after a very long immersion time. On the other hand, larger pores, macropores detected by MIP, which are often found in limestone like DG, will drain after taking the specimen out of the water (Siegesmud & Dürrast, 2014).

Hydric curves have been plotted according to two directions, X and Z, parallel and perpendicular to the anisotropy. CS reached the highest absorption rate (Table 6.9 and Fig.6.9). The capillary absorption is closely linked to the anisotropy (Sousa *et al.*, 2002; Vázquez *et al.*, 2010). According to Fig. 6.9 and to the anisotropy indices (P waves velocities), it is observed as the anisotropic material, which is AF with a total anisotropy value 17.4% (Table 6.12), behaves differently in both tested directions. Conversely, DG, which appears to be the most compact material for its low porosity and more isotropic for the total and relative anisotropy indices (1.1% and 0.5%, respectively), exhibits the same capillary behavior in both directions.

According to the Figs. 6.10 a, 6.10 b, 6.14 a, 6.16 a, 6.16 b, GF and DG, during hydric test, present three principal phases of hydric absorbing, both for capillary and absorption/desorption test. In all cases the first phase presents highest values of water absorbing, while the last phase the lowest. Moreover, GF and DG present air impermeability. So, GF and DG demonstrated better hydric behavior than CS and AF. In fact, CS has the fastest capillary absorption while AF an anisotropic hydric behavior.

Correlation between ultrasonic velocities, petrographic properties and stiffness

The P-wave velocity is affected by the orientation of microcracks and minerals and by grain size (Suárez del Río, 1982). In fact, comparing GF with other similar granites, this material shows lower values of ultrasonic pulse velocity. UPV obtained values show that GF belongs to the category of “middle velocity” (Anon, 1979; Vasaneli *et al.*, 2015). These values can be explained by the compactness of this building stone. But the lowest obtained values compared to other granites are explained by the microcracks system. Moreover, due to the presence of microcracks, the obtained anisotropy values are higher than other granites, examined with a similar methodology (Fort *et al.*, 2011). These anisotropy values indicate that in the stone a preferential orientation of planes would be appreciable according to the petrographic analysis. Probably, the XY plane is more prone to alteration processes, due to the presence of discontinuities related to microcracks (Fort *et al.*, 2011).

The presence of the intracrystalline microcracks and their different orientation along the three spatial directions, is in accordance with the registered ultrasonic velocities. In fact, along the X-direction the ultrasonic velocities are the highest because: microcracks are well oriented and parallel; there isn't a secondary system of microcracks; there are few microcracks, mainly concentrated in quartz crystals.

Along the Y-direction the ultrasonic velocities are medium because: there are two systems of microcracks, perpendicular to each other; microcracks of the principal system are well oriented and parallel; microcracks of the second system are less developed and shorter than the first one.

Whereas along the Z-direction the ultrasonic velocities are the lowest, due to: the presence of three sets of microcracks; they are not well oriented; there are lots of microcracks in number; there are also intercrystalline microcracks.

In other words the oriented analyzed thin sections, highlighting the complex system of microcracks, show how GF has a significant anisotropy, due to the orientation of its microcracks: the

average values of the ultrasonic wave propagation is about 3500 m/s along the Z-direction; and about 3700m/s and 4000m/s along the Y and X-direction, respectively. The coefficient of total anisotropy is high, about 8.4% and 6.9% for the P and S-velocities as well as the coefficient of relative anisotropy, 8.7% and 8.1%, for the P and S-wave velocities respectively. So, GF has an anisotropic ultrasonic behaviour.

Regarding the building material durability, the direction of exfoliation microcracks should be taken into consideration when applying conservation treatments on granite sculptures or ashlar. The surface parallel to such microcracks is the one most vulnerable to decay, where treatments penetrate least deeply due to the low capillarity in the perpendicular direction. Conversely, the surface perpendicular to the microcracks is the one less vulnerable and most permeable to conservation treatments (Freire-Lista & Fort, 2016). For these reasons, it is very important to taking into account the anisotropy of this building material in order to improve its petrophysical and mechanical behavior.

While for GF has been possible to notice the different orientation of intracrystalline microcracks, for the other materials (DG, CS and AF) has not been observed any internal orientation. This fact is in agreement with the ultrasonic velocities and the anisotropy indices. Grisolia stone (DG) and San Lucido calcarenite (CS) registered very low values of anisotropy coefficients, less than 1%. So, it can be said that Grisolia stone and San Lucido stone have an isotropic ultrasonic behavior. The anisotropy should be taken into account especially when evaluating treatments through laboratory tests.

Only for Fuscaldo sandstone (AF) a slight and parallel orientation of phyllosilicates along the X-direction has been noticed, according to the petrographic analysis. This different orientation inside the material has been confirmed by the anisotropic ultrasonic behavior detected by the ultrasound propagation test. For AF high anisotropy values for the total anisotropy have been reached, 17.4% and 9.4% for P and S-wave velocities and low values of relative anisotropy. This may be explained as AF

has a prevalent anisotropy direction corresponding to the X-direction where the orientation of the layers of phyllosilicates has been observed, while the other directions, Y and Z, are not affected by a prevalent internal orientation. So, it can be said that AF has an anisotropic behavior, emphasized along the X-direction.

The propagation velocity of the ultrasound waves is higher in DG and CS than in GF and AF (V_p and V_s , [Table 6.12](#)). This difference is in part due to the mineralogy of each stone (Molina *et al.*, 2015), which in the case of DG and CS is composed above all of calcite, while feldspars and above all quartz dominate in GF and AF, as calcite propagates the waves more quickly (approx. 6660 m/s) than quartz (approx. 5800 m/s) (Carmichel, 1989; Siegesmund & Dürrast, 2014). It is clear that the measured V_p values in the stones are lower than those of these mineral phases taken individually, due to the presence of other minor mineral phases (feldspars, clay minerals, etc.), which together with the textural factors (crystal size, crystal edges, porosity, laminations, preferential orientations, microcracks, etc.) lead to a fall in velocity (Martínez-Martínez, 2008).

This can be clearly seen if the V_p and V_s values are observed in the three spatial directions (V_{pX} , V_{pY} and V_{pZ} , [Table 6.12](#)). Moreover, in the direction of propagation normal to the lamination (the Z axis), the velocity of V_{pZ} and of V_{sZ} is quite a lot lower than in the other two directions. This occurs in all samples, which means that even though in some cases, no preferential orientation can be visually observed, ultrasounds show some discontinuity. In GF and AF samples the lowest velocity values have been reached along the Z direction. This result confirms the possible influence of the orientation of the stones on their hydric behavior and the strong influence of the fabric on these properties. The relative anisotropy coefficient ($\Delta m\%$) and especially, the total anisotropy coefficient ($\Delta M\%$), confirm the textural heterogeneity of the two r stones. In GF total and relative anisotropy are quite similar. Indeed the $\Delta M\%$ value is higher than the $\Delta m\%$ value in AF, as the lamination is much more pronounced.

Probably, in AF it is also necessary to take into account the existence of fine levels that are rich in clay and oxyhydroxides that influence the wave propagation velocity, especially in this direction.

The anisotropy behavior of GF and AF has been also confirmed by the elastic modulus (Table 6.13). The mineral composition probably has also influenced the Poisson coefficient in AF and GF, leading to a lower value than DG and CS due to the presence of quartz and feldspar compared to calcite (Ji *et al.*, 2009). The other coefficients (G, E and K) indicate that AF exhibits worse physical-mechanical behavior than GF, DG and CS.

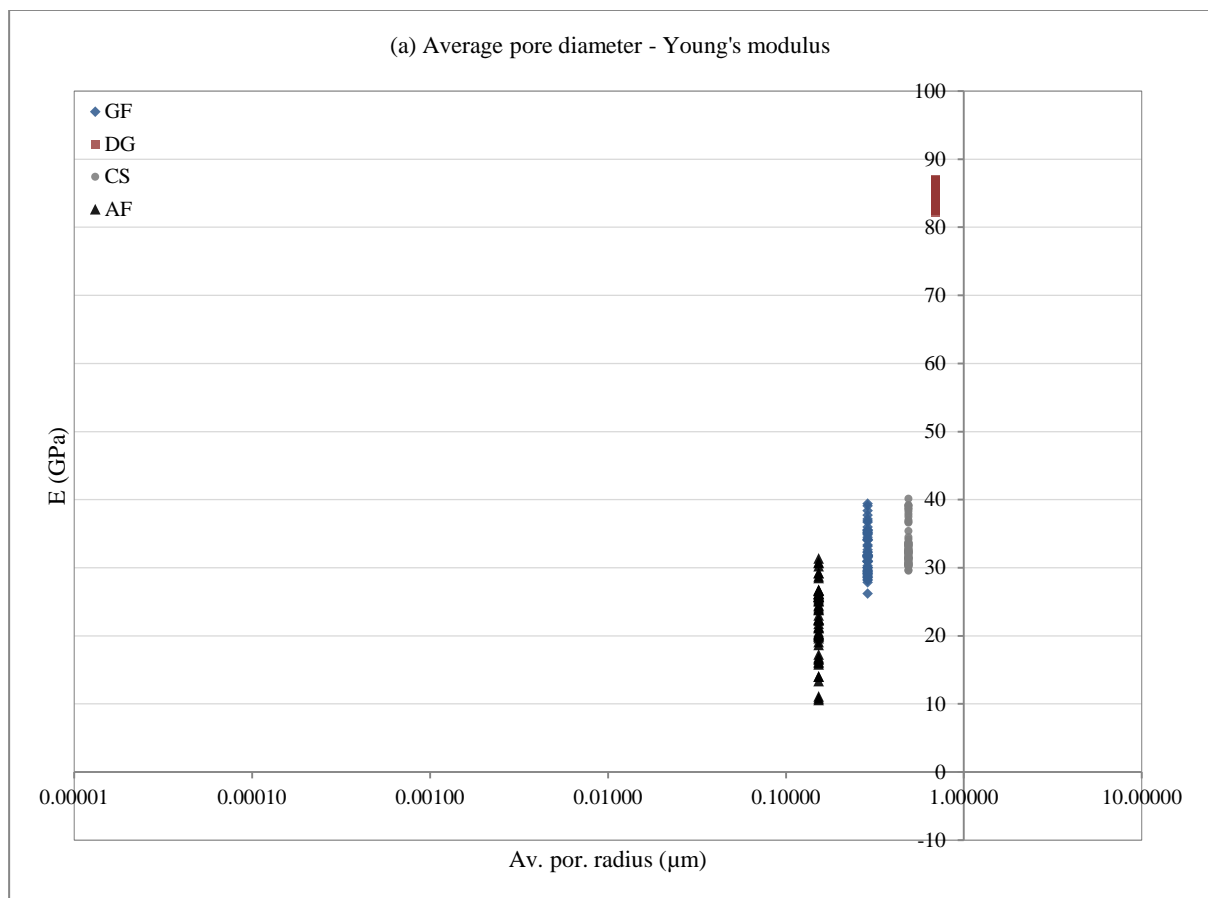
Regarding the stiffness¹⁷ of the analyzed samples it depends on the crystal size and on the porosity, while in the case of carbonates like DG, it is independent from the mineralogical composition (Martínez-Martínez, 2008). Young's modulus (E) measures the resistance of a material to elastic deformation under load. A stiff material has a high Young's modulus and changes its shape only slightly under elastic loads like stones in general, while, on the contrary, a flexible material has a low Young's modulus and changes its shape considerably. Analyzing E values reported in Table 6.13, the stiffest material is DG followed by CS and GF. The most flexible material is AF. This result is coherent with the porosity values. In fact the higher the porosity, the lower is the stiffness (Martínez-Martínez, 2008). So, AF, that exhibits the highest porosity values, is the most plastic material. The direction where all samples exhibited the stiffest behavior is the X direction, where the highest values have been recorded.

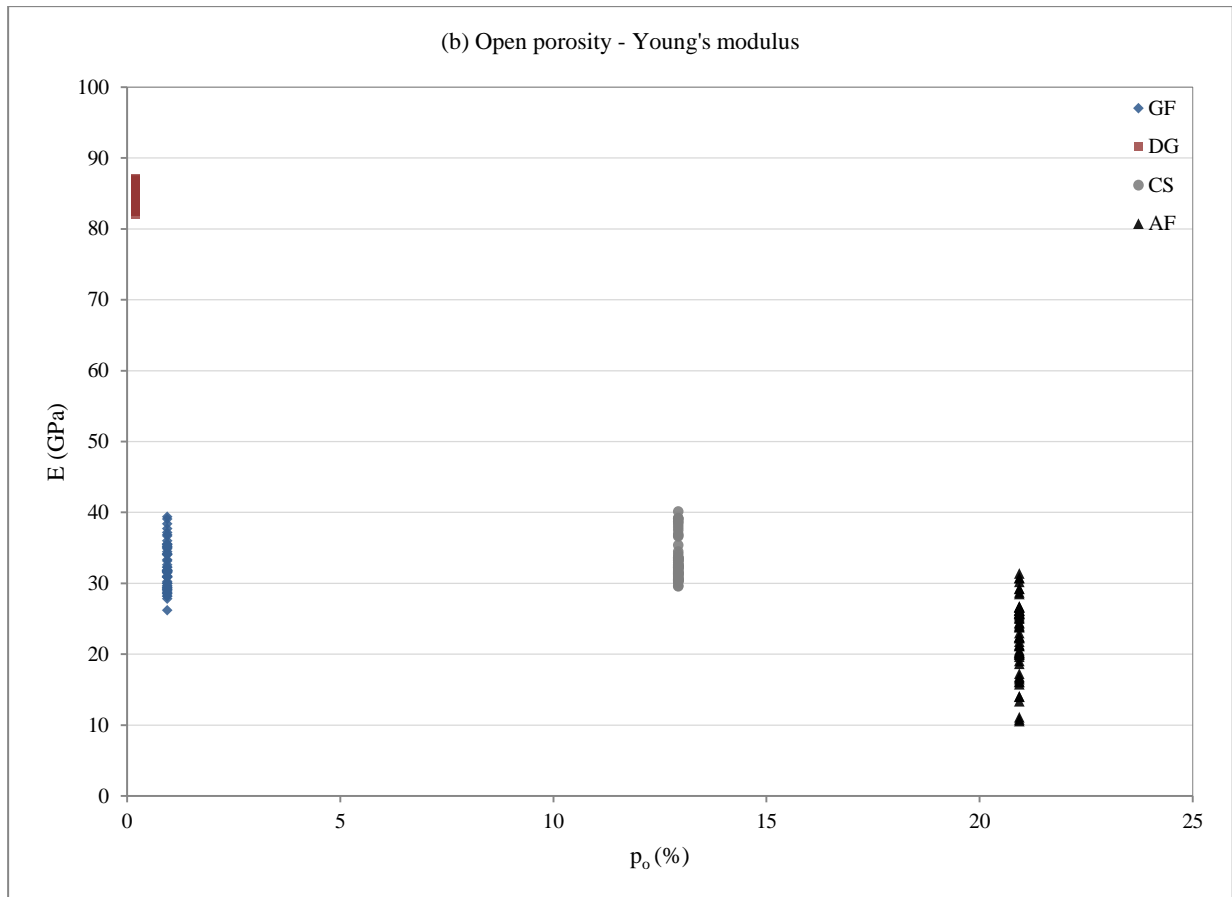
Specific stiffness is obtained as the ratio between Young's modulus and density (but should more properly be called “specific modulus”). Obtained values of specific stiffness are: 12.10 for GF; 31.14 for DG; 14.56 for CS; 10.10 for AF. These results confirm that DG is the stiffest material while AF is the stone with the lowest stiffness value. Comparing granite stiffness, GF reached low values that could be explained with the presence of its microcracks. In fact, one of the factors affecting the stiffness is the

¹⁷ *Stiffness* is defined as the rigidity of a material - the extent to which it resists deformation in response to an applied force (Baumgart, 2000). The complementary concept is *flexibility* or *pliability*: the more flexible an object is, the less stiff it is (Wenham, 2001).

porosity and, consequently, the presence of microcracks, because the space among crystals gives to the stone the possibility of displacements under loading conditions. For this reason, porosity, fractures and microcracks are responsible of the stones plastic behavior (Meng & Pan, 2007; Walsh, 1965). The internal set of microcracks in GF could explain the more plastic behavior of GF compared to other granitic stones (p.180 Table 3.9, Siegesmund & Dürrast, 2014).

As shown in Figs. 7.6 a, b, stiffness is dependent on the porosity and the average pore diameter. The higher the pore diameter, the higher the Young's modulus and consequently the stiffness. On the contrary, the higher the porosity, the lower the Young's modulus, so the material shows a more plastic behavior. These graphs are coherent with results of other studies (pp.198-199, Martínez-Martínez, 2008).





Figs. 7.6 a, b. Diagrams showing the relationship, for all investigated samples, between Young's modulus and: average pore diameter (a); open porosity (b).

Correlation between Drilling resistance and mechanical properties

To obtain the relationship between drilling resistance and UCS, the strength values obtained along the same loading direction have been considered. In fact, the direction of drilling was along the X axis and for UCS have been reported in [Fig. 7.7 a](#) the obtained values along the same axis in order to compare the obtained results.

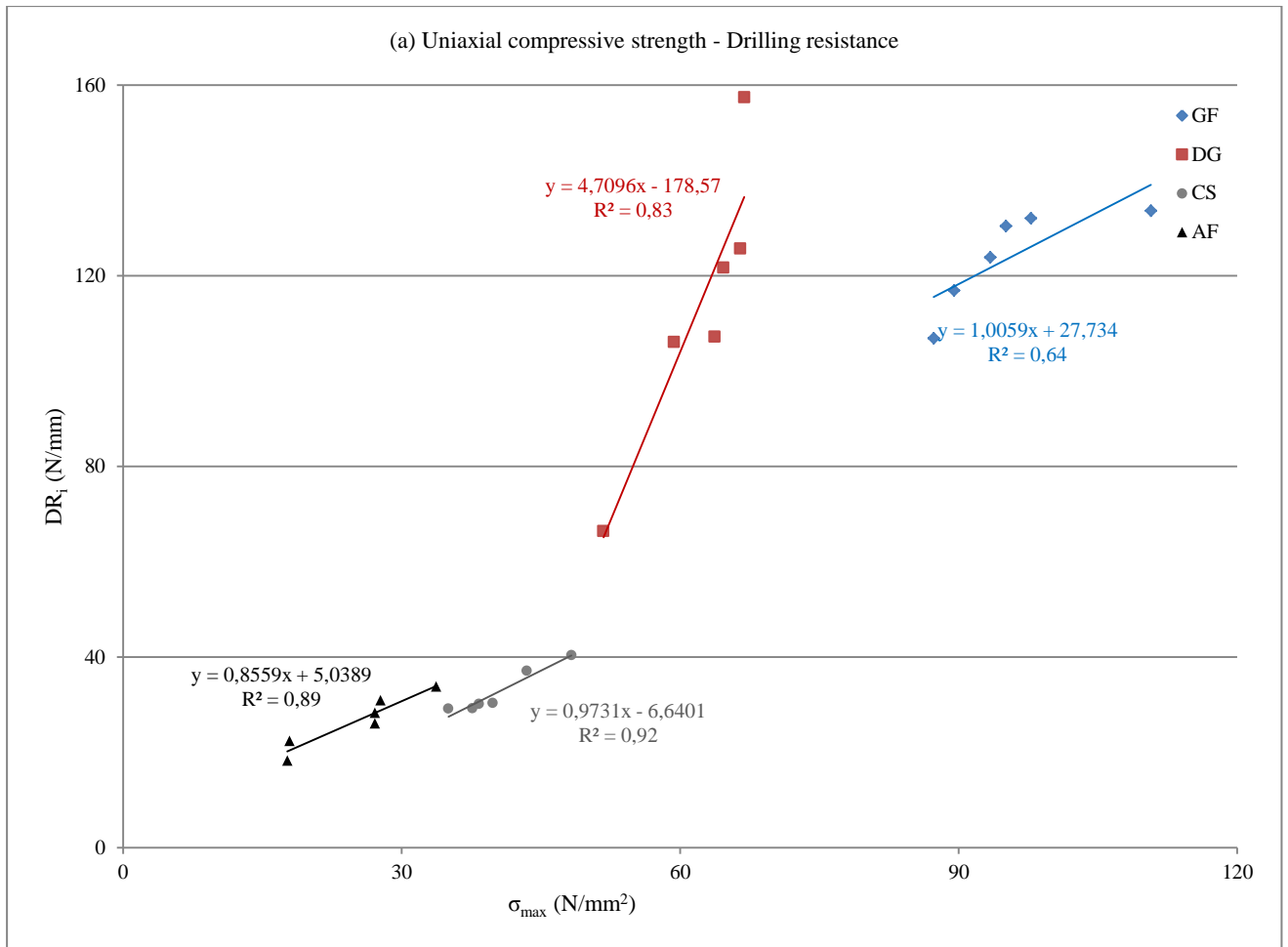
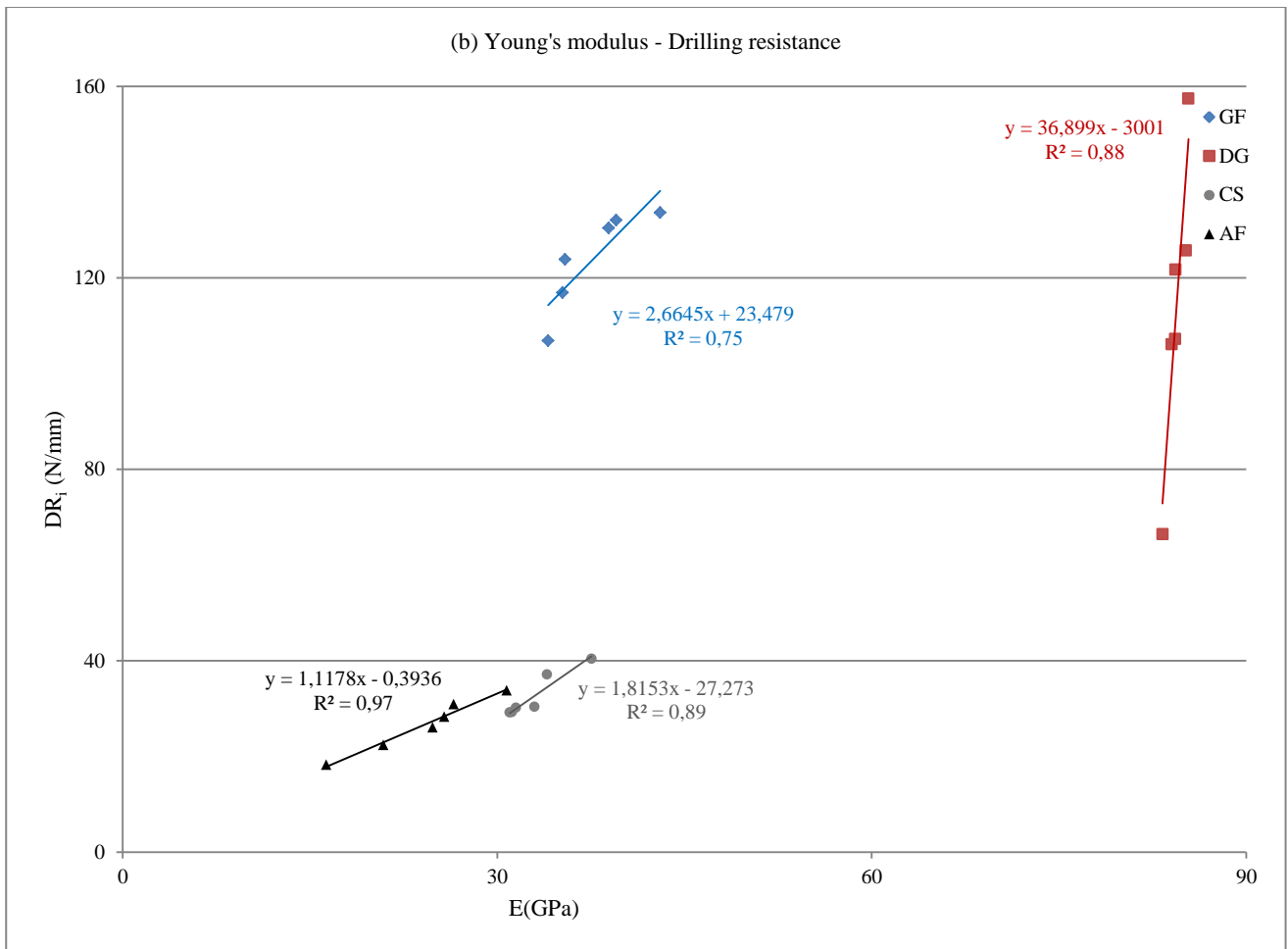
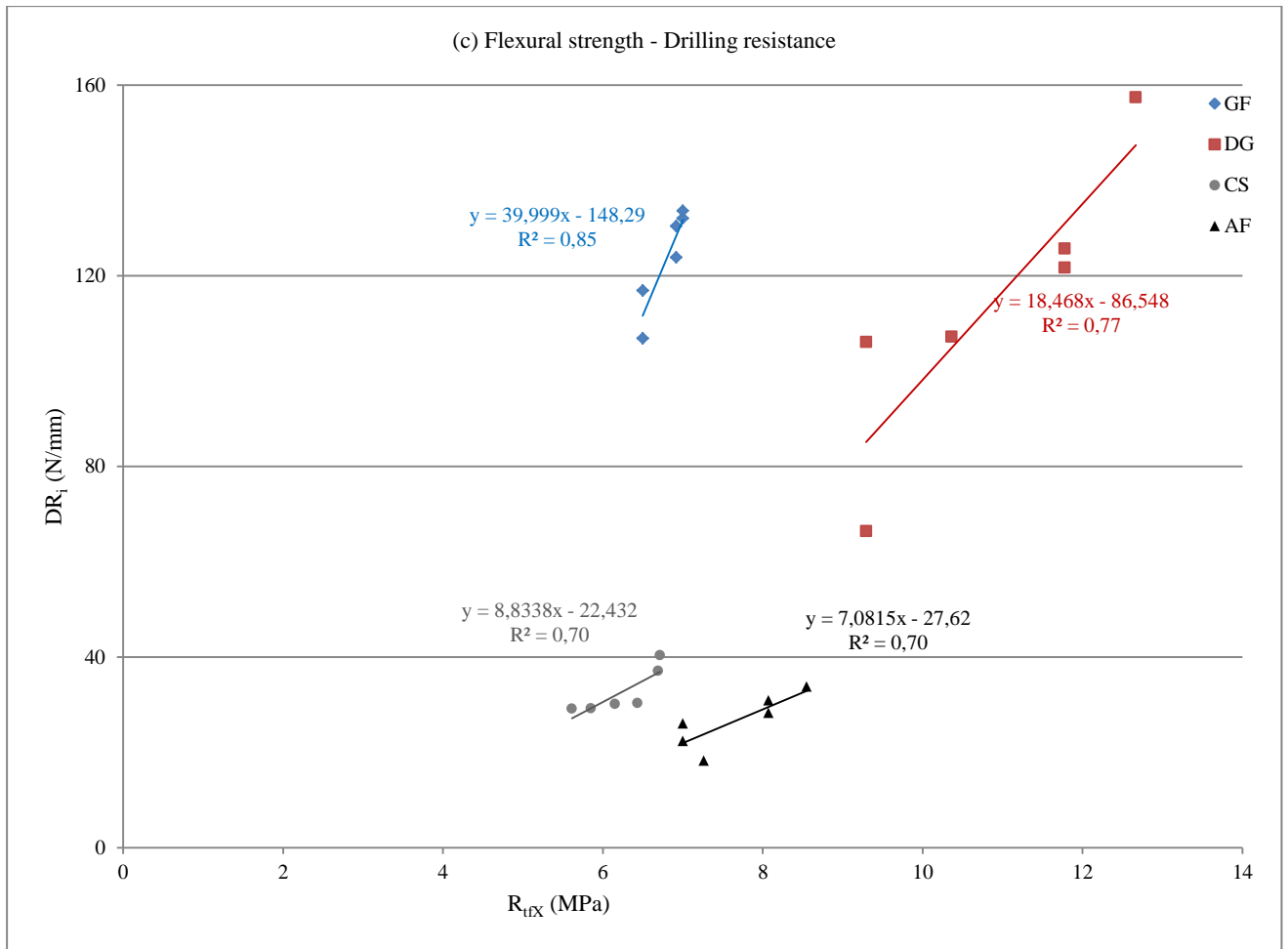


Fig. 7.7 a. Correlation of the micro-drilling results, expressed by drilling resistance (DR_i) with the uniaxial compressive strength along the X-axis (σ_{maxX}).

In Fig. 7.7 a, a high correlation coefficient is observed for the relationship between drilling resistance and uniaxial compressive strength for all samples. Only GF shows lower values with a correlation coefficient <0.7 even though it shows a linear relationship ($R^2 = 0.64$) between drilling resistance and mechanical properties, according to the linear correlation obtained by Delgao *et al.* (2002) under the same drilling test conditions. The other materials registered very high correlation values with $R^2 > 0.85$. Therefore, sufficiently accurate predictions of compressive strength could be yielded via the portable, micro-destructive application of the micro-drilling test using the equations reported in Fig. 7.7 a. This result is in agreement with other authors that have successfully used drilling measurements for determining the compressive strength (Exadaktylos *et al.*, 2000; Fernandes &

Lourenço, 2007). Strong associations are also shown between drilling resistance and the rest of the properties measured (Figs. 7.7 b, c, d). This can be explained by the fact that, during the interaction of the drilling bit with the material's matrix, voids such as pores can affect the measurements taken (Theodoridou *et al.*, 2012).



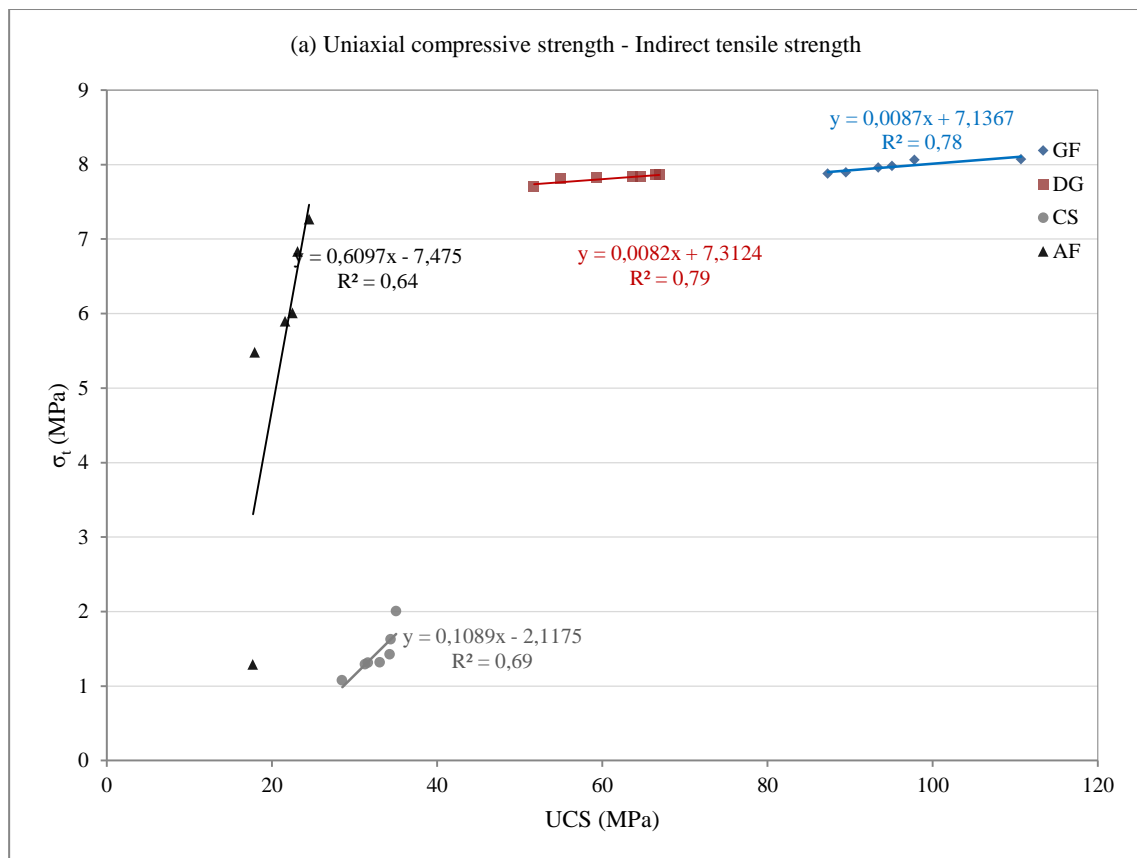


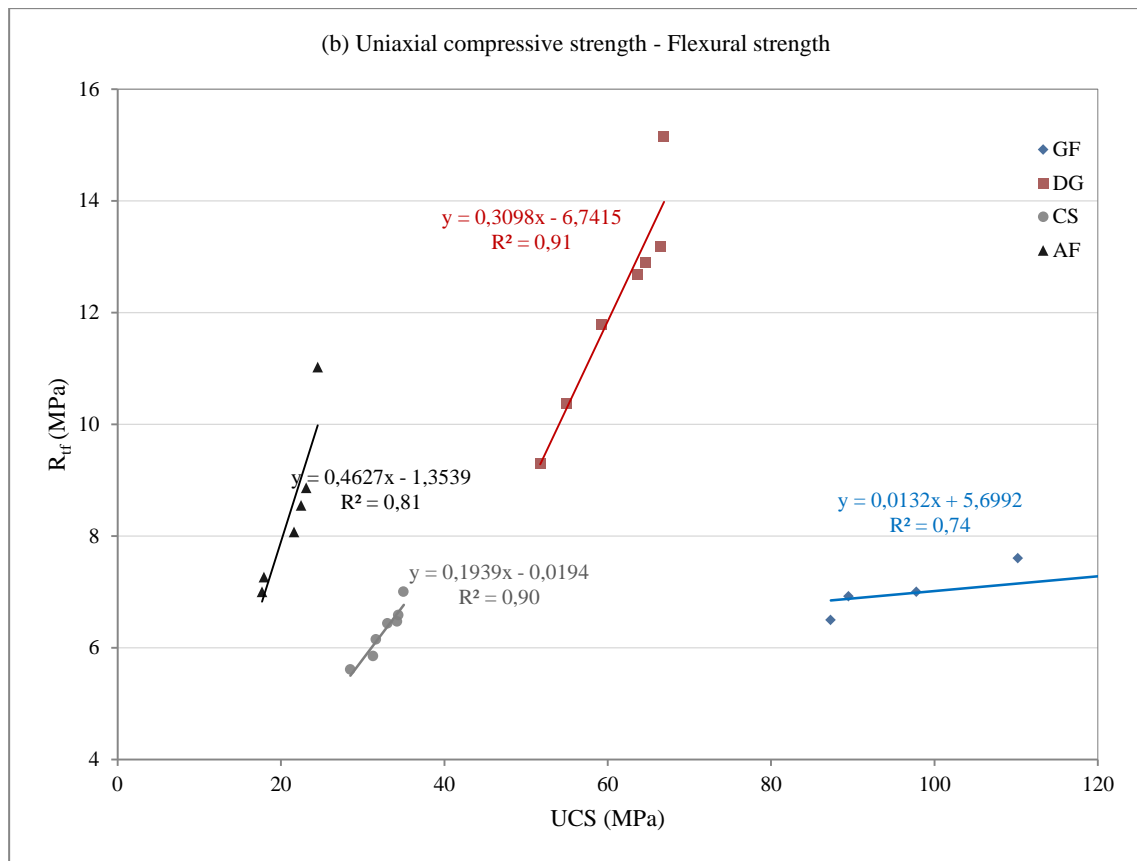
Figs. 7.7 b, c. Correlation of the micro-drilling results, expressed by drilling resistance (DR_t) with: (b) Young's modulus along the X-axis (E_x); (c) flexural strength along the X-axis (R_{tfx}).

As well as for UCS, also for R_{tf} , only the strength values obtained in the same direction of the drilling test (X-axis) have been chosen in order to compare values. As shown in Fig. 7.7 c, the correlation values between these two properties are high for all the analyzed samples. The highest correlation values have been registered by GF, followed by DG and the same values have been reached by CS and AF. Moreover, it can be seen that there is a linear relationship between the two considered properties. So, the higher the flexural strength, the higher the drilling resistance. DG showed the best mechanical behavior, while AF the worst, coherently with the results obtained by the other performed tests. Thanks to the high correlation values, flexural strength could be determined through the micro-drilling test adopting the equations reported in Fig. 7.7 c.

Correlation between compressive, tensile and flexural strengths

The correlation between the uniaxial compressive and tensile strength for all samples is very significant ($R^2=0.79$ for DG; $R^2=0.78$ for GF; $R^2=0.69$ for CS; $R^2=0.64$ for AF). There is a linear relationship between these two properties (Fig. 7.8 a). The same correlation between these two properties was obtained for basaltic stones by D'Andrea *et al.* (1965) and Tuğrul & Zarif (1999). High correlation values, statistically significant, have been also obtained for the relationship between UCS and flexural strength as shown in Fig. 7.8 b. The highest values have been recorded for DG and CS, followed by AF and GF.





Figs. 7.8 a, b. Relationship between uniaxial compressive strength (UCS) and: (a) tensile strength (σ_t); (b) flexural strength (R_{tf}).

In Fig. 7.9, the modulus of elasticity was plotted vs. the uniaxial compressive strength, determined by loading to failure. To draw the graph the X-axis has been considered because along this direction the E values have been calculated for the same samples that have been successively broken along the same axis.

The relationship between compressive strength and modulus of elasticity is direct and linear for CS and AF. Judd & Huber (1962), D'Andrea *et al.* (1965) and Deere & Miller (1966) obtained similar relationships. On the contrary, for GF and DG samples, it can be said that these lithotypes do not follow an elastic mechanical behavior as UCS and E are not directly correlated (Fig. 7.9). The modulus of elasticity of stone, as well as tensile strength, is controlled by the same factors as compressive strength: composition and texture. Probably, the presence of microcracks in GF within the intact specimen,

lowers tensile strength as it lowers compressive strength (Table 6.16) and causes the lack of a direct relationship between Young's modulus and compressive strength. Moreover, the presence of microcracks also explains the reason why for GF the maximum strength values of UCS have been obtained along the Z axis that is in contrast with other authors that have obtained the maximum values along the X-axis (Prikryl, 2001) and the minimum ones along the Z-axis. But, on the contrary, the same result is in agreement with other authors that recognized the Z-axis as to be the strong direction for granites (Siegesmund & Dürrast, 2014; Kudo *et al.*, 1987).

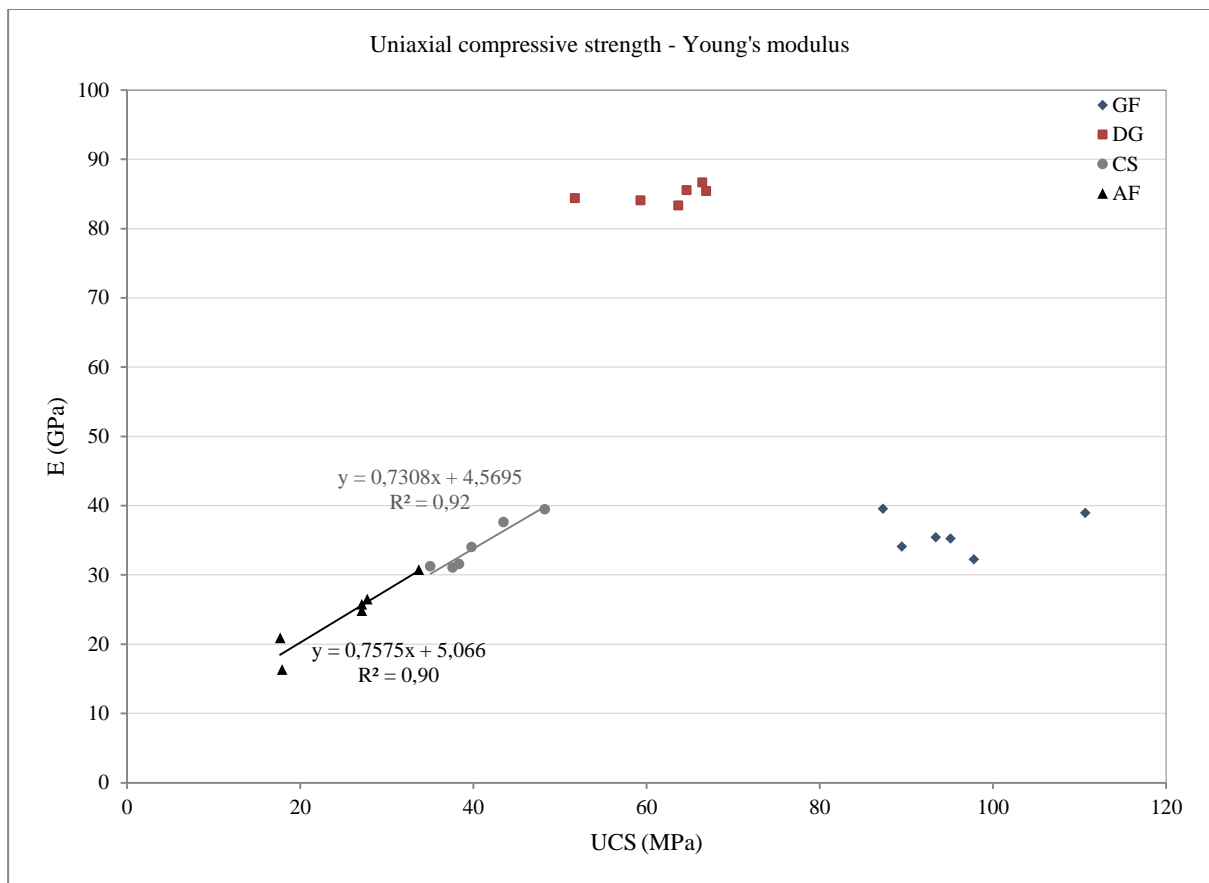
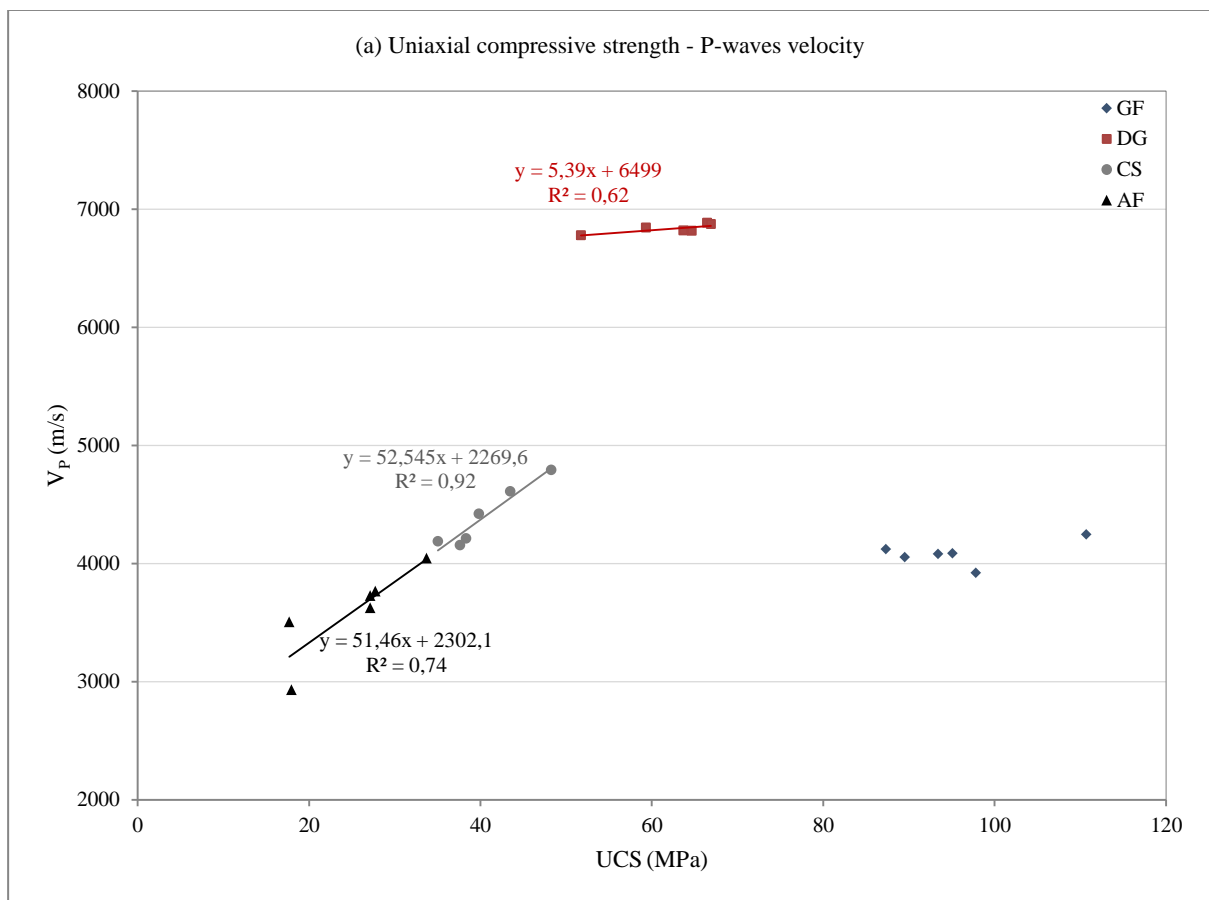
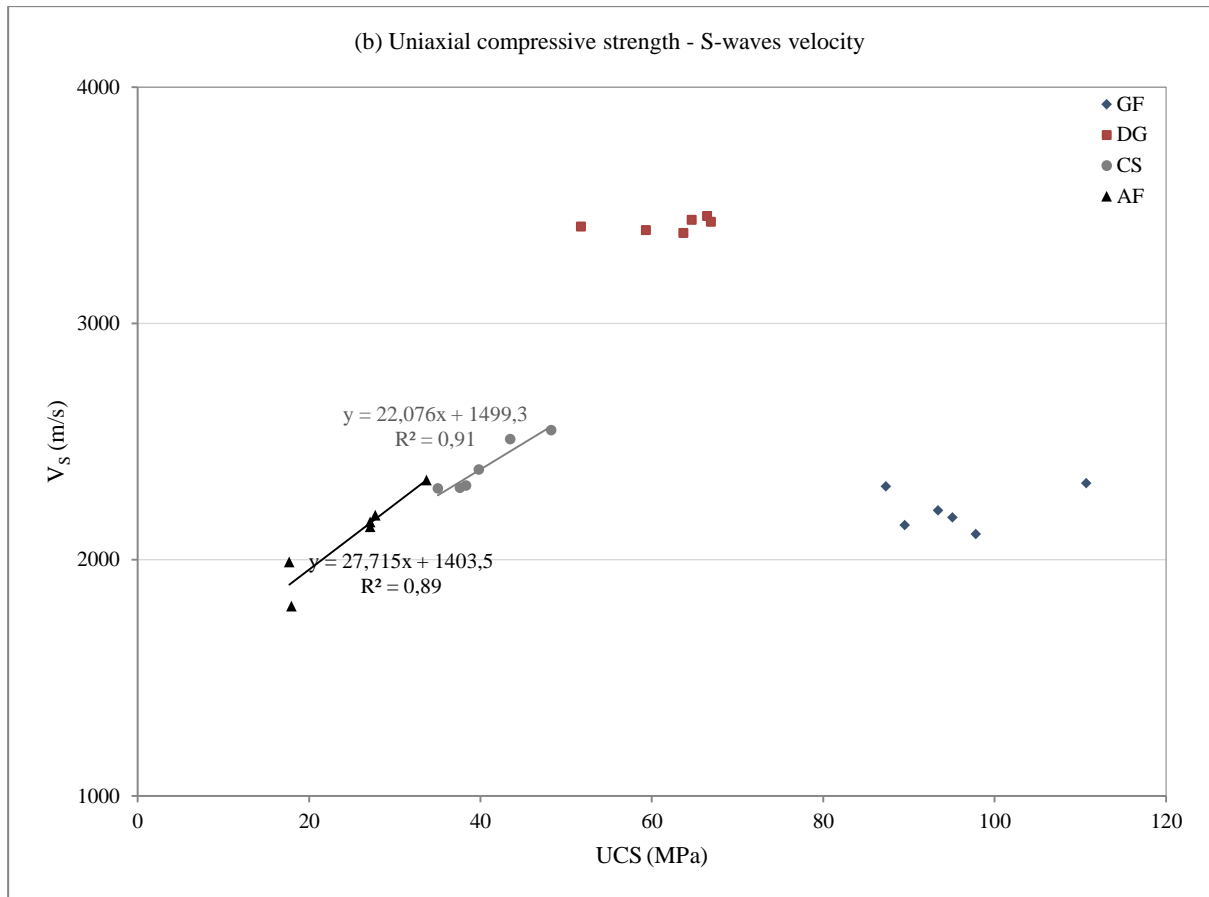


Fig. 7.9. Relationship between uniaxial compressive strength (UCS) and Young's modulus (E).

The relationship between uniaxial compressive strength and ultrasound wave velocity is shown in Figs. 7.10 a, b. As expected, the lower the uniaxial compressive strength, the lower the P and S-wave

velocity and vice versa. The presence of pores and cracks makes the stone less continuous, thereby decreasing ultrasonic velocity and increasing breakability under compression (Sousa *et al.*, 2005). CS and AF have registered strong correlation both for V_p and V_s . DG reached a linear relationship only between UCS and V_p while GF did not show any correlation between the measured properties. This fact could be explicated with the granite alteration. In fact, as resulted by many tests performed, GF has been classified as fresh stone but with the presence of microcracks. So, as demonstrated by other authors (Sousa *et al.*, 2005) and as reported in Figs. 7.10 a, b, the good trend in the relationship between these considered properties (UCS and V_p or V_s) for sound granites changes as they become altered, decreasing the linear relationship among them.





Figs. 7.10 a, b. Relationship between uniaxial compressive strength (UCS) and: (a) P-waves velocity (V_p); (b) S-waves velocity (V_s).

The ratio between unconfined compression and tensile strength is reported in [Table 7.1](#).

Table 7.1. Ratio between uniaxial compressive strength (UCS) and: tensile strength (σ_t); flexural strength (R_{tf}); point load ($Is_{(50)}$).

Samples	UCS/ σ_t	UCS/ R_{tf}	UCS/ $Is_{(50)}$
GF	13.0	13.3	50.7
DG	8.7	5.6	59.2
CS	21.9	5.0	44.5
AF	5.3	3.9	65.2

For all materials the obtained ratio (UCS/ σ_t) was in agreement with data reported in the literature for stones (e.g. 8 to 27, Okubo & Fukui, 1996; e.g. 11.60 to 44.35 for granitic stones, Günes Yılmaz *et al.*, 2009; e.g. 8.71 to 18.6 for limestones and 13.6 to 17.96 for sandstones, Siegesmund & Dürrast,

2014). Only AF showed a lower value (5.3). This can be due to the fact that because of the uniformity of the stress state there is no stress concentration, thus preventing an early failure of the specimen. The tensile strength is therefore likely to be higher than usual as well as found by other authors (Coviello *et al.*, 2005).

Regarding the ratio between UCS and R_{tf} , GF showed higher values than those obtained by other authors for the same lithotypes (*e.g.* 6.85 to 11.62 for granitic stones, Günes Yılmaz *et al.*, 2009). On the contrary, DG, CS and AF presented lower values than those of other authors (*e.g.* 7.36 to 24.0 for limestones and 8.03 to 12.0 for sandstones, Siegesmund & Dürrast, 2014). This means that GF shows lower flexural strength values, while DG, CS and AF show higher flexural strength values compared to data in literature. This could be explicated by the relationship between the Navier's theory and the fracture's position, as explicated in Par. 6.6. The consequence is that in the three pointed flexural strength test, in many cases when the fracture did not develop in the loaded section, the flexural strength is overestimated (Coviello *et al.*, 2005).

Analyzing the strength values of UCS, R_{tf} and σ_t (Tables 6.16, 6.17, 6.18) for the four lithotypes, it can be observed that stones that recorded the highest UCS values (*e.g.* GF) did not registered coherently the highest tensile strength values and *viceversa* (*e.g.* AF registered the lowest UCS values but higher tensile strength values, if compared with GF). This difference between UCS and tensile values among lithotypes, is in agreement with other authors that explained this fact with the theory of the mode failure under compressive and tensile stresses. In compressive loading, in fact, the crack failure is more complex compared to that of tensile loading where only a single plane of the sample is involved in the created stress (Tsur-Lavie & Denekamp, 1982; Alehossein & Boland, 2004; Günes-Yılmaz *et al.*, 2011).

Regarding the relationship between tensile and flexural strength (Fig. 7.11), there were registered very strong correlations ($R^2 > 0.80$) except for AF ($R^2 < 0.70$). The flexural strengths of the analyzed samples on all investigated directions are consistently higher than the tensile strength measured from Brazilian tests, as shown in Fig. 7.11 and as numerically reported in Table 6.17 and Table 6.18. This result matches what reported by Dai *et al.* (2013).

Comparing the fracture propagation under uniaxial compressive and tensile (Brazilian and flexural strength tests) conditions, there are some differences. UCS cracks are more irregular, more complex and apparently they have no prevalent direction (Figs. 6.24, 6.25) compared to those provoked by tensile failure (Figs. 6.27, 6.29). This is probably due to the fact that in both the Brazilian tensile strength and flexural strength testing only a single plane of the test specimen is affected by the created stress, whereas in uniaxial compressive strength testing a volume of the specimen is affected by the applied compressive stresses. Consequently, in compressive loading, crack interaction and coalescence mechanism is much more complex due to the interaction and combination of splitting and shear stresses, as better shown in Fig. 6.25, compared to that of the tensile loading where only a limited number of critical cracks are required to induce failure (Tsur-Lavie & Denekamp, 1982; Alehossein & Boland, 2004; Günes Yılmaz *et al.*, 2011).

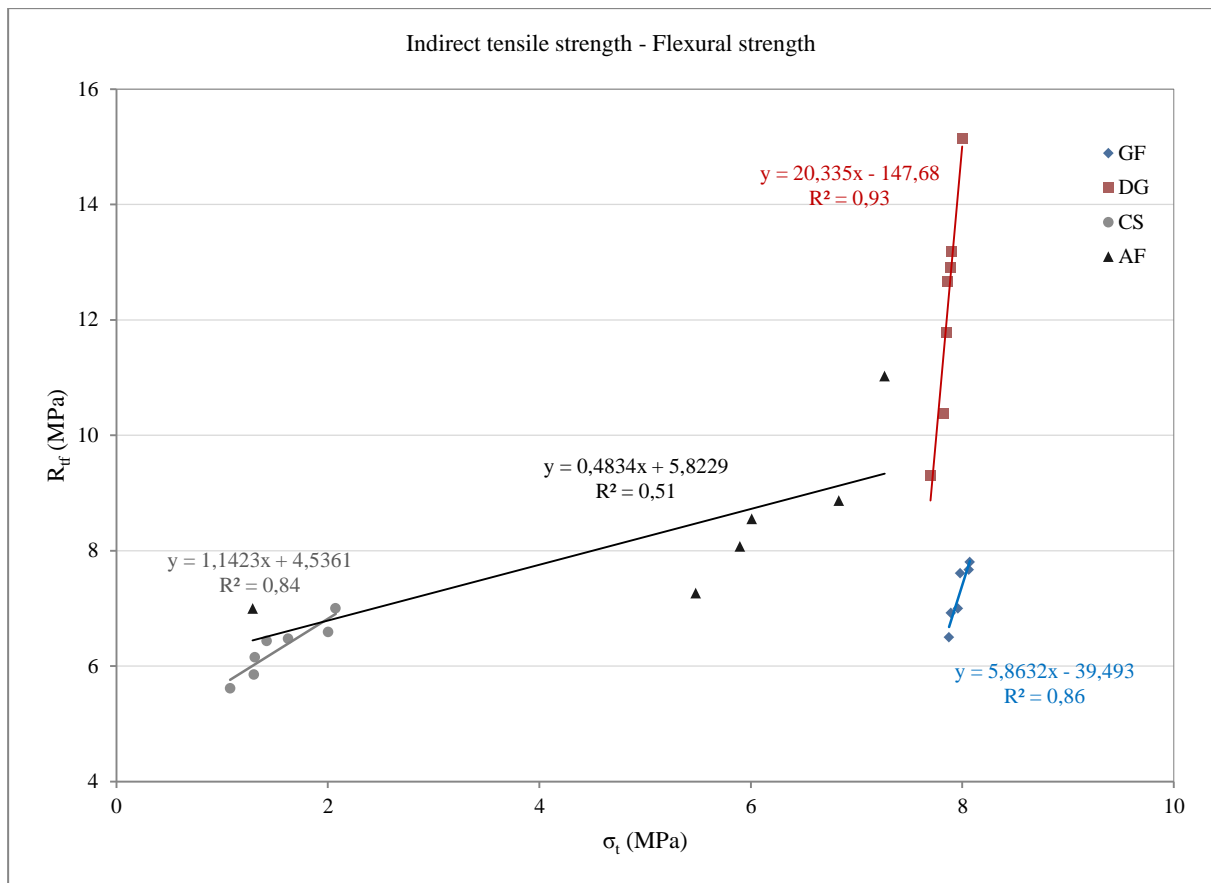


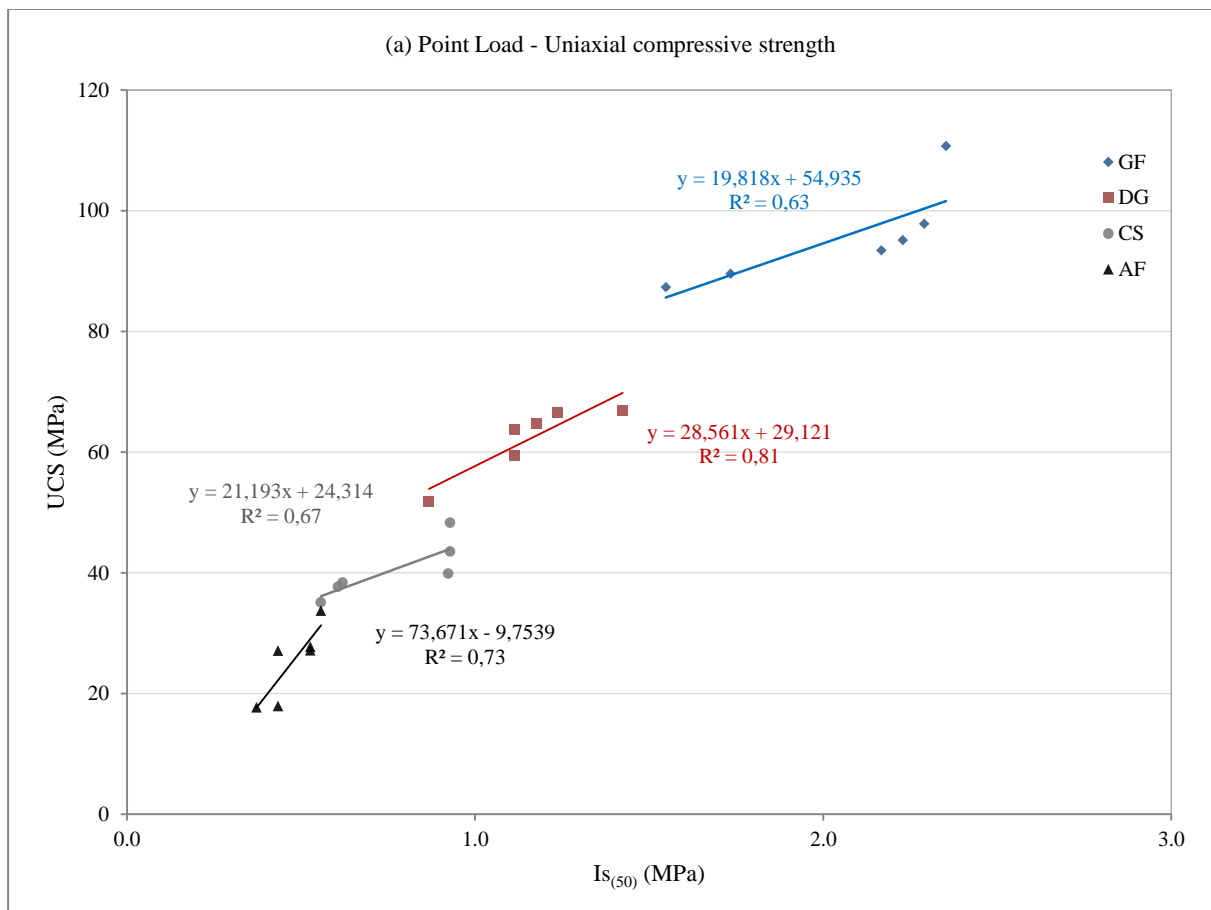
Fig. 7.11. Relationship between tensile strength (σ_t) and flexural strength (R_{ft}).

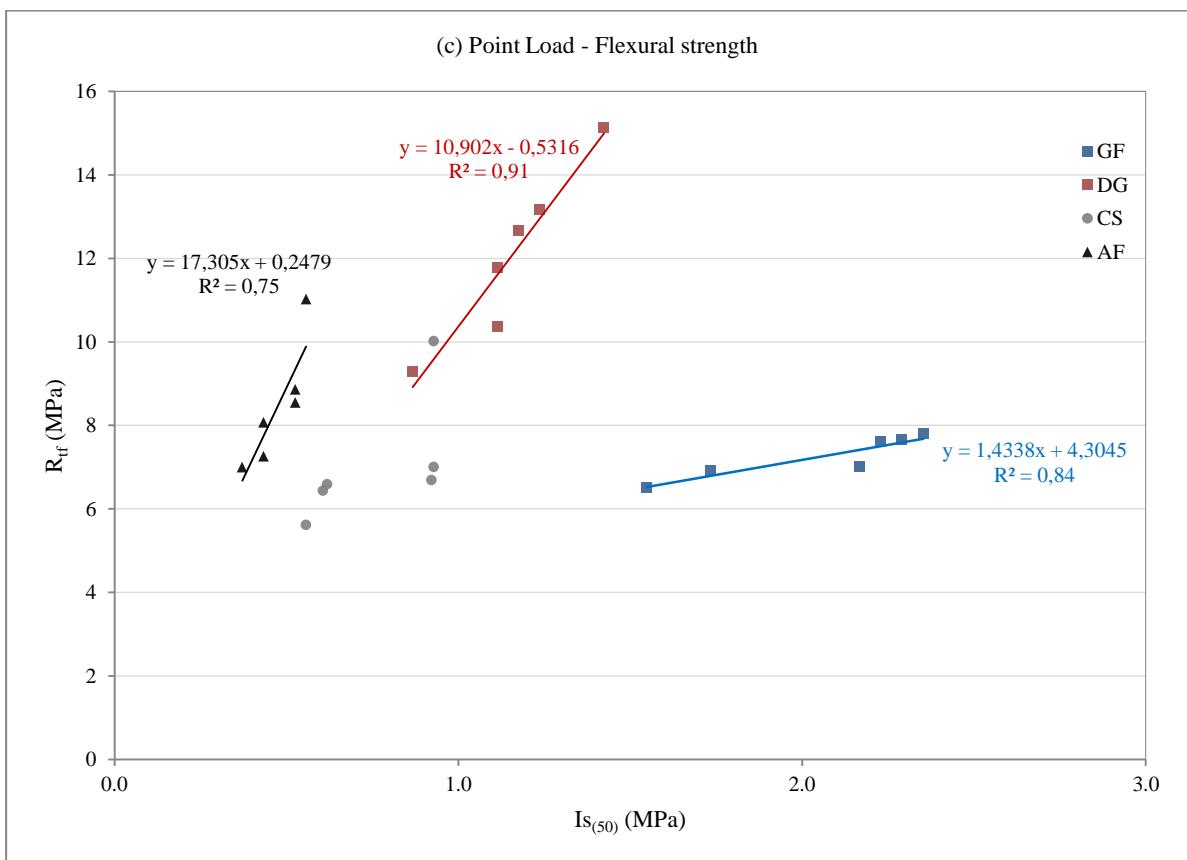
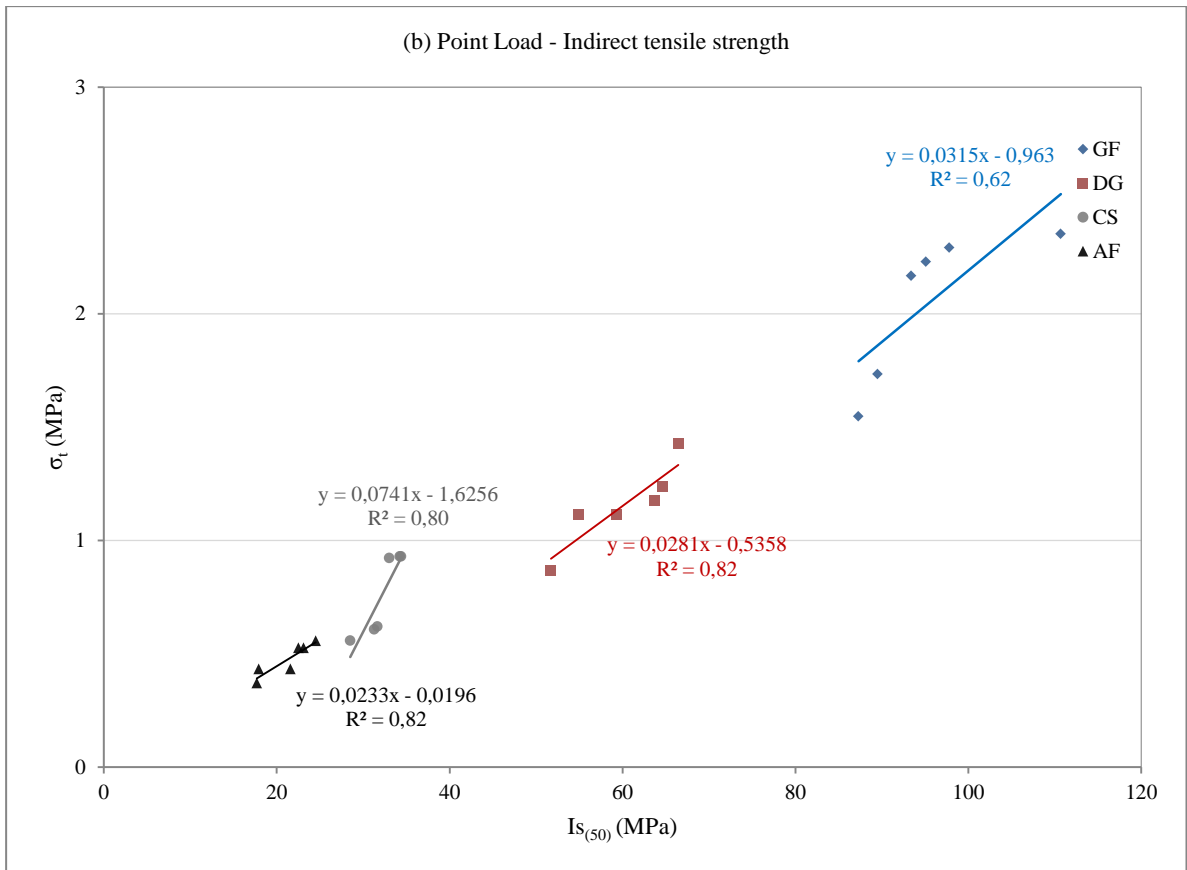
Correlation between Point Load and mechanical properties

The point load strength index has been widely used to estimate the uniaxial compressive strength of stones in the field and laboratory (D'Andrea *et al.*, 1965; Deere & Miller, 1966; Broch & Franklin, 1972; Bieniawski, 1975; Tuğrul & Zarif, 1999).

The correlation between the point load strength ($Is_{(50)}$) index and the compressive strength for DG (Fig. 7.12a) is very significant for DG ($R^2=0.81$) and AF ($R^2=0.73$). D'Andrea *et al.* (1965) and Tuğrul & Zarif (1999) obtained high correlation values for similar lithotypes ($R^2=0.92$). Lower correlation values have been obtained for CS ($R^2=0.67$) and GF ($R^2=0.63$). But for all the samples a strong linear relationship between the two measured properties has been obtained.

Higher correlation values ($R^2 > 0.80$) than for UCS have been obtained between $I_{s(50)}$ and σ_t (Fig. 7.12 b). Only GF showed the same correlation value (Fig. 7.12 a). A power relationship exists between these two mentioned parameters, according to other authors who performed the same tests (e.g. Khanlari *et al.*, 2014). In Fig. 7.12 c the relationship between $I_{s(50)}$ and R_{tf} is shown. DG reported the highest value ($R^2 = 0.91$), followed by GF ($R^2 = 0.84$) and AF ($R^2 = 0.75$). Only CS did not show any relationship. So, for the majority of the analyzed samples a linear correlation among the analyzed properties has been obtained. Starting from the Point load values it is possible to obtain the other considered properties using the correlation equations reported in each graph (Figs. 7.12 a, b, c). According to these test results, values of UCS, σ_t and R_{tf} can be obtained with a high degree of confidence using the point load testing methods. Since the method is simple, fast, and low cost, this is the most useful method for determining UCS, σ_t and R_{tf} in practice.





Figs. 7.12 a, b, c. Relationship between Point load ($Is_{(50)}$) and: (a) uniaxial compressive strength (UCS); (b) indirect tensile strength (σ_t); (c) flexural strength (R_{tf}).

Early studies (Bieniawski, 1975; Broch & Franklin, 1972) were conducted on hard, strong stones, and found that relationship between UCS and the point load strength could be expressed as:

$$UCS = (K) \times Is_{(50)} = 24 \times Is_{(50)}$$

where K is the “conversion factor.” Subsequent studies found that K=24 was not as universal as had been hoped, and that instead there appeared to be a broad range of conversion factors. In this study has been applied the conversion factor for “sedimentary stones” to CS, AF and DG by Bieniawski (1975, K=23.9), Hassani *et al.* (1980, K=29), O' Rourke (1988, K=30), Vallejo *et al.* (1989, K=17.4) and the conversion factor for “various stones” for GF by obtained by Broch & Franklin (1972, K=23.7), that worked well for a variety of stone types and geographic regions. The conversion factors for sedimentary stones were applied for CS, AF and DG while for various stones for GF. These conversions have been used to verify if it possible to obtain the UCS from the Point Load value for the considered stones. Applying these factors no samples verified the correlation conditions, obtaining underestimate UCS values. The indirect UCS values obtained by the correlation factor of O'Rourke (1989) were the most similar to the direct UCS strength values but underestimated the direct UCS values. So, to define exactly values similar to the “real” UCS values, for these types of analyzed stones should be used higher conversion factors as reported in [Table 7.1](#).

8. Durability

In order to achieve a complete study of characterization of stone materials, it is necessary to evaluate the influence of the fabric of a stone on its durability, it is necessary to combine the results of various techniques, in order to obtain a clearer vision of the factors and characteristics that can influence or limit the durability of the stone used in construction (Molina *et al.*, 2013). The durability of stone and stone-like materials is traditionally and relatively efficiently assessed by means of durability tests or ageing tests. The aim of these tests is to avoid the need of several years of testing – necessary in real exposure tests – and so they intend to artificially accelerate the damaging process (Fort, 2009).

The main objective of this experimental part is to evaluate the durability of the selected building stones against the action of salts and ice, because salt and ice crystallization are recognized as the most dangerous decay factors affecting the stone durability (Ruedrich & Siegesmund, 2007 a, b).

8.1 Action of salts

The salts originate from the combination of ions that have been leached out from soils, building stones, mortars, bricks, and other materials used on monuments, they can be also the result of polluted atmospheres or generated by organic metabolism.

The ions are carried in diluted aqueous solutions. They may penetrate into the materials and circulate within or percolate through their cavities and pores. They concentrate and accumulate whenever the water (as solvent) evaporates, where and when the solution gets supersaturated with respect to a certain salt phase within the system, this phase will precipitate on or beneath the material surface and form efflorescences or subflorescences and, even a saline crust (Arnold & Zehnder, 1989).

Practically, all building materials contain soluble salts. They may be dispersed within the porous materials or locally concentrated. They can be present in efflorescences forming different aggregates of crystals with different forms and habits on the surface, as subflorescences forming crystalline aggregates

in a zone behind the surface and as solutes in aqueous solutions on and within the walls. Soluble salts become a risk to the integrity of materials in the presence of water.

8.2 Salt crystallization process

It is known that crystallization of salt solutions is one of the most important decay mechanisms that affects many buildings (Winkler & Singer, 1972; Rodriguez Navarro & Doehne, 1999). Crystallizing salts have a disruptive effect, especially for porous materials (Chabas & Jeannette, 2001), due to the production of physical stress (Benavente *et al.*, 2003 a, 1999, 2007 a, b) as a result of salt crystallization inside the porous system. When efflorescences form on the surface of a porous material, a certain portion of the salt may crystallize underneath the surface. The place where salts precipitates on and beneath a surface of a porous medium depends on the solution supply and the evaporation.

According to Arnold & Zehnder (1989) it is possible to individuate four phases of the salt crystallization process. In a first phase crystals grow favorably in the large pores (about 1 to 10 μm) while smaller pores remain empty (Snethlage, 1984).

In a second phase, the crystals already exceed the pore size and overlap other pores. The pore sizes being exceeded by the crystals provoke a tensile stress perpendicular to the surface.

In a third phase, crystallization is concentrated at fissures, because evaporation is accelerated along the opened and widening structure.

In the fourth phase, as the fissures are widened and the solution retreats, the area where the crystals contact the solution is reduced more and more, and consequently columnar crystal growth thinning out more and more as the solution supply is reduced while the substrate is drying out.

Some of the most common salts that may be found on walls are carbonates, sulphates, chlorides, nitrates and oxalates of sodium, potassium, calcium, magnesium and ammonia.

Sodium sulphate is one of the most damaging salt affecting porous stones. The $\text{Na}_2\text{SO}_4 \cdot n\text{H}_2\text{O}$ includes two phases: if the temperature is higher than 32.4°C thenardite (Na_2SO_4) crystallizes, while if the temperature is lower the crystallization of mirabilite ($\text{Na}_2\text{SO}_4 \cdot 10\text{H}_2\text{O}$) or thenardite happens, depending on the relative humidity. Both mineral phases crystallize as subflorescences, especially for materials with small pores sizes. The crystallization pressure inside the pores provokes the development of microcracking inside the stone. Therefore, even small quantities and precipitation processes can lead to considerable damages in the stone (Benavente, 2003).

8.3 Salt crystallization test

8.3.1 Procedure

Salt crystallization test was carried out to evaluate the decay suffered by the selected stones. This test was selected because it is the most frequently used and is one of the most aggressive tests for assessing stone decay in the laboratory (Molina *et al.*, 2015). Moreover the principal forms of decay that have been observed in the stone surfaces of the analyzed portals and walls reported in Chapters 3 and 4 (*e.g.* growing of some salt species by alternative cycles of wetting and drying; surface oxidation; expansion and contraction; weakness and embrittlement of stone surfaces) are caused by the effect of the salt crystallization (El-Gohary, 2015).

The degree of deterioration was controlled by measuring the weight changes ($\Delta M\%$) every cycle and the loss of fragments along the edges. Salt crystallization test (UNI EN 12370, 2001) was performed on 32 cubic specimens (5 cm sides), 8 for each lithotype, which underwent fifteen 2-h cycles at 20°C of total immersion in an aqueous solution of decahydrate sodium sulphate ($\text{Na}_2\text{SO}_4 \cdot 10\text{H}_2\text{O}$) at 14% v/v and subsequent drying for at least 16h at 105°C . At the end of each cycle, the results were expressed as percentage weight loss ($\Delta M\%$) due to degradation by salts crystallization and samples were photographed for each cycle until reaching the end of the test (Fig. 8.1). Samples, at the end of the 15th

cycle, were washed in order to remove the salts form the void space and dried till constant weight. The percentage weight loss after water washing has been expresses as $\Delta f\%$.

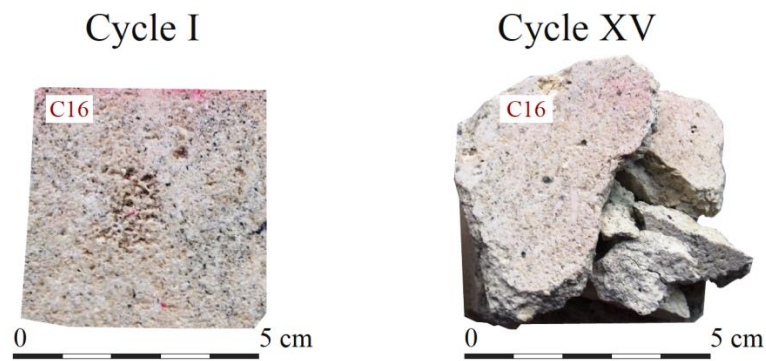


Fig. 8.1. Specimen C16 of San Lucido calcarenite before and after the salt crystallization test.

8.3.2 Results of the salt crystallization test

The results of the salt crystallization test are reported into binary diagrams (Figs. 8.2 a, b, c, d), showing the curves relative to the modification trend of specimens' weight within the fifteen cycles. The weight variations ($\Delta M\%$) for each cycle, at the end of the fifteenth cycle ($\Delta 15$) and after water washing (Δf) are reported in Tables 8.1, 8.2, 8.3, 8.4.

During the crystallization test, GF specimens are characterized by a slight and constant mass increase (Fig. 8.2 a), due to the crystallization of salts within the pore structure and within the microcracks, reaching the maximum value of mass increase at the end of the test with 0.14% for the samples G19 and G21 (Table 8.1). At the end of the fifteenth cycle the specimens display an average weight increase of 0.13% and the final average weight increase after water washing is 0.12%. GF shows an increase of weight during the first 15 cycles and after water washing, which is probably due to the accumulation of salts in the small voids of this material, which could not be removed by washing. None of the sample show changes in shape or broken parts.

Table 8.1. Weight variations ($\Delta M\%$) of San Giovanni in Fiore granite specimens for each cycle, at the end of the 15th cycle and after water washing are listed.

Sample	ΔM_0	ΔM_1	ΔM_2	ΔM_3	ΔM_4	ΔM_5	ΔM_6	ΔM_7	ΔM_8	ΔM_9	ΔM_{10}	ΔM_{11}	ΔM_{12}	ΔM_{13}	ΔM_{14}	Δ_{15}	Δ_f
G15	0.00	0.02	0.03	0.04	0.05	0.07	0.08	0.09	0.09	0.10	0.10	0.10	0.11	0.12	0.12	0.13	0.12
G16	0.00	0.02	0.03	0.04	0.05	0.08	0.09	0.09	0.09	0.10	0.11	0.11	0.11	0.12	0.12	0.13	0.12
G17	0.00	0.02	0.03	0.04	0.05	0.07	0.08	0.09	0.10	0.10	0.10	0.11	0.11	0.11	0.12	0.13	0.12
G18	0.00	0.02	0.03	0.04	0.04	0.07	0.08	0.09	0.09	0.09	0.10	0.11	0.11	0.12	0.12	0.13	0.12
G19	0.00	0.02	0.03	0.04	0.05	0.08	0.09	0.10	0.11	0.11	0.11	0.11	0.12	0.12	0.13	0.14	0.13
G20	0.00	0.02	0.03	0.04	0.04	0.07	0.08	0.08	0.09	0.10	0.10	0.10	0.11	0.11	0.12	0.12	0.11
G21	0.00	0.02	0.03	0.05	0.05	0.07	0.08	0.10	0.10	0.11	0.11	0.11	0.12	0.13	0.13	0.14	0.13
G22	0.00	0.02	0.03	0.04	0.04	0.07	0.08	0.08	0.08	0.09	0.08	0.08	0.09	0.09	0.09	0.10	0.09
mean value	0.00	0.02	0.03	0.04	0.05	0.07	0.08	0.09	0.09	0.10	0.10	0.10	0.11	0.12	0.12	0.13	0.12
st. dev.	0.00	0.00	0.00	0.00	0.00	0.00	0.00	0.01	0.01	0.01	0.01	0.01	0.01	0.01	0.01	0.01	0.01

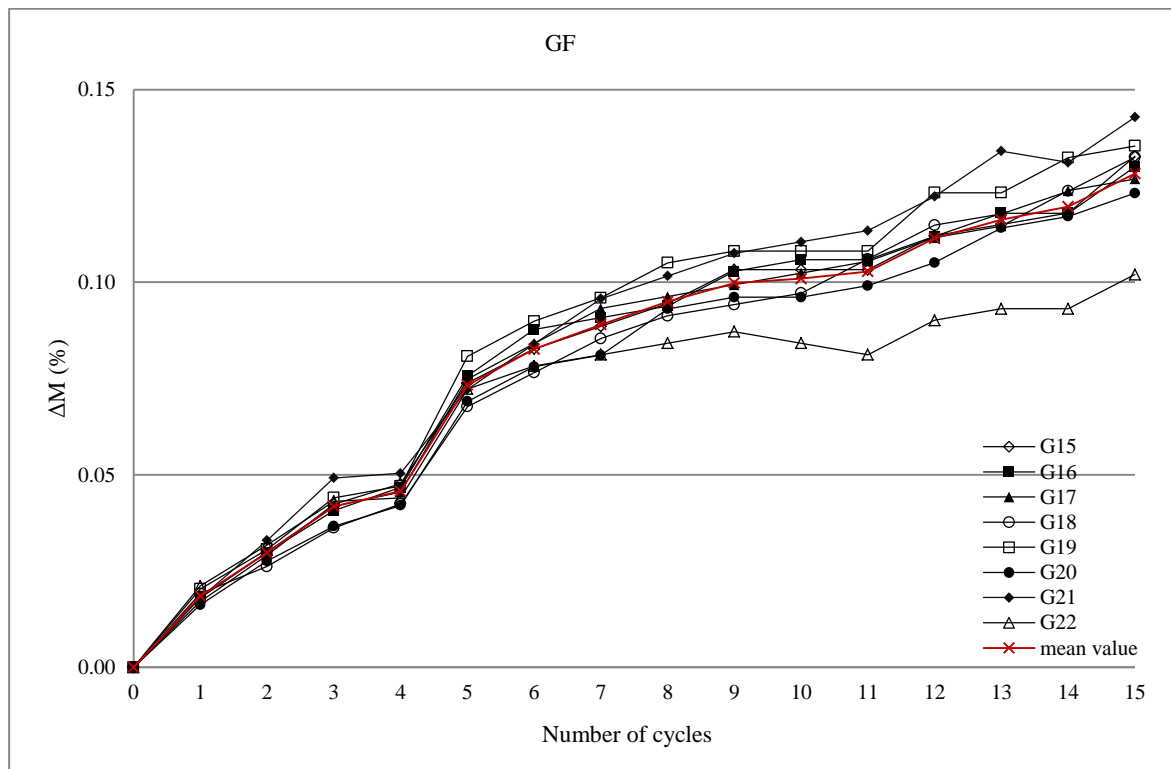


Fig. 8.2 a. Binary diagram showing the weight variation ($\Delta M\%$) of San Giovanni in Fiore granite specimens during the salt crystallization test.

During the first five cycle, all Grisolia stone specimens are characterized by a very slight mass increase (Fig. 8.2 b) ($\approx 0\%$), due to the crystallization of salts within the few pores. From the sixth cycle, a mass loss that remains almost constant for the entire test can be observed. At the end of the fifteenth cycle the specimens display an average weight loss of -0.17% with maximum value of -0.19% for the

sample D21 (Table 8.2). The final average weight loss after water washing is -0.18%. Between the 4th and the 5th cycle a mass decrease is registered, as can be seen in Fig. 8.2 b, probably related to the mass loss observed along the edges of the specimens. None of the sample show changes in shape or broken parts as well as San Giovanni in Fiore granite specimens.

Table 8.2. Weight variations ($\Delta M\%$) of Grisolia stone specimens for each cycle, at the end of the 15th cycle and after water washing are listed.

Sample	ΔM_0	ΔM_1	ΔM_2	ΔM_3	ΔM_4	ΔM_5	ΔM_6	ΔM_7	ΔM_8	ΔM_9	ΔM_{10}	ΔM_{11}	ΔM_{12}	ΔM_{13}	ΔM_{14}	ΔM_{15}	Δ_f
D15	0.00	0.01	0.01	0.01	0.00	-0.18	-0.18	-0.18	-0.18	-0.17	-0.16	-0.15	-0.14	-0.13	-0.13	-0.17	-0.17
D16	0.00	0.00	0.00	0.00	0.00	-0.18	-0.18	-0.18	-0.18	-0.18	-0.17	-0.17	-0.17	-0.16	-0.16	-0.17	-0.19
D17	0.00	0.01	0.01	0.00	0.00	-0.18	-0.18	-0.18	-0.17	-0.14	-0.14	-0.14	-0.13	-0.11	-0.12	-0.14	-0.16
D18	0.00	0.01	0.00	0.01	0.01	-0.18	-0.18	-0.17	-0.17	-0.15	-0.15	-0.14	-0.13	-0.13	-0.13	-0.16	-0.17
D19	0.00	0.01	0.00	0.00	0.00	-0.18	-0.18	-0.18	-0.18	-0.18	-0.17	-0.16	-0.16	-0.15	-0.14	-0.17	-0.18
D20	0.00	0.00	0.01	0.01	0.00	-0.18	-0.17	-0.16	-0.16	-0.16	-0.15	-0.15	-0.14	-0.13	-0.13	-0.17	-0.18
D21	0.00	0.01	0.01	0.00	0.00	-0.19	-0.18	-0.18	-0.18	-0.18	-0.17	-0.16	-0.16	-0.16	-0.16	-0.19	-0.20
D22	0.00	0.01	0.00	0.00	0.00	-0.18	-0.18	-0.18	-0.18	-0.17	-0.16	-0.16	-0.15	-0.15	-0.15	-0.18	-0.19
mean value	0.00	0.01	0.01	0.00	0.00	-0.18	-0.18	-0.17	-0.17	-0.17	-0.16	-0.15	-0.15	-0.14	-0.14	-0.17	-0.18
st. dev.	0.00	0.00	0.00	0.00	0.00	0.00	0.00	0.01	0.01	0.01	0.01	0.01	0.01	0.02	0.01	0.01	0.01

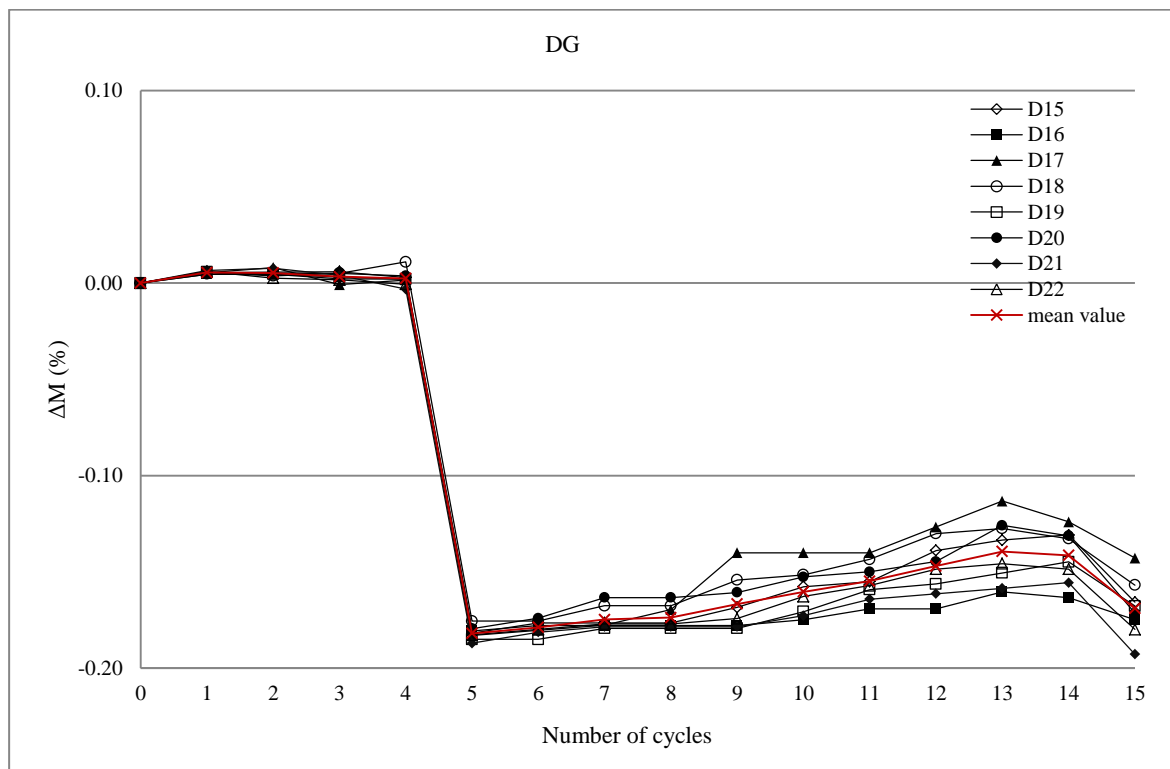


Fig. 8.2 b. Binary diagram showing the weight variation ($\Delta M\%$) of Grisolia stone specimens during the salt crystallization test.

During the first five cycles, all San Lucido calcarenite specimens are characterized by a slight mass increase (Fig. 8.2 c) due to the crystallization of salts within the pore structure. The maximum value of mass increases from the initial weight is 0.74% for the sample C21 (Table 8.3). From the sixth cycle, a mass loss (which is particularly evident from the tenth cycle) can be observed and the specimens begin to degrade, mainly exhibiting smoothing of corners and edges, granular disaggregation and selective degradation dependent on fossil fragments. At the end of the fifteenth cycle the specimens display an average weight loss of -0,18% with maximum value of -0.48% for the sample C16. The final average weight loss after water washing is -0.24%. The sample C16 at the end of the test has broken. In the first stage (up until the 2nd cycle), the porous system was saturated with salt solution; from the 3rd and 4th cycle onwards, fragments began to fall off the samples. This decay continued until it reached the Cycle 10, by which time the sample had already lost more material. In these cycles the decay took the form of spalling on planes parallel to the preferential orientation of the clasts and the loss of small fragments. This form of decay could be defined as *delamination* or even *exfoliation* and *sanding* (Vergès-Belmin, 2008). From Cycle 11 the loss of material resumed and continued until the end of the test. This further decay was due to new salt solution getting into the fissures that had developed between the sedimentary planes, so producing an increase in salt crystallization pressure (Anania *et al.*, 2012).

Table 8.3. Weight variations ($\Delta M\%$) of San Lucido calcarenite specimens for each cycle, at the end of the 15th cycle and after water washing are listed. The averages at the 15th cycle (Δ_{15}) and after water washing (Δ_f) are calculated by excluding the broken samples.

Sample	ΔM_0	ΔM_1	ΔM_2	ΔM_3	ΔM_4	ΔM_5	ΔM_6	ΔM_7	ΔM_8	ΔM_9	ΔM_{10}	ΔM_{11}	ΔM_{12}	ΔM_{13}	ΔM_{14}	Δ_{15}	Δ_f
C15	0.00	0.22	0.40	0.55	0.63	0.69	0.64	0.60	0.57	0.53	0.31	0.17	0.08	-0.09	-0.23	-0.27	-0.29
C16	0.00	0.26	0.47	0.64	0.68	0.54	0.38	0.33	0.22	0.09	-0.10	-0.30	-0.34	-0.37	-0.40	-0.48	/
C17	0.00	0.27	0.49	0.67	0.73	0.65	0.63	0.57	0.45	0.38	0.34	0.20	0.15	0.07	0.05	0.00	-0.20
C18	0.00	0.26	0.47	0.58	0.63	0.66	0.62	0.60	0.55	0.45	0.33	0.25	0.23	0.15	-0.02	-0.08	-0.16
C19	0.00	0.23	0.40	0.55	0.63	0.65	0.61	0.61	0.48	0.44	0.36	0.24	0.19	0.05	-0.05	-0.21	-0.26
C20	0.00	0.24	0.44	0.61	0.63	0.59	0.50	0.45	0.42	0.35	0.20	0.07	0.00	-0.05	-0.19	-0.31	-0.43
C21	0.00	0.26	0.47	0.65	0.73	0.74	0.68	0.55	0.42	0.34	0.27	0.23	0.13	0.06	-0.01	-0.11	-0.27
C22	0.00	0.21	0.36	0.51	0.59	0.64	0.61	0.53	0.44	0.37	0.27	0.14	0.10	0.05	0.04	0.01	-0.09
mean value	0.00	0.24	0.44	0.59	0.66	0.65	0.58	0.53	0.44	0.37	0.25	0.13	0.07	-0.01	-0.10	-0.18	-0.24
st. dev.	0.00	0.02	0.04	0.06	0.05	0.06	0.10	0.10	0.11	0.13	0.15	0.18	0.18	0.16	0.16	0.17	0.11

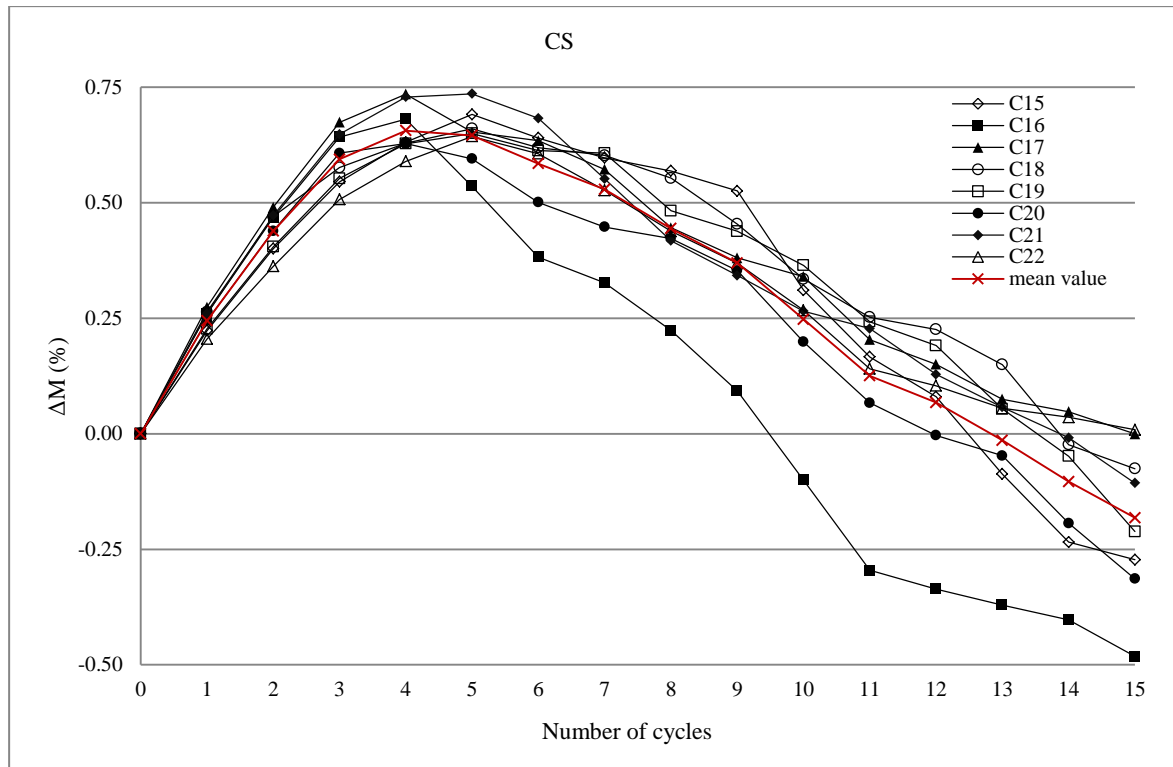


Fig. 8.2 c. Binary diagram showing the weight variation ($\Delta M\%$) of San Lucido calcarenite specimens during the salt crystallization test.

During the salt test, all Fuscaldo sandstone specimens are characterized by a mass increase (Fig. 8.2 d) due to the crystallization of salts within the pore structure, except for the sample A21 that shows a mass loss since the seventh cycle. The maximum value of mass increases from the initial weight is 2.36% for the sample A20 (Table 8.4). Only two specimens, A15 and A20, reach the end of the test. The majority of the samples broke during the test, starting from the seventh cycle. The specimens degraded, mainly exhibiting smoothing of corners and edges, granular disaggregation, selective degradation and evident fractures. At the end of the fifteenth cycle the average weight increase is of 2.06% and the final average weight increase after water washing is 1.90%.

Table 8.4. Weight variations ($\Delta M\%$) of Fuscaldo sandstone specimens for each cycle, at the end of the 15th cycle and after water washing are listed. The averages at the 15th cycle (Δ_{15}) and after water washing (Δ_f) are calculated by excluding the broken samples.

Sample	ΔM_0	ΔM_1	ΔM_2	ΔM_3	ΔM_4	ΔM_5	ΔM_6	ΔM_7	ΔM_8	ΔM_9	ΔM_{10}	ΔM_{11}	ΔM_{12}	ΔM_{13}	ΔM_{14}	Δ_{15}	Δ_f
A15	0.00	0.23	0.43	0.69	0.85	0.98	1.11	1.25	1.35	1.39	1.38	1.47	1.59	1.72	1.71	1.73	1.44
A16	0.00	0.16	0.40	0.75	0.97	1.17	1.39	1.64	1.91	/	/	/	/	/	/	/	/
A17	0.00	0.30	0.60	0.98	1.19	1.13	1.17	1.25	/	/	/	/	/	/	/	/	/
A18	0.00	0.30	0.57	0.92	1.10	1.10	1.22	1.38	1.56	1.61	/	/	/	/	/	/	/
A19	0.00	0.32	0.61	1.02	1.27	1.41	1.65	1.80	1.71	/	/	/	/	/	/	/	/
A20	0.00	0.20	0.38	0.61	0.78	0.90	1.06	1.20	1.36	1.60	1.60	1.75	1.93	2.08	2.21	2.38	2.36
A21	0.00	0.29	0.56	0.92	0.99	0.76	0.63	0.48	0.31	/	/	/	/	/	/	/	/
A22	0.00	0.24	0.48	0.79	0.98	1.06	1.28	1.47	1.68	1.80	1.80	1.70	1.70	/	/	/	/
mean value	0.00	0.25	0.50	0.84	1.02	1.06	1.19	1.31	1.41	1.60	1.59	1.64	1.74	1.90	1.96	2.06	1.90
st. dev.	0.00	0.06	0.09	0.15	0.16	0.20	0.29	0.39	0.53	0.17	0.21	0.15	0.17	0.26	0.35	0.46	0.65

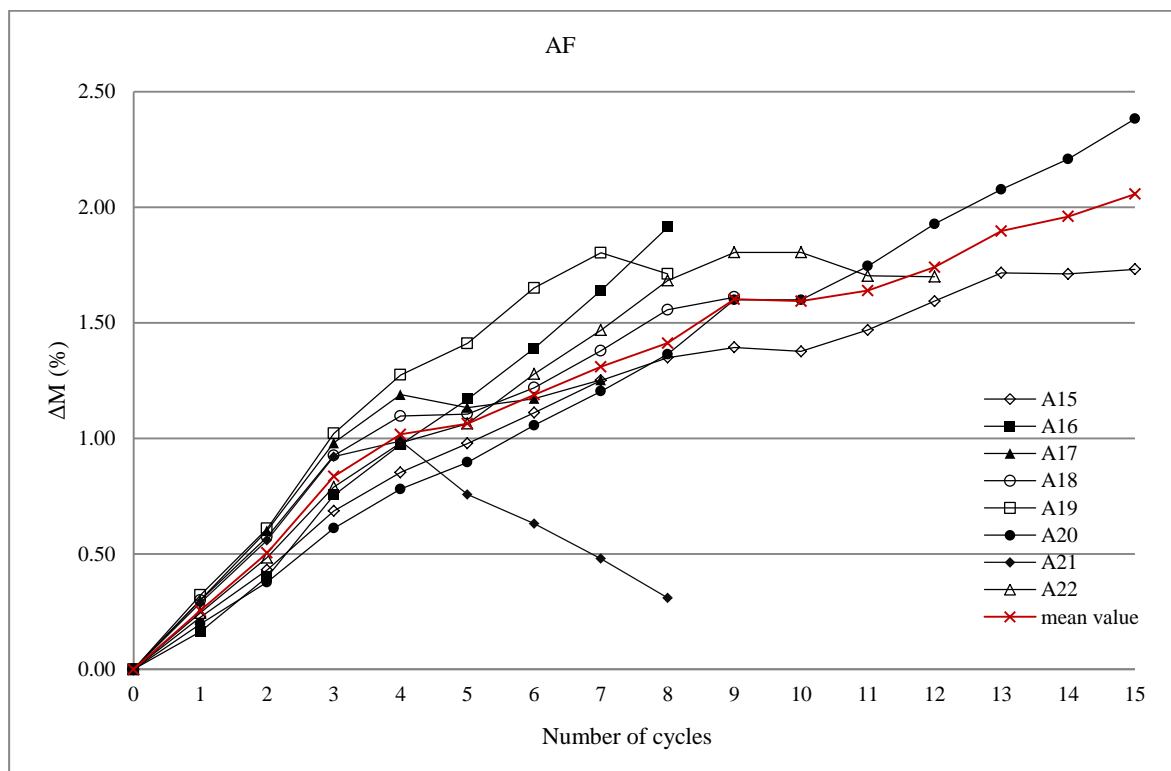


Fig. 8.2 d. Binary diagram showing the weight variation ($\Delta M\%$) of Fuscaldo sandstone specimens during the salt crystallization test.

Mean values of the weight variation (%) for all investigated lithotypes are reported in [Table 8.5](#), both at the end of the 15th cycle and after water washing.

Table 8.5. Mean values and standard deviation of the weight variations ($\Delta M\%$) of all specimens (GF, DG, CS and AF) at the end of the 15th cycle and after water washing are listed. The averages at the 15th cycle (Δ_{15}) and after water washing (Δ_f) are calculated by including all the samples (broken samples too).

Sample		Δ_{15}	Δ_f
GF	mean value	0.13	0.12
	<i>st.dev.</i>	0.01	0.01
DG	mean value	-0.17	-0.18
	<i>st.dev.</i>	0.01	0.01
CS	mean value	-0.18	-0.24
	<i>st.dev.</i>	0.17	0.11
AF	mean value	1.58	1.90
	<i>st.dev.</i>	0.60	0.65

8.3.3 Discussion of the salt crystallization test

The damage caused by the ageing tests of salt crystallization is conditioned by the voids. After 15 cycles of salt crystallization, San Giovanni in Fiore granite and Grisolia stone, with an effective porosity of less than 1.35% and 0.54%, respectively, were practically unaffected and maintained their original shape (Fig. 8.3). As can be observed in Table 8.5, the mean values of the weight variations are very low, less than <1%. Sousa *et al.* (2005) observed that since salt crystallization is conditioned by voids or porosity, the damage caused by ageing tests in granites with open porosities of under 1.5% was practically zero after 100 salt crystallization cycles. This would explain why GF was undeteriorated after the salt crystallization test.

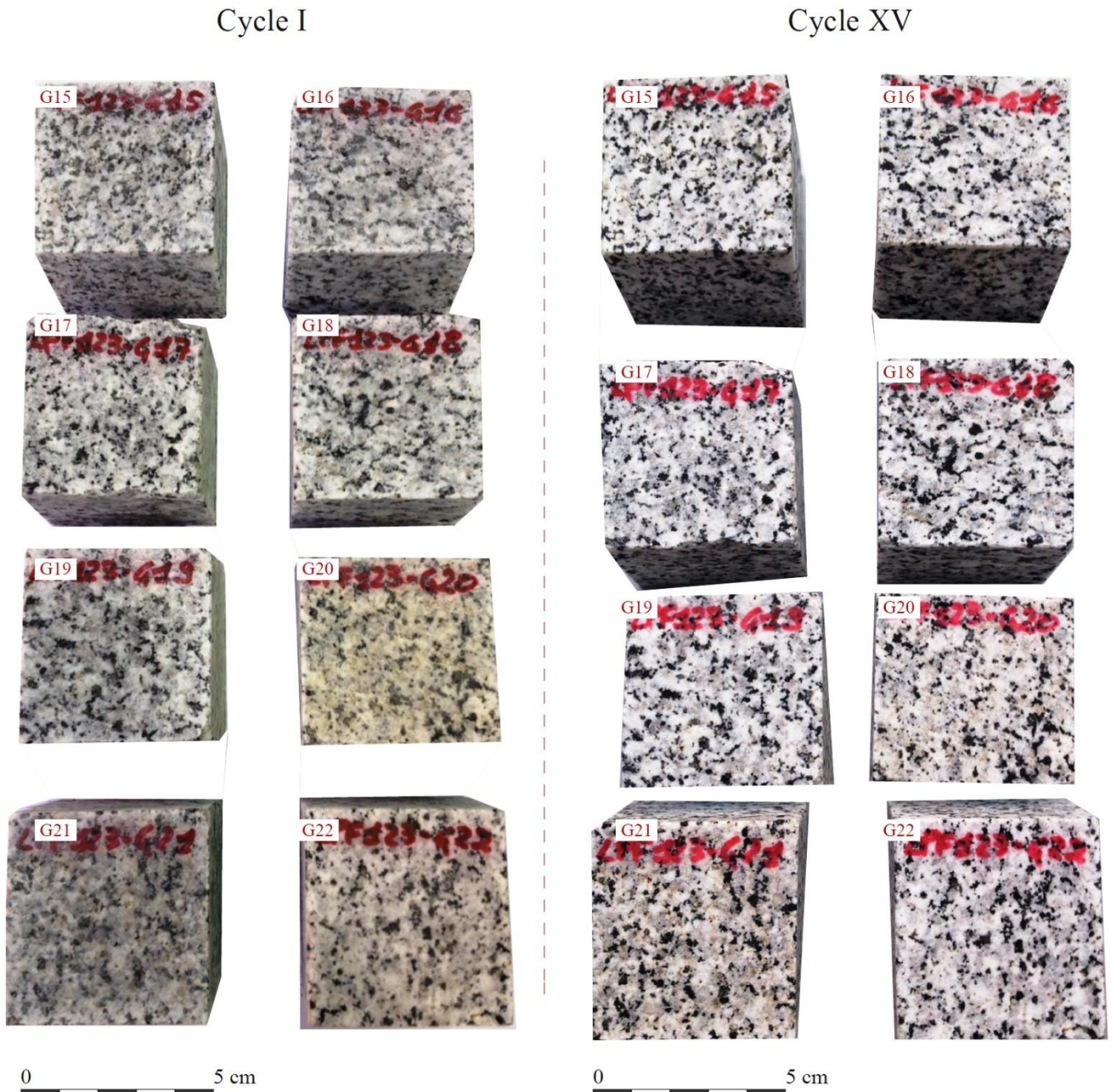


Fig. 8.3. San Giovanni in Fiore granite specimens before and after the salt crystallization test.

As can be seen in Fig. 8.3 and Fig. 8.4, samples of GF and DG maintained their original forms. Only edges have been slightly rounded. As can be observed in Fig. 8.4, an increase in surface roughness of DG specimens is observed, and the presence of components and structures not visible before the aging test could be also observed at the end of the 15th cycle.

Cycle I

Cycle XV

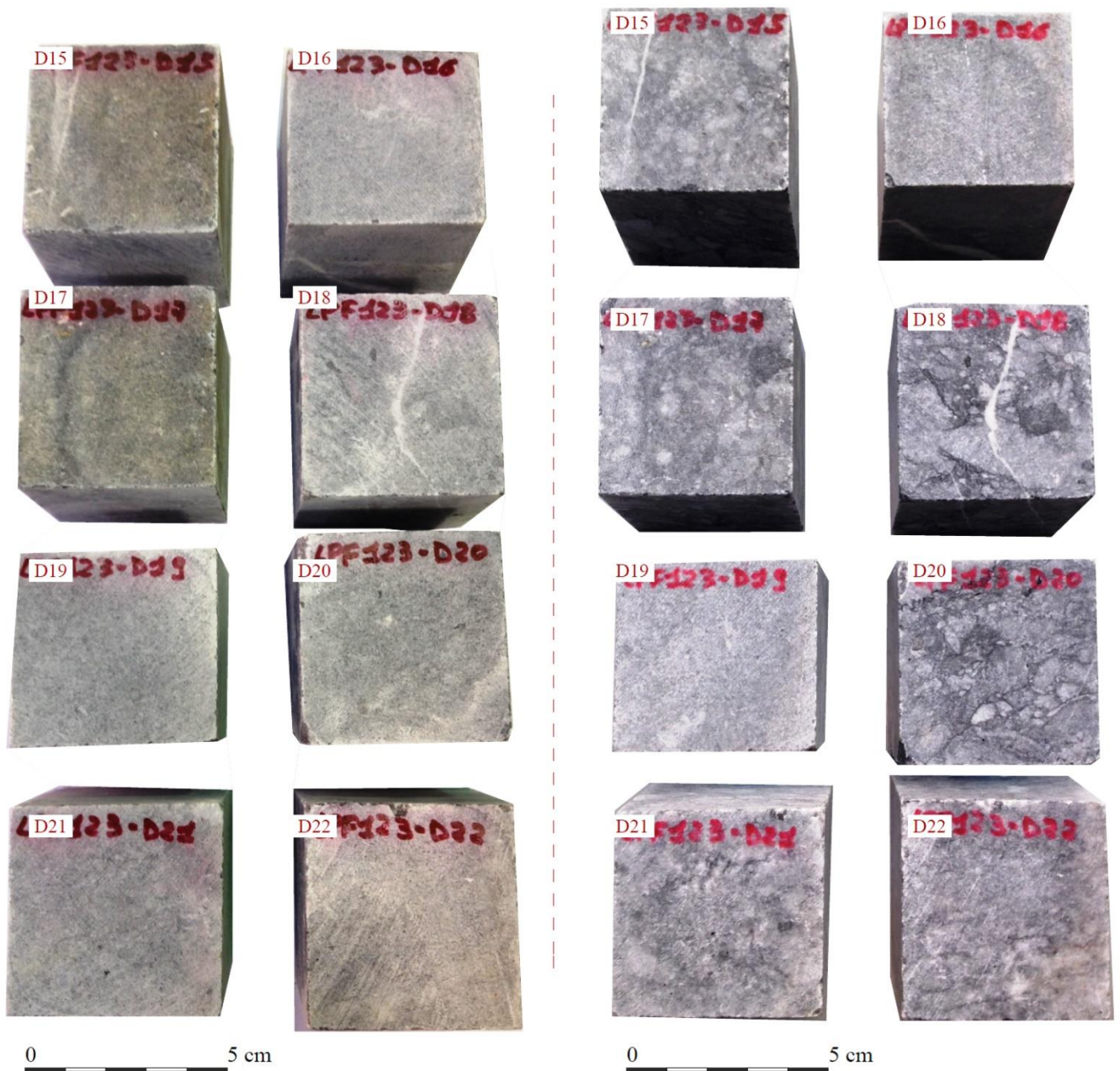


Fig. 8.4. Grisolia stone specimens before and after the salt crystallization test.

San Lucido calcarenite reached at the end of the test a very low weight loss but samples were affected by starting form of degradation, especially with the smoothing of the corners and one sample broke. When porosity increases, material weight variation becomes more significant (Sousa *et al.*, 2005). This is the case of San Lucido calcarenite and Fuscaldó sandstone. In fact, a final weight loss of -

0.24% and a weight increase of 1.90%, have been registered, respectively. For both investigated stone types an increase in weight was observable for the first cycles, which is the consequence of salt enrichment. Granular disintegration occurred at the edges of the majority of specimens.

The visual deterioration observed after ageing (Fig. 8.5) consisted in morphologies similar to those defined in limestone by other authors (Ordoñez *et al.*, 1997; Fort *et al.*, 2008). San Lucido calcarenite specimens showed dimensional losses essentially around the vertices and edges of the stone cubes, ranging from 2.0 to 5.0 mm in depth. The face opposite the side on which the cubes rested during the crystallization test, exhibited the severest deterioration, rounding down to a final size of about 20 mm in diameter. This top-side concentration of deterioration was favoured by test conditions and characteristics. Where deterioration was most intense, cracks perpendicular to this side appeared, which developed into loose membranes. The studied calcarenite is slight sensitive to degradation induced by salt crystallization. The mass loss, even though is not very high, during the test mostly depends on the open porosity of 16.18±0.81%. As known, in fact, only the open pores are interested by salt crystallization, so that the higher the open porosity, the higher the amount of salts which crystallizes causing the disaggregation of the sample and the consequent mass loss (Anania *et al.*, 2012). The calcarenite of this study is characterized not only by high porosity, but also by a chemical composition dominated by calcium carbonates, which, is known, gives the stone a high susceptibility to acid attack by gaseous atmospheric pollutants (Zaouia *et al.*, 2005). The possible interaction between calcarenite and atmospheric pollutants could be accompanied by structural degradation. The most frequent weathering minerals for buildings are gypsum and salts of Na, Cl and K. It can be said that their crystallization could be responsible for most of the damages in the monuments built with San Lucido calcarenite as in the calcareous monumental stones of the Mediterranean region exposed to weathering agents (Zezza, 1993).

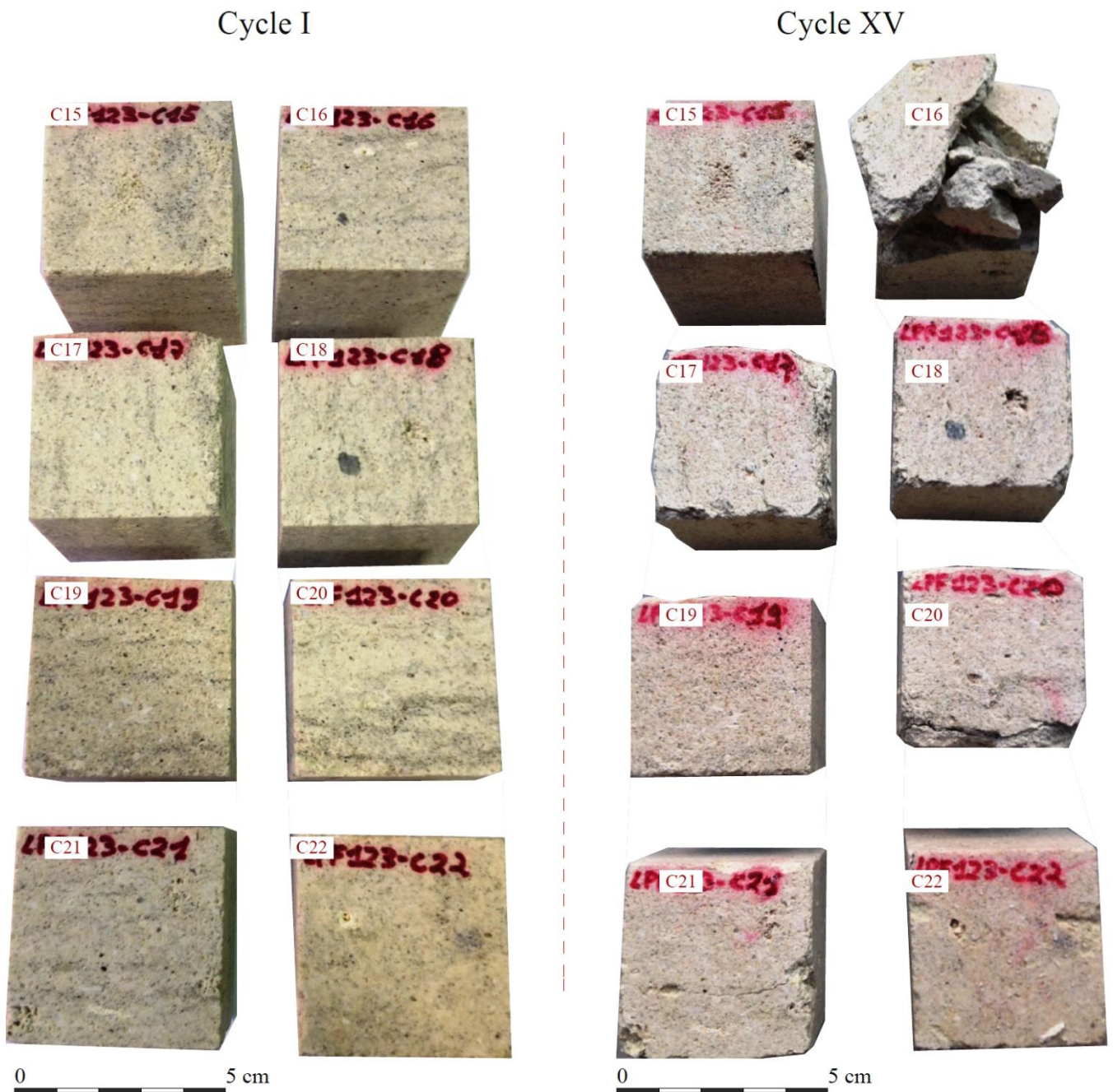


Fig. 8.5. San Lucido calcarenite specimens before and after the salt crystallization test.

Concerning the deterioration of Fuscaldo sandstone it can be observed that specimens broke according to preferential directions, along planes parallel to each other (Fig. 8.6). Fissures were produced by the pressure caused by salt crystallization (Molina *et al.*, 2015). The result is the delamination of the sample in layers with an average thickness of 10-15 mm. This form of deterioration is in accordance with the anisotropy values obtained; in particular, the high value of total anisotropy that

indicates the presence of a prevalent anisotropic direction, probably corresponding to those planes. Maximum deterioration occurred when the top eroded and the patches worked loose from the surface (spalling). The result on the specimens surface is the disaggregation and powdery. The lateral faces were also rounded as well as the edges.

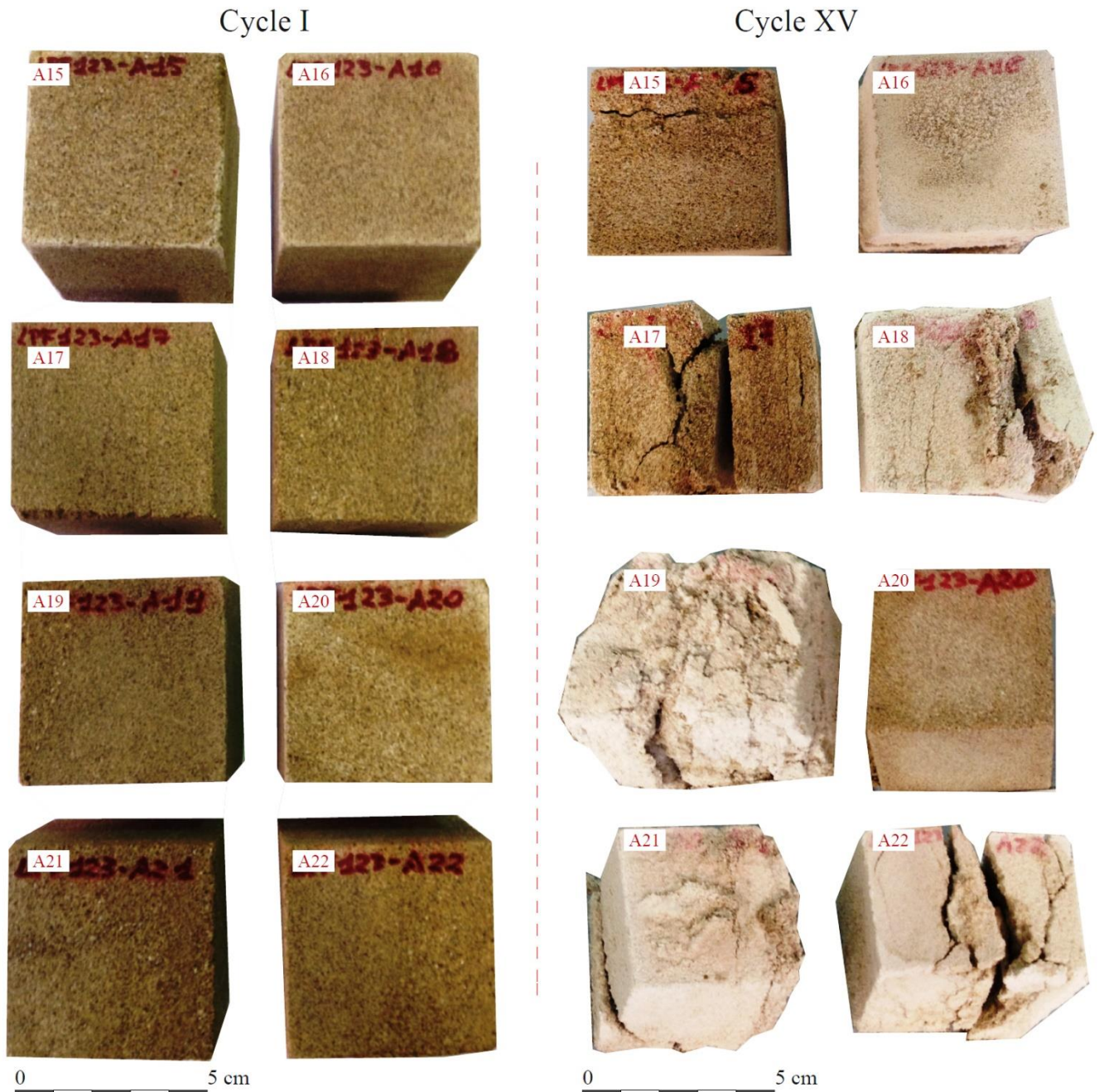


Fig. 8.6. Fuscaldo sandstone specimens before and after the salt crystallization test.

The correlation between open porosity and weight variation is shown in Fig. 8.7. The mass loss during the test mostly depends on the open porosity as well as on the dimensional distribution of pores that determine the crystallization pressure. As known, in fact, only the open pores are interested by salt crystallization so that the higher open porosity the higher amount of salts which crystallize causing the disaggregation of the sample and the consequent mass loss. In all the investigated samples, pores with sizes in the range 1–10 μm predominate, except in the case of GF and DG samples where the greater average diameter of pores determines a loss of the linear relationship between the open porosity and the weight loss, as shown in Fig. 8.7. This is due to the fact that the crystallization stress and, consequently, the mass loss in a large pore is lower than in a smaller one (Zehnder & Arnold, 1989).

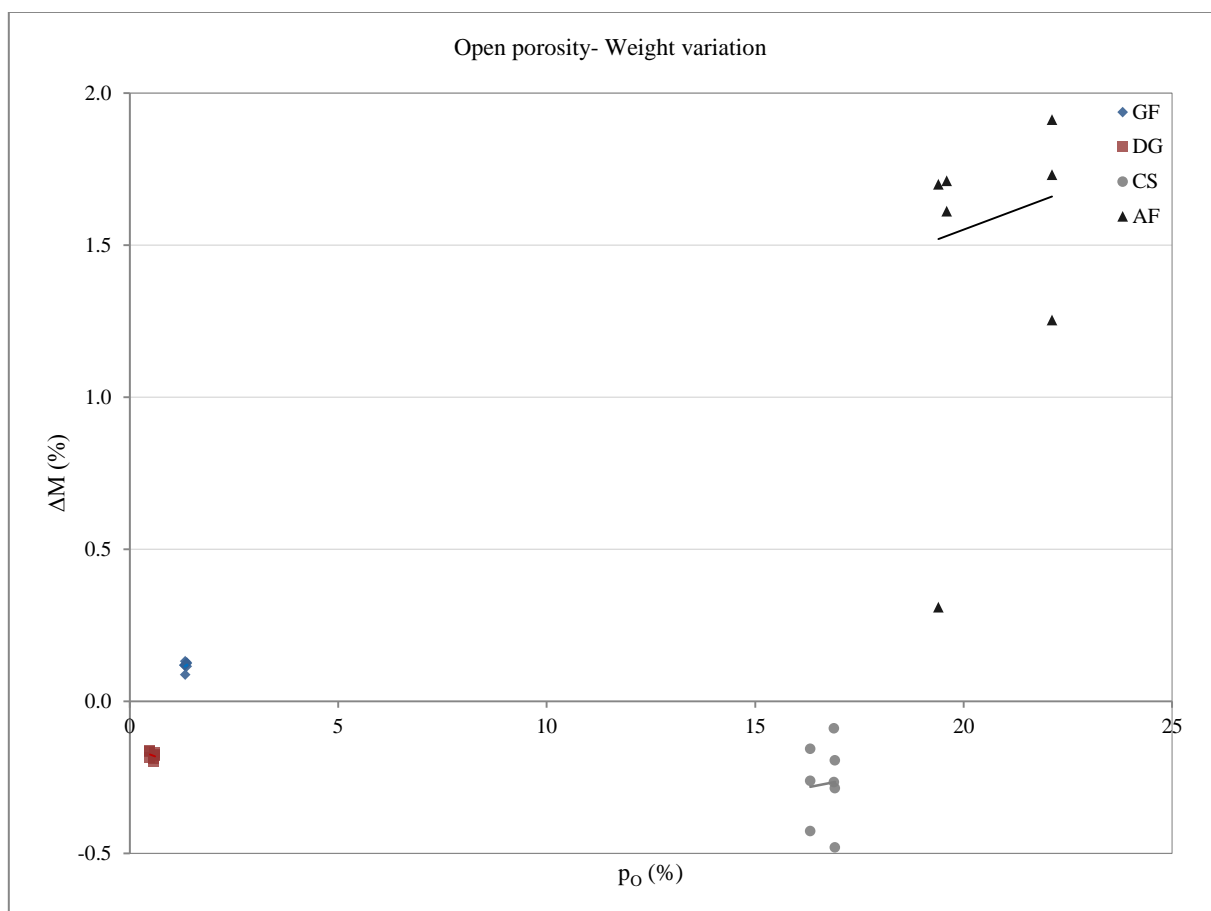


Fig. 8.7. Diagram showing the mass variation of samples due to salt crystallization vs. open porosity.

In conclusion, as expected (Fort *et al.*, 2008), specimens with the highest open porosity values exhibited a more severe deterioration, even though mean values of weight loss reached at the end of the fifteenth cycle are not very high for building materials, as demonstrated by many authors for (Anania *et al.*, 2012; Freire-Lista *et al.*, 2015). So, it can be said that: GF and DG are resistant to salt crystallization; CS is slightly more sensitive to weathering processes due to salt crystallization; while AF, taking into account the high specimens decay (the loss of significant fragments and the rupture of some of them, as shown in Fig. 8.6), is not a durable stone towards decay processes.

8.4 Ice crystallization process

Frost damage – due to alternating water freeze and thaw events - is one of the major causes of building material decay (Molina *et al.*, 2015). Its importance evidently depends on the meteorology but in the majority of European countries this type of decay process is an important issue. The volume expansion during freezing of water, is the primary cause of frost damage (Taber, 1929; Everett, 1961; Walder & Hallet, 1986). The mechanisms of frost damage have been reviewed by Scherer & Valenza (2004). A strong argument that crystallization pressure is the primary source of stress during freezing comes from experiments with organic liquids that contract upon freezing (Taber, 1930; Beaudoin & MacInnis, 1974; Litvan, 1978). In these experiments, dilation and damage of various porous materials were observed with liquids that were less dense than their respective solid phase. In this case, the damage can only be explained in terms of crystallization pressure.

In a porous material, there is no uniform temperature at which the pore water freezes. Apart from the concentration of dissolved salts, the freezing temperature is also affected by pore size. A small ice crystal, *i.e.* a crystal growing in a small pore, has a higher chemical potential and, therefore, a lower freezing temperature than a large crystal.

It is obvious that there is a strong depression of the freezing temperature with decreasing pore size. Therefore, in a porous stone, pure water starts to freeze in large pores and at temperatures only slightly below 0 °C. In small pores (<0.1 μm), water only freezes at significantly lower temperatures. In contrast, there is a significant depression of the freezing temperature in large pores. This means that the ice will only be able to penetrate into a given void size when the temperature is lower than the equilibrium temperature. Consequently, the water in a porous body will crystallize progressively with the decreasing temperature starting in the largest pores (Camuffo, 1996).

There are many theories concerning the ice damage once the ice is formed or has started to form inside the porous material.

The first and most evident cause of damaging – already considered by Hirschwald (1908) – is the 9 per cent volume increase suffered by the water as it solidifies. If the void space is completely (or at least to 91%) filled with water, this volume expansion will exert pressure on the walls of the voids. The explanation seems straightforward enough, but the fact that building materials hardly ever reach such degree of saturation in reality, requires other solutions.

A second theory, strongly connected to the first one, is that when the expansion in some of the pores takes place, it causes the drainage of the still liquid water towards other pores inducing a hydraulic pressure in the material (Powers, 1945). For saturated materials, the generation of hydraulic pressures is commonly considered to be the most important cause of frost deterioration (Pigeon *et al.*, 2003).

A third theory, concerning the frost heave, was introduced to explain the swelling of frozen soil. As explained by Torraca (1982), this model is based on the notion that ice crystals, or ice lenses, grow in relatively large voids (fractures or large pores) but are unable to develop in the small pores, unless under pressure. Water present in the small pores is fed by the growing crystals by diffusion instead of freezing on the spot. If water is still available in the small pores when all the large spaces are occupied, a

pressure is developed which should allow ice crystals to grow also in the small pores. It is interesting to note that the frost heave pressure does not depend upon the fact that water increases in volume when it freezes (Buj Fandos, 2009).

8.5 Freeze-thaw test

8.5.1 Procedure

The freeze-thaw test has been performed only on two lithotypes, granite GF and limestone DG, because they were used as structural and decorative elements in the parts of the Region where the temperature is lower, Sila and Pollino area, respectively.

Freeze-thaw test, together with salt crystallization test, are the most frequently used and the most aggressive tests for assessing stone decay in the laboratory (Molina *et al.*, 2015).

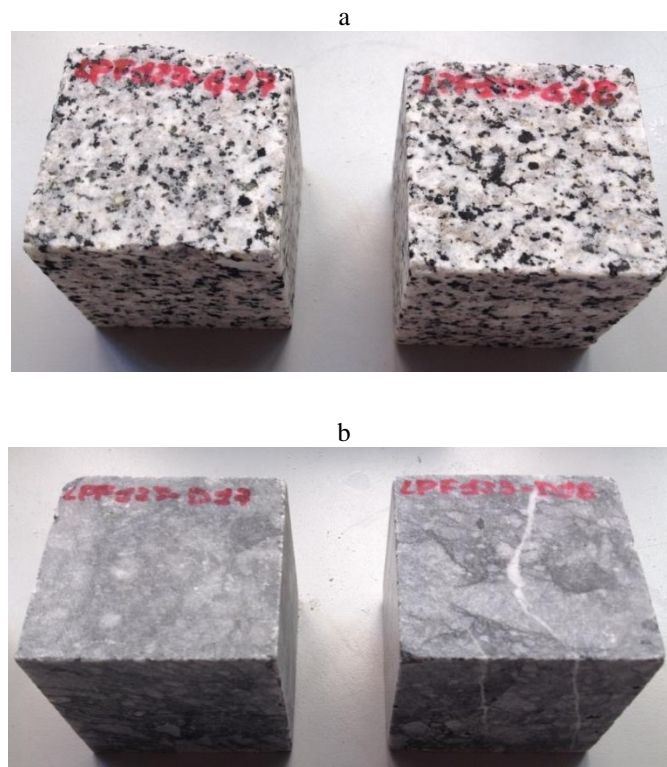
The determination of frost resistance has been carried out according to the European standard UNE-EN 12371 (2011) on 54 cubic orientated specimens (5 cm sides), 27 for each stone type (GF and DG), in an ACS-Angelantoni Environmental test chamber fitted with a control system to programme the freeze-thaw cycles to an accuracy of ± 1.0 °C. Samples were dried till constant weight at 60°C before the test and, after recording their dry weight (w_0), they were saturated by water. A single cycle consisted of two parts: 6 hours of freezing at -15°C and 6 hours of thawing at 20°C. The velocity of heating and cooling was 0.5°C/min. 250 cycles were carried out. The degree of deterioration was controlled by measuring the weight changes (wt.%) in every cycle. The evaluation of the changes were monitored by continuous visual inspection, by the measurement of weight loss and the measurement of the US propagation at the 100th, 200th and 250th cycle, the measurement of the mechanical properties (UCS and R_{tf}) at the end of the test.

8.5.2 Results of the freeze-thaw test

Visual changes

The visual observation of the cubic samples was carried out continuously during the 250 cycles of freeze-thaw test in order to detect the macro scale superficial changes, such as the loss of material and the possible colour changes.

The two stone types showed slight differences to the freeze-thaw process, even though the differences and in general the visual changes are not as pronounced as during the salt crystallization test. The most significant material loss, observable by the naked eye, corresponds to GF. The loss of grains – granular disintegration – could be observed from the 100th cycle, and was getting gradually more severe resulting in a slight material loss on the corners and the edges of the cubes (Fig. 8.8 a). The material loss of DG mostly occurs on the corners and edges of the samples and only after the 250th cycles (Fig. 8.8 b).

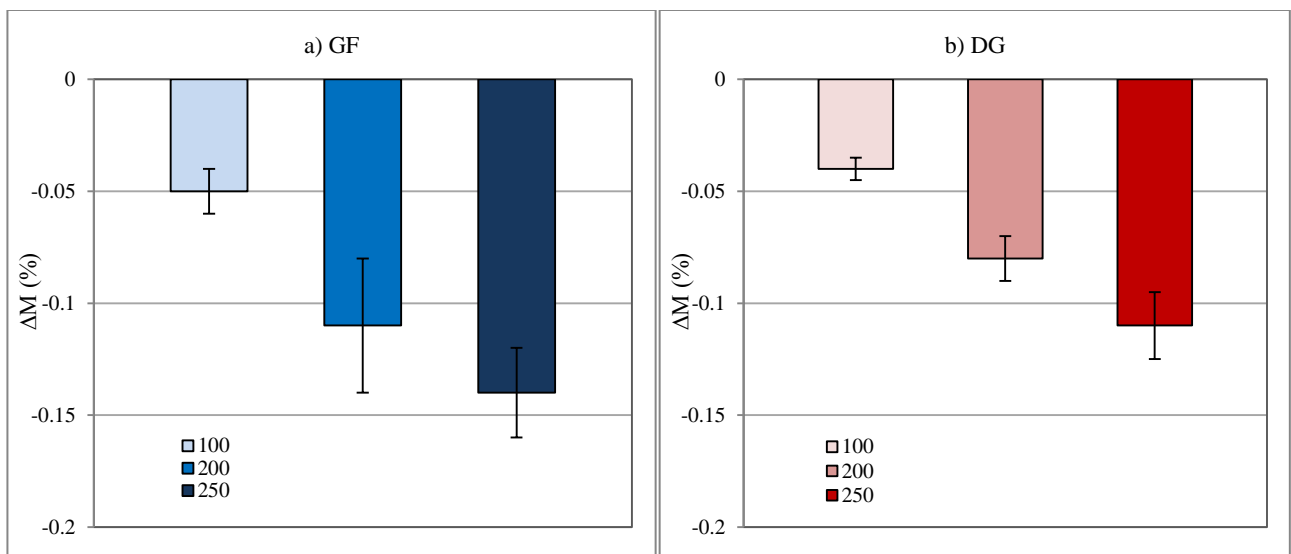


Figs. 8.8 a, b. Slight granular disintegration can be observed on GF after 250 freeze-thaw cycles (a). DG does not show any significant visual changes after 250 freeze-thaw cycles.

Weight loss

In Figs. 8.9 a, b the weight loss – expressed in percentage – is shown after 100 cycles, which means more or less the middle of the test, after 200 cycles and at the end of the test, after 250 cycles.

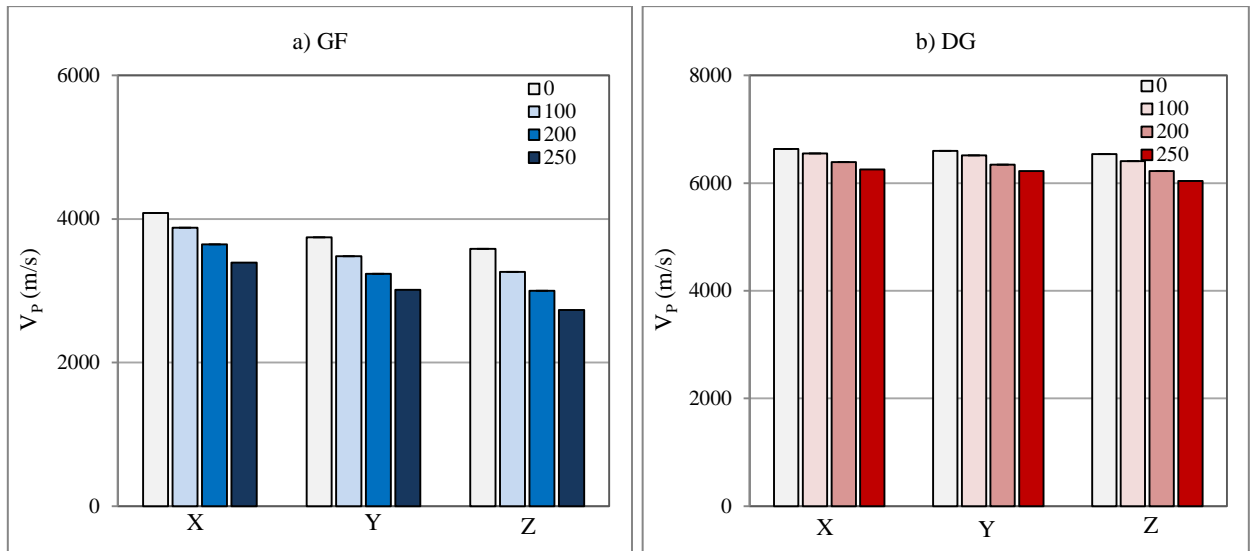
As it can be noticed, all both stones suffer a gradually increasing weight loss during the test. For the highest value is reached by GF, coherently to the visual observations, which reached a weight loss - $0.14 \pm 0.01\%$ at the end of the test while, on the contrary, the material weight increased during the salt crystallization test. For DG samples has been detected a final weight loss of -0.11% , while during the salt crystallization test it showed a higher weight loss value ($-0.18 \pm 0.01\%$). GF showed the highest weight variations.



Figs. 8.9 a, b. Weight loss during the freeze-thaw test for San Giovanni in Fiore granite (a) and Grisolia stone (b).

Ultrasound velocity

The measurement of velocity of P waves provides information about the changes inside the material after the ageing test. It was measured on the dry samples after 100, 200 and 250 cycles. The velocities are shown in Figs. 8.10 a, b in the three spatial directions.



Figs. 8.10 a, b. V_P variations during the freeze-thaw test, along the three axes, for San Giovanni in Fiore granite (a) and Grisolia stone (b).

The highest V_P change for GF occurs almost exclusively during the first 100 cycles, according to other authors that studied similar granites (Freire-Lista *et al.*, 2015 b). Afterwards, the V_P values decrease constantly. Along the Z direction, where the values were originally lower, the decrease is higher as the anisotropy of the stone increases.

The maximum V_P decrease of DG is very low, presenting similar values in all directions, confirming one again the isotropy of the stone. As well as for GF, along the Z axis the highest variation has been registered. The V_P values reached along the three directions are reported in Table 8.6. The final V_P loss is of 20% and 6.4% for GF and DG respectively.

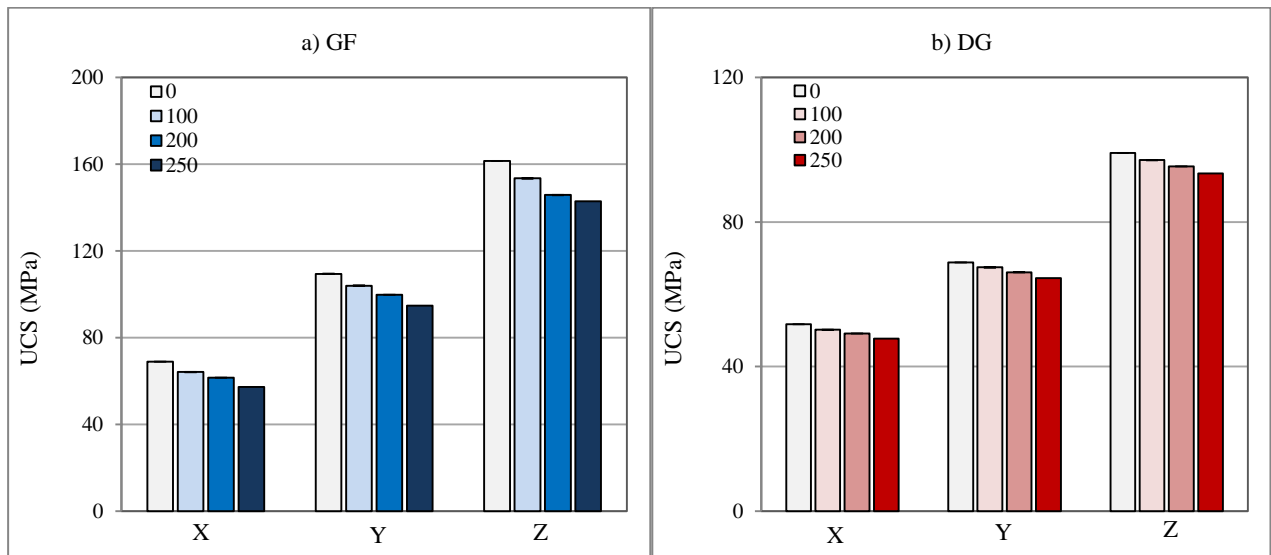
Table 8.6. V_p values during the freeze-thaw test, along the three axes, for San Giovanni in Fiore granite (GF) and Grisolia stone (DG). V_{Px} , V_{Py} , V_{Pz} = ultrasonic velocity (m/s) registered in the directions X, Y and Z; V_p = average ultrasonic velocity (m/s); dM_{Vp} %: total anisotropy index and dm_{Vp} % relative anisotropy index; Δ (%) = V_p variation.

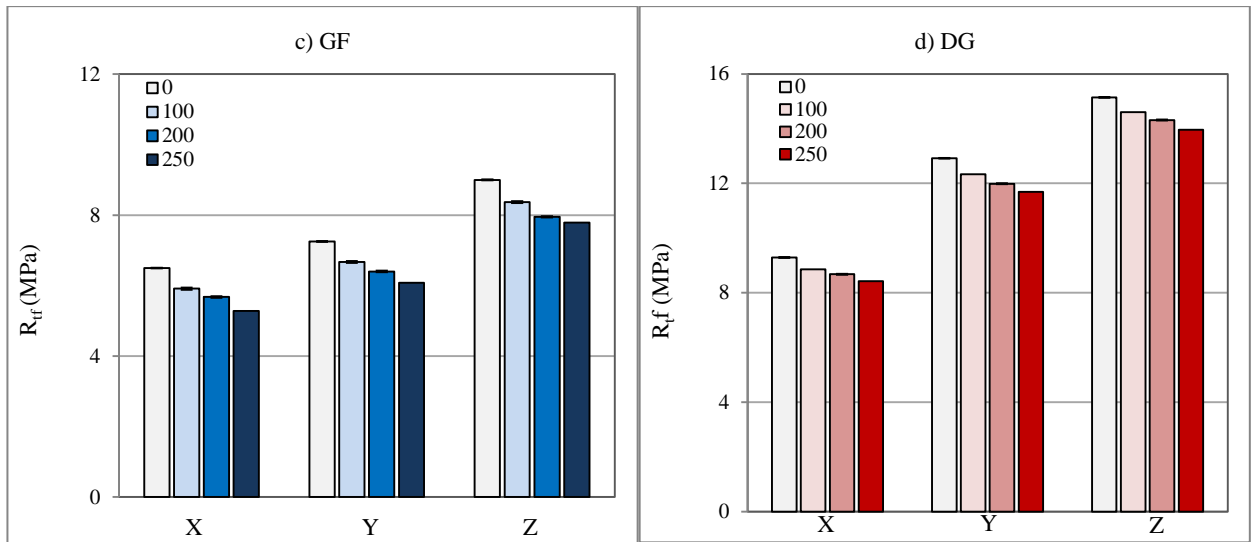
Cycle	V_{Px} (m/s)	V_{Py} (m/s)	V_{Pz} (m/s)	V_p (m/s)	dM_{Vp} (%)	dm_{Vp} (%)
	GF					
0	4082	3744	3585	3804	8.4	8.7
100	3878	3482	3263	3541	11.3	10.8
200	3646	3238	3002	3295	12.8	11.8
250	3390	3011	2731	3044	14.7	11.8
Δ (%)	-17.0	-19.6	-23.8	-20.0		
Cycle	DG					
	V_{Px} (m/s)	V_{Py} (m/s)	V_{Pz} (m/s)	V_p (m/s)	dM_{Vp} (%)	dm_{Vp} (%)
0	6633	6600	6542	6592	1.1	0.5
100	6553	6515	6411	6493	1.9	0.6
200	6389	6345	6225	6320	2.2	0.7
250	6255	6225	6038	6173	3.2	0.5
Δ (%)	-5.7	-5.7	-7.7	-6.4		

Mechanical properties

Uniaxial compressive strength and flexural strength values, UCS and R_{tf} , are reported in [Figs.](#)

8.11 a, b, c, d.





Figs. 8.11 a, b, c, d. UCS (a, b) and R_{tf} (c, d) variations during the freeze-thaw test along the three axes.

As expected, the mechanical properties decreased after the ageing test. Coherently to the visual observations and the V_p test, GF suffered the highest variations, while DG the lowest. As well as the mechanical tests performed on the fresh samples, the highest strengths were reached along the Z-axis while the lowest along the X-axis.

At the end of the test, the UCS decrease was of 5.5% for GF and of 6.4% for DG while the R_{tf} registered higher decrease variations, of 18.5% and 6.8%, for GF and DG, respectively (Table 8.7).

Table 8.7. Mechanical values during the freeze-thaw test, along the three axes, for San Giovanni in Fiore granite (GF) and Grisolia stone (DG). UCS_x , UCS_y , UCS_z = uniaxial compressive strength (MPa) registered in the directions X, Y and Z; UCS = average uniaxial compressive strength (MPa); R_a and max/min: uniaxial compressive anisotropy indices; R_{tfx} , R_{tfy} , R_{tfz} = flexural strength (MPa) registered in the directions X, Y and Z; R_{tf} = average flexural strength (MPa); $R_{a_{tf}}$ and max/min: flexural anisotropy indices; Δ (%) = mechanical values variation.

	UCS_x (MPa)	UCS_y (MPa)	UCS_z (MPa)	UCS (MPa)	R_a	max/min
Cycle	GF					
0	69.00	109.44	161.50	104.07	0.9	2.3
100	64.17	103.97	153.43	107.19	0.8	2.4
200	61.60	99.81	145.75	102.39	0.8	2.4
250	57.29	94.82	142.84	98.32	0.9	2.5
Δ (%)	-17.0	-13.4	-11.6	-5.5		
	DG					
0	51.74	68.83	99.10	73.22	0.6	1.9
100	50.18	67.46	97.12	71.59	0.7	1.9
200	49.18	66.11	95.37	70.22	0.7	1.9
250	47.70	64.45	93.46	68.54	0.7	2.0
Δ (%)	-7.8	-6.4	-5.7	-6.4		
	GF					
	R_{tfX} (MPa)	R_{tfY} (MPa)	R_{tfZ} (MPa)	R_{tf} (MPa)	$R_{a_{tf}}$	max/min
Cycle	GF					
0	6.50	7.25	9.00	7.83	0.3	1.4
100	5.91	6.67	8.37	6.98	0.4	1.4
200	5.68	6.40	7.95	6.68	0.3	1.4
250	5.28	6.08	7.79	6.38	0.4	1.5
Δ (%)	-18.8	-16.1	-13.4	-18.5		
	DG					
0	9.29	12.91	15.14	12.19	0.5	1.6
100	8.86	12.33	14.61	11.93	0.5	1.6
200	8.68	11.99	14.32	11.66	0.5	1.6
250	8.42	11.69	13.96	11.35	0.5	1.7
Δ (%)	-9.4	-9.5	-7.8	-6.8		

8.5.3 Discussion of results of freeze-thaw test

The freeze–thaw test did not cause any significant visible damage and there were no very important changes in the weight of the samples. However, the ultrasound readings show that the stones did suffer the ageing test, with a fall in V_p , especially from Cycle 100 onwards. Similarly to the salt crystallization test, this fall is probably due to the rise of small cracks that cannot be observed with the naked eye (Molina *et al.*, 2015).

GF suffered the highest damage out of the two stone types taking into account all the evaluated parameters.

The V_p values suggest an increasing number of cracks in the material, because the P-wave velocity – among other parameters – depends on the number of discontinuities inside the material (Delgado Rodrigues, 2000). So, the detected decrease could be related to the appearance of new cracks and the growing of the existing ones. The appearance of new discontinuities may be due to the internal stress among the crystals due to their anisotropic expansion during the thermal cycles (Weiss et al., 2003).

Also the anisotropy increases after the test, especially in the Z direction where the lowest V_p values for both stones have been registered. In the case of DG, this means that the new cracks are parallel to the foliation, as observed by other authors (Martínez-Martínez, 2008).

DG, analogously to salt crystallization test, does not exhibit any significant visual changes of damage. The weight loss, such as the ultrasonic velocity decrease, or the changes in the mechanical properties are lower than those registered in GF. The lack of damage could mostly be attributed to the fact that probably the salt solution did not reach the inner pores due to the low porosity values registered.

According to the classification based on the saturation value obtained by hydric tests, DG and GF were classified as *frost resistant* and *probably frost resistant*, respectively. Through the freeze-thaw test, DG confirmed its frost resistant behavior while GF resulted sensitive to the freeze-thaw test, as demonstrated by the UPV decrease during the cycles.

Results can be summarized in the following points:

- GF is more susceptible to frost weathering than DG probably due to the lower open porosity value and to the larger average pore size of DG;

- freeze-thaw cycles probably cause the opening of new microcracks in GF, which allow the damaging effect of the ice formation. This statement may be favored by the existence of anisotropy planes that do not have DG;
- frost weathering is less damaging than the salt crystallization test for both stones; because salt crystallization produced worse fissures by the salt pressure more intense than the ice action
- anisotropy increases with the number of cycles;
- mechanical properties decreased for both materials, more for GF than DG;
- among the mechanical properties, higher losses were registered for the uniaxial compressive strength than the flexural strength at the end of the freeze-thaw test;
- the lowest V_P values and the highest mechanical strength, for both stones, were obtained along the Z-direction.

9. Limitations of the study and techniques used

The European Committee for Standardization (CEN), has produced a great effort to unify the stone industrial procedures within its member countries and is aiming to the development of a harmonized stone industry market.

Standardization could facilitate to share the scientific results of different investigations and furnishes common guidelines for different laboratories. “Repeatability”, “comparability” and “harmonization” are the key-words of standardization (Exadaktylos, 1998).

On the other hand, standardization has also disadvantages. Within the natural stone field, the variability of materials and their properties is so high that the approach of taking into account the “average” values to characterize stone materials inevitably leads to errors. Therefore, slight modifications of measurement procedures are necessary in accordance with the properties of the tested material (Kovács, 2009).

In this chapter, an attempt is made to consider possible modifications of current standards and performed non-destructive techniques, strictly focusing on the applied methods and the tested material of this research.

Surface properties

The Spectrophotometer has been largely employed for superficial measurements of chromatic parameters of stones. Limitations of this technique are related to its use:

- when measuring very heterogeneous material, such as granites (*i.e.* GF), whose minerals are varied in composition and colour, it may require an accurate location of each measured point to repeat the measurement after other tests, especially ageing tests, as well as precise location of a point with the same characteristics when comparing treated and untreated areas, in order to

obtain a representative mean value. The current standards suggest only to use a different medium diameter like the MAV one (UNI-EN 15886, 2010), but do not indicate any information about the minimum number of measurements. Heterogeneous materials usually require a higher number of measurements than homogeneous ones to get representative results;

- the instrument must be tight against the surface to prevent light from entering and distorting the measurements as the daily light could influence the measurement (Perez Ema *et al.*, 2013);
- the surface roughness influences colour measurements. Surfaces to be measured must be smooth because roughness affects the colour properties. So, when comparing non-rough and rough surfaces, the influence of roughness on colour properties should be taken into account (Benavente *et al.*, 2003 b).

Hydric properties

The most important hydric properties were found to be the *water absorption* (under vacuum and at atmospheric pressure), the *capillary uptake* and the *evaporation* or *drying*. While there are European standards concerning the first two properties, for the evaporation only national (like the Italian) standards exist. So, it is suggested to emphasize the drying process in the European standards.

Another issue concerning these standards is the way of measurement. The standard procedure is still “wiping the surface of the samples with a wet cloth” before detecting the weight. In the case of a stone of less than 1% open porosity (like DG), the quantity of water inside the material and on the surface are almost in the same range. So, the errors resulting from this “wiping method” – for example the degree of humidity of the cloth, the intensity of wiping, etc. – can be enormous. It is suggested to avoid the human error and to improve automatic measurements for stone materials with low porosity. Actually, some laboratories resort to automated measuring methods (*e.g.* Benavente *et al.*, 2007a).

Hardness properties

Hardness properties and drilling resistance have been evaluated through many techniques, like the Schmidt hammer test and the micro-hardness (hardness properties) and the Drilling Measurement tests (drilling resistance). They are very useful techniques, especially in situ, because they allow to define indirectly mechanical properties. But they have some limitations:

- Schmidt hammer and micro-hardness are considered NDT, nevertheless they could leave marks, little dots, on flat and soft surfaces. The Schmidt hammer, in particular, could provoke serious damages like microcracks and fissures inside the material, due to the strength of the impact of the instrument against the analyzed surface;
- the influence of the support should be taken into account, since the way in which the object being measured bears on its base may vary the rebound energy value (Viles *et al.*, 2011);
- there are no clear standards about their best use. For example, in the case of drilling test, there is no recommendation about the suitable test conditions. So, the consequence is that in the case of testing very hard materials, like GF and DG, the maximum reached depth of drilling is very low and it is impossible to evaluate what happens in the inner part of the sample. So, a standardization of the micro-destructive techniques for stones ¹⁸will facilitate comparison of the experimental findings internationally.

Ultrasound propagation velocity

This technique is very useful to investigate physical and mechanical properties of building stones. Its limitations are:

¹⁸ A standardization exists in the case of the Leeb hardness test, but only for metallic materials (UNI-EN ISO 16859-1 and -2:2015).

- there is no data about the type of coupling agent placed between the transducer and the material surface generally used in these measurements (plasticine, gel, honey, etc.) (Giuzio *et al.*, 2015);
- there are differences between the results obtained from direct and those obtained from indirect mode, so they are not strictly comparable. In the indirect mode, the wave velocity is slightly slower than in the direct mode, due both to the longer path in the former than in the latter and because in the direct mode the measurement refers to the volume while in the indirect mode it refers only to the surface.

It is suggested to provide in the ultrasonic standards, more information about the couplant and the correlation between the indirect and direct mode.

Mechanical properties

The numerous mechanical tests which have been performed in this study have shown some limitations.

First of all, is to be emphasized that data on mechanical properties of commercially used stone ignore the anisotropy during sampling and testing. Hence, appropriate CEN standards should be proposed. It is suggested that before any destructive mechanical test on natural building stones ultrasonic measurements (P and S-waves) must be carried out for characterization of anisotropy and pre-existing defects. Up-to-now such standard does not exist in ASTM, ISRM or CEN for such a procedure.

A general conclusion that is drawn from this research is that companies publish elastic moduli for the stones at 50% of the peak uniaxial compressive strength whereas they do not provide stone elasticities at low loads. Moreover, in the case loading is performed normal to the rift plane, the Young's modulus at small compression or tension loads is significant lower.

Brazilian tests provided tensile strength results which strongly depended on specimen shape (Coviello *et al.*, 2005). In this study has been observed that fracture always develop at the edge of the disk specimens, where stress concentrations are higher. So, results did underestimate σ_t values.

The brittleness of 3-point bend stone specimens depends on the size of the specimen. The two effects which have been investigated by many authors (Exadaktylos, 1998; Coviello *et al.*, 2005), namely the size and notch effects, have important consequences in design. Three point bending tests (TPBT) do not appear to be an appropriate method for determining the tensile strength of materials. Experimental results by Coviello *et al.* (2005) were strongly dependent on specimen shape and slenderness. No standard considers the size and notch effects, therefore the results of this project will feed future committees inside European Committee for Standardization (CEN).

It is also suggested to take into account the influence of fatigue cycles on the stone mechanical behavior. Results regarding the behavior of stones to (cyclic) uniaxial compression loading fatigue and its relation with microstructure have been demonstrated by Exadaktylos (1998). Fatigue tests are not supposed to reproduce the exact conditions that a natural stone will have to withstand during its life, but rather will measure an intrinsic property of the material, namely the integrity of connection between the grains. This is a critical parameter whenever the stone is thermally, chemically or mechanically loaded. Cyclic test data in conjunction with scanning electron microscope observations of fractured surfaces may be used to reveal the effect of microstructure on the integrity of building stones.

10. Use suggestions and conclusions

In this research four lithotypes with different mineralogical composition and textural features have been examined: a granite (San Giovanni in Fiore granite - GF), a crystalline carbonate (Grisolia stone - DG), a biocalcarene (San Lucido calcarenite - CS) and a sandstone (Fuscaldo sandstone - AF). Their petrophysical, chemical, mineralogical and mechanical characteristics have been determined by means of many tests. Moreover, their durability has been investigated through the salt crystallization and freeze-thaw tests.

Tests results and related properties, for each lithotype, are summarized in [Table 10.1](#).

Table 10.1. Test results and related properties for each performed test and for each lithotype.

		GF		DG		CS		AF	
		<i>Granite</i>		<i>Crystalline carbonate</i>		<i>Greywacke</i>		<i>Biopelmicrite or packstone</i>	
Petrographic classification									
Chromatic parameters	L*	70.5 ± 3.6		71.3 ± 1.1		85.2 ± 1.3		66.6 ± 2.5	
	a*	-0.5 ± 0.4		-0.2 ± 0.2		0.1 ± 0.2		2.4 ± 0.4	
	b*	1.6 ± 2.1		-1.4 ± 1.4		6.9 ± 0.6		13.3 ± 1.2	
	C*	1.9 ± 1.9		2.0 ± 0.5		6.9 ± 0.6		13.5 ± 1.2	
	WI	36.8 ± 8.5		47.7 ± 5.5		36.2 ± 3.7		-1.2 ± 3.5	
	YI	3.0 ± 4.1		-3.0 ± 3.0		11.5 ± 1.1		25.9 ± 2.4	
	B	40.5 ± 5.4		43.7 ± 2.1		59.4 ± 2.6		27.5 ± 3.0	
Real or skeletal density (g/cm³)	ρ_{sk}	2.7 ± 0.0		2.7 ± 0.0		2.7 ± 0.0		2.7 ± 0.0	
Apparent or bulk density (g/cm³)	ρ_b	2.7 ± 0.0		2.7 ± 0.0		2.3 ± 0.0		2.2 ± 0.1	
Open porosity (%)	p_o	1.3 ± 0.1		0.5 ± 0.1		16.2 ± 0.8		20.1 ± 2.3	
Water absorption vacuum (%)	W_{vac}	0.5 ± 0.0		0.2 ± 0.0		7.0 ± 0.4		9.4 ± 1.3	
Compactness Index (%)	I_c	1.0 ± 0.0		1.0 ± 0.0		0.8 ± 0.0		0.8 ± 0.0	
Average pore diameter (μm)		0.3 ± 0.1		0.7 ± 0.0		0.5 ± 0.1		0.2 ± 0.0	
Open porosity by MIP (%)	P_o	0.9 ± 0.1		0.2 ± 0.2		12.9 ± 2.5		20.9 ± 0.7	
Air permeability (mD)	AirP	/		/		6.6 ± 2.5		5.1 ± 2.5	
	X	/		/		11.0 ± 7.9		11.6 ± 6.1	
	Z	/		/		3.5 ± 5.3		1.7 ± 4.1	
Capillary water absorption (g/m²s^{0.5})	C_c	3.3 ± 0.1		1.3 ± 0.1		48.9 ± 0.8		29.2 ± 6.1	
	C ₂	3.4 ± 0.9		1.3 ± 0.2		49.4 ± 10.0		33.5 ± 9.4	
	C ₁	3.3 ± 0.4		1.2 ± 0.1		48.3 ± 3.4		24.9 ± 5.8	
Water absorption at atmospheric pressure (%)	W_{ab}	0.4 ± 0.0		0.1 ± 0.0		4.3 ± 0.3		5.3 ± 0.9	
	S_i	90.9 ± 1.6		91.1 ± 4.1		83.1 ± 0.4		77.7 ± 1.7	
	W_{DS}	-0.2 ± 0.0		-0.1 ± 0.0		-2.0 ± 0.1		-2.5 ± 0.3	
	S	0.8		0.6		0.6		0.6	
Static contact angle (°)		45.2 ± 7.2		46.2 ± 4.7		/		/	
Ultrasound propagation velocity (Vp) (m/s)	V_P	3804 ± 258		6592 ± 76		4281 ± 234		3293 ± 517	
	V _{Px}	4083 ± 124		6633 ± 57		4325 ± 235		3528 ± 350	
	V _{Py}	3744 ± 191		6600 ± 77		4282 ± 229		3463 ± 331	
	V _{Pz}	3585 ± 160		6542 ± 73		4237 ± 240		2888 ± 611	
Ultrasonic anisotropy (Vp) (%)	dM	8.4 ± 1.2		1.1 ± 0.5		1.6 ± 0.9		17.4 ± 10.8	

		GF	DG	CS	AF
	dm	8.7 ± 2.4	0.5 ± 0.5	1.0 ± 0.6	1.9 ± 1.3
Ultrasound propagation velocity (Vs) (m/s)	V_s	2225 ± 199	3404 ± 25	2374 ± 84	2037 ± 214
	V _{Sx}	2370 ± 279	3416 ± 26	2386 ± 91	2110 ± 169
	V _{Sy}	2185 ± 83	3406 ± 23	2376 ± 88	2096 ± 161
	V _{Sz}	2120 ± 49	3388 ± 15	2359 ± 73	1905 ± 244
	<i>Ultrasonic anisotropy (Vs) (%)</i>	dM	6.9 ± 4.1	0.7 ± 0.4	0.9 ± 0.7
	dm	8.1 ± 14.3	0.3 ± 0.6	0.4 ± 0.6	0.7 ± 2.6
Young's modulus (GPa)	E	32.4 ± 2.1	84.1 ± 1.2	33.3 ± 2.8	21.8 ± 5.9
	E _X	36.6 ± 3.6	84.8 ± 1.1	33.8 ± 3.0	24.1 ± 4.4
	E _Y	31.7 ± 2.5	84.2 ± 1.2	33.4 ± 2.9	23.6 ± 4.2
	E _Z	29.0 ± 1.4	83.2 ± 0.8	32.8 ± 2.6	17.9 ± 6.7
	Poisson's ratio	ν	0.24 ± 0.01	0.34 ± 0.00	0.29 ± 0.01
ν _X		0.27 ± 0.01	0.35 ± 0.00	0.29 ± 0.01	0.24 ± 0.03
ν _Y		0.24 ± 0.01	0.34 ± 0.00	0.29 ± 0.01	0.23 ± 0.03
ν _Z		0.20 ± 0.01	0.34 ± 0.00	0.28 ± 0.02	0.08 ± 0.19
Shear modulus (GPa)		G	13.4 ± 1.2	31.3 ± 0.4	13.0 ± 1.0
	G _X	15.3 ± 3.0	31.5 ± 0.5	13.1 ± 1.1	9.7 ± 1.7
	G _Y	12.8 ± 1.0	31.3 ± 0.4	13.0 ± 1.1	9.6 ± 1.6
	G _Z	12.1 ± 0.5	31.0 ± 0.3	12.8 ± 0.9	8.0 ± 2.2
	Bulk modulus (GPa)	K	20.3 ± 1.3	89.4 ± 2.6	26.1 ± 3.5
K _X		24.2 ± 3.0	91.4 ± 1.5	27.1 ± 3.4	15.6 ± 3.7
K _Y		20.2 ± 2.1	89.4 ± 2.3	26.1 ± 3.3	14.7 ± 3.3
K _Z		16.5 ± 1.3	87.5 ± 2.1	25.1 ± 3.7	8.6 ± 4.5
Micro-hardness (Leeb)		L_s	761 ± 13	609 ± 14	438 ± 32
Drilling resistance (N/mm)	DRi	54 ± 8	65 ± 36	42 ± 7	37 ± 6
Uniaxial compressive strength (MPa)	UCS	104.1 ± 30.5	73.2 ± 14.2	33.8 ± 5.9	31.0 ± 11.0
	UCS _X	69.0 ± 6.3	51.7 ± 9.0	48.3 ± 5.4	17.7 ± 6.3
	UCS _Y	109.4 ± 23.7	68.8 ± 5.4	33.1 ± 1.9	44.1 ± 3.1
	UCS _Z	161.5 ± 28.7	99.1 ± 25.2	23.8 ± 5.3	50.6 ± 11.8
	<i>Compressive strength anisotropy (%)</i>	Ra	0.9	0.7	0.7
Flexural strength (MPa)	R_{tf}	7.8 ± 1.0	12.2 ± 1.9	6.8 ± 1.2	7.9 ± 1.0
	R _{tfX}	6.5 ± 0.5	9.3 ± 0.8	5.6 ± 2.0	6.7 ± 2.5
	R _{tfY}	7.2 ± 0.6	12.9 ± 0.3	6.4 ± 0.1	8.5 ± 0.8
	R _{tfZ}	9.0 ± 0.5	15.1 ± 2.4	7.0 ± 0.5	11.0 ± 2.1
	<i>Flexural strength anisotropy (%)</i>	Ra_{tf}	0.3	0.5	0.2
Indirect tensile strength (MPa)	σ_t	8.0 ± 0.1	7.9 ± 0.1	1.5 ± 0.4	5.8 ± 2.1
	σ _t (0°)	7.9 ± 0.1	7.7 ± 0.0	1.1 ± 0.0	1.3 ± 2.0
	σ _t (45°)	8.0 ± 0.1	7.9 ± 0.1	1.4 ± 0.3	6.0 ± 2.5
	σ _t (90°)	8.2 ± 0.1	8.0 ± 0.1	2.1 ± 0.0	7.8 ± 2.0
	<i>Tensile strength anisotropy (%)</i>	BAI	1.0	1.0	1.9
Point Load Index (MPa)	I_{S(50)}	2.1 ± 0.1	1.2 ± 0.2	0.8 ± 0.2	0.5 ± 0.1
	I _{S(50)X}	1.5 ± 0.3	0.9 ± 0.2	0.6 ± 0.2	0.4 ± 0.1
	I _{S(50)Y}	2.1 ± 0.2	1.2 ± 0.2	0.8 ± 0.2	0.5 ± 0.1
	I _{S(50)Z}	2.4 ± 0.2	1.4 ± 0.2	0.9 ± 0.1	0.5 ± 0.1
	<i>Point Load anisotropy (%)</i>	Ia₍₅₀₎	1.5	1.6	1.7
Polished stone value	PSV	59.6 ± 2.9	/	/	/
Los Angeles (%)	LA	51.2 ± 6.4	/	/	/
Micro-Deval (%)	M_{DE}	23.1 ± 6.6	/	/	/
Salt crystallization (%)	ΔM	0.12 ± 0.01	-0.18 ± 0.01	-0.24 ± 0.11	1.90 ± 0.65
Frosting (%)	ΔM	-0.14 ± 0.01	-0.18 ± 0.01	/	/

10.1 Use suggestions

Once defined petrophysical and mechanical properties of each stone, it is possible to propose their use suggestions. Each stone could be used as building material taking into account its properties, its required function and site characteristics.

As reported in Fig. 3.18, the principal uses of building stones in the actual Italian market are: slabs for external or internal paving; cladding for façade or internal walls; masonries; aggregates for concrete or for engineering purposes; ornamental uses especially gravestones.

In Table 10.2 the principal characterization tests useful to employ stones as building materials for floor tiles, cladding, masonries and aggregates are summarized.

Table 10.2. Summary of the main tests for building stone uses.

Test	Cladding		Slabs/Floor tiles		Masonry	Aggregate
	Internal	External	Internal	External		
Petrographic analysis						
Water absorption						
Capillary water absorption						
Open porosity						
Apparent/real density						
Uniaxial compressive strength						
Flexural strength						
Indirect Tensile strength			Recommended			
Abrasion resistance						
Slip resistance						
Micro-hardness						
Reaction to fire						
Anisotropy						
Frost resistance						
Water vapour permeability						
Thermal shock resistance						

Then some examples of use suggestions, according to the current UN-EN standards are reported.

10.1.1 Water absorption and porosity

Water absorption and porosity are two important stone properties, especially for their external use. The lower the absorption, the higher the durability of stones vs. decay processes (*i.e.* freeze-thaw, salt crystallization and others).

A direct relationship between absorption and/or porosity and stone decay, has not been assessed, because decay processes related to the presence of water are influenced more by the type and the pore size distribution rather than the total porosity (Buj Fandos, 2009).

Due to the major susceptibility of porous stones to decay, it is suggested to use stones with a low porosity. All the analyzed samples registered a porosity <25% and some of them (GF and DG) an open porosity less than 2%. For masonries uses, Lopez Mesones G. *et al.* (2001) recommend stone porosity values <45% to realize walls. Therefore, all the analyzed samples are suitable for being employed in masonry, especially GF and DG for their low porosity values.

10.1.2 Uniaxial compressive strength

The uniaxial compressive strength test, as reported in Table 10.2, it is recommended for floors, cladding and masonries.

A) Slabs

The minimum uniaxial compressive strength values recommended for floor uses, depending on the traffic characteristics (Cerdeño del Castillo *et al.*, 2007), are reported below:

Uniaxial compressive strength	Use
UCS > 55 MPa	Heavy vehicles
40 MPa < UCS < 55 MPa	Not heavy vehicles
30 MPa < UCS < 45 MPa	Pedestrian traffic

According to these values, all the analyzed samples are suitable for pedestrian traffic. DG can be also used for not heavy vehicles traffic, while GF is the only stone that can be used for all the three traffic categories: pedestrian, not heavy and heavy vehicles.

When using stones as slabs, it is important not only taking into account their strength properties and durability but also their correct placement and the behavior of the mortar which is employed as substrate. Therefore, it is suggested to use many layers (Fig. 10.1) with different functions to obtain a durable paving stratigraphy (García de los Ríos & Baez, 2001).

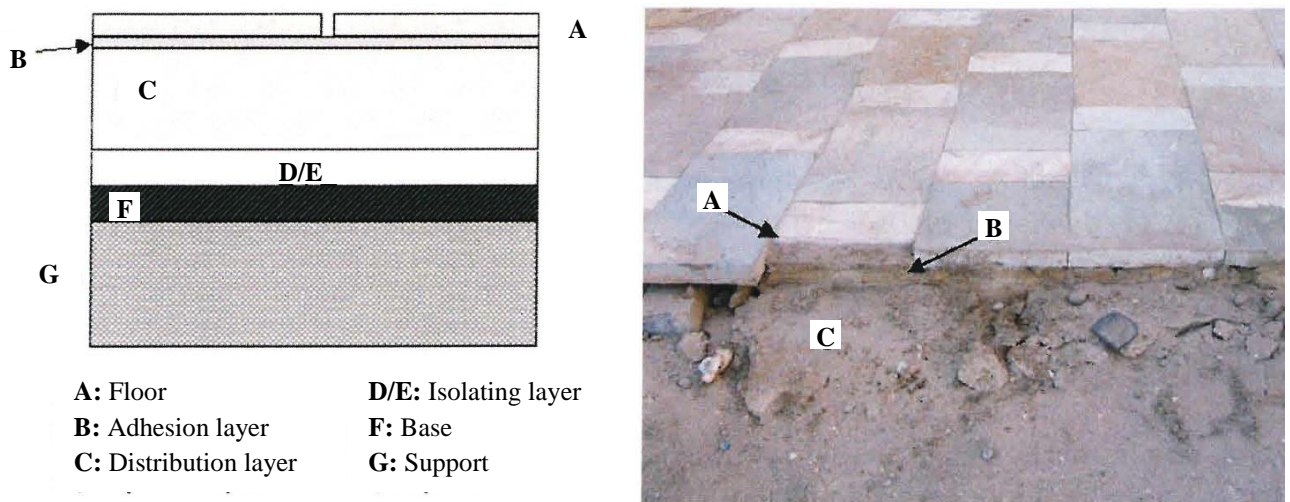


Fig.10.1. Schematic representation of a correct stratigraphy for slab uses (a); example of an external floor realized with stone tiles.

The first layer (A) it is the stone layer and the tile thickness is determined according to the stone characteristics and its strength properties (*i.e.* UCS and R_{tf}), as reported in Table 10.3. The layer B or adhesion layer is a mortar layer joining the upper floor and the lower distribution layer. The distribution layer C has the function to transmit the upper loads to the support. It is made of cement mortar with electro-welded nets. Its thickness depends both on the type of the support and on the traffic characteristics. The layers C and D are optional layers constituted by isolating materials. They are laid on a base layer (E) composed by cement mortar and sand. All the layers are laid on a structural support (F) made of soil or concrete (depending on traffic characteristics).

B) Masonry

For masonry uses the minimum uniaxial compressive strength value recommended is 20 MPa (Lopez Mesones G. *et al.*, 2001; Buj Fandos, 2009).

All the analyzed samples reached higher values than 20 MPa. So, they are suitable for being employed as masonry structural elements.

The general principles that should be followed in the construction of stone masonry are (Sharma, 1960; Barry, 1999):

- the stone used shall be hard and durable. All stones should be laid on their natural bed;
- the pressure acting on the stones should not act parallel to the bedding planes (like stones used in corbels), as this will try to split the stones;
- the bond stones and headers should not be of dumb-bell shape;
- large flat stones should be laid under the ends of girders, roof trusses, etc.;
- in all sloping retaining walls, the beds of the stones and the plan of the courses should be at right angles to the slope;
- all laid fine dressed stone work should be protected against damage during further construction by means of wooden boxes;
- jambs for door and window openings should be made of quoins equal in height to the course. They should be in breadth equal to at least 1½ times the height of the course and their length should be at least twice the height;
- all the surfaces should be kept enough wet¹⁹, with the just amount of water, while the work is in progress and also till the mortar has set. On one hand, in the case of porous stones, the mortar should contain enough water because porous stones may absorb excess amounts of the water

¹⁹ Masonry Technical guidelines, 5.6. Grapevine, Texas, pp.1-9. <http://www.grapevinetexas.gov/DocumentCenter/View/128>

contained in the mortar during the construction of the masonry and cause damages like shrinkage and fractures within the wall (Antonacci *et al.*, 2009). On the other hand, for not porous stone, the amount of water contained in the mortar should be lower than in the first case, in order to avoid serious consequences (*e.g.* ice crystallization processes²⁰) if construction work is being carried out in winter or in cold areas;

- double scaffolding will be used wherever it is difficult to fit in the stones later on;
- all the portions of the masonry should be raised uniformly. Wherever this is not possible, the stone work built earlier should be raked (stepped), so that the new work can be bonded well with the old;
- sufficient thorough stones should be used and they should form $\frac{1}{4}$ th of the area in elevation;
- vertical faces of the masonry walls should be checked with a plumb rule and the battered faces should be tested with wooden template corresponding to the batter and a plumb rule to ensure a constant batter;
- the stones used in the masonry should be wetted before use to avoid moisture being sucked from the mortar;
- masonry should not be allowed to take tension;
- the hearting of the masonry should be properly packed with mortar and chips, if necessary, to avoid any hollows or very thick mortar joints.

Regarding the last point, it is well known that mortar strength increases with increasing cement content. It is suggested to use mortars with a compressive mortar strength in a range of 1.9 up to 13.8 MPa and water absorption in a wide range from 10 V/V% to 22 V/V% (Domaslowski, 2000; Sneath, 2014). As the mortar compositions cover a wide range of properties, it should be possible to find an

²⁰ <http://www.stastier.co.uk/nhl/guides/protection.htm>

appropriate mortar for nearly any kind of stone. Joint mortars within masonry have to fulfill certain requirements concerning compressive strength because they have to withstand the load of the above masonry. The new standard UNI-EN 998-2 (2010) requires the following minimum values (Table 10.3):

Table 10.3. Minimum compressive strength β_{CS} (MPa) requirements for mortar groups 1-25 (UNI-EN 998-2:2010).

Mortar group	M 1	M 2.5	M 5	M 10	M 15	M 20	M d
β_{CS}	1	2.5	5	10	15	20	>25

Concerning cement mortar, it is known that cement nearly reaches its maximum hardness after 28 days of storage in appropriate climate of 20°C and 65 % of relative humidity and that the subsequent strength increase is only minor. So, relative strength measurements are carried out on cement or cement containing mortars at the time of 28 days. There are, however, exceptions for pure lime mortars and mortars with pozzolanic additives. Pure lime mortars harden through evaporation of the water admixed for mortar preparation and subsequent carbonation. The latter process is slow and may take years within a thick masonry. For this reason, strength requirements for pure lime mortars do not exist. However, as a compromise, curing time of 90 days has been proposed. Similar difficulties are found in the case of latent hydraulic additives, *i.e.* pozzolans. The hydration reaction of the reactive silica within the additive with the Ca(OH)_2 is also very slow and may take weeks or months. It will even cease when the mortar dries too quickly, without reaching the final and desired strength. It is, therefore, recommended to test cement mortars containing latent hydraulic additives only after a curing time of 90 days. Moreover, the workability of mortars containing latent hydraulic additives under practical building conditions is often very problematic. Many failures have been produced because curing time and curing conditions (regular wetting of the mortar) have not been carefully observed (Snethlage, 2014).

10.1.3 Flexural strength

Flexural strength test allows evaluating the stone suitability as floor slabs or kerbs, cladding or for masonry uses. Depending on the breaking load and on the specific use, the minimum stone thickness requirements are fixed.

In general, for façade, it is important to evaluate the flexural strength for the lateral wind or seismic action against the cladding elements. In this study, flexural strength values for slabs and kerbs for external paving have been considered. For these elements, the two European standards, the UNI-EN 1341 (2003) for slabs and the UNI-EN 1343 (2003) for kerbs, have been considered. These standards recommend to take into account the following breaking loads for different classes of use (Table 10.4).

Table 10.4. Suggested breaking loads of slabs and kerbs for different classes of use where P_{\min} is the minimum breaking load (kN).

Class	P_{\min} (kN)	Typical Use
0	/	Decoration
1	0.75	Slabs Bedded in mortar, pedestrian areas only
2	3.5	Pedestrian and cycle areas. Gardens, balconies
3	6.0	Occasional car, light vehicle and motorcycle access. Garage entrances
4	9.0	Walking areas, market places occasionally used by delivery vehicles and emergency vehicles
5	14.0	Pedestrian areas often used by heavy vehicles
6	25.0	Roads and streets, petrol stations

The minimum strength of slabs and kerbs is defined in terms of breaking loads for different classes of use. The breaking load is calculated using the following equation (UNI-EN 1341 and 1343, 2003):

$$P = \frac{(R_{tf} \times W \times t^2)}{(1500 \times L \times 1.6)}$$

where P is the minimum breaking load (kN); R_{tf} is the flexural strength (MPa); W is the width (mm); t is the thickness (mm); L is the length (mm); 1.6 is a safety factor. This equation is valid for all work dimensions up to 900 mm. Once the flexural strength and the minimum breaking load for each category are known and supposing standard dimensions for a stone slab (e.g. 800x800 mm) and for a kerb (e.g.

200x900 mm), the thickness of slab or kerb has been evaluated as follows (UNI-EN 134 and 1343, 2003):

$$t = \sqrt{\frac{(1.6 \times 1500 \times L \times P)}{(R_{tf} \times W)}}$$

For each lithotype, according to the equation above, slabs and kerbs thickness suggested values are reported in Table 10.5 and Table 10.6, respectively.

Table 10.5. Minimum thickness values obtained for standard stone slabs of 800x400 mm, for each lithotype and for each use. The slab thickness t (mm) has been determined knowing the maximum flexural strength R_{tf} (MPa) of each lithotype, obtained by the flexural strength test, and the minimum breaking load P (kN) that varies from 0.75 kN to 25 kN for the different classes of use.

Slabs - UNI-EN 1341:2003 t = thickness (mm)							
Stone	R_{tf} (MPa)	P(kN)25	P(kN)14	P(kN)9	P(kN)6	P(kN)3.5	P(kN)0.75
GF	7.8	123.8	92.6	74.3	60.6	42.9	21.4
DG	12.2	99.2	74.3	59.5	48.6	34.4	17.2
CS	6.8	133.3	99.8	80.0	65.3	46.2	23.1
AF	7.9	123.4	92.4	74.1	60.5	42.8	21.4

Table 10.6. Minimum thickness values obtained for standard stone kerbs of 200x900 mm, for each lithotype and for each use. The kerb thickness t (mm) has been determined knowing the maximum flexural strength R_{tf} (MPa) of each lithotype, obtained by the flexural strength test, and the minimum breaking load P (kN) that varies from 0.75 kN to 25 kN for the different classes of use.

Kerbs - UNI-EN 1343:2003 t = thickness (mm)							
Stone	R_{tf} (MPa)	P(kN)25	P(kN)14	P(kN)9	P(kN)6	P(kN)3.5	P(kN)0.75
GF	7.8	185.6	138.9	111.4	90.9	64.3	32.1
DG	12.2	148.8	111.3	89.3	72.9	51.5	25.7
CS	6.8	199.9	149.6	119.9	97.9	69.2	34.6
AF	7.9	185.1	138.5	111.1	90.7	64.1	32.0

Regarding the different classes of uses, it is possible to individuate two stone categories for each use (Tables 10.5 and 10.6):

– **Roads and streets (P=25 kN)**

Group 1: slab thickness <10 cm and kerb thickness <15 cm: DG

Group 2: slab thickness 10< t <15 cm and kerb thickness 15< t <20 cm: GF, CS and AF.

- **Pedestrian areas often used by heavy vehicles** (P=14 kN)
 - Group 1: slab thickness <8 cm and kerb thickness <12 cm: DG
 - Group 2: slab thickness 8<t<10 cm and kerb thickness 12<t<15 cm: GF, CS and AF.
- **Walking areas, delivery vehicles and emergency vehicles** (P=9 kN)
 - Group 1: slab thickness <7 cm and kerb thickness <9 cm: DG
 - Group 2: slab thickness 7<t<8 cm and kerb thickness 10<t<12 cm: GF, CS and AF.
- **Light vehicles** (P=6 kN)
 - Group 1: slab thickness <5 cm and kerb thickness <8 cm: DG
 - Group 2: slab thickness 5<t<7 cm and kerb thickness 9<t<10 cm: GF, CS and AF.
- **Pedestrian and cycle areas** (P=3 kN)
 - Group 1: slab thickness <4 cm and kerb thickness <6 cm: DG
 - Group 2: slab thickness 4<t<5 cm and kerb thickness 6<t<7 cm: GF, CS and AF.
- **Pedestrian areas only** (P=0.75 kN)
 - Group 1: slab thickness <2 cm and kerb thickness <3 cm: DG
 - Group 2: slab thickness 2<t<3 cm and kerb thickness 3<t<4 cm: GF, CS and AF.

10.1.4 Micro-hardness

Micro-hardness is a useful test for external paving uses. The obtained micro-hardness values expressed as Vickers hardness (HV) have been converted to MPa multiplying by 9,807.

Reguerio (2005) distinguishes three groups of stones according to their micro-hardness:

Micro-hardness Knoop	MPa
Low	<1000
Intermediate	1000-2500
High	>2500

The obtained micro-hardness values for each lithotype are reported in [Table 10.7](#). According to the Knoop values, GF is the material with the highest hardness, so suitable for paving floors. The Knoop hardness values have been obtained, for each lithotype, from the Vickers hardness values multiplying for the correlation factor of 9.871.

Table 10.7. Micro-hardness values converted to Knoop values for each lithotype.

Samples	Vickers (HV)	Knoop (MPa)
GF	212	2094
DG	170	1675
CS	122	1205
AF	102	1007

The other materials with lower hardness values should be used for floors but preferably for internal uses.

10.1.5 Frosting

The durability of the studied stone materials has been evaluated through the flexural and uniaxial compressive strength variation before and after the freeze-thaw test according to the UNE-EN 12371 (2011) standards. The suitability of GF and DG has been obtained considering the residual flexural or compressive resistance value after the ageing test to establish if that materials could be used for cold areas or not.

The UNI-EN 1341 and the UNI-EN 1343 (2003) standards define stones as *frost resistant* if they show a flexural resistance decrease after 48 cycles of the freeze-thaw test lower than 20% of their initial flexural strength value for being used as slabs and kerbs, respectively.

According to [Table 8.7](#) both stones, GF and DG, showed very low flexural strength loss variations, so that they may be considered suitable as slabs and kerbs for external paving uses in cold areas.

The UNI-EN 1342 (2003) standard defines as frost resistant for external paving uses stones that show a compressive resistance decrease after 48 cycles of the freeze-thaw test lower than 20% of their initial uniaxial compressive strength value. According to [Table 8.7](#) both stones, GF and DG, exhibited low uniaxial compressive strength loss variations. So they are suitable as setts for external paving uses in cold areas.

10.2 Conclusions

The obtained results of the four selected stones (summarized in Table 10.8) indicate very distinctive behaviors. Therefore, each lithotype is discussed individually.

Table 10.8. Conclusions summarized for each performed test and for each lithotype, according to stone classifications.

		GF	DG	CS	AF
Name		<i>San Giovanni in Fiore granite</i>	<i>Grisolia stone</i>	<i>San Lucido calcarenite</i>	<i>Fuscaldo sandstone</i>
Petrographic analysis		oriented sets of microcracks; slightly altered	homogeneous, isotropic & compact	homogeneous, isotropic & compact	oriented phyllosilicates
Linear microcrack density	LMD	sound stone	/	/	/
Chromatic parameters		heterogeneous	homogeneous	homogeneous	heterogeneous
Open porosity	p _o	few pores; low porosity	compact; low porosity	many pores; high porosity	a lot of pores; high porosity
Pore size distribution	μm	microporosity	macroporosity	microporosity	microporosity
Air permeability	AirP	air-impermeable	air-impermeable	air-permeable	air-permeable
Capillary water absorption	C _c	slightly absorbing	slightly absorbing	medium absorbing	medium absorbing
Frost resistance	S	weather & probably frost resistant	weather & frost resistant	weather & frost resistant	weather & frost resistant
Hydrophobicity	(°)	not hydrophobic	not hydrophobic	not hydrophobic	not hydrophobic
Ultrasound propagation velocity	class	middle velocity - class 3	high velocity - class 5	high velocity - class 4	low velocity - class 2
Young's modulus	E	low deformability	very low deformability	low deformability	moderate deformability
Micro-hardness (Leeb)	L _s	high	intermediate	intermediate	intermediate
Drilling resistance	DRi	high	high	low	low
Weathering class	Hs	class II	/	/	/
Uniaxial compressive strength	UCS	very strong	strong	moderately strong	moderately strong
Flexural strength	R _{tf}	moderate	high	moderate	moderate
Tensile strength	σ _t	moderate	high	low	moderate
Point Load Index	IS ₍₅₀₎	high strength	high strength	high strength	high strength
Polished stone value	PSV	not polished	/	/	/
Sal crystallization resistance		durable	durable	slightly sensitive	not durable
Freeze-thaw resistance	S	frost resistant	frost resistant	/	/
Hydric behavior		isotropic	isotropic	isotropic	anisotropic
Ultrasonic behavior		anisotropic	isotropic	isotropic	anisotropic
Mechanical behavior		slightly anisotropic	isotropic	isotropic	anisotropic
Use suggestions					
<i>structural element (masonry)</i>		√	√	√	√
<i>floor tile pedestrian areas</i>		√	√	√	√
<i>floor tile not heavy traffic</i>		√	√	X	X
<i>floor tile heavy traffic</i>		√	X	X	X
<i>slab</i>		√	√	√	√
<i>kerb</i>		√	√	√	√
<i>sett in cold areas</i>		√	√	X	X
<i>external uses (water & salts)</i>		√	√	X	X
<i>ornamental uses</i>		X	X	√	√
<i>aggregate</i>		X	/	/	/
<i>Z-direction // loading direction</i>		Yes	/	/	Yes

San Giovanni in Fiore granite (GF)

- (1) The use of GF has evolved throughout history. Building granites have endured over time, due to the presence of traditional quarries and to the presence of the school of stonemasons of San Giovanni in Fiore. This stone is present in the architectural and engineering heritage of Cosenza Province and form part of the architectural landscape of many old towns. This stone has been used until the 20th century; not only for decorative purposes but also for engineering uses (bridges, ports, milestones).
- (2) The petrographic analysis showed that GF is slightly altered, even though it is recognized as belonging to the category of fresh stones. The oriented thin sections demonstrate the presence of microcracks and their different orientation along the three spatial directions (anisotropy), and classified as *granite*. The chromatic parameters indicate that GF is a heterogeneous material, for the high standard deviations.
- (3) According to stone classifications, one can say that GF is/has: *sound stone* (LMD: Sousa et al., 2005); *few pores* (p_0 : von Moos & De Quervain, 1948); *low porosity* (p_0 : Anon, 1979); *microporosity* (μm : De Quervain, 1967); *slightly absorbing* (C_c : Siegesmund & Dürrast, 2014); *weather and probably frost resistant* (S: Hirschwald, 1912); *middle velocity – class 3* (UPV: Anon, 1979); *low deformability* (E: Bell & Lindsay, 1999); *high micro-hardness* (Knoop: Reguerio, 2005); *moderately weathered – class II* (H_S : Irfan & Dearman, 1978); *very strong* (UCS: Anon, 1977); *high strength* ($Is_{(50)}$: Bell & Lindsay, 1999); *not polishing* (PSV: Dokic et al., 2015).
- (4) According to the obtained results, anisotropy influences GF's durability, together with other properties (*i.e.* texture and composition). GF's anisotropy depends on its structure and texture, and is directly related to the effective porosity and capacity to absorb water by capillary action.
- (5) The oriented sets of microcracks demonstrate that they influence the physical and mechanical GF behavior. Furthermore, the most influential factor affecting GF's strength anisotropy is the presence

of oriented sets of microcracks. Comparing GF with other similar granites, this stone presented worse properties. With regards to the UPV values and tensile strength, GF is classified as belonging to the “middle velocity” category and as “not strong” granite, respectively. In contrast, GF’s UCS and $I_s(50)$ values are classified as “very strong” and with a “high strength”, respectively.

- (6) With regards to hydric behavior, GF is classified as “isotropic” as it did not demonstrate significant variations along the two investigated directions. Moreover, the low porosity value (compared to other non-granitic stones) indicates that this stone can be used for both inside and outside purposes. This resistance is also confirmed by the salt crystallization test. Furthermore, GF is an air-impermeable material.
- (7) Physical and mechanical tests highlighted a slight anisotropic behavior. The highest V_p and V_s values are registered along the X direction and the lowest along the Z direction. In contrast, the highest mechanical values are registered along the XY or “rift plane” (Z axis) and the lowest along the YZ or “hard-way plane” (X axis). In addition, the review of the Brazilian test results demonstrated that the maximum value of σ_t was obtained at $\beta = 90^\circ$ for all tested samples. Instead, the minimum value of σ_t was obtained at $\beta = 0^\circ$ in different tested samples. Therefore, with regards to the mechanical strength, the rift plane is individuated as the strongest plane and the hard-way as the weakest plane. In summary, GF displayed intermediate-good values of strength properties along the three splitting planes, for all the performed mechanical tests.
- (8) The splitting plane named *rift*, is determined by the orientation of the exfoliation microcracks. Stonemasons prefer using the rift plane for the fascia of historic buildings as rift is easily split.
- (9) The good correlation factors among physical and mechanical properties indicated that it is possible to obtain mechanical strength values by means of non-destructive tests with less costs, less samples, and without wasting specimens.

(10) According to the performed ageing tests (salt crystallization and freeze-thaw), GF has been classified as *durable* (i.e. salt resistant) and *probably frost resistant* material, suitable for indoor and exterior uses. The term “*probably frost resistant*” suggests that GF has not a clear behavior in relation to ice crystallization processes. Moreover, taking into account its significant microporosity (a possible weak factor for decay processes connected to water) and the mechanical strength decreases registered during the frost test cycles, it is suggested to use GF preferably in places where the freeze-thaw variations are not present.

(11) Due to good mechanical properties, durability, and slight anisotropic behavior demonstrated in all performed tests, GF should be employed in the constructions as building material whilst considering the direction of anisotropy. For reasons presented, the recommendation is made to use San Giovanni in Fiore’s granite as building material due to the beneficial properties and for the lack of decay processes observed. Alternatively, with regards to the few number of active quarries of this material, the suggestion is for local use. Studying the different V_p and V_s values and strengths values along the three directions, it is important to consider, e.g. the granite ashlar orientation in masonries to improve GF properties as a building stone. The results of this study suggest that in general, granite cannot be considered as a continuum isotropic material. This fact is reflected not only in the laboratory testing but also for engineering and architectural design projects. Typically, the values of the obtained anisotropy indices indicated that anisotropy is more accentuated in one spatial direction. In particular, the rift plane (XY) resulted the strongest direction where GF demonstrated better performance than the others. Thus, GF is positioned in a structural element or for ornamental purposes, vertically along this direction (Z axis). Furthermore, considering decay agents (e.g. water), capillary water uptake is influenced by the direction in which this stone is laid, even though for GF the capillary water uptake resulted quite similar along the different spatial

directions. The direction of microcracks must be also taken into consideration when applying conservation treatments on sculptures or ashlar and applied along the hard-way plane (YZ), as this is the plane with the lowest number of microcracks; a lower prone to alteration processes.

- (12) Identified usage suggestions for GF is for many building purposes: structural element in masonry; floor tiles for pedestrian paths, not heavy and heavy vehicles' traffic; as GF resulted salt and frost resistant, this stone can be used as slabs (minimum thickness of 2.14 cm), kerbs (minimum thickness of 3.21 cm), and setts for external paving in cold areas. GF exhibits numerous uses except as aggregate as this stone demonstrated a low abrasion resistance outside of engineering limits. Measurements obtained by the performed tests make this granite a high quality building material with a good answer to decay agents; and thus, durable.

Grisolia stone (DG)

- (1) According to the historical study, DG was used by the Schools of stonemasons of Basilicata and the northern part of Calabria as a structural element, principally for masonries, floor tiles and portals. DG's ornamental use was very limited due to hardness and concentrated, in certain details, such as the lateral volutes or the stoke emblem of portals.
- (2) The petrographic analysis identified that DG is a very compact and homogenous limestone. The oriented thin sections demonstrated the absence of variations along the three spatial directions; is classified as *crystalline carbonate*. DG's chromatic parameters displayed that it is a homogeneous stone, for the low standard deviations.
- (3) According to the stone classifications, it can be said that DG is/has: *compact* (p₀: von Moos & De Quervain, 1948); *low porosity* (p₀: Anon, 1979); *macroporosity* (μm: De Quervain, 1967); *slightly absorbing* (C_C: Siegesmund & Dürrast, 2014); *weather and frost resistant* (S: Hirschwald, 1912);

very high velocity – class 5 (UPV: Anon, 1979); *very low deformability* (E: Bell & Lindsay, 1999); *intermediate micro-hardness* (Knoop: Reguerio, 2005); *strong* (UCS: Anon, 1977); *high strength* ($Is_{(50)}$: Bell & Lindsay, 1999).

- (4) DG's hydric behavior is classified as *isotropic* as there was no significant variation along the two investigated directions. Moreover, the low porosity value (similar to marble) indicates that DG can be used for inside and outside purposes. Furthermore, it is naturally air-impermeable.
- (5) According to the ageing performed tests (salt crystallization and freeze-thaw) and to its void structure, DG is a *durable* material suitable for both indoor and exterior uses. This stone displays high durability due to its very low open porosity, to the presence of macropores that are more resistant than micropores, for processes that consist of the movement of fluids or of crystallization in the void space, such as the crystallization of salts or of ice. DG is highly durable to any kind of decay factor where the damaging agent acts via fluids entering into the material, such as salt or frost damage. The fluid movement kinetics is so slow and the open porosity is so low, that the circulation of fluids in this limestone is almost zero. The salt solution and the ice hardly reach the void space during the tests and thus minimal salt or ice crystallization takes place inside the material, as observed by the registered small weight variations during the two performed tests. Moreover, DG high mechanical strength and the low mechanical strength variations pre- and post-durability tests, confirm DG resistance to decay factors.
- (6) Due to DG's good physical-mechanical properties and to isotropic behavior, demonstrated in all performed tests, DG can be employed in construction as a building material. Considering the active quarries, DG can be employed for local uses.
- (7) DG owes its long durability and resistance to decay to its physical properties. Because of this stone's petrophysical and mechanical characteristics, DG is highly resistant to the agents of decay and

consequently durable. The low anisotropy, capillary water absorption, porosity and high mechanical strength and durability characterizing DG, render the stone exceptionally durable and resistant. DG is highly durable to any kind of decay where the damaging agent acts via fluids entering into the material, such as salt or frost damage. The fluid movement kinetics is so slow and the void space so poorly connected that the circulation of fluids in this limestone is almost zero. The salt solution hardly reaches the void space during testing and thus minimal crystallization occurs inside the material. The depression of freezing point due to the small average void size is another reason why this stone is highly resistant to the effect of frost.

- (8) The high mechanical strength of DG further improves its durability to physical damage. High values of uniaxial compressive, tensile and flexural strength are obtained; especially DG's flexural strength is very high along the Z-direction. Contrarily to other similar limestones that under mechanical and environmental loading are known to fail by fracture of a tensile character and seriously damaged, DG is suitable for ashlar elements and also for "flexural" members (architraves, corbels, cantilevers), due to its high compactness.
- (9) The good correlation factors among physical and mechanical properties indicated the possibility to obtain mechanical strength values by means of non-destructive tests with less costs, less samples, and without wasting specimens.
- (10) DG exhibited an isotropic behavior for all performed tests, except for the flexural strength, where a slight anisotropic behavior is displayed. Thus, regarding this specific property to improve DG's good mechanical properties, DG can be used in constructions, although considering the anisotropic directions. In particular, DG must be positioned with the Z-direction vertically to transmit loads perpendicular to the XY plane when the structural element is subjected to flexural stresses, in order to improve DG flexural resistance.

- (11) Due to intermediate micro-hardness and thus workability, DG should not be used as an ornamental material.
- (12) Due to the high value of brightness obtained by the chromatic test, DG can be used both for external uses exposed to weathering agents and for polished surfaces. Furthermore, according to the performed ageing tests (salt crystallization and freeze-thaw), DG is a durable material suitable for indoor and exterior uses, and for all kinds of finishing.
- (13) In addition to GF and with regards to use suggestions, DG can be used for many building purposes: structural element in masonry; floor tile for pedestrian paths but not for heavy traffic; and as resulted salt and frost resistant, DG can be also used as slabs (minimum thickness of 1.72 cm), kerbs (minimum thickness of 2.58 cm), and setts for external paving in cold areas.

San Lucido calcarenite (CS)

- (1) This stone, which is commercially known as “Pietra di San Lucido” or as “Mendicino calcarenite or tuff”, was employed in the last centuries by the most important School of stonemasons of Rogliano and Altilia; principally, to realize portals and masonries. Due to CS’s easy workability, it was also widely employed as an ornamental stone. Many Calabrian historical centers of the Coastal Tyrrhenian area and of the central area of the Crati River (Italy), are built with this building stone.
- (2) The petrographic analysis indicated that CS is a compact carbonate stone with a large amount of fossils. The oriented thin sections demonstrated that CS is petrographically *isotropic* and is classified as *biopelmicrite/biopelsparite* or *packstone*; chromatic parameters indicated that CS is a homogeneous stone, for the low standard deviations.
- (3) CS stone’s classifications is/has: *many pores* (p_o : von Moos & De Quervain, 1948); *high porosity* (p_o : Anon, 1979); *microporosity* (μm : De Quervain, 1967); *medium absorbing* (C_c : Siegesmund &

Dürrast, 2014); *weather and frost resistant* (S: Hirschwald, 1912); *high velocity – class 4* (UPV: Anon, 1979); *low deformability* (E: Bell & Lindsay, 1999); *intermediate micro-hardness* (Knoop: Reguerio, 2005); *moderately strong* (UCS: Anon, 1977); *high strength* ($I_{s(50)}$: Bell & Lindsay, 1999).

- (4) With regards to hydric behavior, CS is classified as *isotropic*, since significant variations along the two investigated directions were not apparent. On the contrary, the porosity value and the fast capillary absorption indicate that CS can be used for inside rather than outside purposes.
- (5) On one hand, the low hardness value, low drilling resistance, easy workability, indicate that CS can be used as ornamental stone. On the other hand, its chromatic parameters indicate that CS should not be used as ornamental stone because the light colour of the stone is especially sensitive to colour changes, which is a very important aspect in the field of monumental and/or ornamental stones. Moreover, due to low hardness, low drilling resistance, and high capillary coefficient values, it is not suggested to use CS in the lower parts of the building, to avoid mechanical damages provoked by impacts and to prevent capillary rise.
- (6) The results of water absorption by capillary test and ultrasound speed determination, performed along different directions of the same sample, highlight that the studied calcarenite is isotropic with respect to the mechanical and hydric behavior. Moreover, CS exhibited a fairly low anisotropy and high ultrasound values. As isotropic stone, CS can be used without regarding orientation.
- (7) According to the salt crystallization test performed, CS is slightly sensitive to degradation induced by salt crystallization. Even though CS did not display a significant weight loss, at the end of testing several specimens broke. Results of salt crystallization tests are conditioned by the heterogeneity of the stone texture. All samples at the end of the 15th cycle of crystallization displayed degradation forms, mainly consisting of differential degradation and detachment around bioturbations.

Moreover, CS's high open porosity, the relevant presence of microporosity and its chemical composition (prevalently calcium carbonate) make this stone sensitive to decay processes (pollutant agents and any process in which water is involved). The recommendation is to use this stone for inside purposes and where no salts are present.

- (8) With regards to suggested usage, CS can be used for many building uses: structural element in masonry; floor tiles for pedestrian traffic; floor but preferably for internal uses; and also as slabs (minimum thickness of approximately 2.3 cm) and kerbs (minimum thickness of approximately 3.5 cm).
- (9) Finally, since CS displays better mechanical properties than petrophysical features, the recommended use is for structural purposes, especially inside rather than for ornamental and external uses. Taking into consideration the number of active quarries, CS should be employed for large scale uses.

Fuscaldo sandstone (AF)

- (1) Commercially known as "Pietra di Fuscaldo" or as "Pietra dolce", this stone was employed by the most important Schools of stonemasons of Fuscaldo, from the 12th until the 18th century. Fuscaldo sandstone, commonly named as "tuff", was utilized to realize structural and ornamental elements, such as buildings, arches and portals of many Calabrian historical centers.
- (2) Petrographic analyses indicated that AF is a compact sandstone. The oriented thin sections demonstrated that AF presents a slight orientation of phyllosilicates, prevalently in the X-direction and is classified as *greywacke*. AF's chromatic parameters indicated that it is a heterogeneous stone, for the high standard deviations.

- (3) With regards to the stone classification, it can be said that AF is/has: *a lot of pores* (p_o: von Moos & De Quervain, 1948); *high porosity* (p_o: Anon, 1979); *microporosity* (μm: De Quervain, 1967); *medium absorbing* (C_C: Siegesmund & Dürrast, 2014); *weather and frost resistant* (S: Hirschwald, 1912); *low velocity – class 2* (UPV: Anon, 1979); *moderate deformability* (E: Bell & Lindsay, 1999); *intermediate micro-hardness* (Knoop: Reguerio, 2005); *moderately strong* (UCS: Anon, 1977); *high strength* (I_{S(50)}: Bell & Lindsay, 1999).
- (4) The micro-porosity, ranging between 1 and 10μm of AF, allows the formation of ice or salts on relatively low sub-zero temperatures or salt crystallization conditions. The presence of phyllosilicates and their orientation indicate other weak points of the stone, in front of physical damage, due both to the susceptibility of phyllosilicates and to the variability of AF properties along the spatial directions. The presence of phyllosilicates affects decay processes like the salt crystallization due to the high susceptibility of these minerals to physical damage, as testified by the amount of broken samples during the performed salt test. As the mechanical strength of the stone is also not very high, it cannot resist the stress exerted by the precipitating or growing crystals. Therefore, the application of this material under conditions where it can be subjected to salt weathering or frosting, is not recommended.
- (5) The hydric and the ultrasound test results displayed low ultrasonic velocity values and anisotropic behavior, with high water capillary coefficients pronounced in the X-direction. Thus, concerning building uses, this stone must be laid with the plane of greatest anisotropy or lowest V_p parallel to the direction in which the capillary water is absorbed (typically vertical and ascending), so as to minimize decay induced by water ingress.
- (6) The anisotropic behavior is also confirmed by mechanical tests. Strength values are very different along the three spatial directions. The mechanical properties were found to be greatly influenced by

anisotropy. The longitudinal and transverse wave velocity perpendicular to the anisotropy plane is approximately 40% lower than that parallel to that plane. The highest values are registered along the Z-direction (XY plane) while, on the contrary, the lowest ones along the X-direction (YZ plane). Thus, to improve AF mechanical behavior, the stone must be laid with the Z-axis vertical to the loading direction.

- (7) The low hardness values, low drilling resistance, and easy workability indicate that AF can be used as ornamental stone, as employed in the past by stonemasons. Furthermore, due AF's low hardness and high capillary coefficient values, it is not recommended to use this stone in the lower parts of buildings to avoid mechanical damages provoked by impacts and to prevent capillary rise.
- (8) According to the salt crystallization performed test, AF is very sensitive to degradation induced by salt crystallization, with the majority of specimens breaking by the end of testing. It has been classified as a not durable stone towards salt crystallization processes. Moreover, AF's high open porosity make this stone sensitive to decay processes and the recommendation is to use this stone for inside purposes and where no salts are present.
- (9) With regards to usage suggestions, AF can be used for these building purposes: structural element in masonry; floor tiles for pedestrian traffic; floor, however, preferably for internal uses; and as slabs (minimum thickness of approximately 2.1 cm) and kerbs (minimum thickness of approximately 3.2 cm).
- (10) In conclusion, AF did not display good petrophysical and mechanical properties when compared to the other investigated lithotypes. Moreover, AF's anisotropic behavior influenced performed tests. Therefore, it is recommended for building uses to consider AF's anisotropy. In particular, it is suggested positioning AF ashlar with the Z-direction parallel to the loading direction to obtain

higher strengths and, simultaneously, to minimize water absorption. Considering the number of active quarries, this stone should be employed for local uses.

General conclusions

Conclusively, anisotropy resulted an influencing factor for the stone behavior. Building material anisotropy determines the variability of petrophysical and mechanical properties along splitting planes, and the resistance to the agents inducing decay. Construction material anisotropy determines resistance to the agents inducing decay. The way in which these materials are positioned can contribute to decay by facilitating water ingress. Capillary water uptake is also influenced by the direction in which the stone is laid: absorption is greater in more anisotropic, more porous varieties, and in the direction parallel to the plane of anisotropy, where water is absorbed more quickly and with a higher coefficient.

The determination of the direction of anisotropy in a material is a simple, repetitive process that entails very low costs after the initial investment in equipment. This provides medium to long-term savings by delaying decay and lengthening the durability of materials and, therefore, buildings or infrastructures. This is a preventive conservation method in line with actual trends, as opposed to interventional or corrective conservation, which is always costlier and more invasive. Therefore, determining anisotropy is imperative to understanding behavior mechanisms in construction materials and that information must be considered, especially when using stones for building purposes. Evaluating anisotropy is also beneficial as a preventive conservation method by delaying decay and lengthening the durability of stone materials and, therefore, buildings or infrastructures. Moreover, to improve building durability, the suggestion is to place building stones with both a low degree of anisotropy and with similar petrophysical and mechanical behavior together, to prevent differential decay processes. In the first case, the degree of anisotropy, in fact, may expedite material decay, for it often favors water ingress

through slip planes (structural, textural or mineralogical orientations), generating differential decay among similar stone blocks. In the second case, small variations in the stone characteristics (e.g. mechanical strengths, coefficient of thermal expansion, durability resistance, capillary water absorption, modulus of elasticity, etc.) among more lithotypes employed in the same construction, may provoke differential decay processes due to the different behavior of each lithotype towards external agents. Ideally, considering, for example, the coefficient of thermal expansion and the modulus of elasticity, if two or more types of stone are to be used in juxtaposition in the same large structure, then to prevent differences in displacement occurring due to temperature change and due to loading, the coefficients of thermal expansion and the moduli of elasticity of the different stones should be chosen to be of similar magnitude.

The durability of the examined lithotypes has been determined as a function of several stone properties. The most important ones resulted: the mineralogical composition (*e.g.* the presence of phyllosilicates for their susceptibility or the presence of calcite for its solubility in solution); the pore size distribution (*e.g.* stones like AF with micropores between 1 and 10 μm resulted to be more sensitive than those, like DG, with higher amount of macropores); the open porosity and the hydric properties (*e.g.* the water uptake is determined by the open porosity, which controls the amount of absorbed fluid and by the capillary uptake, which controls the velocity of the stone saturation; the water uptake is directly connected to the amount of crystallizing salts or ice, and thus to the degree of damage); the mechanical properties (salt or ice crystallization produces stress over the pore surface; consequently, stone durability is closely related to both pore structure and strength, which is the material resistance to crystallization pressure; the higher the mechanical strength, the higher the stone resistance in front of decay processes).

Therefore, porosity resulted another important influencing factor for the stone behavior. In particular, accelerated aging tests highlighted that the studied lithotypes are sensitive or not to degradation induced by salt or ice crystallization depending on the open porosity and the pore size distribution. The mass loss during the test mostly depends on the open porosity as well as on the dimensional distribution of pores that determine the crystallization pressure. As demonstrated by the performed tests, in fact, only the open pores are interested by salt or ice crystallization, so that the higher open porosity the higher amount of salts or ice which crystallize causing the disaggregation of the sample and the consequent mass loss. In the investigated samples, micropores predominate (especially in AF with sizes in the range 1–10 μm), except in the case of DG samples where the greater average diameter of pores determines a higher resistance of DG to decay processes than the other lithotypes. Microporous stones (*e.g.* AF) or stones with high capillary porosity (*e.g.* CS) are more susceptible to salt crystallization- and frost-induced decay. This is due to the fact that the crystallization stress and, consequently, the mass loss in a large pore is lower than in a smaller one. Furthermore, insofar as porosity constitutes gaps in the solid phase of the stone creating weak areas, porosity has an obvious impact on its mechanical properties. Therefore, this study demonstrates that porosity plays a decisive role in the stone behavior and in decay processes.

In the field of new constructions and stone conservation, a solid background of the studied ideas in this thesis, assists the selection of the most adequate stones and uses. In addition, portable techniques employed in this thesis are vital for the evaluation of stone properties, especially in cases where sampling is limited, such as cultural heritage objects and architecture. These techniques are also essential to identify the optimum arrangement for stone properties in replacement or new construction works. The achieved results in this thesis contributes to the knowledge concerning the characterization, the durability, the use suggestions of building stones and their most important properties that influence petrophysical and mechanical behavior.

Symbols used

LMD	linear microcrack density
L*	lightness
a*	red-green coordinate
b*	yellow-blue coordinate
C*	Chroma
WI	whiteness index
YI	yellowness index
B	brightness
ρ_{sk}	real or skeletal density (g/cm^3)
ρ_b	apparent or bulk density (g/cm^3)
ρ_o	open porosity (%)
W_{vac}	water absorption vacuum (%)
I_c	compactness Index (%)
p_{tot}	total porosity (%)
AirP	air permeability (mD)
C_c or C_2 or C_1	capillary water absorption ($\text{g/m}^2\text{h}^{0.5}$)
W_{ab}	water absorption at atmospheric pressure (%)
S_i	saturation coefficient
W_{Ds}	water content evaporated
S	saturation degree
V_p	ultrasound propagation P-waves velocity (V_p) (m/s)
dM	total anisotropy index (%)
dm	relative anisotropy index (%)
V_s	ultrasound propagation S-waves velocity (m/s)
E	Young's modulus (GPa)
ν	Poisson's ratio
G	Shear modulus (GPa)
K	Bulk modulus (GPa)
L_s	Micro-hardness (Leeb)
DRi	Drilling resistance (N/mm)
UCS	Uniaxial compressive strength (MPa)
Ra	Compressive strength anisotropy (%)
R_{tf}	Flexural strength (MPa)
$R_{a_{tf}}$	Flexural strength anisotropy (%)
σ_t	Indirect tensile strength (MPa)
BAI	Tensile strength anisotropy (%)
$I_{S(50)}$	Point Load Index (MPa)
$I_{a(50)}$	Point Load anisotropy (%)
PSV	Polished stone value
LA	Los Angeles (%)
M_{DE}	Micro-Deval (%)

Bibliography

Bibliography

- (1) AA.VV. Basilicata Calabria. Guida D'Italia, Touring Club Italiano, Centro Grafico Ambrosiano, Milano, 1980, p. 427
- (2) AA.VV. La pietra, il mestiere e l'arte del decorare. Storia della lavorazione della pietra nella provincia di Cosenza, Pellegrini Editore, Cosenza, 2015, p.262
- (3) Adams A. E., MacKenzie W. S. A Colour Atlas of Carbonate Sediments and Rocks Under the Microscope, 1998. London: Manson.
- (4) Alehossein H., Boland J.N. Strength toughness and fatigue of rock. In: Atrens A., Boland J.N., Clegg R., Griffiths J.R. (Eds.). Structural Integrity and Fracture International Conference (SIF'04), Brisbane, Australia, 26th-29th September 2004
- (5) Allen T..Particle Size Measurement,4thed.Chapman and Hall, 1990, Chapter 19, pp.653-678
- (6) Altomare C. L'utilizzo della pietra per l'uso quotidiano tra XVI e XIX secolo: Matri fabbricatori, Muratori e Manipoli semplici, in "La pietra, il mestiere e l'arte del decorare. Storia della lavorazione della pietra nella provincia di Cosenza", Pellegrini Editore, Cosenza, 2015, pp. 74-91
- (7) Alvarez Manilla Aceves A., Garnica Anguas P., Pérez Salazar A. Evaluación indirecta de los módulos elásticos de rigidez in situ y la relación entre V_p/V_s y el ángulo de fricción interna, Publicación Técnica, Sanfandila, Qro, 2003, n. 225
- (8) Almeida L.C.R., Marques E.A.G., Vargas Jr. E.A., Barros W.T. Characterization and utilization of tensile strength and toughness of granitic and gneissic rocks of Rio de Janeiro City—a proposal for optimizing rock blasting processes. In: Moore, D.P, Hungr, O. (Eds.), Proc. 8th Int. Cong. of IAEG, 1998, vol. 1. Balkema, Vancouver, pp. 351-357
- (9) Ameduri M. Su alcuni portali litici barocchi dell'attuale provincia di Cosenza, in "La pietra, il mestiere e l'arte del decorare. Storia della lavorazione della pietra nella provincia di Cosenza", Pellegrini Editore, Cosenza, 2015, pp. 130-136
- (10) Amodio-Morelli L., Bonardi G., Colonna V., Dietrich D., Giunta G., Ippolito F., Liguori V., Lorenzoni S., Paglionico A., Perrone V., Piccarreta G., Russo M., Scandone P., Zanetti-Lorenzoni E., Zuppetta A. The Calabrian-Peloritan Arc in the Apennine-Maghrebide orogen. Memorie della Società Geologica Italiana, 1976, 17, pp.1-60
- (11) Anania L., Badalà A., Barone G., Belfiore C. M., Calabrò C., La Russa M. F., Mazzoleni P., Pezzino A. The stones in monumental masonry buildings of the "Val di Noto" area: New data on the relationships between petrographic characters and physical-mechanical properties, Construction and Building Materials, 2012, n.33, pp. 122-132
- (12) Anastasio M. Fuscaldo: Cento Portali - Raccolta di documenti per apprendere la saggezza di una cultura antica e raccoglierne l'irresistibile messaggio, Rho, 1996, pp. 1-79
- (13) Anon. The description of rock masses for engineering purposes. Quarterly Journal of Engineering Geology, 1977, 10, pp.355-388.
- (14) Anon. Classification of rocks and soils for engineering geological mapping. Part 1 – Rock and soil materials, Bull. Int. Assoc. Eng. Geol. 19, 1979, pp. 364-371
- (15) Antonacci E., Avola S., De Leo A., Fanale L., Galeota D., Gregori A., Romagnoli A., Quaresima R., Tohme D. L'attività del DICEAA nella ricostruzione dopo sisma 2009: alcuni esempi di ricerche e applicazioni. INGENIO, 2014 LF, v2 rev sg, pp.1-28. <http://www.ingenio-web.it/immagini/Articoli/PDF/eHKxGXoBmh.pdf>
- (16) Aoki H., Matsukura Y. A new technique for non-destructive field measurement of rock-surface strength: an application of the Equotip hardness tester to weathering studies, Earth Surf. Processes Landforms 32 (12), 2007, pp.1759-1769

- (17) Apollaro C., Accornero M., Marini L., Barca D., De Rosa R. The impact of dolomite and plagioclase weathering on the chemistry of shallow groundwaters circulating in a granodiorite-dominated catchment of the Sila Massif (Calabria, Southern Italy). *Applied Geochemistry*, 2009, 24, pp.957–979
- (18) Argentieri B., I ponti di San Giovanni. *Nuovo Corriere della Sila*, 03 febbraio 2013, <http://www.ilnuovocorrieredellasila.it/?p=1247>
- (19) Arikan F., Ulusay R. and Aydin N. Characterization of weathered acidic volcanic rocks and a weathering classification based on a rating system. *Bulletin of Engineering Geology and the Environment*, 66, 2007, pp. 415-430
- (20) Arnold A., Zehnder K. Salt weathering on monuments. In Fulvio Zezz (Ed.) “Estratti: La conservazione dei monumenti nel bacino del Mediterraneo. Influenza dell'ambiente costiero e dello spray marino sulla pietra calcarea e sul marmo. Atti del I Simposio internazionale Bari 7-10 giugno 1989, pp.31-58
- (21) Ashmole I., Motloung M. Dimension stone: the latest trends in exploration and production technology, The Southern African Institute of Mining and Metallurgy, Surface Mining, 2008, pp. 35-70
- (22) ASTM E313-98. Standard Practice for Calculating Yellowness and Whiteness Indices from Instrumentally Measured Colour Coordinates, 1998
- (23) ASTM D5731-08. Standard Test Method for Determination of the Point Load Strength Index of Rock and Application to Rock Strength Classifications, 2008
- (24) ASTM D5873-14. Standard Test Method for Determination of Rock Hardness by Rebound Hammer Method, 2014
- (25) Aydin A., Basu A. The Schmidt hammer in rock material characterization. *Engineering Geology* 81, 2005, pp. 1 –14
- (26) Ayuso R. A., Messina A., De Vivo B., Russo S., Woodruff L. G., Sutter J. F., Belkin H. E. Geochemistry and argon thermochronology of the Variscan Sila Batholith, southern Italy: source rocks and magma evolution. *Contrib Mineral Petrol*, 1994, 117, pp.87-109
- (27) Barla G., Innaurato N. Indirect tensile strength of anisotropic rocks. *Rock Mech.*, 1973, 5, pp.215–230.
- (28) Barrio G. *Antichità e luoghi della Calabria*, Cosenza, Brenner, 1979
- (29) Barry R. *The construction of buildings – Volume 2*. 5th Edition, Blackwell Science, United Kingdom, 1999, 202 pp.
- (30) Barton N. *Rock quality, seismic velocity, attenuation and anisotropy*. Taylor and Francis, London, 2007, p. 104
- (31) Baumgart F. *Stiffness--an unknown world of mechanical science?*. Injury. Elsevier, 2000, 31, doi:10.1016/S0020-1383(00)80040-6
- (32) Beaudoin J.J., MacInnis C. The mechanism of frost damage in hardened cement paste. *Cem. Concr. Res.*, 1974, 4, pp.139–147
- (33) Behrestaghi M.H.N., Rao K.S., Ramamurthy T. Engineering geological and geotechnical responses of schistose rocks from dam project areas in India. *Eng. Geol.*, 1996, 44 (1–4), pp.183–201
- (34) Bell F.G., Dearman W.R. Assesment of the durability of sandstones with illustrations from some buildings in the North of England. *Engineering Geology of Ancient Works, Monuments and Historical Site*, Rotterdam, 1988, pp. 707-716
- (35) Bell F.G., Lindsay P. The petrographic and geomechanical properties of some sandstones from the Newspaper Member of the Natal Group near Durban, South Africa. *Engineering Geology* 53, 1999, pp.57–81
- (36) Benavente D. *Modelización y estimación de la durabilidad de materiales pétreos porosos frente a la cristalización de sales*. Tesis doctoral Universidad de Alicante, 2003, 289 pp.
- (37) Benavente D., García-del-Cura M. A., Fort R., Ordoñez S. Thermodynamic modelling of changes induced by salt pressure crystallization in porous media of stone. *Journal of Crystal Growth*, 204, 2003 (a), pp.168-178

- (38) Benavente D., Martínez-Verdú F., Bernabéu A., Viqueira V., Fort R., García del Cura M. A., Illueca C., Ordóñez S. Influence of Surface Roughness on Color Changes in Building Stones. Volume 28, Number 5, October 2003 (b), pp.1-9
- (39) Benavente D., Cueto N., Martínez-Martínez J., García-del-Cura M. A., Cañaveras J.C. The influence of petrophysical properties on salt weathering of porous building rocks. *Environmental Geology*, 52(2), 2007a, pp. 197-206
- (40) Benavente D., Martínez-MARTÍNEZ J., Jáuregui P., Rodríguez M.A., García del Cura M.A. Assessment of the strength of building rocks using signal processing procedures. *Construction and Building Materials*, 2006, 20 pp.562-568
- (41) Benavente D., Martínez-Martínez J., Cueto N., García-del-Cura M. A. Salt weathering in dual-porosity building dolostones. *Engineering Geology*, 94, 2007b, pp.215-226
- (42) Benavente D., Medina-Lapeña F. J., Martínez-Martínez J., Cueto N., García-del-Cura M. A. Influencia de la petrografía en las propiedades petrofísicas y de durabilidad del Travertino Clásico. Valoración de su anisotropía, *GEOGACETA*, 2009, 46, 147-250.
- (43) Benson P. M., Meredith P.G., Platzman E.S., White R.E. Pore fabric shape anisotropy in porous sandstones and its relation to elastic wave velocity and permeability anisotropy under hydrostatic pressure. *International Journal of Rock Mechanics and Mining Sciences*, 2005, 42 pp. 890-899
- (44) Bieniawski Z.T. Mechanism of brittle fracture of rock. *Int. J. Rock Mech. Min. Sci.* 1967, n. 4, pp.395–430
- (45) Bieniawski Z.T. Point load in geotechnical practice. *Eng Geol*, 1975, 9, pp.1–11
- (46) Bieniawski Z.T., *Rock mechanics design in mining and tunneling*, A.A. Balkema, 1984, p.227
- (47) Binda L., Drdácky M., Kasal B. (eds). In-situ evaluation and non-destructive testing of historic wood and masonry structures. Institute of Theoretical and Applied Mechanics of the Academy of Science of the Czech Republic. Prague, 2007, pp. 253
- (48) Bitonti T. Appunti per la lettura di una chiesa medievale: l'Abbazia di San Giovanni in Fiore. *Calabria sconosciuta: rivista trimestrale di cultura e turismo*, 1994, 61(gen-mar), pp. 61-62
- (49) Bläuer C., Kueng A. Examples of microscopic analysis of historic mortars by means of polarising light microscopy of dispersions and thin sections. Special issue, *Materials Characterization*, 2007, 58 (11–12): 1199–207.
- (50) Borrelli E., Urland A. *ARC Laboratory Handbook*. Rome: ICCROM, 1999. http://www.iccrom.org/pdf/ICCROM_14_ARCLabHandbook00_en.pdf
- (51) Borrelli L., Coniglio S., Critelli S., La Barbera A., Gullà G. Weathering grade in granitoid rocks: The San Giovanni in Fiore area (Calabria, Italy). *Journal of Maps*, 2015, <http://dx.doi.org/10.1080/17445647.2015.1010742>
- (52) Bourgès A. Holistic correlation of physical and mechanical properties of selected natural stones for assessing durability and weathering in the natural environment. PhD diss., Universität München, 2006. http://edoc.ub.uni-muenchen.de/5505/1/Bourges_Ann.pdf
- (53) Bourgès A., Fehr K.T., Simon S., Snelthage R. Correlation between the micro-structure and the macroscopic behavior of sandstones. *Restoration of Buildings and Monuments*, 2008. An International Journal = Bauinstandsetzen und Baudenkmalpflege: Eine internationale Zeitschrift 2008, 14 (3): 157–66
- (54) Brandi C. *Teoría de la restauración*, Alianza Editorial, 1977
- (55) Broch E. Estimation of strength anisotropy using the point-load test. *Int. J. Rock Mech. Min. Sci. Geomech. Abstr.*, 1983, 20(4):181–7
- (56) Broch E., Franklin J.A. Point load strength test. *Int J Rock Mech Min Sci* 9, 1972, pp.669–697
- (57) Brosch F.J., Schachner K., Bluemel M., Fasching A., Fritz H. Preliminary investigation results on fabrics and related mechanical properties of an anisotropic gneiss. *J Struct Geol*, 2000, 22, pp.1773–1787
- (58) Bruno E. (Ed.). *Scalpellini a San Giovanni in Fiore*, Centro Servizi Culturali, San Giovanni in Fiore, 1993
- (59) Bruno E. *Scalpellini di Calabria – I cantieri e le scuole*, La petite Académie, Fuscaldo Marina (CS), 1995

- (60) Buj Fandos O. Caracterización tecnológica de las rocas aragonesas de usos constructivos: propiedades hídras y durabilidad de las rocas con uso ornamental. 1st Edition, Zaragoza, Consejo Económico y social de Aragón, 2009, 250 pp.
- (61) Buj Fandos O., Gisbert J., Colucci M. F. Variaciones en el sistema poroso de materiales pétreos tras la aplicación de productos de conservación. *Revista de la sociedad española de mineralogía MACLA*, 2007, 7: 85
- (62) Camuffo D. Limits of stone sensitivity to freezing-thawing cycles. In: Vicente M.A., Delgado-Rodriguez J., Acevedo J. (Eds.). *Proceedings of the European Commission Research Workshop on Degradation and Conservation of Granitic Rocks in Monuments*, Spain, 1996, pp.455-462
- (63) Cardani G., Meda A. Marble behaviour under monotonic and cyclic loading in tension. *Construction Building Materials* 2004, 18, pp.419–424
- (64) Cargill J.S., Shakoor A. Evaluation of empirical methods for measuring the uniaxial compressive strength of rock. *Int. J. Rock Mech. Min. Sci. Geomech. Abstr.*, 1990, 27, pp.495–503
- (65) Carmichel R.S. *Practical handbook of physical properties of rocks and mineral*. CRS Press Inc., 1989, USA
- (66) Casmez. *Carta Geologica della Calabria - Foglio 236, IV N.O. – San Lucido (in scale 1/25000)*. Poligrafica & CarteValori, Ercolano, Napoli, Italy, 1967 (a)
- (67) Casmez. *Carta Geologica della Calabria - Foglio 229, III S.O. – Paola (in scale 1/25000)*. Poligrafica & CarteValori, Ercolano, Napoli, Italy, 1967 (b)
- (68) Ceraudo G. Le maestranze roglianesi. *Calabria Letteraria: periodico mensile di cultura regionale*, 1996, n.4-6 (apr-giu), pp.44-45
- (69) Cerdeño del Castillo F.J., Díaz R., González I., López González-Mesones F., Obis J., Pérez A., Regueiro M., Tirado A., Vera R. *La piedra en la arquitectura contemporánea*, 2007, Edita Aitemin, 245 pp.
- (70) Ceruti F., Di Gregorio A. Risorse minerarie e sostenibilità in Italia, *Ecoscienza*, 2014, n.6, pp.36-37
- (71) Chabas A., Jeannette D. Weathering of marbles and granites in marine environment: petrophysical properties and special role of atmospheric salts. *Environmental Geology*, 40 (3), 2001, pp.359-368
- (72) Chabertlain P.G., Van E., Podmięks E.R. Four factors influencing observed rock properties. *Soil Specimen Preparation Lab Test ASTM STP*, 1976, 599, pp.21–36.
- (73) Chen C.S., Pan E., Amadei B. Determination of deformability and tensile strength of anisotropic rock using Brazilian tests. *Int. J. Rock Mech. Min. Sci.*, 1998, 35 (1), pp. 43–61
- (74) Chen S., Yue Z.Q., Tham L.G., Lee P.K.K. Modelling of the indirect tensile test for inhomogeneous granite using a digital image-based numerical method. *Int. J. Rock. Mech.*, 2004, 41(S1), pp.466–471.
- (75) Chuanchenga Y., Wenxia C., Haiyue D. Research on Comparison of the Maximum Dynamic Shear Modulus Test. *International Conference on Modern Hydraulic Engineering*, 2012, n. 28, pp.230-234
- (76) Colella A. Sedimentation, deformational events and eustasy in the perityrrhenian Amantea Basin: preliminary synthesis, *Giorn. Geol.*, 57, I-2, 1995, pp. 179-193
- (77) Coviello A., Lagioia R., Nova R. On the Measurement of the Tensile Strength of Soft Rocks. *Rock Mech. Rock Engng.*, 2005, 38 (4), pp.251–273, DOI 10.1007/s00603-005-0054-7
- (78) Crisci G.M., Davoli M., De Francesco A.M., Gagliardi F., Gattuso C., Mercurio P., Miriello D. L'analisi composizionale delle malte, un valido mezzo per risalire alle fasi costruttive. Risultati preliminari. *Atti del II Congresso Nazionale di Archeometria*, Bologna, 2002
- (79) Crisci G.M., De Francesco A.M., Gattuso C., Miriello D. Un metodo geochimico per la determinazione della provenienza di lapidei macroscopicamente omogenei. Un esempio di applicazione sui monumenti del centro storico di Cosenza, *Arkos – Scienze e Restauro dell'architettura* 2, anno IV, aprile/giugno 2003, pp.52-59

- (80) Critelli S., Di Nocera S., Le Pera E. Approccio metodologico per la valutazione petrografica del grado di alterazione degli gneiss del Massiccio Silano (Calabria settentrionale). *Geologia Applicata e Idrogeologia*, 1991, 26, pp.41–70
- (81) Critelli S., Le Pera E. Geological Map of Calabria, scale 1:330,000, in S. Gabriele (Ed.), *Valutazione delle Piene in Calabria. Caratteristiche morfometriche dei bacini della Calabria*, Rubbettino, Soveria Mannelli (CZ), 2000
- (82) Critelli S., Muto F., Tripodi V., Perri F. Link between thrust tectonics and sedimentation processes of stratigraphic sequences from the southern Apennines foreland basin system, Italy. *Rendiconti Online della Società Geologica Italiana*, 2013, 25, pp.21–42
- (83) Croci G., Delgado Rodrigues J. Surface and structural stability for the conservation of historic buildings. In *Science and Technology of the Environment for Sustainable Protection of Cultural Heritage*, 2002, EC Advanced Study Course, London: University College London. http://www.ucl.ac.uk/sustainableheritage/Archive_0906/sustainableheritage/sustainableheritage/learning/asc/delegates/coursematerials.html
- (84) D'Andrea D.V., Fischer R.L., Fogelson D.E. Prediction of compressive strength of rock from other properties. US Bureau of Mines Report, 1965, Investigation n. 6702
- (85) Dai F. Xia K., Zuo J. P., Zhang R., Xu N. W. Static and Dynamic Flexural Strength Anisotropy of Barre Granite, *Rock Mech Rock Eng*, 2013, 46, pp.1589–1602, [DOI 10.1007/s00603-013-0390-y](https://doi.org/10.1007/s00603-013-0390-y)
- (86) Damiani A. V. Osservazioni geologiche in alcune tavolette del F° 220 della Calabria nord-occidentale. Parte I: Stratigrafia, *Boll. Soc. Geol. It.*, 1970, 89, pp.65-80
- (87) Davis J.C. *Statistics and Data Analysis in Geology*. John Wiley and Sons, 1986, New York
- (88) De Quervain F. *Technische Gesteinskunde. Lehrbücher und Monographien aus dem Gebiete der exakten Wissenschaften. Mineralogisch-geotechnische Reihe, Bd 1*. Birkhäuser, Basel, 1967
- (89) Deere D.U., Miller R.P. Engineering classification and index properties for intact rock. Technical Report n. AFWLTR- 65–116. Air Force Weapons Lab, Kirkland Air Force Base, 1966, 308 pp
- (90) Delgado Rodrigues J. Evaluación del comportamiento expansivo de las rocas y su interés en conservación = Swelling behaviour of stones and its interest in conservation. An appraisal. *Materiales de construcción*, 2001, (263–64): 183–95
- (91) Delgado Rodrigues J., Ferreira Pinto A., Costa, D. Tracing of decay profiles and evaluation of stone treatments by means of microdrilling techniques. *Int. J. Cultural Heritage*, 2002, 3, pp.117–125
- (92) Di Benedetto D. Un esempio di geomorfologia calabrese: gli sferoidi granitici della Sila. *Calabria Libri*, Rubbettino Editore, Catanzaro, 1982, n.3-4
- (93) Di Benedetto D., Greco A. Notizie storico-documentarie sui materiali lapidei ornamentali della Calabria: situazione attuale e prospettive future della industria estrattiva. *Quarry and Construction*, 1990, n.5, Parma, Ed. Pei
- (94) Doehne E., Price C.A. *Stone Conservation An Overview of Current Research*. 2nd Edition. The Getty Conservation Institute Los Angeles, California, 2010, 175 pp., ISBN 978-1-60606-046-9, http://www.getty.edu/conservation/publications_resources/pdf_publications/pdf/stoneconservation.pdf
- (95) Dokic O., Matovic V., Eric S., Šaric K. Influence of engineering properties on Polished Stone Value (PSV): A case study on basic igneous rocks from Serbia. *Construction and Building Materials*, 101, 2015, pp.1088–1096
- (96) Domasłowski W. Investigations on technology of joint mortars in brick. In: Fassina V. (Ed.) *Proceedings of the 9th international congress on deterioration and conservation of stone*, Venice, 19–24 June, 2000. Elsevier, Amsterdam, pp.843–852
- (97) Dorn R.I., Whitley D.S., Cerveny N.V., Gordon S.J., Allen C.D., Gutbrod E. The Rock Art Stability Index: A new strategy for maximizing the sustainability of rock art. *Heritage Management*, 2008, 1 (1), pp.37–70
- (98) Douglass P.M., Voight B. Anisotropy of granites: a reflection of microscopic fabric. *Geotechnique*, 1969, 19(3), pp. 376–98

- (99) Dubois C., Couchot P., Alvaret Calleja A., Boeglin E., Chambaudet A. Specific mercury porosimetry for low-porosity materials. *Measurement Science Technology*, 1998, 9, pp. 2016-2022
- (100) Duffus P., Wangler T., Scherer G. W. Swelling damage mechanism for clay-bearing sandstones. In *Proceedings of the 11th International Congress on Deterioration and Conservation of Stone*, 15–20 September 2008, Torun, Poland. J. W. Lukaszewicz and P. Niemcewicz (Eds.), 2008, 65–72. Torun, Poland: Nicolaus Copernicus University
- (101) Dunham R. J. Classification of carbonate rocks according to depositional texture. In: Ham W.E. (Ed.), *Classification of carbonate rocks*, *Am Assoc Petrol Geol Memo*, 1962, pp. 108–210
- (102) Dürrast H., Siegesmund S. Correlation between rock fabrics and physical properties of carbonate rocks. *International Journal of Earth Sciences*, 88, 1999, pp. 392-408
- (103) El-Gohary M. Effective roles of some deterioration agents affecting Edfu Royal birth house "Mammisi". *International Journal of Conservation Science*, v.6, Issue 3, July-September 2015, pp. 349-368
- (104) Engelder T., Plumb R. Changes in in situ ultrasonic properties of rock on strain relaxation. *Int. J. Rock Mech. Min. Sci. Geomech. Abstr.* 1984, 21 (2), 75– 82.
- (105) Erichsen E., Ulvik A., Sævik K. Mechanical Degradation of Aggregate by the Los Angeles, the Micro-Deval and the Nordic Test Methods. *Rock Mechanics and Rock Engineering*, 2011, 44:333
- (106) Esbert R.M., Ordaz J. Alteración y alterabilidad de las piedras de la constricción: criterios petrofísicos y ensayos de laboratorio. *Primer Congreso de Patología de la Edificación*, C.O.A.C., Barcelona, 1985, p. 15
- (107) Esbert R.M., Valdeón L. Relación entre porosidad, contenido en arcillas y durabilidad de areniscas. *Materiales de construcción*, 35, 1985, pp. 15-22
- (108) Esbert R.M., Ordaz J., Alonso F.J., Montoto M. *Manual de diagnosis y tratamiento de materiales pétreos y cerámicos*. Col·legi d'Aparelladors i Arquitectes Tècnics de Barcelona, Barcelona, 1997, p. 139
- (109) Evangelista V., Foschia M., Montani M. Study for the HFC criteria revision and SFC criteria development – Preliminary Report, *Life Cycle Engineering*, 2007
- (110) Everett D.H. The thermodynamics of frost damage to porous solids. *Trans. Faraday Soc.*, 1961, 57, pp.1541–1551
- (111) Exadaktylos G. Characterization of mechanical properties and damage of natural building stones in historical monuments – Report of the MONUMENTS PROJECT – SMT4-CT96-2130, 1998. <http://www.mred.tuc.gr/projects/monuments/monuments.html>
- (112) Exadaktylos G., Tiano P., Filareto C., Validation of a model of rotary drilling of rocks with the drilling force measurement. *International Journal for Restoration of Buildings and Monuments*, 2000, 3, pp.307-340
- (113) Fernandes, F. Lourenço, P. Evaluation of the Compressive Strength of Ancient Clay Bricks Using Microdrilling. *Journal of Materials in Civil Engineering*, 2007, 19, pp.791-800
- (114) Fernandez-Revuelta B., Galán L., Fort R., Varas M. J., Alvarez de Buergo M. Influencia de la anisotropía en la caracterización hídrica de la Pizarra de Bernardos *Geotemas*, 2008, 10, 1539–42
- (115) Ferreira Pinto A., Delgado Rodrigues J. Assessment of the durability of water repellents by means of exposure tests. In: Fassina V. (Ed) *Proceedings of the 9th international congress on deterioration and conservation of stone*, vol 2, Venice, 19–24 June. Elsevier, Amsterdam, 2000, pp 273–285
- (116) Filomena C. M., Hornung J., Stollhofen H., Assessing accuracy of gas-driven permeability measurements: a comparative study of diverse Hassler-cell and probe permeameter devices, in “Solid Earth”, 2014, n.5, pp.1-11
- (117) Fitzner B. Documentation and evaluation of stone damage on monuments. In: D. Kwiatkowski, Löfvendahl R. (Eds.), *Proceedings of the 10th International Congress on Deterioration and Conservation of Stone*, Stockholm, June 27–July 2, 2004, vol. 2, 677–90. Stockholm: ICOMOS Sweden

- (118) Fitzner B., Heinrichs K., Kownatzki R. Weathering forms at natural stone monuments: Classification, mapping and evaluation. *Restoration of Buildings and Monuments: An International Journal = Bauinstandsetzen und Baudenkmalpflege: Eine internationale Zeitschrift*, 1997, 3 (2): 105–24
- (119) Fitzner B., Heinrichs K., La Bouchardiere D. The Bangudae Petroglyph in Ulsan, Korea: Studies on weathering damage and risk prognosis. *Environmental Geology*, 2004, 46 (3– 4): 504–26
- (120) Folk R. L. Practical petrographic classification of limestone, *Bull. Am. Assoc. Pet. Geol.*, 1959, 43, pp.1–38
- (121) Forestieri G., Tedesco A., Ponte M., Olivito R. S. Relationship between stone characteristics and weathering. Case study: sandstone elements of the old town of Fuscaldo (Italy) In: Campanella L., Piccioli C. (Eds.) “Diagnosis, Conservation and Valorization of Cultural Heritage – Proceedings of the VIth International Conference”, December 2015, Naples (Italy), pp.173-185, ISBN:978-88-86208-69-7
- (122) Forestieri G., Campolongo A., Ponte M. La pietra e l’architettura. Analisi storica e materica del materiale lapideo nel territorio di Cosenza. In D’Agostino S. (Ed.), Proceedings of the 2nd International Conference “History of Engineering”, 22nd-23rd April 2016 (a), Naples (Italy), v.1, pp. 213-222, ISBN:978-88-86638-33-3
- (123) Forestieri G., Tedesco A., Ponte M., Olivito R.S. Local building stones used in Calabrian architecture: calcarenite and sandstone of the Thyrrhenian Coastal Range of Cosenza Province (Italy). In: Gambardella C. “Le Vie dei Mercanti - XIV International Forum: World Heritage and Degradation, Smart Design, Planning and Technologies”, La scuola di Pitagora editrice, Napoli, 16th-17th-18th June 2016 (b), Aversa/Naples/Capri, ISBN/ISSN: 978-88-6542-257-1
- (124) Fort R. Caracterización cromática de los materiales de construcción. Degradación y conservación del Patrimonio Arquitectónico, Madrid, Editorial Complutense, 1996, pp. 213-226
- (125) Fort R. La piedra natural y su presencia en el Patrimonio Histórico. *Enseñanzas de las Ciencias de la Tierra* 17, 2009, pp. 16–25.
- (126) Fort R., Fernández-Revuelta B., Álvarez Varas M.J., de Buergo M., Taborda-Duarte M. Influence of anisotropy on the durability of Madrid-region Cretaceous dolostone exposed to salt crystallization processes, *Materiales de Construcción*, 58(289–290), 2008, pp.161–178.
- (127) Fort R., Varas M. J., Álvarez de Buergo M., Martín-Freire D. Determination of anisotropy to enhance the durability of natural stone. *Journal of Geophysics and Engineering* 8, 2011, pp. 132-144
- (128) Fort R., Álvarez de Buergo M., Pérez-Monserrat E.M. The reading of Non-destructive testing for the assessment of granite decay in heritage structures compared to quarry stone. *Int J Rock Mech Min*, 2013, 61, pp.296-305
- (129) Fort R., Álvarez de Buergo M., Pérez-Monserrat E.M., Gómez-Heras M., Varas-Muriel M.J., Freire-Lista D.M. Evolution in the use of natural building stone in Madrid Spain. *Q. J. Eng. Geol. Hydrogeol.*, 2013, 46, pp. 421–429. <http://dx.doi.org/10.1144/qjegh2012-041>
- (130) Frangipane A. *Maestranze di Calabria. Il Ponte: rivista mensile diretta da Pietro Calamandrei*, 1950, n.9-10 (sett-ott), pp.1.136-1.143
- (131) Franklin J.L., Broch E. The point load test. *International Journal of Rock Mechanics and Mining Science*, 9, 1972, 669–697
- (132) Franzen C., Mirwald P.W. Moisture content of natural stones: static and dynamic equilibrium with atmospheric humidity. *Environ Geol*, 2004, 46, pp.391–401
- (133) Fratini F., Rescic S., Tiano P. A new portable system for determining the state of conservation of monumental stones. *Materials and Structures*, 2006, 39: 139-147
- (134) Freire-Lista D.M., Fort R. Decay in heritage granite ashlars. Its dependence with exfoliation microcracks. *Rend. Online Soc. Geol. It.*, 2015, Suppl. n. 2 al Vol. 35, p.340
- (135) Freire-Lista D.M., Fort R. Causes of scaling on bush-hammered heritage ashlars: a case study—Plaza Mayor of Madrid (Spain), *Environ. Earth Sci.*, 2016, 75:932, DOI 10.1007/s12665-016-5688-0

- (136) Freire-Lista D.M., Fort R., Varas-Muriel M.J. Berroqueña stone of Madrid (Spain). A traditional and contemporary building stone, *Geophysical Research Abstracts* Vol. 16, EGU2014-13039, 2014
- (137) Freire-Lista D.M., Fort R., Varas-Muriel M.J. Alpedrete granite (Spain). A nomination for the “Global Heritage Stone Resource” designation, *IUGS*, June 2015 a, 106-113
- (138) Freire-Lista D.M., Fort R., Varas-Muriel M.J. Freeze–thaw fracturing in building granites, *Cold Regions Science and Technology*, 2015 b, 113, pp.40–51
- (139) García de los Ríos J., Baez J.M. *La Piedra de Castilla y León*. Junta de Castilla y León, 2001, 345 pp.
- (140) Gauri K. L., Bandyopadhyay J.K. *Carbonate Stone: Chemical Behavior, Durability, and Conservation*, 1999, New York: Wiley
- (141) Gebrande H. Elasticity and inelasticity. In: Augenheister G. (Ed.) *Landolt-Börnstein, Band 1, Physikalische Eigenschaften der Gesteine*, 1982, Springer, Berlin
- (142) Giesche H. Mercury porosimetry: a general (practical) overview. *Part. Part. Syst. Charact.* 23, 2006, pp. 1–11, <http://dx.doi.org/10.1002/ppsc.200601009>
- (143) Giuzio B., Alvarez de Buergo M., Fort R., Masini N. Influence of coupling substances in the measurement of ultrasound velocity in stone materials. Poster EGU General Assembly, 2015
- (144) *Geophysical Research Abstracts*, Vol. 17, EGU2015-6623-1, 2015
- (145) Goldsmith W., Sackman J.L., Ewert C. Static and dynamic fracture strength of Barre granite. *Int J Rock Mech Min*, 1976, 13(11), pp.303–309
- (146) Goudie A.S. Experimental salt weathering of limestones in relation to rock properties. *Earth Surface Processes and Landforms*, 24, 1999, pp. 715-724
- (147) Gramberg J. *A Non-conventional View on Rock Mechanics and Fracture Mechanics*. Balkema, Rotterdam, 1989, (published for the Commission of European Communities, Rotterdam)
- (148) Grandjacquet C. Données nouvelles sur la tectonique tertiaire des massifs calabro-lucaniens, *Bull. Soc. Geol. De France*, 1962, 7 set, 4, pp.695-706
- (149) Grandjacquet M. J. Geologie de la zone Diamante-Verbicaro (Calabrie), *Geol. Romana*, 1962, 1, pp.297-312
- (150) Grimmer A.E. (Ed.) *A Glossary of Historic Masonry Deterioration Problems and Preservation Treatments*. Washington, DC: Dept. of the Interior, National Park Service, Preservation Assistance Division (US Government Printing Office), 1984
- (151) Grossi C.M., Brimblecombe P., Esbert M. R., Alonso F. J. Colour Changes in Architectural Limestones from Pollution and Cleaning. *Colour research and application*, V. 32, Number 4-August 2007, pp. 320-331
- (152) Günes Yılmaz N. The Influence of Testing Procedures on Uniaxial Compressive Strength Prediction of Carbonate Rocks from Equotip Hardness Tester (EHT) and Proposal of a New Testing Methodology: Hybrid Dynamic Hardness (HDH). *Rock Mech Rock Eng*, 2013, 46, pp.95–106, DOI 10.1007/s00603-012-0261-y
- (153) Günes Yılmaz N., Karaca Z., Goktan R. M., Akal C. Relative brittleness characterization of some selected granitic building stones: Influence of mineral grain size, *Construction and Building Materials*, Volume 23, Issue 1, 2009, pp. 370-375
- (154) Günes Yılmaz N., Goktan R. M., Kibici Y. Relations between some quantitative petrographic characteristics and mechanical strength properties of granitic building stones. *International Journal of Rock Mechanics & Mining Sciences*, 2011, pp. 506–513
- (155) Gupta A. S., Seshagiri Rao K. Weathering effects on the strength and deformational behaviour of crystalline rocks under uniaxial compression state, *Engineering Geology*, n. 56, 2000, pp. 257–274
- (156) Guydader J., Denis A. Propagation des ondes dans les roches anisotropes sous contrainte évaluation de la qualité des schistes ardoisiers. *Bull. Eng. Geo.* Vol. 33, 1986, pp. 49-55

- (157) Habekost M. Which colour differencing equation should be used?. In: International Circular of Graphic Education and Research, 2013, Number 6, pp. 20-33
- (158) Hammam A.H., Eliwa M. Comparison between results of dynamic & static moduli. HBRC Journal, n. 9, 2013, pp.144-149
- (159) Hassan M., Burdet O., Favre R., Ultrasonic measurements and static load tests in bridge evaluation, NDT&E International, 1995, 28 (6), pp. 331–337
- (160) Hassani F.P., Whittaker B.N., Scoble M.J. Application of the Point Load Index Test to Strength Determination of Rock, Proposals for a New Size Correlation Chart. Proceeding of the 21st U.S. Symp. on Rock Mech., Rolla, MO, 1980
- (161) Hills E.S. Elements of structural geology, 2nd ed. Chapman and Hall Ltd., London, 1972, pp. 502
- (162) Hirschwald J. Die Prüfung der natürlichen Bausteine auf ihre Wetterbeständigkeit. Ernst and Sohn, Berlin, 1908
- (163) Hirschwald J. Die Prüfung der natürlichen Bausteine auf ihre Verwitterungsbeständigkeit. Verlag W Ernst & Sohn, Berlin, 1912
- (164) Hisashi A., Yukinori M., A new technique for non-destructive field measurement of rock-surface strength: an application of the Equotip hardness tester to weathering studies. Earth Surface Processes and Landforms, 2007, 32, pp. 1759-1769
- (165) Hobbs D.W. The tensile strength of rocks. Int. J. Rock Mech. Min. Sci., 1963, 1, pp.385–396
- (166) Hooker J.N., Laubach S.E., Marrett R. A universal power-law scaling exponent for fracture apertures in sandstones. GSA Bulletin v.126 (9/10), 2014, pp.1340–1362, doi: 10.1130/B30945.1
- (167) Hora Z.D. Dimension Stone “Granite” RO3, in Selected British Columbia Mineral Deposit Profiles, British Columbia Geological Survey, Victoria, B.C., Canada, 2007
- (168) ICR CNR NORMAL 7/81. Assorbimento d’acqua per immersione totale e capacità d’imbibizione, Roma, 1981
- (169) ICR CNR NORMAL 29/88. Misura Dell’Indice di Ascugamento, Roma, 1988
- (170) Ietto A., Ietto F. Age and history of the weathering of granitoids in southern Calabria. Geografia Fisica e Dinamica Quaternaria, 2004, 27, pp.37–45
- (171) Irfan T.Y., Dearman, W.R. Engineering classification and index properties of a weathered granite. Int. Assoc. Eng. Geol. Bull., 1978, 17, pp. 79–90
- (172) ISPRA. Carta geologica d’Italia. Foglio 561 – San Giovanni in Fiore, 2010 (a)
- (173) ISPRA. Carta geologica d’Italia. Foglio 542 – Verbicaro, 2010 (b)
- (174) ISRM-1981. Raccomandazioni ISRM per la misura della resistenza al punzonamento. R.I.G., 1, 1994, pp. 62-71
- (175) ISRM-1997. Raccomandazioni ISRM- Metodologie di prova per la determinazione della resistenza a trazione di materiali rocciosi, R.I.G., 3-4, 1997, pp. 111-114
- (176) ISRM-2007. The blue book: the complete ISRM suggested methods for rock characterization, testing and monitoring: 1974–2006. In: Ulusay, R., Hudson, J.A. (Eds.), Compilation Arranged by the ISRM Turkish National Group, Ankara, Turkey. Kazan Offset Press, Ankara
- (177) Jacobs Engineering U.K. Limited (Jacobs), Code of Practice on Skid Resistance for Local Authority Roads. Project n.41. Document control sheet BPP04F8, 2009
- (178) Jackson M. D., Marra F., Hay R.L., Cawood C., Winkler E.M. The judicious selection and preservation of tuff and travertine building stone in ancient Rome. Archaeometry, 2005, 47 (3), pp.485–510
- (179) Jermy C.A., Bell F.G. Durability of some dolerites from South Africa. In: Moore, D.P., Hungr, O. (Eds.), Proc. 8th Inter. Cong. of IAEG, vol. 4. Balkema, Vancouver, 1998, pp.2869– 2875

- (180) Ji S., Wang Q., Salisbury M.H. Composition and tectonic evolution of the Chinese continental crust constrained by Poisson's ratio. *Tectonophysics*, 2009, 463, pp.15–30.
- (181) Judd W.R., Huber C. Correlation of rock properties by statistical methods. *Proc Int Symp of Mining Resources*, University of Missouri, Rolla, 1962, pp 621–648
- (182) Kahraman S. Evaluation of simple methods for assessing the uniaxial compressive strength of rock. *International Journal of Rock Mechanics and Mining Sciences*, 2001, 38 (7), pp. 981-994
- (183) Kahraman S., Gunaydin O. The effect of rock classes on the relation between uniaxial compressive strength and point load index. *Bull. Eng. Geol. Environ.*, 2009, 68, pp.345–353
- (184) Kelsall P.C., Watters R., Franzone J.G. Engineering characterization of fissured, weathered dolerite and vesicular basalt. *Proc. 27th U.S. Symposium*, 1986, pp.77– 84
- (185) Khanlari G.R., Heidari M., Sepahigero A.A., Fereidooni D., Quantification of strength anisotropy of metamorphic rocks of the Hamedan province, Iran, as determined from cylindrical punch, point load and Brazilian tests. *Engineering Geology*, 2014, 169, pp. 80–90
- (186) Komloš C., Popovics S., Nürnbergerová T., Babál B., Popovics J. S. Ultrasonic pulse velocity test of concrete properties as specified in various standards. *Cement and Concrete Composites*, 1996, 18 (5), pp. 357-364
- (187) Kovács T. Durability of crystalline monumental stones in terms of their petrophysical characteristics (PhD Thesis), University of Bologna, 2009, 242 pp.
- (188) Kudo Y., Hashimoto K.I., Sano O., Nakagawa K. Relation between physical anisotropy and microstructures of granitic rocks in Japan. *Proceedings of the 6th Congress of the International Society of Rock Mechanics*, Montreal, Canada, August 30–September 3, 1987. vol. 1, 1987. p. 429–32
- (189) Kühnel R.A. Driving forces of rock degradation. In: Galán E., Zezza F. (Eds.) *Protection and Conservation of the Cultural Heritage of Mediterranean Cities*, Swets and Zeitlinges, Lisse, 2002, pp.11-17
- (190) Kühnel R.A. Cause and consequence: volume changes behing building material deterioration. *Materials Characterization*, 53, 2004, pp. 171-180
- (191) Laboritt. Linee guida per il recupero e la riqualificazione ambientale dei siti di cava nella Regione Calabria, Laboratorio Regionale di Ricerca Scientifica e Industriale per l’Innovazione, il Trasferimento Tecnologico e la sperimentazione di materiali costruttivi locali (aperto alle PMI), Dipartimento Attività Produttive, University of Reggio Calabria, 2014
- (192) Le Pera E., Sorriso-Valvo G. M. Weathering, erosion and sediment composition in a high gradient river, Calabria, Italy. *Earth Surface Processes and Landforms*, 2000, 25, pp. 277-292
- (193) Legambiente. Rapporto Cave 2014: I numeri, il quadro normativo, il punto sull’impatto economico e ambientale dell’attività estrattiva nel territorio italiano, Roma, 2014
- (194) Leone G. Pietra di Calabria: una introduzione storiografica per lo studio del patrimonio degli scalpellini dell’attuale provincia di Cosenza in età medioevale e moderna in “La pietra, il mestiere e l’arte del decorare. Storia della lavorazione della pietra nella provincia di Cosenza”, Pellegrini Editore, Cosenza, 2015, pp. 94-103
- (195) Li D., Wong L.N.Y., The Brazilian disc test for rock mechanics applications: review and New insights. *Rock Mech. Rock Eng*, 2013, 46 (2), pp. 269–287
- (196) Lico A. Materiali lapidei e cave di approvvigionamento degli scalpellini roglianesi: risorse in Calabria e nella Provincia di Cosenza, in “La pietra, il mestiere e l’arte del decorare. Storia della lavorazione della pietra nella provincia di Cosenza”, Pellegrini Editore, Cosenza, 2015, pp. 74-91
- (197) Litvan G.G. Adsorption systems at temperatures below the freezing point of the adsorptive. *Adv. Colloid Interface Sci.*, 1978, 9, pp.253–302

- (198) López-Arce P., Garcia-Guinea J., Benavente D., Tormo L., Doehne E. Deterioration of dolostone by magnesium sulphate salt: an example of incompatible building materials at Bonaval Monastery, Spain. *Constr Build Mater* 2009, 23(2), pp. 846–55
- (199) López-Arce P., Gomez-Villalba L.S., Pinho L., Fernández-Valle M.E., Álvarez de Buergo M., Fort R. Influence of porosity and relative humidity on consolidation of dolostone with calcium hydroxide nanoparticles: Effectiveness assessment with non-destructive techniques. *Materials characterization*, 2010, 61, pp. 168–184
- (200) López Mesones F., Escribano J., Nieves G. *Manual para el uso de la piedra en la arquitectura*, 2001, 393 pp.
- (201) MacAdam D.L. *Colour Measurement –Theme and Variations*, Second Revised Edition, Springer-Verlag, 1985, p.228
- (202) Martínez-Martínez J. Influencia de la alteración sobre las propiedades mecánicas de calizas, dolomías y mármoles. Evaluación mediante estimadores no destructivos (Ultrasonidos). PhD Thesis, University of Alicante, 2008, 295 pp.
- (203) Massa S., Naldini S., Rorro A. A system of classification of the decay of stone monuments. In: Baer N.S., Sabbioni C., Sors A. I. (Eds), *Science, Technology, and European Cultural Heritage: Proceedings of the European Symposium*, Bologna, Italy, 13–16 June 1989, 859–62. Oxford and Boston: Published in 1991 for the Commission of the European Communities by Butterworth-Heinemann Publishers.
- (204) Mastandrea A., Muto F., Neri C., Papazzoni C.A., Perri E., Russo F. Deep-Water Coral Banks: an Example from the “Calcare di Mendicino” (Upper Miocene, Northern Calabria, Italy), *FACIES*, 47, Erlangen, 2002, pp.27-42
- (205) Mastandrea A., Perri E., Neri C., Russo F. Conodont biostratigraphy of the Norian-Rhaetian deposits in the Northern Calabria. The Valle Corvino and Grisolia sections, *Bollettino della Società Paleontologica Italiana*, 2003, 42 (1-2), pp.39-47
- (206) Matano F., Di Nocera S. Weathering patterns in the Sila Massif (northern Calabria, Italy). *Italian Journal of Quaternary Sciences*, 1999, 12, pp.141–148
- (207) McWilliams J.R. The role of microstructure in the physical properties of rock. *Testing techniques for rock mechanics*, 1966, ASTM STP 402, 175–189
- (208) Meng Z., Pan J. Correlation between petrographic characteristics and failure duration in clastic rocks. *Engineering Geology*, 2007, 89(3/4), pp.258-265
- (209) Merke G. Sustainable development in the natural stone industry, *Roc. Maquina*, June 2000, pp56-58
- (210) Messina A., Barbieri M., Compagnoni R., De Vivo B., Perrone V., Russo S., Scott B. A. Geological and petrochemical study of the Sila Nappe granitoids (northern Calabria, Italy). *Boll Soc Geol Ital*, 1991 (a), 110, pp.165-206.
- (211) Messina A., Russo S., Perrone, Giacobbe A. Calc-alkaline late Variscan two mica-cordierite- Al-silicate-bearing intrusions of the Sila batholith (northern sector of the Calabrian- Peloritani Arc- Italy). *Boll Soc Geol Ital*, 1991 (b), 110, pp.365-389
- (212) Messina A., Russo S., Borghi A., Colonna V., Compagnoni R., Caggianelli A., Fornelli A., Piccarreta G. Il Massiccio della Sila Settore settentrionale dell’Arco Calabro-Peloritano. *Bollettino della Società Geologica Italiana*, 1994, 113, pp.539–586
- (213) Modestou S., Theodoridou M., Ioannou I., Fournari R. Micro-destructive mapping of salt crystallization in stone. *Proceedings of the 12th International Conference on the Deterioration and Conservation of Stone*, Columbia University, New York, 2012
- (214) Molina E., Cultrone G., Sebastián E., Alonso F.J. Evaluation of stone durability using a combination of ultrasound, mechanical and accelerated aging tests. *Journal of Geophysics and Engineering*, 2013, n.10
- (215) Molina E., Benavente D., Sebastián E., Cultrone G. The influence of rock fabric in the durability of two sandstones used in the Andalusian Architectural Heritage (Montoro and Ronda, Spain). *Engineering Geology* 197, 2015, 67–81
- (216) Montani C. *Stone 2007: World Marketing Handbook*, Gruppo Editoriale Faenza Editrice s.p.a., Faenza, Italy, 2007

- (217) Moomivand H., Development of a New Method for Estimating the Indirect Uniaxial Compressive Strength of Rock Using Schmidt Hammer, *BHM*, Vol. 156(4), 2011, pp.142–146
- (218) Moraes Rodrigues D., Emery S.D. Revisiting the conservation of the flooring of the Great Stone Church: Results of the use of ethyl silicate five years after treatment. In: Delgado Rodrigues J., Mimoso J.M. (Eds.), *Stone Consolidation in Cultural Heritage: Research and Practice; Proceedings of the International Symposium, Lisbon, 6–7 May, 2008*, 241–50. Lisbon: LNEC (Laboratório Nacional de Engenharia Civil).
- (219) Mosch S., Siegesmund S. Statistische Bewertung gesteintechnischer Kenndaten von Natursteinen. *Z dtsh Ges Geowiss*, 2007, 158(4), pp. 821–868
- (220) Nooruddin H.A., Hossain E., Al-Yousef H., Okasha T. Comparison of permeability models using mercury injection capillary pressure data on carbonate rock samples. *Journal of Petroleum Science and Engineering* 121, 2014, pp. 9–22
- (221) O'Rourke J.E. Rock Index Properties for Geoenvironmental Design in Underground Development. SME preprint 88-48, 1988, 5 pp.
- (222) Okubo F., Fukui K. Complete stress-strain curves for various rock types in uniaxial tension. *Int. J. Rock Mech. Min. Sci. Geomech. Abstr.*, 1996, 33(6), pp.549–556
- (223) Ordóñez, S., Fort, R., García del Cura, M. A. Pore size distribution and the durability of a porous limestone. *Q J Engin. Geol.* Vol. 30, nº 3, 1997, pp. 221-230
- (224) Kwasniewski M.A. Mechanical behaviour of anisotropic rocks. In: Hudson JA, editor. *Comprehensive rock engineering. Principles, practice & projects*. 1st ed., vol. 1. Pergamon Press, Oxford, 1993, pp. 285–312.
- (225) Pamplona M., Kocher M., Snethlage R., Aires Barros L. Drilling resistance: overview and outlook. *Z. dt. Ges. Geowiss.*, 2007, 158/3, 665–676
- (226) Pigeon M., Zuber B., Marchand J. Freeze/thaw resistance. In: Newmann J., Choo B.S. (Eds.) *Advanced Concrete Technology: Concrete Properties*. Butterworth-Heinemann, 2003, pp.11/2-11/17
- (227) Primavori P. *Planet stone*, Giorgio Zusi Editore S.A.S, 1999, Verona
- (228) Pender R.J. The behaviour of water in porous building materials and structures. *Reviews in Conservation*, 2004, 5 pp. 49-62
- (229) Pérez Bernal J.L., Bello López M.A. Fractal dimension of stone pore surface as weathering descriptor. *Applied Surface Science*, 2000, 161 (1), pp.47–53
- (230) Perez Ema N., Alvarez De Buergo M., Bustamante R.. Integrated studies for the evaluation of conservation treatments on building materials from archaeological sites. Application to the case of Merida (Spain). *International Journal of Conservation Science*, 2013, Volume 4, Special Issue, pp. 693-700
- (231) Perri F., Scarciglia F., Apollaro C., Marini L. Characterization of granitoid profiles in the Sila Massif (Calabria, southern Italy) and reconstruction of weathering processes by mineralogy, chemistry, and reaction path modeling. *J. Soils Sediments.*, 2015, 15, 1351–1372. DOI 10.1007/s11368-014-0856-x
- (232) Peschel A. *Natursteine*. VEB Deutscher Verlag für Grundstoffindustrie, Leipzig, 1983
- (233) Petagna L., Terrone G., Tenore M. Viaggio in alcuni luoghi della Basilicata e della Calabria Citeriore effettuato nel 1826, *Tip. Francese, Napoli*, 1827, pp. 78-86
- (234) Pettijohn F. J., *Sedimentary rocks*. Third ed. Harper and Brothers Publisher, New York, 1975, 618 pp.
- (235) Phillips W.J., Phillips N. *An introduction to mineralogy for geologists*, 1980, Wiley, New York
- (236) Poblador M.P. Legislación intenacional sobre patrimonio y restauración: Convenios y Cartas Internacionales. In: J. Gisbert Aguilar (Ed.), *Jornadas se Caracterización y Restauración de Materiales Pétreos en Arquitectura, Escultura y Restauración*, Universidad de Zaragoza, 2001, pp. 3-58
- (237) Poschlod K. *Das Wasser im Porenraum kristalliner Naturwerksteine*, Münchener Geowiss Abh B 7, Verlga Dr. Friedrich Pfeil, Munich, 1990

- (238) Powers T.C. A working hypothesis for further studies of frost resistance of concrete. *American Concrete Institute Journal Proc.*, 1945, 41, pp.245-272
- (239) Prikryl R. Some microstructural aspects of strength variation in rocks. *International Journal of Rock Mechanics & Mining Sciences*, 2001, 38, pp. 671–682
- (240) Primavori P. *Planet stone*, Giorgio Zusi Editore S.A.S, Verona, 1999
- (241) Rammamurthy T. Strength and modulus responses of anisotropic rocks. In: Brown ET, editor. *Comprehensive rock engineering. Principles, practice & projects*. 1st ed. Fundamentals, vol. 1. Pergamon Press, Oxford, 1993. p. 313–29
- (242) Reedy C. L. *Thin-Section Petrography of Stone and Ceramic Cultural Materials*. London, 2008, Archetype.
- (243) Regueiro M. *Minerales y Rocas: ¿De qué está hecho este planeta? Muy Especial*. Abril 2005, 62- 67. Editorial Muy Interesante. España. ISSN 1885.5180
- (244) Rigopoulos I., Tsikouras B., Pomonis P., Hatzipanagiotou K. Determination of the interrelations between the engineering parameters of construction aggregates from ophiolite complexes of Greece using factor analysis, *Construction and Building Materials*, 2013, 49, pp. 747–757
- (245) RILEM 1980, Recommended test to measure the deterioration of stone and to assess the effectiveness of treatment methods. Commission 25-PEM: Protection et Erosion des Monuments, pp. 175-253
- (246) Robertson E. C. Physical properties of building stone. In *Conservation of Historic Stone Buildings and Monuments: Report of the Committee on Conservation of Historic Stone Buildings and Monuments*, National Materials Advisory Board, Commission on Engineering and Technical Systems, National Research Council, 1982, pp.62–86. Washington, DC: National Academy Press.
- (247) Rodolico F. *Le pietre delle città d’Italia*, Second Edition, Firenze, Ed. Le Monnier, 1995, pp. 427-429
- (248) Rodríguez-Navarro C., Doehne E. Salt weathering: influence of evaporation rate supersaturation and crystallization pattern. *Earth Surface Processes and Landforms*, 1999, 24, pp. 191-209
- (249) Ruedrich J., Bartelsen T., Dohrmann R., Siegesmund S. Building sandstone integrity affected by the process of hygric expansion, *Environ Earth Sci*, 2010
- (250) Ruedrich J., Seidel M., Kirchner D. Salzverwitterung, hygrische und thermische Dehnung als auslösende Schadensquantitäten. *Z dtsch geol Ges*, 2005, 156(1), pp. 59–74
- (251) Ruedrich J., Siegesmund S. Fabric dependence of length change behaviour induced by ice crystallization in the pore space of natural building stones. In: Fort A, Alvarez de Buergo M, Gomez-Heras M et al (eds) *Heritage, weathering and conservation*. Taylor & Francis Group, London, 2006
- (252) Ruedrich J., Siegesmund S. Salt-induced weathering: an experimental approach. *Environ. Geol*, 2007 (a), 52, pp.225–249
- (253) Ruedrich J., Siegesmund S. Salt and ice crystallization in porous sandstones, *Environmental Geology*, 52, 2007 (b), pp. 225-249.
- (254) Sack D. A., Olson L. D. Advanced NDT methods for evaluating concrete bridges and other structures, *NDT&E International*, 1995, 28 (6), pp. 349–357
- (255) Saka M., Uchikawa T. Simplified NDE of a closed vertical crack using electronics, *NDT&E International*, 1995, 28 (5), pp. 289–296
- (256) Salerno M. “Facere et portare petra”:l’economia della pietra nella Calabria medievale, in “La pietra, il mestiere e l’arte del decorare. Storia della lavorazione della pietra nella provincia di Cosenza”, Pellegrini Editore, Cosenza, 2015, pp. 46-50
- (257) Saroglou H., Marinos P., Tsiambaos G. The anisotropic nature of selected metamorphic rocks from Greece. *J S Afr I Min Metall* 2004, 104(4):217–22

- (258) Scarciglia F., Vecchio G., De Rosa R., Robustelli G., Muto F., Le Pera E., Critelli S. The contribution of pedology to geomorphological analysis. The case of Sila (Calabria, southern Italy). *Mem. Descr. Carta Geol. d'It.*, 2008, pp. 253-276
- (259) Scarciglia F., Saporito N., La Russa M. F., Le Pera E., Macchione M., Puntillo D., Crisci G. M., Pezzino A. Role of lichens in weathering of granodiorite in the Sila uplands (Calabria, southern Italy). *Sedimentary Geology* 2012, 280, pp. 119–134
- (260) Scherer G.W., Valenza J.J. Mechanisms of frost damage. In: Young F., Skalny J. (Eds.) *Materials science of concrete VII. The American Ceramic Society*, Westerville, 2004, pp 209–246
- (261) Schilling, M.R. Colour Measurement of the Wall Painting in the Tomb of Nefertati. *The 10th Triennial Meeting for ICOM Committee for Conservation*, 1993, Washington: James & James
- (262) Schmidt E. A non-destructive concrete tester. *Concrete*, 1951, 59, pp. 34–35
- (263) Shadmon A. *Stone: an Introduction*, Intermediate Technology Publications, New York, 1989
- (264) Shalabi F.I., Cording E.J., Al-Hattamleh O.H. Estimation of rock engineering properties using hardness tests. *Eng. Geol.*, 2007, 90, pp. 138–147
- (265) Sharma S.K. *A textbook of building construction*. S. Chand Publishing, New Delhi, 1960
- (266) Sheremeti-Kabashi F., Snethlage R. Determination of structural anisotropy of Carrara marble with ultrasonic measurements 9th Int. Congress on Deterioration and Conservation of Stone vol 1 ed V Fassina (Amsterdam: Elsevier), 2000, pp 247–53
- (267) Siegesmund S. The significance of rock fabrics for the geophysical interpretation of geophysical anisotropies. *Geotekt Forsch*, 1996, 85:1–123
- (268) Siegesmund S., Dürrast H. Physical and Mechanical Properties of Rocks. In Siegesmund S., Snethlage R.. (Eds.). *Stone in Architecture. Properties, Durability 5th Edition*, Springer, Berlin, 2014, pp.107-224
- (269) Siegesmund S., Török Á. Building Stones. In Siegesmund S., Snethlage R.. (Eds.). *Stone in Architecture. Properties, Durability 5th Edition*, Springer, Berlin, 2014, pp. 34-43
- (270) Siegesmund S., Weiss T., Vollbrecht A. (Eds.) *Natural Stone, Weathering Phenomena, Conservation Strategies and Case Studies. Geological Society Special Publication*, 25, 2002, London, 448 pp.
- (271) Simmons G. Velocity of compressional waves in various minerals at pressures to 10 kbars. *J. Geophys. Res.*, 1964, 69, pp.1117–1121
- (272) Singh M.M. Strength of rock. In: Toulonkia YS, Judd WR, Roy RF, editors. *Physical properties of rocks and minerals. CINDAS data series on material properties*, vol. II-2, Hemisphere Publ Corp, New York, 1989, pp. 83–121.
- (273) Snethlage R. *Steinkonservierung, Forschungsprogramm des Zentrallabors für Denkmalpflege 1979–1983. Bericht für die Stiftung Volkswagenwerk. Arbeitsheft Bayr Landesamt Denkmalpflege*, Lipp, Munich, 1984, 22
- (274) Snethlage R. Stone conservation. In: Siegesmund S., Snethlage R.. (Eds.). *Stone in Architecture. Properties, Durability 5th Edition*, Springer, Berlin, 2014, pp.415-550
- (275) Snethlage R., Wendler E. Methoden der Steinkonservierung Anforderungen und Bewertungskriterien. In: Snethlage R (ed) *Denkmalpflege und Naturwissenschaft Natursteinkonservierung I*. Ernst & Sohn, Berlin, 1996, pp. 3–40
- (276) Sole G., *Viaggio nella Calabria Citeriore dell'800*, Amministrazione Provinciale di Cosenza, 1985, pp. 355-356
- (277) Sousa L.M.O., Calleja L., Suárez de Río L.M., Rey A.R. Anisotropia de propagação das ondas sísmicas em granitos. In: *Sociedade portuguesa de Geotecnia*, editors. *Annais do 8º Congresso Nacional de Geotecnia*, Lisboa, 2002. p. 507–16.
- (278) Sousa L.M.O. Evaluation of joints in granitic outcrops for dimension stone exploitation. *Q. J. Eng. Geol. Hydrogeol.*, 2010, 43, pp. 85–94

- (279) Sousa L.M.O., Suárez del Río L.M., Calleja L., Ruiz de Argandoña, Rodríguez Rey A. Influence of microfractures and porosity on the physico-mechanical properties and weathering of ornamental granites. *Engineering Geology*, 2005, 77, pp. 153-168
- (280) Steiger M., Charola A.E., Sterflinger K. Weathering and Deterioration. In Siegesmund S., Snethlage R. (Eds.). *Stone in Architecture. Properties, Durability 5th Edition*, Springer, Berlin, 2014, pp.225-316
- (281) Stone Federation of Great Britain. *Natural Stone Glossary*. London: Linked Advertising & Marketing, 1991
- (282) Streckeisen A.L. Plutonic rocks, classification and nomenclature recommended by the IUGS subcommission on the systematics of igneous rocks. *Geotimes*, 1973, 18 (10), pp. 26-30
- (283) Suárez del Río L.M. Estudio petrofísico de materiales graníticos geomecánicamente diferentes. Tesis Doctoral. Departamento de Petrología, Universidad de Oviedo, Spain, 1982
- (284) Sutphin D.M, Orris, G.J. Dimension Stone, in Preliminary Non-Fuel Mineral Resource Assessment of Afghanistan, Peters, S.G. et al (eds), United States Geological Survey Open-File Report, 2007, 1214, pp. 677-702
- (285) Svahn H. Non-Destructive Field Tests in Stone Conservation: Field and Laboratory Tests: Final Report for the Research and Development Project. Rapport från Riksantikvarieämbetet, 2006:4. Stockholm: Riksantikvarieämbetet. <http://www.raa.se/publicerat/9172094354.pdf>
- (286) Taber S. Frost heaving. *J. Geol.*, 1929, 37, pp.428–461
- (287) Taber S. The mechanics of frost heaving. *J. Geol.*, 1930, 38, pp.303–317
- (288) Takemura T., Golshani A., Oda M., Suzuki K. Preferred orientations of open microcracks in granite and their relation with anisotropic elasticity. *Int. J. Rock Mech. Min. Sci.*, 2003, 40, pp. 443–454
- (289) Tansi C., Muto F., Critelli S., Iovine G. Neogene-Quaternary strike-slip tectonics in the central Calabrian Arc (Southern Italy). *Journal of Geodynamics*, 2007, 43, pp.393–414
- (290) Theodoridou M., Dagrain F., Ioannou I. Correlation of stone properties using standardized methodologies and non-standardized micro-destructive techniques. *Proceedings of 12th International Congress on the Deterioration and Conservation of Stone*, Columbia University, New York, 2012
- (291) Thompson A., Burrows A., Flavin D., Walsh I. The sustainable use of high specification aggregates for skid resistant road surfacing in England, Report to the Office of the Deputy Prime Minister and the Mineral Industry Research Organisation, Capita Symonds Ltd., East Grinstead, 2004.
- (292) Thompson A. High specification aggregates for road surfacing materials in England – updating the Travers Morgan report, in: G. Walton (Ed.) *Proceedings of the 14th Extractive Industry Geology Conference, Resistance of marginal durability aggregates skid resistance of marginal durability aggregates*, 2008, pp. 91–98
- (293) Tiano P., Rodrigo J., De-Witte E., Verges-Belmin V., Massey S., Snethlage R., Costa D., Cadot-Leroux L., Garrod E., Singer B. The conservation of monuments: A new method to evaluate consolidating treatments. *International Journal for Restoration of Buildings and Monuments*, 2000, 6: 133-150
- (294) Torraca G. Porous building materials. *Materials science for architectural conservation*. ICCROM, Rome, Italy, 1982, 145pp.
- (295) Tournier B., Jeannette D., Destrigenville C. Stone drying: an approach of the effective evaporation surface area. In: Fassina V. (ed) *9th international congress on deterioration and conservation of stone*. Elsevier, Amsterdam, 2000
- (296) Tsur-Lavie Y., Denekamp S.A. Comparison of size effect for different types of strength tests. *Rock Mechanics*, December 1982, V. 15, Issue 4, pp 243–254, doi:10.1007/BF01240592
- (297) Tuğrul A. The effect of weathering on the pore geometry and compressive strength of selected rock types from Turkey. *Engineering Geology*, 2004, 75, pp. 215-227
- (298) Tuğrul A., Zarif I. H. Correlation of mineralogical and textural characteristics with engineering properties of selected granitic rocks from Turkey. *Engineering Geology*, 1999,51, pp. 303-317

- (299) Tourenq C., Fourmaintraux D., Denis A. Propagation des ondes et discontinuités des roches. Proceedings of International Symposium on Rock Mechanics, 1971, Nancy, I-1
- (300) Tucker M.E. Geologia del sedimentario: rocce, strutture sedimentarie, ambienti deposizionali. Dario Flaccovio Editore, Palermo, 1st Edition, 2010, 366 pp.
- (301) Uchida E., Ogawa Y., Maeda N., Nakagawa T. Deterioration of stone materials in the Angkor monuments, Cambodia, Engineering Geology, 1999, 55, pp. 101–112
- (302) Ugur I., Demirdag S., Yavuz H. Effect of rock properties on the Los Angeles abrasion and impact test characteristics of the aggregates. Materials Characterization, 2010, 61, pp. 90-96
- (303) UNI-EN 1097-1:1996. Tests for mechanical and physical properties of aggregates – Part 1: determination of the resistance to wear (micro-Deval). European Committee for Standardization, Brussels, 1996.
- (304) UNI-EN 1097-2:1999. Prove per determinare le proprietà meccaniche e fisiche degli aggregati - Metodi per la determinazione della resistenza alla frammentazione. Ente Nazionale Italiano di Unificazione, Milano, 1999
- (305) UNI-EN 1925:2000. Metodi di prova per pietre naturali - Determinazione del coefficiente di assorbimento d'acqua per capillarità. Ente Nazionale Italiano di Unificazione, Milano, 2000
- (306) UNI-EN 1926:2000. Metodi di prova per pietre naturali - Determinazione della resistenza a compressione. Ente Nazionale Italiano di Unificazione, Milano, 2000
- (307) UNI EN 12370:2001. Metodi di prova per pietre naturali - Determinazione della resistenza alla cristallizzazione dei Sali. Ente Nazionale Italiano di Unificazione, Milano
- (308) UNI-EN 12372:2001. Metodi di prova per pietre naturali - Determinazione della resistenza a flessione sotto carico concentrato. Ente Nazionale Italiano di Unificazione, Milano, 2001
- (309) UNI EN 12670:2001. Pietre naturali – Terminologia. Ente Nazionale Italiano di Unificazione, Milano, 2001
- (310) UNI-EN 1936:2001. Metodi di prova per pietre naturali - Determinazione delle masse volumiche reale e apparente e della porosità totale e aperta. Ente Nazionale Italiano di Unificazione, Milano, 2001
- (311) UNI EN 13755:2002. Metodi di prova per pietre naturali - Determinazione dell'assorbimento d'acqua a pressione atmosferica. Ente Nazionale Italiano di Unificazione, Milano, 2002
- (312) UNI-EN 1341:2003. Lastre di pietra naturale per pavimentazioni esterne - Requisiti e metodi di prova. Ente Nazionale Italiano di Unificazione, Milano, 2003
- (313) UNI-EN 1342:2003. Cubetti di pietra naturale per pavimentazioni esterne - Requisiti e metodi di prova. Ente Nazionale Italiano di Unificazione, Milano, 2003
- (314) UNI-EN 1343:2003. Cordoli di pietra naturale per pavimentazioni esterne - Requisiti e metodi di prova. Ente Nazionale Italiano di Unificazione, Milano, 2003
- (315) UNI EN 1097-1:2004. Prove per determinare le proprietà meccaniche e fisiche degli aggregati - Determinazione della resistenza all'usura (micro-Deval). Ente Nazionale Italiano di Unificazione, Milano, 2004.
- (316) UNI-EN 14579:2005. Metodi di prova per pietre naturali - Determinazione della velocità di propagazione del suono. Ente Nazionale Italiano di Unificazione, Milano
- (317) UNI-EN 11182:2006. Descrizione della forma di alterazione; Termini e definizioni = Cultural heritage: Natural and artificial stone; Description of the alteration; Terminology and definition. Ente Nazionale Italiano di Unificazione, Milano and Roma
- (318) UNI-EN 12407:2007. Natural Stone Test Methods - Petrographic Examination. Ente Nazionale Italiano di Unificazione, Milano
- (319) UNI-EN 998-2:2010. Specifiche per malte per opere murarie - Parte 2: Malte da muratura. Ente Nazionale Italiano di Unificazione, Milano, 2010

- (320) UNI-EN 15886:2010. Conservation of cultural property - Test methods - Colour measurement of surfaces. Ente Nazionale Italiano di Unificazione, Milano, 2010
- (321) UNI-EN ISO 16859-1:2015. Metallic materials - Leeb hardness test - Part 1: Test method. International Organization for Standardization, 2015
- (322) UNI-EN ISO 16859-2:2015. Metallic materials - Leeb hardness test - Part 2: Verification and calibration of the testing devices. International Organization for Standardization, 2015
- (323) UNE-EN 15802:2010. Conservación del patrimonio cultural - Métodos de ensayo - Determinación del ángulo de contacto estático. AENOR, Madrid, 2010
- (324) UNE-EN 12371:2011. Natural stone test methods. Determination of frost resistance. AENOR, Madrid, 2011
- (325) Valdeón L., Montoto M., Calleja L., Esbert R.M. A method to assess spatial coordinates in art and archaeological objects: Application of tomography to a dolmen. *Journal of Archaeological Science*, 1997, 24 pp. 337-346
- (326) Vallejo L.E., Walsh R.A., Robinson M.K. Correlation Between Unconfined Compressive and Point Load Strength for Appalachian Rocks. In the Proceeding of the 30th U.S. Symposium on Rock Mechanics, 1989, pp.461-468
- (327) Van Balen K. Expert system for evaluation of deterioration of ancient brick masonry structures. *Science of the Total Environment*, 1996, 189–190: 247–54
- (328) Van Balen K. Expert System for the Evaluation of the Deterioration of Ancient Brick Structures: Scientific Background of the Damage Atlas and the Masonry Damage Diagnostic System. Research Report (European Commission, Directorate-General XII, Science, Research, and Development) 8. Luxembourg: Office for Official Publications of the European Communities, and Lanham, MD: Bernan Associates (distributor), 1999
- (329) Van Dijk J. P., Bello M., Brancaleoni G. P., Cantarella G., Costa V., Frixia A., Golfetto F., Merlini S., Riva M, Torricelli S., Toscano C., Zerilli A. A regional structural model for the northern sector of the Calabria Arc (Southern Italy). *Tectonophysics*, 2000, 324, pp.267–320
- (330) Van Hees R., Naldini S., Lubelli B. The development of MDDS-COMPASS. Compatibility of plasters with salt loaded substrates. *Construction and Building Materials*, 2009, 23 (5): 1719–30
- (331) Van Hees R.P.J., Naldini S., Sanders M. An expert system for analysis of damage to plasters due to salt and moisture. In *Sais solúveis em argamassas de edifícios antigos: Danos, processos e soluções*, Lisboa, LNEC, 14 e 15 de Fevereiro de 2005, 16.1–16.11. *Cursos e seminários 32*. Lisbon: Laboratório Nacional de Engenharia Civil, 2006
- (332) Vasanelli E., Colangiuli D., Calia A., Sileo M., Aiello M.A. Ultrasonic pulse velocity for the evaluation of physical and mechanical properties of a highly porous building limestone, *Ultrasonics* 60, 2015, pp. 33–40
- (333) Vasconcelos G., Lourenço P.B., Alves C.A.S., Pamplona J. Analysis of weathering and internal texture on the engineering properties of granites, in: 11th International Congress of the International Society of Rock Mechanics, Workshop W3-Preservation of Natural Stone and Rock Weathering, 2007, pp. 75–83
- (334) Vasconcelos G., Lourenço P.B., Alves C.A.S., Pamplona J. Ultrasonic evaluation of the physical and mechanical properties of granites. *Ultrasonics* 48, 2008, pp. 453–466
- (335) Vázquez P., Alonso F.J., Esbert R.M., Ordaz J. Ornamental granites: Relationships between p-waves velocity, water capillary absorption and the crack network. *Construction and Building Materials* 24, 2010, pp. 2536–2541
- (336) Vergès-Belmin, V. Répartition des sels et cartographie des altérations sur la façade de l'église Notre-Dame-La-Grande à Poitiers, France = Salts distribution and mapping of stone surface weathering on the facade of Notre-Dame-La-Grande in Poitiers, France. In: Delgado Rodrigues J., Henriques F., Telmo Jeremias F. (Eds.). *Proceedings of the 7th International Congress on Deterioration and Conservation of Stone*, Lisbon, 15–18 June 1992, 927–36
- (337) Vergès-Belmin V. *Illustrated Glossary on Stone Deterioration Patterns=Glossaire illustré sur les formes d'altération de la pierre*, English-French ed. *Monuments & Sites* 15, 2008, ICOMOS (International Council on Monuments and Sites) and ISCS (International Scientific Committee for Stone), Paris (80 pp.)

- (338) Vicente M.A., Delgado-Rodrigues J., Acevedo J. (Eds). Degradation and conservation of granitic rocks in monuments – Proceedings of EC workshop Environmental protection and conservation of the European cultural heritage, Santiago de Compostela, Spain, 1996, p. 471
- (339) Viles H. Goudie A., Grab S., Lalley J. The use of the Schmidt Hammer and Equotip for rock hardness assessment in geomorphology and heritage science: a comparative analysis. *Earth Surf Proc Land* 2011;36:320–33
- (340) Vollbrecht A., Dürrast H., Weber K. Open microcracks: indicators for in-situ stress directions, 1993, KTB-Report 93–2, pp.227–230
- (341) von Moos A., De Quervain F. *Technische Gesteinskunde*. Birkhäuser, Basel, 1948
- (342) Vos B.H. Hygric methods for the determination of the behaviour of stones. International symposium on deterioration of stone monuments. UNESCO-RILEM, Paris, 1978
- (343) Walder J.S., Hallet B. The physical basis of frost weathering: toward a more fundamental and unified perspective. *Arct. Alp. Res.*, 1986, 18, pp.27–32
- (344) Walsh J.B. The effect of cracks on the uniaxial elastic compression of rocks. *Journal of Geophysical Research*, 1965, 70(2), pp.399-411
- (345) Washburn E.W. A method of determining the distribution of pore sizes in a porous material. *Proc Nat Acad Sci*, 1921, 7, p. 115
- (346) Weiss G. Die Eis- und Salzkristallisation im Porenraum von Sandsteinen und ihre Auswirkungen auf das Gefüge unter besonderer Berücksichtigung gesteinspezifischer Parameter. *Münchner Geowiss Abh B 9*, Verlag Dr. Friedrich Pfeil, Munich, 1992
- (347) Wendler E., Sattler L. Bohrwiderstandsmessung als zerstörungssarmes Prüfverfahren. Proceeding of the 4th Int. Koll. Werkstoffwissenschaften und Bauinstandsetzen, 1996, Esslingen, Germany
- (348) Wenham M. Stiffness and flexibility. 200 science investigations for young students, 2001, p. 126, ISBN 978-0-7619-6349-3
- (349) Wenk H.R. Preferred orientation in deformed metals and rocks. An introduction to modern texture analysis. Academic, Orlando, 1985
- (350) Winkler E.M. A durability index for stone. In *Ve Congrès international sur l'altération et la conservation de la Pierre*, Lausanne, 25–27, 9, 1985: Actes = 5th International Congress on Deterioration and Conservation of Stone, Lausanne, 25–27.9.1985. G. Félix (Ed.), 151–56. Lausanne: Presses polytechniques romandes
- (351) Winkler E.M. *Stone in Architecture: Properties, Durability*, 3rd ed. Springer-Verlag, Berlin, 1997, 309 p.
- (352) Winkler E.M., Singer P.C. Crystallization pressure of salts in stone and concrete. *Geology Society American Bulletin*, 1972, 83, pp. 3509-3514
- (353) Yerrapragada S.S., Tambe S.S., Gauri K.L. Fractals, pore potential and Sphinx limestone durability. In *Rock for Erosion Control*. McElroy C.H., Lienhart D.A. (Eds.), 38–45. ASTM Special Technical Publication 1177, 1993, Philadelphia: ASTM.
- (354) Yasar E., Erdogan Y. Correlating sound velocity with density, compressive strength and Young modulus of carbonate rocks, *International Journal of Rock Mechanics and Mining Sciences*, 2004, 41 (5), pp. 871–875
- (355) Zaouia N., Elwartiti M., Baghdad B. Superficial alteration and soluble salts in the calcarenite weathering. case study of almohade monuments in Rabat: Morocco, *Environ. Geol.*, 48, 2005, pp. 742–747
- (356) Zehnder K., Arnold A. Crystal growth in salt efflorescence. *J Cryst Growth* 1989, 97, pp.513–52
- (357) Zezza F. Computerized analysis of stone decay in monuments. In: Veniale F., Zezza U. (Eds.), *Advanced Workshop: Analytical Methodologies for the Investigation of Damaged Stones*, Pavia University, Italy, 14–21 September 1990 (a), 163–84

- (358) Zezza U. Physical-mechanical properties of quarry and building stones. In: Veniale F., Zezza U. (Eds.), *Advanced Workshop: Analytical Methodologies for the Investigation of Damaged Stone*, Pavia University, Italy, 14-21 September 1990 (b)
- (359) Zezza F., The E.C. Project Marine spray and polluted atmosphere as factors of damage to monuments in the Mediterranean coastal environment: objectives and results, *Eur. Cultural Herit. Newslett. Res.*, 7, 1-4, 1993, pp. 49-52
- (360) Zezza F. Stone decay diagnosis and control of treatments by computerized analytical techniques. In: Fassina V., Ott H., Zezza F. (Eds.), *Conservation of Monuments in the Mediterranean Basin: Stone Monuments, Methodologies for the Analysis of Weathering and Conservation; Proceedings of the 3rd International Symposium, Venice, 22-25 June, 1994*, pp.77-81 and plates
- (361) Zezza F. Non-destructive technique for the assessment of the deterioration processes of prehistoric rock art in karstic caves: The paleolithic paintings of Altamira (Spain). In: Galán Huertos E., Zezza F. (Eds.), *Protection and Conservation of the Cultural Heritage of the Mediterranean Cities*, Lisse, Netherlands, and Exton, PA, Balkema, 2002, 377-88

Websites

<http://www.stonehengeandaveburywhs.org/about-us/stonehenge-avebury/>
<https://en.wikipedia.org/wiki/Stonehenge>
https://en.wikipedia.org/wiki/Great_Pyramid_of_Giza
<https://en.wikipedia.org/wiki/Trullo>
https://en.wikipedia.org/wiki/Roman_aqueduct
https://en.wikipedia.org/wiki/Modena_Cathedral
[https://it.wikipedia.org/wiki/Cattedrale_di_Notre-Dame_\(Tournai\)](https://it.wikipedia.org/wiki/Cattedrale_di_Notre-Dame_(Tournai))
<http://www.archdaily.com/372492/ad-classics-stephanuskirche-alvar-aalto>
<http://www.archdaily.com/124725/ad-classics-neue-staatsgalerie-james-stirling>
<http://www.archdaily.com/206751/bajo-martin-county-magen-arquitectos>
<https://www.dezeen.com/2007/09/09/dominus-winery-by-herzog-de-meuron/>
<http://www.arcspace.com/features/renzo-piano-/padre-pio-pilgrimage-church/>
https://en.wikipedia.org/wiki/Joachim_of_Fiore
http://www.florense.it/Inglese/San_Giovanni_in_Fiore-Italy.asp
<http://www.visitsitaly.com/calabria/grisolia/>
http://web.provincia.cs.it/ptcp/struttura_ambiente/sist_ris_stor_cult/ralazione1.pdf
<http://www.europietra.it>
<http://www.architetturadi Pietra.it>
<http://www.grapevintexas.gov/DocumentCenter/View/128>
<http://www.stastier.co.uk/nhl/guides/protection.htm>